

**Investigating the role of small RNAs in the interaction between  
the model grass *Brachypodium distachyon* and the  
endosymbiont *Serendipita indica* (syn. *Piriformospora indica*)**

Dissertation zur Erlangung des Doktorgrades (Dr. rer. nat.) der  
Naturwissenschaftlichen  
Fachbereiche der Justus-Liebig-Universität Gießen

durchgeführt am Institut für Phytopathologie

vorgelegt von  
M. Sc. Ena Šečić  
Gießen, 2021

1. Gutachter: Prof. Dr. Karl-Heinz Kogel
2. Gutachter: Prof. Dr. Volker Wissemann



**Investigating the role of small RNAs in the interaction between  
the model grass *Brachypodium distachyon* and the  
endosymbiont *Serendipita indica* (syn. *Piriformospora indica*)**

Dissertation zur Erlangung des Doktorgrades (Dr. rer. nat.) der  
Naturwissenschaftlichen  
Fachbereiche der Justus-Liebig-Universität Gießen  
durchgeführt am Institut für Phytopathologie

vorgelegt von  
M. Sc. Ena Šečić  
Gießen, 2021

1. Gutachter: Prof. Dr. Karl-Heinz Kogel
2. Gutachter: Prof. Dr. Volker Wissemann

## Abstract

Plants and microbes readily establish interactions resulting in varying outcomes, ranging from antagonistic to beneficial for both organisms. Mutualistic interactions with reciprocal benefits are called symbioses, and they include an exchange of nutrients between plant and microbe, as well as growth promotion and priming against biotic and abiotic stresses within the host. The rhizosphere is a microbe-rich environment in which roots come in contact with many organisms, including beneficial endophytes that can colonize and proliferate inside plants.

Recent discoveries emphasized the role of small RNAs (sRNAs) and RNA interference (RNAi) in modulating gene expression by cross-kingdom (ck) communication. In plant-pathogen ck communication, sRNAs are exchanged between a plant and a microbe in a bidirectional fashion, targeting virulence genes of the pathogen and defense-related transcripts in the plant. Beyond this exogenous role of sRNAs, it is known that both plants and microbes reprogram their transcriptional landscape in response to their interactions, by deploying endogenous gene silencing via micro RNAs (miRNAs). RNAi-associated proteins, which facilitate both endogenous and ck-guided gene silencing, are encoded by Argonaute (*AGO*) and Dicer-like (*DCL*) gene families. Since these gene families are expanded in many plant species, we analyzed the genome of the model grass plant *Brachypodium distachyon* to detect its putative AGOs and DCLs and elucidate on their structures.

Subsequently, a novel model system for plant-endophyte research, between *B. distachyon* and the endosymbiont *Serendipita indica* (syn. *Piriformospora indica*) was established. Concurrent mRNA and sRNA sequencing of the colonized roots and control samples within this interaction was performed, and a previously established bioinformatics pipeline applied to predict putative sRNAs with ck and endogenous roles. Target prediction and analysis of downregulation indicate that sRNA-mediated silencing might be involved in growth, development, modulation of plant immunity and fungal nutrient acquisition during the colonization. Thus, RNAi-based regulation in this system provides novel insight into sRNAs in mutualistic interactions, and also promises target discovery and translation to crop species that can be colonized by *S. indica*.

The role of sRNA-mediated silencing during infection of *B. distachyon* tissues with the fungal pathogens *Magnaporthe oryzae* and *Fusarium graminearum* also indicated control of plant immune responses. Evidently, sRNAs are widely utilized to navigate the transcriptional landscape in plant-microbe interactions. Conserved plant miRNA families are also variably responsive to pathogens and mutualists, reinforcing both the parallels and differences in plant responses. RNAi-based plant protection, which utilizes this pathway to silence pathogenic virulence genes, is an attractive addition to existing plant protection strategies. We concluded that the requirements for efficient RNAi-based application against fungal pathogens converge on stability of applied sRNA, uptake and expression of fungal RNAi proteins.

## Zusammenfassung

Pflanzen und Mikroben gehen leicht Wechselbeziehungen ein, die zu unterschiedlichen Ergebnissen führen, die von antagonistisch bis vorteilhaft für beide Organismen reichen. Mutualistische Interaktionen werden als Symbiosen bezeichnet und umfassen den Austausch von Nährstoffen zwischen Pflanze und Mikrobe sowie die Förderung des Wachstums und die Vorbeugung gegen biotische und abiotische Stressfaktoren im Wirt. Die Rhizosphäre ist eine an Mikroben reiche Umgebung, in der Wurzeln mit vielen Mikroben in Kontakt kommen, darunter auch nützliche Endophyten, die sich in Pflanzen ansiedeln und vermehren können.

Jüngste Entdeckungen zeigen die Rolle von kleinen RNAs (sRNAs) und RNA-Interferenz (RNAi) bei der Modulation der Genexpression durch Cross-Kingdom Kommunikation (ck). Bei der ck-Kommunikation zwischen Pflanze und Pathogen werden sRNAs zwischen einer Pflanze und einer Mikrobe bidirektional ausgetauscht, wobei sie auf Virulenzgene des Pathogens und auf verteidigungsrelevante Transkripte in der Pflanze abzielen. Neben dieser exogenen Rolle von sRNAs ist bekannt, dass sowohl Pflanzen als auch Mikroben ihre Transkriptionslandschaft als Reaktion auf ihre Interaktion umprogrammieren, indem sie endogenes Gen-Silencing über Mikro-RNAs (miRNAs) einsetzen. RNAi-assoziierte Proteine, die sowohl endogenes als auch ck-gesteuertes Gen-Silencing ermöglichen, werden von den Genfamilien Argonaute (*AGO*) und Dicer-like (*DCL*) kodiert. Da diese Genfamilien in vielen Pflanzenarten verbreitet sind, haben wir das Genom der Modellgraspflanze *Brachypodium distachyon* analysiert, um ihre mutmaßlichen AGOs und DCLs aufzuspüren und ihre Proteinstrukturen aufzuklären.

Anschließend wurde eine neue Modellinteraktion für die Pflanzen-Endophytenforschung zwischen *B. distachyon* und dem Endosymbionten *Serendipita indica* (syn. *Piriformospora indica*) etabliert. Es wurde eine gleichzeitige mRNA- und sRNA-Sequenzierung der kolonisierten Wurzeln und der Kontrollproben durchgeführt, und es wurde eine zuvor eingerichtete Bioinformatik-Pipeline zur Vorhersage mutmaßlicher sRNAs mit ck- und endogenen Funktionen eingesetzt. Die Zielvorhersage und die Analyse der Herunterregulierung deuten darauf hin, dass das sRNA-vermittelte Silencing an Wachstum, Entwicklung, Modulation der Pflanzenimmunität und Pilznährstoffakquisition während der Kolonisierung beteiligt sein könnte. Die RNAi-basierte Regulierung in diesem System liefert somit neue Erkenntnisse über sRNAs in mutualistischen Interaktionen und verspricht auch die Entdeckung von Zielmolekülen und deren Übertragung auf Pflanzenarten, die ebenfalls von *S. indica* besiedelt werden können.

Die Rolle des sRNA-vermittelten Silencing während der Infektion von *B. distachyon*-Gewebe mit den Pilzpathogenen *Magnaporthe oryzae* und *Fusarium graminearum* deutet ebenfalls auf die Kontrolle der pflanzlichen Immunreaktionen hin. Offensichtlich werden sRNAs in großem Umfang genutzt, um die Transkriptionslandschaft bei Interaktionen zwischen Pflanzen und Mikroben zu

steuern. Auch konservierte miRNA Familien reagieren unterschiedlich auf Pathogene und Mutualisten, was sowohl die Parallelen als auch die Unterschiede in den pflanzlichen Reaktionen unterstreicht.

RNAi-basierter Pflanzenschutz, der diesen Weg nutzt, um Virulenzgene eines Pathogens zu silencen, ist eine attraktive Ergänzung zu bestehenden Pflanzenschutzstrategien. Ich komme zu dem Schluss, dass die Voraussetzungen für eine effiziente RNAi-basierte Anwendung gegen Pilzpathogene in der Stabilität der applizierten sRNA und der effizienten Expression von Pilz-RNAi-Proteinen liegen.

## Contents

Abbreviations	7
General introduction to plant-microbe interactions	8
Plant – mutualist interactions	9
Basic outline of plant immunity	10
Plant response to mutualistic microbes	12
Plant-microbe symbioses in agriculture	13
<i>Serendipita indica</i> (syn. <i>Piriformospora indica</i> ) – a model root endophyte	14
<i>Magnaporthe oryzae</i> and <i>Fusarium graminearum</i> – major cereal pathogens	16
<i>Brachypodium distachyon</i> – a model grass plant	17
RNA Interference and associated proteins in plants and fungi	18
Small RNAs in plant-microbe interactions	19
Cross-kingdom communication between plants and microbes	20
miRNAs in plant-microbe interactions	21
Bioinformatics approaches to analysis of plant-microbe sequencing datasets	22
Applications of RNAi-based plant protection	23
General discussion and conclusions	24
References	28
List of publications	36
A bioinformatics pipeline for the analysis and target prediction of RNA effectors in bidirectional communication during plant–microbe interactions	37
Further elucidation of the Argonaute and Dicer protein families in the model grass species <i>Brachypodium distachyon</i>	44
Comparative analysis of transcriptome and sRNA expression patterns in the <i>Brachypodium distachyon</i> - <i>Magnaporthe oryzae</i> pathosystems	59
Requirements for fungal uptake of dsRNA and gene silencing in RNAi-based crop protection strategies	91
Biotic stress-associated microRNA families in plants	98
A novel plant-fungal association reveals fundamental sRNA and gene expression reprogramming at the onset of symbiosis	109

<b><i>Fusarium graminearum</i> DICER-like-dependent sRNAs are required for the suppression of host immune genes and full virulence</b>	<b>131</b>
<b>Selbstständigkeitserklärung</b>	<b>156</b>
<b>Acknowledgments</b>	<b>157</b>
<b>Supplementary material</b>	<b>158</b>

## Abbreviations

<b>AGO</b>	Argonaute
<b>AMF</b>	arbuscular mycorrhizal fungi
<b>ck</b>	cross-kingdom
<b>DAMP</b>	danger-associated molecular pattern
<b>DCL</b>	Dicer-like
<b>DON</b>	deoxynivalenol
<b>DPI</b>	day post infection/inoculation
<b>dsRNA</b>	double-stranded RNA
<b>ETI</b>	effector-triggered immunity
<b>ETS</b>	effector-triggered susceptibility
<b>EV</b>	extracellular vesicle
<b>exRNA</b>	extracellular RNA
<b>FHB</b>	Fusarium head blight
<b>GMO</b>	genetically modified organism
<b>HIGS</b>	host-induced gene silencing
<b>HR</b>	hypersensitive response
<b>ISR</b>	induced systemic resistance
<b>JA</b>	jasmonic acid
<b>LCO</b>	lipochitooligosaccharide
<b>lncRNA</b>	long non-coding RNA
<b>mRNA</b>	messenger RNA
<b>MAMP</b>	microbe-associated molecular pattern
<b>Mb</b>	megabase (pair)
<b>MBCA</b>	microbial biological control agent
<b>MF</b>	mycorrhizal fungi
<b>Mo</b>	<i>Magnaporthe oryzae</i>
<b>miRNA</b>	micro RNA
<b>milRNA</b>	miRNA-like RNA
<b>NB-LRR</b>	nucleotide-binding-leucine-rich-repeat
<b>ncRNA</b>	non-coding RNA
<b>nt</b>	nucleotide
<b>PAMP</b>	pathogen-associated molecular pattern
<b>PR gene</b>	pathogenesis-related gene
<b>PRR</b>	pattern recognition receptor
<b>PTGS</b>	post-transcriptional gene silencing
<b>PTI</b>	PAMP/pattern-triggered immunity
<b>R-gene</b>	resistance gene
<b>RdRP</b>	RNA-dependent RNA polymerase
<b>RNAi</b>	RNA interference
<b>rRNA</b>	ribosomal RNA
<b>SA</b>	salicylic acid
<b>SAR</b>	systemic acquired resistance
<b>SIGS</b>	spray induced gene silencing
<b>sRNA</b>	small RNA
<b>ss sRNA</b>	single-stranded sRNA
<b>ta-siRNA</b>	trans-acting small interfering RNA
<b>TGS</b>	transcriptional gene silencing
<b>tRF</b>	tRNA-derived RNA fragment
<b>tRNA</b>	transfer RNA

## General introduction to plant-microbe interactions

Plants commonly establish interactions with microbial organisms such as bacteria, archaea, viruses, fungi and oomycetes, as well as with complex microbial networks composed of a multitude of microbes simultaneously (van der Heijden and Hartmann, 2016). Ubiquitous in nature, these interactions significantly contribute to the chemical and physiological landscape of the phytobiome.

Because of their complexity, existing research on relationships between plants and microbes is based on an array of diverse and multifaceted approaches. Outside the oversimplified conditions of laboratory research, plants in nature come in contact with microbes on a spectrum of varying character and life styles. This spectrum, classified by the effect the microbes have on the plant, contains plant pathogens, beneficial plant mutualists and commensal organisms. Additionally, depending on whether the microbes obtain nutrients from living or dead plants, they are classified as biotrophic or saprophytic, respectively, and, in case the microbes themselves kill plant cells, necrotrophic organisms. All of them survive and, if conditions are favorable, proliferate in and/or around plant tissues, thus forming what is known as the holobiont. Plant interactions are a multidirectional signaling exchange network, in which individual organisms form specific hubs within diverse communities. Additionally, both the host and the microbe interact and depend on environmental conditions. Thus, understanding the qualitative and quantitative composition of these microbial communities is necessary to present a complete picture of the plant holobiont.

In response to microbial presence, signaling cascades and corresponding genetic reprogramming of plant cells, as well as the microbes themselves, are under scrutiny of a multitude of genomic and transcriptomic research approaches. While some pathways, especially in study of well-established pathosystems (e.g. *Arabidopsis thaliana* with the bacterium *Pseudomonas syringae*, the oomycete *Hyaloperonospora arabidopsidis* or the fungus *Botrytis cinerea*), are well understood, the differences in response to pathogens and beneficial microbes is less so, as well as the translation of known pathways to crop plants with more complex genomes (Harris et al., 2020). The advent of fast and high-throughput sequencing approaches and accompanying bioinformatics tools developed to predict and analyze these discrepancies are powerful allies in furthering knowledge about plant-microbe interactions.

Lastly, stable and long-term exposure to specific microbes often results in macroscopic changes in plant phenotypes, often in agronomically relevant traits such as yield and resistance to stresses. Predicting this final, quantifiable outcome of the interaction is not an easy matter though, since many factors, including microbial community composition, plant life stage, previous exposure to biotic stresses and environmental conditions result in a multitude of variables to consider (Cheng et al., 2019). Thus, elucidation of the intricacies in the interactions between plants and microbes is a pillar of both basic and applied research in plant biology.

## **Plant – mutualist interactions**

Plant-microbe interactions exist on an interaction continuum ranging from antagonism to mutualism, held in balance by the microbial load, perceived environmental signals and nutritional requirements. Antagonistic interactions pit the host and the microbe against each other in an arms race for survival, and result either in severe disease development and/or death of the host, or successful mounting of defense responses towards exclusion of the microbe. In turn, direct and complex interactions of hosts with microbes that are beneficial for both participants are called mutualistic symbioses. In plants, these relationships are established with bacterial and/or fungal microbial partners, which form specialized organelles to optimize nutrient exchange. For example, intracellular structures similar to those of mycorrhizal fungi (MF) were found associated with the earliest land plants ca. 400 million years ago (Martin et al., 2017), indicating symbioses and their advantageous assimilation of scarce nutrients to be an important factor in terrestrial plant evolution. Interestingly, a common symbiotic pathway shared between the two major but evolutionarily distant types of plant-microbe symbioses, the MF and nitrogen-fixing bacteria has been indicated (Oldroyd, 2013), with clear similarities in the triggered signaling cascades, evasion of plant immune responses and the localization in root tissues. Interactions start with signal exchange that allows the specific recognition of the microbe and progress to formation of nutrient exchange interfaces (e.g. arbuscules and nodules) within a delicate temporal and spatial balance. Finally, a complex network of microbial and plant cells interacting throughout all life stages is maintained.

Mycorrhizal fungi associate with roots of over 90% of land plants and are generally classified into ectomycorrhiza, colonizing the root intercellularly, and endomycorrhiza, colonizing the inside of the root cells (Bonfante and Genre, 2010). The fungi provide minerals such as phosphorus and nitrogen to the plants, in exchange for photosynthetic carbon fixed by plants, a nutrient-rich food source for the fungus (Genre et al., 2020).

The character of a plant-mutualist interaction is strongly influenced by chemical signals exchanged at its beginning, aiming to attract the beneficial microbe to the plant and exclude the pathogens, followed by activation of microbe-recognition receptors and subsequently of signaling cascades in the plant cells. The result of this activation depends on multiple receptors that are simultaneously activated, identifying the type and life style of the microbe (Thoms et al., 2021). For example, chitin or flagellin will indicate to the plant that the microbe is a fungus or a bacterium, respectively, while the presence of a lipochitooligosaccharide (LCO) will indicate that the fungus with which the plant comes in contact with is not a pathogen, but a mutualist. Lastly, the balance of the established interactions is further influenced by additional biotic and abiotic factors, such as other microbes in the community, plant age, microbial load, environmental conditions, nutrient abundance and others.

## Basic outline of plant immunity

As sessile organisms rich in sugars and other nutrients, plants are highly exposed to microbe and pathogen pressure during all life stages. Plant-generated response to this microbial exposure has famously been described as a “two-branched innate immune system” (Jones and Dangl, 2006), in which one branch recognizes general microbial molecular patterns and the second one responds to pathogenic virulence factors. While the mammalian immune responses depend on mobile defensive cells and adaptive immunity, plants respond to microbial challenge with local innate response of each cell and systemic signals dispersing through the plant tissues afterwards. At its foundation, plant immunity is based on a wide range of recognition strategies, both of universal, conserved microbial molecular traits, and variable molecules specific to a microbe species or strain (Dodds and Rathjen, 2010).

Microbe-associated molecular patterns (MAMPs; otherwise known as pathogen-associated molecular patterns - PAMPs), are highly conserved molecules shared within the classes of microbes, which act as elicitors of plant responses in the initial stages of microbial recognition (Dodds and Rathjen, 2010). For example, flg22, a 22 amino acid long part of the bacterial protein flagellin is a component of the bacterial motility apparatus – the flagellum, and is sufficient to trigger an immune response and subsequent gene expression reprogramming (Jones and Dangl, 2006). Another well-known MAMP is chitin, the major component of the fungal cell wall. Additionally, plants also generate a response to molecules of endogenous origin that have been released due to microbial-induced damage, called danger-associated molecular patterns (DAMPs; Dodds and Rathjen, 2010).

Recognized by plant transmembrane pattern recognition receptors (PRRs), MAMP/PAMP presence on the outside of the plant cell triggers the first branch of the plant immune response – pattern or PAMP-triggered immunity – PTI. Within the scope of this work, the term “pattern-triggered immunity” is preferred, because it includes non-pathogenic microbes (i.e. plant mutualists), which are also known to trigger plant immune responses.

Virulence factors typical for the second branch of plant immune response are called effectors. The corresponding competitive edge that their secretion provides for the pathogen over plant-generated PTI responses is the effector-triggered susceptibility (ETS). Typically, effectors are small hormone-like or proteinaceous molecules secreted into the plant cell with the aid of a specialized apparatus such as the T3 secretion system of bacteria. Eukaryotic organisms like fungi and oomycetes also deliver effectors into plant cells, probably across invaginated structures such as fungal haustoria, but the exact pathways have yet to be elucidated (Dodds and Rathjen, 2010). Effectors commonly have enzymatic activity on a host target in order to block PTI-initiated signaling cascades. Plant response is facilitated by disease *R*(resistance)-genes, which encode NB (nucleotide-binding)-LRR (leucine-rich-repeat) proteins. In case of biotrophic and hemi-biotrophic plant-microbe interactions, these

proteins recognize the microbial effectors directly, or the effect on their cellular targets indirectly (Jones and Dangl, 2006), thus deploying effector-triggered immunity - ETI.

Pathways activated in plant cells after direct exposure to a pathogen converge on early or late response gene expression, production of reactive oxygen species, increase in cytosolic calcium concentration and others, facilitated by kinase cascades from the the initial point of microbial recognition. They result in many downstream effects, including secretion of defense proteins, structural changes in plant cells, hormonal regulation and others. For example, pathogenesis related (*PR*) genes are a typical part of the plant response to microbial presence. Cell wall appositions at the site of pathogen attack are an example of a physical barrier and a structural change in plant cells as a defense mechanism. Hypersensitive response (HR), the cell death occurring in compromised plant cells is the typical result of a successfully generated ETI response of the plant. Regulation of plant hormonal networks is also in an interplay with immune responses, with salicylic acid (SA) as a known regulator of defense against biotrophic pathogens and jasmonic acid (JA) and ethylene, regulating defense against necrotrophic pathogens (Jones and Dangl, 2006).

Beyond the local PTI/ETI interplay of plant immune responses, commonly represented as a “zig-zag model“ of plant immunity (Jones and Dangl, 2006), systemic signals with mobile molecules that trigger responses in tissues far away from the initial site of microbial recognition are crucial to expand and utilize the full strength of immune responses. Systemic acquired resistance (SAR) is an SA-dependent long distance signaling pathway, induced by exposure to a pathogen, and resulting in resistance to future infections throughout the entire plant (Ryals et al., 1996). Induced systemic resistance (ISR) is a similar systemic transduction pathway, but JA and ethylene dependent, and known to be caused by exposure of plant roots to beneficial soil microbes (Pieterse et al., 2014).

Taking all the pathways intersecting during plant-microbe interactions into account, it becomes obvious that they occur in a delicate balance between molecular recognition, attack, evasion mechanisms, and corresponding genes evolving at a fast rate in order to provide advantage to the plant or the pathogen through natural selection (Jones and Dangl, 2006). This arms-race of modifications in effectors and corresponding plant genes is an ever-evolving war of signals and pathway deployment, including many cellular factors and extensive transcriptional reprogramming, all for the purpose of successful evasion of plant defenses on the the microbe side, and exclusion of harmful pathogens on the host side. Additionally, even though many specifics of plant-pathogen co-evolution have been elucidated in model pathosystems, their scope, diversity and exact mechanistic outline remain unexplored in many non-model plant organisms, including major crop species. These gaps in knowledge extend further into the microbial world of non-pathogenic organisms, whose interactions with plants have to be elucidated without the aid of clear disease markers and symptomatic phenotypes in functional genomics and molecular studies.

## Plant response to mutualistic microbes

The main principle behind any plant-beneficial organism interaction is permitted growth of a mutualistic microbe in symbiosis with the plant, while recognition, general and specific defenses against pathogenic microbes can still occur. Generally, establishment of a plant-mutualist interaction occurs through evasion of recognition as a harmful microbe and suppression of induced plant defense response (Soto et al., 2009). Regarding signal variability, exclusion of pathogenic microbes operates on universal plant recognition and response cascades, while establishment of a mutualistic interaction requires more specific and targeted signaling. For example, molecular patterns of AMF, called lipochitooligosaccharides (LCOs), resemble chitin as a general fungal MAMP in molecular structure, but have the crucial distinction of present and specific lipid modifications (Zipfel and Oldroyd, 2017). Recognition of LCOs, alongside several other types of oligosaccharides, is facilitated by a plant gene family of LysM-receptor kinases (Buendia et al., 2018).

Recognition of mutualist-typical LCOs on the plant cell membrane triggers a signaling cascade within the cells, in part similar to a MAMP-triggered response, especially in generation of reactive oxygen species and calcium signaling (Zipfel and Oldroyd, 2017). However, many of the proteins responsible for signaling in symbiosis have not yet been identified. Downstream of this initial recognition, cytosolic and nuclear receptors, as well as transcriptional factors involved in symbiosis signaling differ from pathogen-induced signaling cascades, resulting in crucial gene expression distinctions.

A hallmark of mutualistic interactions with plants is the modulation and suppression of immune responses by the microbe, which is still recognized as an intruder organism. However, symbiotic organisms also secrete corresponding effectors in order to regulate immunity and signaling of the plant during the interaction (Deakin and Broughton, 2009; Zipfel and Oldroyd, 2017). Interestingly, in the case of the AMF *Glomus intraradices*, the secreted effector SP7 interacts with the pathogenesis-related transcription factor ERF19, resulting in suppression of the plant immune system and drawing another link between pathogenic and mutualistic effectors in their ability to promote biotrophic growth (Kloppholz et al., 2011).

After exposure to a beneficial microbe and establishment of a successful colonization, plants benefit in more than acquisition of necessary nutrients. One of the benefits is broad resistance to future pathogen exposure through activation of systemic signaling pathways in the plant. This physiological state is called “priming” by beneficial microbes and results in the plant being in a “primed” state, with quicker and/or stronger activation of defense responses towards pathogens (Conrath et al., 2006). Changes within the scope of the primed plant state can be of physiological and/or transcriptional nature, but also epigenetic ones, which implies transmission of the state to progeny and a type of “immunological memory” (Mauch-Mani et al., 2017).

## Plant-microbe symbioses in agriculture

The most important outcome of stable plant-mutualist interactions for agriculture is the sequestration of valuable nutrients in food and feed crop yields. Biological fixation of nitrogen by the nitrogenase enzymes in soil bacteria and in symbiosis with legume plants is a main source of naturally fixed nitrogen. However, cereals such as wheat, rice and maize, grown as food staples worldwide, are non-legume plants, and do not form symbioses with rhizobial bacteria. In order to fertilize the soil in which those cereals are grown, crop rotation systems commonly include legume cultivation, and efforts towards introducing root nodulation symbioses in non-legume crops are a major focus of plant genetic engineering (Pankievicz et al., 2019). Mycorrhizal fungi also associate with major crop and food staple plants and increase plant biomass, yield and nutrient acquisition, through augmentation of uptake surfaces for water and phosphorus, regulation of plant hormones, protection against stresses and improvement of soil composition (Benami et al., 2020). Additionally, most of terrestrial carbon stocks and crucial biomass relevant for all ecosystems are stored in mycorrhizal plant symbioses (Soudzilovskaia et al., 2019).

Especially in the case of emerging plant diseases for which there is no established chemical treatment, genetic transformation of the host plant is not accepted or realistic and the breeding processes for resistances are too time-consuming, wealth of management strategies commonly branches out to beneficial microbes as control. Currently, most prevalent examples of beneficial organisms used as microbial biological control agents (MBCA) are the bacterial mutualists *Bacillus subtilis* and *Pseudomonas fluorescens*, as well as the fungus *Trichoderma harzianum* (Singh et al., 2021). Utilized for their antagonistic influence against plant pathogens, MBCAs act by antibiosis, hyperparasitism, plant priming and competition for nutrients in order to limit the proliferation of plant pathogens (Köhl et al., 2019). More and more, research efforts within phytopathology are turning towards beneficial microbial species or communities for integration in pathogen and pest management strategies. For example, a highly damaging bacterial pathogen *Xylella fastidiosa* has recently been detected in Southern Europe and is predicted to potentially spread over vast climatically suitable areas of the continent (Godefroid et al., 2019). *X. fastidiosa* subsp. *pauca* is the causative agent of Olive Quick Decline Syndrome, and while there is no curative treatment established currently, research indicates biocontrol agents such as *Bacillus* bacteria to be a viable option (Zicca et al., 2020).

Maintenance of a plant-microbe interaction is a balanced process, highly sensitive to environmental and anthropogenic influences. Intensive agriculture practices, which include elevated agrochemical use, fertilizer applications, mineral depletion and soil contamination have been shown to influence the establishment and maintenance of plant soil symbioses (Soudzilovskaia et al., 2019; Genre et al., 2020).

## ***Serendipita indica* (syn. *Piriformospora indica*) – a model root endophyte**

*Serendipita indica* is a fungal root endophyte belonging to the order of Sebaciniales and division Basidiomycota, discovered in the Indian Thar desert in a serendipitous (hence the name) fashion, during a scan for AM fungi (Verma et al., 1998). *S. indica* has an extremely broad host range, forming symbioses with roots of an “unlimited” number of plant species (Qiang et al., 2012), including the non-mycorrhizal model plant *Arabidopsis thaliana* and many staple food and crop species. Fungi from the order Sebaciniales are generally considered to be ubiquitous in association with plant species, with no host or geographical pattern distinguishable (Weiß et al., 2011). Considering the narrow host range and dependence on environmental conditions of mycorrhizal fungi, *S. indica* presents as a highly interesting endophyte candidate for elucidation of colonization and symbiosis pathways conserved or adapted to a spectrum of plant species.

*S. indica* can be cultivated axenically, is genetically transformable (Zuccaro et al., 2009) and has a sequenced genome of approx. 25 Mb (Zuccaro et al., 2011; Šečić et al., 2021c), making it genetically accessible for functional and transcriptomic studies. Interestingly, *S. indica* is itself colonized with the endofungal bacterial strain *Rhizobium radiobacter* F4 (syn. *Agrobacterium tumefaciens* F4), and while the fungus can't be cured from the bacteria, its quantity increases during plant colonization, relative to axenically cultivated *S. indica* (Guo et al., 2017). Within its genome, *S. indica* shows traits of a biotrophic organism, with deficiencies in metabolic enzymes indicating the inability to assimilate nutrients without a host, but also expansion of gene families of plant cell wall degradation and hydrolytic enzymes, indicating saprophytic traits (Zuccaro et al., 2011; Lahrmann et al., 2015). As in any other plant-mutualist interaction, at its basis is a mutually beneficial nutrient exchange between the host and the microbe. *S. indica* colonization changes the expression of *A. thaliana* invertase and sucrose synthase genes in order to adjust the plant sugar production to endophyte needs (Opitz et al., 2021).

After germination of *S. indica* chlamydospores, an extensive hyphal network grows on the surface of the root and between root cells, especially in the rhizodermal and cortical tissues of the differentiation zone. At a later stage, extensive intracellular growth is detected, with hyphal tips producing single *S. indica* spores, especially in dead root cells (Deshmukh et al., 2006). Thus, the colonization strategy of *S. indica* has a biphasic character, with an early biotrophic stage of colonization and a cell-death associated, saprophytic one, in which dead root cells contain a hyphal network, but with no macroscopic negative symptoms visible on the colonized plants (Deshmukh et al., 2006; Schäfer et al., 2009; Zuccaro et al., 2011). The shift between the two phases, as well as gene expression during their course is tightly controlled by the fungus, in order to achieve colonization, nutrient acquisition, and proliferation in a mixture of living and dead cells of root tissue.

In order to navigate the colonization course without triggering the plant immune system (especially considering the possibility of exclusion by any of the plant species from its broad host range), *S. indica* has to employ successful strategies for repression or bypassing of innate immune responses. Endophyte-induced regulation of hormone synthesis and signaling, as well as modulation of immunity-related gene expression was detected during colonization of barley (Schäfer et al., 2009). In the case of *A. thaliana* as the host, *S. indica* has also been shown to suppress, rather than bypass immune responses (Jacobs et al., 2011), reinforcing on the hypothesis that the host immune response is not absent but modulated by *S. indica*. A set of *S. indica*-specific DELD proteins, identified by the seven amino acid motif (RSIDELD) within their sequence are predicted to be secreted effectors during this mutualistic association (Zuccaro et al., 2011). *S. indica* effector PIIN\_08944 was shown to promote the symbiotic interaction by interfering with SA-mediated immune response of the plant host (Akum et al., 2015).

Besides the broad host range, elucidated colonization strategies and gene expression patterns, as well as the sequenced genome, *S. indica* also provides an array of beneficial advantages to plant growth, yield development and resistance to stresses. Increase in grain yield of barley plants was detected upon *S. indica* colonization, as well as the resistance to root rot caused by the necrotrophic pathogen *Fusarium culmorum*, powdery mildew caused by the biotrophic leaf pathogen *Blumeria graminis* and tolerance to mild salt stress (Waller et al., 2005), indicating the multi-beneficial potential of this endophyte. Resistance of barley to root rot caused by *Fusarium graminearum* has also been shown (Deshmukh and Kogel, 2007). Tolerance to salt stress has been attributed to increases in ascorbic acid and antioxidant enzyme activity in barley roots (Baltruschat et al., 2008). *S. indica* also confers resistance against *Golovinomyces orontii*, the powdery mildew of *A. thaliana* (Stein et al., 2008). Induction of resistance to oomycete pathogens (Trzewik et al., 2020) and influence on viral concentrations (Fakhro et al., 2010) in *S. indica* colonized plants has also been shown.

Taking into account this unique combination of (a) a broad host range encompassing plant species not colonized by other beneficial microbes, (b) genetic transformation possibilities, (c) availability of -omics data sets, (d) ability to suppress plant immunity, (e) provide benefits for growth, yield and (f) priming against stresses, it is obvious that *S. indica* establishes itself as a model root endophyte. It is especially interesting to look into aspects of its interactions that would unlock conserved and divergent molecular mechanisms and signaling pathways during *S. indica* colonization of phylogenetically distant plant species, as well as mechanisms that this endophyte uses to suppress and/or bypass all of their immune responses. Additionally, basic research utilizing this fungus as a model is at an excellent position to be translated to agronomically relevant crops that it also colonizes.

## ***Magnaporthe oryzae* and *Fusarium graminearum* – major cereal pathogens**

*Magnaporthe oryzae* (Mo, syn. *Magnaporthe grisea*, anamorph: *Pyricularia grisea*) is a filamentous fungal hemibiotroph from the division Ascomycota, causative agent of rice blast, a devastating disease that typically causes 10-30 % of grain losses in rice (Dean et al., 2012). The fungus belongs to a species complex that can also infect wheat, thus jeopardizing two main staple food crops (Urashima, 1993). The fungal conidia commonly attach to foliar tissues, germinate and utilize an infection structure called a melanized appressorium to apply localized turgor pressure and penetrate the plant cells (Dean et al., 2012). Typical blast lesions that indicate a switch from a biotrophic to a necrotrophic stage of infection are visible after several days. While it visibly attacks all the aerial parts of the plant, root infections have also been detected (Sesma and Osbourn, 2004). Management strategies rely on application of fungicides, resistance cultivar breeding and farming management practices like crop rotation (Asibi et al., 2019).

Genome of the strain Mo 70-15 has been sequenced in 2005, resulting in total size (including the assembled scaffolds and gaps) of approx. 40 Mb (Dean et al., 2005). A large protein secretome was predicted based on this genome, containing plant cell degrading enzymes and fungal effector families, and current research focuses on identification of effector pools available in different isolates and pathotypes (Kim et al., 2019). Since *M. oryzae* is genetically transformable, functional genomics and phenotyping studies on a large mutant library were preformed (Jeon et al., 2007), resulting in identification of pathogenicity genes. Taking advantage of these resources, we studied the interaction and transcriptomic landscape of this major plant pathogen with the model grass *Brachypodium distachyon* (Zanini et al., 2021).

*Fusarium graminearum* (teleomorph: *Gibberella zeae*, Ascomycota) is another major fungal plant pathogen (Dean et al., 2012), the causative agent of Fusarium head blight (FHB), affecting all major cereal species. Fungal ascospores infect through natural openings and soft tissues, and grow asymptotically at first, with eventual intracellular invasion and secretion of mycotoxins such as deoxynivalenol (DON), which aids with tissue necrosis (Trail, 2009). Infection at the head/florets of the plant occurs early during the growing season, but the disease becomes apparent much later, making management strategies and timing of fungicide application extremely challenging. The fungus significantly reduces grain quality by mycotoxin production, making the yield unsafe for human or live stock consumption (Dean et al., 2012). *F. graminearum* genome has been sequenced (isolate PH1, 36.5 Mb; Cuomo et al., 2007) and later completed and annotated (King et al., 2015). Integrated management strategies, which include growing of tolerant cultivars, well-timed fungicide application, utilization of harvesting, storage and cultural practices adjusted to infection prevention and mycotoxin detection are recommended (Wegulo et al., 2015). We investigated the involvement of small RNA (sRNA) species in the virulence of *F. graminearum* (Werner et al., 2021).

## ***Brachypodium distachyon* – a model grass plant**

*Brachypodium distachyon* (purple false brome) is a wild grass from the subfamily of Pooideae, with a short life cycle, small size and simple growth requirements (Vogel and Hill, 2008). Because of these traits, highly efficient transformation protocols (Vogel and Hill, 2008), mutant libraries (Hsia et al., 2017) and germplasm collections (Filiz et al., 2009) have been established. With a sequenced genome of approx. 272 Mb (diploid inbred line Bd21; The International Brachypodium Initiative, Vogel et al., 2010), *B. distachyon* is considered a good model grass species for cereals, temperate grasses and biofuel crop grasses. Majority of gene families annotated in *B. distachyon* are shared among the major grass subfamilies and despite a significantly lower ploidy level and chromosome number relative to cereals such as rice and wheat, there are broad synteny links between *B. distachyon* and these crops (Huo et al., 2009; Vogel et al., 2010). It is important to note that, while *B. distachyon* can be used to study certain molecular mechanisms and gene groups (e.g. synthesis and degradation of cell wall polymers; Douché et al., 2013, cell wall architecture and seed development; Girin et al., 2014), the evolutionary path of this wild grass does not overlap with others in all cases (e.g. low temperature adaptations; Li et al., 2012), making its use as a model organism limited to case-by-case examination.

Since *B. distachyon* is a self-fertile plant, majority of the germplasm collections consist of inbred lines with sufficient genetic variability to be a valuable phenotyping resource (Tyler et al., 2014). These differences are made visible in the *B. distachyon* pangenome, composed of 54 sequenced lines, in which genes not present in all the lines show variation in adaptation to selection pressure, for example in defense responses (Gordon et al., 2017). These traits of the *B. distachyon* germplasm make it an attractive host target for study of plant-microbe interactions.

*B. distachyon* interacts and shows broad susceptibility to plant cereal pathogens, including viruses, bacteria, fungi and oomycetes, and is colonized by some mycorrhizal fungi, making it an excellent model for grass responses to microbial presence (Scholthof et al., 2018). Importantly, not only is susceptibility to *Magnaporthe grisea* (Routledge et al., 2004), *Fusarium graminearum* and *F. culmorum* reported (Peraldi et al., 2011), but the course of infection and symptoms observed on *B. distachyon* tissues closely resemble those of rice and wheat, respectively, indicating the importance of *B. distachyon* as a model for highly relevant crop pathosystems. Thus, while the two cereal pathogens investigated within the scope of this thesis, *M. oryzae* (Zanini et al., 2021) and *F. graminearum* (Werner et al., 2021) have been shown to infect *B. distachyon*, an interaction with *S. indica* has not been shown until Šečić et al., 2021c. Because of the combined advantageous traits of *S. indica* as a model for fungal endophytes with a broad host range, and *B. distachyon* as a model grass with translational possibilities to agriculturally more relevant crops, an in-depth look into the intricacies of the interaction between these two organisms was of high importance.

## RNA Interference and associated proteins in plants and fungi

RNA interference (RNAi) is an eukaryotic gene silencing mechanism at the transcriptional and post-transcriptional level, ensuring fast and efficient inhibition of protein synthesis guided by small RNA (sRNA) molecules complementary to the target mRNA transcript (Wilson and Doudna, 2013). It can occur in response to environmental stimuli or developmental cues, with endogenous sRNA sequences, but also as a protective tool against viruses and transposable elements. Post-transcriptional gene silencing (PTGS) via RNAi occurs in the cytoplasm, resulting in mRNA degradation or translation inhibition by preventing binding of translational machinery to the transcript. On the other hand, transcriptional gene silencing (TGS) is localized to the nucleus of the cell, resulting in epigenetic changes introduced by sRNA-guided recognition. Since sRNA-guided processes discussed further occur within the framework of PTGS, the sequence and functions of RNAi processes involved in this type of RNAi will be explained in more detail.

The trigger of the PTGS pathway is recognition of a double-stranded RNA (dsRNA) fragment, either exogenous or endogenous, by an enzyme called Dicer (Dicer-like – DCL in plants), an RNase III endonuclease that processes the longer dsRNA into smaller fragments. These smaller fragments are loaded onto Argonaute (AGO) proteins within the RNA-induced silencing complex (RISC), where they are processed into single-stranded (ss) sRNAs and guided to target silencing (Fang and Qi, 2016). In some cases, RNA-dependent RNA polymerases (RdRPs) generate dsRNAs from ss RNAs, thus amplifying the primary silencing. Functional domains of these proteins are highly conserved among eukaryotes, providing means for their novel prediction and detection in new and non-model organisms.

Due to gene duplication and high ploidy levels in many species, plant genomes usually contain expanded gene families of DCLs and AGOs, with specific and at least partly redundant expression patterns and functions. For example, *A. thaliana* has 10 AGOs and 4 DCLs, which are known to have variable roles in gene silencing (Fang and Qi, 2016). In order to estimate the RNAi machinery of *B. distachyon*, we searched its genome (Šečić et al., 2019) and our prediction concludes presence of 6 DCL and 16 AGO-like genes, phylogenetically classified by their similarity to better characterized *A. thaliana* RNAi proteins. For the AGO family, corresponding predicted 3D structures and organ/tissue-specific expression imply functional specialization and thus indicate that determination of exact proteins involved in a specific RNAi-mediated process has to premeditate any deeper functional or molecular studies.

In fungi, RNAi-based processes (initially called “quelling”) also utilize DCL and AGO proteins and are involved in maintenance of genome integrity and response to stimuli (Dang et al., 2011). Based on similarity with the better known RNAi components of the model fungus *Neurospora crassa*, we predicted a set of RNAi-associated proteins in the genome of *S. indica* (Šečić et al., 2021c).

## Small RNAs in plant-microbe interactions

Any RNA that is not translated into a protein is defined as a “non-coding” RNA (ncRNA), and the subtypes are identified based on abundant RNA pools with the same function and usually similar length measured in nucleotides (nt). Major components of the ncRNA pool are transfer RNAs (tRNAs), ribosomal RNAs (rRNAs) and various types of sRNAs, including microRNAs (miRNAs), with endogenous targets within the organism of biogenesis and exRNAs (extracellular RNAs), presumed to be exchanged between cells while packed in extracellular vesicles (EVs). While they are all processed from stem-loop structures or longer dsRNA fragments, sRNAs in plants differ in biogenesis pathways and functions. For example, different DCL proteins process the sRNA precursors in *A. thaliana* to form resulting pools of miRNAs (DCL1) and trans-acting small interfering RNAs (ta-siRNAs, DCL4, Singh et al., 2018), both of which target silencing of mRNAs different than the regions they are derived from. Regardless of their type, if the sRNAs are assumed to: i) be induced in an interaction between a plant and a microbe, ii) can be detected by sequencing approaches and iii) can be certainly classified as originating from one of the interacting organisms, they are studied as “interaction-responsive” sRNAs within the scope of this thesis.

During plant-microbe interactions, speed and efficiency of expression modification are crucial, and sRNAs have been shown to be highly involved, both as endogenous and exogenous responses (Song et al., 2021). The advent of sRNA sequencing projects focused on plant microbes included major pathogens like *Magnaporthe oryzae*, where sRNA sequencing of mycelium and appressoria revealed a differential accumulation of sRNAs in the infection-specialized tissue of appressoria, namely the 28-35 nt sRNAs classified as tRNA-derived RNA fragments (tRFs; Nunes et al., 2011). Interestingly, sRNA studies on fungal mutants compromised in sRNA biogenesis imply the role of these non-coding RNAs in fungal growth and virulence (Raman et al., 2017). In the case of *F. graminearum*, sRNA production and expression has been shown in response to mycoviruses (Wang S et al., 2016) and functional genomics studies on the RNAi machinery proteins regulate processes relevant for ascospore formation, virulence and mycotoxin production (Son et al., 2017; Gaffar et al., 2019). Additionally, we have shown the requirement for silencing of barley and *B. distachyon* genes by *F. graminearum* sRNAs for full fungal virulence (Werner et al., 2021).

In order to study the sRNA involvement in fungal virulence and plant colonization, we applied a simultaneous sRNA and mRNA sequencing approach to three pathosystems of *M. oryzae* infecting *B. distachyon*: leaf infection at the biotrophic stage of 2 days post infection (DPI) and the necrotrophic one at 4 DPI, as well as root infection at 4 DPI (Zanini et al., 2021). In order to study the involvement of sRNA silencing regulation in the same plant, but in response to the model endophyte *S. indica*, we utilized the same combined sRNA and mRNA sequencing at 4 days post *S. indica* inoculation of *B. distachyon* roots (Šečić et al., 2021c).

## Cross-kingdom communication between plants and microbes

Small RNAs are known to be involved in plant defense against viruses, but their role in plant interaction with other microbes has not been elucidated until the groundbreaking discovery of cross-kingdom exchange between plants and fungi (Weiberg et al., 2013). This landmark study showed that *Botrytis cinerea* (causative agent of gray mold disease) expresses sRNAs that are transported “cross-kingdom” into the plant host and then loaded into the plant AGO to silence immunity-related genes in *A. thaliana* and tomato. Another landmark study in 2016 revealed that this process occurs in the other direction too, with cotton plants utilizing their miRNAs to silence virulence genes in the vascular wilt pathogen *Verticillium dahliae* (Zhang et al., 2016). Thus, the process of bidirectional cross-kingdom (ck) communication via RNAi was unveiled, in which microbial sRNAs act as RNA effector molecules delivered into the plant to silence specific genes, and plants in turn utilize their sRNAs for silencing of virulence or essential genes of microbes. Interaction-responsive sRNAs that originate from the plant or the microbe (“organism of origin”) are presumably cut by the “origin” DCL, but load into the “target organism” AGO after transport. The exact mechanistic background of this process has not been elucidated yet, but transport probably (at least partly) occurs through secretion and uptake of extracellular vesicles (Cai et al., 2020).

Since these initial studies, ck communication has been predicted or uncovered in other pathosystems too, including *Puccinia striiformis* and wheat (Wang et al., 2017) and the oomycete *Hyaloperonospora arabidopsidis* and *A. thaliana* (Dunker et al., 2020). There have also been first indications that this communication is not limited to plant-pathogen interactions, focused on identifying the putative plant targets of AM fungus sRNAs (Silvestri et al., 2019) and even showing that rhizobial bacteria utilize tRFs to silence plant host genes in order to control the nodulation process (Ren et al., 2019). However, the role of sRNAs in *S. indica* colonization has not been studied until we analyzed the sequenced sRNA and mRNA pools from *B. distachyon* roots colonized with the model endophyte and the corresponding control samples (Šečić et al., 2021c). Similarly, even though the importance of sRNAs and RNAi machinery in *M. oryzae* virulence was already indicated (Raman et al., 2017), we took advantage of the sRNA and mRNA sequencing datasets in three pathosystems with *B. distachyon* and predicted the ck targets in both interacting organisms (Zanini et al., 2021). In both of the datasets, we utilized a previously established bioinformatics analysis pipeline (Zanini et al., 2018), in order to combine the data about sRNA expression with predicted mRNA target downregulation, since we sequenced both types of RNA from shared biological samples.

While it was previously shown that a *F. graminearum* sRNA silences a wheat resistance-related gene in order to aid the infection process (Jian and Liang, 2019), we found strong hints that *F. graminearum* sRNAs also target host genes in barley and *B. distachyon* (Werner et al., 2021).

## miRNAs in plant-microbe interactions

Regulation of endogenous gene expression in response to environmental and/or developmental stimuli is under control of eukaryotic small RNAs with a distinct biogenesis pathway, commonly called miRNAs. Among many other ncRNA types, miRNAs are identified as originating from hairpin structures formed by folded repeats, but are still cut by DCLs and loaded into AGO proteins as mature miRNAs (Wang et al., 2019). miRNA families, groups of miRNAs with shared ancestry and similar functions, are partly highly conserved across a multitude of plant species, while others are specific for a single or a few species (Fahlgren et al., 2010). miRNA regulation often converges on the same major pathways of transcriptional and hormonal regulation that are triggered within basic immune responses, adding another layer to the fast and mobile signaling cascades. We comprehensively reviewed well-known and conserved plant miRNA families in terms of their function and typical expression pattern in response to pathogenic and beneficial bacteria, fungi and oomycetes (Šečić et al., 2021b). For example, miR393, miR160, miR164 and miR167 are differently responsive to pathogenic bacteria relative to fungi, but there is also a clear difference in responses to pathogens and mutualists in these families (Table 1 and Figure 2, Šečić et al., 2021b). Since these miRNA families regulate plant immune and hormonal networks, this outcome implies that differentiation signals and pathways that plants employ to elucidate the character of the microbe in an interaction incorporate endogenous RNAi-based regulation.

In our model species, *B. distachyon* miRNAs differentially expressed under various types of stress exposure originate both from conserved miRNA families and specific ones (Jeong et al., 2013). Induction and differential regulation of miRNAs associated with growth promotion in the *Oncidium* hybrid orchid was detected upon colonization with *S. indica*, signifying that the signaling and downstream gene expression, as well as the phenotype observed after exposure to this endophyte include miRNA regulation (Ye et al., 2014). In the sRNAs generated from our sequencing approaches with *S. indica* and *M. oryzae*, we predicted miRNA-generating loci in *B. distachyon* colonized by these two fungi (Šečić et al., 2021c; Zanini et al., 2021). After colonization by both fungi, known miRNAs associated with growth and developmental regulation were present, some during both interactions and some exclusive to the pathogen or the mutualist. For example, members of the miRNA family miR159 were found in *B. distachyon* colonized with *S. indica*, and also in leaves infected with *M. oryzae*. This miRNA family regulates MYB transcription factor expression, but was also found to be one of the cotton miRNAs transported to *V. dahliae* for ck-based silencing of the pathogen virulence genes (Zhang et al., 2016).

In fungi, miRNA-like RNAs (miRNAs) are produced by several biogenesis pathways, somewhat different than in plants, and their prediction and identification from sRNA data and animal/plant miRNA prediction criteria remains challenging (Chen et al., 2014).

## Bioinformatics approaches to analysis of plant-microbe sequencing datasets

With sequencing technology becoming widely accessible and applicable in recent years, so is the number of available RNA and sRNA datasets from many eukaryotic organisms. Study of plant-microbe interactions requires a dual-sequencing approach though, in which both the expression and sequence data can be untangled and attributed to one of the interacting organisms correctly. While there are plenty of advanced analysis pipelines focused on exactly this goal on the mRNA level, sRNAs are more complicated to analyze. Well-known tools for plant ncRNA analysis are focused on sequences with presumed endogenous function, such as miRNAs and long non-coding RNAs (lncRNAs; Liao et al., 2018). However, in the case of exchange-based ck communication, the elucidation of exogenous roles is essential. Additionally, sRNAs have to be clearly assigned to one of the two interacting organisms. With that in mind, we reviewed and recommended an analysis pipeline for selection and target prediction of sRNA “effectors” in bidirectional ck communication (Zanini et al., 2018). This is the exact analysis pipeline applied to selection of optimal, most likely effective sRNA datasets in *B. distachyon* with *S. indica* (Šečić et al., 2021c) and *M. oryzae* (Zanini et al., 2021). One of the main advantages of an integrated mRNA and sRNA sequencing approach is the immediate accessibility of predicted target downregulation data for initial validation. Additionally, both of these analyses benefit from sequenced controls (including the axenic fungal cultures), which greatly decrease the “noise” of sequenced sRNA sequences and allow focus on “induced” subsets, which are present exclusively or in a greater quantity in the colonized plant tissue. For two studies that are based on the same model plant, application of a common analysis pipeline is crucial for later comparative analyses. In the case of *F. graminearum* (Werner et al., 2021), the sRNAs with which the initial target prediction was done was derived from axenic fungal culture, and confirmation of target downregulation and degradation was thus done at a later stage, and at a significantly smaller number of targets than in the case of mRNA sequencing. However, to truly benefit from an optimal sequencing strategy for sRNA-based silencing prediction, the biological sample would have to provide an additional sample to sRNA and mRNA – namely the degradome dataset, which would allow for automatic confirmation of AGO-guided target degradation on a large, bidirectional scale,

Genome sequencing of previously neglected plant hosts and their interacting microbes is crucial for effector discovery, target prediction and validation, as well as elucidation of expression patterns present and fluctuating during the establishment and maintenance of colonization. While *B. distachyon*, *M. oryzae* and *F. graminearum* had assembled genomes available, that was not the case with *S. indica*. Because of this fact, we also resequenced the genome of *S. indica* with Oxford Nanopore sequencing, managing to reduce the contig number from 2,359 to 57 (Zuccaro et al., 2011; Šečić et al., 2021c).

## Applications of RNAi-based plant protection

Due to the lack of effective and sustainable protection strategies against novel pathogens, development of pathogen resistance to established agrochemicals, as well as missing resistance genes for plant breeding strategies, plant protection efforts are always on the lookout for new, effective solutions. Silencing of target genes via the RNAi machinery can be deployed as a plant protection strategy, utilizing dsRNAs complementary to virulence or other essential genes of a pest or a pathogen. Based on the origin of the dsRNA, these strategies are either Host-Induced Gene Silencing (HIGS; Nowara et al., 2010), or Spray-Induced Gene Silencing (SIGS; Koch et al., 2016; Wang M et al., 2016). In HIGS strategies, dsRNA is produced within the plant host, which has been genetically modified to include the sequence of the pest/pathogen target. On the other hand, in SIGS, dsRNA is applied by means of spray or similar exogenous mechanisms onto the plant surface. Up to date, these strategies have been successfully applied against obligate biotrophic fungi (*B. graminis*; Nowara et al., 2010), as well as necrotrophs (Koch et al., 2013; Koch et al., 2016; Wang M et al., 2016), making them a viable alternative to chemical fungicide use. The first, and currently only, commercial product utilizing an RNAi-protection strategy is targeted against the corn rootworm in transgenic maize plants (Head et al., 2017), in an integrated pest management approach alongside insecticidal proteins. Thus, RNAi-based protection is another tool to be used against pests and pathogens. However, the HIGS-based genetic transformation approach in use of the RNAi is, as is the case with all other genetically modified (GM) approaches, impeded by lack of transformation technology for all economically relevant plant species and consumer resistance to GM foods and products. In that regard, SIGS as a GMO-free approach would be a clearly better choice, but there are obstacles of efficiency and stability of the applied dsRNA to consider, as well as the safety and application formulation issue. Ideally, an efficient SIGS strategy would have to contain dsRNA that targets a gene highly specific for the organism that is the causative agent of the disease, and effective targets in any other organism that can come in contact with the dsRNA have to be excluded. Additionally, the dsRNA applied would have to remain stable long enough for uptake into the target organism to occur. Lastly, it is yet unknown what is the risk of pathogen resistance development against RNAi-based plant protection strategies.

Revising the basic requirements for establishment and development of an RNAi-based gene protection strategy against fungal pathogens we summarized that i) the dsRNA has to remain stable until either direct environmental or indirect (from the plant host) uptake occurs, and ii) an expressed and efficient RNAi machinery in the fungal cells has to exist, in order for recognition of the target to occur (Šečić et al., 2021a). Additionally, iii) exact knowledge of optimal dsRNA design, target selection, dsRNA structure and length is highly desirable, alongside possible applications with stabilizing formulations.

## General discussion and conclusions

Working at the intersection of RNAi-based communication and plant-microbe interactions, we conducted research on the model grass *Brachypodium distachyon* and associated microbes, including a novel interaction with the endophyte *Serendipita indica* (Šečić et al., 2021c), and major cereal pathogens *Magnaporthe oryzae* (Zanini et al., 2021) and *Fusarium graminearum* (Werner et al., 2021). Besides establishment and characterization of the interaction at the phenotypic level, we investigated the transcriptomic and sRNA expression landscapes in the plant and microbe(s), with a specific focus on prediction of interaction-induced sRNAs with gene silencing function. As preparatory work for these analyses, we established an analysis pipeline for putative sRNA effectors exchanged between plants and microbes (Zanini et al., 2018) and analyzed the *Argonaute* and *Dicer-like* gene families in *B. distachyon* (Šečić et al., 2019). During these research projects, we took advantage of the accumulated literature and expert insight to review the response of endogenous gene silencing via conserved miRNA families induced upon exposure to various biotic stresses (Šečić et al., 2021b). Additionally, we clarified upon the requirements necessary for dsRNA uptake into fungal cells (Šečić et al., 2021a), thus touching upon the application aspect of RNAi-based communication. Figure 1 summarizes the connections among these publications.

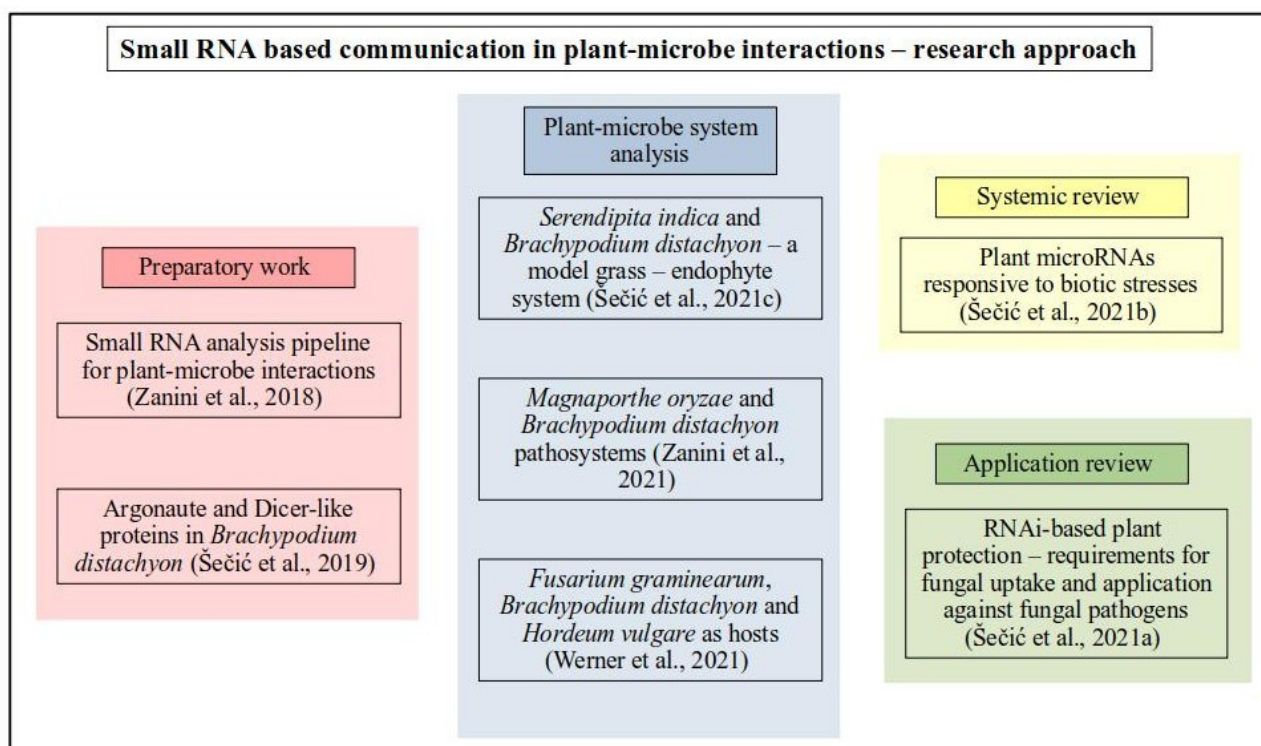


**Figure 1:** RNAi and sRNAs in plant-microbe interactions: basic and applied research aspects (own work)

Main conclusions and discussion points resulting from this work will be considered in the following paragraphs.

### **Ck RNAi in plant-microbe interactions – how to see the full picture?**

Considering all the plant-microbe interaction systems in which ck communication has been shown or hinted at by prediction analyses, it seems that there is no restriction of a microbe type or lifestyle that limits the presence of putative sRNA effectors. Indeed, it has been identified as a mechanism by which microbes with both biotrophic and necrotrophic lifestyles silence defense-related genes in plant hosts, and our research supports the indication that beneficial microbes also utilize sRNAs to control the course of mutualist colonization. Because of this, a reproducible sequencing analysis pipeline, adjustable to specific plant-microbe system requirements and availability of samples, which can facilitate easier validation of ck-based gene silencing remains a crucial first accomplishment of our work (Zanini et al., 2018).

### **The RNAi protein landscape of a monocot model organism – which gene family members are involved?**

While our analysis of *AGO* and *DCL* gene families in *B. distachyon* yielded a finite gene copy number per family (Šečić et al., 2019), the question of true expression and function in various plant tissues remains. For example, a specific study of the *AGO* gene family in *B. distachyon* that is focused on root microbial interactions would need to identify: i) which AGO protein has the highest expression in the root, ii) are there redundant functions in the absence of it that are taken over by other family members, iii) is the sRNA loading into that AGO sequence or length preferential and iv) does the protein level change upon exposure to the microbe in the interaction. Additional to time-point, life-stage and tissue-specific expression patterns, major interaction partners of the RNAi proteins would have to be clarified, for example the connection between sRNA transport pathways and the RNAi machinery. For these questions, experimental analyses such as AGO pull-down sRNA sequencing and plant knock-out mutant analysis should prove useful.

### **Interaction analyses of a plant-endophyte model system – what have we learned?**

We established a novel plant-endophyte interaction between two broadly applicable model species: *B. distachyon* and *S. indica* (Šečić et al., 2021c). After confirming the beneficial character of this interaction for plant growth and yield promotion, we detected extensive transcriptional reprogramming in both interacting organisms, following the known pattern of *S. indica* switching between biotrophic and saprophytic traits during plant colonization. According to our analysis of induced sRNA pools in both organisms, *S. indica* putative sRNA effectors have predicted targets in circadian clock, flowering regulation and immunity of the plant, while *B. distachyon* sRNAs have predicted targets in fungal genes controlling nutrient acquisition and development. Even though the degradation of the target transcripts and sRNA transport still have to be confirmed experimentally,

this work provides initial hints of a communication mechanism between a grass and an endophyte that can eventually be translated to other, more agronomically relevant plant species that *S. indica* also interacts with.

### **A peek into plant-pathogen interactions with different microbe lifestyles**

We studied the transcriptional and sRNA landscape of both plant and microbe during three different pathosystems/lifestyles of *M. oryzae* on *B. distachyon* (Zanini et al., 2021). While molecular reprogramming on both sides of the interaction was extensive, and in character of a biotrophic or necrotrophic interaction, the putative sRNA pools induced in these pathosystems were only partly overlapping. This might be an indication that sRNA-based silencing follows infection-dependent cues to accompany its course, and further implies a variable and modifiable role for putative sRNA effectors within the interaction. In the case of *F. graminearum*, targets in defense genes of both *B. distachyon* and barley were found (Werner et al., 2021), indicating that fungi evolved ck-RNAi infection strategies towards multiple hosts and the research is thus translatable from model to crop species. Within further research, a question of whether the cellular targets of protein and sRNA effectors are conserved or not, arises.

### **Further steps in the analysis of the role of sRNAs in plant-microbe interactions**

Crucial further questions to answer in study of the role of sRNAs in plant-microbe interactions are: i) how conserved are the putative sRNA effectors and their target hubs across phylogenetically related and distant species, ii) how conserved are plant responses to microbial presence, iii) how does the transport of sRNAs occur mechanistically and iv) is this communication present in species that have lost the RNAi machinery (e.g. the fungus *Ustilago maydis*).

There are many sub-types of sRNA sequences detectable by various sequencing approaches, depending on length, structure or trait selection during library preparation. However, in a general case of size selection from a plant-microbe interaction sample, classification of the subtype by bioinformatic analyses is necessary. For example, to analyses of sRNAs with presumed ck or endogenous function during *B. distachyon* – *S. indica* interaction we applied two different filtering-dependent analysis pipelines (Šečić et al., 2021c). Lastly, knowledge of sequence similarity to conserved miRNA families responsive to biotic stress (Šečić et al., 2021b) was crucial in identifying sRNA-generating loci in *B. distachyon*. Assignment of sRNA origin for other sRNA sub-species, especially in the fungus *S. indica* was not as successful, indicating that optimization of existing approaches for sRNA origin determination is necessary. Ideally, combined analyses from unanswered questions about sRNA origin, classification and target prediction would all contribute to a fuller, more exact picture of sRNA-based gene regulation during plant-microbe interactions.

Further on, tissue and even single-cell resolution of sRNA activity and expression would be desirable, in order to resolve signals for cell and tissue types that are affected locally and distantly by microbial presence. In our sequencing approaches, sRNA concentration from the cells where uptake initially occurs is necessarily diluted by sampling of the entire root and/or leaf tissue. Additionally, while addition of degradome sequencing to the used set-up would contribute information about mRNAs that are silenced by transcript degradation, that still does not account for the portion of silencing that occurs via translation inhibition.

### **Application of RNAi in plant protection**

Detected as a naturally-present communication mechanism between plants and microbes, cross-kingdom sRNA exchange affirms that the use of RNAi-based plant protection has a foreseeable application in many plant pathosystems. The model organisms we selected for analysis in our research certainly accumulated knowledge necessary for many translation approaches to crop species. For this to occur however, further studies are necessary, both on the plant and the microbe side. For example, obstacles of dsRNA design optimization, stability and fungal uptake all have to be conquered before a HIGS or SIGS-based strategy is applied against a fungal pathogen (Šečić et al., 2021a). Additionally, targets of fungal sRNA silencing in plants offer an attractive pool of candidates for plant immunity and growth regulation research, especially in response to beneficial endophyte colonization.

## References (in alphabetical order)

- Akum FN, Steinbrenner J, Biedenkopf D, Imani J, Kogel K-H: The *Piriformospora indica* effector PIIN\_08944 promotes the mutualistic Sebacinalean symbiosis. *Front Plant Sci* 2015, 6:906.
- Asibi AE, Chai Q, Coulter JA: Rice Blast: A Disease with Implications for Global Food Security. *Agron* 2019, 9.
- Baltruschat H, Fodor J, Harrach BD, Niemczyk E, Barna B, Gullner G, Janeczko A, Kogel K-H, Schäfer P, Schwarczinger I, et al.: Salt tolerance of barley induced by the root endophyte *Piriformospora indica* is associated with a strong increase in antioxidants. *New Phytol* 2008, 180:501–510.
- Benami M, Isack Y, Grotzky D, Levy D, Kofman Y: The Economic Potential of Arbuscular Mycorrhizal Fungi in Agriculture BT - Grand Challenges in Fungal Biotechnology. In Edited by Nevalainen H. Springer International Publishing; 2020:239–279.
- Bonfante P, Genre A: Mechanisms underlying beneficial plant–fungus interactions in mycorrhizal symbiosis. *Nat Commun* 2010, 1:48.
- Buendia L, Girardin A, Wang T, Cottret L, Lefebvre B: LysM Receptor-Like Kinase and LysM Receptor-Like Protein Families: An Update on Phylogeny and Functional Characterization. *Front Plant Sci* 2018, 9:1531.
- Cai Q, He B, Weiberg A, Buck AH, Jin H: Small RNAs and extracellular vesicles: New mechanisms of cross-species communication and innovative tools for disease control. *PLOS Pathog* 2020, 15:e1008090.
- Chen R, Jiang N, Jiang Q, Sun X, Wang Y, Zhang H, Hu Z: Exploring microRNA-like small RNAs in the filamentous fungus *Fusarium oxysporum*. *PLoS One* 2014, 9:e104956–e104956.
- Cheng YT, Zhang L, He SY: Plant-Microbe Interactions Facing Environmental Challenge. *Cell Host Microbe* 2019, 26:183–192.
- Conrath U, Beckers GJM, Flors V, García-Agustín P, Jakab G, Mauch F, Newman M-A, Pieterse CMJ, Poinssot B, Pozo MJ, et al.: Priming: Getting Ready for Battle. *Mol Plant-Microbe Interact* 2006, 19:1062–1071.
- Cuomo CA, Güldener U, Xu JR, Trail F, Turgeon BG, Di Pietro A, Walton JD, Ma LJ, Baker SE, Rep M, Adam G, Antoniw J, Baldwin T, Calvo S, Chang YL, Decaprio D, Gale LR, Gnerre S, Goswami RS, Hammond-Kosack K, Harris LJ, Hilburn K, Kennell JC, Kroken S, Magnuson JK, Mannhaupt G, Mauceli E, Mewes HW, Mitterbauer R, Muehlbauer G, Münsterkötter M, Nelson D, O'donnell K, Ouellet T, Qi W, Quesneville H, Roncero MI, Seong KY, Tetko IV, Urban M, Waalwijk C, Ward TJ, Yao J, Birren BW, Kistler HC: The *Fusarium graminearum* Genome Reveals a Link Between Localized Polymorphism and Pathogen Specialization. *Science* (80- ) 2007, 317:1400–1402.
- Dang Y, Yang Q, Xue Z, Liu Y: RNA Interference in Fungi: Pathways, Functions, and Applications. *Eukaryot Cell* 2011, 10:1148 LP – 1155.
- Deakin WJ, Broughton WJ: Symbiotic use of pathogenic strategies: rhizobial protein secretion systems. *Nat Rev Microbiol* 2009, 7:312–320.

Dean RA, Talbot NJ, Ebbole DJ, Farman ML, Mitchell TK, Orbach MJ, Thon M, Kulkarni R, Xu J-R, Pan H, et al.: The genome sequence of the rice blast fungus *Magnaporthe grisea*. *Nature* 2005, 434:980–986.

Dean R, Van Kan JA, Pretorius ZA, Hammond-Kosack KE, Di Pietro A, Spanu PD, Rudd JJ, Dickman M, Kahmann R, Ellis J, Foster GD.: The Top 10 fungal pathogens in molecular plant pathology. *Mol Plant Pathol* 2012, 13:414–430.

Deshmukh S, Hükelhoven R, Schäfer P, Imani J, Sharma M, Weiss M, Waller F, Kogel K-H: The root endophytic fungus *Piriformospora indica* requires host cell death for proliferation during mutualistic symbiosis with barley. *Proc Natl Acad Sci U S A* 2006, 103:18450–18457.

Deshmukh SD, Kogel K-H: *Piriformospora indica* protects barley from root rot caused by *Fusarium graminearum*. *J Plant Dis Prot* 2007, 114:263–268.

Dodds PN, Rathjen JP: Plant immunity: towards an integrated view of plant–pathogen interactions. *Nat Rev Genet* 2010, 11:539–548.

Douché T, Clemente HS, Burlat V, Roujol D, Valot B, Zivy M, Pont-Lezica R, Jamet E: *Brachypodium distachyon* as a model plant toward improved biofuel crops: Search for secreted proteins involved in biogenesis and disassembly of cell wall polymers. *Proteomics* 2013, 13:2438–2454.

Dunker F, Trutzenberg A, Rothenpieler JS, Kuhn S, Pröls R, Schreiber T, Tissier A, Kemen A, Kemen E, Hükelhoven R, et al.: Oomycete small RNAs bind to the plant RNA-induced silencing complex for virulence. *Elife* 2020, 9:e56096.

Fahlgren N, Jogdeo S, Kasschau KD, Sullivan CM, Chapman EJ, Laubinger S, Smith LM, Dasenko M, Givan SA, Weigel D, et al.: MicroRNA gene evolution in *Arabidopsis lyrata* and *Arabidopsis thaliana*. *Plant Cell* 2010, 22:1074–1089.

Fakhro A, Andrade-Linares DR, von Barga S, Bandte M, Büttner C, Grosch R, Schwarz D, Franken P: Impact of *Piriformospora indica* on tomato growth and on interaction with fungal and viral pathogens. *Mycorrhiza* 2010, 20:191–200.

Fang X, Qi Y: RNAi in Plants: An Argonaute-Centered View. *Plant Cell* 2016, 28:272 LP – 285.

Filiz E, Ozdemir BS, Budak F, Vogel JP, Tuna M, Budak H: Molecular, morphological, and cytological analysis of diverse *Brachypodium distachyon* inbred lines. *Genome* 2009, 52:876–890.

Gaffar FY, Imani J, Karlovsky P, Koch A, Kogel K-H: Different Components of the RNA Interference Machinery Are Required for Conidiation, Ascosporeogenesis, Virulence, Deoxynivalenol Production, and Fungal Inhibition by Exogenous Double-Stranded RNA in the Head Blight Pathogen *Fusarium graminearum*. *Front Microbiol* 2019, 10:1662.

Genre A, Lanfranco L, Perotto S, Bonfante P: Unique and common traits in mycorrhizal symbioses. *Nat Rev Microbiol* 2020, 18:649–660.

Girin T, David LC, Chardin C, Sibout R, Krapp A, Ferrario-Méry S, Daniel-Vedele F: *Brachypodium*: a promising hub between model species and cereals. *J Exp Bot* 2014, 65:5683–5696.

- Godefroid M, Cruaud A, Streito J-C, Rasplus J-Y, Rossi J-P: *Xylella fastidiosa*: climate suitability of European continent. *Sci Rep* 2019, 9:8844.
- Gordon SP, Contreras-Moreira B, Woods DP, Des Marais DL, Burgess D, Shu S, Stritt C, Roulin AC, Schackwitz W, Tyler L, et al.: Extensive gene content variation in the *Brachypodium distachyon* pan-genome correlates with population structure. *Nat Commun* 2017, 8:2184.
- Guo H, Glaeser SP, Alabid I, Imani J, Haghighi H, Kämpfer P, Kogel K-H: The Abundance of Endofungal Bacterium *Rhizobium radiobacter* (syn. *Agrobacterium tumefaciens*) Increases in Its Fungal Host *Piriformospora indica* during the Tripartite Sebacinalean Symbiosis with Higher Plants. *Front Microbiol* 2017, 8:629.
- Harris JM, Balint-Kurti P, Bede JC, Day B, Gold S, Goss EM, Grenville-Briggs LJ, Jones KM, Wang A, Wang Y, et al.: What are the Top 10 Unanswered Questions in Molecular Plant-Microbe Interactions? *Mol Plant-Microbe Interact* 2020, 33:1354–1365.
- Head GP, Carroll MW, Evans SP, Rule DM, Willse AR, Clark TL, Storer NP, Flannagan RD, Samuel LW, Meinke LJ: Evaluation of SmartStax and SmartStax PRO maize against western corn rootworm and northern corn rootworm: efficacy and resistance management. *Pest Manag Sci* 2017, 73:1883–1899.
- Hsia MM, O'Malley R, Cartwright A, Nieu R, Gordon SP, Kelly S, Williams TG, Wood DF, Zhao Y, Bragg J, et al.: Sequencing and functional validation of the JGI *Brachypodium distachyon* T-DNA collection. *Plant J* 2017, 91:361–370.
- Huo N, Vogel JP, Lazo GR, You FM, Ma Y, McMahon S, Dvorak J, Anderson OD, Luo M-C, Gu YQ: Structural characterization of *Brachypodium* genome and its syntenic relationship with rice and wheat. *Plant Mol Biol* 2009, 70:47–61.
- Jacobs S, Zechmann B, Molitor A, Trujillo M, Petutschnig E, Lipka V, Kogel K-H, Schäfer P: Broad-Spectrum Suppression of Innate Immunity Is Required for Colonization of Arabidopsis Roots by the Fungus *Piriformospora indica*. *Plant Physiol* 2011, 156:726–740.
- Jeon J, Park S-Y, Chi M-H, Choi J, Park J, Rho H-S, Kim S, Goh J, Yoo S, Choi J, et al.: Genome-wide functional analysis of pathogenicity genes in the rice blast fungus. *Nat Genet* 2007, 39:561–565.
- Jeong D-H, Schmidt SA, Rymarquis LA, Park S, Ganssmann M, German MA, Accerbi M, Zhai J, Fahlgren N, Fox SE, et al.: Parallel analysis of RNA ends enhances global investigation of microRNAs and target RNAs of *Brachypodium distachyon*. *Genome Biol* 2013, 14:R145–R145.
- Jian J, Liang X: One Small RNA of *Fusarium graminearum* Targets and Silences CEBiP Gene in Common Wheat. *Microorganisms* 2019, 7:425.
- Jones JDG, Dangl JL: The plant immune system. *Nature* 2006, 444:323–329.
- Kim K-T, Ko J, Song H, Choi G, Kim H, Jeon J, Cheong K, Kang S, Lee Y-H: Evolution of the Genes Encoding Effector Candidates Within Multiple Pathotypes of *Magnaporthe oryzae*. *Front Microbiol* 2019, 10:2575.
- King R, Urban M, Hammond-Kosack MCU, Hassani-Pak K, Hammond-Kosack KE: The completed genome sequence of the pathogenic ascomycete fungus *Fusarium graminearum*. *BMC Genomics* 2015, 16:544.

- Koch A, Kumar N, Weber L, Keller H, Imani J, Kogel K-H: Host-induced gene silencing of cytochrome P450 lanosterol C14 $\alpha$ -demethylase–encoding genes confers strong resistance to *Fusarium* species. *Proc Natl Acad Sci* 2013, 110:19324 LP – 19329.
- Koch A, Biedenkopf D, Furch A, Weber L, Rossbach O, Abdellatef E, Linicus L, Johannsmeier J, Jelonek L, Goesmann A, et al.: An RNAi-Based Control of *Fusarium graminearum* Infections Through Spraying of Long dsRNAs Involves a Plant Passage and Is Controlled by the Fungal Silencing Machinery. *PLOS Pathog* 2016, 12:e1005901.
- Köhl J, Kolnaar R, Ravensberg WJ: Mode of Action of Microbial Biological Control Agents Against Plant Diseases: Relevance Beyond Efficacy. *Front Plant Sci* 2019, 10:845.
- Kloppholz S, Kuhn H, Requena N: A Secreted Fungal Effector of *Glomus intraradices* Promotes Symbiotic Biotrophy. *Curr Biol* 2011, 21:1204–1209.
- Lahrmann U, Strehmel N, Langen G, Frerigmann H, Leson L, Ding Y, Scheel D, Herklotz S, Hilbert M, Zuccaro A: Mutualistic root endophytism is not associated with the reduction of saprotrophic traits and requires a noncompromised plant innate immunity. *New Phytol* 2015, 207.
- Li C, Rudi H, Stockinger EJ, Cheng H, Cao M, Fox SE, Mockler TC, Westereng B, Fjellheim S, Rognli OA, et al.: Comparative analyses reveal potential uses of *Brachypodium distachyon* as a model for cold stress responses in temperate grasses. *BMC Plant Biol* 2012, 12:65.
- Liao P, Li S, Cui X, Zheng Y: A comprehensive review of web-based resources of non-coding RNAs for plant science research. *Int J Biol Sci* 2018, 14:819–832.
- Martin F, Uroz S, Barker D: Ancestral alliances: Plant mutualistic symbioses with fungi and bacteria. *Science* 2017, 356(6340):eaad4501.
- Mauch-Mani B, Baccelli I, Luna E, Flors V: Defense Priming: An Adaptive Part of Induced Resistance. *Annu Rev Plant Biol* 2017, 68:485–512.
- Nowara D, Gay A, Lacomme C, Shaw J, Ridout C, Douchkov D, Hensel G, Kumlehn J, Schweizer P: HIGS: Host-Induced Gene Silencing in the Obligate Biotrophic Fungal Pathogen *Blumeria graminis*. *Plant Cell* 2010, 22:3130 LP – 3141.
- Nunes CC, Gowda M, Sailsbery J, Xue M, Chen F, Brown DE, Oh Y, Mitchell TK, Dean RA: Diverse and tissue-enriched small RNAs in the plant pathogenic fungus, *Magnaporthe oryzae*. *BMC Genomics* 2011, 12:288.
- Oldroyd GED: Speak, friend, and enter: signalling systems that promote beneficial symbiotic associations in plants. *Nat Rev Microbiol* 2013, 11:252–263.
- Opitz MW, Daneshkhah R, Lorenz C, Ludwig R, Steinkellner S, Wieczorek K: *Serendipita indica* changes host sugar and defense status in *Arabidopsis thaliana*: cooperation or exploitation? *Planta* 2021, 253:74.
- Pankievicz VCS, Irving TB, Maia LGS, Ané J-M: Are we there yet? The long walk towards the development of efficient symbiotic associations between nitrogen-fixing bacteria and non-leguminous crops. *BMC Biol* 2019, 17:99.

- Peraldi A, Beccari G, Steed A, Nicholson P: *Brachypodium distachyon*: a new pathosystem to study Fusarium head blight and other Fusarium diseases of wheat. BMC Plant Biol 2011, 11:100.
- Pieterse CMJ, Zamioudis C, Berendsen RL, Weller DM, Van Wees SCM, Bakker PAHM: Induced Systemic Resistance by Beneficial Microbes. Annu Rev Phytopathol 2014, 52:347–375.
- Qiang X, Weiss M, Kogel KH, Schäfer P: *Piriformospora indica*—a mutualistic basidiomycete with an exceptionally large plant host range. Mol Plant Pathol 2012, 13:508–518.
- Raman V, Simon SA, Demirci F, Nakano M, Meyers BC, Donofrio NM: Small RNA Functions Are Required for Growth and Development of *Magnaporthe oryzae*. Mol Plant-Microbe Interact 2017, 30:517–530.
- Ren B, Wang X, Duan J, Ma J: Rhizobial tRNA-derived small RNAs are signal molecules regulating plant nodulation. Science (80) 2019, 365.
- Routledge APM, Shelley G, Smith JV, Talbot NJ, Draper J, Mur LAJ: *Magnaporthe grisea* interactions with the model grass *Brachypodium distachyon* closely resemble those with rice (*Oryza sativa*). Mol Plant Pathol 2004, 5:253–265.
- Ryals JA, Neuenschwander UH, Willits MG, Molina A, Steiner HY, Hunt MD: Systemic Acquired Resistance. Plant Cell 1996, 8:1809–1819.
- Soudzilovskaia NA, van Bodegom PM, Terrer C, Zelfde M van't, McCallum I, Luke McCormack M, Fisher JB, Brundrett MC, de Sá NC, Tedersoo L: Global mycorrhizal plant distribution linked to terrestrial carbon stocks. Nat Commun 2019, 10:5077.
- Sesma A, Osbourn A: The rice leaf blast pathogen undergoes developmental processes typical of root-infecting fungi. Nature 2004, 431:582–586.
- Schäfer P, Pfiffi S, Voll LM, Zajic D, Chandler PM, Waller F, Scholz U, Pons-Kühnemann J, Sonnewald S, Sonnewald U, et al.: Manipulation of plant innate immunity and gibberellin as factor of compatibility in the mutualistic association of barley roots with *Piriformospora indica*. Plant J 2009, 59:461–474.
- Scholthof K-BG, Irigoyen S, Catalan P, Mandadi KK: *Brachypodium*: A Monocot Grass Model Genus for Plant Biology. Plant Cell 2018, 30:1673–1694.
- Silvestri A, Fiorilli V, Miozzi L, Accotto GP, Turina M, Lanfranco L: In silico analysis of fungal small RNA accumulation reveals putative plant mRNA targets in the symbiosis between an arbuscular mycorrhizal fungus and its host plant. BMC Genomics 2019, 20:1–18.
- Singh A, Gautam V, Singh S, Sarkar Das S, Verma S, Mishra V, Mukherjee S, Sarkar AK: Plant small RNAs: advancement in the understanding of biogenesis and role in plant development. Planta 2018, 248:545–558.
- Singh S, Balodi R, Meena PN, Singhal S: Biocontrol activity of *Trichoderma harzianum*, *Bacillus subtilis* and *Pseudomonas fluorescens* against *Meloidogyne incognita*, *Fusarium oxysporum* and *Rhizoctonia solani*. Indian Phytopathol 2021, 74:703–714.
- Son H, Park AR, Lim JY, Shin C, Lee Y-W: Genome-wide exonic small interference RNA-mediated gene silencing regulates sexual reproduction in the homothallic fungus *Fusarium graminearum*. PLOS Genet 2017, 13:e1006595.

Song L, Fang Y, Chen L, Wang J, Chen X: Role of non-coding RNAs in plant immunity. *Plant Commun* 2021, 2:100180.

Soto MJ, Domínguez-Ferreras A, Pérez-Mendoza D, Sanjuán J, Olivares J: Mutualism versus pathogenesis: the give-and-take in plant–bacteria interactions. *Cell Microbiol* 2009, 11:381–388.

Soudzilovskaia NA, van Bodegom PM, Terrer C, Zelfde M van't, McCallum I, Luke McCormack M, Fisher JB, Brundrett MC, de Sá NC, Tedersoo L: Global mycorrhizal plant distribution linked to terrestrial carbon stocks. *Nat Commun* 2019, 10:5077.

Stein E, Molitor A, Kogel K-H, Waller F: Systemic Resistance in Arabidopsis Conferred by the Mycorrhizal Fungus *Piriformospora indica* Requires Jasmonic Acid Signaling and the Cytoplasmic Function of NPR1. *Plant Cell Physiol* 2008, 49:1747–1751.

Šečić E, Zanini S, Kogel K-H: Further Elucidation of the Argonaute and Dicer Protein Families in the Model Grass Species *Brachypodium distachyon*. *Front Plant Sci* 2019, 10:1332.

Šečić E, Kogel K-H: Requirements for fungal uptake of dsRNA and gene silencing in RNAi-based crop protection strategies. *Curr Opin Biotechnol* 2021a, 70:136–142.

Šečić E, Kogel K-H, Ladera-Carmona MJ: Biotic stress-associated microRNA families in plants. *J Plant Physiol* 2021b, 263:153451.

Šečić E, Zanini S, Wibberg D, Jelonek L, Busche T, Kalinowski J, Nasfi S, Thielmann J, Imani J, Steinbrenner J, Kogel K-H: A novel plant-fungal association reveals fundamental sRNA and gene expression reprogramming at the onset of symbiosis. *BMC Biol* 2021c, 19:171.

Thoms D, Liang Y, Haney CH: Maintaining Symbiotic Homeostasis: How Do Plants Engage With Beneficial Microorganisms While at the Same Time Restricting Pathogens? *Mol Plant-Microbe Interact* 2021, 34:462–469.

Trail F: For blighted waves of grain: *Fusarium graminearum* in the postgenomics era. *Plant Physiol* 2009, 149:103–110.

Trzewik A, Maciorowski R, Klocke E, Orlikowska T: The influence of *Piriformospora indica* on the resistance of two rhododendron cultivars to *Phytophthora cinnamomi* and *P. plurivora*. *Biol Control* 2020, 140:104121.

Tyler L, Fangel JU, Fagerström AD, Steinwand MA, Raab TK, Willats WGT, Vogel JP: Selection and phenotypic characterization of a core collection of *Brachypodium distachyon* inbred lines. *BMC Plant Biol* 2014, 14:25.

Urashima A: Host Range, Mating Type, and Fertility of *Pyricularia grisea* from Wheat in Brazil. *Plant Dis* 1993, 77:1211.

van der Heijden MGA, Hartmann M: Networking in the Plant Microbiome. *PLOS Biol* 2016, 14:e1002378.

Verma S, Varma A, Rexer K-H, Hassel A, Kost G, Sarbhoy A, Bisen P, Bütehorn B, Franken P: *Piriformospora indica*, gen. et sp. nov., a new root-colonizing fungus. *Mycologia* 1998, 90:896–903.

- Vogel J, Hill T: High-efficiency *Agrobacterium*-mediated transformation of *Brachypodium distachyon* inbred line Bd21-3. *Plant Cell Rep* 2008, 27:471–478.
- Vogel JP, Garvin DF, Mockler TC, Schmutz J, Rokhsar D, Bevan MW, Barry K, Lucas S, Harmon-Smith M, Lail K, et al.: Genome sequencing and analysis of the model grass *Brachypodium distachyon*. *Nature* 2010, 463:763–768.
- Waller F, Achatz B, Baltruschat H, Fodor J, Becker K, Fischer M, Heier T, Hückelhoven R, Neumann C, von Wettstein D, et al.: The endophytic fungus *Piriformospora indica* reprograms barley to salt-stress tolerance, disease resistance, and higher yield. *Proc Natl Acad Sci U S A* 2005, 102:13386–13391.
- Wang B, Sun Y, Song N, Zhao M, Liu R, Feng H, Wang X, Kang Z: *Puccinia striiformis* f. sp. *tritici* microRNA-like RNA 1 (Pst-miR1), an important pathogenicity factor of Pst, impairs wheat resistance to Pst by suppressing the wheat pathogenesis-related 2 gene. *New Phytol* 2017, 215:338–350.
- Wang J, Mei J, Ren G: Plant microRNAs: Biogenesis, Homeostasis, and Degradation. *Front Plant Sci* 2019, 10:360.
- Wang M, Weiberg A, Lin F-M, Thomma BPHJ, Huang H-D, Jin H: Bidirectional cross-kingdom RNAi and fungal uptake of external RNAs confer plant protection. *Nat Plants* 2016, 2:16151.
- Wang S, Li P, Zhang J, Qiu D, Guo L: Generation of a high resolution map of sRNAs from *Fusarium graminearum* and analysis of responses to viral infection. *Sci Rep* 2016, 6:26151.
- Weiberg A, Wang M, Lin F-M, Zhao H, Zhang Z, Kaloshian I, Huang H-D, Jin H: Fungal Small RNAs Suppress Plant Immunity by Hijacking Host RNA Interference Pathways. *Science* (80) 2013, 342:118 LP – 123.
- Weiß M, Sýkorová Z, Garnica S, Riess K, Martos F, Krause C, Oberwinkler F, Bauer R, Redecker D: Sebaciniales Everywhere: Previously Overlooked Ubiquitous Fungal Endophytes. *PLoS One* 2011, 6:e16793.
- Wegulo SN, Baenziger PS, Hernandez Nopsa J, Bockus WW, Hallen-Adams H: Management of *Fusarium* head blight of wheat and barley. *Crop Prot* 2015, 73:100–107.
- Werner BT, Koch A, Šečić E, Engelhardt J, Jelonek L, Steinbrenner J, Kogel K-H: *Fusarium graminearum* DICER-like-dependent sRNAs are required for the suppression of host immune genes and full virulence. *PLOS One* 2021, 16(8): e0252365.
- Wilson RC, Doudna JA: Molecular mechanisms of RNA interference. *Annu Rev Biophys* 2013, 42:217–239.
- Ye W, Shen C-H, Lin Y, Chen P-J, Xu X, Oelmüller R, Yeh K-W, Lai Z: Growth Promotion-Related miRNAs in *Oncidium* Orchid Roots Colonized by the Endophytic Fungus *Piriformospora indica*. *PLoS One* 2014, 9:e84920.
- Zanini S, Šečić E, Jelonek L, Kogel K-H: A bioinformatics pipeline for the analysis and target prediction of RNA effectors in bidirectional communication during plant–microbe interactions. *Front Plant Sci* 2018, 9.

Zanini S, Šečić E, Busche T, Galli M, Zheng Y, Kalinowski J, Kogel K-H: Comparative analysis of transcriptome and sRNA expression patterns in the *Brachypodium distachyon* - *Magnaporthe oryzae* pathosystems. *Int J Mol Sci* 2021, 22.

Zhang T, Zhao YL, Zhao JH, Wang S, Jin Y, Chen ZQ, Fang YY, Hua CL, Ding SW, Guo HS: Cotton plants export microRNAs to inhibit virulence gene expression in a fungal pathogen. *Nat Plants* 2016, 2:1–6.

Zicca S, De Bellis P, Masiello M, Saponari M, Saldarelli P, Boscia D, Sisto A: Antagonistic activity of olive endophytic bacteria and of *Bacillus* spp. strains against *Xylella fastidiosa*. *Microbiol Res* 2020, 236:126467.

Zipfel C, Oldroyd GED: Plant signalling in symbiosis and immunity. *Nature* 2017, 543:328–336.

Zuccaro A, Basiewicz M, Zurawska M, Biedenkopf D, Kogel K-H: Karyotype analysis, genome organization, and stable genetic transformation of the root colonizing fungus *Piriformospora indica*. *Fungal Genet Biol* 2009, 46:543–550.

Zuccaro A, Lahrmann U, Güldener U, Langen G, Pfiffi S, Biedenkopf D, Wong P, Samans B, Grimm C, Basiewicz M, et al.: Endophytic Life Strategies Decoded by Genome and Transcriptome Analyses of the Mutualistic Root Symbiont *Piriformospora indica*. *PLOS Pathog* 2011, 7:e1002290.

## List of publications\*

1. Zanini S, Šečić E, Jelonek L, Kogel K-H: A bioinformatics pipeline for the analysis and target prediction of RNA effectors in bidirectional communication during plant–microbe interactions. *Front Plant Sci* 2018, 9. <https://doi.org/10.3389/fpls.2018.01212> (review, writing – 40%)
2. Šečić E, Zanini S, Kogel K-H: Further elucidation of the Argonaute and Dicer protein families in the model grass species *Brachypodium distachyon*. *Front Plant Sci* 2019, 10:1332. <https://doi.org/10.3389/fpls.2019.01332> (research paper, experiments – 60 %, writing – 50%)
3. Zanini S, Šečić E, Busche T, Galli M, Zheng Y, Kalinowski J, Kogel K-H: Comparative analysis of transcriptome and sRNA expression patterns in the *Brachypodium distachyon* - *Magnaporthe oryzae* pathosystems. *Int J Mol Sci* 2021, 22. <https://doi.org/10.3390/ijms22020650> (research paper, experiments – 20 %, writing – 10%)
4. Šečić E, Kogel K-H: Requirements for fungal uptake of dsRNA and gene silencing in RNAi-based crop protection strategies. *Curr Opin Biotechnol* 2021, 70:136–142. <https://doi.org/10.1016/j.copbio.2021.04.001> (review, writing – 70 %)
5. Šečić E, Kogel K-H, Ladera-Carmona MJ: Biotic stress-associated microRNA families in plants. *J Plant Physiol* 2021, 263:153451. <https://doi.org/10.1016/j.jplph.2021.153451> (review, writing – 50%)
6. Šečić E, Zanini S, Wibberg D, Jelonek L, Busche T, Kalinowski J, Nasfi S, Thielmann J, Imani J, Steinbrenner J, Kogel K-H: A novel plant-fungal association reveals fundamental sRNA and gene expression reprogramming at the onset of symbiosis. *BMC Biol* 2021, 19:171. <https://doi.org/10.1186/s12915-021-01104-2> (research paper, experiments – 70%, writing – 60%)
7. Werner BT, Koch A, Šečić E, Engelhardt J, Jelonek L, Steinbrenner J, Kogel K-H: *Fusarium graminearum* DICER-like-dependent sRNAs are required for the suppression of host immune genes and full virulence. *PLOS One* 2021, 16(8): e0252365. <https://doi.org/10.1371/journal.pone.0252365> (research paper, experiments – 10%, writing – 5%).

\* Publications listed in order of acceptance. Authors contribution to experiments and writing indicated in %.



# A Bioinformatics Pipeline for the Analysis and Target Prediction of RNA Effectors in Bidirectional Communication During Plant–Microbe Interactions

Silvia Zanini<sup>1</sup>, Ena Šečić<sup>1</sup>, Lukas Jelonek<sup>2</sup> and Karl-Heinz Kogel<sup>1\*</sup>

<sup>1</sup> Institute of Phytopathology, Centre for BioSystems, Land Use and Nutrition, Justus Liebig University Giessen, Giessen, Germany, <sup>2</sup> Institute of Bioinformatics and Systems Biology, Justus Liebig University Giessen, Giessen, Germany

## OPEN ACCESS

### Edited by:

Mahmut Tör,  
University of Worcester,  
United Kingdom

### Reviewed by:

David John Studholme,  
University of Exeter, United Kingdom  
Laura Baxter,  
University of Warwick,  
United Kingdom

### \*Correspondence:

Karl-Heinz Kogel  
karl-heinz.kogel@agr.uni-giessen.de

### Specialty section:

This article was submitted to  
Plant Microbe Interactions,  
a section of the journal  
Frontiers in Plant Science

**Received:** 17 May 2018

**Accepted:** 27 July 2018

**Published:** 20 August 2018

### Citation:

Zanini S, Šečić E, Jelonek L and  
Kogel K-H (2018) A Bioinformatics  
Pipeline for the Analysis and Target  
Prediction of RNA Effectors  
in Bidirectional Communication  
During Plant–Microbe Interactions.  
*Front. Plant Sci.* 9:1212.  
doi: 10.3389/fpls.2018.01212

Small RNA (sRNA) molecules are key factors in the communication between hosts and their interacting pathogens, where they function as effectors that can modulate both host defense and microbial virulence/pathogenicity through a mechanism termed cross-kingdom RNA interference (*ck*-RNAi). Consistent with this recent knowledge, sRNAs and their double-stranded RNA precursor have been adopted to control diseases in crop plants, demonstrating a straight forward application of the new findings to approach agricultural problems. Despite the great interest in natural *ck*-RNAi, it is astonishing to find just a few additional examples in the literature since the first report was published in 2013. One reason might be that the identification of sRNA effectors is hampered both by technical challenges and lack of routine bioinformatics application strategies. Here, we suggest a practical procedure to find, characterize, and validate sRNA effectors in plant–microbe interaction. The aim of this review is not to present and discuss all possible tools, but to give guidelines toward the best established software available for the analysis.

**Keywords:** small RNA, cross-kingdom RNAi, bidirectional communication, RNA targets, plant disease, virulence

## INTRODUCTION

Natural cross-kingdom RNA interference (*ck*-RNAi) is an emerging field of research in plant–microbe interactions and plant pathology (Cai et al., 2018). The phenomenon includes small RNA (sRNA) (Borges and Martienssen, 2015) that are mutually transferred between interacting hosts and pathogens to eventually target and thus modulate respective host defense and pathogen virulence functions by RNAi (Weiberg et al., 2013; Zhang et al., 2016). RNAi is the process by which 21–24 nucleotide (nt) sRNAs are used by ARGONAUTE (AGO) proteins to guide an RNA-Induced Silencing Complex (RISC) toward a complementary messenger RNA (mRNA), resulting either in mRNA cleavage and degradation, or impairment of its transcription by acting as a physical block (Fire et al., 1998; Hamilton and Baulcombe, 1999).

Recent studies have shown that fungal pathogens can produce and deliver sRNAs to host plants in order to suppress their immunity and thus aid colonization (Weiberg et al., 2013; Wang B. et al., 2017). During infection, *Botrytis cinerea* transfers sRNAs to Arabidopsis and tomato cells, targeting

host genes known to be involved in plant defense responses, including transcription factors and receptor-like kinases (Wang M. et al., 2017). This silencing is possible due to the fungus hijacking the RNAi machinery of the host, in particular AtAGO1. Consequently, the fertile hypomorphic *ago1-27* Arabidopsis mutant shows increased resistance to *Botrytis* infection. Interestingly, the *ago1-27* mutant is similarly less infected compared to wild type (wt) plants when infected with *Verticillium dahliae* (Vd), suggesting a role for RNAi also in this interaction.

Furthermore, the causal agent of stripe rust in wheat, *Puccinia striiformis* (Ps), delivers fungal microRNA (miRNA)-like RNAs into host cells to suppress the defense response by targeting and downregulating wheat *Pathogenesis-related 2* (*PR-2*) expression. Silencing of the sRNA precursor showed enhanced resistance to the virulent Ps isolate in wheat adult plants (Wang B. et al., 2017).

Preliminary results indicate the bidirectionality of this process in the interaction between Vd and cotton plants. In Vd samples recovered from infected cotton plants, 28 different sRNAs were predicted to originate not from Vd, but from the cotton plant, implying that host-derived sRNAs had been transferred into the pathogen during infection (Zhang et al., 2016). Despite the great interest in natural *ck*-RNAi and its agronomic application (Koch et al., 2013, 2016; Koch and Kogel, 2014; Wang et al., 2016; Niehl et al., 2018), it is astonishing to find just a few examples in the literature since the first report was published by Weiberg and colleagues in 2013 (Weiberg et al., 2013). One reason might be that the identification of sRNA effectors is hampered both by technical challenges and lack of routine bioinformatics application strategies. Here we suggest a practical procedure to find, characterize, and validate sRNA effectors in plant-microbe interactions. The aim of this review is not to present and discuss all possible tools, but to give guidelines toward the establishment of a suitable pipeline for the analysis.

## STRATEGIES TO FIND, CHARACTERIZE, AND VALIDATE sRNA EFFECTORS IN PLANT-MICROBE INTERACTIONS

### Sample Preparation and sRNA Sequencing

In all cases, identification and confirmation of cross-kingdom sRNAs (*ck*-sRNAs) starts with the preparation of suitable biological samples. When planning which and how many samples to sequence, control samples of uninfected plants and, when possible, axenic cultures of the microbe should be included in order to verify the infection-related upregulation/induction of the candidate *ck*-sRNAs in bidirectional fashion. The preparation also requires to fix the number of replicates and of reads per sample (typically three biological replicates with 5–10 million reads each, Conesa et al., 2016).

While sequencing can be carried out using a variety of machines, the focus of this review is on sequencing with Illumina

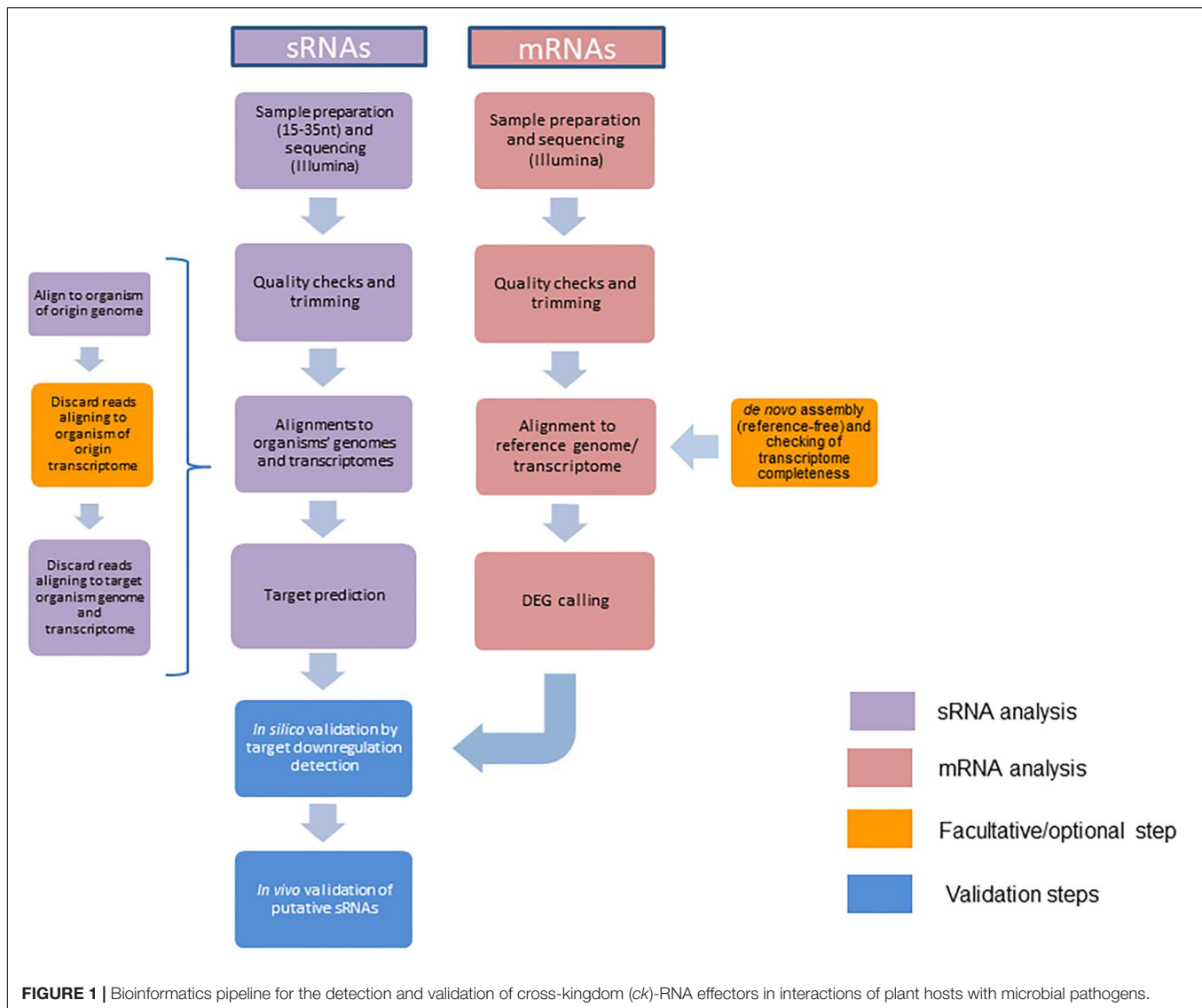
technology. With TruSeq Small RNA Library Preparation by Illumina it is possible to create indexed libraries of sRNAs both from total RNA and from pre-size-selected fractions, depending on the need to preserve mRNA for further sequencing or not. Libraries can then be pooled and sequenced on various Illumina systems, including MiSeq and NextSeq, depending on the output range and total reads per run required. Subsequent analysis of this data is the critical point toward discovery of candidate *ck*-sRNAs. There are numerous detailed papers comparing the performances of the programs mentioned in this review, which are recommended for reading once a preliminary pipeline is chosen, as the fine tuning of the software settings is specific for each project/organism analyzed (Dai et al., 2011a; Srivastava et al., 2014; Li et al., 2015; Conesa et al., 2016).

Although known *ck*-sRNAs are between 21 and 24 nt long (Weiberg et al., 2013; Wang M. et al., 2017; Wang B. et al., 2017), the range for the size selection can be increased to 18–35 nt for detection of all other known regulatory sRNAs. Sequencing depth, number of replicates, and type of libraries are all experiment-specific and highly variable depending on the aim of the study and the resources available. For example, for adequate statistical power in the data analysis, a minimum of three biological replicates is required (Love et al., 2014) and, while for mRNA it is usually recommended to explore the option of longer read length or paired-end (PE) sequencing, single-end (SE) short reads are perfectly suitable for sRNAseq. Regardless of the specific datasets, some measures have to be taken to ensure the removal of unwanted fragments that would outweigh the sequences of interest. In particular, size selection prior to sRNA sequencing is required to avoid sequencing longer fragments that would not be the focus of the study.

### Determination of Candidate *ck*-sRNA

Acquisition of the raw reads is the first step of the bioinformatics analysis and is immediately followed by quality check. FastQC (Andrews, 2010) is the most frequently used program for this task, as it is recommended by Illumina for the analysis of Illumina NGS data and it is compatible also with PacBio and 454 datasets. Alternatively, programs such as NGS-QC can also be used for the analysis of data obtained from several sequencing platforms (Dai et al., 2010). With these the overall quality of the sequencing can be assessed, in particular the sequence quality, GC content, N content, and overrepresented sequences. While there are no universal cutoffs for some of these tests, as the values vary based on the organisms and the sequencing setups, similar results should be obtained throughout the same kind of datasets both for “failed” k-mer and duplication tests.

When analyzing sRNA datasets, a test that will most likely fail is the adapter content test: given that the fragments sequenced (usually 18–35 nt) are often shorter than the read length (36 bp), the machine is bound to read into the adapter. There are number of software programs designed to do the necessary trimming, such as Cutadapt or FASTX-Toolkit (Martin, 2011). At this point of the analysis, low quality reads/bases should be removed, as well as adapters and PCR artifacts. The workflow proposed,



summarized in **Figure 1**, can be used to identify the sRNAs originating from either the host or the microbe by assigning the “sRNA source” organism and the “sRNA target” organism at the beginning of the analysis. Afterward, the same pipeline can be applied with the roles inverted to obtain information about both sides of the bidirectional cross-kingdom communication.

Trimmed reads can now be mapped with short read un-gapped mappers such as Bowtie (Langmead, 2010) and SOAP (Li et al., 2008) to reference genomes and transcriptomes; by this way one gains information on the origin of the potential *ck*-sRNA and its localization in the respective genome. Given that it is crucial to find the sRNAs from the source organism that target the interacting organism, this alignment step includes the removal of reads that align to both organisms. In particular, sRNAs are kept only if (i) they align 100% of the full read length to the source organism’s genome (bowtie settings: -v0 -al), and (ii) have at least two mismatches to the target organism’s genome or transcriptome (bowtie settings: -v1 -un). As an additional step,

the removal of sequences aligning 100% to the source organism’s transcriptome can be done in order to select exclusively sRNAs originating from non-coding regions (bowtie settings: -v0 -un), removing short sequences derived from mRNA degradation. After the alignments, sRNAs can be additionally filtered based on their presence in the sample of the pure source organism as they are expected to be either upregulated in the sample from the interacting organisms compared to the control (pure organism), or present exclusively in that sample (Weiberg et al., 2013).

## ***ck*-sRNA Target Detection and Evaluation**

The remaining sequences can be further analyzed for target prediction. There are various software platforms available for small interfering RNA (siRNA) and microRNA (miRNA) detection, originally tailored for mammal sRNAs. While these

can be customized for plant and microbe studies, two well established tools are designed specifically for plants: psRNATarget and TAPIR (Bonnet et al., 2010; Dai and Zhao, 2011b). Both are comparable regarding sRNA identification rates at their default settings and are widely used in plant miRNA analysis and discovery research, making them the best options for this analysis. While TAPIR offers a standalone and an online version, psRNATarget is only available online, making it less convenient for automatized workflows. On the other hand, psRNATarget provides more options for customizing settings and parameters of the prediction, making it more adaptable to different organisms and systems. Both programs work by aligning sRNA sequences to the target transcriptome and assigning penalties for mismatches, gaps, and G:U pairs, in particular in the seed region (between positions 2 and 12 of the sRNA for TAPIR and 2–13 for psRNATarget), which is critical for target recognition. The resulting score is between 0 and 5, and can be decreased from the default value to further reduce the risk of false positives. Additionally, TAPIR separately scores the free energy ratio, represented by the free energy of the predicted sRNA:target duplex divided by the free energy of the corresponding duplex having a perfect complementarity (Bonnet et al., 2010). In this case, the minimal value cutoff suggested is 0.7 (range between 0 and 1). The default output of both programs is a table containing all scores of the sRNA:mRNA duplexes, the alignment itself and, if available, a description of the target mRNA.

## Analysis of Target Transcript Expression

The first validation step of candidate *ck*-sRNAs is the confirmation of target gene downregulation in the colonized tissue as a result of the cleavage of the corresponding mRNA by the RISC enzymatic complex. Plant and microbial mRNA levels can be checked by mRNA sequencing analysis from the same biological samples the sRNA was obtained from. Since the library preparation for sRNA libraries is based on size separation and excision of a specific nt length interval, the longer RNA fraction from the same samples can be used to prepare mRNA libraries. Read length and sequencing depth selected can vary depending on the experimental design and resources available, but the mRNA sequences are primarily obtained from the large RNA fraction after polyA affinity selection, as more than 90% of total RNA is comprised of ribosomal RNA (rRNA) (Conesa et al., 2016). In bacterial samples or in samples with low RNA integrity number (RIN) values, where polyA selection would not be effective, rRNA depletion can be done instead. The bioinformatic pipeline described in the following paragraph will serve as a primary *in silico* validation step toward confirmation of candidate *ck*-sRNA activity in the target organism.

Since there is a multitude of RNAseq tools available, the experimental design and the availability of published sequence data are the main factors in deciding on a pipeline (Conesa et al., 2016). Quality check and trimming of sequencing artifacts are necessary steps at the beginning of the analysis, following the similar principle as in sRNA analysis, namely the use of FastQC (Andrews, 2010) and cutadapt (Martin, 2011). If reference sequences for the organisms involved are available, the

mapping of RNAseq reads can be done as a straight forward strategy (see below). Depending on available -omics data for the organisms in question, mapping of reads can be done to the reference genome or transcriptome. Without available reference sequences, *de novo* assembly (reference-free) of the transcriptome can be computed from all RNAseq datasets, usually with a De Bruijn graph-based assembler like Trinity (Grabherr et al., 2011), SOAPdenovo-Trans (Xie et al., 2014), Oases (Schulz et al., 2012), or Trans-AbySS (Robertson et al., 2010). Functional annotation and ortholog search can then be performed with common platforms such as BLAST (Altschul et al., 1990) and ENSEMBL (Zerbino et al., 2018) or, specifically developed but harder to install, transcriptome annotation tools like Trinotate (github<sup>1</sup>) and FunctionAnnotator (Chen et al., 2017). Transcriptome completeness can be checked with Busco (Simão et al., 2015). These tools can also be used in case of unsatisfactory annotation of available reference genome or transcriptome.

Spliced alignment to the reference genome is done by mappers that take into account the introns in the genome. TopHat/TopHat2 (Trapnell et al., 2009; Kim et al., 2013) are gapped mappers developed to detect novel splice-sites. They were superseded by a new mapper called HISAT2 (Kim et al., 2015) that is more accurate and much more efficient. Another option is Spliced Transcripts Alignment to a Reference (STAR), which also allows for fast and precise mapping with known and novel splice-sites (Dobin et al., 2013). Correction for exon sizes specific to the respective plant and microbe organism in question are needed, since typically the programs use default settings for the human genome. Un-gapped mappers, such as Bowtie (Langmead, 2010), can be used to map against a reference transcriptome if no novel transcript discovery is needed. However, since the goal of the analysis is to discover a high number of transcripts, including those with a low level of expression, and since organisms in question often are not sufficiently annotated, the gapped mapping on a genome followed by quality control is the recommended strategy. The quality of the mapping can be checked by programs such as Picard (Picard tools<sup>2</sup>, github), RseQC (Wang et al., 2012), and Qualimap (García-Alcalde et al., 2012). Percentage of mapped reads, multi-mapping reads (mapping to the several identical regions), and the uniformity of read coverage are relevant parameters to assess sequencing quality at this point (Conesa et al., 2016).

The first step for differential gene expression (DGE) is determining transcript abundances using program packages like Cufflinks (Trapnell et al., 2010) or htseq-count (Anders et al., 2015). DGE analysis can be done by a variety of programs, including DeSeq (Anders and Huber, 2010), Deseq2 (Love et al., 2014), edgeR (Robinson et al., 2010), and voom (Law et al., 2014). Low replicate numbers of transcripts and outliers among the replicates can complicate the DGE analysis. Thus, a powerful analytical method proves crucial to determine when the fold change in transcripts between the control and treated sample is different. The programs differ in statistical distributions they use for analysis of data and how they treat the variability among the

<sup>1</sup><http://trinotate.github.io/>

<sup>2</sup><http://broadinstitute.github.io/picard>

replications, but a comparison study claims DeSeq2 and edgeR have an advantage when it comes to smaller number of replicates (below 12) (Schurch et al., 2016).

The results of this target prediction and analysis pipeline can be visualized at several levels and by a variety of programs, some of which focus on sRNA-mRNA duplex conformation structure and others on a broader representation of cross-kingdom effects between genomes. ReadXplorer (Hilker et al., 2014) and Integrative Genomics Viewer (IGV) (Thorvaldsdóttir et al., 2013) are used for different types of presentation of sequencing data, and in this case specifically for visualization of mapped reads on the reference genome. miRPlant (An et al., 2014), a tool for prediction of miRNAs from NGS data, provides the visual presentation of the predicted miRNA in the precursor hairpin structure and with the indication of where the mature fragment is. Cummerbund (Goff et al., 2013) is commonly used after the Cufflinks package for visualization of differentially expressed genes in different types of plots. The software package Circos (Krzywinski et al., 2009) is a good choice for circular visualization of entire genomes, transcriptomes, sRNA candidates, and the range of silencing downregulation effects.

## Further Validation of *ck*-RNAs

Having obtained information on differentially expressed genes in the treated sample, the ones which are significantly downregulated and predicted as targets of candidate *ck*-sRNAs are investigated further. Alternative to mRNA sequencing, validation of *ck*-sRNA candidates requires confirmation of downregulation of their putative target by qRT-PCR.

Additional *in vivo* validation of the interaction of *ck*-sRNA candidates with their targets can be based on genetic analysis, e.g., mutational knockdown (KO) strategies of target genes and/or precursor loci of candidate *ck*-sRNAs. Finally, we suggest that the following additional analyzes are required to unequivocally claim a *ck*-RNA-mediated target interaction in *ck*-RNAi: (i) verification of sRNA-target interaction in transient expression systems such as leaves of *Nicotiana benthamiana*; (ii) testing respective AGO and DCL mutants for a loss of *ck*-RNA function in RNAi-mediated target downregulation; and (iii) detection of direct association of *ck*-RNAs or their target mRNA with

the respective microbial or plant AGO1 protein by immunoprecipitation techniques (Jain et al., 2011; Riley et al., 2012; Carbonell, 2017).

## CONCLUSION

RNAi-based bidirectional communication between interacting organisms, also called *ck*-RNAi, has been detected in a few natural plant – microbe systems, but the implications of a novel effector class of sRNA are significant. So far, there is no evidence that the activity of such RNA effectors would be restricted to certain microbial life styles as they were identified in plants interacting with both biotrophic and necrotrophic microbes. The recent finding that mammals also generate RNA effectors to combat parasites suggests that the phenomenon is widespread and prevalent in different types of host–parasite interaction. Besides the exciting discovering of a novel chemical communication strategy, the knowledge on *ck*-RNAs opens new avenues in sustainable and environmentally safe plant protection as sRNAs and their cellular precursors dsRNAs are natural molecules with an anti-microbial activity. However, the detection and validation of RNA-based communication and *ck*-RNAi still relies on the available data about model species and a narrow range of investigated systems. The present review tries to give a practical outline of a pipeline for *ck*-RNA detection focused on plant – microbe systems. A bioinformatics pipeline used to strengthen and accelerate the experimental approaches is of paramount importance for confirmation of sRNA communication between plants and microbes in a multitude of relevant systems.

## AUTHOR CONTRIBUTIONS

SZ, K-HK, EŠ, and LJ wrote the text. SZ and EŠ designed the figure.

## FUNDING

This work was supported by Deutsche Forschungsgemeinschaft to K-HK (project GRK2355) and by the European Union in the Marie Skłodowska-Curie actions “CerealPATH” to K-HK and SZ.

## REFERENCES

- Altschul, S. F., Gish, W., Miller, W., Myers, E. W., and Lipman, D. J. (1990). Basic local alignment search tool. *J. Mol. Biol.* 215, 403–410 doi: 10.1016/S0022-2836(05)80360-2
- An, J., Lai, J., Sajjanhar, A., Lehman, M. L., and Nelson, C. C. (2014). miRPlant: an integrated tool for identification of plant miRNA from RNA sequencing data. *BMC Bioinformatics* 15:275 doi: 10.1186/1471-2105-15-275
- Anders, S., and Huber, W. (2010). Differential expression analysis for sequence count data. *Genome Biol.* 11:R106 doi: 10.1186/gb-2010-11-10-r106
- Anders, S., Pyl, P. T., and Huber, W. (2015). HTSeq—a Python framework to work with high-throughput sequencing data. *Bioinformatics* 31, 166–169 doi: 10.1093/bioinformatics/btu638
- Andrews, S. (2010). *FastQC: A Quality Control Tool for High Throughput Sequence Data*. Available at: <http://www.bioinformatics.babraham.ac.uk/projects/fastqc>
- Bonnet, E., He, Y., Billiau, K., and Van de Peer, Y. (2010). TAPIR, a web server for the prediction of plant microRNA targets, including target mimics. *Bioinformatics* 26, 1566–1568 doi: 10.1093/bioinformatics/btq233
- Borges, F., and Martienssen, R. A. (2015). The expanding world of small RNAs in plants. *Nat. Rev. Mol. Cell Biol.* 16, 727–741. doi: 10.1038/nrm4085
- Cai, Q., He, B., Kogel, K. H., and Jin, H. (2018). Cross-kingdom RNA trafficking and environmental RNAi — nature's blueprint for modern crop protection strategies. *Curr. Opin. Microbiol.* 46, 58–64 doi: 10.1016/j.mib.2018.02.003
- Carbonell, A. (2017). Immunoprecipitation and high-throughput sequencing of ARGONAUTE-bound target RNAs from plants. *Methods Mol. Biol.* 1640, 93–112. doi: 10.1007/978-1-4939-7165-7\_6

- Chen, T. W., Gan, R. C., Fang, Y. K., Chien, K. Y., Liao, W. C., Chen, C. C., et al. (2017). Functionannotator, a versatile and efficient web tool for non-model organism annotation. *Sci. Rep.* 7:10430. doi: 10.1038/s41598-017-10952-4
- Conesa, A., Madrigal, P., Tarazona, S., Gomez-Cabrero, D., Cervera, A., McPherson, A., et al. (2016). A survey of best practices for RNA-seq data analysis. *Genome Biol.* 17:13 doi: 10.1186/s13059-016-0881-8
- Dai, M., Thompson, R. C., Maher, C., Contreras-Galindo, R., Kaplan, M. H., Markovitz, D. M., et al. (2010). NGSQC: cross-platform quality analysis pipeline for deep sequencing data. *BMC Genomics* 11(Suppl. 4):S7. doi: 10.1186/1471-2164-11-S4-S7
- Dai, X., and Zhao, P. X. (2011b). psRNATarget: a plant small RNA target analysis server. *Nucleic Acids Res.* 39 (suppl. 2), W155–W159. doi: 10.1093/nar/gkr319
- Dai, X., Zhuang, Z., and Zhao, P. X. (2011a). Computational analysis of miRNA targets in plants: current status and challenges. *Brief. Bioinform.* 12, 115–121. doi: 10.1093/bib/bbq065
- Dobin, A., Davis, C. A., Schlesinger, F., Drenkow, J., Zaleski, C., and Jha, S. et al. (2013). STAR: ultrafast universal RNA-seq aligner. *Bioinformatics* 29, 15–21. doi: 10.1093/bioinformatics/bts635
- Fire, A., Xu, S., Montgomery, M. K., Kostas, S. A., Driver, S. E., and Mello, C. C. (1998). Potent and specific genetic interference by double-stranded RNA in *Caenorhabditis elegans*. *Nature* 391, 806–811. doi: 10.1038/35888
- García-Alcalde, F., Okonechnikov, K., Carbonell, J., Cruz, L. M., Götz, S., Tarazona, S., et al. (2012). Qualimap: evaluating next-generation sequencing alignment data. *Bioinformatics* 28, 2678–2679. doi: 10.1093/bioinformatics/bts503
- Goff, L., Trapnell, C., and Kelley, D. (2013). *Cummerbund: Analysis, Exploration, Manipulation, and Visualization of Cufflinks High-Throughput Sequencing Data. R Package Version 2.20.0*
- Grabherr, M. G., Haas, B. J., Yassour, M., Levin, J. Z., Thompson, D. A., Amit, I., et al. (2011). Full-length transcriptome assembly from RNA-seq data without a reference genome. *Nat. Biotechnol.* 29, 644–652. doi: 10.1038/nbt.1883
- Hamilton, A. J., and Baulcombe, D. C. (1999). A species of small antisense RNA in posttranscriptional gene silencing in plants. *Science* 286, 950–952. doi: 10.1126/science.286.5441.950
- Hilker, R., Stadermann, K. B., Doppmeier, D., Kalinowski, J., Stoye, J., Straube, J., et al. (2014). Readexplorer—visualization and analysis of mapped sequences. *Bioinformatics* 30, 2247–2254. doi: 10.1093/bioinformatics/btu205
- Jain, R., Devine, T., George, A. D., Chittur, S. V., Baroni, T. E., Penalva, L. O., et al. (2011). RIP-chip analysis: RNA-binding protein immunoprecipitation-microarray (ChIP) profiling. *Methods Mol. Biol.* 703, 247–263. doi: 10.1007/978-1-59745-248-9\_17
- Kim, D., Langmead, B., and Salzberg, S. L. (2015). HISAT: a fast spliced aligner with low memory requirements. *Nat. Methods* 12, 357–360. doi: 10.1038/nmeth.3317
- Kim, D., Pertea, G., Trapnell, C., Pimentel, H., Kelley, R., and Salzberg, S. L. (2013). TopHat2: accurate alignment of transcriptomes in the presence of insertions, deletions and gene fusions. *Genome Biol.* 14:R36. doi: 10.1186/gb-2013-14-4-r36
- Koch, A., Biedenkopf, D., Furch, A., Weber, L., Rossbach, O., Abdellatif, E., et al. (2016). An RNAi-based control of *Fusarium graminearum* infections through spraying of long dsRNAs involves a plant passage and is controlled by the fungal silencing machinery. *PLoS Pathog.* 12:e1005901. doi: 10.1371/journal.ppat.1005901
- Koch, A., and Kogel, K. H. (2014). New wind in the sails: improving the agronomic value of crop plants through RNAi-mediated gene silencing. *Plant Biotechnol. J.* 12, 821–831.
- Koch, A., Kumar, N., Weber, L., Keller, H., Imani, J., and Kogel, K. H. (2013). Host-induced gene silencing of cytochrome P450 lanosterol C14- $\alpha$ -demethylase-encoding genes confers strong resistance to *Fusarium* species. *Proc. Natl. Acad. Sci. U. S. A.* 110, 19324–19329. doi: 10.1073/pnas.1306373110
- Krzywinski, M., Schein, J., Birol, I., Connors, J., Gascoyne, R., Horsman, D., et al. (2009). Circos: an information aesthetic for comparative genomics. *Genome Res.* 19, 1639–1645. doi: 10.1101/gr.092759.109
- Langmead, B. (2010). Aligning short sequencing reads with bowtie. *Curr. Protoc. Bioinformatics* 32, 11.7.1–11.7.14. doi: 10.1002/0471250953.bib1107s32
- Law, C. W., Chen, Y., Shi, W., and Smyth, G. K. (2014). voom: precision weights unlock linear model analysis tools for RNA-seq read counts. *Genome Biol.* 15:R29 doi: 10.1186/gb-2014-15-2-r29
- Li, H., Ruan, J., and Durbin, R. (2008). Mapping short DNA sequencing reads and calling variants using mapping quality scores. *Genome Res.* 18, 1851–1858. doi: 10.1101/gr.078212.108
- Li, P., Piao, Y., Shon, H. S., and Ryu, K. H. (2015). Comparing the normalization methods for the differential analysis of Illumina high-throughput RNA-Seq data. *BMC Bioinformatics* 16:347 doi: 10.1186/s12859-015-0778-7
- Love, M. I., Huber, W., and Anders, S. (2014). Moderated estimation of fold change and dispersion for RNA-seq data with DESeq2. *Genome Biol.* 15:550. doi: 10.1186/s13059-014-0550-8
- Martin, M. (2011). Cutadapt removes adapter sequences from high-throughput sequencing reads. *EMBnet J.* 17, 10–12. doi: 10.14806/embnet.17.1.200
- Niehl, A., Soininen, M., Poranen, M. M., and Heinlein, M. (2018). Synthetic biology approach for plant protection using dsRNA. *Plant Biotechnol. J.* doi: 10.1111/pbi.12904 [Epub ahead of print].
- Riley, K. J., Yario, T. A., and Steitz, J. A. (2012). Association of argonaute proteins and microRNAs can occur after cell lysis. *RNA* 18, 1581–1585. doi: 10.1261/rna.034934.112
- Robertson, G., Schein, J., and Chiu, R. (2010). De novo assembly and analysis of RNA-seq data. *Nat. Methods* 7, 909–912. doi: 10.1038/nmeth.1517
- Robinson, M. D., McCarthy, D. J., and Smyth, G. K. (2010). edgeR: a bioconductor package for differential expression analysis of digital gene expression data. *Bioinformatics* 26, 139–140. doi: 10.1093/bioinformatics/btp616
- Schulz, M. H., Zerbino, D. R., Vingron, M., and Birney, E. (2012). Oases: robust de novo RNA-seq assembly across the dynamic range of expression levels. *Bioinformatics* 28, 1086–1092. doi: 10.1093/bioinformatics/bts094
- Schurich, N. J., Schofield, P., Gierliński, M., Cole, C., Shernstnev, A., Singh, V., et al. (2016). How many biological replicates are needed in an RNA-seq experiment and which differential expression tool should you use? *RNA* 22, 839–851.
- Simão, F. A., Waterhouse, R. M., Ioannidis, P., Kriventseva, E. V., and Zdobnov, E. M. (2015). BUSCO: assessing genome assembly and annotation completeness with single-copy orthologs. *Bioinformatics* 31, 3210–3212. doi: 10.1093/bioinformatics/btv351
- Srivastava, P. K., Moturu, T. R., Pandey, P., Baldwin, I. T., and Pandey, S. P. (2014). A comparison of performance of plant miRNA target prediction tools and the characterization of features for genome-wide target prediction. *BMC Genomics* 15:348. doi: 10.1186/1471-2164-15-348
- Thorvaldsdóttir, H., Robinson, J. T., and Mesirov, J. P. (2013). Integrative Genomics Viewer (IGV): high-performance genomics data visualization and exploration. *Brief. Bioinform.* 14, 178–192. doi: 10.1093/bib/bbs017
- Trapnell, C., Pachter, L., and Salzberg, S. L. (2009). TopHat: discovering splice junctions with RNA-Seq. *Bioinformatics* 25, 1105–1111. doi: 10.1093/bioinformatics/btp120
- Trapnell, C., Williams, B. A., Pertea, G., Mortazavi, A., Kwan, G., van Baren, M. J., et al. (2010). transcript assembly and quantification by RNA-Seq reveals unannotated transcripts and isoform switching during cell differentiation. *Nat. Biotechnol.* 28, 511–515. doi: 10.1038/nbt.1621
- Wang, L., Wang, S., and Li, W. (2012). RSeQC: quality control of RNA-seq experiments. *Bioinformatics* 28, 2184–2185. doi: 10.1093/bioinformatics/bts356
- Wang, M., Weiberg, A., Dellota, E. Jr., Yamane, D., and Jin, H. (2017). Botrytis small RNA Bc-siR37 suppresses plant defense genes by cross-kingdom RNAi. *RNA Biol.* 14, 421–428. doi: 10.1080/15476286.2017.1291112
- Wang, B., Sun, Y. F., Song, N., Zhao, M. X., Liu, R., Feng, H., et al. (2017). *Puccinia striiformis* f. sp. *tritici* microRNA-like RNA 1 (Pst-miR1), an important pathogenicity factor of Pst, impairs wheat resistance to Pst by suppressing the wheat pathogenesis-related 2 gene. *New Phytol.* 215, 338–350. doi: 10.1111/nph.14577
- Wang, M., Weiberg, A., Lin, F. M., Thomma, B. P., Huang, H. D., and Jin, H. (2016). Bidirectional cross-kingdom RNAi and fungal uptake of external RNAs confer plant protection. *Nat. Plants* 2:16151. doi: 10.1038/nplants.2016.151
- Weiberg, A., Wang, M., Lin, F. M., Zhao, H., Zhang, Z., Kaloshian, I., et al. (2013). Fungal small RNAs suppress plant immunity by hijacking host RNA interference pathways. *Science* 342, 118–123. doi: 10.1126/science.1239705

- Xie, Y., Wu, G., Tang, J., Luo, R., Patterson, J., Liu, S., et al. (2014). SOAPdenovo-trans: de novo transcriptome assembly with short RNA-Seq reads. *Bioinformatics* 30, 1660–1666. doi: 10.1093/bioinformatics/btu077
- Zerbino, D. R., Achuthan, P., Akanni, W., Amode, M. R., Barrell, D., Bhai, J., et al. (2018). Ensembl. *Nucleic Acids Res.* 46, D754–D761. doi: 10.1093/nar/gkx1098
- Zhang, T., Zhao, Y. L., Zhao, J. H., Wang, S., Jin, Y., Chen, Z. Q., et al. (2016). Cotton plants export microRNAs to inhibit virulence gene expression in a fungal pathogen. *Nat. Plants* 2:16153. doi: 10.1038/nplants.2016.153

**Conflict of Interest Statement:** The authors declare that the research was conducted in the absence of any commercial or financial relationships that could be construed as a potential conflict of interest.

Copyright © 2018 Zanini, Šečić, Jelonek and Kogel. This is an open-access article distributed under the terms of the Creative Commons Attribution License (CC BY). The use, distribution or reproduction in other forums is permitted, provided the original author(s) and the copyright owner(s) are credited and that the original publication in this journal is cited, in accordance with accepted academic practice. No use, distribution or reproduction is permitted which does not comply with these terms.



# Further Elucidation of the Argonaute and Dicer Protein Families in the Model Grass Species *Brachypodium distachyon*

Ena Šečić, Silvia Zanini and Karl-Heinz Kogel\*

Institute of Phytopathology, Centre for BioSystems, Land Use and Nutrition, Justus Liebig University, Giessen, Germany

## OPEN ACCESS

### Edited by:

Hailing Jin,  
University of California,  
United States

### Reviewed by:

Zhaoqing Chu,  
Shanghai Chenshan Plant Science  
Research Center (CAS), China

Ling Li,  
Mississippi State University,  
United States

### \*Correspondence:

Karl-Heinz Kogel  
Karl-Heinz.Kogel@agrar.uni-giessen.de

### Specialty section:

This article was submitted to  
Plant Microbe Interactions,  
a section of the journal  
Frontiers in Plant Science

**Received:** 13 April 2019

**Accepted:** 25 September 2019

**Published:** 22 October 2019

### Citation:

Šečić E, Zanini S and Kogel K-H  
(2019) Further Elucidation of the  
Argonaute and Dicer Protein  
Families in the Model Grass Species  
*Brachypodium distachyon*.  
Front. Plant Sci. 10:1332.  
doi: 10.3389/fpls.2019.01332

RNA interference (RNAi) is a biological process in which small RNAs regulate gene silencing at the transcriptional or posttranscriptional level. The trigger for gene silencing is double-stranded RNA generated from an endogenous genomic locus or a foreign source, such as a transgene or virus. In addition to regulating endogenous gene expression, RNAi provides the mechanistic basis for small RNA-mediated communication between plant hosts and interacting pathogenic microbes, known as cross-kingdom RNAi. Two core protein components, Argonaute (AGO) and Dicer (DCL), are central to the RNAi machinery of eukaryotes. Plants encode for several copies of AGO and DCL genes; in *Arabidopsis thaliana*, the AGO protein family contains 10 members, and the DCL family contains four. Little is known about the conservation and specific roles of these proteins in monocotyledonous plants, which account for the most important food staples. Here, we utilized *in silico* tools to investigate the structure and related functions of AGO and DCL proteins from the model grass *Brachypodium distachyon*. Based on the presence of characteristic domains, 16 BdAGO- and 6 BdDCL-predicted proteins were identified. Phylogenetic analysis showed that both protein families were expanded in *Brachypodium* as compared with *Arabidopsis*. For BdDCL proteins, both plant species contain a single copy of DCL1 and DCL4; however, *Brachypodium* contains two copies each of DCL2 and DCL3. Members of the BdAGO family were placed in all three functional clades of AGO proteins previously described in *Arabidopsis*. The greatest expansion occurred in the AtAGO1/5/10 clade, which contains nine BdAGOs (BdAGO5/6/7/9/10/11/12/15/16). The catalytic tetrad of the AGO P-element-induced wimpy testis domain (PIWI), which is required for endonuclease activity, is conserved in most BdAGOs, with the exception of BdAGO1, which lacks the last D/H residue. Three-dimensional modeling of BdAGO proteins using tertiary structure prediction software supported the phylogenetic classification. We also predicted a provisional interactome network for BdAGOs, their localization within the cell, and organ/tissue-specific expression. Exploring the specifics of RNAi machinery proteins in a model grass species can serve as a proxy for agronomically important cereals such as barley and wheat, where the development of RNAi-based plant protection strategies is of great interest.

**Keywords:** protein, structure, prediction, RNAi, Argonaute, Dicer, *Brachypodium*

## INTRODUCTION

RNA interference (RNAi) is a regulatory mechanism utilized by most eukaryotes for endogenous gene silencing and protection against mobile repetitive sequences, transposons, and viruses (Fire et al., 1998; Wilson and Doudna, 2013). In contrast to transcriptional gene silencing (TGS), which results in the methylation of DNA and/or histones, posttranscriptional gene silencing (PTGS) operates by transcript degradation or translation inhibition. Selection of the target for silencing is governed by sequence complementarity between a single-stranded small RNA (sRNA) and the target RNA. Beyond its native role, the RNAi machinery has been exploited for developing novel plant protection strategies based on double-stranded (ds)RNA applications. Delivery of artificial dsRNA through transgene expression [host-induced gene silencing (HIGS)] or exogenous application [spray-induced gene silencing (SIGS)] was proven effective against fungal pathogens (Nowara et al., 2010; Koch et al., 2013; Koch et al., 2016; Wang et al., 2016), nematodes (Dutta et al., 2015), insects (Coleman et al., 2014; Abdellatif et al., 2015; Head et al., 2017), and parasitic plants (Tomilov et al., 2008; for review, see Andrade and Hunter, 2016; Cai et al., 2018). A recent discovery revealed that RNAi also is involved in natural cross-kingdom RNA communication (ckRNAi), where sRNA molecules function as mediators that are exchanged bidirectionally between a host plant and a microbial pathogen to silence their target transcripts and impact the outcome of the plant–pathogen interaction (Weiberg et al., 2013; Zhang et al., 2016; Wang et al., 2017a; Wang et al., 2017b).

Regardless of which RNAi-based process or application is involved, evolutionarily conserved protein components, including Dicer [termed Dicer-like (DCL) in plants] and Argonaute (AGO), play key roles in dsRNA processing. Dicers and DCLs are RNase III endonucleases that process exogenously supplied or endogenously generated ds- or hairpin (hp)-containing RNA precursors into various species of dsRNAs, commonly 21–24 nucleotides (nt) in length. These sRNAs are then loaded onto specific AGO proteins, which are components of the RNA-induced silencing complex (RISC). The loaded sRNA is processed into a single-stranded sRNA molecule, which then guides the RISC to complementary targets in the cytoplasm or nucleus. Depending on the biological context, target recognition leads to PTGS *via* RNA degradation, which may be mediated by the AGO protein's slicer activity, or inhibition of translation, or to TGS *via* genomic DNA and/or histone methylation (Carthew and Sontheimer, 2009; Poulsen et al., 2013; Borges and Martienssen, 2015; Fang and Qi, 2016).

Phylogenetic analysis of genes belonging to the Dicer family suggests that they arose early in the evolution of eukaryotes and that their duplication and diversification correlated with the development of multicellularity and the need for complex gene regulation (Mukherjee et al., 2013). In plants, the structure and function of DCL proteins have been investigated most intensively in *Arabidopsis*, which expresses four DCLs (Schauer et al., 2002). The domain architecture of these proteins, like that of other eukaryotic Dicers, generally consists of an amino-terminal DEXDc and helicase-C (HELICc) domain, which are thought

to mediate processive movement along a dsRNA, a dicer-dimer (heterodimerization) domain that facilitates binding with protein partners (Qin et al., 2010), a P-element-induced wimpy testis (PIWI)–Argonaute–Zwille (PAZ) domain, which binds the 3' end of the dsRNA, two RIBOc (ribonuclease III family) domains and at least one dsRNA-binding motif (DSRM) domain at the C terminus (Schauer et al., 2002; Mukherjee et al., 2013; Bologna and Voinnet, 2014; Song and Rossi, 2017).

Analyses of *Arabidopsis* mutants revealed that the four DCLs generate different types of sRNAs, although some functional redundancy was observed (Gascioli et al., 2005; Bologna and Voinnet, 2014; Borges and Martienssen, 2015). AtDCL1 produces microRNAs (miRNAs), a class of sRNAs that regulates endogenous gene expression via PTGS (Bartel, 2004). The remaining AtDCLs generate various subclasses of small interfering RNAs (siRNAs), including i) natural-antisense-transcript (nat)-siRNAs generated by AtDCL2 (Borsani et al., 2005), ii) trans-activating (ta)-siRNAs produced by AtDCL4 (Dunoyer et al., 2005), and iii) TGS-related 24-nt siRNAs generated by AtDCL3, which are responsible for silencing transposons and other repeated DNA sequences (Xie et al., 2004).

Despite the diversity of sRNAs, their association with AGO proteins and the RISC complex is a common feature. AGO proteins were named after the tube-shaped leaves of *Arabidopsis ago1* mutants, which resemble the tentacles of the pelagic octopus, *Argonauta argo* (Bohmert et al., 1998). AGO proteins are highly conserved in nature, although the size of this family varies substantially between species (Höck and Meister, 2008; Zhang et al., 2015; Fang and Qi, 2016; You et al., 2017).

AGOs have a high level of structure and domain conservation between the prokaryotic and eukaryotic variants, even when the biological function clearly differs (Willkomm et al., 2015). Several prokaryotic (Wang et al., 2009; Liu et al., 2018) and eukaryotic (Lingel et al., 2003; Lingel et al., 2004; Boland et al., 2011) complete AGO structures or individual domains have been crystallographically resolved. Several human AGO proteins have been crystallized, namely, AGO2 in complex with a miRNA (Elkayam et al., 2012), AGO1 (Faehnle et al., 2013), and AGO3 (Park et al., 2017), showing that the AGO activity is dependent on conservation of active site residues and their interaction with other protein regions. The structures of AtAGO proteins have been partly resolved, especially the middle (MID) domain of AtAGO1, AtAGO2, and AtAGO5 (Frank et al., 2012; Zha et al., 2012). Functional domains characteristic of all AGO proteins, including the *Arabidopsis* AGOs, are the PAZ, MID, and PIWI domains governing the binding of sRNA ends and the slicer activity (Höck and Meister, 2008; Frank et al., 2012).

In *Arabidopsis*, 10 different AGOs have been identified. Phylogenetic analyses have divided them into three clades, comprising AGO1/5/10, AGO2/3/7, and AGO4/6/8/9 (Vaucheret, 2008). The different clades contain AGOs that mediate PTGS or TGS after they load specific types of sRNAs, which are selected based on length and identity of the 5' nt (Bologna and Voinnet, 2014; Zhang et al., 2015; Fang and Qi, 2016). For example, AtAGO1 is involved in endogenous developmental regulation by miRNAs (Vaucheret et al., 2004), antiviral defense (alongside AtAGO2, Harvey et al., 2011), as well as bidirectional ckRNAi

(Weiberg et al., 2013). AtAGO4 and AtAGO6 are involved in DNA and histone methylation (Zilberman et al., 2003; Zheng et al., 2007). AtAGO9 is known to be involved in female gametogenesis (Olmedo-Monfil et al., 2010), while AtAGO10 competes with AtAGO1 for sRNA loading in regulation of shoot apical meristem development (Zhu et al., 2011). AtAGO7 plays a role in defense against viruses (Qu et al., 2008).

In comparison to *Arabidopsis*, little is known about the RNAi machinery components in monocots. The number of AGO proteins is expanded in cereals, as there are 17 AGOs in maize (*Zea mays*) and 19 in rice (*Oryza sativa*; Fang and Qi, 2016; Mirzaei et al., 2014; Patel et al., 2018). The copy number of DCL2 and/or DCL3 genes also differs between monocot species and *Arabidopsis*. Six predicted DCLs were identified in rice, while five were identified in maize, wheat, and barley (Margis et al., 2006). Furthermore, the DCL3b gene has diverged significantly from its DCL3a paralog (Margis et al., 2006) and, thus, is considered a distinct, monocot-specific class of Dicer, termed DCL5 (Fukudome and Fukuhara, 2017; Borges and Martienssen, 2015).

Cereals are major staple crops worldwide; however, a plethora of pathogens and pests threaten their production (Savary et al., 2012). Recent efforts to develop environmentally friendly plant protection strategies have demonstrated that HIGS and SIGS can be used in major cereal crops, such as barley and wheat, to control necrotrophic fungi (Koch et al., 2013; Koch et al., 2016; Koch et al., 2018) and aphid pests (Abdellatif et al., 2015). Developing a better understanding of the cereal AGO and DCL protein family members and their specific functions is a prerequisite for clarifying the mechanisms undergirding RNAi-mediated plant protection. Here, we use the model species for temperate grass plants, *Brachypodium distachyon* (*Brachypodium*), to investigate cereal AGO and DCL proteins. *Brachypodium* is self-fertile, has a small genome (~272 Mb), a short life cycle, and established transformation protocols (Vogel et al., 2006). The commonly used diploid inbred line Bd21 is fully sequenced (The International Brachypodium Initiative, 2010). In addition, literature data reveal strong responsiveness of *Brachypodium* sRNA pools to abiotic stress, suggesting that the RNAi machinery is sensitive to environmental changes (Wang et al., 2015).

Based on genomic database searches and *in silico* analysis, we identified six BdDCL proteins, as well as 16 previously reported AGO protein sequences in *Brachypodium* (Mirzaei et al., 2014). Since the structure of proteins closely relates to function and thus can serve as an indication of interaction patterns and redundancy in large protein families, we especially looked into domain structure conservation in *Brachypodium* relative to *Arabidopsis*. Similar to the protein structure and interactome analysis applied in Šečić et al. (2015), we subjected Bd AGO and DCL proteins to a series of *in silico* analysis steps. The focus of this study is the structures and related functions of the AGO-like and DCL proteins of *B. distachyon*, with special regard to analysis of the phylogeny and three-dimensional (3D) structure modeling of the AGO family, as compared with the more familiar *Arabidopsis thaliana* AGO protein family. Given that the At AGO1/5/10

clade contains proteins involved in ckRNAi, we were especially interested to define the BdAGO proteins that are structurally most related to this clade and thus potentially have a key function in plant immunity and RNAi-based plant protection.

## MATERIALS AND METHODS

### Acquisition of Sequences and Database Search

AGO and DCL protein sequences corresponding to the primary transcripts of specific genes were acquired by searching the Plant Comparative Genomics portal Phytozome 12 (Goodstein et al., 2012) *B. distachyon* v3.1 database (The International Brachypodium Initiative, 2010). Proteins whose domain architecture resembled those of *Arabidopsis* AGO and DCL proteins were considered. The *Arabidopsis* AGO and DCL protein sequences were taken from The *Arabidopsis* Information Resource database (Rhee et al., 2003; Berardini et al., 2015). Information on resolved protein structures was acquired from the Research Collaboratory for Structural Bioinformatics Protein Data Bank (Berman et al., 2000; Burley et al., 2018). The Brachypodium eFP Browser (Sibout et al., 2017; Winter et al., 2007) was used to assess the expression of transcripts corresponding to proteins involved in this study, based on the expression atlas detailing different organs and developmental stages.

### Phylogenetic Analysis, Interactome Analysis, and Localization

The phylogenetic analysis and tree rendering were done by the Phylogeny.fr web server (Dereeper et al., 2008; Dereeper et al., 2010). The operational sequence is composed of MUSCLE 3.8.31 (Edgar, 2004) for alignment with default settings, Gblocks 0.91b for removal of ambiguous regions (Castresana, 2000), PhyML 3.1/3.0 aLRT for phylogeny (Guindon and Gascuel, 2003; Anisimova and Gascuel, 2006), based on maximum likelihood, and TreeDyn 198.3 for graphical representation (Chevenet et al., 2006). Multiple sequence alignment (MSA) was done using Clustal Omega at European Molecular Biology Laboratory—European Bioinformatics Institute (Sievers et al., 2011; Goujon et al., 2010) and the conserved residues and domains visualized by the Mview multiple alignment viewer (Brown et al., 1998). Pairwise sequence alignments were done using EMBOSS Needle (Rice et al., 2000), utilizing the Needleman–Wunsch algorithm for global alignment. Domain search was conducted using Simple Modular Architecture Research Tool (SMART) in normal SMART mode (Schultz et al., 1998; Letunic and Bork, 2017) and visualized with the Illustrator for Biological Sequences (IBS) online illustrator (Liu et al., 2015). Prediction of protein location was done using the plant subcellular localization integrative predictor (PSI), which shows an integrative result based on the output of an 11-member predictor community (Liu et al., 2013). Prediction of the interactome was done using the STRING database of protein–protein associations, while searching by protein

sequence (Szkarczyk et al., 2019). Resulting associations/possible interactions that originate from text mining have been excluded, and the results show only associations supported by co-expression and/or experimental data.

## Three-Dimensional Structure Modeling and Validation

SWISS-MODEL, a homology-based modeling software available at the ExPASy web server (Waterhouse et al., 2018), and CPHmodels 3.2 protein homology modeling server (Nielsen et al., 2010) were both used for 3D structure prediction from the sequence data. BLAST (Camacho et al., 2009) and HHBlits (Remmert et al., 2011) template search through the SWISS-MODEL template library was done and the models built using ProMod3 (Waterhouse et al., 2018) and the target-template alignment.

QMEAN, used for validation of the predicted 3D structures, is a scoring function that considers single residues and the global model, delivering an estimation of absolute quality of the prediction (Benkert et al., 2011). In order to check the stereochemical quality of predicted structures, we used the PROCHECK program (Morris et al., 1992; Laskowski et al., 1993). One of the stereochemical parameters considered is the fitness of the model in a Ramachandran plot, which maps the allowed backbone dihedral angles of amino acids (aa) in a protein structure (Ramachandran et al., 1963). Further on, we used the WHATCHECK software (Hooft et al., 1996) to calculate the Ramachandran Z-score, which compares the quality of the query structure to structures with high confidence (Hooft et al., 1997). Lastly, we used the dDFIRE/DFIRE2 energy calculation (Yang and Zhou, 2008) to calculate free energy scores for our structure predictions.

PyMOL (The Py-MOL Molecular Graphics System) was used for visualization of the predicted structures (Schrödinger, 2010, Open-Source PyMOL 1.3).

## RESULTS

### Argonaute and Dicer Protein Families Are Expanded in *Brachypodium* Relative to *Arabidopsis*

To identify AGO and DCL proteins, the *B. distachyon* v3.1 database (The International Brachypodium Initiative, 2010) was searched for transcripts whose encoded proteins contain the characteristic domain architecture of each protein family. The accession numbers of the acquired sequences, the names assigned to the corresponding BdAGO proteins, the location of the encoding genes, and a description of the primary transcripts are shown in **Table 1**. The naming convention is similar to that used by Mirzaei et al. (2014) for 16 AGO proteins identified by primary transcripts in the *B. distachyon* Bd21 v3.1 annotation (The International Brachypodium Initiative, 2010). Our search for BdDCL candidates within the Bd21 v3.1 database revealed nine sequences. Clear lack of functional domains or insufficient length of the deduced aa sequence reduced the number of putative DCL genes to six (Bradi1g15440, Bradi1g77087, Bradi2g23187, Bradi5g15337, Bradi1g21030, and Bradi3g29287). Accession numbers and assigned names for the encoded BdDCLs are shown in **Table 2**. The putative AtAGO and AtDCL protein sequences were downloaded from The *Arabidopsis* Information Resource database (**Table S1**) and included in the MSA and phylogenetic analysis.

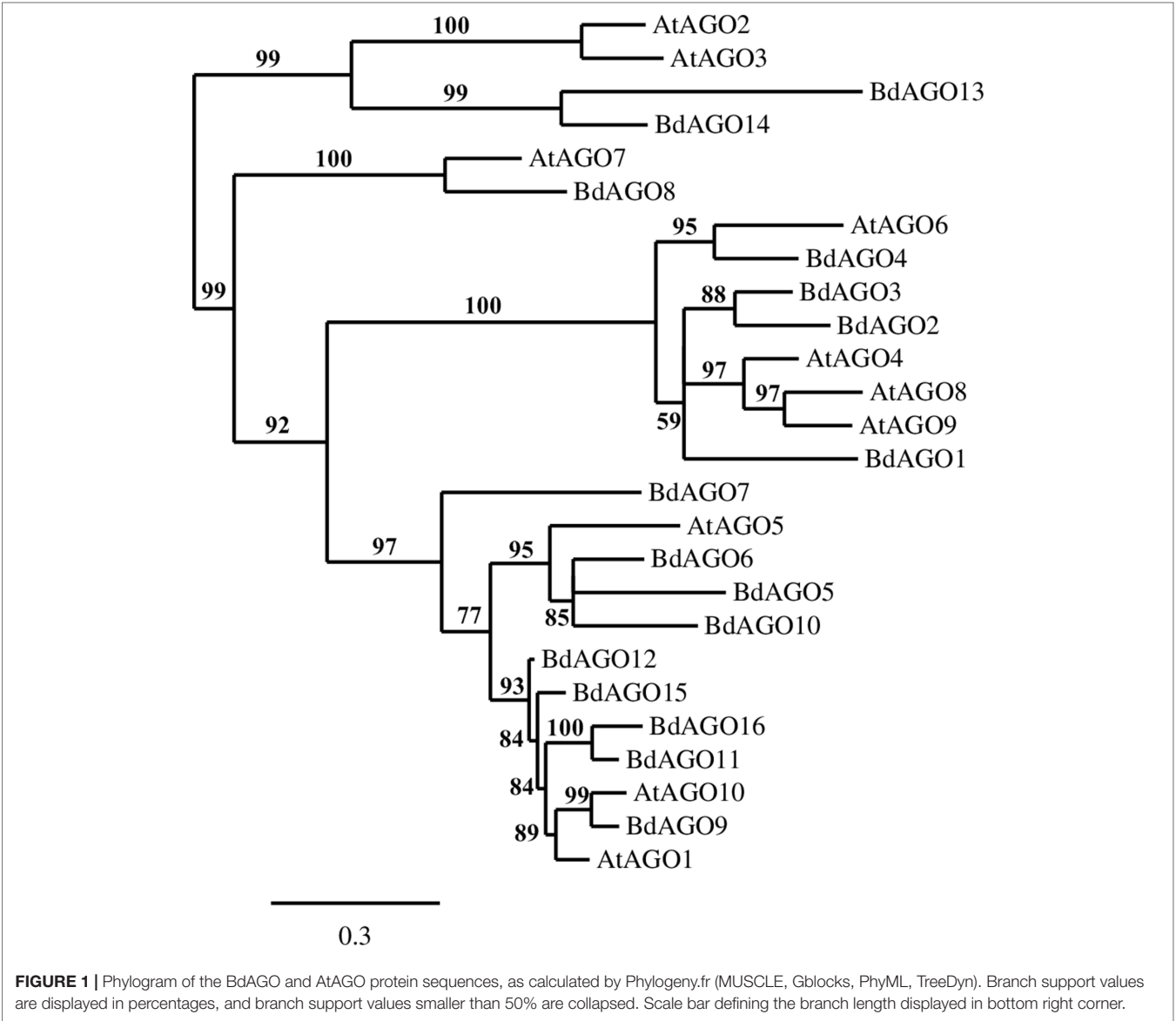
A phylogenetic analysis of the inferred BdAGO protein sequences relative to those of *Arabidopsis* AGOs is shown in **Figure 1**. BdAGO proteins were placed in all three AtAGO clades. Some were grouped with a specific AtAGO member within a clade (e.g., BdAGO8 was grouped with AtAGO7, and BdAGO5/6/7/10 were grouped with AtAGO5), whereas other BdAGOs were distributed throughout an entire clade (e.g., BdAGO1/2/3/4 within the AtAGO4/6/8/9 clade). In the AtAGO1/5/10 clade, BdAGO9/11/12/15/16 were interspersed

**TABLE 1** | Assigned names and accession numbers of BdAGO proteins as well as genomic location and description of the primary transcript (as acquired from Phytozome Bd21 v3.1 database).

Assigned name of protein	Primary transcript ID (Phytozome)	Location	Description (Phytozome)
BdAGO1	Bradi2g10360.2	Bd2:8611187.8615652 reverse	PTHR22891//PTHR22891:SF44 – Eukaryotic translation initiation factor 2C
BdAGO2	Bradi2g14147.1	Bd2:12806099.12812784 reverse	PTHR22891:SF20 – Protein AGO 4-related
BdAGO3	Bradi2g10370.1	Bd2:8620394.8628745 reverse	AGO family, subfamily AGO4
BdAGO4	Bradi4g08587.1	Bd4:7715921.7724879 reverse	PTHR22891:SF35 – Protein AGO 6
BdAGO5	Bradi1g12431.2	Bd1:9307067.9313002 forward	PTHR22891//PTHR22891:SF49 – Eukaryotic translation initiation factor 2C
BdAGO6	Bradi1g05162.2	Bd1:3447373.3455769 forward	PTHR22891//PTHR22891:SF24 – Eukaryotic translation initiation factor 2C
BdAGO7	Bradi1g28260.3	Bd1:23482384.23489131 reverse	AGO family, subfamily monocot-AGO1
BdAGO8	Bradi1g16060.3	Bd1:12986117.12991032 reverse	AGO family, subfamily AGO7
BdAGO9	Bradi1g36907.2	Bd1:32760045.32772130 reverse	PTHR22891//PTHR22891:SF25 – Eukaryotic translation initiation factor 2C
BdAGO10	Bradi1g54977.1	Bd1:53536162.53543236 forward	PTHR22891//PTHR22891:SF36 – Eukaryotic translation initiation factor 2C
BdAGO11	Bradi1g29577.1	Bd1:25162908.25171156 reverse	PTHR22891//PTHR22891:SF57 – Eukaryotic translation initiation factor 2C
BdAGO12	Bradi5g18540.1	Bd5:21720455.21728815 reverse	AGO family, subfamily AGO1
BdAGO13	Bradi5g21810.1	Bd5:24487261.24492250 forward	AGO family, subfamily AGO2/3
BdAGO14	Bradi5g21800.1	Bd5:24479944.24484383 forward	AGO family, subfamily AGO2/3
BdAGO15	Bradi3g51077.3	Bd3:51944662.51956527 forward	PTHR22891//PTHR22891:SF34 – Eukaryotic translation initiation factor 2C
BdAGO16	Bradi3g60697.5	Bd3:59325332.59333596 reverse	PTHR22891//PTHR22891:SF34 – Eukaryotic translation initiation factor 2C

**TABLE 2 |** Assigned names and accession numbers of BdDCL proteins as well as genomic location and description of the primary transcript (as acquired from Phytozome Bd21 v3.1 database).

Assigned name of protein	Primary transcript ID (Phytozome)	Location	Description (Phytozome)
BdDCL1	Bradi1g77087.1	Bd1:73701094.73713218 forward	PTHR14950:SF3 – ENDORIBONUCLEASE DICER HOMOLOG 1
BdDCL2a	Bradi1g15440.1	Bd1:12353426.12376799 forward	DCL family, subfamily DCL2
BdDCL2b	Bradi1g21030.3	Bd1:16934990.16948923 reverse	PTHR14950:SF19 - ENDORIBONUCLEASE DICER HOMOLOG 2
BdDCL3a	Bradi3g29287.1	Bd3:31008845.31020951 forward	PTHR14950//PTHR14950:SF31 - HELICASE-RELATED//SUBFAMILY NOT NAMED
BdDCL3b	Bradi2g23187.3	Bd2:20726122.20733365 reverse	PF00636//PF02170//PF03368 – Ribonuclease III domain (Ribonuclease_3)//PAZ domain (PAZ)//Dicer dimerization domain (Dicer_dimer)
BdDCL4	Bradi5g15337.3	Bd5:18845215.18867304 reverse	PTHR14950:SF15 – DCL 4



with AtAGO1 and AtAGO10. These findings suggest that the structural and functional differences of AtAGO proteins are translated to the expanded *Brachypodium* family. Phylogenetic analysis of the inferred BdDCL proteins showed that they strongly aligned with individual members of the *Arabidopsis* DCL family (Figure 2). Like *Arabidopsis*, *Brachypodium* contains a single ortholog of DCL1 and DCL4; however, expansion of the BdDCL family has led to the presence of two copies of both

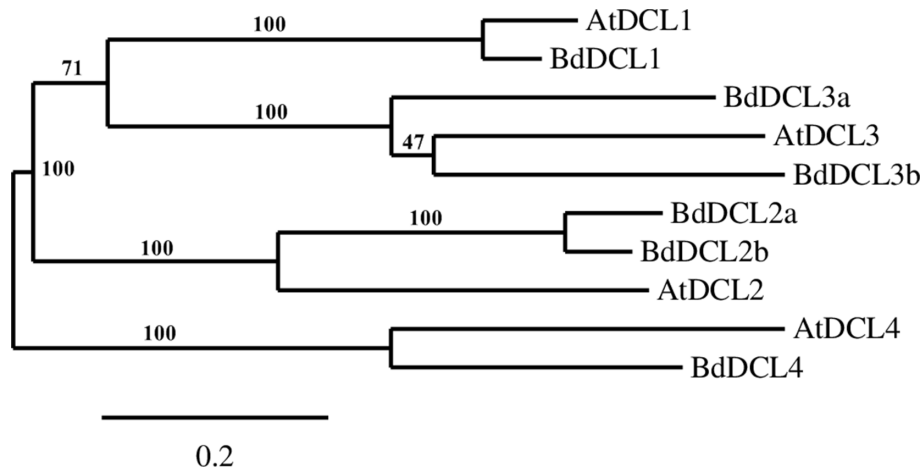


**FIGURE 2 |** Phylogram of the BdDCL and AtDCL protein sequences, as calculated by Phylogeny.fr (MUSCLE, Gblocks, PhyML, TreeDyn). Branch support values are displayed in percentages, and branch support values smaller than 50% are collapsed. Scale bar defining the branch length displayed in bottom right corner.

DCL2 and DCL3, as compared with the single ortholog present in *Arabidopsis*. Sequence comparisons revealed that DCL2a and DCL2b share 82.5% similarity at the aa level, while BdDCL3a and BdDCL3b share 44.2% similarity (aa, global alignment). Together, the phylogenetic trees show distinct branches interspersing *Arabidopsis* and *Brachypodium* homologues in functional clades; to our knowledge, this is the first indication of how the expansion of AGO and DCL protein families in *Brachypodium* relates to the specific clades and/or functional diversity of the corresponding *Arabidopsis* proteins.

### Predicted Domains of BdAGO and BdDCL Proteins Indicate Structure Conservation

Next, we executed a domain search using SMART to elucidate the structures and functions of the 16 BdAGO proteins and six BdDCLs. The domain structure visualization of BdAGO (Figure 3) and BdDCL (Figure 4) proteins highlights the differences between members of each protein family with respect to the positions and presence/absence of the typically conserved domains. Detailed domain prediction data, as acquired by SMART/Pfam search, and the corresponding confidence values

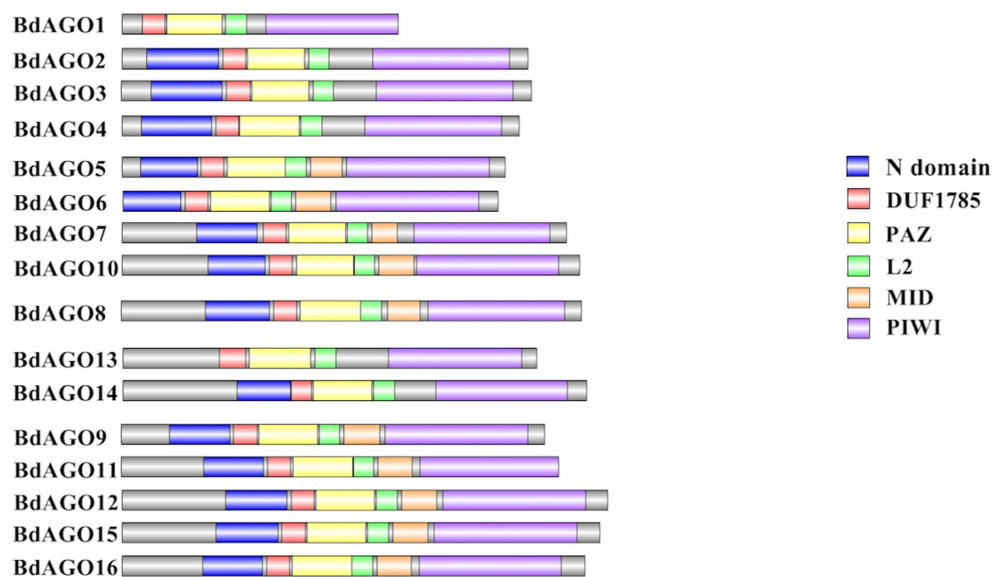


**FIGURE 3 |** Visual representation of domain structure of BdAGO proteins, as identified by domain search by SMART and Pfam. Picture generated with Illustrator for Biological Sequences illustrator. Displayed domains: N-domain, DUF1785 (L1), PAZ (PIWI Argonaut and Zwill), L2, MID, PIWI, sequence, with no domain predicted in gray.

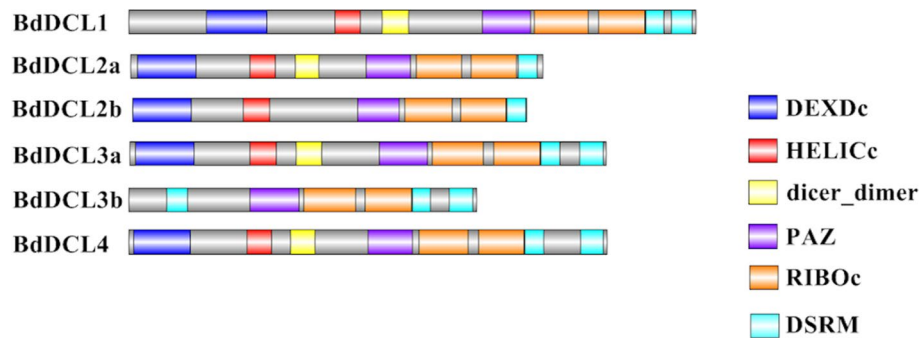


**FIGURE 4 |** Visual representation of domain structure of Bd DCL proteins, as identified by domain search by SMART and Pfam. Picture generated with Illustrator for Biological Sequences illustrator. Displayed domains: DEAD-like helicase superfamily (DEXDc), helicase superfamily c-terminal domain (HELICc), dicer\_dimer, PIWI Argonaut and Zwiille (PAZ), ribonuclease III family (RIBOc), double-stranded RNA-binding motif (DSRM), sequence with no domain predicted in gray.

are shown for BdAGO (Table S2) and BdDCL proteins (Table S3). Consistent with other eukaryotic AGO proteins, many members of the BdAGO family are predicted to have four characteristic functional domains, including the N-terminal domain, PAZ, MID, and PIWI domain (Zhang et al., 2014). However, while the domain prediction results identified a variable N-t domain in most BdAGOs that consisted of both an N-domain and a DUF1785 domain (Poulsen et al., 2013), BdAGO1 and BdAGO13

contained only the DUF1785 domain. In addition, BdAGO1, BdAGO2, BdAGO3, BdAGO4, BdAGO13, and BdAGO14 were not predicted to contain a MID domain, in comparison to a previous report (Mirzaei et al., 2014). MSA performed by Clustal Omega on the PIWI domain of BdAGO proteins (Figure 5) showed a typical pattern of conservation for the DEDD/H catalytic tetrad required for slicer activity and a conserved QF-V motif in all aligned sequences except BdAGO1, which has the

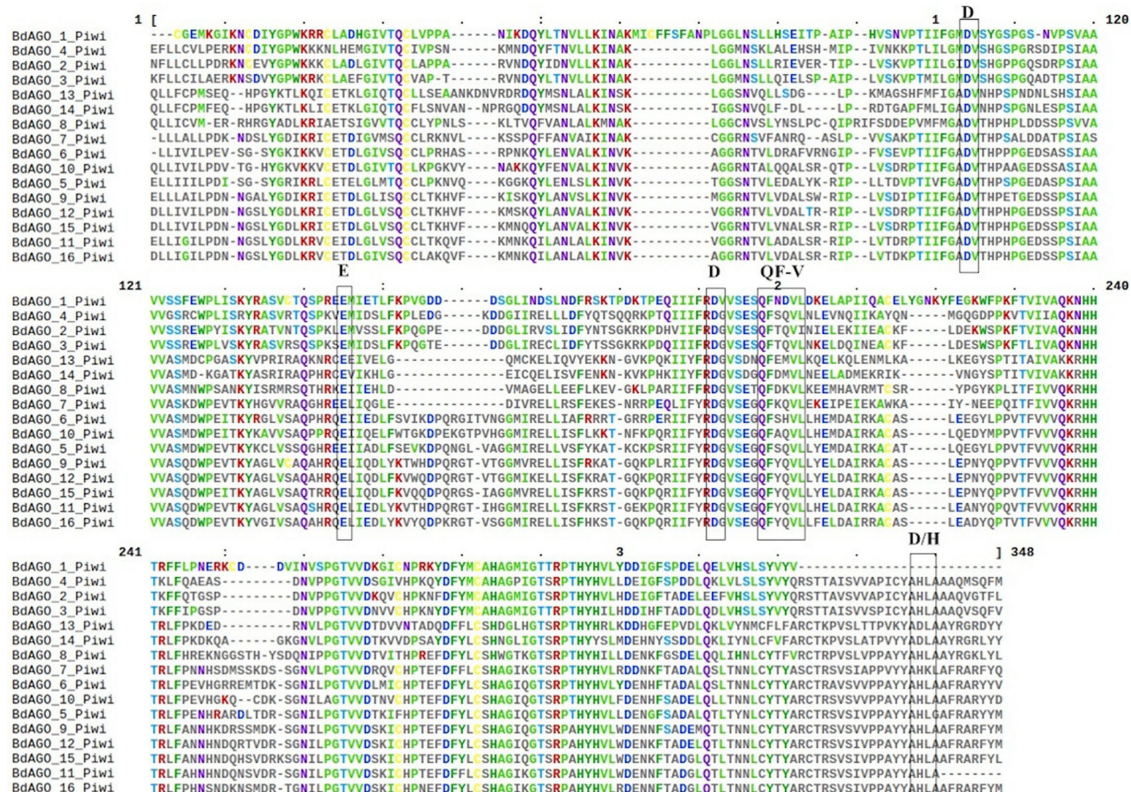


**FIGURE 5 |** Multiple sequence alignment (MSA) of the PIWI domain of BdAGO proteins, as acquired by Clustal Omega and Mview visualization. The catalytic tetrad DEDD/H (Asp-Glu-Asp-Asp or Asp-Glu-Asp-His) and the QF-V (Gln-Phe-Val) motifs are boxed.

shortest protein sequence of all the BdAGO proteins and lacks the D/H residue of the catalytic tetrad.

Analysis of the predicted domains in BdDCL proteins revealed that the characteristic DEXDc, HELICc, Dicer-dimer (DUF283, Qin et al., 2010), PAZ, RIBOc, and DSRM domains are present in most family members. However, BdDCL2b and BdDCL3b lack the dimerization domain; BdDCL3b additionally lacks both the DEXDc and HELICc domains and instead contains an additional DSRM domain at the N terminus (position: 131-218, E-value: 8.6e-17; **Figure 4** and **Table S3**). By contrast, BdDCL2a and BdDCL2b contain only one DSRM domain (**Figure 4**, **Table S3**).

### Three-Dimensional Modeling Supports Phylogenetic Data Showing a Strong Expansion in the BdAGOs in the AGO1/5/10-Related Clade

In order to obtain an optimal homology-based 3D model of the studied proteins, we used SWISS-MODEL and CPHmodels 3.2. When choosing between models generated by alternative software programs or based on different templates, validation of the predicted structures is crucial for generating a consensus on the optimal model and further comparison. In case of

BdAGOs, validation of the predicted structures was done using four different measurements, the results of which are shown in **Table S4**. While a 0-1 QMEAN value gives an absolute scoring of the predicted model, the Z-score shown in **Table S4** serves as a comparison of the quality of the prediction of the query model relative to expected from a high-resolution X-ray crystallography structure. Typically, the more negative the Z-score is, the lower the quality of the predicted structure. Using PROCHECK, we report on the percentage of residues that fall into the most favored regions of the Ramachandran plot. The free energy score of the conformation of the predicted protein calculated by dDFIRE usually indicates lower values for a better model. Based on validation of the 3D models by the software, SWISS-MODEL was chosen as the preferred modeling tool for BdAGO proteins (**Table S4**). The corresponding AtAGO 3D structures, predicted and validated in the same fashion (**Table S5**), were subsequently used alongside the visualization of the BdAGO proteins by PyMOL. **Figures 6, 7, and S1** display the models, in which the PAZ, MID, and PIWI domains (where predicted) and residues comprising the DEDD/H catalytic tetrad are indicated for all BdAGOs and a corresponding AtAGO representing the appropriate branch of the phylogenetic tree depicted in **Figure 1**. Overall, the predicted structures of the BdAGOs mirror the

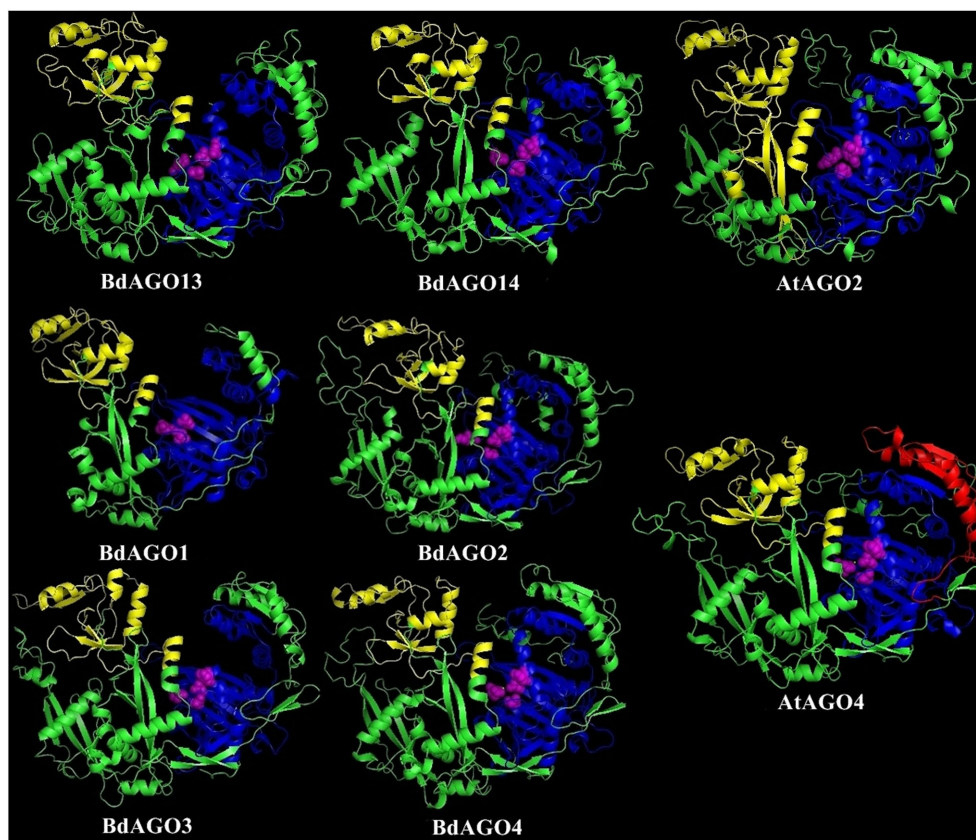


**FIGURE 6 |** Three-dimensional structure predictions for BdAGO13 and BdAGO14 (with AtAGO2 as the closest homolog in *Arabidopsis*) and BdAGO1, BdAGO2, BdAGO3, BdAGO4 (with AtAGO4 as the closest homolog in *Arabidopsis*), as modeled by SWISS-MODEL. PAZ (yellow), PIWI (blue), and MID (red) domains as predicted by SMART and Pfam displayed. The catalytic tetrad within the PIWI domain (DEDD) is marked by magenta spheres. Visualization by PyMOL.

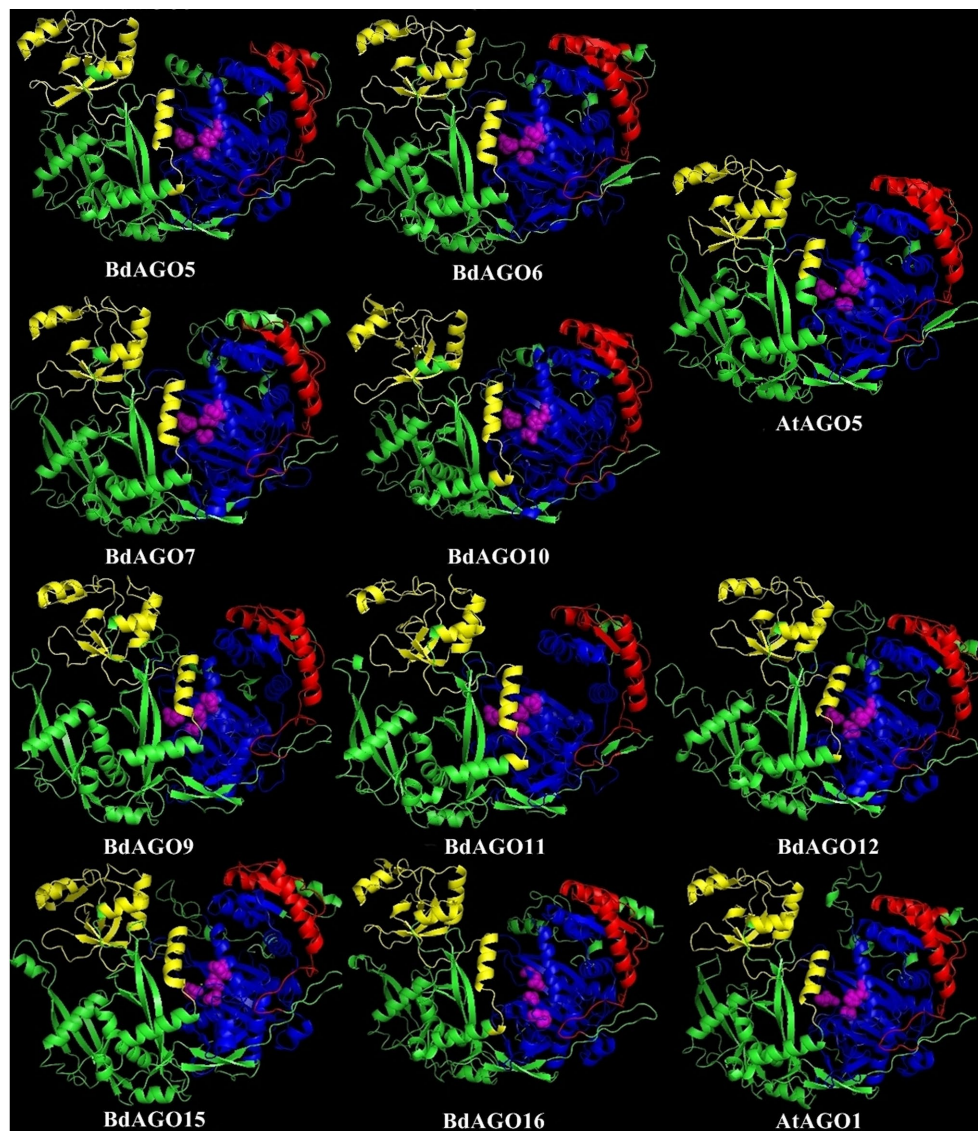


**FIGURE 7 |** Three-dimensional structure predictions for BdAGO5, BdAGO6, BdAGO7, and BdAGO10 (with AtAGO5 as the closest homolog in *Arabidopsis*) and BdAGO9, BdAGO11, BdAGO12, BdAGO15, and BdAGO16 (with AtAGO1 as the closest homolog in *Arabidopsis*), as modeled by SWISS-MODEL. PAZ (yellow), PIWI (blue), and MID (red) domains as predicted by SMART and Pfam displayed. The catalytic tetrad within the PIWI domain (DEDD) is marked by magenta spheres. Visualization by PyMOL.

corresponding AtAGO structures, suggesting a functional conservation. The PIWI domain and the catalytic tetrad especially show similarity between the clade members shown together in **Figures 6 and 7**. The BdDCL proteins did not have successfully modeled structures predicted by either software and thus are not shown.

## Expression Analysis and Putative Interactors of BdAGO Proteins

We addressed the question of tissue-specific expression of *BdAGO* and *BdDCL* genes by utilizing the *B. distachyon* eFP Browser (Sibout et al., 2017; Winter et al., 2007) in **Table 3**.

Stronger expression of *BdAGO* and *BdDCL* genes was observed in seed and stem tissue compared with roots or leaves. The plant subcellular localization integrative predictor used for protein localization predicted that all BdAGOs reside in the cytosol, except for BdAGO3, BdAGO14 (predicted to localize in the nucleus), and BdAGO7 (predicted to localize in plastids), with varying scores of confidence (**Table S7**).

Finally, prediction of proteins that interact with BdAGOs was carried out using STRING (**Table S6**). All predicted BdAGOs were found to be either co-expressed or experimentally shown to interact with three proteins: Bradi1g36340.1, Bradi2g30160.1, and Bradi4g45065.1. BLASTP search of these protein sequences identified them as a 110-kDa U5 small nuclear ribonucleoprotein

**TABLE 3 |** Gene expression data as displayed on the *B. distachyon* eFP Browser (Winter et al., 2007; Sibout et al., 2017).

Gene ID	Assigned name	<sup>1</sup> Highest expression signal	<sup>2</sup> Peduncle, spikelet and stem nodes	<sup>2</sup> Root	<sup>2</sup> Leaf	<sup>2</sup> Seed
Bradi2g10360	BdAGO1	Whole_grain_11_DAF				
Bradi2g14147	BdAGO2	First_node_27_DAG				
Bradi2g10370	BdAGO3	First_node_10_DAG				
Bradi4g08587	BdAGO4	Whole_grain_2_years				
Bradi1g12431	BdAGO5	Not found in browser				
Bradi1g05162	BdAGO6	Endosperm_31_DAF				
Bradi1g28260	BdAGO7	Endosperm_11_DAF				
Bradi1g16060	BdAGO8	First_node_10_DAG				
Bradi1g36907	BdAGO9	First_node_10_DAG				
Bradi1g54977	BdAGO10	Whole_grain_11_DAF				
Bradi1g29577	BdAGO11	Upper_part_of_inclined_node_42_DAG				
Bradi5g18540	BdAGO12	Last_internode_35_DAG				
Bradi5g21810	BdAGO13	Last_node_35_DAG				
Bradi5g21800	BdAGO14	Last_internode_35_DAG				
Bradi3g51077	BdAGO15	Roots_10_DAG				
Bradi3g60697	BdAGO16	Roots_10_DAG				
Bradi1g77087	BdDCL1	Whole_grain_2_years				
Bradi1g15440	BdDCL2a	First_internode_27_DAG				
Bradi1g21030	BdDCL2b	Whole_grain_2_years				
Bradi3g29287	BdDCL3a	Lower_part_of_inclined_node_42_DAG				
Bradi2g23187	BdDCL3b	First_node_10_DAG				
Bradi5g15337	BdDCL4	Whole_grain_2_years				

<sup>1</sup>The tissue with the highest absolute expression level per gene ID is indicated (DAF, day after fertilization; DAG, day after germination).

<sup>2</sup>Summary of relative expression level per gene ID displayed for tissues; color indicates relative expression levels (log2, the control is calculated from all the samples displayed on the particular eFP browser view); dark blue (high for the transcript relative to control) to light blue (low for the transcript relative to control).

component CLO (Bradi1g36340.1), a putative GTP-binding/transcription factor (Bradi2g30160.1), and DNA-directed RNA polymerase V subunit 1 or DNA-directed RNA polymerase V subunit 1 (Bradi4g45065.1). In addition to the aforementioned proteins, BdAGO9 (classified in the AtAGO1/5/10 clade) was predicted to interact with seven other proteins, identified as three homeobox proteins knotted-1-like (Bradi1g12677.1, Bradi1g12690.1, Bradi1g57607.1), two GATA transcription factors (Bradi2g14890.1, Bradi2g45750.1), and two putative uncharacterized proteins (Figure S2).

## DISCUSSION

In the present work, we investigated the phylogenetic relationships, domain, structure conservation, and predicted redundancy of AGO and DCL proteins in the model grass plant *B. distachyon*. Our findings imply that BdAGOs and BdDCLs have more copies and possibly greater diversification relative to *Arabidopsis*. One known example of such diversification in monocotyledonous plants is the rice AGO18, which confers antiviral immunity by sequestration of an miRNA (Wu et al., 2015). Since the presence of domains typical for AGO and DCL protein families serves as a selection criterion for proteins within this uninvestigated grass model species, we discuss phylogenetic relationships and predicted domain occurrence in detail.

Our analyses show that *Brachypodium*, like other grasses, contains one protein (BdDCL1) whose sequence groups with AtDCL1, one with AtDCL4 (BdDCL4), and two proteins each that group with AtDCL2 and AtDCL3 (Margis et al., 2006). Analysis

of their predicted domain structures showed that BdDCL2b and BdDCL3b lack the dicer-dimer (DUF283) domain, known to mediate heterodimerization of AtDCL4 with its protein partners (Qin et al., 2010), but it is partially missing in two other DCLs (AtDCL3 and OsDCL2b, Margis et al., 2006). The second DSRM domain also was not predicted in either of the BdDCL2s. This finding is consistent with the previous discovery that AtDCL2 in *Arabidopsis* and OsDCL2a and OsDCL2b in rice also contain only one DSRM (Margis et al., 2006). This second DSRM domain has only a weak affinity for dsRNA, but it specifically binds to proteins of the HYPONASTIC LEAVES 1/dsRNA-binding protein family (Hiraguri et al., 2005; Margis et al., 2006). Since the DSRM domains mediate the transfer of the newly generated sRNA to the appropriate AGO protein (Parker et al., 2008), variations in the C-terminal architecture may influence which downstream partners and RNAi pathways are utilized by specific DCLs. The high level of divergence between DCL3a and DCL3b in several monocot species has led to the classification of DCL3b as a distinct type of DCL, termed DCL5. This monocot-specific class of DCLs has been retained for over 60 million years (Margis et al., 2006). It is responsible for generating 24-nt-phased sRNAs in the male reproductive organs (Song et al., 2012). Interestingly, the predicted domain structure of BdDCL3b differs substantially from that of BdDCL3a, as it lacks both the DEXDc and HELICc domains (alongside the dicer-dimer domain) but contains an additional N-terminal DSRM (Figure 4, Table S3). Since the helicase domains are thought to mediate unwinding of the dsRNA (Zhang et al., 2004), the functionality of BdDCL3b is unclear. Mutations in AtDCL1 that impair helicase activity were previously shown to suppress miRNA accumulation (Liu

et al., 2012). However, comparable levels of transcripts for two splice variants of AtDCL2, one of which contains an altered helicase region, were detected throughout the *Arabidopsis* life cycle (Margis et al., 2006). Additional structural and biochemical analyses are therefore required to assess the role of BdDCL3b.

Phylogenetic analysis of the BdAGO protein family placed members in all three clades defined by *Arabidopsis* AGOs. Thus, the structural and functional differences of AtAGO proteins appear to be translated to the expanded *Brachypodium* family. For two of the three clades, the number of BdAGO and AtAGO family members was equivalent. By contrast, the AtAGO1/5/10 clade was highly expanded in *Brachypodium*, with four members (BdAGO9/11/12/15/16) grouped with AtAGO1. This member of the *Arabidopsis* family is associated with a range of functions, including processing of dsRNA from transgenes and exogenous sources, and RNAs involved in ckRNAi (Vaucheret et al., 2004; Weiberg et al., 2013). If the corresponding BdAGO members of this clade are found to have similar functions in PTGS-mediated transgene silencing, this information would be highly useful for developing RNAi-based protection strategies for cereal crops. AtAGO10 groups with the same BdAGOs, as expected considering the clade association with AtAGO1. AtAGO5, which is the third member of the AtAGO1/5/10 clade, groups with BdAGO5/6/7/10. By contrast, BdAGO1/2/3/4 were interspersed within the AtAGO4/6/8/9 clade, raising the possibility that these *Brachypodium* proteins are involved in TGS.

As displayed in our domain visualization (Figure 3), all 16 BdAGOs have a predicted PAZ domain. In AGOs, this domain recognizes the 3' end of the guide sRNA molecule, made accessible to the hydrophobic pocket of this nucleotide-binding domain by the typical 2'-O-methyl modification of the final sugar (Lingel et al., 2003; Cenik and Zamore, 2011). The MID domain recognizes the 5' nucleotide of the sRNA, thus giving preference of an AGO protein into which the sRNA will be loaded (Frank et al., 2012). In *Arabidopsis*, sRNA with a 5' U are sorted into AtAGO1, while AtAGO2 and AtAGO4 load sRNAs with a 5' A and AtAGO5 loads sRNAs with a 5' C (Mi et al., 2008). Our SMART/Pfam domain architecture search failed to identify a MID domain in any of the BdAGOs grouped in the AtAGO4/6/8/9 clade (BdAGO1/2/3/4) and with the AtAGO2/3 (BdAGO13/14) (Table S2), although this domain was reported in these proteins in a different study (Mirzaei et al., 2014). The specificity of sRNA sorting into particular AGOs can be further determined by the recognition of the sRNA secondary structure/base pairing by a QF-V motif present in the PIWI domain (Zhang et al., 2014). All *Arabidopsis* AGOs have the conserved QF-V motif, as do all 16 BdAGOs (Figure 5). The DEDD/H catalytic tetrad in the PIWI domain is also present in all but one of the BdAGOs. These active-site residues are critical for the RNase H-like endonuclease (slicer) activity exhibited by certain AGOs, which mediates sequence-specific cleavage of the target transcript. AtAGO1, AtAGO2, AtAGO4, AtAGO7, and AtAGO10 have been shown to have endonucleolytic activity toward target RNAs (Fang and Qi, 2016). Originally identified as a catalytic triad consisting of the residues DDH in most AtAGOs, but DDD in AtAGO2 and AtAGO3 (Höck and Meister, 2008), studies of yeast AGO revealed the importance of an invariant glutamate (E)

residue, creating a catalytic tetrad (Nakanishi et al., 2012). This E residue is conserved in all *Arabidopsis* AGOs (Zhang et al., 2014). Consistent with these findings, MSA visualization of the BdAGO PIWI domains indicated that the majority of BdAGO proteins have the DEDH tetrad, except BdAGO13 and BdAGO14, which like their closest homologues AtAGO2 and AtAGO3, contain the DEDD tetrad (Figure 5). The only exception is BdAGO1, which is a short protein that terminates after 624 residues and lacks the last catalytic residue of the tetrad. Without the conserved catalytic residues, a specific AGO protein might induce gene silencing through means other than cutting, but Höck and Meister (2008) also discuss that the presence of a conserved catalytic triad does not mean the protein indeed has endonuclease activity. If an AGO does not display endonuclease activity, it may mediate PTGS via translation inhibition of the target RNA (Carthew and Sontheimer, 2009). Interestingly, the L1 and L2 linkers are predicted in all 16 BdAGOs as well (Table S2).

3D structure visualizations of all BdAGOs (Figures 6, 7 and S1) reinforce the conservation of the PAZ, PIWI, and MID domains (when predicted by SMART) and the catalytic tetrad residues in proximity within the PIWI domain (magenta spheres). The differences in the folding and looping linker regions within a certain group, relative to *Arabidopsis* AGOs, are shown in the model visualizations. Furthermore, the similarity between the 3D structures of BdAGOs that were predicted either to contain or lack a MID domain by the SMART/Pfam domain architecture search (e.g., Figure 6) reinforces the importance of comparing entire 3D models in order to gain insight into structure/function conservation. These structures are based on templates with better-known functional specificity and thus hint at the functions of the orthologs in Bd. As shown in Table S4, the templates used for modeling are based on either Argonaute 1 or Argonaute 2, with varying coverage and confidence values.

To assess the expression levels and locations of BdAGO and BdDCL family members, we analyzed the microarray-based expression data in the *B. distachyon* eFP browser (Table 3). Expression of BdAGO genes was observed in all four tissues assayed, although to varying extents. The expression patterns across the gene families indicate potential for functional redundancy. Notably, all members of the AtAGO1 clade (BdAGO9/11/12/15/16) show high and intermediate levels of expression in stem nodes and root tissue, respectively, while the BdAGO1/2/3/4 proteins generally display high expression in stem nodes and seeds. Analysis of BdDCL gene expression revealed that most members of this family are highly expressed in stem nodes and/or seeds. *In vivo* experimental approaches are necessary to decipher whether the apparent co-expression of these genes indicates specific compartmentalization or complete/partial redundancy in the various RNAi processes, including environmental RNAi and ckRNAi pathways.

Finally, we used STRING to predict the interactome for members of the BdAGO family. This analysis indicates that all BdAGOs interact with three proteins (Table S6), as was expected because of the domain conservation within the family. In addition, several potential interactors were identified for BdAGO9, based on co-expression or experimental data (Figure S2, Table S6). Of these, DNA-directed RNA polymerase V subunit 1 was previously

shown to co-localize with, and possibly directly bind to, AtAGO4 via a so-called “Ago hook” (GW-rich domain), in order to facilitate the recruitment of AGO4 to chromatin to mediate TGS (El-Shami et al., 2007; Fang and Qi, 2016). Poulsen et al. (2013) have discussed that the binding of GW interactors to AGO make the loop with the E residue of the catalytic tetrad unavailable to the otherwise rigid DDD/H triad within the PIWI domain, thus offering an explanation of how the slicing activity is prevented in cases of silencing by translational inhibition. Moreover, GW containing proteins Needed for RDR2-independent DNA methylation and Silencing Defective 3 have been indicated in pathways bringing DNA/chromatin silencing together with RNAi proteins (Garcia et al., 2012; Pontier et al., 2012). Protein co-expression and interaction studies *in vivo* are necessary to confirm the identity and locations of these putative BdAGO interacting proteins. Due to the stringency of the prediction (excluding text mining data) and the lack of knowledge about the *Brachypodium* RNAi machinery, we were unable to predict additional interactions or to detect RNAi-related proteins that are known to interact with members of the AGO family in *Arabidopsis*. These include DCLs, HEN1 (involved in the methylation of sRNA 3' ends to prevent degradation), RDRs (RNA-dependent RNA polymerases that synthesize dsRNAs from single-stranded RNAs), and HSP90, the heat shock protein that binds to AtAGO1 and AtAGO4 to aid the loading of the sRNAs and RISC assembly (Fang and Qi, 2016; Nakanishi, 2016). Moreover, the predicted localization of the BdAGOs places the majority of them in the cytosol, except for BdAGO3 and BdAGO14, which are predicted to localize in the nucleus (Table S7). From what is known about *Arabidopsis* AGOs, AtAGO1 is proposed to have a localization in the nucleus and the cytoplasm (Vaucheret, 2008), while AtAGO4 localizes to the nuclear Cajal bodies (Höck and Meister, 2008).

In sum, based on *in silico* prediction, our data provide the first detailed functional insight into the AGO and DCL protein families in *Brachypodium*. In the context of plant-microbe interactions and ckRNAi, the *Brachypodium* orthologs of AtAGO1 are of special interest because microbial sRNAs are shown to be loaded onto AtAGO1 (Weiberg et al., 2013). Our predictions indicate a clade of BdAGOs structurally similar to AtAGO1, consisting of BdAGO9/11/12/15/16 (Figure 7). Elaborating on such similarities with the well-established clades of *Arabidopsis* AGOs and DCLs is a valuable basis for testing the hypothesis that BdAGO9/11/12/15/16 proteins are required for exogenous and endogenous dsRNA processing in HIGS, SIGS, and bidirectional ckRNAi in the grass model. Beyond what is

predictable by *in silico* analysis, more data on expression patterns and interacting proteins are needed to further understand the role of these pillar proteins of RNAi pathways in cereals.

## DATA AVAILABILITY STATEMENT

All datasets for this study are included in the article/Supplementary Files.

## AUTHOR CONTRIBUTIONS

EŠ, SZ, and KHK wrote the text. EŠ and SZ performed analysis and designed the figures.

## FUNDING

This work was funded by the Deutsche Forschungsgemeinschaft in the program GRK2355 to KHK and by of the European Union in the Marie Skłodowska-Curie Actions CEREALPATH to KHK and SZ.

## ACKNOWLEDGMENTS

We thank Sebastien Santini—CNRS/AMU IGS UMR7256, for administration of Phylogeny.fr, used for phylogenetic analysis within this study. We are very thankful to D'Maris Dempsey for her assistance in text editing. This manuscript summarizes EŠ's and KHK's contribution during the Organisation for Economic Cooperation and Development Conference on RNAi-Based Pesticides, which was sponsored by the Organisation for Economic Cooperation and Development Co-operative Research Programme: Biological Resource Management for Sustainable Agricultural Systems whose financial support made it possible for the author KHK to participate in the conference.

## SUPPLEMENTARY MATERIAL

The Supplementary Material for this article can be found online at: <https://www.frontiersin.org/articles/10.3389/fpls.2019.01332/full#supplementary-material>

## REFERENCES

- Abdellatef, E., Will, T., Koch, A., Imani, J., Vilcinskis, A., and Kogel, K.-H. (2015). Silencing the expression of the salivary sheath protein causes transgenerational feeding suppression in the aphid Sitobion avenae. *Plant Biotechnol. J.* 13 (6), 849–857. doi: 10.1111/pbi.12322
- Andrade, E. C., and Hunter, W. B. (2016). “RNA interference—natural gene-based technology for highly specific pest control (HiSPeC).” *RNA interference (Ch.19)*. Ed. I. Y. Abdurakhmonov (IntechOpen), 391–409. doi: 10.5772/61612
- Anisimova, M., and Gascuel, O. (2006). Approximate likelihood-ratio test for branches: a fast, accurate, and powerful alternative. *Syst. Biol.* 55 (4), 539–552. doi: 10.1080/10635150600755453
- Bartel, D. P. (2004). MicroRNAs: genomics, biogenesis, mechanism, and function. *Cell* 116 (2), 281–297. doi: 10.1016/S0092-8674(04)00045-5
- Benkert, P., Biasini, M., and Schwede, T. (2011). Toward the estimation of the absolute quality of individual protein structure models. *Bioinformatics* 27 (3), 343–350. doi: 10.1093/bioinformatics/btq662
- Berardini, T. Z., Reiser, L., Li, D., Mezheritsky, Y., Muller, R., Strait, E., et al. (2015). The aArabidopsis information resource: Making and mining the “gold standard” annotated reference plant genome. *Genesis* 53 (8), 474–485. doi: 10.1002/dvg.22877
- Berman, H., Gilliland, G. M., Weissig, H., Shindyalov, I. N., Westbrook, J., Bourne, P. E., et al. (2000). The protein data bank. *Nucleic Acids Res.* 28 (1), 235–242. doi: 10.1093/nar/28.1.235

- Bohmert, K., Camus, I., Bellini, C., Bouchez, D., Caboche, M., and Benning, C. (1998). AGO1 defines a novel locus of Arabidopsis controlling leaf development. *EMBO J.* 17 (1), 170–180. doi: 10.1093/emboj/17.1.170
- Boland, A., Huntzinger, E., Schmidt, S., Izaurralde, E., and Weichenrieder, O. (2011). Crystal structure of the MID-PIWI lobe of a eukaryotic Argonaute protein. *Proc. Natl. Acad. Sci.* 108 (26), 10466 LP–10471. doi: 10.1073/pnas.1103946108
- Bologna, N. G., and Voinnet, O. (2014). The diversity, biogenesis, and activities of endogenous silencing small RNAs in Arabidopsis. *Annu. Rev. Plant Biol.* 65, 473–503. doi: 10.1146/annurev-arplant-050213-035728
- Borges, F., and Martienssen, R. A. (2015). The expanding world of small RNAs in plants. *Nat. Rev. Mol. Cell Biol.* 16 (12), 727–741. doi: 10.1038/nrm4085
- Borsani, O., Zhu, J., Verslues, P. E., Sunkar, R., and Zhu, J.-K. (2005). Endogenous siRNAs derived from a pair of natural cis-Antisense transcripts regulate salt tolerance in Arabidopsis. *Cell* 123 (7), 1279–1291. doi: 10.1016/j.cell.2005.11.035
- Brown, N. P., Leroy, C., and Sander, C. (1998). MView: a web-compatible database search or multiple alignment viewer. *Bioinformatics* 14 (4), 380–381. doi: 10.1093/bioinformatics/14.4.380
- Burley, S. K., Yang, H., Tan, L., Sala, R., Hudson, B. P., Bhikadiya, C., et al. (2018). RCSB Protein Data Bank: biological macromolecular structures enabling research and education in fundamental biology, biomedicine, biotechnology and energy. *Nucleic Acids Res.* 47 (D1), D464–D474. doi: 10.1093/nar/gky1004
- Cai, Q., He, B., Kogel, K.-H., and Jin, H. (2018). Cross-kingdom RNA trafficking and environmental RNAi — nature's blueprint for modern crop protection strategies. *Curr. Opin. Microbiol.* 46, 58–64. doi: 10.1016/j.mib.2018.02.003
- Camacho, C., Coulouris, G., Avagyan, V., Ma, N., Papadopoulos, J., Bealer, K., et al. (2009). BLAST+: architecture and applications. *BMC Bioinformatics* 10 (1), 421. doi: 10.1186/1471-2105-10-421
- Carthew, R. W., and Sontheimer, E. J. (2009). Origins and mechanisms of miRNAs and siRNAs. *Cell* 136 (4), 642–655. doi: 10.1016/j.cell.2009.01.035
- Castresana, J. (2000). Selection of conserved blocks from multiple alignments for their use in phylogenetic analysis. *Mol. Biol. Evol.* 17 (4), 540–552. doi: 10.1093/oxfordjournals.molbev.a026334
- Cenik, E. S., and Zamore, P. D. (2011). Argonaute proteins. *Curr. Biol.* 21 (12), R446–R449. doi: 10.1016/j.cub.2011.05.020
- Chevenet, F., Brun, C., Bañuls, A.-L., Jacq, B., and Christen, R. (2006). TreeDyn: towards dynamic graphics and annotations for analyses of trees. *BMC Bioinformatics* 7, 439. doi: 10.1186/1471-2105-7-439
- Coleman, A. D., Wouters, R. H. M., Mugford, S. T., and Hogenhout, S. A. (2014). Persistence and transgenerational effect of plant-mediated RNAi in aphids. *J. Exp. Bot.* 66 (2), 541–548. doi: 10.1093/jxb/eru450
- Dereeper, A., Audic, S., Claverie, J.-M., and Blanc, G. (2010). BLAST-EXPLORER helps you building datasets for phylogenetic analysis. *BMC Evol. Biol.* 10, 8. doi: 10.1186/1471-2148-10-8
- Dereeper, A., Guignon, V., Blanc, G., Audic, S., Buffet, S., Chevenet, F., et al. (2008). Phylogeny.fr: robust phylogenetic analysis for the non-specialist. *Nucleic Acids Res.* 36 (Web Server issue), W465–W469. doi: 10.1093/nar/gkn180
- Dunoyer, P., Himber, C., and Voinnet, O. (2005). DICER-LIKE 4 is required for RNA interference and produces the 21-nucleotide small interfering RNA component of the plant cell-to-cell silencing signal. *Nat. Genet.* 37, 1356. doi: 10.1038/ng1675
- Dutta, T. K., Papolu, P. K., Banakar, P., Choudhary, D., Sirohi, A., and Rao, U. (2015). Tomato transgenic plants expressing hairpin construct of a nematode protease gene conferred enhanced resistance to root-knot nematodes. *Front. Microbiol.* 6, 260. doi: 10.3389/fmicb.2015.00260
- Edgar, R. C. (2004). MUSCLE: multiple sequence alignment with high accuracy and high throughput. *Nucleic Acids Res.* 32 (5), 1792–1797. doi: 10.1093/nar/gkh340
- Elkayam, E., Kuhn, C.-D., Tocilj, A., Haase, A. D., Greene, E. M., Hannon, G. J., et al. (2012). The structure of human argonaute-2 in complex with miR-20a. *Cell* 150 (1), 100–110. doi: 10.1016/j.cell.2012.05.017
- El-Shami, M., Pontier, D., Lahmy, S., Braun, L., Picart, C., Vega, D., et al. (2007). Reiterated WG/GW motifs form functionally and evolutionarily conserved ARGONAUTE-binding platforms in RNAi-related components. *Genes Dev.* 21 (20), 2539–2544. doi: 10.1101/gad.451207
- Faehnle, C. R., Elkayam, E., Haase, A. D., Hannon, G. J., and Joshua-Tor, L. (2013). The making of a slicer: activation of human Argonaute-1. *Cell Rep.* 3 (6), 1901–1909. doi: 10.1016/j.celrep.2013.05.033
- Fang, X., and Qi, Y. (2016). RNAi in Plants: an argonaute-centered view. *Plant Cell.* 28 (2), 272 LP–272285. doi: 10.1105/tpc.15.00920
- Fire, A., Xu, S., Montgomery, M. K., Kostas, S. A., Driver, S. E., and Mello, C. C. (1998). Potent and specific genetic interference by double-stranded RNA in *Caenorhabditis elegans*. *Nature* 391 (6669), 806–811. doi: 10.1038/35888
- Frank, F., Hauver, J., Sonenberg, N., and Nagar, B. (2012). Arabidopsis Argonaute MID domains use their nucleotide specificity loop to sort small RNAs. *EMBO J.* 31 (17), 3588 LP–3595. doi: 10.1038/emboj.2012.204
- Fukudome, A., and Fukuhara, T. (2017). Plant dicer-like proteins: double-stranded RNA-cleaving enzymes for small RNA biogenesis. *J. Plant Res.* 130 (1), 33–44. doi: 10.1007/s10265-016-0877-1
- Garcia, D., Garcia, S., Pontier, D., Marchais, A., Renou, J. P., Lagrange, T., et al. (2012). Ago hook and RNA helicase motifs underpin dual roles for SDE3 in antiviral defense and silencing of nonconserved intergenic regions. *Mol. Cell* 48 (1), 109–120. doi: 10.1016/j.molcel.2012.07.028
- Gascioli, V., Mallory, A. C., Bartel, D. P., and Vaucheret, H. (2005). Partially redundant functions of Arabidopsis DICER-like enzymes and a role for DCL4 in producing trans-acting siRNAs. *Curr. Biol.* 15 (16), 1494–1500. doi: 10.1016/j.cub.2005.07.024
- Goodstein, D. M., Shu, S., Howson, R., Neupane, R., Hayes, R. D., Fazo, J., et al. (2012). Phytozome: a comparative platform for green plant genomics. *Nucleic Acids Res.* 40 (Database issue), D1178–D1186. doi: 10.1093/nar/gkr944
- Goujon, M., McWilliam, H., Li, W., Valentin, F., Squizzato, S., Paern, J., et al. (2010). A new bioinformatics analysis tools framework at EMBL-EBI. *Nucleic Acids Res.* 38 (suppl\_2), W695–W699. doi: 10.1093/nar/gkq313
- Guindon, S., and Gascuel, O. (2003). A simple, fast, and accurate algorithm to estimate large phylogenies by maximum likelihood. *Syst. Biol.* 52, 696–704. doi: 10.1080/10635150390235520
- Harvey, J. J. W., Lewsey, M. G., Patel, K., Westwood, J., Heimstädt, S., Carr, J. P., et al. (2011). An antiviral defense role of AGO2 in plants. *PLoS One* 6 (1), e14639. doi: 10.1371/journal.pone.0014639
- Head, G. P., Carroll, M. W., Evans, S. P., Rule, D. M., Willse, A. R., Clark, T. L., et al. (2017). Evaluation of SmartStax and SmartStax PRO maize against western corn rootworm and northern corn rootworm: efficacy and resistance management. *Pest Manag. Sci.* 73 (9), 1883–1899. doi: 10.1002/ps.4554
- Hiraguri, A., Itoh, R., Kondo, N., Nomura, Y., Aizawa, D., Murai, Y., et al. (2005). Specific interactions between Dicer-like proteins and HYL1/DRB-family dsRNA-binding proteins in Arabidopsis thaliana. *Plant Mol. Biol.* 57 (2), 173–188. doi: 10.1007/s11103-004-6853-5
- Höck, J., and Meister, G. (2008). The Argonaute protein family. *Genome Biol.* 9 (2), 210. doi: 10.1186/gb-2008-9-2-210
- Hooft, R. W. W., Sander, C., and Vriend, G. (1997). Objectively judging the quality of a protein structure from a Ramachandran plot. *Bioinformatics* 13 (4), 425–430. doi: 10.1093/bioinformatics/13.4.425
- Hooft, R. W. W., Vriend, G., Sander, C., and Abola, E. E. (1996). Errors in protein structures. *Nature* 381 (6580), 272. doi: 10.1038/381272a0
- Koch, A., Biedenkopf, D., Furch, A., Weber, L., Rossbach, O., Abdellatif, E., et al. (2016). An RNAi-based control of fusarium graminearum infections through spraying of long dsRNAs involves a plant passage and is controlled by the fungal silencing machinery. *PLOS Pathog.* 12 (10), e1005901. doi: 10.1371/journal.ppat.1005901
- Koch, A., Kumar, N., Weber, L., Keller, H., Imani, J., and Kogel, K.-H. (2013). Host-induced gene silencing of cytochrome P450 lanosterol C14 $\alpha$ -demethylase-encoding genes confers strong resistance to Fusarium species. *Proc. Natl. Acad. Sci.* 110 (4), 19324 LP–19329. doi: 10.1073/pnas.1306373110
- Koch, A., Stein, E., and Kogel, K.-H. (2018). RNA-based disease control as a complementary measure to fight Fusarium fungi through silencing of the azole target Cytochrome P450 Lanosterol C-14  $\alpha$ -Demethylase. *Eur. J. Plant Pathol.* 152 (4), 1003–1010. doi: 10.1007/s10658-018-1518-4
- Laskowski, R., MacArthur, M. W., Moss, D. S., and Thornton, J. (1993). PROCHECK: A program to check the stereochemical quality of protein structures. *J. Appl. Crystallogr.* 26, 283–291. doi: 10.1107/S0021889892009944
- Letunic, I., and Bork, P. (2017). 20 years of the SMART protein domain annotation resource. *Nucleic Acids Res.* 46 (D1), D493–D496. doi: 10.1093/nar/gkx922
- Lingel, A., Simon, B., Izaurralde, E., and Sattler, M. (2003). Structure and nucleic-acid binding of the Drosophila Argonaute 2 PAZ domain. *Nature* 426 (6965), 465–469. doi: 10.1038/nature02123

- Lingel, A., Simon, B., Izaurralde, E., and Sattler, M. (2004). Nucleic acid 3'-end recognition by the Argonaute2 PAZ domain. *Nat. Struct. Mol. Biol.* 11, 576. doi: 10.1038/nsmb777
- Liu, C., Axtell, M. J., and Fedoroff, N. V. (2012). The helicase and RNaseIIIa domains of Arabidopsis Dicer-Like1 modulate catalytic parameters during microRNA biogenesis. *Plant Physiol.* 159 (2), 748–758. doi: 10.1104/pp.112.193508
- Liu, L., Zhang, Z., Mei, Q., and Chen, M. (2013). PSI: a comprehensive and integrative approach for accurate plant subcellular localization prediction. *PLOS ONE* 8 (10), e75826. doi: 10.1371/journal.pone.0075826
- Liu, W., Xie, Y., Ma, J., Luo, X., Nie, P., Zuo, Z., et al. (2015). IBS: an illustrator for the presentation and visualization of biological sequences. *Bioinformatics*. 31 (20), 3359–3361. doi: 10.1093/bioinformatics/btv362
- Liu, Y., Eshyunina, D., Olovnikov, I., Teplova, M., Kulbachinskiy, A., Aravin, A. A., et al. (2018). Accommodation of helical imperfections in rhodospirillum rubrum argonaute ternary complexes with guide RNA and target DNA. *Cell Rep.* 24 (2), 453–462. doi: 10.1016/j.celrep.2018.06.021
- Margis, R., Fusaro, A. F., Smith, N. A., Curtin, S. J., Watson, J. M., Finnegan, E. J., et al. (2006). The evolution and diversification of Dicers in plants. *FEBS Lett.* 580 (10), 2442–2450. doi: 10.1016/j.febslet.2006.03.072
- Mi, S., Cai, T., Hu, Y., Chen, Y., Hodges, E., Ni, F., et al. (2008). Sorting of Small RNAs into Arabidopsis argonaute complexes is directed by the 5' terminal nucleotide. *Cell* 133 (1), 116–127. doi: 10.1016/j.cell.2008.02.034
- Mirzaei, K., Bahramnejad, B., Shamsifard, M. H., and Zamani, W. (2014). In silico identification, phylogenetic and bioinformatic analysis of argonaute genes in plants. *Int. J. Genomics*. 2014, 967461. doi: 10.1155/2014/967461
- Morris, A. L., MacArthur, M. W., Hutchinson, E. G., and Thornton, J. M. (1992). Stereochemical quality of protein structure coordinates. *Proteins Struct. Funct. Bioinf.* 12 (4), 345–364. doi: 10.1002/prot.340120407
- Mukherjee, K., Campos, H., and Kolaczowski, B. (2013). Evolution of animal and plant dicers: early parallel duplications and recurrent adaptation of antiviral RNA binding in plants. *Mol. Biol. Evol.* 30 (3), 627–641. doi: 10.1093/molbev/mss263
- Nakanishi, K. (2016). Anatomy of RISC: how do small RNAs and chaperones activate Argonaute proteins? *Wiley Interdiscip. Rev. RNA*. 7 (5), 637–660. doi: 10.1002/wrna.1356
- Nakanishi, K., Weinberg, D. E., Bartel, D. P., and Patel, D. J. (2012). Structure of yeast Argonaute with guide RNA. *Nature* 486, 368. doi: 10.1038/nature11211
- Nielsen, M., Lundegaard, C., Lund, O., and Petersen, T. N. (2010). CPHmodels 3.0—remote homology modeling using structure-guided sequence profiles. *Nucleic Acids Res.* 38 (Web Server issue), W576–W581. doi: 10.1093/nar/gkq535
- Nowara, D., Gay, A., Lacomme, C., Shaw, J., Ridout, C., Douchkov, D., et al. (2010). HIGS: Host-Induced Gene Silencing in the obligate biotrophic fungal pathogen blumeria graminis. *Plant Cell*. 22 (9), 3130 LP–3141. doi: 10.1105/tpc.110.077040
- Olmedo-Monfil, V., Durán-Figueroa, N., Arteaga-Vázquez, M., Demesa-Arévalo, E., Autran, D., Grimanelli, D., et al. (2010). Control of female gamete formation by a small RNA pathway in Arabidopsis. *Nature* 464, 628. doi: 10.1038/nature08828
- Park, M. S., Phan, H.-D., Busch, F., Hinckley, S. H., Brackbill, J. A., Wysocki, V. H., et al. (2017). Human Argonaute3 has slicer activity. *Nucleic Acids Res.* 45 (20), 11867–11877. doi: 10.1093/nar/gkx916
- Parker, G. S., Maity, T. S., and Bass, B. L. (2008). dsRNA binding properties of RDE-4 and TRBP reflect their distinct roles in RNAi. *J. Mol. Biol.* 384 (4), 967–979. doi: 10.1016/j.jmb.2008.10.002
- Patel, P., Mathioni, S., Kakrana, A., Shatnay, H., and Meyers, B. (2018). Reproductive phasiRNAs in grasses are compositionally distinct from other classes of small RNAs. *New Phytol.* 220, 851–864. doi: 10.1111/nph.15349
- Pontier, D., Picart, C., Roudier, F., Garcia, D., Lahmy, S., Azevedo, J., et al. (2012). NERD, a Plant-Specific GW Protein, Defines an Additional RNAi-Dependent Chromatin-Based Pathway in Arabidopsis. *Mol. Cell* 48 (1), 121–132. doi: 10.1016/j.molcel.2012.07.027
- Poulsen, C., Vaucheret, H., and Brodersen, P. (2013). Lessons on RNA silencing mechanisms in plants from eukaryotic argonaute structures. *Plant Cell*. 25 (1), 22–37. doi: 10.1105/tpc.112.105643
- Qin, H., Chen, F., Huan, X., Machida, S., Song, J., and Yuan, Y. A. (2010). Structure of the Arabidopsis thaliana DCL4 DUF283 domain reveals a noncanonical double-stranded RNA-binding fold for protein-protein interaction. *RNA* 16 (3), 474–481. doi: 10.1261/rna.1965310
- Qu, F., Ye, X., and Morris, T. J. (2008). Arabidopsis DRB4, AGO1, AGO7, and RDR6 participate in a DCL4-initiated antiviral RNA silencing pathway negatively regulated by DCL1. *Proc. Natl. Acad. Sci. U. S. A.* 105 (38), 14732–14737. doi: 10.1073/pnas.0805760105
- Ramachandran, G. N., Ramakrishnan, C., and Sasisekharan, V. (1963). Stereochemistry of polypeptide chain configurations. *J. Mol. Biol.* 7 (1), 95–99. doi: 10.1016/S0022-2836(63)80023-6
- Remmert, M., Biegert, A., Hauser, A., and Söding, J. (2011). HHblits: lightning-fast iterative protein sequence searching by HMM-HMM alignment. *Nat. Methods* 9, 173. doi: 10.1038/nmeth.1818
- Rhee, S. Y., Beavis, W., Berardini, T. Z., Chen, G., Dixon, D., Doyle, A., et al. (2003). The Arabidopsis Information Resource (TAIR): a model organism database providing a centralized, curated gateway to Arabidopsis biology, research materials and community. *Nucleic Acids Res.* 31 (1), 224–228. doi: 10.1093/nar/gkg076
- Rice, P., Longden, I., and Bleasby, A. (2000). EMBOS: the European molecular biology open software suite. *Trends Genet.* 16 (6), 276–277. doi: 10.1016/S0168-9525(00)00204-2
- Savary, S., Ficke, A., Aubertot, J.-N., and Hollier, C. (2012). Crop losses due to diseases and their implications for global food production losses and food security. *Food Secur.* 4, 519–537. doi: 10.1007/s12571-012-0200-5
- Schauer, S. E., Jacobsen, S. E., Meinke, D. W., and Ray, A. (2002). DICER-LIKE1: blind men and elephants in Arabidopsis development. *Trends Plant Sci.* 7 (11), 487–491. doi: 10.1016/S1360-1385(02)02355-5
- Schrödinger, L. L. C. (2010). The PyMOL Molecular Graphics System, Version~1.3.
- Schultz, J., Milpetz, F., Bork, P., and Ponting, C. P. (1998). SMART, a simple modular architecture research tool: identification of signaling domains. *Proc. Natl. Acad. Sci.* 95 (11), 5857 LP–5864. doi: 10.1073/pnas.95.11.5857
- Secic, E., Sutkovic, J., and Abdel Gawwad, M. (2015). Interactome analysis and docking sites prediction of radiation sensitive 23 (RAD 23) proteins in Arabidopsis thaliana. *Curr. Proteomics* 12 (1), 28–44. doi: 10.2174/1570164612666150225234240
- Sibout, R., Proost, S., Hansen, B. O., Vaid, N., Giorgi, F. M., Ho-Yue-Kuang, S., et al. (2017). Expression atlas and comparative coexpression network analyses reveal important genes involved in the formation of lignified cell wall in Brachypodium distachyon. *New Phytol.* 215 (3), 1009–1025. doi: 10.1111/nph.14635
- Sievers, F., Wilm, A., Dineen, D., Gibson, T. J., Karplus, K., Li, W., et al. (2011). Fast, scalable generation of high-quality protein multiple sequence alignments using Clustal Omega. *Mol. Syst. Biol.* 7 (1), 539. doi: 10.1038/msb.2011.75
- Song, M. S., and Rossi, J. J. (2017). Molecular mechanisms of Dicer: endonuclease and enzymatic activity. *Biochem. J.* 474, 1603–1618. doi: 10.1042/BCJ20160759
- Song, X., Li, P., Zhai, J., Zhou, M., Ma, L., Liu, B., et al. (2012). Roles of DCL4 and DCL3b in rice phased small RNA biogenesis. *Plant J.* 69 (3), 462–474. doi: 10.1111/j.1365-3113.2011.04805.x
- Szklarczyk, D., Gable, A. L., Lyon, D., Junge, A., Wyder, S., Huerta-Cepas, J., et al. (2019). STRING v11: protein-protein association networks with increased coverage, supporting functional discovery in genome-wide experimental datasets. *Nucleic Acids Res.* 47 (D1), D607–D613. doi: 10.1093/nar/gky1131
- The International Brachypodium Initiative (2010). Genome sequencing and analysis of the model grass Brachypodium distachyon. *Nature* 463, 763–768. doi: 10.1038/nature08747
- Tomilov, A. A., Tomilova, N. B., Wroblewski, T., Micheltore, R., and Yoder, J. I. (2008). Trans-specific gene silencing between host and parasitic plants. *Plant J.* 56 (3), 389–397. doi: 10.1111/j.1365-3113.2008.03613.x
- Vaucheret, H. (2008). Plant ARGONAUTES. *Trends Plant Sci.* 13 (7), 350–358. doi: 10.1016/j.tplants.2008.04.007
- Vaucheret, H., Vazquez, F., Crété, P., and Bartel, D. P. (2004). The action of ARGONAUTE1 in the miRNA pathway and its regulation by the miRNA pathway are crucial for plant development. *Genes Dev.* 18 (10), 1187–1197. doi: 10.1101/gad.1201404
- Vogel, J. P., Garvin, D. F., Leong, M. O., and Hayden, D. M. (2006). Agrobacterium-mediated transformation and inbred line development in the model grass Brachypodium distachyon. *Plant Cell Tissue Organ Culture* 84, 199–211. doi: 10.1007/s11240-005-9023-9

- Wang, B., Sun, Y., Song, N., Zhao, M., Liu, R., Feng, H., et al. (2017b). Puccinia striiformis f. sp. tritici microRNA-like RNA 1 (Pst-milR1), an important pathogenicity factor of Pst, impairs wheat resistance to Pst by suppressing the wheat pathogenesis-related 2 gene. *New Phytol.* 215 (1), 338–350. doi: 10.1111/nph.14577
- Wang, H.-L. V., Dinwiddie, B. L., Lee, H., and Chekanova, J. A. (2015). Stress-induced endogenous siRNAs targeting regulatory intron sequences in *Brachypodium*. *RNA (New York, N.Y.)* 21 (2), 145–163. doi: 10.1261/rna.047662.114
- Wang, M., Weiberg, A., Dellota, E., Yamane, D., and Jin, H. (2017a). Botrytis small RNA Bc-siR37 suppresses plant defense genes by cross-kingdom RNAi. *RNA Biol.* 14 (4), 421–428. doi: 10.1080/15476286.2017.1291112
- Wang, M., Weiberg, A., Lin, F.-M., Thomma, B. P. H. J., Huang, H.-D., and Jin, H. (2016). Bidirectional cross-kingdom RNAi and fungal uptake of external RNAs confer plant protection. *Nat. Plants* 2, 16151. doi: 10.1038/nplants.2016.151
- Wang, Y., Juranek, S., Li, H., Sheng, G., Wardle, G. S., Tuschl, T., et al. (2009). Nucleation, propagation and cleavage of target RNAs in Ago silencing complexes. *Nature* 461, 754. doi: 10.1038/nature08434
- Waterhouse, A., Bertoni, M., Bienert, S., Studer, G., Tauriello, G., Gumienny, R., et al. (2018). SWISS-MODEL: homology modelling of protein structures and complexes. *Nucleic Acids Res.* 46 (W1), W296–W303. doi: 10.1093/nar/gky427
- Weiberg, A., Wang, M., Lin, F.-M., Zhao, H., Zhang, Z., Kaloshian, I., et al. (2013). Fungal small RNAs suppress plant immunity by hijacking host RNA interference pathways. *Science* 342 (6154), 118 LP–118123. doi: 10.1126/science.1239705
- Willkomm, S., Zander, A., Gust, A., and Grohmann, D. (2015). A prokaryotic twist on argonaute function. *Life (Basel, Switzerland)* 5 (1), 538–553. doi: 10.3390/life5010538
- Wilson, R. C., and Doudna, J. A. (2013). Molecular mechanisms of RNA interference. *Annu. Rev. Biophys.* 42, 217–239. doi: 10.1146/annurev-biophys-083012-130404
- Winter, D., Vinegar, B., Nahal, H., Ammar, R., Wilson, G. V., and Provart, N. J. (2007). An “Electronic Fluorescent Pictograph” browser for exploring and analyzing large-scale biological data sets. *PLoS One* 2 (8), e718. doi: 10.1371/journal.pone.0000718
- Wu, J., Yang, Z., Wang, Y., Zheng, L., Ye, R., Ji, Y., et al. (2015). Viral-inducible Argonaute18 confers broad-spectrum virus resistance in rice by sequestering a host microRNA. *Elife* 4, e05733. doi: 10.7554/eLife.05733
- Xie, Z., Johansen, L. K., Gustafson, A. M., Kasschau, K. D., Lellis, A. D., Zilberman, D., et al. (2004). Genetic and functional diversification of small RNA pathways in plants. *PLOS Biol.* 2 (5), e104. doi: 10.1371/journal.pbio.0020104
- Yang, Y., and Zhou, Y. (2008). Specific interactions for ab initio folding of protein terminal regions with secondary structures. *Proteins Struct. Funct. Bioinf.* 72 (2), 793–803. doi: 10.1002/prot.21968
- You, C., Cui, J., Wang, H., Qi, X., Kuo, L.-Y., Ma, H., et al. (2017). Conservation and divergence of small RNA pathways and microRNAs in land plants. *Genome Biol.* 18, 158. doi: 10.1186/s13059-017-1291-2
- Zha, X., Xia, Q., and Adam Yuan, Y. (2012). Structural insights into small RNA sorting and mRNA target binding by Arabidopsis argonaute mid domains. *FEBS Lett.* 586 (19), 3200–3207. doi: 10.1016/j.febslet.2012.06.038
- Zhang, H., Kolb, F. A., Jaskiewicz, L., Westhof, E., and Filipowicz, W. (2004). Single processing center models for human dicer and bacterial RNase III. *Cell* 118 (1), 57–68. doi: 10.1016/j.cell.2004.06.017
- Zhang, H., Xia, R., Meyers, B. C., and Walbot, V. (2015). Evolution, functions, and mysteries of plant ARGONAUTE proteins. *Curr. Opin. Plant Biol.* 27, 84–90. doi: 10.1016/j.pbi.2015.06.011
- Zhang, T., Zhao, Y.-L., Zhao, J.-H., Wang, S., Jin, Y., Chen, Z.-Q., et al. (2016). Cotton plants export microRNAs to inhibit virulence gene expression in a fungal pathogen. *Nat. Plants* 2, 16153. doi: 10.1038/nplants.2016.153
- Zhang, X., Niu, D., Carbonell, A., Wang, A., Lee, A., Tun, V., et al. (2014). ARGONAUTE PIWI domain and microRNA duplex structure regulate small RNA sorting in Arabidopsis. *Nat. Commun.* 5, 5468. doi: 10.1038/ncomms6468
- Zheng, X., Zhu, J., Kapoor, A., and Zhu, J. (2007). Role of Arabidopsis AGO6 in siRNA accumulation, DNA methylation and transcriptional gene silencing. *EMBO J.* 26 (6), 1691 LP–1701. doi: 10.1038/sj.emboj.7601603
- Zhu, H., Hu, F., Wang, R., Zhou, X., Sze, S.-H., Liou, L. W., et al. (2011). Arabidopsis Argonaute10 specifically sequesters miR166/165 to regulate shoot apical meristem development. *Cell* 145 (2), 242–256. doi: 10.1016/j.cell.2011.03.024
- Zilberman, D., Cao, X., and Jacobsen, S. E. (2003). ARGONAUTE4 control of locus-specific siRNA accumulation and DNA and histone methylation. *Science* 2995607, 716 LP–716719. doi: 10.1126/science.1079695

**Conflict of Interest:** The authors declare that the research was conducted in the absence of any commercial or financial relationships that could be construed as a potential conflict of interest.

Copyright © 2019 Šečić, Zanini and Kogel. This is an open-access article distributed under the terms of the Creative Commons Attribution License (CC BY). The use, distribution or reproduction in other forums is permitted, provided the original author(s) and the copyright owner(s) are credited and that the original publication in this journal is cited, in accordance with accepted academic practice. No use, distribution or reproduction is permitted which does not comply with these terms.



Article

# Comparative Analysis of Transcriptome and sRNAs Expression Patterns in the *Brachypodium distachyon*—*Magnaporthe oryzae* Pathosystems

Silvia Zanini <sup>1</sup>, Ena Šečić <sup>1</sup> , Tobias Busche <sup>2</sup>, Matteo Galli <sup>1</sup> , Ying Zheng <sup>1</sup> , Jörn Kalinowski <sup>2</sup> and Karl-Heinz Kogel <sup>1,\*</sup>

<sup>1</sup> Institute of Phytopathology, Centre for BioSystems, Land Use and Nutrition, Justus Liebig University (iFZ), 35392 Giessen, Germany; Silvia.F.Zanini@agrar.uni-giessen.de (S.Z.); Ena.Secic@agrar.uni-giessen.de (E.Š.); Matteo.Galli@agrar.uni-giessen.de (M.G.); Ying.Zheng@agrar.uni-giessen.de (Y.Z.)

<sup>2</sup> Center for Biotechnology (CeBiTec), Bielefeld University, 33615 Bielefeld, Germany; tbusche@cebitec.uni-bielefeld.de (T.B.); joern@cebitec.uni-bielefeld.de (J.K.)

\* Correspondence: Karl-Heinz.Kogel@agrar.uni-giessen.de

**Abstract:** The hemibiotrophic fungus *Magnaporthe oryzae* (Mo) is the causative agent of rice blast and can infect aerial and root tissues of a variety of Poaceae, including the model *Brachypodium distachyon* (Bd). To gain insight in gene regulation processes occurring at early disease stages, we comparatively analyzed fungal and plant mRNA and sRNA expression in leaves and roots. A total of 310 Mo genes were detected consistently and differentially expressed in both leaves and roots. Contrary to Mo, only minor overlaps were observed in plant differentially expressed genes (DEGs), with 233 Bd-DEGs in infected leaves at 2 days post inoculation (DPI), compared to 4978 at 4 DPI, and 138 in infected roots. sRNA sequencing revealed a broad spectrum of Mo-sRNAs that accumulated in infected tissues, including candidates predicted to target Bd mRNAs. Conversely, we identified a subset of potential Bd-sRNAs directed against fungal cell wall components, virulence genes and transcription factors. We also show a requirement of operable RNAi genes from the DICER-like (DCL) and ARGONAUTE (AGO) families for fungal virulence. Overall, our work elucidates the extensive reprogramming of transcriptomes and sRNAs in both plant host (Bd) and fungal pathogen (Mo), further corroborating the critical role played by sRNA species in the establishment of the interaction and its outcome.

**Keywords:** argonaute; dicer; RNAi; plant disease; small RNA; virulence; gene expression



**Citation:** Zanini, S.; Šečić, E.; Busche, T.; Galli, M.; Zheng, Y.; Kalinowski, J.; Kogel, K.-H. Comparative Analysis of Transcriptome and sRNAs Expression Patterns in the *Brachypodium distachyon*—*Magnaporthe oryzae* Pathosystems. *Int. J. Mol. Sci.* **2021**, *22*, 650. <https://doi.org/10.3390/ijms22020650>

Received: 14 December 2020

Accepted: 1 January 2021

Published: 11 January 2021

**Publisher's Note:** MDPI stays neutral with regard to jurisdictional claims in published maps and institutional affiliations.



**Copyright:** © 2021 by the authors. Licensee MDPI, Basel, Switzerland. This article is an open access article distributed under the terms and conditions of the Creative Commons Attribution (CC BY) license (<https://creativecommons.org/licenses/by/4.0/>).

## 1. Introduction

The ascomycete fungus *Magnaporthe oryzae* (Mo) (anamorph: *Pyricularia grisea*) is the causal agent of rice blast, one of the most devastating and widespread diseases of cultivated rice, reducing yields up to 30% annually [1–3]. Members of the *Magnaporthe* genus can also infect a variety of other cereals, including barley, rye and wheat, making Mo a major threat to global food security [4,5]. Currently, blast management strategies rely on a combination of fungicide applications (e.g., azoles), development of resistant cultivars, and agronomic practices such as removal of crop residues, water management and crop/land rotation [6,7].

In the early stage of foliar infection Mo behaves as a biotroph, forming a biotrophic interfacial complex (BIC) between the primary invasive hyphae (derived from the penetration peg) and the infected host cell, where it secretes small molecules (effectors) to modulate the interaction [8,9]. Subsequently the fungus forms secondary hyphae and spreads to neighboring cells, undertaking a lifestyle change switching to a necrotrophic growth, with the appearance of the characteristic blast lesions on leaves [5]. Mo is able to infect all aerial parts of rice including nodes, panicles and necks, and has been shown to produce necrotic lesions on both rice and barley roots, although its lifestyle in roots seems to depend on the inoculation method [4,10]. Mo infections have also been established

in *Brachypodium distachyon* (Bd), which has been proposed as a model for cereals as it is preferable for research over more complex crops such as wheat and barley [11,12]. Bd has a smaller genome (272 Mb in Bd21-3 v1.0 assembly) with low genome complexity, a short life cycle, simple growth requirements and a vast T-DNA insertion library available [13–15].

Small RNAs (sRNAs), such as small interfering RNAs (siRNAs) and micro RNA (miRNAs), are systemic signals that modulate distal gene regulation and epigenetic events in response to biotic and abiotic environmental cues in plants [16–18]. Particularly, sRNA-mediated gene silencing is one of the main defense mechanisms against viral attack and genome damaging effects of transposons. The action of sRNAs rests upon their role in RNA interference (RNAi), a conserved mechanism of gene regulation in eukaryotes at the transcriptional (TGS or transcriptional gene silencing) and post-transcriptional (PTGS or post-transcriptional gene silencing) levels [19–21]. In plants, the trigger for RNAi is either endogenous or exogenous (e.g., viral) double-stranded RNA (dsRNA) or hairpin RNA (hpRNA) that is processed into short 20 to 24 nucleotide (nt) double-stranded sRNAs by DICER-like (DCL) enzymes [22,23]. These sRNAs are incorporated into an RNA-induced silencing complex (RISC), containing an RNase III-type endonucleolytic ARGONAUTE (AGO) protein to target complementary RNAs for degradation/inhibition or epigenetic modification by RNA-dependent DNA methylation (RdDM), histone modification and chromatin remodeling. Additionally, secondary sRNAs are generated in plants by RNA-dependent RNA polymerases (RdRPs) [21,24].

The genome of Mo encodes a complete RNAi machinery, comprised of two *DCL* genes, three *AGO* genes and three *RdRP* genes [25–27]. Knock-out (KO) of RNAi pathway components severely affected sRNA production in axenic culture, with deletion of *MoDCL2*, *MoRdRP2* and *MoAGO3* genes reducing sRNA expression levels. In particular, *MoDCL2*, but not *MoDCL1*, was necessary for siRNA production from dsRNA precursor molecules [27]. Of note, loss of *MoAGO3* and *MoRdRP1* function reduced both sRNAs and fungal virulence on barley leaves. sRNA-mediated alterations of TGS and PTGS have been detected *in vitro* both during starvation/different nutrient availability, and *in planta* during different stages of rice leaf infection [27]. Additionally, Mo sRNAs differentially accumulate in mycelia and appressoria [28], further supporting the notion that sRNAs regulate Mo's development, growth and virulence. Similar to Mo, the formation of endogenous sRNAs in Bd is also subject to changes in response to external factors, where miRNAs have been proven to vary during exposure to abiotic stress and between vegetative vs. reproductive tissues [29], pointing to operable RNAi-based regulatory mechanisms in the model grass [30]. A total of 328 Bd miRNA precursor sequences have been identified so far and deposited in the miRBase database, corresponding to 536 mature miRNAs with predicted regulatory functions in cold [31], heat [32] and drought stress [33] and morphological alterations [34]. While knowledge about the RNAi machinery of Bd is not comprehensive and there is currently no data on RNAi KO mutants available from this organism, our recent work characterized the major RNAi genes *in silico*, resulting in 16 BdAGO-like and six BdDCL candidates [35]. Thus, the study showed that the RNAi machinery follows the trend that cereals have extended families of key enzymes involved in RNAi.

Consistent with the exchange of RNAs during animal-parasitic interactions [36–38], sRNAs are also exchanged in host plant–pathogen interactions. The plant–pathogenic fungus *Verticillium dahliae* (Vd) accumulated plant miRNAs when recovered from infected cotton samples, indicating that host-derived sRNAs were transmitted into the pathogen during infection [39]. Two of those cotton miRNAs, miR166 and miR159, target the fungal genes *Ca2+-dependent cysteine protease calpain* (*VdClp-1*) and *isotricondromin C-15 hydroxylase* (*VdHiC-15*), respectively, which are known to contribute to fungal virulence. Similarly, *Arabidopsis* cells secrete vesicles to deliver sRNAs into grey mold fungal pathogen *Botrytis cinerea* (Bc), where they cause silencing of fungal genes critical for pathogenicity [40]. Consistent with the bidirectional move of sRNAs in plant-microbe interactions, Bc also produces sRNA effectors that downregulate *Arabidopsis* and tomato genes involved in

immunity [41]. Some of these sRNAs, for example Bc-siR37, downregulate a large set of host immunity genes to enhance Bc pathogenicity [42].

Here we investigate the induction of sRNAs and transcriptome changes in the early stages of interaction of Bd and Mo based on data generated by parallel sequencing of sRNA and mRNA from infected leaf and root tissues. Using a previously published bioinformatics pipeline to characterize sRNA and its targets [43], we predict potential sRNA effectors whose targets were downregulated in the respective recipient organism.

## 2. Results

### 2.1. Requirement for Functional RNAi Genes in the Interaction of *Brachypodium distachyon* Bd21-3 and *Magnaporthe oryzae* 70-15

The *Magnaporthe oryzae* (Mo) 70-15 genome encodes three putative AGO and two DCL proteins, previously identified by domain search and phylogeny with known *Neurospora crassa* (Nc) RNAi machinery genes [25–27]. The corresponding protein sequences were obtained from NCBI: XP\_003714515.1 (MGG\_01541T0, MoDCL1), XP\_003715365.1 (MGG\_12357T0, MoDCL2), XP\_003716704.1 (MGG\_14873T0, MoAGO1), XP\_003717504.1 (MGG\_13617T0, MoAGO2) and XP\_003714217.1 (MGG\_01294T0, MoAGO3); they were included in new phylogenetic trees to corroborate previous findings (Figure S1A,B). To assess the conservation of key AGO and DCL domains, prediction was carried out with Simple Modular Architecture Research Tool (SMART). All three AGOs have conserved domain structures with five characteristic domains: N-terminal domain, DUF1785, PAZ (Piwi Argonaut and Zwillig), L2 and PIWI (P-element Induced Wimpy testis) (Figure S1C; Table S1). Additionally, multiple sequence alignment (MSA) confirmed the conservation of the DEDD catalytic tetrad (Asp/Glu/Asp/Asp) and the QF-V motif (Glu/Phe/Val) in the MoAGO PIWI domains (Figure S2). Likewise, both MoDCLs have the four conserved domains required for the cleavage of dsRNAs: DEXDc, HELICc, dicer-dimer and RIBOc (Figure S1D; Table S1). Subcellular localization of MoAGOs and MoDCLs was assessed using PSI-predictor; MoDCL1, MoAGO1 and MoAGO3 were predicted to primarily localize in the nucleus, while MoDCL2 and MoAGO2 were predicted to primarily localize in the cytosol. MoAGO1 and MoAGO2 also had secondary predicted localizations, the first in the cytosol and the second in plastids (Table S2).

Protein interaction analysis with STRING did not highlight any experimentally proven interaction for MoAGO and MoDCL proteins, but probable interactions could be inferred from data derived from homologs, found to either interact or co-express with several proteins in other species (Table S3A,B). In particular, all MoAGOs were predicted to interact with the two MoDCL proteins, a U5 small nuclear ribonucleoprotein component (MGG\_13500) and a cell cycle control protein cwf14 (MGG\_06309). For MoAGO1, additional interaction was predicted with Pumilio-family RNA-binding repeat protein (MGG\_03158), ATP-dependent RNA helicase DED1 (MGG\_02762), high-affinity glucose transporter (MGG\_13651) and four uncharacterized proteins. In addition to interaction with AGO proteins, both fungal MoDCLs were predicted to interact with ATP-dependent DNA helicase MPH1 (MGG\_04429), 30S ribosomal protein S16 (MGG\_02598), WD domain-containing protein (MGG\_06727) and three uncharacterized proteins.

3D protein structure modeling for both MoDCL and MoAGO was performed with SWISS-MODEL. While no acceptable QMEAN Z-scores ( $>-4$ ) values were obtained for the two DCLs and AGO2 models due to the lack of suitable reference structures, two models for AGO1 (model 1 based on hAGO1, GMQE = 0.52 QMEAN =  $-3.98$  and model 3, based on hAGO2, GMQE = 0.51 QMEAN =  $-3.31$ ) and model 6 for AGO3 (based on hAGO4 template, GMQE = 0.46 QMEAN =  $-3.50$ ) passed the first quality check and were further validated with PROCHECK and WHATCHECK. Model 1 of AGO1 had a higher percentage of residues in the core region of the Ramachandran plot (88.4%) and a better Ramachandran Z-score ( $-1.808$ ) compared to model 3 (87.6% and  $-1.531$  Z-score), while the AGO3 model scored 86.7% and  $-2.088$ , respectively. As a result, model 1 of AGO1 and model 6 of AGO3 were selected as the best models and visualized with PyMOL (Figure 1A,B).

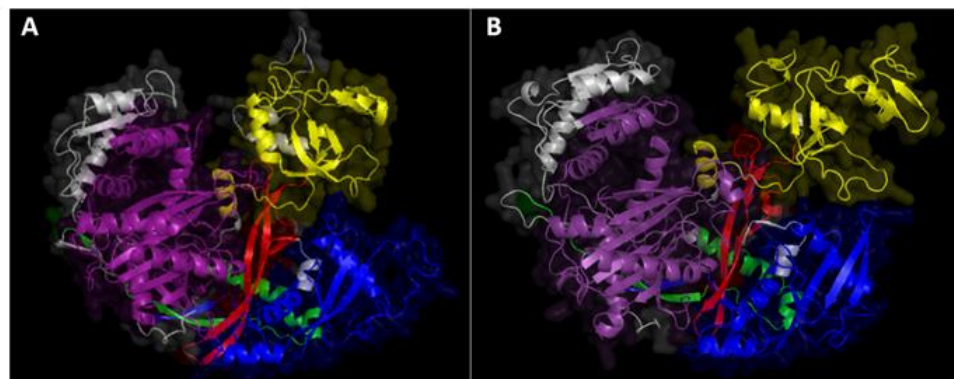


**Figure 1.** Predicted 3D structures of (A) *M. oryzae* MoAGO1 and (B) MoAGO3. Structures were modeled with SWISS-MODEL and domains were highlighted with PyMOL: blue = N-domain, red = DUF1785, yellow = PAZ (Piwi Argonaut and Zwiller), green = L2, purple = PIWI (P-element Induced WImpy testis), the rest of the sequence with no domain predicted is colored in grey.

Next, we assessed the virulence of  $\Delta moago1$ ,  $\Delta moago2$ ,  $\Delta modcl1$ ,  $\Delta modcl2$  and the double mutant  $\Delta modcl1/2$  using Bd21-3 as a host. Negative effects on vitality of the five mutants vs. Mo wildtype (wt) could not be detected when inspecting conidia germination and appressorium formation on poly-L-lysine coated glass slides by 24 h after the onset of germination (Figure S3). In contrast, virulence of these mutants was compromised both on Bd leaves and roots (Figure S4). Since we expected differences in infection phenotypes depending on test conditions, three different leaf inoculation protocols were tested: (i.) upon drop inoculation of detached leaves all mutants showed significant (Kruskal–Wallis test,  $p < 0.05$ ) reduction in necrotic lesion size, ranging from a  $-20\%$  to  $-48\%$  reduction of relative necrotic area compared to Mo wt ( $\Delta moago1$   $-48\%$ ;  $\Delta moago2$   $-32\%$ ;  $\Delta modcl1$   $-39\%$ ;  $\Delta modcl2$   $-24\%$ ;  $\Delta modcl1/2$   $-20\%$ ; Figure 2A); (ii.) upon spray inoculation of detached leaves, virulence of  $\Delta moago1$  and  $\Delta modcl1$  was virtually unaffected as they showed the typical necrotic lesions at 5 days post inoculation (DPI), compared to  $\Delta moago2$ ,  $\Delta modcl2$  and  $\Delta modcl1/2$ , showing significantly reduced necrotic lesion areas (compared to Mo wt:  $\Delta moago2$   $-40\%$ ;  $\Delta modcl2$   $-83\%$ ;  $\Delta modcl1/2$   $-68\%$  necrotic lesion sizes; Figure 2B); (iii.) similar phenotypes were observed in the whole seedling spray assay, with the exception of  $\Delta modcl2$  and  $\Delta modcl1/2$  that appeared avirulent and did not show any detectable lesions (reduction in the necrotic lesion size compared to Mo wt:  $\Delta moago2$   $-79\%$ ;  $\Delta modcl2$   $-100\%$ ;  $\Delta modcl1/2$   $-100\%$ ; Figure 2C). Finally, mutants were inoculated on Bd roots and fungal presence was measured at 5 DPI by qPCR based on the fungal actin. All mutants showed a significant reduction in fungal biomass, with  $\Delta moago2$ ,  $\Delta modcl2$  and  $\Delta modcl1/2$  being the most severely affected (reduction in MoActin levels compared to wt:  $\Delta moago1$   $-70\%$ ;  $\Delta moago2$   $-78\%$ ;  $\Delta modcl1$   $-47\%$ ;  $\Delta modcl2$   $-87\%$ ;  $\Delta modcl1/2$   $-87\%$ ; Figure 2D). These results confirm and extend previous findings that Mo's RNAi machinery is required for disease development in cereals and, in particular, that DCL2 is a key factor not only for sRNA biogenesis but also for fungal virulence.

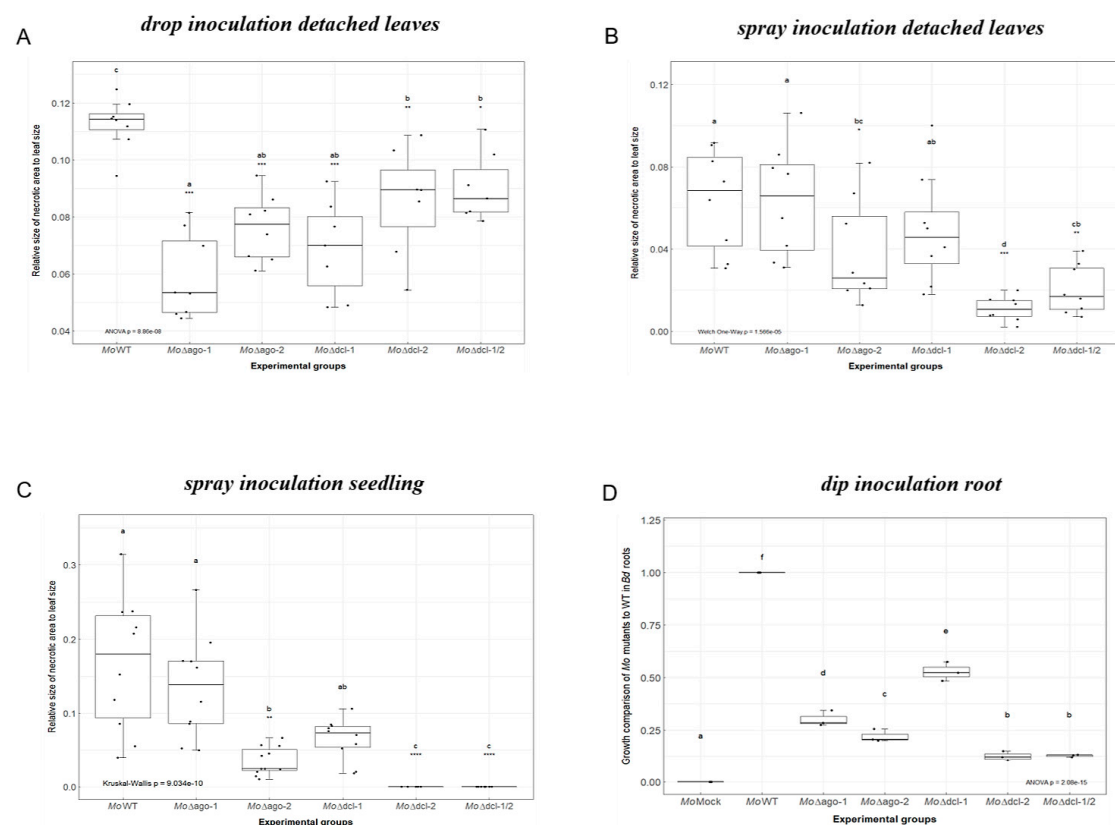


**Figure 2.** Infection assays of *M. oryzae* RNAi mutants. **(A)** Detached second youngest leaves of three-week-old Bd seedlings were drop inoculated with 10  $\mu$ L Mo conidia suspension  $50 \times 10^3$  spores  $\text{mL}^{-1}$  in 0.002% Tween20 and kept under high humidity at 16 h light/8 h dark cycle at 22 °C/18 °C. Fungal pathogenicity was assayed via ImageJ software at 5 DPI. The experiment was conducted two times ( $n = 8$  plants per experimental group) with similar results. Comparisons between groups was performed via ANOVA and Tukey's range test for multiple comparisons. **(B)** Detached Bd leaves were spray inoculated with a total of 250  $\mu$ L Mo conidia suspension  $50 \times 10^3$  spores  $\text{mL}^{-1}$  in 0.002% Tween20 and kept and evaluated as in (A). The experiment was conducted two times ( $n = 8$  plants per experimental group) with similar results. Comparisons between groups was performed via Welch one-way test coupled with pairwise t-tests with Benjamini–Hochberg  $p$ -value adjustment. **(C)** Three-week-old Bd seedlings were spray inoculated with Mo conidia suspension  $120 \times 10^3$  spores  $\text{mL}^{-1}$  in 0.002% Tween20 and kept and evaluated as in (A). The experiment was conducted two times ( $n = 18$  plants per experimental group) with similar results. Comparisons between groups was performed via Kruskal–Wallis test and Dunn's test of multiple comparisons. **(D)** Roots of seven-day-old Bd seedlings were inoculated with 1 mL of Mo conidia suspension  $125 \times 10^3$  spores  $\text{mL}^{-1}$  in 0.002% Tween20 for 3 h. Afterwards, seedlings were transplanted in small pots (3 cm  $\varnothing$ ) and grown for an additional 5 days before harvesting. Fungal amount was calculated by qPCR based on the ratio of fungal actin (*MoActin*). The experiment was conducted two times ( $n = 6$  roots per experimental group) with similar results. Comparisons between groups was performed via ANOVA and Tukey's range test for multiple comparisons. **(A–D)** Letters represent statistical difference among all groups' means ( $\alpha < 0.05$ ). Asterisks represent statistical difference of each group against wildtype (wt) (\*  $p < 0.05$ ; \*\*  $p < 0.01$ ; \*\*\*  $p < 0.001$ ; \*\*\*\*  $p < 0.0001$ ).

## 2.2. Differentially Expressed Genes (DEGs) in the Early Stages of Leaf and Root Infections

TruSeq® Stranded mRNA libraries were produced from (i.) Mo axenic culture, (ii.) Mo-infected and mock-treated Bd roots (4 DPI) and (iii.) Mo-infected and mock-treated Bd leaves (2 DPI and 4 DPI) (Figure 3). These early time points were chosen to assess gene expression patterns both in the foliar biotrophic and necrotrophic growth phase of hemibiotrophic Mo [5]. mRNAseq analysis revealed a total of 233 Bd-DEGs (Wald test, Benjamini–Hochberg (BH) adjustment, adjusted  $p$ -value (padj)  $< 0.05$ ) in leaves at 2 DPI (224 upregulated and 9 downregulated), compared to 4978 at 4 DPI (3023 upregulated and 1955 downregulated) and 128 in roots (89 upregulated and 39 downregulated) (Figure 4; Table 1; Figure S5).

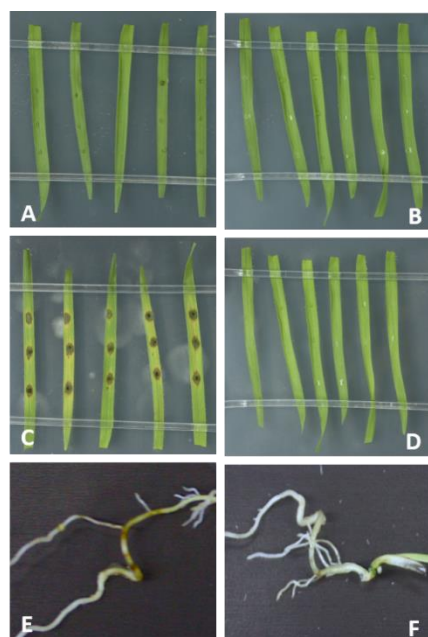


**Figure 3.** Brachypodium blast caused by *M. oryzae* Mo 70-15 on leaves and roots of *B. distachyon* Bd21-3. (A,D) Detached 21-day-old Bd leaves were drop-inoculated with 10  $\mu$ L of Mo suspension (50,000 conidia/mL) and kept for (A) 2 and (C) 4 days at high humidity, or mock-inoculated (B,D) with Tween water. Roots of 7-day-old Bd seedlings were (E) drop-inoculated with 1 mL of Mo suspension (250,000 conidia/mL) or (F) mock-inoculated or and kept for 4 days under high humidity at 16 h light/8 h dark cycle at 22 °C/18 °C.

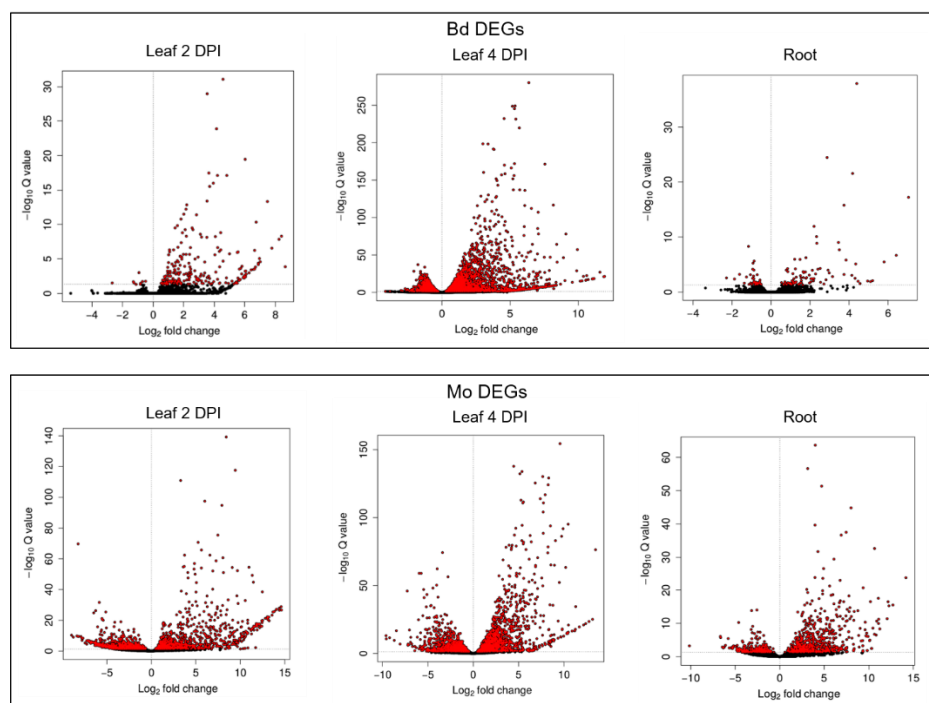


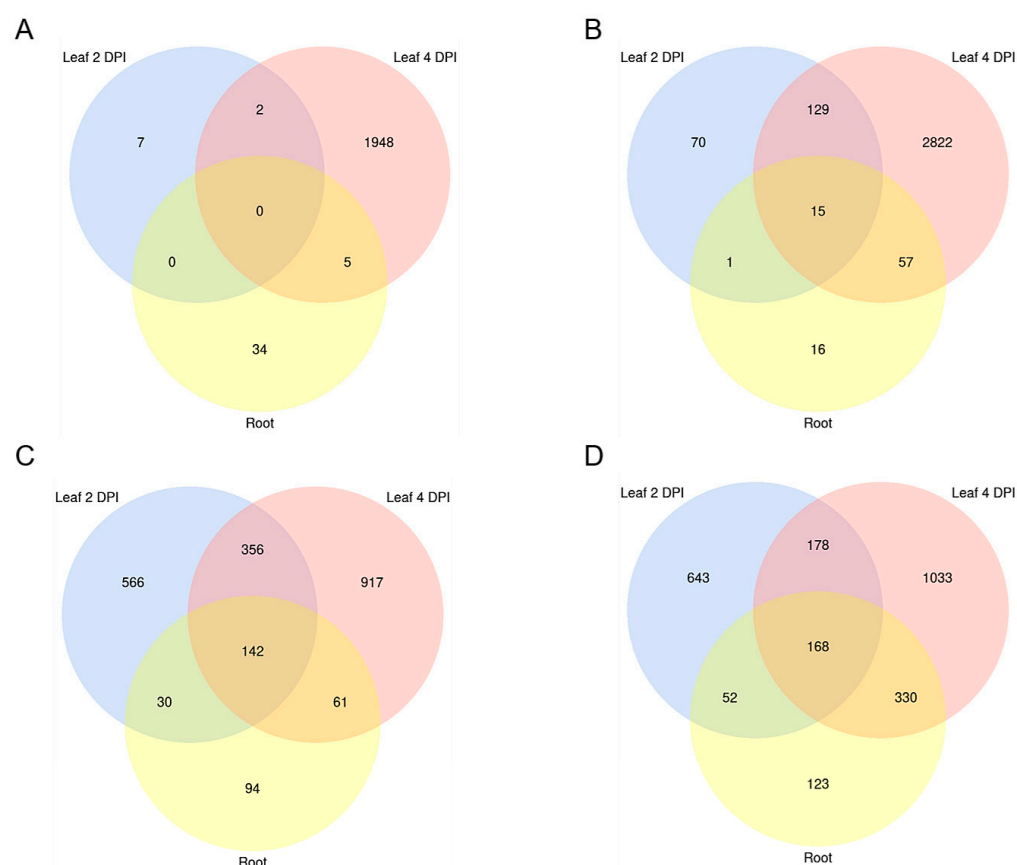
**Figure 4.** Volcano plots of DESeq2 results based on mRNAseq analysis of *M. oryzae*-infected leaves and roots of *B. distachyon* vs. control. Differentially expressed genes (DEGs) are highlighted in red with significant adjusted  $p$ -values ( $padj < 0.05$ ).

**Table 1.** Total numbers of significantly ( $\text{padj} < 0.05$ ) upregulated or downregulated genes in the *B. distachyon*–*M. oryzae* interaction.

Setup	Total Mo Genes (Up)	Total Mo Genes (Down)	Total Bd Genes (Up)	Total Bd Genes (Down)
Leaf 2 DPI	1041	1094	224	9
Leaf 4 DPI	1710	1476	3023	1955
Root	673	327	89	39

Overview of DESeq2 results. DESeq2 test for differential expression based on negative binomial distribution. Abbreviation: DPI = days post inoculation.

Minor overlaps were observed comparing downregulated Bd genes between the biological setups, with only two shared between the foliar infections, and five between the leaf (4 DPI) and the root setup (Figure 5A). Among the upregulated genes, the highest overlap was seen between the foliar infections, sharing 134 DEGs, compared to 16 DEGs shared between root and leaf 2 DPI, and 72 between root and leaf 4 DPI (Figure 5B). Interestingly, 15 Bd genes were upregulated in all setups, including defense-related *ABC transporter* (BdiBd21-3.3G0465100.1), *anthranilate synthase component II* (BdiBd21-3.5G0159100.1), *protein kinase xa21* (BdiBd21-3.3G0144800.1) and *secologanin synthase-like* (BdiBd21-3.2G0563800.1) (Table 2).

**Figure 5.** Venn diagram of differentially expressed *B. distachyon* and *M. oryzae* genes. Significantly (A) downregulated (fold change (FC)  $< 0$   $\text{padj} < 0.05$ ) and (B) upregulated (FC  $> 0$   $\text{padj} < 0.05$ ) Bd genes shared between setups. Significantly (C) downregulated (FC  $< 0$   $\text{padj} < 0.05$ ) and (D) upregulated (FC  $> 0$   $\text{padj} < 0.05$ ) Mo genes shared between setups (“Leaf 2 DPI”, “Leaf 4 DPI” and “Root”). Transcript downregulation was calculated from mRNAseq data with DESeq2.

**Table 2.** Selected defense-related Bd DEGs ( $\text{padj} < 0.05$ ) during infection of leaves and roots by *M. oryzae*.

Gene	Description	Log <sub>2</sub> FC- Leaf 2 DPI	Log <sub>2</sub> FC- Leaf 4 DPI	Log <sub>2</sub> FC- Root
BdiBd21-3.3G0465100	ABC transporter a family member 2-like	1.15	3.38	0.79
BdiBd21-3.3G0464900	ABC transporter a family member 7-like		2.64	0.71
BdiBd21-3.2G0605400	ABC transporter b family member 4-like	2.15	5.08	
BdiBd21-3.2G0550500	Pleiotropic drug resistance protein 3-like	1.78	6.82	1.51
BdiBd21-3.5G0159100	Anthranilate synthase component ii	0.76	2.75	0.88
BdiBd21-3.3G0344500	Chitinase 1		2.70	
BdiBd21-3.2G0371800	Cytochrome p450 71c4		1.32	2.12
BdiBd21-3.1G0952300	Disease resistance response		2.07	
BdiBd21-3.3G0144800	Protein kinase xa21	1.77	2.41	1.24
BdiBd21-3.2G0545400	LRR receptor-like serine threonine-protein kinase gso1		1.59	1.79
BdiBd21-3.2G0632400	Receptor-like protein kinase hsl1-like		3.15	
BdiBd21-3.1G0713100	Proton-coupled amino acid transporter 3-like	0.85	1.97	0.97
BdiBd21-3.2G0114800	Pathogenesis related protein	1.34	1.25	
BdiBd21-3.1G0165000	Pathogenesis-related protein 1	6.06	8.19	
BdiBd21-3.4G0068000	Pathogenesis-related protein 10		3.47	3.75
BdiBd21-3.4G0043000	Pathogenesis-related protein 5		2.91	
BdiBd21-3.1G0772600	Pathogenesis-related protein class i		5.29	4.47
BdiBd21-3.1G0772700	Pathogenesis-related protein prb1-2-like		3.41	6.42
BdiBd21-3.3G0422200	PR3-like 1		2.63	
BdiBd21-3.3G0639500	PR3-like 2		3.96	
BdiBd21-3.4G0025400	PR5-like		1.37	
BdiBd21-3.2G0600500	PR5-like		2.28	
BdiBd21-3.1G0875700	Pathogenesis-related protein Bet v I family		2.14	
BdiBd21-3.1G0054700	NAC1 transcription factor		2.49	
BdiBd21-3.3G0652700	MYB-related protein myb4-like		3.33	
BdiBd21-3.2G0688100	Probable WRKY transcription factor 33-like		2.69	
BdiBd21-3.2G0615100	Probable WRKY transcription factor 51-like	1.45	3.44	
BdiBd21-3.3G0669400	Ethylene-responsive transcription factor 1a		2.16	
BdiBd21-3.4G0171000	Multicopper oxidase family expressed	4.35	9.93	2.35
BdiBd21-3.4G0387000	Cationic peroxidase spc4-like	3.17	3.72	
BdiBd21-3.1G0233900	Peroxidase		2.11	
BdiBd21-3.2G0563800	Secologanin synthase-like	0.57	0.54	1.08

In total, we found 2135 Mo DEGs (Wald test, Benjamini–Hochberg adjustment,  $\text{padj} < 0.05$ ) in leaves at 2 DPI (1041 up and 1094 down), 3186 DEGs at 4 DPI (1710 up and 1476 down) and 1000 DEGs in infected roots (673 up and 327 down) (Figure 4; Table 1; Figure S5). A notable overlap of fungal DEGs was detected between the two foliar infections, with 346 up- and 498 downregulated genes shared, compared to 220 up- and 172 downregulated DEGs shared between leaf 2 DPI and root infection, and 498 up- and 203 downregulated DEGs shared between leaf 4 DPI and root infection. Overall, 142 genes were significantly downregulated in all setups, while 168 were consistently upregulated in all

samples, including genes involved in fungal development, metabolism and pathogenicity (Figure 5C,D).

Expression of *DCL* and *AGO* genes was assessed in both organisms in leaves and roots, which showed that *BdDCL1* and *MoDCL2* had the highest expression among the *DCL* family, and *BdAGO3* and *MoAGO3* among the *AGO* family (Figure 6).

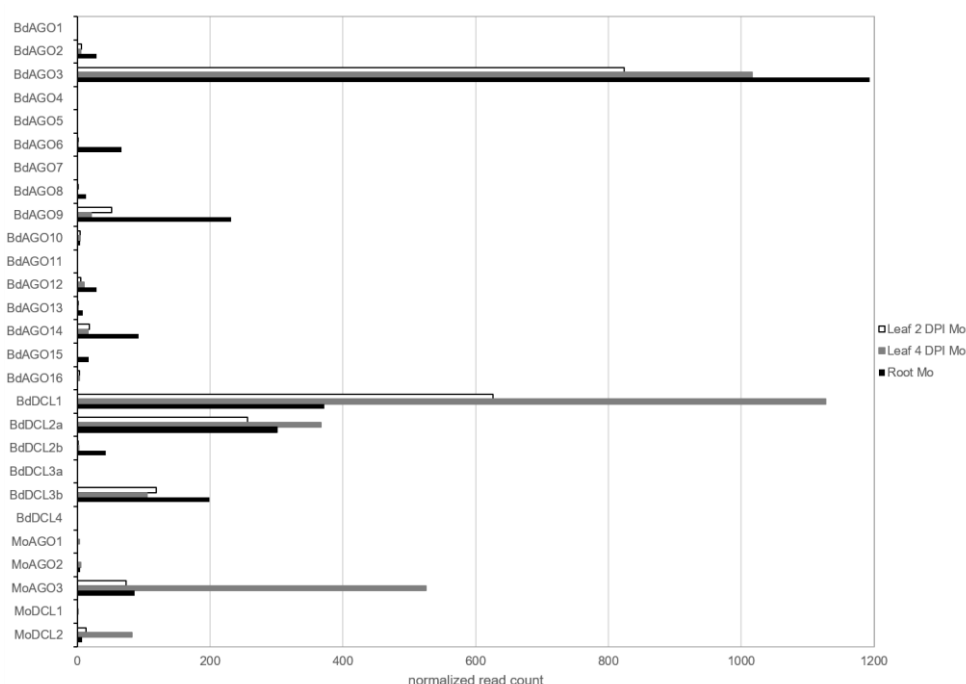


**Figure 6.** Expression of predicted *ARGONAUTE* (*AGO*) and *DICER-like* (*DCL*) during the interaction of *B. distachyon* and *M. oryzae* from mRNAseq results. Normalized read counts of each RNAi component were retrieved from DESeq2 analyses of infected datasets: leaf 2 DPI (white), leaf 4 DPI (grey) and root (black).

Interestingly, *BdAGO9*, which is the closest homolog to *AtAGO1* [35], was detected expressed in all three setups and had the highest read count of the *AtAGO1*-like clade. Moreover, *BdAGO1*, *BdAGO5* and *BdAGO15* were only expressed in the root samples, while *BdAGO4*, *BdAGO7*, *BdAGO11*, *BdDCL3a* and *BdDCL4* were not detected in any of the datasets. Finally, the majority of *DCL* and *AGO* genes were not differentially regulated during the infection, with the exception of *BdDCL3b* and *BdAGO3* (minor downregulation;  $> -1 \log_2FC$ ) and *BdDCL1-2a* and *MoAGO3* (minor upregulation;  $< 1 \log_2FC$ ) (Table S4).

### 2.3. Gene Ontology Enrichment (GOE) and Defense-Related Gene Expression in Mo-Infected Bd

GOE analysis using AgriGO v2 was performed on all *Bd* DEGs identified in leaves and roots by mRNAseq. In all three datasets, GO:0003824 (catalytic activity), GO:0016491 (oxidoreductase activity) and GO:0044710 (single-organism metabolic process) were enriched (Table S5). The highest number of Gene Ontology (GO) terms enrichment—in particular those related to various cellular metabolic processes—was recorded in leaves at 4 DPI, which corresponds to the necrotrophic fungal growth phase (Figure S6). Consistent with the extensive metabolic reprogramming highlighted in the GOE analysis, the highest number of DEGs also was observed in these samples. Specifically, we detected significant upregulation of known *Bd* defense response genes such as *pathogenesis-related 1* (*PR1*), *PR3* and *PR5*, receptor-like protein kinases and *Myb* and *WRKY* transcription factors (Table 2). Only minor overlap was observed between defense-related genes expression patterns in the leaf 2 DPI and root samples. Three predicted PR proteins were upregulated in both 4 DPI and root setups, including *PR10* and *PRB1-2* ( $\log_2FC > 3$  in both, while not induced at

2 DPI) and two were found significantly upregulated in the two foliar datasets, including PR1 (with a  $\log_2FC > 6$  in these datasets and not induced in the roots).

#### 2.4. GOE and Gene Expression in Mo during Bd Infection

Next, significantly up- and downregulated Mo genes were subjected to GOE analysis, showing the highest number of enriched GO terms in the root samples, including several terms relating to the interaction with the host (Table S6; Figure S7). Overall, many infection-related genes were significantly upregulated, including effectors *AVR Pita1* and *PWL2* (*Pathogenicity toward Weeping Lovegrass*) and *NOXs* (*superoxide-generating NADPH oxidases*) (Table 3).

**Table 3.** Selected significantly ( $\text{padj} < 0.05$ ) upregulated pathogenicity-/virulence-related *M. oryzae* genes during *B. distachyon* leaves and roots infection.

Gene Stable ID	Description	Log <sub>2</sub> FC- Leaf 2 DPI	Log <sub>2</sub> FC- Leaf 4 DPI	Log <sub>2</sub> FC- Root
MGG_00750	Cytochrome b-245 heavychain subunit beta	2.23	2.12	2.80
MGG_01081	Peroxin 14/17		1.05	
MGG_01092	Homocitrate synthase	1.35		
MGG_01748	Putative protease		1.28	
MGG_02074	Potassium/sodium efflux P-type ATPase		1.28	2.55
MGG_03356	Ricin B lectin:Parallel beta-helix		7.08	5.06
MGG_04202	MAS3 protein	2.27		2.75
MGG_04212	L-ornithine 5-monooxygenase	2.81	3.46	3.17
MGG_04301	Pwl2 protein (PWL2) gene	8.53		
MGG_04545	Cytochrome c peroxidase, mitochondrial	3.26	0.95	
MGG_06011	S-(Hydroxymethyl)glutathione dehydrogenase		2.53	
MGG_06648	Hsp70 (LHS1) gene	1.25		
MGG_07514	3-oxoacyl-[acyl-carrier-protein] reductase		1.49	
MGG_07971	Calcium-transporting ATPase 1		1.80	
MGG_08315	1-phosphatidylinositol-4,5-bisphosphate phosphodiesterase delta-1	8.83	7.94	
MGG_08409	Cellulose-growth-specific protein		3.78	
MGG_09022	Transmembrane CFEM domain-containing protein	5.41	7.42	7.88
MGG_09559	Autophagy-related protein 9		1.07	
MGG_09956	PRO41 protein	1.93	1.91	2.62
MGG_10097	Intracellular hyphae protein 1	5.42		
MGG_10510	Ribonuclease T2	3.90		
MGG_10730	Potassium/sodium efflux P-type ATPase		4.75	
MGG_11882	Sensor protein zRas		1.60	3.15
MGG_11899	SH3 domain-containing protein	1.93	1.52	
MGG_15370	Metalloproteinase	11.86		
MGG_15972	AVR-pik/pikm/pikp	14.63	6.33	

#### 2.5. sRNA Reprogramming in Bd and Mo at Early Infection Stages

We assessed the expression of sRNAs in the same biological material utilized for mRNAseq. Before high-throughput next generation sequencing (NGS), multiplexed sRNA libraries were size selected for 15 to 35 nt fragments (140–160 nt including TruSeq adapters).

Single end sequencing on Illumina HiSeq1500 platform generated between 22 million (mil) and 38 mil reads each (Table S7). Quality check of raw reads was performed with FastQC, adapters were removed with cutadapt and reads were size selected between 18 to 32 nt. The organism of origin of the trimmed reads was predicted by mapping via Bowtie alignments to both Bd21-3 and Mo 70-15 genomes [44] (Bd21-3 v1.1 DOE-JGI, <http://phytozome.jgi.doe.gov/>). Ambiguous reads that could not be assigned to the organism of origin with high confidence were excluded to avoid miscalling. As expected, most reads in Mo-infected samples were assigned to Bd (with 100% match) and not to the fungus (with at least two nucleotide mismatches) (Table S7). Size distribution of genome matched unique sRNA reads followed a similar trend throughout samples, with the Mo reads showing a minor peak around 20 nt and Bd reads a considerable peak at 24 nt (Figure 7A,B). Fungal unique sRNA reads were then compared among datasets derived from Mo axenic culture and Mo-infected plant tissues and classified as either exclusive or shared between samples (Figure 8A). Some 5708 Mo-sRNAs were identified in Mo-infected roots, of which 3263 (57.15%) were found exclusively in the infected sample and not in the axenic culture. A total of 7215 Mo-sRNAs were identified in infected leaves during the biotrophic phase (2 DPI), of which 4399 (60.97%) were found exclusively in infected samples. Finally, a total of 63,017 were found in infected leaf tissue during the necrotrophic phase (4 DPI), of which 46,212 (73.33%) were exclusively found in infected samples.

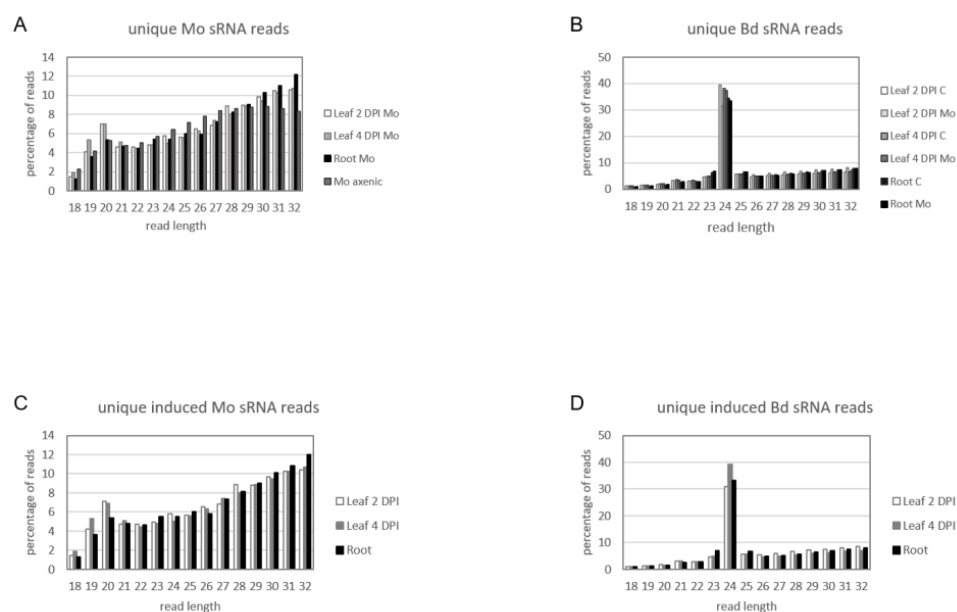


**Figure 7.** Size distribution of unique sRNA reads in the interaction of *M. oryzae* and *B. distachyon*. Relative size distribution (in percentage) of unique filtered sRNA reads assigned to (A) Mo or (B) Bd. Reads were assigned to either Mo or Bd only if aligning 100% to the organism of origin genome and had at least two mismatches to the interacting organism genome. (C,D) Relative size distribution of unique filtered sRNA reads assigned to (C) Mo or (D) Bd and induced or increased in infected samples compared to controls (i.e., axenic fungal cultures and non-inoculated plants, respectively). Samples for sRNA sequencing by Illumina HiSeq1500 were taken from different setups: leaf biotrophic phase (“2 DPI”), leaf necrotrophic phase (“4 DPI”) and root (“root”).

Next, we compared unique Bd-sRNA reads in leaf and root samples from Mo-infected and mock-treated Bd (Figure 8B). A large number of sRNAs were found in infected tissues: 571,644 in leaves at 2 DPI, of which 326,657 (72.24%) were specific for infection; 415,469 at 4 DPI, of which 265,172 (69.06%) were specific for infection; and 597,158 Bd-sRNAs in infected roots, of which 346,259 (77.92%) were specific for infection. These data show that the majority of unique sRNAs of both interacting organisms are expressed exclusively during the interaction, suggesting that they are relevant to the establishment and outcome

of the disease. We further selected unique Bd-sRNAs that (i.) were either found exclusively in infected plant tissues or (ii.) showed higher reads in infected vs. mock-inoculated tissue. Interestingly, the size distribution of these induced Bd-sRNA did not show a change in length preference compared to the total unique reads (Figure 7C,D).

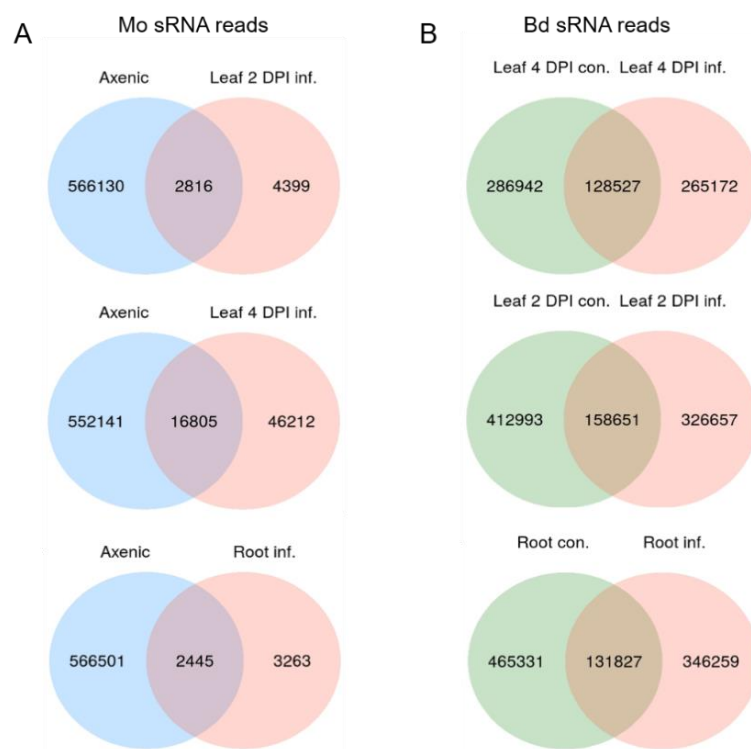


**Figure 8.** Venn diagrams of unique filtered sRNAs reads from *M. oryzae* and *B. distachyon*. (A) Venn diagram of Mo sRNA reads (18–32 nt) from axenic culture and Mo-infected Bd leaves (2 DPI, 4 DPI) and roots (4 DPI). (B) Venn diagram of Bd sRNA reads (18–32 nt) in non-infected and Mo-infected Bd leaves.

## 2.6. Infection-Related Bd miRNAs

Filtered Bd-sRNA reads were analyzed with Shortstack 3.8.5 to identify infection-related upregulation of potential plant miRNAs. The program identified 14 putative miRNA-generating loci in leaves at 2 DPI, 15 at 4 DPI and 16 in the roots. Matching predicted miRNA generating clusters in the uninfected samples were identified via their genomic coordinates, and numbers of total reads per cluster were compared between infected and uninfected samples to select exclusively expressed or upregulated miRNA loci. The selected clusters' sequences were aligned to known Bd miRNA stem loop precursor sequences obtained from the miRBase database: three known miRNAs were upregulated in leaves at 2 DPI, six at 4 DPI and four in the roots (Table 4). Structures of the miRNA precursors are shown in Figure S8.

**Table 4.** *B. distachyon* miRNA identification.

Setup	Cluster Number	miRNA	Cluster RPM	Mature miRNA Name
Leaf 2 DPI	3086	Bdi-miR159b	118.27	miR159b-3p.2
				miR159b-3p.1
	3421	Bdi-MIR531	15.03	MIR531
	6495	Bdi-MIR156b	2.61	miR156b-3p
	7687	Bdi-miR9481b	19.12	miR9481b -5p miR9481b-3p
Leaf 4 DPI	7744	Bdi-MIR156h	13.79	MIR156h-5p
	3312	Bdi-MIR159b	184.31	miR159b-3p.1
				miR159b-3p.2
				miR159b-5p.1
				miR159b-5p.2
	3162	Bdi-MIR171d	0.58	MIR171d-3p
	7470	Bdi-MIR529	30.80	MIR529-5p
	2384	Bdi-miR7723a	13.02	miR7723a-3p
	10592	Bdi-MIR156d	8.31	MIR156d-5p
	8229	Bdi-MIR156i	2.87	MIR156i-5p
				MIR156i -3p
Root	5121	Bdi-MIR168	310.27	MIR168-5p
	9081	Bdi-MIR156d	1.15	miR156d-5p
	4330	bdi-MIR9484	3.90	MIR9484

miRNA-generating clusters were identified with Shortstack in all datasets. Genomic coordinates were used to detect and compare the same loci in infected and control samples, and only clusters exclusive or increased in the infected samples were selected. Clusters and mature miRNAs were compared to known miRNA/miRNA precursor from miRBase. Abbreviation: RPM = reads per million.

## 2.7. In Silico Prediction of Mo-sRNA Targeting *Bd* Transcripts

sRNAs that were either exclusively produced or increased in infected tissues and had a normalized read count of at least five reads per million (RPM) were further investigated. Induced 20–22 nt sRNAs originating from non-coding regions of the Mo 70-15 genome (Figure 9) were selected as candidate cross-kingdom effectors with potential targets in the *Bd* transcriptome. Target prediction for these Mo-sRNAs was performed with psRNA target using modified settings and a default score cut-off of 5.0. Target prediction data were then compared with the DEGs information derived from the concomitant mRNA sequencing. Of the total downregulated *Bd* transcripts, five were predicted to be targeted by Mo-sRNAs in the leaf 2 DPI setup, 1128 in the 4 DPI setup and 10 in the root (Table 5), with only one target shared between the root and the leaf 4 DPI datasets (Figure 10A). Predicted plant targets in leaves (4 DPI) included transcription factors such as *transcriptional regulator algH*, *myb-related protein Zm38* and *NIGTH1*, along with aquaporin transporters and RNA helicases, including the putative *BdDCL3b* (BdiBd21-3.2G0305700), along with resistance genes *RGA3* (BdiBd21-3.2G0771500.1), *RGA4* (BdiBd21-3.3G0396200.1) and *RPP13-like protein 3* (BdiBd21-3.3G0776700.1) (Table 6).

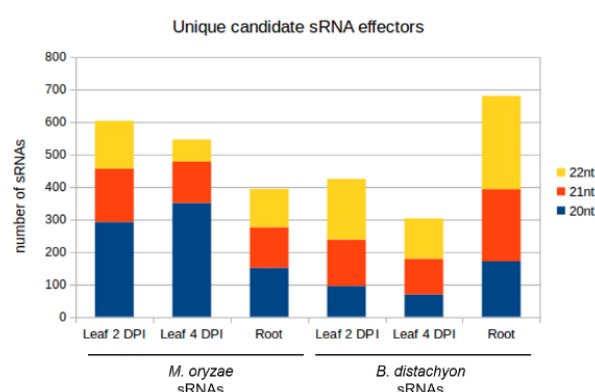


**Figure 9.** Size composition of unique candidate sRNA effectors from *M. oryzae* and *B. distachyon*. The number of unique reads is reported on the y-axis.

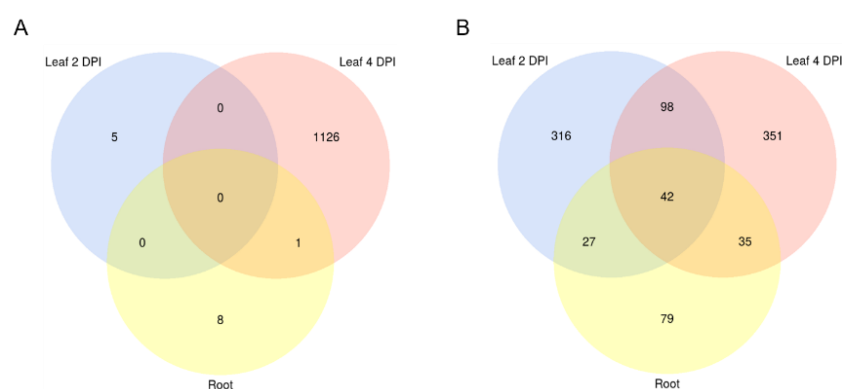


**Figure 10.** Venn diagram of downregulated predicted RNAi targets in *M. oryzae* and *B. distachyon*. Significantly downregulated ( $FC < 0$ ,  $padj < 0.05$ ) (A) *Bd* mRNA targets with complementarity to putative *Mo* sRNAs effectors shared between setups. (B) *Mo* mRNA targets with complementarity to putative *Bd* sRNA effectors. Setups: Leaf biotrophic phase (2 DPI) Leaf necrotrophic phase (4 DPI), and root. Transcript downregulation was assessed from mRNAseq data with DESeq2.

**Table 5.** Overview of the number of predicted cross-kingdom sRNA candidates (20–22 nt) and their corresponding target mRNAs after target downregulation confirmation ( $FC < 0$ ,  $padj < 0.05$ ).

	Setup	Number of sRNA Candidates	Number of sRNA Candidates with Downregulated Targets	Number of Targets Predicted	Number of Targets Down-regulated	
Mo sRNAs	Leaf 2 DPI	604	7	25106	5	Bd mRNAs
	Leaf 4 DPI	546	490	25415	1128	
	Root	394	14	17335	10	
Bd sRNAs	Leaf 2 DPI	424	314	4621	484	Mo mRNAs
	Leaf 4 DPI	302	236	4431	527	
	Root	681	263	6730	183	

Table 6. Selection of Mo sRNA/Bd mRNA duplexes from different leaf and roots setups.

Setup	sRNA	RPM I	Target	Log <sub>2</sub> FC	Description
Leaf 2 DPI	TTTCGACGCTGCCCTGACTT	31.9	BdiBd21-3.1G0045900.1	−0.49	Bowman–Birk type trypsin inhibitor
	TTTCGACGCTGCCCTGACTT	31.9	BdiBd21-3.4G0610700.1	−1.25	probable apyrase 3
	GGTTATCATCGTCCCAGCCC	15.9	BdiBd21-3.4G0347500.1	−0.70	abscisic stress-ripening protein 3
	TGGCAGCGCGGCAGGATCTCG	8.5	BdiBd21-3.5G0309700.1	−1.39	ABC transporter B family member 19
	CAATCGTTGTCTGGCAATGA	83.4	BdiBd21-3.4G0207200.1	−0.72	ABC transporter F family member 5
	TTGTGTCCAAAGCGTTCTGAAA	13.3	BdiBd21-3.2G0019400.1	−0.88	ABC transporter G family member 7
	TGATTAAAGGAGAAAGCGGGG	6.0	BdiBd21-3.5G0286800.1	−0.95	auxin-responsive protein SAUR71
	TCGCTTTGGCGGCGCGCCGCG	27.8	BdiBd21-3.1G0937800.1	−1.15	cytochrome P450 94B3
	TCGCAC TTCGGCGCGTTGGCG	16.9	BdiBd21-3.3G0497100.1	−1.11	cytokinin dehydrogenase 11
	AGGGGCTACGATCTTTGAGAA	18.1	BdiBd21-3.3G0787100.1	−1.13	DexH-box ATP-dependent RNA helicase DEXH15
Leaf 4 DPI	TTTCGAGATTGGAAACGGCT	12.1	BdiBd21-3.2G0305700.1	−0.69	dicer homolog 3b
	TGACGGGATAGGTAAAGAACTA	8.5	BdiBd21-3.2G0095300.1	−0.72	G-type lectin S-receptor-like serine/threonine-protein kinase
	TAGATCGGTTGGTGTCTCGGC	109.9	BdiBd21-3.1G0507400.1	−0.66	GATA transcription factor 21
	TGGCGGCGGTCATTCGGC	6.0	BdiBd21-3.3G0739100.1	−1.86	peroxidase 1
	AGAAGAAATTCATGCCCGGCCAG	8.5	BdiBd21-3.1G0796400.1	−0.71	peroxidase 50
	CCGGCATGAAATTCTTCTCGAA	7.2	BdiBd21-3.1G0093800.1	−0.99	photosystem I reaction center subunit III, chloroplastic
	TAGTAGGGCTGCAAGATCTA	10.9	BdiBd21-3.5G0116500.1	−0.91	photosystem I subunit Psao
	TAGTTGAGTTCGGCCTGCTG	58.0	BdiBd21-3.1G0118800.1	−0.60	photosystem II D1 precursor processing protein PSB27-H2, chloroplastic
	TGGCTGTGAATTCGGCGAGGG	59.2	BdiBd21-3.5G0237900.1	−0.62	probable aquaporin PIP1-2
	CCAATCGTTGTCTGGCAATTGA	105.1	BdiBd21-3.2G0771500.1	−1.33	putative disease resistance protein RGA3
	TTTCGGATAGAGGCACCCAA	10.9	BdiBd21-3.3G0396200.1	−0.54	putative disease resistance protein RGA4
	TATCGTCGCGCAGTTGGTCG	7.2	BdiBd21-3.3G0461000.1	−0.56	RNA exonuclease 4

Table 6. Cont.

Setup	sRNA	RPM I	Target	Log <sub>2</sub> FC	Description
	TGAGCCGGGGTATAATCGG	6.0	BdiBd21-3.4G0029600.1	−0.65	stress-induced-phosphoprotein 1
	TGATTCGGCGGCAGGTCTGGC	14.5	BdiBd21-3.1G0170300.1	−1.17	transcription factor bHLH25
	TCGGTTTCGGCTTCTGGGGT	10.9	BdiBd21-3.2G0063400.1	−1.19	transcription factor NIGTH1
	TAAATACCGTCCCGGCAAGG	9.7	BdiBd21-3.4G0018600.1	−0.66	wall-associated receptor kinase 5
	TGACGGAGCTCGGCCTGGAA	45.9	BdiBd21-3.5G0304000.1	−0.90	wound-induced protein
	TAGGGTGGCCTGAATTATAGT	10.4	BdiBd21-3.2G0378400.1	−0.74	glycine-rich cell wall structural protein 1
Root	AGTATTCGGTCGTCGCCGTA	20.7	BdiBd21-3.3G0257600.1	−0.78	xyloglucan endotransglycosylase/hydrolase protein 8
	TGAACCAAGCCGTTGAGTAAG	10.4	BdiBd21-3.3G0280200.1	−0.55	fatty acyl-CoA reductase 1

Abbreviations: RPM = reads per million; I = infected sample; FC = fold change.

### 2.8. In Silico Prediction of Bd-sRNAs Targeting Mo Transcripts

Given that plant-derived sRNAs can move into fungal pathogens during fungal infections [39,40], we further explored the possibility that Bd-sRNAs have corresponding downregulated Mo transcripts. In total, 20–22 nt Bd-sRNAs (Figure 9) that (i.) originate from the non-coding regions of the Bd21-3 genome, and (ii.) show a higher read count in the Mo-infected compared to non-infected sample were selected. We found 424, 302 and 681 Bd-sRNA in leaves at 2 DPI and 4 DPI and in roots, respectively, with predicted targets in the Mo transcriptome (Table 5). In the next step, we selected for targets found downregulated in the mRNAseq analysis, which further reduced the predicted Mo ck-sRNAs to 314 in leaves at 2 DPI, 236 at 4 DPI and 263 in roots, respectively, corresponding to potentially targeted mRNAs downregulated in leaves at 2 DPI (484), 4 DPI (527) and roots (183) (Table 5). Downregulated Mo targets include cell wall-related genes such as *chitin deacetylase 1* (MGG\_05023), *cell wall protein* MGG\_09460 and virulence genes, such as *CAP20* (MGG\_11916) (Table 7). By comparing predicted Mo targets in infected tissues, we found a considerable overlap between leaf and root samples (42 Mo mRNAs) and between the two leaf samples (140 Mo mRNAs) (Table 7; Figure 10B).

**Table 7.** Selected *M. oryzae* mRNA targets of predicted cross-kingdom *B. distachyon* sRNAs from leaf and root setups.

Predicted Target			Target ID	Target Description	Log <sub>2</sub> FC		
Leaf 2 DPI	Leaf 4 DPI	Root			Leaf 2 DPI	Leaf 4 DPI	Root
X	X	X	MGG_02127	alcohol oxidase	−5.46	−2.53	−3.11
X	X	X	MGG_02695	cysteine proteinase 1	−4.72	−1.35	−2.46
X	X	X	MGG_06494	D-arabinitol 2-dehydrogenase	−5.52	−1.16	−3.21
X	X	X	MGG_01386	FAD dependent oxidoreductase superfamily protein	−5.19	−2.16	−4.51
X	X	X	MGG_05981	glutamine amidotransferase subunit pdxT	−4.79	−2.34	−4.25
X	X	X	MGG_10400	GPI-anchored cell wall beta-1,3-endoglucanase EglC	−0.99	−2.05	−2.11
X	X	X	MGG_01361	PHO85 cyclin-1	−5.81	−1.27	−2.85
	X		MGG_15576	DNA repair protein rhp51	n.s.	−1.05	n.s.
	X		MGG_03587	essential for mitotic growth 1	n.s.	−0.60	n.s.
X	X		MGG_04345	cytochrome P450 17A1	−4.40	−1.06	n.s.
X		X	MGG_03201	acetyl-coenzyme A synthetase	−1.39	0.86	−1.84
	X		MGG_09950	C2H2 type zinc finger domain-containing protein	n.s.	−1.49	n.s.
	X	X	MGG_16901	ATP-dependent RNA helicase DBP2	n.s.	−1.04	−1.18
X	X	X	MGG_07667	autophagy-related protein 17	−2.45	−1.33	n.s.
X	X	X	MGG_01391	ent-kaurene oxidase	−3.90	−2.44	n.s.
X	X	X	MGG_11962	G-protein coupled receptor	−5.75	−3.42	n.s.
X	X	X	MGG_04378	integral membrane protein	−3.99	−1.04	n.s.
X	X	X	MGG_04935	integral membrane protein	−3.58	−1.40	n.s.
X	X	X	MGG_03123	MATE efflux family protein subfamily	−4.68	−1.11	n.s.
X	X	X	MGG_14872	calpain-9	−4.19	−1.17	n.s.

Table 7. Cont.

Predicted Target			Target ID	Target Description	Log <sub>2</sub> FC		
Leaf 2 DPI	Leaf 4 DPI	Root			Leaf 2 DPI	Leaf 4 DPI	Root
X	X	X	MGG_09460	cell wall protein	−4.72	−3.92	n.s.
X	X	X	MGG_03186	1,4-alpha-glucan-branching enzyme	−1.52	n.s.	−1.36
X	X	X	MGG_14154	RETRO5, retrotransposons MoTeR1s and MoTeR2	−6.04	−1.15	n.s.
X		X	MGG_06393	serine/threonine-protein kinase ATG1	−3.24	n.s.	n.s.
	X	X	MGG_04938	C-3 sterol dehydrogenase/C-4 decarboxylase	n.s.	−1.85	n.s.
X	X	X	MGG_10568	sterol 24-C-methyltransferase	n.s.	n.s.	−1.24
X		X	MGG_06371	pyruvate dehydrogenase E1 component subunit alpha	n.s.	n.s.	−1.75

X is assigned if the gene is predicted to be targeted by candidate sRNA in the corresponding setup. Abbreviations: FC = fold change; n.s. = not significant.

We searched the Pathogen-Host Interactions Database (PHI-base) for available information on loss-of-virulence mutants for the predicted Mo target genes. A list of down-regulated predicted Mo targets and corresponding PHI-base phenotypes is shown in Table 8. Of note, the predicted Mo genes are involved in virulence and pathogenicity, including *CON7* transcription factor (MGG\_05287) predicted to be targeted in the Mo-infected root, the effector *AvrPiz-t* (MGG\_09055) predicted to be targeted in the leaf at 4 DPI and the *vacuolar glucoamylase SGA1* (MGG\_01096) predicted to be targeted in the leaf at 2 DPI. Additionally, potential targets shared between more than one setup included (MGG\_00620), *Sso1* (MGG\_04090) encoding a SNARE protein and *YHM2* (MGG\_07201) encoding mitochondrial DNA replication protein (2 DPI leaf vs. root), as well as *MoATG17* (MGG\_07667) encoding an autophagy-related protein (biotrophic vs. necrotrophic leaves), whose respective mutants are also known to be compromised in pathogenicity [45,46] (Tables 7 and 8).

Table 8. Predicted RNAi targets with known infection-impaired phenotypes in the corresponding *M. oryzae* knock-out (KO) mutants.

Transcript ID	Gene ID	Description	Phenotype	Host Species	Reference Phi-Base
MGG_00063T0	AGL1	glycogen debranching enzyme	reduced_virulence	Os_Hv	PHI:3814
MGG_00365T0	MAGB	G alpha protein subunit	reduced_virulence	Os	PHI:83
MGG_00620T0	MoDac	GlcNAc-6-phosphate deacetylase	reduced_virulence	Os	PHI:5471
MGG_01096T0	SCA1	vacuolar glucoamylase	loss_of_pathogenicity	Os_Hv	PHI:2138
MGG_01180T0	MoSCAD3	short-chain specific acyl-CoA dehydrogenase	reduced_virulence	Os_Hv	PHI:8929
MGG_01285T0	Tpc1	transcription factor for Polarity Control 1	reduced_virulence	Os_Hv	PHI:7317
MGG_01819T0	Gph1	phosphorylase	loss_of_pathogenicity/reduced_virulence	Os_Hv	PHI:2062/3815
MGG_02444T0	MoPLC1	modulator of calcium flux	loss_of_pathogenicity	Os	PHI:2057
MGG_02457T0	RHO2	Rho GTPase	reduced_virulence	Os	PHI:8752
MGG_02884T0	MoFLP1	fasciclin-like protein	reduced_virulence	Os_Hv	PHI:4231
MGG_03148T0	TDG4	trigalactosyl/diacylglycerol-4	reduced_virulence	Os_Hv	PHI:3811
MGG_03198T0	TIG1	histone deacetylation	loss_of_pathogenicity	Os_Hv	PHI:2002
MGG_03670T0	SPM1	subtilisin-like proteinase Spm1	reduced_virulence	Os_Hv	PHI:2117
MGG_03860T0	TPS1	trehalose-6-phosphate synthase	loss_of_pathogenicity/reduced_virulence	Os_Hv	PHI:322/1064
MGG_04895T0	ICL1	isocitrate lyase	reduced_virulence	Os	PHI:305
MGG_05344T0	MgSM1	effector	increased_virulence	At	PHI:2118/5540
MGG_06393T0	ATG1	autophagy-related protein 1	loss_of_pathogenicity	Os_Hv	PHI:2035/2069/8612
MGG_07667T0	Moatg17	autophagy-related protein 17	loss_of_pathogenicity	Os_Hv	PHI:2083
MGG_08054T0	MoChi1	chitinase 1	reduced_virulence	Os_Hv	PHI:8753/8806
MGG_08370T0	gel3	1,3-beta-glucanosyltransferase	loss_of_pathogenicity	Os	PHI:6713
MGG_09471T0	NTH1	neutral trehalase	reduced_virulence	Os_Hv	PHI:123/775/794
MGG_10859T0	MoLDS1	heme peroxidase	reduced_virulence	Os	PHI:5189
MGG_11862T0	ABC4	ABC transporter	reduced_virulence/loss_of_pathogenicity	Hv	PHI:1017/2067
MGG_12122T0	MoGSK1	glycogen synthase kinase 1	loss_of_pathogenicity	Os_Hv	PHI:7117
MGG_12814T0	MoAPI	BZIP domain-containing protein	loss_of_pathogenicity	Os_Hv	PHI:2142
MGG_17909T0	ATG3	autophagy-related protein 3	loss_of_pathogenicity	Os	PHI:2071
MGG_05287T0	CON7	transcription factor CON7	loss_of_pathogenicity	Os_Hv	PHI:2039
MGG_09055T0	AvrPiz-t	avrpiz-tgene, effector protein	increased_virulence	Os	PHI:7896

Information derived from Pathogen-Host Interactions Database (PHI-base) search.

### 3. Discussion

Based on the work done to elucidate the function and 3D structure of *Brachypodium distachyon* AGO and DCL proteins published by Šečić et al. [35], we set out to investigate these RNAi machinery components in *Magnaporthe oryzae*. Mo has been extensively studied as a model for RNAi in fungi, and it is known to encode three AGOs, two DCLs and three RdRPs [25,26]. Interestingly, while the phylogeny with other fungal RNAi machineries such as *N. crassa*, *Mucor circinelloides*, *Cryphonectria parasitica* and *Schizosaccharomyces pombe* and the domain conservation have been reported, we found no information regarding the proteins' predicted interactome, subcellular localization and 3D protein structures, which would help elucidate the function and relevance of these proteins in vivo. We confirmed that all three fungal AGOs have the characteristic PAZ (Piwi Argonaut and Zwillig) and PIWI (P-element Induced Wimpy testis) domains: the first is involved in the recognition of the 3' end of the guide sRNA molecule [47], while the second is an RNase H domain that confers AGOs the ability to cleave single-stranded RNAs complementary to the guide sRNA sequence [48]. A closer look at the PIWI domains via MSA confirmed the conservation of both the QF-V motif, involved in the sorting of sRNAs based on their sequence and secondary structure [49] and the DEDD catalytic tetrad, critical for the protein 'slicer' activity [48]. Similar to NcDCLs, both MoDCLs lacked predicted PAZ domain but differed from the *N. crassa* ortholog showing predicted dicer-dimer domains and lacking predicted dsRNA-specific ribonuclease and ds-RNA binding (DSRM) domains [27]. At this point of the analysis, no major differences were recorded among either Mo protein families, which would help elucidate the differences in both sRNA production and virulence reported in the RNAi KO mutants by Raman et al. [50]. Interestingly, protein subcellular localization helped shed additional light on MoAGO3 and MoDCL2 non-redundant roles within their families, with MoAGO3 predicted to localize exclusively in the nucleus, compared to MoAGO1, predicted in both the nucleus and the cytosol, and MoAGO2, predicted to localize in the cytosol and plastid. Moreover, we predicted MoDCL2 to exclusively localize in the cytosol, while MoDCL1 in the nucleus, confirming the distinct roles for these proteins in contrast with their redundant function *N. crassa* [51]. Additionally, predicted interactomes of MoAGOs showed significant differences between MoAGO1 vs. MoAGO2 and MoAGO3, which would point to a unique role of this protein. Specifically, the predicted interaction with an ATP-dependent RNA helicase DED1 (MGG\_02762) and a Pumilio-family RNA-binding repeat protein (MGG\_03158) would suggest a unique role for MoAGO1 in translation regulation [52,53]. KO mutants of these RNAi components have been previously characterized both for their sRNA accumulation patterns and their virulence on barley [27,50]. Except for  $\Delta moago3$ , which did not sporulate and could not be further utilized, we tested the morphology and virulence of the available mutants in our newly established Bd pathosystems. While all five RNAi mutants showed unaltered growth, morphology and conidiation in axenic cultures, we detected significant differences in their ability to infect Bd tissues. Interaction between plants and its host pathogen is a dynamic system, influenced by several genetic and environmental factors which may alter the course of the infection and its reproducibility. The inoculation method proved to be critical for the assessment of virulence alterations, with the drop inoculation on detached leaves resulting in the most stable assay, and the spray on whole seedlings resulting in the most extreme phenotypes, with  $\Delta modcl2$  and  $\Delta modcl1/2$  showing a complete loss of pathogenicity. These results both confirm and expand the key role of MoDCL2 first hypothesized by Raman and colleagues in a variety of fungal biological processes, including: sRNA biogenesis, fungal development and, as shown here, fungal virulence [27,50]. The reduction of virulence observed among RNAi mutants throughout the different setups further substantiate the importance of a fully functioning fungal silencing machinery and sRNAs generated for a successful infection of Bd tissues.

GOE analysis of Mo DEGs highlighted an enrichment of terms mainly related to fungal growth and development in all infected tissues. Especially in the root GO, terms related to interactions with other organisms, particularly via protein secretion, were found

overrepresented. By assessing expression of protein effectors, we confirmed upregulation of known avirulence genes, including *AVR Pita1* (coding for a metalloprotease) and *PWL2* (a glycine-rich protein recognized by weeping lovegrass and finger millet R proteins), both found highly upregulated in the foliar biotrophic phase (2 DPI), and *Avr-Pik/km/kp*, upregulated at 2 and 4 DPI.

Genes involved in appressorium and penetration peg functionality were upregulated in all three setups, including *WISH* (Water wettability, Infection, Surface sensing and Hyper-conidiation) G-protein coupled receptor protein, whose KO renders the fungus unable to develop appressoria and establishes the infection on intact rice leaves [54] and superoxide-generating NADPH oxidases *NOX1* (MGG\_00750) and *NoxD* (MGG\_09956). *NOX1* is involved in cell wall biogenesis, affecting both chitin and melanin biosynthesis and deposition. KO of this gene resulted in a complete loss of appressorium-mediated cuticle penetration and failure of *in planta* proliferation even when inoculated onto wounded rice seedlings [55]. Similar defects were detected in rice leaves and roots inoculated with  $\Delta noxD$  [56], confirming the key role played by NOX proteins not only in growth and sexual reproduction, but also in fungal virulence. *PLC3*, significantly upregulated at both timepoints in leaves, is also required for normal conidiation and appressorium function, but contrary to NOXs normal infection was observed when  $\Delta moplc3$  was inoculated by infiltration into wounded rice leaves, excluding a function of *PLC3* in fungal growth once inside host cells [57]. As expected, we detected in the later timepoint of the leaf infection (4 DPI) upregulation of genes known to be required for infection maintenance and expansion. One of these genes, *S-(hydroxymethyl) glutathione dehydrogenase* (MGG\_06011), was exclusively upregulated in the 4 DPI dataset and it is known to be involved in the growth of infectious hyphae on barley leaves [58].

Overall, our analysis shows that *Mo* undergoes an extensive reprogramming during the establishment and maintenance of the infection and highlights the commonalities and differences in expression patterns depending on the inoculated tissue and the progression of the colonization. Of note and consistent with the detection of necrotrophic lesions on *Bd* roots (Figure S4), fungal reprogramming during the root infection is closer to the one reported in the foliar necrotrophic phase (with 701 DEGs shared between the setups) compared to the biotrophic phase (only 392 DEGs shared between the setups).

mRNA sequencing of *Mo*-infected and non-infected *Bd* leaves and root samples allowed for a systemic analysis and comparison of expression pattern alterations of *Bd* genes in response to the fungal pathogen. As predicted, the highest amount of DEGs was observed at 4 DPI in leaves, when the infection is spreading outside of the inoculation point and the fungus has switched to a more aggressive necrotrophic lifestyle [5,12,59]. The relatively low amount of DEGs in the other two setups is consistent with the early infection stages and the limited amount of fungal biomass both in the root and at 2 DPI in leaves. Interestingly, in all three setups the percentage of upregulated DEGs was higher compared to downregulated DEGs, with 96% upregulated in leaves at 2 DPI, 60.7% at 4 DPI and 69.5% in the roots, indicating an overall strong induction of gene expression. Consistent with the highest numbers of DEGs detected at 4 DPI, most GO terms reported in Table S5 belong to this dataset, with terms related to metabolic and biosynthetic processes being the most prevalent. Interestingly, all datasets had enriched terms related to oxidoreductase activities (GO:001649) confirmed also by the upregulation of *BdiBd21-3.4G0171000*, coding for a multicopper oxidase, in all setups, and *BdiBd21-3.1G0233800* and *BdiBd21-3.1G0233900*, coding for peroxidases, in the leaf 4 DPI datasets. Peroxidases are commonly associated with plant responses to stress and specifically fungal infection, as they are involved in a variety of processes including the synthesis of phenols such as tannins and melanins, reactive oxygen species (ROS) removal, lignin biosynthesis and induction of defense responses by stimulating intracellular  $Ca^{2+}$  signaling [60]. Another gene upregulated in all three setups is *secologanin synthase-like* (*BdiBd21-3.2G0563800*), encoding an enzyme involved in the biosynthesis of monoterpenoid indole alkaloids (MIAs), also reported upregulated in *Bd* following *F. pseudograminearum* infection [61]. Expression of other

defense-related genes was induced in one or more of our datasets, including known pathogenesis-related proteins, receptor kinases, transcription factors and ABC transporters. Once again, 2 DPI and root samples were found overlapping in only a few of these genes. Examples of genes consistently found upregulated in all three setups are BdiBd21-3.3G0144800, encoding a protein kinase xa21 which confers resistance to *Xanthomonas oryzae* pv. *oryzae* race 6 [62], an ABC transporter A family member 2-like (BdiBd21-3.3G0465100) and the pleiotropic drug resistance protein 3-like (BdiBd21-3.2G0550500).

Interestingly, all PR genes shown in Table 5 were upregulated in leaves at 4 DPI, while leaf 2 DPI and root PR protein expression patterns did not overlap, with only two (PR-like and PR1-like) upregulated at 2 DPI, and three (two PR1-like and PR10) in the root datasets. Similarly, the strongest and most widespread upregulation in the other pathogen sensing/defense-related genes was observed at 4 DPI, with an upregulation of transcription factors belonging to MYB, WRKY and NAC families consistent with the upregulation observed in Bd after *F. pseudograminearum* infection [61], and the knowledge that these families regulate a variety of plant responses, including those to biotic stresses [63–65]. In line with the considerable overlap in Mo gene expression patterns between leaf 4 DPI and root datasets, the majority of genes found upregulated in Bd roots (80.9%) are also detected upregulated in leaves at 4 DPI, compared to 18% shared with the 2 DPI sample. Altogether, these results highlight differences in the upregulation of specific protein family members depending on the infected tissue and fungal lifestyle, while confirming the relevance of these families in response to Mo infections.

Candidate Bd miRNA-generating loci were identified with Shortstack from both control and infected filtered sRNA datasets. Given that the program-assigned cluster IDs are specific to the dataset analyzed and are not comparable between different files, we compared clusters based on their genomic coordinates, and further analyzed loci from the infected sample that had higher RPM (reads per million) than in control, or that were found exclusively in the presence of Mo. This resulted in the identification of 12 miRNA stem loop precursor sequences and 17 mature miRNAs across setups.

Specifically, we identified five mature miRNAs belonging to the MIR156 family, shown to be induced by *F. oxysporum* in *Persicaria minor* [66] and known to be induced by environmental stress, resulting in the cleavage of a SPL (SQUAMOSA promoter binding protein-like) transcription factor and overall modulation of anthocyanin biosynthesis [34,67]. Bd-MIR529, also predicted to target this gene, was found upregulated at 4 DPI in our datasets. Another miRNA involved in the plant response to abiotic stress is miR159b, found upregulated during Mo leaf infection both at 2 and 4 DPI, and known to target two MYB transcription factors in cucumber (*CsGAMYB1* and *CsMYB29-like*), involved in ABA signaling [68]. Finally, four additional miRNA families were detected as induced by Mo infection (MIR9484, miR9481b, MIR531 and miR7723a).

To establish the origin of the sRNA reads detected in the different leaf and root setups of the Mo—Bd interaction, sRNAseq datasets from infected samples were aligned to both the Bd 21-3 and the Mo 70-15 genome. Only reads aligning without mismatches to Mo and with at least two mismatches to Bd were assigned to the fungus and vice-versa, only reads aligning without mismatches to Bd and with at least two mismatches to Mo were assigned to the plant. As expected from the low amount of Mo in infected samples from leaves at 2 DPI, most of the reads were assigned to Bd, whereas higher levels of Mo reads were detected at 4 DPI (leaf) consistent with proliferating infection. All assigned reads were then filtered based on their read counts to select only reads either induced or upregulated in the datasets of infected tissues compared to uninfected tissues and axenic mycelia. We noted that most of the reads (>50%) found in infected samples are specific and are not detected in healthy tissues and axenic culture, showing that sRNA production both in the plant and the fungus is strongly responsive to infection. It follows that sRNA datasets from healthy plants and axenic fungal culture do not represent the full diversity of infection-related sRNA communities. As an additional step, we selected for sRNAs that were not aligning to the coding sequences of the organism of origin. The reasoning behind

this filtering step is that we avoided accidental mRNA degradation to be kept as candidate ck-sRNAs, and more important, removed the sRNA sequences more likely to play an endogenous role. Given that the size distribution of upregulated/induced sRNA reads did not show variation in peaks compared to the total sRNA reads, we decided to select 20–22 nt sRNAs (canonical length range for PTGS) for further analysis. Target prediction was carried out with psRNATarget, a web-based prediction software specifically designed for plant sRNA investigations, which allowed for the identification of complementary mRNA sequences in the interacting organism. In PTGS, sRNAs are loaded onto AGO proteins, which guide them towards a complementary mRNA sequence that will then be degraded or sequestered, resulting in reduced levels of the encoded protein. Knowing the expression levels of the predicted targets from the same biological samples used for the sRNA sequencing, we proceeded with further selection of candidate ck-sRNAs based on the significant downregulation of their mRNA targets. Most of the predicted Mo sRNA effectors in the 2 DPI leaf (biotrophic phase) and root samples did not pass this filtering step, as their predicted targets were either upregulated or had comparable expression levels in the corresponding control datasets. There are a few possible explanations as to why the potential targets would not be significantly downregulated in our mRNAseq datasets, including: (i.) the sRNA has not yet been transported throughout the tissue, so the downregulation occurs only at the penetration site, where the fungus is physically interacting with the plant cells, and that is masked by the upregulation in distal parts of the tissue; (ii.) the target mRNA is not cleaved, but its translation is inhibited by the RISC complex acting as a physical barrier, in which case the measurable effect would not be at the mRNA level but only at the protein level; and (iii.) the target is indeed cleaved, but concurrently with the downregulating effect of the sRNA, there is a stronger endogenous upregulation of the gene, leading to either similar levels of mRNA as the control, or even higher.

Comparison of lists with predicted fungal mRNA targets of Bd-sRNAs between the different setups highlights substantial target conservation between the leaf biotrophic and necrotrophic phases, with 140 predicted shared Mo targets between the two, and 42 Mo targets conserved among all three setups. Subjecting the shortlisted predicted fungal target genes to a PHI-base survey for mutations in Mo with lethal or detrimental outcome, we found a clear indication for a reduction in pathogenicity or loss of virulence in respective KO mutants, including *MoATG17* (MGG\_07667), an autophagy-related protein whose KO impaired appressorium formation and function, resulting in a complete lack of disease symptoms on rice leaves [45]. Similarly, *MoATG1* (MGG\_06393) was also predicted to be targeted by Bd sRNAs and downregulated at 2 DPI, with *Mgatg1* mutant reported by Liu et al. to be unable to infect rice and barley leaves [69]. Additionally, we predicted sRNAs targeting the avirulence effector *AvrPiz-t* (MGG\_09055). *AvrPiz-t* suppresses rice PTI signaling pathway by targeting the E3 ubiquitin ligase APIP6 and suppressing its ligase activity, resulting in reduced flg22-induced ROS generation and overall enhanced susceptibility in vivo [70].

Interestingly, we detected *Calpain-9* to be targeted in all three datasets and significantly downregulated in the foliar ones, both at 2 and 4 DPI. While downregulation in the root setup did not reach a significant padj value, targeting of this transcript would match the finding in the cotton–*V. dahliae* pathosystem, where the host was found to be expressing and exporting miRNAs to the infecting fungus to inhibit its virulence via the targeting of *Clp-1* [39].

Additional predicted targets included integral membrane proteins (MGG\_04378T0, MGG\_04935T0), ergosterol biosynthesis enzymes (ERG6, MGG\_10568T0; ERG26, MGG\_04938T0) and fungal cell wall related genes, such as *GPI-anchored cell wall beta-1,3- endoglucanase EglC* (MGG\_10400T0, targeted and significantly downregulated in all three datasets), *cell wall protein* MGG\_09460T0 (targeted and significantly downregulated in both foliar samples), *chitin deacetylase* (MGG\_08774T0) and *chitinase 1* (MGG\_08054T0). Targeting fungal membrane components and ergosterol homeostasis has already been proven to be a

successful strategy in crop protection against fungal pathogens, both via the application of DMI (sterol demethylation inhibitors) fungicides [71] and with the RNAi-based HIGS (Host-Induced Gene Silencing) and SIGS (Spray Induced Gene Silencing) approaches, where artificial sRNAs are introduced in the plant either via transformation or external application is then transferred to the fungal cells during infection [72–74]. It is interesting to observe how the plant appears to have naturally evolved to produce sRNAs potentially able to target fungal essential and pathogenicity related genes. However, Mo is still able to progress its infection both in Bd leaves and roots, and the most likely factors behind this fungal success are the countermeasures it employs in this crosstalk, from the extensive reprogramming of gene expression to the release of effectors and sRNAs.

To substantiate the hypothesis that fungal sRNAs function as effectors to aid the establishment and maintenance of infection, we investigated the role of downregulated Bd targets. Targeting conserved sequences, such as ribosome- and photosynthesis-related ones, and hampering gene expression and biosynthetic processes would prove to be a more effective strategy than specific defense/immunity genes, which are more prone to mutate in the arms race between plants and pathogens.

We confirmed the targeting of a variety of RNA helicases genes, including *BdDCL3b* (BdiBd21-3.2G0305700), identified in our recent work [35] and involved in the preprocessing of sRNA precursor molecules involved in chromatin modification [75]. Specific plant targets included gene families involved in the plant response to both biotic and abiotic stresses, including hormone responsive proteins (BdiBd21-3.5G0286800.1, BdiBd21-3.4G0347500.1), transcription factors such as members of the GATA bHLH families (BdiBd21-3.1G0507400.1, BdiBd21-3.1G0170300.1), peroxidases (BdiBd21-3.3G0739100.1, BdiBd21-3.1G0796400.1, BdiBd21-3.3G0559700.1), disease resistance proteins (BdiBd21-3.2G0771500.1, BdiBd21-3.3G0396200.1) and ABC transporters (BdiBd21-3.5G0309700.1, BdiBd21-3.4G0207200.1, BdiBd21-3.2G0019400.1) [61,63,76,77]. Interestingly, *Brachypodium* aquaporins (BdiBd21-3.5G0237900.1) were also downregulated and predicted targets of Mo sRNAs during the infection, consistent with the knowledge that aquaporins play a role in the interaction between plants and microbial pathogens, most likely by modulating both H<sub>2</sub>O availability and transport of ROS [78].

Altogether, the prediction of Mo ck-sRNAs and corresponding Bd targets involved in the plant response to biotic and abiotic stress paves the way for further validation of predicted sRNA/mRNA interactions, including: (i.) proof of target cleavage via RACE or degradome sequencing; (ii.) verification of sRNA–target interaction in transient expression systems such as leaves of *Nicotiana benthamiana*; (iii.) mutational KO strategies of predicted target genes and/or precursor loci of predicted ckRNAs; and (iv.) detection of direct association of sRNAs or their target mRNA with the respective fungal or plant AGO1-like protein by immunopurification techniques [79,80].

#### 4. Materials and Methods

##### 4.1. AGO and DCL Protein Analysis and 3D Structure Modeling

Known ARGONAUTE and DICER-like protein sequences were downloaded from the NCBI database and analyzed following the workflow utilized for *B. distachyon* AGOs and DCLs [35]. The phylogenetic analysis and tree rendering were done by the Phylogeny.fr web server [81]. Multiple sequence alignment (MSA) of AGO PIWI domains was done using Clustal Omega [82,83] and visualized with the Mview multiple alignment viewer [84]. Protein domains were identified by using Simple Modular Architecture Research Tool (SMART) including PFAM domains in the search [85,86] and visualized with the Illustrator for Biological Sequences (IBS) online illustrator [87]. Prediction of protein location was done using the plant subcellular localization integrative predictor (PSI) [88], and prediction of the interactome was done using the STRING database [89], excluding text mining as indication of putative interaction. Finally, AGOs and DCLs amino acid (aa) sequences were utilized for predicting the proteins' 3D structure utilizing SWISS-MODEL [90]. Predictions were selected for further validations based on the GMQE and QMEAN Z-score values [91].

PROCHECK [92,93] and WHATCHECK [94] were used to check the stereochemical quality of the selected structures and calculate the Ramachandran Z-score [95]. Open-Source Py-MOL (The Py-MOL Molecular Graphics System Version 2.4.0a0) was used for visualization of the predicted structures [96].

#### 4.2. *Mo Mutants Cultivation and Inoculation*

The *Magnaporthe oryzae* wild type Mo 70-15 and mutants  $\Delta moago1$ ,  $\Delta moago2$ ,  $\Delta moago3$ ,  $\Delta modcl1$ ,  $\Delta modcl2$  and  $\Delta modcl1/2$  obtained from N. Donofrio, Newark, NJ, USA, were grown as described [12]. Conidia germination and appressoria development was assessed by incubating conidial suspension ( $2 \times 10^3$  spores  $\text{mL}^{-1}$ ) in distilled water on poly-L-lysine coated glass slides (Sigma-Aldrich, St. Louis, MO, USA) in a damp chamber at room temperature for 24 h and examined via inverted microscopy. Fungal stock was prepared on oatmeal agar (OMA) in a regime of 26 °C/24 °C (day/night cycle) and a light intensity of 70  $\mu\text{mol m}^{-2} \text{s}^{-1}$  photon flux density. Seeds of *Brachypodium distachyon* cv. 'Bd21-3' [97] were germinated in soil (Fruhstorfer Erde Typ T) and cultivated in a growth chamber at 22 °C/18 °C (day/night cycle) with 60% relative humidity and a photoperiod of 240  $\mu\text{mol m}^{-2} \text{s}^{-1}$  photon flux density. Three methods were utilized to assess disease progression and phenotype of the mutants on leaves: (i.) spray infection of whole seedlings on three-week-old Bd plants with Mo conidia suspension of  $120 \times 10^3$  spores  $\text{mL}^{-1}$  in 0.002% Tween20 and assayed on the second youngest leaf; (ii.) spray infection of second youngest detached leaves of three-week-old Bd plants with 250  $\mu\text{L}$  *Magnaporthe oryzae* conidia suspension  $50 \times 10^3$  spores  $\text{mL}^{-1}$  in 0.002% Tween20; (iii.) drop inoculation on second youngest detached leaves of three-week-old Bd with 10  $\mu\text{L}$  of conidia solution (50,000 conidia/mL in 0.002% Tween water) on 1% agar plates. Control leaves/seedlings were mock-inoculated with 0.002% Tween water in all setups. Leaves were kept at 16 h light (160  $\mu\text{mol m}^{-2} \text{s}^{-1}$ )/8 h dark cycle at 22 °C/18 °C. Score disease progression and analysis of the necrotic spots was assayed 5 DPI via ImageJ software [98]. For root inoculation, sterilized seeds (3% NaClO for 15 min, followed by three times 5 min washes in sterile water) of Bd21-3 were vernalized in the dark at 4 °C for two days on half strength MS medium [99] and then moved to a 16 h light (160  $\mu\text{mol m}^{-2} \text{s}^{-1}$ )/8 h dark cycle at 22 °C/18 °C. Roots of one-week-old seedlings were dip-inoculated in 1 mL of conidia solution (125,000 conidia/mL in 0.002% Tween water) for 3 h and transplanted in a (2:1) mixture of vermiculite (Deutsche Vermiculite GmbH, Sprockhövel, Germany) and Oil-Dri (Damolin, Mettmann, Germany). Control roots were mock-inoculated with 1 mL of 0.002% Tween water solution. Quantification of Mo DNA presence in roots was performed at 5 DPI by quantitative PCR based on the fungal actin (*MoActin*). The experiment was repeated two times, each time with  $n = 10$  roots per experimental group.

#### 4.3. *Sample Preparation from Mo–Bd Interaction Sequencing*

Mo was grown on oatmeal agar (OMA) for two weeks at 26 °C with 16 h light/8 h dark cycles both for sampling of mycelium and conidia production. Samples from axenic cultures were collected by scraping a mixture of mycelia and spores from three plates, followed by immediate freezing in liquid nitrogen. For root inoculation, sterilized seeds (3% NaClO for 15 min, followed by three times 5 min washes in sterile water) of Bd21-3 were vernalized in the dark at 4 °C for two days on half strength MS medium and then moved to a 16 h light (160  $\mu\text{mol m}^{-2} \text{s}^{-1}$ )/8 h dark cycle at 22 °C/18 °C. Roots of one-week-old seedlings were dip-inoculated in 1 mL of conidia solution (250,000 conidia/mL in 0.002% Tween water) for 3 h, transplanted in a (2:1) mixture of vermiculite (Deutsche Vermiculite GmbH, Sprockhövel, Germany) and Oil-Dri (Damolin, Mettmann, Germany) and grown for an additional 4 days before harvesting. Control roots were mock-inoculated with 1 mL of Tween water solution. For leaf inoculation, third leaves of three-week-old Bd were detached and drop-inoculated with 10  $\mu\text{L}$  of conidia solution (50,000 conidia/mL in 0.002% Tween water) on 1% agar plates. Control leaves were mock-inoculated with Tween

water. Leaves were kept at 6 h light ( $160 \mu\text{mol m}^{-2} \text{s}^{-1}$ )/8 h dark cycle at 22 °C/18 °C and collected for sequencing at 2 days post inoculation (DPI) and 4 DPI.

#### 4.4. RNA Extraction, Library Preparation and Sequencing

Three roots or two leaves, respectively, were pooled per sample for RNA extraction and for each condition three pooled biological samples were prepared. Frozen tissue stored at −80 °C was ground in liquid nitrogen using mortar and pestle. Total RNA was isolated with ZymoBIOMICS™ RNA Mini Kit (Zymo Research, Irvine, CA, USA) according to the manufacturer's instructions. Quantity and integrity of the RNA were assessed with DropSense16/Xpose (BIOKÉ, Leiden, Netherlands) and Bioanalyzer 2100 (Agilent, Santa Clara, CA, USA), respectively. Purification of small and large RNAs into separate fractions was carried out using RNA Clean & Concentrator™ -5 (Zymo Research, Irvine, CA, USA) and concentration and quality of the fractions were checked again, using the Agilent 2100 Bioanalyzer Pico Chip and the Qubit fluorometer (Invitrogen, Carlsbad, CA, USA) for the sRNA fraction. A total of 50 ng of sRNA (17 to 200 nt) were used for cDNA library preparation with TruSeq® Small RNA Library Prep (Illumina, San Diego, CA, USA) and 1.5 µg of large RNA were used for cDNA library preparation with TruSeq® Stranded mRNA (Illumina, San Diego, CA, USA). Constructed cDNA libraries of sRNAs were further size selected with BluePippin (Sage Science, Beverly, MA, USA) for fragments between 140 and 160 nt (15–35 nt without adapters). Quality of polyA mRNA libraries was assessed using the Fragment Analyzer™ Automated CE System (Advanced Analytical Technologies, Heidelberg, Germany). The Illumina HiSeq1500 sequencing platform was used to sequence the Illumina TruSeq® Small RNA libraries single end with 35 nt read length and the Illumina TruSeq® Stranded mRNA libraries (paired-end [PE] sequencing, 70 nt) of all samples.

#### 4.5. Transcriptome Analysis

Paired end sequenced cDNA reads of Illumina TruSeq® Stranded mRNA libraries were analyzed through the quality check in FastQC and alignment in the junction mapper HISAT2 [100]. *Magnaporthe oryzae* MG8 release 38 [101] and *Brachypodium distachyon* Bd21-3 v1.1 (DOE-JGI, <http://phytozome.jgi.doe.gov/>) assemblies were utilized throughout this study as references. Htseq-count [102] and DESeq2 [103] were then used for read counting and differential gene expression calling (DGE) between the infected and control sample genes and to generate volcano plots. Heatmaps for selected DEGs were obtained with the pheatmap package for R [104]. Gene Ontology Enrichment (GOE) analysis on DEGs was done with AgriGO v2 [105]. Gene descriptions were integrated from the organism genome assembly, ENSEMBL Biomart, Phytozome and Blast2GO [106].

#### 4.6. sRNA Analysis, Prediction of Endo- and Cross-Kingdom sRNA

The single end sequenced cDNA reads of Illumina TruSeq® Small RNA libraries were analyzed starting with quality check with FastQC [107] and trimming of adapter artifacts with cutadapt [108]. The alignment of the reads to reference genomes and transcriptomes of Bd and Mo was done using the short read aligner Bowtie [109]. Reads with a 100% alignment to the genome of the organism of origin were selected, alongside the reads with at least two mismatches in the alignment to the target organism genome. Venn diagrams for sRNA and target overlaps were obtained with the VennDiagram package for R [110].

To identify interaction-related Bd sRNAs with endogenous function, both infected and control datasets were analyzed with ShortStack [111] to identify potential miRNA generating loci. Genomic coordinates and corresponding reads per million (RPM) of the identified clusters were compared between infected and control datasets to select clusters exclusively present or increased during infection. Both potential precursors and mature miRNAs deriving from these clusters were compared to known miRNA sequences, obtained from miRBase [112]. The structure of miRNA generating clusters was visualized with strucVis (version 0.4, Michael J. Axtell).

Bioinformatics analysis of candidate ck-sRNAs was done as described in Zanini et al. [43]. Only sRNA reads of 20–22 nt originating from non-coding regions and with a higher count in the organism of origin control datasets compared to the infected ones were analyzed further for ck-sRNA effector identification by the target prediction software psRNATarget used with customized settings [113].

Expression levels obtained for each gene were used as confirmation of downregulation of predicted targets from the psRNATarget software. PHI-base, a collection of experimentally verified pathogenicity/virulence genes from fungal and microbial pathogens [114], was used to gather information regarding phenotype and virulence of fungal mutants carrying a mutation in the identified Mo gene targets.

## 5. Conclusions

In the present work, we analyzed and characterized the interaction between *Brachypodium distachyon* and *Magnaporthe oryzae* at different fungal lifestyles and infection sites, both from a transcriptomic and sRNA expression profiles' point of view. The pathosystem has been studied as a model for the effect of blast disease on staple crops leaves (e.g., rice, wheat and barley), owing to Bd's short maturation phase, smaller genome and space-saving production [11,12,14]. In addition to foliar infections, we also established and characterized the interaction and responses to Bd root colonization by Mo. Additional to the confirmation of the extensive reprogramming in both organisms throughout the interaction, our results support the possibility that major staple crops co-evolved mechanisms of RNA-based communication with their microbial pathogens. Based on concomitant deep sequencing of mRNA and sRNA fractions, our work provides the first indication of both plant and fungal sRNAs involvement in the communication between *Magnaporthe oryzae* with the model grass *Brachypodium distachyon*, further supporting the theory of ckRNAi participation in plant–pathogen interactions. Interestingly, sRNAs induced during infection setups show only partial overlap both among the different tissues (leaves, roots) and the different infection phases (leaf: biotrophic, necrotrophic), raising the possibility that ckRNAi in a given host–pathogen interaction exhibits tissue- and lifestyle-specificity.

**Supplementary Materials:** The following are available online at <https://www.mdpi.com/1422-0067/22/2/650/s1>, Figure S1: Analysis of MoAGO and MoDCL protein sequences, Figure S2: Multiple sequence alignment of the PIWI domain of MoAGO proteins, Figure S3: Development of appressoria from conidia of Mo wt and RNAi mutants, Figure S4: Phenotypic analysis of Mo wt and RNA interference mutants, Figure S5: Heatmap for Mo and Bd DEG calling with DESeq2, Figure S6: Results of gene ontology enrichment (GOE) analysis for significantly DE Bd genes in the 4 DPI leaf setup, Figure S7: Results of gene ontology enrichment (GOE) analysis for significantly DE Mo genes in the root setup, Figure S8: Visual representation of the identified upregulated Bd clusters (miRNA precursors) structures, Table S1: Domain structures and coordinates of MoAGOs and MoDCLs as detected by SMART+PFAM search, Table S2: MoAGOs and MoDCLs protein localization prediction results by PSI, Table S3: Prediction of protein interactome for MoDCLs and MoAGOs, Table S4: Expression changes of AGOs and DCLs during the interaction of (A) *B. distachyon* and (B) *M. oryzae* from mRNAseq results, Table S5: Selection of significantly enriched Bd GO terms from 2 DPI, 4 DPI and root Bd DEG datasets, Table S6: Selection of significantly enriched Mo GO terms from 2 DPI, 4 DPI and root Mo DEG datasets, Table S7: Overview of total sRNA and mRNA reads in the *Brachypodium distachyon*–*Magnaporthe oryzae* interaction.

**Author Contributions:** Conceptualization, S.Z., E.Š., T.B. and K.-H.K.; Data curation, S.Z. and E.Š.; Formal analysis, S.Z. and E.Š.; Funding acquisition, K.-H.K.; Investigation, S.Z., E.Š., T.B., M.G., Y.Z. and J.K.; Methodology, S.Z., E.Š., T.B., J.K. and K.-H.K.; Project administration, S.Z. and K.-H.K.; Resources, K.-H.K.; Validation, S.Z., E.Š. and M.G.; Visualization, S.Z., E.Š. and M.G.; Writing—original draft, S.Z. and K.-H.K.; Writing—review & editing, S.Z., E.Š., T.B., M.G., Y.Z., J.K. and K.-H.K. All authors have read and agreed to the published version of the manuscript.

**Funding:** This work was supported by the Deutsche Forschungsgemeinschaft (DFG) in the project RU5116 to K.-H.K. by the European Union's Horizon 2020 research and innovation programme under the Marie Skłodowska-Curie grant agreement No. 674964 to K.-H.K. and S.Z.

**Institutional Review Board Statement:** Not applicable.

**Informed Consent Statement:** Not applicable.

**Data Availability Statement:** The data presented in this study are openly available in ArrayExpress, accessions E-MTAB-9985 and E-MTAB-9984.

**Acknowledgments:** We thank Elke Stein, Dagmar Biedenkopf and Christina Birkenstock for technical assistance. We thank John Vogel and the DOE-JGI for permission to use the Bd21-3 genome under early access conditions. We are grateful to Nicole M. Donofrio, Department of Plant & Soil Sciences, University of Delaware, Newark, for sharing the *Magnaporthe oryzae* mutants. *Brachypodium distachyon* Bd21-3 is a gift of R. Sibout, INRA Versaille. A previous version of this manuscript has been released as a Pre-Print at BioRxiv (Zanini et al. 2019).

**Conflicts of Interest:** The authors declare no conflict of interest.

## References

- Dean, R.; Van Kan, J.A.L.; Pretorius, Z.A.; Hammond-Kosack, K.E.; Di Pietro, A.; Spanu, P.D.; Rudd, J.J.; Dickman, M.; Kahmann, R.; Ellis, J.; et al. The Top 10 fungal pathogens in molecular plant pathology. *Mol. Plant Pathol.* **2012**. [\[CrossRef\]](#)
- Donofrio, N.M.; Hu, J.; Mitchell, T.K.; Wilson, R.A. Facilitating the fungus: Insights from the genome of the rice blast fungus, *Magnaporthe Oryzae*. *Genom. Plant-Assoc. Fungi Monocot Pathog.* **2014**. [\[CrossRef\]](#)
- Fisher, M.C.; Henk, D.A.; Briggs, C.J.; Brownstein, J.S.; Madoff, L.C.; McCraw, S.L.; Gurr, S.J. Emerging fungal threats to animal, plant and ecosystem health. *Nature* **2012**. [\[CrossRef\]](#) [\[PubMed\]](#)
- Sesma, A.; Osbourn, A.E. The rice leaf blast pathogen undergoes developmental processes typical of root-infecting fungi. *Nature* **2004**. [\[CrossRef\]](#)
- Wilson, R.A.; Talbot, N.J. Under pressure: Investigating the biology of plant infection by *Magnaporthe oryzae*. *Nat. Rev. Microbiol.* **2009**, *7*, 185–195. [\[CrossRef\]](#)
- Nalley, L.; Tsiboe, F.; Durand-Morat, A.; Shew, A.; Thoma, G. Economic and environmental impact of rice blast pathogen (*Magnaporthe oryzae*) alleviation in the United States. *PLoS ONE* **2016**. [\[CrossRef\]](#) [\[PubMed\]](#)
- Asibi, A.E.; Chai, Q.; Coulter, J.A. Rice blast: A disease with implications for global food security. *Agronomy* **2019**, *9*, 451. [\[CrossRef\]](#)
- Osés-Ruiz, M.; Talbot, N.J. Cell cycle-dependent regulation of plant infection by the rice blast fungus *Magnaporthe oryzae*. *Commun. Integr. Biol.* **2017**, *10*, e1372067. [\[CrossRef\]](#) [\[PubMed\]](#)
- Talbot, N.J. Having a blast: Exploring the pathogenicity of *Magnaporthe grisea*. *Trends Microbiol.* **1995**, *3*, 9–16. [\[CrossRef\]](#)
- Marcel, S.; Paszkowski, U.; Sawers, R.; Oakeley, E.; Angliker, H. Tissue-adapted invasion strategies of the rice blast fungus *Magnaporthe oryzae*. *Plant Cell* **2010**, *22*, 3177–3187. [\[CrossRef\]](#)
- Routledge, A.P.M.; Shelley, G.; Smith, J.V.; Talbot, N.J.; Draper, J.; Mur, L.A.J. *Magnaporthe grisea* interactions with the model grass *Brachypodium distachyon* closely resemble those with rice (*Oryza sativa*). *Mol. Plant Pathol.* **2004**. [\[CrossRef\]](#)
- Parker, D.; Beckmann, M.; Enot, D.P.; Overy, D.P.; Rios, Z.C.; Gilbert, M.; Talbot, N.; Draper, J. Rice blast infection of *Brachypodium distachyon* as a model system to study dynamic host/pathogen interactions. *Nat. Protoc.* **2008**. [\[CrossRef\]](#) [\[PubMed\]](#)
- Fitzgerald, T.L.; Powell, J.J.; Schneebeli, K.; Hsia, M.M.; Gardiner, D.M.; Bragg, J.N.; McIntyre, C.L.; Manners, J.M.; Ayliffe, M.; Watt, M.; et al. *Brachypodium* as an emerging model for cereal-pathogen interactions. *Ann. Bot.* **2015**. [\[CrossRef\]](#) [\[PubMed\]](#)
- Vogel, J.P.; Garvin, D.F.; Leong, O.M.; Hayden, D.M. Agrobacterium-mediated transformation and inbred line development in the model grass *Brachypodium distachyon*. *Plant Cell. Tissue Organ Cult.* **2006**. [\[CrossRef\]](#)
- Brutnell, T.P.; Bennetzen, J.L.; Vogel, J.P. *Brachypodium distachyon* and *Setaria viridis*: Model Genetic Systems for the Grasses. *Annu. Rev. Plant Biol.* **2015**, *66*, 465–485. [\[CrossRef\]](#) [\[PubMed\]](#)
- Molnar, A.; Melnyk, C.W.; Bassett, A.; Hardcastle, T.J.; Dunn, R.; Baulcombe, D.C. Small silencing RNAs in plants are mobile and direct epigenetic modification in recipient cells. *Science* **2010**, *328*, 872–875. [\[CrossRef\]](#)
- Borges, F.; Martienssen, R.A. The expanding world of small RNAs in plants. *Nat. Rev. Mol. Cell Biol.* **2015**. [\[CrossRef\]](#)
- Kehr, J.; Kragler, F. Long distance RNA movement. *New Phytol.* **2018**. [\[CrossRef\]](#)
- Fire, A.; Xu, S.; Montgomery, M.K.; Kostas, S.A.; Driver, S.E.; Mello, C.C. Potent and specific genetic interference by double-stranded RNA in *Caenorhabditis elegans*. *Nature* **1998**. [\[CrossRef\]](#)
- Vaucheret, H.; Fagard, M. Transcriptional gene silencing in plants: Targets, inducers and regulators. *Trends Genet.* **2001**. [\[CrossRef\]](#)
- Castel, S.E.; Martienssen, R.A. RNA interference in the nucleus: Roles for small RNAs in transcription, epigenetics and beyond. *Nat. Rev. Genet.* **2013**. [\[CrossRef\]](#) [\[PubMed\]](#)
- Hamilton, A.J.; Baulcombe, D.C. A species of small antisense RNA in posttranscriptional gene silencing in plants. *Science* **1999**, *286*, 950–952. [\[CrossRef\]](#) [\[PubMed\]](#)
- Baulcombe, D. RNA silencing in plants. *Nature* **2004**. [\[CrossRef\]](#) [\[PubMed\]](#)
- Vaucheret, H.; Vazquez, F.; Crété, P.; Bartel, D.P. The action of ARGONAUTE1 in the miRNA pathway and its regulation by the miRNA pathway are crucial for plant development. *Genes Dev.* **2004**. [\[CrossRef\]](#) [\[PubMed\]](#)

25. Kadotani, N.; Nakayashiki, H.; Tosa, Y.; Mayama, S. RNA silencing in the phytopathogenic fungus *Magnaporthe oryzae*. *Mol. Plant-Microbe Interact.* **2003**. [[CrossRef](#)]
26. Murphy, D.; Dancis, B.; Brown, J.R. The evolution of core proteins involved in microRNA biogenesis. *BMC Evol. Biol.* **2008**. [[CrossRef](#)]
27. Raman, V.; Simon, S.A.; Demirci, F.; Nakano, M.; Meyers, B.C.; Donofrio, N.M. Small RNA functions are required for growth and development of *magnaporthe oryzae*. *Mol. Plant-Microbe Interact.* **2017**, *30*, 517–530. [[CrossRef](#)]
28. Nunes, C.C.; Gowda, M.; Sailsbery, J.; Xue, M.; Chen, F.; Brown, D.E.; Oh, Y.Y.; Mitchell, T.K.; Dean, R.A. Diverse and tissue-enriched small RNAs in the plant pathogenic fungus, *Magnaporthe oryzae*. *BMC Genom.* **2011**, *12*, 1–20. [[CrossRef](#)]
29. Wei, B.; Cai, T.; Zhang, R.; Li, A.; Huo, N.; Li, S.; Gu, Y.Q.; Vogel, J.; Jia, J.; Qi, Y.; et al. Novel microRNAs uncovered by deep sequencing of small RNA transcriptomes in bread wheat (*Triticum aestivum* L.) and *Brachypodium distachyon* (L.) Beauv. *Funct. Integr. Genom.* **2009**. [[CrossRef](#)]
30. Wang, H.L.V.; Dinwiddie, B.L.; Lee, H.; Chekanova, J.A. Stress-induced endogenous siRNAs targeting regulatory intron sequences in *Brachypodium*. *RNA* **2015**. [[CrossRef](#)]
31. Zhang, J.; Xu, Y.; Huan, Q.; Chong, K. Deep sequencing of *Brachypodium* small RNAs at the global genome level identifies microRNAs involved in cold stress response. *BMC Genom.* **2009**, *10*, 449. [[CrossRef](#)] [[PubMed](#)]
32. Franke, K.R.; Schmidt, S.A.; Park, S.; Jeong, D.H.; Accerbi, M.; Green, P.J. Analysis of *Brachypodium* miRNA targets: Evidence for diverse control during stress and conservation in bioenergy crops. *BMC Genom.* **2018**. [[CrossRef](#)] [[PubMed](#)]
33. Bertolini, E.; Verelst, W.; Horner, D.S.; Gianfranceschi, L.; Piccolo, V.; Inzé, D.; Pè, M.E.; Mica, E. Addressing the role of microRNAs in reprogramming leaf growth during drought stress in *brachypodium distachyon*. *Mol. Plant* **2013**, *6*, 423–443. [[CrossRef](#)] [[PubMed](#)]
34. Jeong, D.H.; Schmidt, S.A.; Rymarquis, L.A.; Park, S.; Ganssmann, M.; German, M.A.; Accerbi, M.; Zhai, J.; Fahlgren, N.; Fox, S.E.; et al. Parallel analysis of RNA ends enhances global investigation of microRNAs and target RNAs of *brachypodium distachyon*. *Genome Biol.* **2013**, *14*, 1–22. [[CrossRef](#)] [[PubMed](#)]
35. Šečić, E.; Zanini, S.; Kogel, K.H. Further Elucidation of the Argonaute and Dicer Protein Families in the Model Grass Species *Brachypodium distachyon*. *Front. Plant Sci.* **2019**, *10*, 1–15. [[CrossRef](#)]
36. Buck, A.H.; Coakley, G.; Simbari, F.; McSorley, H.J.; Quintana, J.F.; Le Bihan, T.; Kumar, S.; Abreu-Goodger, C.; Lear, M.; Marcus, Y.; et al. Exosomes secreted by nematode parasites transfer small RNAs to mammalian cells and modulate innate immunity. *Nat. Commun.* **2014**. [[CrossRef](#)]
37. Lamonte, G.; Philip, N.; Reardon, J.; Lacsina, J.R.; Majoros, W.; Chapman, L.; Thornburg, C.D.; Telen, M.J.; Ohler, U.; Nicchitta, C.V.; et al. Translocation of sickle cell erythrocyte MicroRNAs into *Plasmodium falciparum* inhibits parasite translation and contributes to malaria resistance. *Cell Host Microbe* **2012**. [[CrossRef](#)]
38. Garcia-Silva, M.R.; Cura Das Neves, R.F.; Cabrera-Cabrera, F.; Sanguinetti, J.; Medeiros, L.C.; Robello, C.; Naya, H.; Fernandez-Calero, T.; Souto-Padron, T.; De Souza, W.; et al. Extracellular vesicles shed by *Trypanosoma cruzi* are linked to small RNA pathways, life cycle regulation, and susceptibility to infection of mammalian cells. *Parasitol. Res.* **2014**. [[CrossRef](#)]
39. Zhang, T.; Zhao, Y.L.; Zhao, J.H.; Wang, S.; Jin, Y.; Chen, Z.Q.; Fang, Y.Y.; Hua, C.L.; Ding, S.W.; Guo, H.S. Cotton plants export microRNAs to inhibit virulence gene expression in a fungal pathogen. *Nat. Plants* **2016**. [[CrossRef](#)]
40. Cai, Q.; Qiao, L.; Wang, M.; He, B.; Lin, F.M.; Palmquist, J.; Huang, S.D.; Jin, H. Plants send small RNAs in extracellular vesicles to fungal pathogen to silence virulence genes. *Science* **2018**, *360*, 1126–1129. [[CrossRef](#)]
41. Weiberg, A.; Wang, M.; Lin, F.M.; Zhao, H.; Zhang, Z.; Kaloshian, I.; Huang, H.D.; Jin, H. Fungal small RNAs suppress plant immunity by hijacking host RNA interference pathways. *Science* **2013**, *342*, 118–123. [[CrossRef](#)] [[PubMed](#)]
42. Wang, M.; Weiberg, A.; Dellota, E.; Yamane, D.; Jin, H. Botrytis small RNA Bc-siR37 suppresses plant defense genes by cross-kingdom RNAi. *RNA Biol.* **2017**. [[CrossRef](#)]
43. Zanini, S.; Šečić, E.; Jelonek, L.; Kogel, K.H. A bioinformatics pipeline for the analysis and target prediction of RNA effectors in bidirectional communication during plant–microbe interactions. *Front. Plant Sci.* **2018**, *9*, 1212. [[CrossRef](#)]
44. Zerbino, D.R.; Achuthan, P.; Akanni, W.; Amode, M.R.; Barrell, D.; Bhai, J.; Billis, K.; Cummins, C.; Gall, A.; Girón, C.G.; et al. Ensembl 2018. *Nucleic Acids Res.* **2018**. [[CrossRef](#)]
45. Kershaw, M.J.; Talbot, N.J. Genome-wide functional analysis reveals that infection-associated fungal autophagy is necessary for rice blast disease. *Proc. Natl. Acad. Sci. USA* **2009**. [[CrossRef](#)] [[PubMed](#)]
46. Giraldo, M.C.; Dagdas, Y.F.; Gupta, Y.K.; Mentlak, T.A.; Yi, M.; Martinez-Rocha, A.L.; Saitoh, H.; Terauchi, R.; Talbot, N.J.; Valent, B. Two distinct secretion systems facilitate tissue invasion by the rice blast fungus *Magnaporthe oryzae*. *Nat. Commun.* **2013**, *4*, 1–12. [[CrossRef](#)]
47. Cenik, E.S.; Zamore, P.D. Argonaute proteins. *Curr. Biol.* **2011**, *21*, R446–R449. [[CrossRef](#)]
48. Song, J.J.; Smith, S.K.; Hannon, G.J.; Joshua-Tor, L. Crystal structure of argonaute and its implications for RISC slicer activity. *Science* **2004**, *305*, 1434–1437. [[CrossRef](#)] [[PubMed](#)]
49. Zhang, X.; Niu, D.D.; Carbonell, A.; Wang, A.; Lee, A.; Tun, V.; Wang, Z.; Carrington, J.C.; Chang, C.E.A.; Jin, H. ARGONAUTE PIWI domain and microRNA duplex structure regulate small RNA sorting in *Arabidopsis*. *Nat. Commun.* **2014**. [[CrossRef](#)] [[PubMed](#)]

50. Raman, V.; Simon, S.A.; Romag, A.; Demirci, F.; Mathioni, S.M.; Zhai, J.; Meyers, B.C.; Donofrio, N.M. Physiological stressors and invasive plant infections alter the small RNA transcriptome of the rice blast fungus, *Magnaporthe oryzae*. *BMC Genom.* **2013**, *14*. [[CrossRef](#)] [[PubMed](#)]
51. Kadotani, N.; Murata, T.; Nguyen, B.Q.; Adachi, Y.; Nakayashiki, H. Transcriptional control and protein specialization have roles in the functional diversification of two dicer-like proteins in *Magnaporthe oryzae*. *Genetics* **2008**. [[CrossRef](#)] [[PubMed](#)]
52. Chuang, R.Y.; Weaver, P.L.; Liu, Z.; Chang, T.H. Requirements of the DEAD-box protein Ded1p for messenger RNA translation. *Science* **1997**, *275*, 1468–1471. [[CrossRef](#)] [[PubMed](#)]
53. Spassov, D.S.; Jurecic, R. The PUF Family of RNA-binding Proteins: Does Evolutionarily Conserved Structure Equal Conserved Function? *IUBMB Life* **2003**, *55*, 359–366. [[CrossRef](#)] [[PubMed](#)]
54. Sabnam, N.; Roy Barman, S. WISH, a novel CFEM GPCR is indispensable for surface sensing, asexual and pathogenic differentiation in rice blast fungus. *Fungal Genet. Biol.* **2017**, *105*, 37–51. [[CrossRef](#)]
55. Egan, M.J.; Wang, Z.Y.; Jones, M.A.; Smirnoff, N.; Talbot, N.J. Generation of reactive oxygen species by fungal NADPH oxidases is required for rice blast disease. *Proc. Natl. Acad. Sci. USA* **2007**, *104*, 11772–11777. [[CrossRef](#)]
56. Galhano, R.; Illana, A.; Ryder, L.S.; Rodríguez-Romero, J.; Demuez, M.; Badaruddin, M.; Martinez-Rocha, A.L.; Soanes, D.M.; Studholme, D.J.; Talbot, N.J.; et al. Tpc1 is an important Zn(II)2Cys6transcriptional regulator required for polarized growth and virulence in the rice blast fungus. *PLoS Pathog.* **2017**, *13*, e1006516. [[CrossRef](#)]
57. Choi, J.; Kim, K.S.; Rho, H.S.; Lee, Y.H. Differential roles of the phospholipase C genes in fungal development and pathogenicity of *Magnaporthe oryzae*. *Fungal Genet. Biol.* **2011**, *48*, 445–455. [[CrossRef](#)]
58. Zhang, Z.; Wang, J.; Chai, R.; Qiu, H.; Jiang, H.; Mao, X.; Wang, Y.; Liu, F.; Sun, G. An S-(hydroxymethyl)glutathione dehydrogenase is involved in conidiation and full virulence in the rice blast fungus *Magnaporthe oryzae*. *PLoS ONE* **2015**. [[CrossRef](#)]
59. Tucker, S.L.; Besi, M.I.; Galhano, R.; Franceschetti, M.; Goetz, S.; Lenhert, S.; Osbourn, A.; Sesma, A. Common genetic pathways regulate organ-specific infection-related development in the rice blast fungus. *Plant Cell* **2010**, *22*, 953–972. [[CrossRef](#)]
60. Kawano, T. Roles of the reactive oxygen species-generating peroxidase reactions in plant defense and growth induction. *Plant Cell Rep.* **2003**. [[CrossRef](#)]
61. Powell, J.J.; Carere, J.; Sablok, G.; Fitzgerald, T.L.; Stiller, J.; Colgrave, M.L.; Gardiner, D.M.; Manners, J.M.; Vogel, J.P.; Henry, R.J.; et al. Transcriptome analysis of Brachypodium during fungal pathogen infection reveals both shared and distinct defense responses with wheat. *Sci. Rep.* **2017**. [[CrossRef](#)] [[PubMed](#)]
62. Song, W.-Y.; Wang, G.-L.; Chen, L.L.; Kim, H.-S.; Pi, L.-Y.; Holsten, T.; Gardner, J.; Wang, B.; Zhai, W.-X.; Zhu, L.-H.; et al. A receptor Kinase-Like Protein Encoded by the Rice Disease Resistance Gene, Xa21. *Science* **1995**, *270*, 1804–1806. [[CrossRef](#)] [[PubMed](#)]
63. Ambawat, S.; Sharma, P.; Yadav, N.R.; Yadav, R.C. MYB transcription factor genes as regulators for plant responses: An overview. *Physiol. Mol. Biol. Plants* **2013**. [[CrossRef](#)] [[PubMed](#)]
64. Bakshi, M.; Oelmüller, R. Wrky transcription factors jack of many trades in plants. *Plant Signal. Behav.* **2014**. [[CrossRef](#)] [[PubMed](#)]
65. Murozuka, E.; Massange-Sánchez, J.A.; Nielsen, K.; Gregersen, P.L.; Braumann, I. Genome wide characterization of barley NAC transcription factors enables the identification of grain-specific transcription factors exclusive for the Poaceae family of monocotyledonous plants. *PLoS ONE* **2018**. [[CrossRef](#)] [[PubMed](#)]
66. Samad, A.F.A.; Ali, N.M.; Ismail, I.; Murad, A.M.A. Analysis of miRNAs targeting transcription factors in *Persicaria minor* induced by *Fusarium oxysporum*. *AIP Conf. Proc.* **2016**. [[CrossRef](#)]
67. Cui, L.G.; Shan, J.X.; Shi, M.; Gao, J.P.; Lin, H.X. The miR156-SPL9-DFR pathway coordinates the relationship between development and abiotic stress tolerance in plants. *Plant J.* **2014**, *80*, 1108–1117. [[CrossRef](#)]
68. Li, H.; Wang, Y.; Wang, Z.; Guo, X.; Wang, F.; Xia, X.J.; Zhou, J.; Shi, K.; Yu, J.Q.; Zhou, Y.H. Microarray and genetic analysis reveals that csa-miR159b plays a critical role in abscisic acid-mediated heat tolerance in grafted cucumber plants. *Plant Cell Environ.* **2016**, *39*, 1790–1804. [[CrossRef](#)]
69. Liu, X.H.; Lu, J.P.; Zhang, L.; Dong, B.; Min, H.; Lin, F.C. Involvement of a *Magnaporthe grisea* serine/threonine kinase gene, MgATG1, in Appressorium turgor and pathogenesis. *Eukaryot. Cell* **2007**, *6*, 997–1005. [[CrossRef](#)]
70. Park, C.H.; Chen, S.; Shirsekar, G.; Zhou, B.; Khang, C.H.; Songkumarn, P.; Afzal, A.J.; Ning, Y.; Wang, R.; Bellizzi, M.; et al. The *magnaporthe oryzae* effector avrpiz-t targets the RING E3 ubiquitin ligase APIP6 to suppress pathogen-associated molecular pattern-triggered immunity in rice. *Plant Cell* **2012**. [[CrossRef](#)]
71. Bossche, H.V.; Lauwers, W.; Willemsens, G.; Marichal, P.; Cornelissen, F.; Cools, W. Molecular basis for the antimycotic and antibacterial activity of N-substituted imidazoles and triazoles: The inhibition of isoprenoid biosynthesis. *Pestic. Sci.* **1984**. [[CrossRef](#)]
72. Koch, A.; Kumar, N.; Weber, L.; Keller, H.; Imani, J.; Kogel, K.H. Host-induced gene silencing of cytochrome P450 lanosterol C14 $\alpha$ -demethylase-encoding genes confers strong resistance to *Fusarium* species. *Proc. Natl. Acad. Sci. USA* **2013**. [[CrossRef](#)] [[PubMed](#)]
73. Koch, A.; Biedenkopf, D.; Furch, A.; Weber, L.; Rossbach, O.; Abdellatef, E.; Linicus, L.; Johannsmeier, J.; Jelonek, L.; Goesmann, A.; et al. An RNAi-Based Control of *Fusarium graminearum* Infections Through Spraying of Long dsRNAs Involves a Plant Passage and Is Controlled by the Fungal Silencing Machinery. *PLoS Pathog.* **2016**. [[CrossRef](#)] [[PubMed](#)]

74. Koch, A.; Höfle, L.; Werner, B.T.; Imani, J.; Schmidt, A.; Jelonek, L.; Kogel, K.H. SIGS vs. HIGS: A study on the efficacy of two dsRNA delivery strategies to silence *Fusarium* FgCYP51 genes in infected host and non-host plants. *Mol. Plant Pathol.* **2019**. [\[CrossRef\]](#)
75. Margis, R.; Fusaro, A.F.; Smith, N.A.; Curtin, S.J.; Watson, J.M.; Finnegan, E.J.; Waterhouse, P.M. The evolution and diversification of Dicers in plants. *FEBS Lett.* **2006**. [\[CrossRef\]](#)
76. Feller, A.; MacHemer, K.; Braun, E.L.; Grotewold, E. Evolutionary and comparative analysis of MYB and bHLH plant transcription factors. *Plant J.* **2011**. [\[CrossRef\]](#)
77. Kang, J.; Park, J.; Choi, H.; Burla, B.; Kretschmar, T.; Lee, Y.; Martinoia, E. Plant ABC Transporters. *Arab. Book/Am. Soc. Plant Biol.* **2011**, 9, e0153. [\[CrossRef\]](#)
78. Afzal, Z.; Howton, T.C.; Sun, Y.; Mukhtar, M.S. The roles of aquaporins in plant stress responses. *J. Dev. Biol.* **2016**, 9. [\[CrossRef\]](#)
79. Riley, K.J.; Yario, T.A.; Steitz, J.A. Association of argonaute proteins and microRNAs can occur after cell lysis. *RNA* **2012**. [\[CrossRef\]](#)
80. Carbonell, A. Plant ARGONAUTES: Features, functions, and unknowns. *Methods Mol. Biol.* **2017**. [\[CrossRef\]](#)
81. Dereeper, A.; Guignon, V.; Blanc, G.; Audic, S.; Buffet, S.; Chevenet, F.; Dufayard, J.F.; Guindon, S.; Lefort, V.; Lescot, M.; et al. Phylogeny.fr: Robust phylogenetic analysis for the non-specialist. *Nucleic Acids Res.* **2008**. [\[CrossRef\]](#) [\[PubMed\]](#)
82. Goujon, M.; McWilliam, H.; Li, W.; Valentin, F.; Squizzato, S.; Paern, J.; Lopez, R. A new bioinformatics analysis tools framework at EMBL-EBI. *Nucleic Acids Res.* **2010**. [\[CrossRef\]](#)
83. Sievers, F.; Wilm, A.; Dineen, D.; Gibson, T.J.; Karplus, K.; Li, W.; Lopez, R.; McWilliam, H.; Remmert, M.; Söding, J.; et al. Fast, scalable generation of high-quality protein multiple sequence alignments using Clustal Omega. *Mol. Syst. Biol.* **2011**. [\[CrossRef\]](#) [\[PubMed\]](#)
84. Brown, N.P.; Leroy, C.; Sander, C. MView: A web-compatible database search or multiple alignment viewer. *Bioinformatics* **1998**. [\[CrossRef\]](#) [\[PubMed\]](#)
85. Schultz, J.; Milpetz, F.; Bork, P.; Ponting, C.P. SMART, a simple modular architecture research tool: Identification of signaling domains. *Proc. Natl. Acad. Sci. USA* **1998**. [\[CrossRef\]](#)
86. Letunic, I.; Bork, P. 20 years of the SMART protein domain annotation resource. *Nucleic Acids Res.* **2018**. [\[CrossRef\]](#)
87. Liu, W.; Xie, Y.; Ma, J.; Luo, X.; Nie, P.; Zuo, Z.; Lahrmann, U.; Zhao, Q.; Zheng, Y.; Zhao, Y.; et al. IBS: An illustrator for the presentation and visualization of biological sequences. *Bioinformatics* **2015**. [\[CrossRef\]](#)
88. Liu, L.; Zhang, Z.; Mei, Q.; Chen, M. PSI: A Comprehensive and Integrative Approach for Accurate Plant Subcellular Localization Prediction. *PLoS ONE* **2013**. [\[CrossRef\]](#)
89. Szklarczyk, D.; Gable, A.L.; Lyon, D.; Junge, A.; Wyder, S.; Huerta-Cepas, J.; Simonovic, M.; Doncheva, N.T.; Morris, J.H.; Bork, P.; et al. STRING v11: Protein-protein association networks with increased coverage, supporting functional discovery in genome-wide experimental datasets. *Nucleic Acids Res.* **2019**. [\[CrossRef\]](#)
90. Waterhouse, A.; Bertoni, M.; Bienert, S.; Studer, G.; Tauriello, G.; Gumienny, R.; Heer, F.T.; De Beer, T.A.P.; Rempfer, C.; Bordoli, L.; et al. SWISS-MODEL: Homology modelling of protein structures and complexes. *Nucleic Acids Res.* **2018**. [\[CrossRef\]](#)
91. Benkert, P.; Biasini, M.; Schwede, T. Toward the estimation of the absolute quality of individual protein structure models. *Bioinformatics* **2011**. [\[CrossRef\]](#) [\[PubMed\]](#)
92. Morris, A.L.; MacArthur, M.W.; Hutchinson, E.G.; Thornton, J.M. Stereochemical quality of protein structure coordinates. *Proteins Struct. Funct. Bioinforma* **1992**. [\[CrossRef\]](#) [\[PubMed\]](#)
93. Laskowski, R.A.; MacArthur, M.W.; Moss, D.S.; Thornton, J.M. PROCHECK: A program to check the stereochemical quality of protein structures. *J. Appl. Crystallogr.* **1993**. [\[CrossRef\]](#)
94. Hooft, R.W.W.; Vriend, G.; Sander, C.; Abola, E.E. Errors in protein structures. *Nature* **1996**. [\[CrossRef\]](#) [\[PubMed\]](#)
95. Ramachandran, G.N.; Ramakrishnan, C.; Sasisekharan, V. Stereochemistry of polypeptide chain configurations. *J. Mol. Biol.* **1963**. [\[CrossRef\]](#)
96. Delano, W.L. *The PyMOL Molecular Graphics System*, version 1.8; Schrödinger LLC: New York, NY, USA, 2002.
97. Vogel, J.; Hill, T. High-efficiency *Agrobacterium*-mediated transformation of *Brachypodium distachyon* inbred line Bd21-3. *Plant Cell Rep.* **2008**. [\[CrossRef\]](#)
98. Schneider, C.A.; Rasband, W.S.; Eliceiri, K.W. NIH Image to ImageJ: 25 years of image analysis. *Nat. Methods* **2012**. [\[CrossRef\]](#)
99. Murashige, T.; Skoog, F. A Revised Medium for Rapid Growth and Bio Assays with Tobacco Tissue Cultures. *Physiol. Plant.* **1962**. [\[CrossRef\]](#)
100. Kim, D.; Langmead, B.; Salzberg, S.L. HISAT: A fast spliced aligner with low memory requirements. *Nat. Methods* **2015**. [\[CrossRef\]](#)
101. Yates, A.D.; Achuthan, P.; Akanni, W.; Allen, J.; Allen, J.; Alvarez-Jarreta, J.; Amode, M.R.; Armean, I.M.; Azov, A.G.; Bennett, R.; et al. Ensembl 2020. *Nucleic Acids Res.* **2020**. [\[CrossRef\]](#)
102. Anders, S.; Pyl, P.T.; Huber, W. HTSeq-A Python framework to work with high-throughput sequencing data. *Bioinformatics* **2015**. [\[CrossRef\]](#) [\[PubMed\]](#)
103. Love, M.I.; Huber, W.; Anders, S. Moderated estimation of fold change and dispersion for RNA-seq data with DESeq2. *Genome Biol.* **2014**. [\[CrossRef\]](#)
104. Kolde, R. Package 'pheatmap'. *Bioconductor* **2015**, 7, 790.
105. Tian, T.; Liu, Y.; Yan, H.; You, Q.; Yi, X.; Du, Z.; Xu, W.; Su, Z. AgriGO v2.0: A GO analysis toolkit for the agricultural community, 2017 update. *Nucleic Acids Res.* **2017**. [\[CrossRef\]](#) [\[PubMed\]](#)

106. Conesa, A.; Götz, S.; García-Gómez, J.M.; Terol, J.; Talón, M.; Robles, M. Blast2GO: A universal tool for annotation, visualization and analysis in functional genomics research. *Bioinformatics* **2005**. [[CrossRef](#)]
107. Andrews, S. FastQC:—A quality control tool for high throughput sequence data. *Babraham Bioinforma* **2010**. Available online: <http://www.bioinformatics.babraham.ac.uk/projects/fastqc/> (accessed on 11 January 2018).
108. Martin, M. Cutadapt removes adapter sequences from high-throughput sequencing reads. *EMBnet. J.* **2011**. [[CrossRef](#)]
109. Langmead, B. Aligning short sequencing reads with Bowtie. *Curr. Protoc. Bioinforma* **2010**. [[CrossRef](#)]
110. Chen, H.; Boutros, P.C. VennDiagram: A package for the generation of highly-customizable Venn and Euler diagrams in R. *BMC Bioinform.* **2011**. [[CrossRef](#)]
111. Johnson, N.R.; Yeoh, J.M.; Coruh, C.; Axtell, M.J. Improved placement of multi-mapping small RNAs. *G3 Genes Genomes Genet.* **2016**. [[CrossRef](#)]
112. Griffiths-Jones, S.; Grocock, R.J.; van Dongen, S.; Bateman, A.; Enright, A.J. miRBase: microRNA sequences, targets and gene nomenclature. *Nucleic Acids Res.* **2006**. [[CrossRef](#)] [[PubMed](#)]
113. Dai, X.; Zhao, P.X. PsRNATarget: A plant small RNA target analysis server. *Nucleic Acids Res.* **2011**. [[CrossRef](#)] [[PubMed](#)]
114. Baldwin, T.K.; Winnenburg, R.; Urban, M.; Rawlings, C.; Koehler, J.; Hammond-Kosack, K.E. The Pathogen-Host Interactions Database (PHI-base) provides insights into generic and novel themes of pathogenicity. *Mol. Plant-Microbe Interact.* **2006**. [[CrossRef](#)] [[PubMed](#)]



# Requirements for fungal uptake of dsRNA and gene silencing in RNAi-based crop protection strategies

Ena Šečić and Karl-Heinz Kogel

Growing evidence indicates that RNAi is an effective control strategy for agronomically important fungi. To implement RNAi-based crop protection strategies, dsRNA molecules are either sprayed on foliage or generated by genetically engineered plants. Here, we summarize current knowledge of the mechanisms governing dsRNA uptake and RNAi-mediated gene silencing in fungi, as well as the factors that influence these phenomena. Of primary importance is dsRNA design, as identifying an appropriate gene for silencing and determining which region of the gene to target are critical for maximizing efficiency. Strategies for enhancing dsRNA uptake, potentially by using formulations and/or carriers that prevent dsRNA degradation by (a)biotic factors and possibly facilitate translocation, also are a key consideration. Finally, determining whether the fungal pathogen of interest contains a functional RNAi machinery is a major consideration. Integrated experimental confirmation of these important factors is necessary for the successful development of crop protection strategies against fungal pathogens.

## Address

Institute of Phytopathology, Centre for BioSystems, Land Use and Nutrition, Justus Liebig University, Heinrich-Buff-Ring 26, 35392 Giessen, Germany

Corresponding author:

Kogel, Karl-Heinz ([Karl-Heinz.Kogel@agr.uni-giessen.de](mailto:Karl-Heinz.Kogel@agr.uni-giessen.de))

**Current Opinion in Biotechnology** 2021, **70**:136–142

This review comes from a themed issue on **Plant biotechnology**

Edited by **Robert Schuurink** and **Harro Bouwmeester**

For a complete overview see the [Issue](#) and the [Editorial](#)

Available online 14th May 2021

<https://doi.org/10.1016/j.copbio.2021.04.001>

0958-1669/© 2021 The Author(s). Published by Elsevier Ltd. This is an open access article under the CC BY-NC-ND license (<http://creativecommons.org/licenses/by-nc-nd/4.0/>).

## Introduction

RNA interference (RNAi)-based plant protection strategies were established on the knowledge that plant-derived or exogenous double-stranded RNA (dsRNA) molecules can silence essential or virulence genes in microbial pathogens and pests. These strategies are advantageous due to the highly specific, environmentally friendly and malleable nature of dsRNAs. Moreover, RNAi implemented via transgenic Host-Induced Gene Silencing (HIGS) [1] or environmental uptake (ex. Spray-

Induced Gene Silencing; SIGS) [2] has been proven effective in several plant-pathogen/pest systems [3,4,5\*,6]. Beyond these plant protection strategies, a natural mechanism, called cross-kingdom communication, has been shown to involve bidirectional exchange of small RNA duplexes (sRNA; equiv. 20–24 nt long dsRNAs) between plant and microbial cells and thereby lead to silencing of immune response or virulence genes [7–11, reviewed in Refs. 2 and 12]. After transfer of dsRNA from plant cells into fungi, whether during cross-kingdom communication, HIGS, or SIGS, gene silencing occurs by exploiting the microbial RNAi machinery [13,14]. The RNAi pathway in fungi is involved in maintenance of genome integrity, response to environmental signals, development and pathogenesis, and branches into several subpathways that result in post-transcriptional mRNA degradation/inhibition or epigenetic modifications on the transcriptional level [15]. Based on considerations in current research and application, we focus here on the canonical post-transcriptional gene silencing (PTGS) subpathway.

While physical and physiological hurdles for RNAi-based strategies aimed at regulating plant genes [16\*] or providing insect control [5\*] have been reviewed recently, a detailed assessment of the obstacles for RNA-based biofungicides as a plant protection strategy is lacking. Although there is undeniable potential for RNAi-based protection against harmful fungi, especially for (SIGS-based) control of cereal pathogens [1,2], applications are currently more advanced in RNAi-based insecticides [5\*]. Here, we focus on recently published studies that shed light on the issues that must be addressed in order to develop a successful RNAi-based protection strategy against fungal pathogens. Since fungal cells can internalize exogenous dsRNA either directly from the environment, liquid culture or foliar surface (SIGS); or indirectly following its synthesis/movement through plant tissue (HIGS or SIGS), potential obstacles related to both direct and indirect uptake will be addressed. Specific considerations for dsRNA design, stability, formulation and the activity of fungal RNAi machinery also will be covered.

## Before uptake — physical barriers, endocytosis and RNA stability

A critical requirement for RNAi-mediated plant protection against fungal pathogens is the successful uptake of dsRNA by the fungal cells. This requires the dsRNA to pass through the hyphal cell wall, which is composed of chitin, polysaccharides and glycoproteins, and the plasma

membrane, which consists of lipids and protein/lipid heterogeneous domains [17–19], while remaining stable from environmental degradation and evading potentially secreted fungal nucleases. Direct uptake of dsRNA and/or sRNA has been detected in various fungi [20\*\*], which suggests the existence of uptake pathways that are not impeded by the hyphal cell wall and/or membrane. For example, uptake of fluorescein-labelled dsRNA or shorter sRNA fragments was detected in germinating *Botrytis cinerea* spores grown on agar medium and in protoplasts isolated from liquid fungal culture co-incubated with dsRNA after 12 hours or 20 hours of dsRNA application, respectively [14]. Moreover, this uptake correlated with silencing of the targeted fungal genes *DCL1* (DICER-LIKE1) and *DCL2*, as well as inhibition of *B. cinerea* virulence after external application on plants. Treatment of *Fusarium graminearum* conidia with dsRNA for 24 hours also resulted in silencing of targeted fungal ergosterol biosynthesis genes [13]. More recently, the uptake and silencing efficiency of various dsRNAs applied over a dose gradient was assessed in liquid cultures of *Sclerotinia sclerotiorum* [21]. Uptake and silencing of target genes after *in vitro* treatment with dsRNA also was recently demonstrated in *Fusarium* spp., *B. cinerea*, *Magnaporthe oryzae* and *Colletotrichum truncatum* [22,23\*\*].

A landmark study investigating the mechanism for exogenous dsRNA uptake in fungi recently demonstrated that clathrin-mediated endocytosis (CME), a well-known and conserved eukaryotic pathway [24], is responsible for dsRNA uptake in *S. sclerotiorum* [25\*\*]. Using fluorescence imaging, labeled dsRNA uptake was detected as early as two hours after co-incubation, especially at newly growing hyphal branches. In humans, extracellular dsRNA binds to surface receptors and then is internalized by CME, before it is further recognized by endosomal or cytosolic receptors [26]. CME of dsRNA also has been identified in *Drosophila* cells [27], and in other insect species [20\*\*]. Interestingly, sRNA uptake in some insect groups can involve systemic RNA interference deficient-1 (Sid-1)-like (SIL) transmembrane proteins [28], while fungi lack their orthologs, and thus greatly rely on CME [20\*\*].

In comparison to direct dsRNA uptake, the ability of fungal cells to internalize dsRNA synthesized by or transited through plant tissue requires overcoming several additional, potential obstacles. These include dsRNA stability *in planta*, as well as its ability to pass through the plant cuticle, cell wall, plasma membrane and/or avoid digestion by plant-generated nucleases [16\*]. An additional concern for SIGS-mediated pathogen control is whether untreated portions of the plant are protected. Importantly, SIGS-induced mitigation of *F. graminearum* infection in barley was associated with semi-systemic transport of the sprayed dsRNA [13]. The mechanism (s) supporting indirect dsRNA uptake by fungi is not

well understood. Based on current knowledge of cross-kingdom RNAi, it is hypothesized that sRNAs are released from the plant cell in exosomes or extracellular vesicles (EVs). Uptake of EVs by fungal cells presumably occurs via endocytic fusion with the plasma membrane [29,9,30], comprehensively reviewed in Cai *et al.* [4].

Since hyphal elongation occurs mostly at the tips, and this process requires rapid and extensive cell-to-cell molecular transport, endocytosis-based membrane recycling and secretion of vesicles [17], this region may be involved in dsRNA uptake. Indeed, internalization of fluorescent-labelled dsRNA by *S. sclerotiorum* hyphae occurred predominantly at the hyphal tip [25\*\*]. In some pathogenic fungi, the hyphal tips differentiate into specialized infection organelles such as appressoria and haustoria during plant colonization [17,31,32]. Whether these sites are primary locations of sRNA-based cross-kingdom vesicle exchange is unknown.

To develop a successful HIGS-based or SIGS-based anti-fungal protection strategy, several critical aspects of dsRNA design must be considered. The first decision involves selecting an effective fungal target gene. The dsRNA sequence must then be designed to *i.* minimize off-target effects [33], *ii.* optimize silencing efficiency, since this varied substantially for dsRNA molecules from different parts of the target genes, and *iii.* maximize dsRNA stability. For example, dsRNA derived from several regions of the *Myosin 5* gene in *Fusarium asiaticum* varied in efficiency of reducing fungal growth [22] and application of dsRNAs from several regions of *F. asiaticum*-derived  $\beta 2$ -tubulin gene also resulted in differential silencing efficiency and reduction of growth and virulence [23\*\*]. Further on, dsRNA-degrading nucleases are known to affect dsRNA stability and silencing efficiency in several insect species [34–36]. Currently, no extracellular fungal nucleases that are specifically secreted to degrade dsRNA and impair RNAi silencing have been identified. However, a fungal extracellular S1 nuclease that degrades ssDNA, RNA and dsDNA [37] and dsRNA mycoviruses have been detected [38], implying that the existence of secreted dsRNA nucleases in fungi cannot be excluded. Environmental factors also can cause dsRNA degradation. The rules for designing dsRNA with optimal stability are poorly understood; however, formulations and/or chemical carriers for dsRNA molecules can help minimize degradation by (a)biotic agents [39]. In pertinent examples, nanoparticles have been applied for stable and controlled release of dsRNA mediating protection against plant viruses [40,41], DNA nanostructures have been used to aid silencing of constitutively expressed plant genes [42], and carbon dots for silencing of plant transgenes [43]. While assessing formulations and carriers, it is crucial to include variable environmental conditions to assess stability, as shown with chitosan and dsRNA nanoparticles in *Caenorhabditis elegans* [44].

Manipulating growth conditions to place fungi under stress also may modify the efficiency of RNAi-based silencing, as reported in the case of *Macrophomina phaseolina* [45]. In this example, growing the fungus under suboptimal conditions for temperature and nutrient supply hinted to a higher sensitivity of the fungus to dsRNA, indicating that: i) successful application of dsRNA as a biofungicide can be achieved under variable climate conditions and ii) application of dsRNA in coordination with planting times and weather/soil temperatures should improve the success of RNAi-based protection strategies. Lastly, there is a dsRNA dose/concentration effect to be considered within an uptake/silencing study, in order to determine the minimum dose necessary for significant growth reduction [45] or transcript silencing [21].

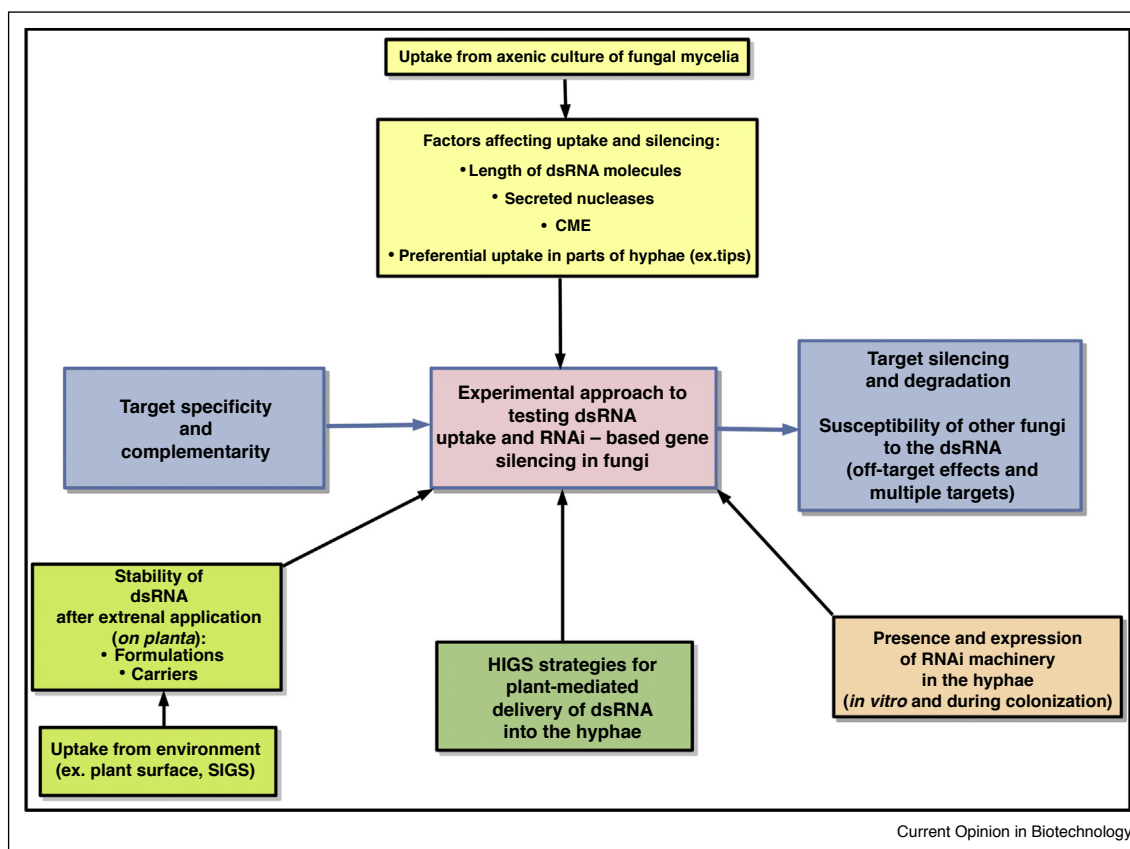
Together, these findings indicate that dsRNA uptake and RNAi silencing are influenced by environmental conditions. Since the dsRNA must be internalized into the hyphae to interact with the RNAi machinery [20<sup>••</sup>], all of

the barriers and factors impeding uptake have to be surpassed successfully. Developing an RNAi-based control strategy therefore requires assessing a wide range of factors, including endocytosis pathways, potential nuclease activity, fungal life-style and stage of growth. We summarize the major factors to take into consideration in Figure 1.

### After uptake – fungal RNAi machinery and gene silencing

For exogenously supplied or plant-associated dsRNAs to mediate target gene silencing and thereby reduce fungal infection, they must not only be internalized by a sufficient number of fungal cells, but these cells must possess functional RNAi machinery. RNAi silencing, which is broadly conserved in eukaryotes, encompasses several related pathways that mediate post-transcriptional gene silencing [20<sup>••</sup>], as well as maintenance of genome stability and regulation of physiological and developmental processes and responses to (a)biotic stresses [15]. The

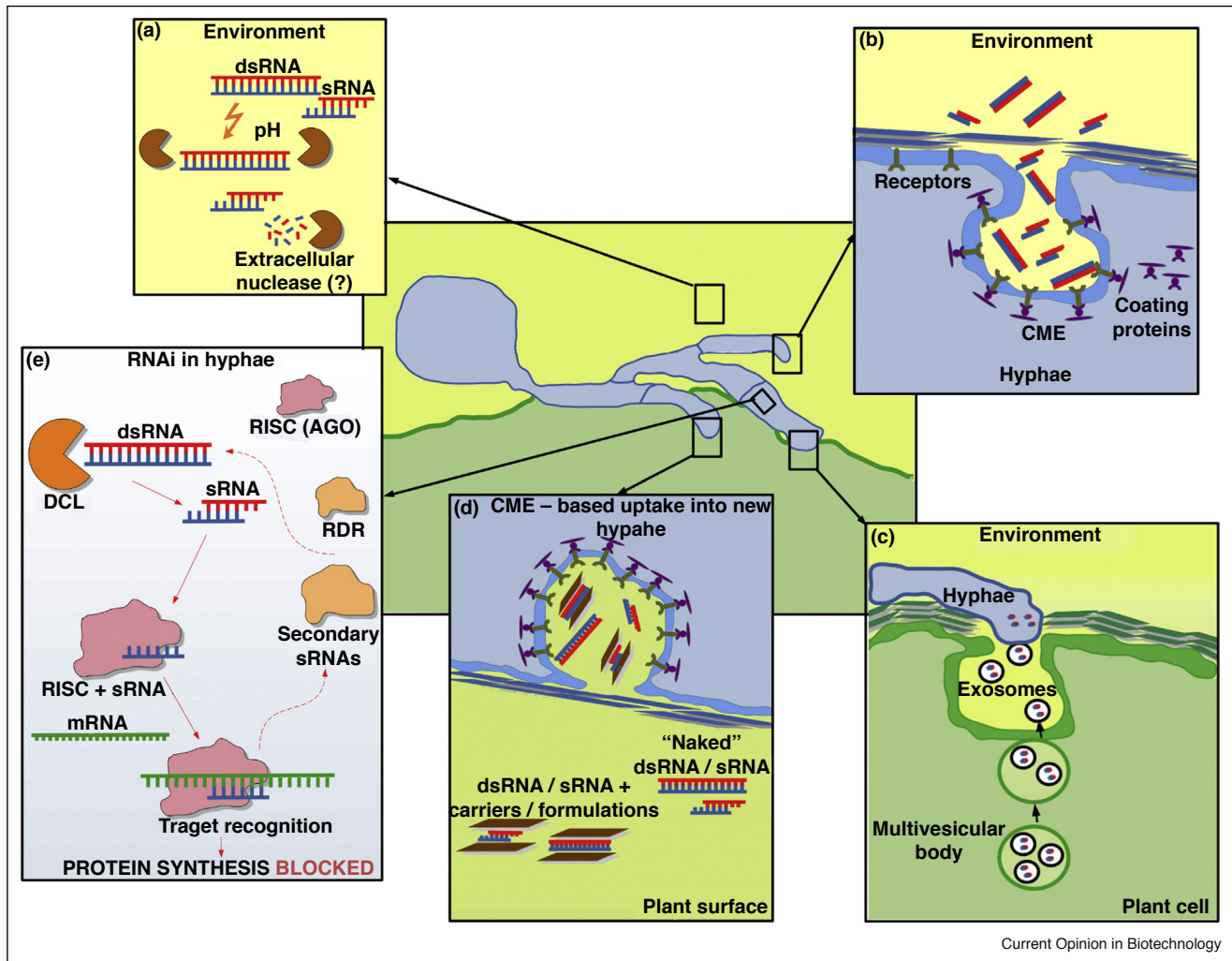
Figure 1



Important factors influencing dsRNA uptake and RNAi-based gene silencing in fungi.

The process of dsRNA design is represented by three central boxes connected by blue arrows: a designed dsRNA that can specifically target an mRNA (blue box, left), which leads to experimental approaches to test dsRNA uptake and gene silencing in fungi (pink box). Finally, the effectiveness of the dsRNA is validated by confirming target silencing and degradation (blue box, right). Important aspects of the experimental setup are indicated with black arrows: testing and improving *i.* stability and uptake of dsRNA in axenic fungal mycelia (yellow), *ii.* uptake and silencing after external application to the plant surface (lighter green), or *iii.* uptake from plant tissue (darker green), and *iv.* assessing the expression and activity of the fungal RNAi machinery after uptake (orange).

Figure 2



Current Opinion in Biotechnology

Schematic representation of dsRNA uptake and processing in fungi.

Deployed dsRNA molecules must successfully overcome a number of obstacles before uptake and come in contact with the RNAi machinery after uptake. **(a)** Stability to degradation (ex. liquid media) by potentially secreted fungal nucleases (which have not been described so far, thus marked with a '?') and abiotic factors is necessary; **(b)** the plasma membrane has to be bypassed, for example by clathrin-mediated uptake (CME) of dsRNA/sRNA molecules from the environment, or **(c)** uptake of extracellular vesicles from plant tissue; **(d)** with potential use of formulations and carriers to ensure stability. Lastly, **(e)** access to fungal RNAi proteins after uptake in the cytoplasm is necessary for silencing to occur.

canonical RNAi machinery includes DICER or DCL endonucleases, which process the dsRNA into shorter sRNAs. These sRNAs are then loaded onto ARGONAUTE (AGO) proteins. Recruitment of additional proteins, along with release of the passenger RNA strand, leads to formation of an active RNA-induced silencing complex (RISC), which uses the retained guide RNA strand to identify complementary target transcript sequences for silencing. In addition, RNA-DEPENDENT RNA POLYMERASES (RDRs) are involved in generating and/or amplifying dsRNAs in many organisms, including fungi [15].

Although RNAi is an important regulatory mechanism in eukaryotes, key components of this pathway are lacking in some fungi [46]. For example, genomic analyses have indicated that some or all of the genes encoding canonical RNAi machinery components are missing in the plant pathogen *Ustilago maydis*; this correlates with the failure of introduced dsRNAs to suppress target gene expression [47]. Thus, ensuring that a particular fungal pathogen contains functional RNAi machinery is an essential consideration for developing a successful RNAi-mediated control strategy. Current knowledge of typical protein domains for major RNAi proteins should facilitate

bioinformatics analyses to assess gene copy number, as well as its structural and functional details, followed by confirmation of expression in the life stage and conditions under which the application of dsRNA is planned [48].

In plants, initial uptake of dsRNA is followed by production of secondary sRNAs. This process, which is mediated by RDRs and 22 nt long sRNAs [16<sup>\*</sup>], enables a small number of primary sRNAs to effect wide-spread changes in gene expression. While RDRs exist in fungi, a recently published study on *F. asiaticum* indicated insufficient sRNA secondary amplification to maintain the silencing after the initially applied exogenous dsRNA was removed [49]. This finding raises questions about the viability of an RNAi-based crop protection against some fungi, when the dsRNA is not continuously produced by the plant (HIGS), or repeatedly supplied exogenously (SIGS).

Finally, it should be noted that RNAi-based control strategies may not be a suitable option for some fungal pathogens even if they contain a RNAi machinery. A recent study of *Zymoseptoria tritici* failed to detect either dsRNA uptake or HIGS-induced silencing of the targeted genes [50]. Furthermore, no cross-kingdom communication was observed between this pathogen and wheat [50,51]. As this result could be due to an obstacle in the internalization of dsRNAs, the importance of the uptake as a critical prerequisite for RNAi-based applications in crop protection is once again underlined. On the other hand, if several types of RNAi strategies can be successfully applied to a plant-pathogen system, a comparison of their efficiency in silencing the same gene is desirable, as shown by the example of HIGS versus SIGS strategies in barley against *F. graminearum* [52].

## Conclusion

Although our understanding of non-coding RNA communication mechanisms and their application to plant protection strategies is growing (for comprehensive reviews see Refs. [2,12]), insights into many fungal-plant systems, especially those of major agricultural significance, are still missing. As currently understood, the basic requirements for successful RNAi-mediated gene silencing in fungal cells are: *i.* maintenance of dsRNA stability long enough for uptake to occur, *ii.* successful uptake of dsRNA molecules into fungal cells, either directly from the environment or indirectly from plant cells that contact the fungal hyphae or infection structures, and *iii.* presence of a functional fungal RNAi machinery that will mediate the silencing process. These basic requirements are depicted in Figure 2. Future efforts to develop dsRNAs for use as novel biofungicides will require assessing different targets in a wide range of fungal species, and evaluating parameters, including but not limited to: target choice optimization, dsRNA length adjustments, simultaneous measurement of target silencing and degradation, the functionality of CME, and the differential dsRNA

uptake in newly growing hyphae versus mature mycelium. The information gathered from these studies will not only provide a deeper understanding of dsRNA uptake and silencing mechanisms in fungal cells, but also should facilitate the translation of proof-of-concept studies to agricultural applications. Before applications are realized, the challenges of specific targeting (avoidance of off-targets) and enhancing stability under field conditions, as well as finding improved formulations and reducing production costs remain. Overall, it is perhaps most realistic that a future commercial RNAi biofungicide will be incorporated into an integrated/stacked plant protection strategy that provides some safety against development of compound resistance, as has been the case with RNAi insecticides [53].

## Funding statement

Research of KHK was supported by the Deutsche Forschungsgemeinschaft (DFG RU5116).

## Conflict of interest statement

Nothing declared.

## CRedit authorship contribution statement

**Ena Sečić:** Conceptualization, Visualization, Writing - review & editing. **Karl-Heinz Kogel:** Conceptualization, Funding acquisition, Supervision, Writing - review & editing.

## Acknowledgements

The authors acknowledge funding from the Deutsche Forschungsgemeinschaft (DFG RU5116). We thank D'Maris Dempsey for assistance in editing the manuscript.

## References and recommended reading

Papers of particular interest, published within the period of review, have been highlighted as:

- of special interest
- of outstanding interest

1. Qi T, Guo J, Peng H, Liu P, Kang Z, Guo J: **Host-Induced Gene Silencing: a powerful strategy to control diseases of wheat and barley.** *Int J Mol Sci* 2019, **20**:206.
2. Cai Q, He B, Kogel K-H, Jin H: **Cross-kingdom RNA trafficking and environmental RNAi – nature's blueprint for modern crop protection strategies.** *Curr Opin Microbiol* 2018, **46**:58-64.
3. Rosa C, Kuo Y-W, Wuriyangan H, Falk BW: **RNA interference mechanisms and applications in plant pathology.** *Annu Rev Phytopathol* 2018, **56**:581-610.
4. Cai Q, He B, Weiberg A, Buck AH, Jin H: **Small RNAs and extracellular vesicles: new mechanisms of cross-species communication and innovative tools for disease control.** *PLoS Pathog* 2019, **15**:e1008090.
5. Liu S, Jaouannet M, Dempsey DA, Imani J, Coustau C, Kogel K-H: **RNA-based technologies for insect control in plant production.** *Biotechnol Adv* 2020, **39**:107463.
6. Sang H, Kim J-I: **Advanced strategies to control plant pathogenic fungi by host-induced gene silencing (HIGS) and**

This paper comprehensively reviews the use of dsRNA in insect control by discussing both major aspects of dsRNA uptake and safety issues related to future applications.

- spray-induced gene silencing (SIGS).** *Plant Biotechnol Rep* 2020, **14**:1-8.
7. Weiberg A, Wang M, Lin F-M, Zhao H, Zhang Z, Kaloshian I, Huang H-D, Jin H: **Fungal small RNAs suppress plant immunity by hijacking host RNA interference pathways.** *Science* (80-) 2013, **342**:118-123.
  8. Zhang T, Zhao YL, Zhao JH, Wang S, Jin Y, Chen ZQ, Fang YY, Hua CL, Ding SW, Guo HS: **Cotton plants export microRNAs to inhibit virulence gene expression in a fungal pathogen.** *Nat Plants* 2016, **2**:1-6.
  9. Cai Q, Qiao L, Wang M, He B, Lin F-M, Palmquist J, Huang H-D, Jin H: **Plants send small RNAs in extracellular vesicles to fungal pathogen to silence virulence genes.** *Science* (80-) 2018, **360**:eaar4142.
  10. Ren B, Wang X, Duan J, Ma J: **Rhizobial tRNA-derived small RNAs are signal molecules regulating plant nodulation.** *Science* (80-) 2019, **365**.
  11. Dunker F, Trutzenberg A, Rothenpieler JS, Kuhn S, Pröls R, Schreiber T, Tissier A, Kemen A, Kemen E, Hückelhoven R *et al.*: **Oomycete small RNAs bind to the plant RNA-induced silencing complex for virulence.** *eLife* 2020, **9**:e56096.
  12. Zeng J, Gupta VK, Jiang Y, Yang B, Gong L, Zhu H: **Cross-kingdom small RNAs among animals, plants and microbes.** *Cells* 2019, **8**:371.
  13. Koch A, Biedenkopf D, Furch A, Weber L, Rossbach O, Abdellatef E, Linicus L, Johannsmeier J, Jelonek L, Goessmann A *et al.*: **An RNAi-based control of *Fusarium graminearum* infections through spraying of long dsRNAs involves a plant passage and is controlled by the fungal silencing machinery.** *PLoS Pathog* 2016, **12**:e1005901.
  14. Wang M, Weiberg A, Lin F-M, Thomma BPHJ, Huang H-D, Jin H: **Bidirectional cross-kingdom RNAi and fungal uptake of external RNAs confer plant protection.** *Nat Plants* 2016, **2**:16151.
  15. Torres-Martínez S, Ruiz-Vázquez RM: **The RNAi universe in fungi: a varied landscape of small RNAs and biological functions.** *Annu Rev Microbiol* 2017, **71**:371-391.
  16. Bennett M, Deikman J, Hendrix B, Iandolo A: **Barriers to efficient foliar uptake of dsRNA and molecular barriers to dsRNA activity in plant cells.** *Front Plant Sci* 2020, **11**:816
- This paper systematically describes the barriers dsRNA may overcome when applied directly to leaves.
17. Riquelme M, Aguirre J, Bartnicki-García S, Braus GH, Feldbrügge M, Fleig U, Hansberg W, Herrera-Estrella A, Kämper J, Kück U *et al.*: **Fungal morphogenesis, from the polarized growth of hyphae to complex reproduction and infection structures.** *Microbiol Mol Biol Rev* 2018, **82**:e00068-17.
  18. Kang X, Kirui A, Muszyński A, Widanage MCD, Chen A, Azadi P, Wang P, Mentink-Vigier F, Wang T: **Molecular architecture of fungal cell walls revealed by solid-state NMR.** *Nat Commun* 2018, **9**:2747.
  19. Athanasopoulos A, André B, Sophianopoulou V, Gournas C: **Fungal plasma membrane domains.** *FEMS Microbiol Rev* 2019, **43**:642-673.
  20. Wytinck N, Manchur CL, Li VH, Whyard S, Belmonte MF: **dsRNA uptake in plant pests and pathogens: insights into RNAi-based insect and fungal control technology.** *Plants* 2020, **9**
- This review comprehensively discusses dsRNA uptake mechanisms and examples in insects and fungi, including special focus on topics of resistance development, dsRNA formulations, carriers and nanoparticles.
21. McLoughlin AG, Wytinck N, Walker PL, Girard IJ, Rashid KY, de Kievit T, Fernando WGD, Whyard S, Belmonte MF: **Identification and application of exogenous dsRNA confers plant protection against *Sclerotinia sclerotiorum* and *Botrytis cinerea*.** *Sci Rep* 2018, **8**:7320.
  22. Song X-S, Gu K-X, Duan X-X, Xiao X-M, Hou Y-P, Duan Y-B, Wang J-X, Zhou M-G: **A myosin5 dsRNA that reduces the fungicide resistance and pathogenicity of *Fusarium asiaticum*.** *Pestic Biochem Physiol* 2018, **150**:1-9.
  23. Gu K-X, Song X-S, Xiao X-M, Duan X-X, Wang J-X, Duan Y-B, Hou Y-P, Zhou M-G: **A  $\beta$ 2-tubulin dsRNA derived from *Fusarium asiaticum* confers plant resistance to multiple phytopathogens and reduces fungicide resistance.** *Pestic Biochem Physiol* 2019, **153**:36-46
- This paper shows that Fa $\beta$ 2Tub-3 dsRNA derived from different regions of the  $\beta$ 2-tubulin gene of *F. asiaticum* had broad-spectrum antifungal activity against *Fusarium* spp., *Botrytis cinerea*, *Magnaporthe oryzae* and *Colletotrichum truncatum*, affecting mycelial growth, asexual reproduction, virulence and sensitivity to the fungicide carbendazim.
24. Kaksonen M, Roux A: **Mechanisms of clathrin-mediated endocytosis.** *Nat Rev Mol Cell Biol* 2018, **19**:313-326.
  25. Wytinck N, Sullivan DS, Biggar KT, Crisostomo L, Pelka P, Belmonte MF, Whyard S: **Clathrin mediated endocytosis is involved in the uptake of exogenous double-stranded RNA in the white mold phytopathogen *Sclerotinia sclerotiorum*.** *Sci Rep* 2020, **10**:12773
- This paper shows that application of exogenous dsRNA to the necrotrophic fungus *Sclerotinia sclerotiorum* leads to RNAi-mediated knock-down of target transcripts. Additionally, live cell imaging, transgenic fungal cultures and use of endocytosis inhibitors show that uptake occurs through clathrin-mediation.
26. Tatematsu M, Funami K, Seya T, Matsumoto M: **Extracellular RNA sensing by pattern recognition receptors.** *J Innate Immun* 2018, **10**:398-406.
  27. Saleh M-C, van Rij RP, Hekele A, Gillis A, Foley E, O'Farrell PH, Andino R: **The endocytic pathway mediates cell entry of dsRNA to induce RNAi silencing.** *Nat Cell Biol* 2006, **8**:793-802.
  28. Cappelle K, de Oliveira CFR, Van Eynde B, Christiaens O, Smagghe G: **The involvement of clathrin-mediated endocytosis and two Sid-1-like transmembrane proteins in double-stranded RNA uptake in the Colorado potato beetle midgut.** *Insect Mol Biol* 2016, **25**:315-323.
  29. Rutter BD, Innes RW: **Extracellular vesicles as key mediators of plant-microbe interactions.** *Curr Opin Plant Biol* 2018, **44**:16-22.
  30. Bielska E, Birch PRJ, Buck AH, Abreu-Goodger C, Innes RW, Jin H, Pfaffl MW, Robatzek S, Regev-Rudzi N, Tisserant C *et al.*: **Highlights of the mini-symposium on extracellular vesicles in inter-organismal communication, held in Munich, Germany, August 2018.** *J Extracell Vesicles* 2019, **8**:1590116.
  31. Bozkurt TO, Kamoun S: **The plant-pathogen haustorial interface at a glance.** *J Cell Sci* 2020, **133**:jcs237958.
  32. Mentges M, Glasenapp A, Boenisch M, Malz S, Henrissat B, Frandsen RJN, Güldener U, Münsterkötter M, Bormann J, Lebrun M-H *et al.*: **Infection cushions of *Fusarium graminearum* are fungal arsenals for wheat infection.** *Mol Plant Pathol* 2020, **21**:1070-1087.
  33. Lück S, Kreszies T, Strickert M, Schweizer P, Kuhlmann M, Douckov D: **siRNA-finder (si-Fi) software for RNAi-target design and off-target prediction.** *Front Plant Sci* 2019, **10**:1023.
  34. Peng Y, Wang K, Fu W, Sheng C, Han Z: **Biochemical comparison of dsRNA degrading nucleases in four different insects.** *Front Physiol* 2018, **9**:624.
  35. Guan R-B, Li H-C, Fan Y-J, Hu S-R, Christiaens O, Smagghe G, Miao X-X: **A nuclease specific to lepidopteran insects suppresses RNAi.** *J Biol Chem* 2018, **293**:6011-6021.
  36. Cooper AMW, Song H, Shi X, Yu Z, Lorenzen M, Silver K, Zhang J, Zhu KY: **Molecular characterizations of double-stranded RNA degrading nuclease genes from *Ostrinia nubilalis*.** *Insects* 2020, **11**.
  37. Balabanova LA, Gafurov YM, Pivkin MV, Terentyeva NA, Likhatskaya GN, Rasskazov VA: **An extracellular S1-type nuclease of marine fungus *Penicillium melinii*.** *Mar Biotechnol* 2012, **14**:87-95.
  38. Liu C, Li M, Redda ET, Mei J, Zhang J, Wu B, Jiang X: **A novel double-stranded RNA mycovirus isolated from *Trichoderma harzianum*.** *Virol J* 2019, **16**:113.
  39. Vurro M, Miguel-Rojas C, Pérez-de-Luque A: **Safe nanotechnologies for increasing the effectiveness of**

- environmentally friendly natural agrochemicals.** *Pest Manag Sci* 2019, **75**:2403-2412.
40. Mitter N, Worrall EA, Robinson KE, Li P, Jain RG, Taochy C, Fletcher SJ, Carroll BJ, Lu GQ (Max), Xu ZP: **Clay nanosheets for topical delivery of RNAi for sustained protection against plant viruses.** *Nat Plants* 2017, **3**:16207.
  41. Worrall EA, Bravo-Cazar A, Nilon AT, Fletcher SJ, Robinson KE, Carr JP, Mitter N: **Exogenous application of RNAi-inducing double-stranded RNA inhibits aphid-mediated transmission of a plant virus.** *Front Plant Sci* 2019, **10**:265.
  42. Zhang H, Demirer GS, Zhang H, Ye T, Goh NS, Aditham AJ, Cunningham FJ, Fan C, Landry MP: **DNA nanostructures coordinate gene silencing in mature plants.** *Proc Natl Acad Sci U S A* 2019, **116**:7543-7548.
  43. Schwartz SH, Hendrix B, Hoffer P, Sanders RA, Zheng W: **Carbon dots for efficient small interfering RNA delivery and gene silencing in plants.** *Plant Physiol* 2020, **184**:647-657.
  44. Lichtenberg SS, Nuti K, DeRouchey J, Tsyusko OV, Unrine JM: **Efficacy of chitosan/double-stranded RNA polyplex nanoparticles for gene silencing under variable environmental conditions.** *Environ Sci Nano* 2020, **7**:1582-1592.
  45. Forster H, Shuai B: **Exogenous siRNAs against chitin synthase gene suppress the growth of the pathogenic fungus *Macrophomina phaseolina*.** *Mycologia* 2020, **112**:699-710.
  46. Lax C, Tahiri G, Patiño-Medina JA, Cánovas-Márquez JT, Pérez-Ruiz JA, Osorio-Concepción M, Navarro E, Calo S: **The evolutionary significance of RNAi in the fungal kingdom.** *Int J Mol Sci* 2020, **21**.
  47. Laurie JD, Linning R, Bakkeren G: **Hallmarks of RNA silencing are found in the smut fungus *Ustilago hordei* but not in its close relative *Ustilago maydis*.** *Curr Genet* 2008, **53**:49-58.
  48. Jeseničnik T, Štajner N, Radišek S, Jakše J: **RNA interference core components identified and characterised in *Verticillium nonalfalfae*, a vascular wilt pathogenic plant fungi of hops.** *Sci Rep* 2019, **9**:8651.
  49. Song X-S, Gu K-X, Duan X-X, Xiao X-M, Hou Y-P, Duan Y-B, Wang J-X, Yu N, Zhou M-G: **Secondary amplification of siRNA machinery limits the application of spray-induced gene silencing.** *Mol Plant Pathol* 2018, **19**:2543-2560.
  50. Kettles GJ, Hofinger BJ, Hu P, Bayon C, Rudd JJ, Balmer D, Courbot M, Hammond-Kosack KE, Scalliet G, Kanyuka K: **sRNA profiling combined with gene function analysis reveals a lack of evidence for cross-kingdom RNAi in the wheat – *Zymoseptoria tritici* pathosystem.** *Front Plant Sci* 2019, **10**:892.
  51. Ma X, Wiedmer J, Palma-Guerrero J: **Small RNA bidirectional crosstalk during the interaction between wheat and *Zymoseptoria tritici*.** *Front Plant Sci* 2020, **10**:1669.
  52. Koch A, Höfle L, Werner BT, Imani J, Schmidt A, Jelonek L, Kogel K-H: **SIGS vs HIGS: a study on the efficacy of two dsRNA delivery strategies to silence *Fusarium FgCYP51* genes in infected host and non-host plants.** *Mol Plant Pathol* 2019, **20**:1636-1644.
  53. Head GP, Carroll MW, Evans SP, Rule DM, Willse AR, Clark TL, Storer NP, Flannagan RD, Samuel LW, Meinke LJ: **Evaluation of SmartStax and SmartStax PRO maize against western corn rootworm and northern corn rootworm: efficacy and resistance management.** *Pest Manag Sci* 2017, **73**:1883-1899.



Humboldt Review

## Biotic stress-associated microRNA families in plants

Ena Šečić, Karl-Heinz Kogel <sup>\*</sup>, Maria Jose Ladera-Carmona

Institute of Phytopathology, Centre for BioSystems, Land Use and Nutrition, Justus Liebig University, Heinrich-Buff-Ring 26, D-35392, Giessen, Germany

### ARTICLE INFO

#### Keywords:

Biotic stress  
miRNA  
Microbial pathogen  
Plant  
RNAi  
Small RNA  
Symbiosis

### ABSTRACT

Plants and animals utilize various regulatory mechanisms for control of gene expression during development in different tissues and cell types. About 30 years ago, a new mechanism of gene regulation, termed RNA interference (RNAi), was discovered and proved revolutionary for the mechanistic understanding of gene regulation. Noncoding RNAs, including short, 21–24 nucleotide (nt) long microRNAs (miRNAs), endogenously-generated from *MIR* genes, are key components of RNAi processes, by post-transcriptionally controlling transcripts with antisense complementarity through either translational repression or mRNA degradation. Since their discovery, important roles in regulation of ontogenetic development, cell differentiation, proliferation, and apoptosis in eukaryotes have been elucidated. In plants, miRNAs are known regulatory elements of basic endogenous functions and responses to the environmental stimuli. While the role of miRNAs in regulation of nutrient uptake, circadian clock and general response to abiotic stress is already well understood, a comprehensive understanding of their immune-regulatory roles in response to various biotic stress factors has not yet been achieved. This review summarizes the current understanding of the function of miRNAs and their targets in plants during interaction with microbial pathogens and symbionts. Additionally, we provide a consensus conclusion regarding the typical induction or repression response of conserved miRNA families to pathogenic and beneficial fungi, bacteria, and oomycetes, as well as an outlook of agronomic application of miRNAs in plants. Further investigation of plant miRNAs responsive to microbes, aided with novel sequencing and bioinformatics approaches for discovery and prediction in non-model organisms holds great potential for development of new forms of plant protection.

### 1. Introduction and historical background

MicroRNAs (miRNAs) are a class of non-coding RNAs with sequence complementarity to messenger RNAs (mRNAs), making them important components in regulating gene expression and silencing in a variety of signalling pathways within eukaryotic cells (Bartel, 2004). Recent reviews emphasize their involvement in various fundamental processes, ranging from mammalian reproduction and fertility (Salilew-Wondim et al., 2020), human stress diseases (Du et al., 2019) and gut-microbiota interactions (Li et al., 2020) to plant development (Liu et al., 2018) and response to biotic and abiotic stresses (Li et al., 2017). At its basis, miRNA-based gene silencing is an obstruction of protein synthesis and translation of mRNAs in a post-transcriptional manner, commonly called Post-Transcriptional Gene Silencing (PTGS), which is a subtype of a highly conserved silencing pathway of RNA interference (RNAi). While RNAi was discovered in nematodes in 1998 (Fire et al., 1998), and a corresponding Nobel Prize awarded to Fire and Mello in 2006, the

process in which expression of sequences complementary to target genes leads to silencing phenotypes was discovered in plants as early as 1990, then termed “co-suppression” (Napoli et al., 1990; van der Krol et al., 1990), and in fungi in 1992, then termed “quelling” (Romano and Macino, 1992). Following these landmark publications, the first miRNA discovered was from the *lin-4* gene of *Caenorhabditis elegans* in 1993 (Lee et al., 1993) and elucidated a mechanism by which complementary *lin-4* miRNA abrogates translation of *lin-14* mRNA (Wightman et al., 1993). Later, another RNA from the gene *let-7* was discovered with targets involved in temporal regulation of development in *C. elegans* (Reinhart et al., 2000; Pasquinelli et al., 2000). Consequently, these RNAs were initially termed small temporal RNAs (stRNAs), but were then shown to be more widespread and versatile in targeted pathways, occurring throughout the genomes of *Caenorhabditis*, *Drosophila* and humans, so they were renamed microRNAs (Lagos-Quintana et al., 2001; Lau et al., 2001; Lee and Ambros, 2001).

True comprehension of the unique nature of these molecules in

<sup>\*</sup> Corresponding author.

E-mail addresses: [Ena.Secic@agr.uni-giessen.de](mailto:Ena.Secic@agr.uni-giessen.de) (E. Šečić), [Karl-Heinz.Kogel@agr.uni-giessen.de](mailto:Karl-Heinz.Kogel@agr.uni-giessen.de) (K.-H. Kogel), [Maria.Ladera-Carmona@agr.uni-giessen.de](mailto:Maria.Ladera-Carmona@agr.uni-giessen.de) (M.J. Ladera-Carmona).

<https://doi.org/10.1016/j.jplph.2021.153451>

Received 16 April 2021; Received in revised form 25 May 2021; Accepted 27 May 2021

Available online 31 May 2021

0176-1617/© 2021 The Author(s). Published by Elsevier GmbH. This is an open access article under the CC BY-NC-ND license

(<http://creativecommons.org/licenses/by-nc-nd/4.0/>).

eukaryotic organisms emerged in the following years, when first studies revealed developmental and tissue-specific miRNA expression patterns and strong conservation in vertebrate and non-vertebrate genomes (Lagos-Quintana et al., 2002; Wienholds et al., 2005, reviewed comprehensively in Bartel, 2004). First miRNAs in plants were described in 2002, with 16 miRNAs (miR156 to miR171) discovered in the *Arabidopsis* genome, eight of which were also conserved in rice (Reinhart et al., 2002). They were detectable by Northern blot analysis, differentially expressed during plant development and originated from stem-loop precursors.

Even though miRNAs play important regulatory roles in plants and animals, and the pathways they utilize are somewhat similar, the debate about the common ancestry or convergent evolutionary history of the plant and animal miRNAs (Axtell et al., 2011; Moran et al., 2017), as well as the origin of non-coding regulatory mechanisms (Gaiti et al., 2017) is still ongoing. A comprehensive and detailed database of known miRNAs, their nomenclature, precursor and mature sequences and corresponding literature was established in 2002, then called the microRNA Registry (Griffiths-Jones, 2004), and later known as miRBase (Griffiths-Jones et al., 2006). The current release (v22.1) contains 48,885 mature miRNAs from 271 species (Kozomara et al., 2019), including *Arabidopsis thaliana* (428 mature miRNAs), *Medicago truncatula* (756 mature miRNAs), *Brachypodium distachyon* (525), *Oryza sativa* (738), *Triticum aestivum* (125), *Zea mays* (325) and *Solanum lycopersicum* (147).

Meanwhile, aberrant miRNA profiles have been associated with cancer diseases, with the first examples in chronic lymphocytic leukemia shown as early as 2002 (Calin et al., 2002). Following these discoveries, small RNA-based therapeutic approaches that exploit miRNA involvement as oncogenes or tumor suppressors have since been in development, with the first clinical trials on treatment of liver cancer with a miRNA mimic starting in 2013 (Bouchie, 2013; Orellana and Kasinski, 2015; Hashemi and Gorji-Bahri, 2020). Similarly, there have also been considerations and initial studies to use RNAi-based signalling pathways for development of plant protection strategies against microbial pathogens and pests (reviewed in: Cai et al., 2018; Cagliari et al., 2019; Liu et al., 2020). Depending on the origin of non-coding RNA specifically targeting an essential or a virulence gene of a microbial pathogen or a

pest, employed strategies are termed either Host-Induced Gene Silencing (HIGS; Nowara et al., 2010), where the RNA is generated by the crop plant, or Spray-Induced Silencing (SIGS; Koch et al., 2016; Wang et al., 2016), where the RNA is exogenously applied to the plant surface. A first commercial product using the HIGS strategy was first approved in 2017 for corn rootworm control in transgenic corn (Head et al., 2017). Major discoveries and application landmarks in miRNA-based research are displayed in Fig. 1.

## 2. miRNA biogenesis and gene silencing mechanisms in plants

Mature miRNAs both in plants and animals have common characteristics, which serve as classification criteria within the diverse non-coding RNA universe: *i.* mature miRNAs are 20–24 nucleotides (nt) long sequences, *ii.* they originate from precursor inverted repeats that fold into hairpin secondary structures, *iii.* are cleaved by endonucleases, and *iv.* loaded into Argonaute (AGO) proteins in order to guide target recognition (Reinhart et al., 2002; Axtell et al., 2011; Budak and Akpinar, 2015). miRNAs are mostly transcribed from intergenic regions with associated promoters, or intragenic intron sequences (O'Brien et al., 2018) by DNA-dependent RNA polymerase II into primary miRNAs (pri-miRNAs), whose accumulation, stability and splicing serve as pathway checkpoints for miRNA synthesis regulation (Budak and Akpinar, 2015; Zhang et al., 2015). pri-miRNAs fold back onto themselves to form hairpins with stem-loop double-stranded (ds) RNA regions, to be recognized and cleaved with the type III RNA endonuclease Dicer-like (DCL) proteins into precursor miRNAs (pre-miRNAs). Plants commonly have several homologs of DCL proteins and the length of a final processed mature miRNA/miRNA\* duplex depends on the DCL protein cutting the precursor molecule (Budak and Akpinar, 2015). Interestingly, flowering plants also have multiple copies of AGO proteins, grouped into clades by homology to 10 canonical *Arabidopsis* AGOs (Fang and Qi, 2015). Prior to export out of the nucleus, the mature duplex is methylated by Hua Enhancer 1 (HEN1), to protect it from exonucleolytic degradation (Yu et al., 2005). Once in the cytoplasm, the miRNA/miRNA\* duplex is loaded into AGO within the RNA-Induced Silencing Complex (RISC), the passenger strand is degraded and the

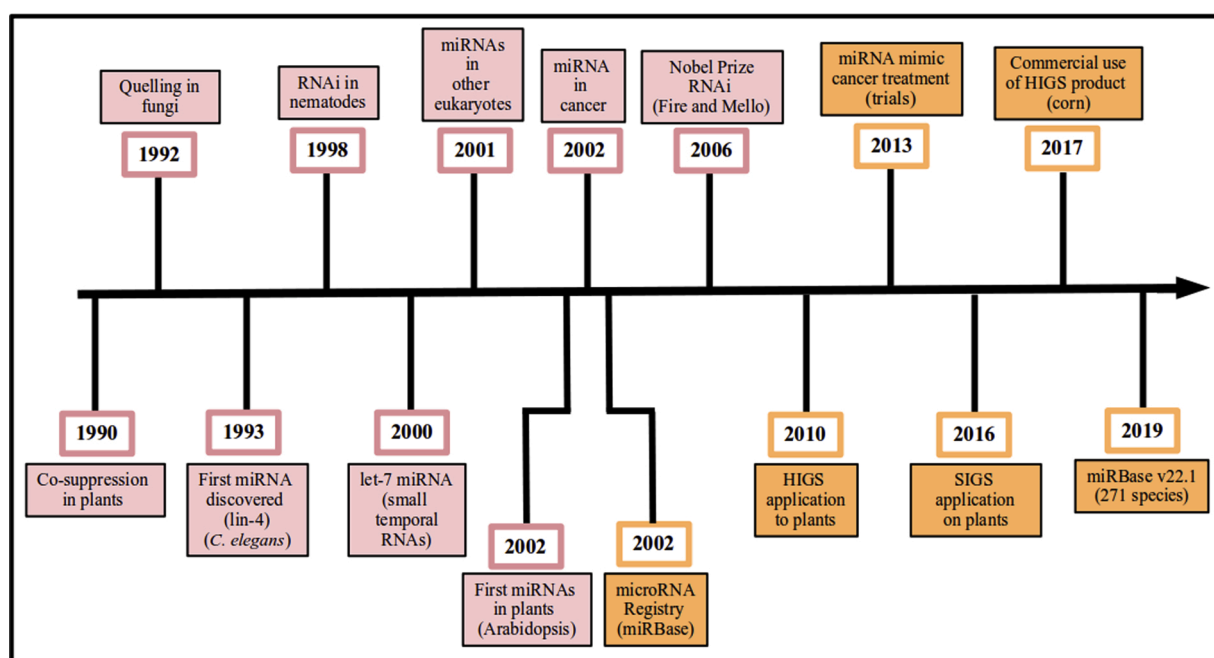


**Fig. 1.** Timeline of major discoveries and applications of miRNAs since the discovery of RNAi-based regulatory mechanisms. First proof/discovery of a term is displayed in pink and the application breakthroughs and miRNA-based tools are displayed in orange. (For interpretation of the references to colour in this figure legend, the reader is referred to the web version of this article.)

guide strand remains in a mature RISC (Fang and Qi, 2015). This miRNA strand facilitates recognition and translational inhibition or cleavage of the target mRNA (Rogers and Chen, 2013). In contrast to animal miRNAs, the pairing between the single-stranded miRNA and its target is mostly near-perfect, leading to AGO-catalyzed cleavage or translation inhibition of the targeted transcript (Axtell et al., 2011). Because the recognition of the target relies on sequence conservation between the miRNA and the mRNA, regulation of a target by multiple miRNAs or vice versa multiple targets by one miRNA are both possible silencing scenarios (Srivastava et al., 2014). The success of miRNA-induced silencing depends on the expression, abundance and localization of both miRNAs and their targets, as well as the stability of the silencing and expression of proteins with redundant function to the target. Major regulatory checkpoints in miRNA biogenesis and homeostasis are the *i.* miRNA transcription, *ii.* processing, *iii.* RISC assembly, and *iv.* stability maintenance (Wang et al., 2019).

Adaptive, rapid, and substantial changes in gene expression, as exerted in miRNA-based regulation of physiological processes, are also required in terms of response to biotic and abiotic stresses (Shriram et al., 2016; Chauhan et al., 2017). While some plant miRNAs are grouped in miRNA families, conserved both in sequence and role in targeted pathways across different species, others have diverged and are typical only for a single species or a few close relatives (Dezulian et al., 2005; Fahlgren et al., 2010). Hence, in this review, when possible, we discuss the microbe-responsive miRNAs within families, taking into account their similarities and differences across the compendium of available data in distinct plant species. In addition, we consider here several categories of biotic interactions into which a microbe-induced miRNA response might fall, including taxonomic (bacterial, fungal) and lifestyle (pathogenic, mutualistic) criteria, with the intention of

providing comprehensive insight into the conservation and divergence of miRNA function. We classify the miRNA families into categories of “induced by biotic stress”, “repressed by biotic stress” or “differentially regulated by biotic stress” in Table 1, based on the consensus from available literature, where such a classification was possible. These miRNAs are schematically indicated, within the biotic stress category they respond to, and within the classification criteria from Table 1, in Fig. 2.

### 3. Biotic stress-responsive miRNA families

#### 3.1. miR393 disrupts auxin crosstalk to plant immune networks

Different studies have shown that miR393 is up-regulated in response to abiotic stresses such as cold, heat, salt and dehydration in Arabidopsis and wheat (*Triticum aestivum*) (Sunkar and Zhu, 2004; Zhou et al., 2008; Xin et al., 2010). In connection with this review, it is interesting that miR393 was the first miRNA shown to be regulated under biotic stress (Navarro et al., 2006). This miRNA is identified in 15 plant species (Windels and Vazquez, 2011), encoded by multiple *AtMIR393* loci in Arabidopsis and targets the Transport Inhibitor Response1 (TIR1)/Auxin-signalling F-Box (AFB) auxin co-receptors (Jones-Rhoades and Bartel, 2004; Sunkar and Zhu, 2004). A modified RACE assay confirmed that *TIR1*, *AFB2* and *AFB3* transcripts are cleaved by miR393 (Navarro et al., 2006). In the absence of auxin, Auxin/Indole Acetic Acid (AUX/IAA) proteins are bound to Auxin Response Factor (ARF) proteins, thereby inactivating them. Upon auxin perception, TIR1 along with AFB1, AFB2 and AFB3 mediate AUX/IAA protein ubiquitination, releasing the ARFs that subsequently activate (or repress, depending on the ARF family member) the transcription of auxin

**Table 1**

miRNA families classified by the type of response to various biotic stress factors: induction upon infection or colonization by the microbe (red), repression upon infection or colonization (blue), differential response upon infection or colonization (yellow). The classification and colours have been assigned by a consensus across currently available literature (cited in the appropriate box). (For interpretation of the references to colour in this table legend, the reader is referred to the web version of this article.)

miRNA family	Target	Response to pathogenic fungi	Response to pathogenic bacteria	Response to mutualistic microbes	Response to oomycetes
miR160	ARF	<i>Cronartium quercuum</i> (Lu et al., 2007), <i>Verticillium dahliae</i> (Yang et al., 2013b), <i>Magnaporthe oryzae</i> (Li et al., 2014)	<i>Pseudomonas syringae</i> (Fahlgren et al., 2007), flg22 (Li et al., 2010a)	<i>Bradyrhizobium japonicum</i> (Subramanian et al., 2008), <i>Sinorhizobium meliloti</i> (Lelandais-Briere et al., 2009)	
miR164	NAC	<i>V. dahliae</i> (Hu et al., 2020), <i>Puccinia striiformis</i> (Feng et al., 2014), <i>M. oryzae</i> (Li et al., 2014)	<i>P. syringae</i> (Lee et al., 2017)	<i>B. japonicum</i> (Subramanian et al., 2008)	
miR166	HD-ZIP III	<i>V. dahliae</i> (Zhang et al., 2016), <i>Colletotrichum graminicola</i> (Balmer et al., 2017)		<i>B. japonicum</i> (Subramanian et al., 2008)	<i>Phytophthora sojae</i> (Wong et al., 2014)
miR167	ARF	<i>V. dahliae</i> (Yang et al., 2013b)	<i>P. syringae</i> (Fahlgren et al., 2007), flg22 (Li et al., 2010b)	<i>S. meliloti</i> (Lelandais-Briere et al., 2009), <i>Poconia chlamydosporia</i> (Pentimone et al., 2018)	
miR168	AGO1	<i>C. graminicola</i> (Balmer et al., 2017), <i>M. oryzae</i> (Zanini et al., 2021)		<i>B. japonicum</i> (Subramanian et al., 2008), <i>P. chlamydosporia</i> (Pentimone et al., 2018)	<i>P. sojae</i> (Wong et al., 2014)
miR169	HAP	<i>C. graminicola</i> (Balmer et al., 2017)	flg22 (Li et al., 2010b)	<i>B. japonicum</i> (Subramanian et al., 2008), <i>S. meliloti</i> (Combiere et al., 2006)	
miR393	TIR1	<i>V. dahliae</i> (Yang et al., 2013b), <i>Blumeria graminis</i> (Xin et al., 2010), <i>C. graminicola</i> (Balmer et al., 2017)	flg22 (Navarro et al., 2006; Li et al., 2010b), <i>P. syringae</i> (Fahlgren et al., 2007; Zhang et al., 2011), <i>Agrobacterium tumefaciens</i> (Pruss et al., 2008)	<i>B. japonicum</i> (Subramanian et al., 2008), <i>Rhizophagus irregularis</i> (Etemadi et al., 2014)	<i>Phytophthora capsici</i> (Hou et al., 2019), <i>P. sojae</i> (Wong et al., 2014)
miR398	CSD	<i>M. oryzae</i> (Li et al., 2014)	flg22 (Li et al., 2010b), <i>P. syringae</i> (Jagadeeswaran et al., 2009)	<i>S. meliloti</i> (Lelandais-Briere et al., 2009)	
miR482	NBS-LRR	<i>V. dahliae</i> (Zhu et al., 2013)	<i>P. syringae</i> (Shivaprasad et al., 2012)	<i>B. japonicum</i> (Li et al., 2010a)	<i>P. sojae</i> (Wong et al., 2014)
miR156	SPL	<i>C. quercuum</i> (Lu et al., 2007), <i>B. graminis</i> (Xin et al., 2010)		<i>Serendipita indica</i> (Ye et al., 2014), <i>P. chlamydosporia</i> (Pentimone et al., 2018)	
miR159	MYB	<i>V. dahliae</i> (Zhang et al., 2016), <i>C. quercuum</i> (Lu et al., 2007), <i>B. graminis</i> (Xin et al., 2010)		<i>B. japonicum</i> (Subramanian et al., 2008)	
miR172	AP2	<i>M. oryzae</i> (Li et al., 2014)		<i>B. japonicum</i> (Subramanian et al., 2008; Wang et al., 2014), <i>S. meliloti</i> (Lelandais-Briere et al., 2009), <i>Rhizobium etli</i> (Nova-Franco et al., 2015)	

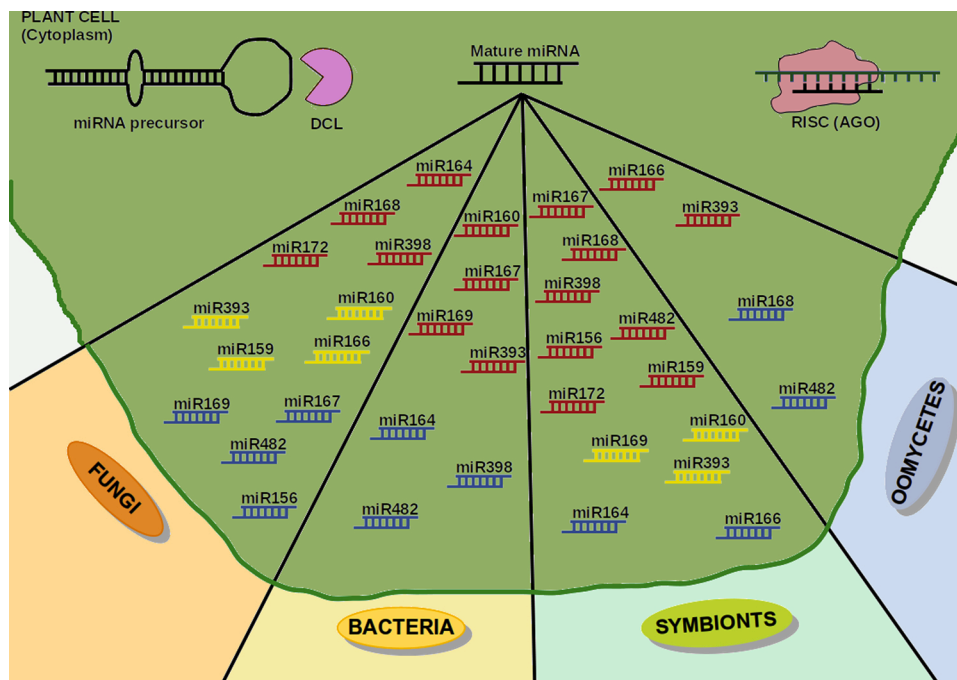


**Fig. 2.** A plant cell can respond to various types of biotic stresses by induction (red), repression (blue) or differential regulation (yellow) of miRNA expression. On top: a schematic representation of Post-Transcriptional-Genetic Silencing in plants: processing of premature miRNA by DCL endonuclease and loading of miRNA into RISC. Below: various pools of miRNAs that are induced, repressed or differentially regulated in response to pathogenic fungi (orange), pathogenic bacteria (yellow), symbiotic/mutualistic microbes (light green), oomycetes (light blue). (For interpretation of the references to colour in this figure legend, the reader is referred to the web version of this article.)

responsive genes (Dharmasiri et al., 2005a,b). miR393 expression is induced by flagellin 22 (flg22), a bacterial Microbe-Associated Molecular Pattern (MAMP), resulting in RNA-mediated repression of TIR1/AFB proteins and modulation of auxin signalling (Navarro et al.,

2006; Li et al., 2010b). Since auxin represses salicylic acid (SA) but not jasmonic acid (JA) signalling, up-regulating miR393 and thus repressing auxin signalling increases the levels of SA, which explains the higher resistance to biotrophic microbes (Naseem et al., 2015). For example,

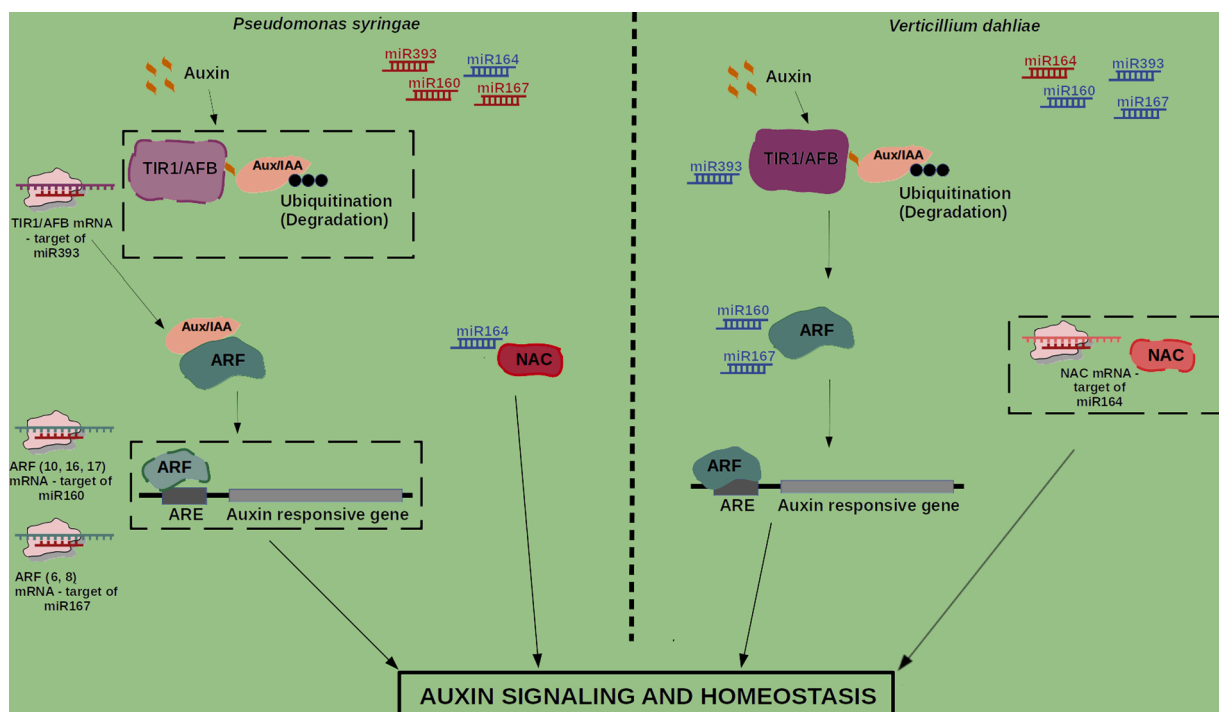


**Fig. 3.** Mechanistic representation of the role played by four selected miRNA families in the regulation of auxin signaling and homeostasis. miR393, miR160, miR164 and miR167 react oppositely towards the pathogenic bacterium *Pseudomonas syringae* on the left (Fahlgren et al., 2007; Lee et al., 2017), and the pathogenic fungus *V. dahliae* on the right (Yang et al., 2013b; Hu et al., 2020). miRNAs induced (red) or repressed (blue) in response to one of the two pathogens are indicated on the top. Black boxes drawn with dashed lines mark the part of the auxin signaling pathway(s) silenced by miRNA-based targeting of crucial transcripts. Loading in RISC (AGO) shown only when the miRNA is known to be induced (red) in response to a pathogen. ARE - Auxin Responsive Element; ARF - Auxin Response Factor; Aux/IAA - Auxin/Indole Acetic Acid protein; NAC - NAM- no apical meristem, ATAF1/2- Arabidopsis transcription activation factor, and CUC- cup-shaped cotyledon; TIR1/AFB - Transport Inhibitor Response1 (TIR1)/Auxin-signalling F-Box (AFB) auxin co-receptors. (For interpretation of the references to colour in this figure legend, the reader is referred to the web version of this article.)

miR393 overexpression in *Arabidopsis* confers resistance towards the biotrophic oomycetes *Hyaloperonospora arabidopsidis* (Robert-Seilanianantz et al., 2011), *Phytophthora capsici* (Hou et al., 2019) and the hemibiotrophic bacterium *Pseudomonas syringae* (Fahlgren et al., 2007), while, in contrast, these plants rendered susceptible to necrotrophic pathogens such as *Alternaria brassicicola* (Robert-Seilanianantz et al., 2011). Similarly, in *Nicotiana tabacum*, miR393 was induced by the gall-forming, but not by the avirulent *Agrobacterium tumefaciens* (Pruss et al., 2008) and in soybean by *Phytophthora sojae* (Wong et al., 2014). Increase in miR393 was observed in roots of susceptible and resistant cultivars, and it was also induced in roots treated with heat-inactivated *P. sojae* cells, further showing that this miRNA is responsive to MAMPs. In maize, expression of miR393 was increased in response to the hemibiotrophic fungus *Colletotrichum graminicola* (Balmer et al., 2017). Consistent with the above observations, miR393 down-regulation was instead found in eggplant challenged with *Verticillium dahliae* (Yang et al., 2013b), suggesting that this is a plant defence strategy. Indeed, blocking auxin transport or treating the seedlings with SA or IAA resulted in enhanced susceptibility to this necrotrophic fungus. Overall, the above reports suggest a pattern in which miR393 is up-regulated by MAMPs, bacterial infection, oomycetes and fungi with biotrophic and hemibiotrophic lifestyle and down-regulated by fungi with a necrotrophic lifestyle. Being one of the few miRNAs responsive to different types of biotic stresses and involved in modulation of auxin signalling pathways, we depicted its role upon plant exposure to *Pseudomonas syringae* (Fahlgren et al., 2007; Lee et al., 2017) and *Verticillium dahliae* (Yang et al., 2013b; Hu et al., 2020) in more detail in Fig. 3.

miR393 also orchestrates a shift in the production of tryptophan-originating secondary metabolites, such as IAA, camalexin (CL) and indole glucosinolates (IG) (Sugawara et al., 2009; Zhao et al., 2002). Even though CL and IG have anti-microbial properties, CL is more effective against necrotrophic fungi through damaging the cell membrane, and IG against insects, biotrophic pathogens and bacteria (Robert-Seilanianantz et al., 2011). Additionally, miR393 is a positive regulator of isoflavonoid biosynthesis, whose activation enhances defence responses due to their direct antimicrobial activity (Wong et al., 2014). These findings together show that miRNA393 is a tool for proper fine-tuning of hormone balance and secondary metabolites, which is crucial for a situation-appropriate response against pathogens and pests.

miR393 was also among the 24 out of a total of 153 miRNAs identified that were responsive to the biotrophic powdery mildew pathogen *Blumeria graminis* (Xin et al., 2010). Interestingly, miR393 was differentially expressed in near-isogenic wheat lines JD8 and JD8-Pm30 (the latter containing the powdery mildew *R* gene *Pm30*), which further strengthens the importance of this miRNA in plant defense responses (González-Lamothe et al., 2012).

Of note, the complementary miR393b\* plays a role in resistance against bacterial infection upon AGO2 loading (Zhang et al., 2011). Induction of the AGO2-miR393\* module, which targets and down-regulates the Golgi-localized SNARE gene MEMB12, was observed after *P. syringae* inoculation in *Arabidopsis* and results in an increase in secretion of pathogenesis-related protein PR1. Thus, this miRNA/miRNA\* duplex serves as an example of layered immunity regulation through different members of the AGO family in *Arabidopsis*.

### 3.2. miR160 and miR167 enhance MAMP responses by interfering with Auxin Response Factors

Like miR393, miR160 and miR167 regulate auxin signaling pathways, though by directly targeting ARFs (Ulmasov et al., 1999). Several studies have shown that miR160 (encoded by *MIR160a/b/c* in *Arabidopsis*) is up-regulated in biotic interactions, leading to differential regulation of *ARF10*, *ARF16* and *ARF17* (Rhoades et al., 2002). miR160 was up-regulated as early as 3 h after *P. syringae* inoculation (Fahlgren et al., 2007) or treatment with flg22 (Li et al., 2010b), suggesting that this miRNA also regulates auxin signaling in response to MAMPs.

Similarly, miR160 induction was observed in rice infected with *Magnaporthe oryzae* (Li et al., 2014) and overexpressing miR160 enhanced resistance to the hemibiotrophic fungus. To add an additional layer of complexity on miR160 function in biotic stress, its down-regulation was observed in the loblolly pine (*Pinus taeda*) infected with pine-oak rust *Cronartium quercuum*, although no corresponding target up-regulation was recorded (Lu et al., 2007). Slight down-regulation of miR160 in eggplant challenged with *V. dahliae* was found by Yang et al. (2013b), suggesting that fine modulation of the miR160-ARF module is crucial for proper response to pathogenic microorganisms.

miR167, encoded by *MIR167a-d* in *Arabidopsis*, targets other members of the ARF family, namely ARF6 and ARF8 (Jones-Rhoades et al., 2006). Like miR167, miR160 is induced upon *P. syringae* and flg22 treatment (Fahlgren et al., 2007; Li et al., 2010b), while it was down-regulated in eggplant when challenged with the pathogenic fungus *V. dahliae* (Yang et al., 2013b). Overall, differential regulation of auxin signaling by miRNAs such as miR160, miR167, miR393 and miR164, depicted in Fig. 3, reinforces the importance of the interplay between biotic stress-responding miRNAs and their role in hormonal signaling, and also seems to be a common strategy used by plants to coordinate their immune response (Jones-Rhoades et al., 2006).

### 3.3. miR164 affects the auxin homeostasis and plant cell death responses by interacting with NAC domain transcription factors

miRNA164 potentially targets five members of the NAC (NAM- no apical meristem, ATAF1/2- *Arabidopsis* transcription activation factor, and CUC- cup-shaped cotyledon) domain-encoding transcription factor (TF) genes in *Arabidopsis* and other plants (Guo et al., 2005; Baker et al., 2005; Sieber et al., 2007). Among them, NAC1 positively regulates lateral root development through auxin signaling, whereby auxin-inducible miR164 controls NAC1 transcription levels (Guo et al., 2005). Up-regulation of this miRNA was observed in cotton and rice in response to both *V. dahliae* and *M. oryzae* (Hu et al., 2020; Li et al., 2014). Further characterization of the miR164-NAC100 module in cotton showed that miR164 directly cleaved NAC100 mRNA in response to *V. dahliae* infection. Moreover, miR164, as well as knockdown of NAC100 positively regulated resistance to this fungus, indicating that miR164-NAC100 modulates plant defense through RNAi (Hu et al., 2020).

Differential miR164 up-regulation in response to *M. oryzae* was observed in a resistant vs. susceptible near-isogenic rice lines, correlating with lower expression of the target gene *Salicylic acid-induced protein 19* (*Os12g4168*), further hinting to a critical role of the miRNA-target gene in plant immunity (Li et al., 2014). Consistent with this, in *Arabidopsis*, miR164 and its target gene *NAC4* play essential roles in the regulation of the hypersensitive cell death response (HR) (Lee et al., 2017). *NAC4* expression was induced by bacterial pathogens after miR164 down-regulation. *LURP1*, *WRKY40* and *WRKY54*, regulated by NAC4, are negative regulators of cell death. Therefore, miR164 is involved in fine-tuning the cell death response. The target gene of miR164 in wheat, *TaNAC21/22*, negatively regulates resistance of wheat to stripe rust (*Puccinia striiformis*; Feng et al., 2014).

### 3.4. miRNA166 is used by cotton plants to interfere with *V. dahliae* virulence

miR166, like miR165, targets mRNAs encoding Class III Homeodomain-Leucine Zipper Gene Family Members (*HD-ZIPIII*) that have overlapping, antagonistic and distinct roles in *Arabidopsis* development (Prigge et al., 2005; Miyashima et al., 2011). Interestingly, miR166 was found in the context of cross-kingdom RNAi (Weiberg et al., 2013), where pathogens and plants use sRNAs to influence the outcome of an interaction in their favor via RNAi. Roots of cotton (*Gossypium hirsutum*) and *Arabidopsis* showed an increase in accumulation of miR166 when infected with *V. dahliae* (Zhang et al., 2016).

Furthermore, this miRNA was exported to fungal hyphae to reduce fungal virulence by silencing a gene encoding a Calcium-dependent cysteine protease (*Clp-1*), involved in microsclerotium formation. Up-regulation of miR166 was also observed in roots from susceptible and resistant soybean in response to *P. sojae* at early interaction stages (Wong et al., 2014). Treatment with heat-inactivated *P. sojae* cells produced the same effect as *P. sojae* infection, indicating that miR166, like many other miRNAs, is responsive to MAMPs. On the contrary, in response to *C. graminicola* in maize, miR166 showed down-regulation (Balmer et al., 2017).

### 3.5. miR168 controls AGO1 homeostasis and thereby affects the mRNA level of targets of other miRNAs

AtAGO1 encodes the crucial enzyme of the miRNA pathway and the RISC (RNAi-induced silencing complex) and is regulated by miR168-mediated AGO1-catalyzed mRNA cleavage (Vaucheret et al., 2006). Thus, AGO1 homeostasis and its availability to silence miRNA targets depends on the AGO1-miR168 module, which influences the mRNA level of other targets of miRNA-based regulation. In addition, AGO1 homeostasis requires transcriptional co-regulation of *MIR168* and *AGO1* genes (Vaucheret et al., 2006).

Consistent with the notion that plant AGO1 is also a key component in host-pathogen interactions (Šečić et al., 2019; Zanini et al., 2021), many reports show up-regulation of miR168 in response to plant hormones and pathogens (Li et al., 2012). In maize, miR168 is up-regulated in response to the hemibiotrophic *C. graminicola*, but only during the necrotrophic stage, while other miRNAs, including miR393, exhibited differential expression only during the biotrophic stage (Balmer et al., 2017). miR168 was also detected in roots of *Brachypodium distachyon* infected with *M. oryzae* (Zanini et al., 2021), though it was down-regulated in soybean roots inoculated with *P. sojae* (Wong et al., 2014). These results suggest that fine-tuning of the expression of AGO1 and the subsequent effect on the RNAi machinery is a common regulatory mechanism deployed during a plant-microbe interaction.

### 3.6. miR169 is an elicitor-responsive miRNA involved in defense hormone homeostasis

miR169 is another flg22 responsive miRNA that is conserved across species (Li et al., 2010b). In Arabidopsis, it targets Heme activator protein2 (HAP2), a transcription factor that forms a complex together with HAP3 and HAP5, recognizing the CCAAT motif, which is widely found in promoters of eukaryotes (Maity and de Crombrughe, 1998; Combier et al., 2006). HAP2 dampens the expression of *Indole-3-pyruvate monooxygenase Yucca2* (*YUC2*) by direct interaction with the *YUC2* promoter, thus regulating auxin biosynthesis (Zhang et al., 2017). In maize, the target of miR169 encodes *Allene oxide synthase*, an enzyme involved in JA biosynthesis. Down-regulation of miR169 in response to *C. graminicola* infection leads to up-regulation of its target, thus enhancing JA production (Balmer et al., 2017). This key position of miR169 in hormone homeostasis and biotic stress regulation is reflected by i. a considerable number of loci encoding this miRNA in Arabidopsis, ii. four mature miRNA sequences and iii. its target genes being involved in many processes related to stress-response, development and defense signaling (Zhang et al., 2017).

### 3.7. miR398 regulates reactive oxygen species (ROS) in response to abiotic and biotic stresses

In eukaryotes, environmental stress leads to the production of ROS (Hückelhoven and Kogel, 2003). ROS accumulation, known as oxidative burst, is a common early plant response to infection by bacteria and fungi (Lamb and Dixon, 1997). Among other enzymes, superoxide dismutases (SODs) regulate the oxidative burst by catalyzing the conversion of the highly reactive superoxide anion  $\cdot\text{O}_2^-$  into  $\text{H}_2\text{O}_2$  and  $\text{O}_2$ . Some

members of the SOD family, such as Zn/Cu superoxide dismutase 1 and 2 (CDS1, CDS2) and cytochrome c oxidase (COX5b.1) are targets of miR398 (Jones-Rhoades and Bartel, 2004; Sunkar and Zhu, 2004). Apart from differential regulation after abiotic stress (Jagadeeswaran et al., 2009; Loreti et al., 2020), miR398 is down-regulated in Arabidopsis in response to flg22 and infection with *P. syringae* (Jagadeeswaran et al., 2009; Li et al., 2010b). Through control of SODs, miR398 negatively regulates  $\text{H}_2\text{O}_2$ -dependent callose deposition and PTI (Li et al., 2010b), and overexpression of miR398 renders plants more susceptible to *P. syringae* infection. On the contrary, *M. oryzae* infection up-regulated miR398 in both susceptible and resistant rice varieties and its overexpression conferred resistance to the hemibiotrophic fungus, probably due to activation of defense genes (Li et al., 2014).

### 3.8. miRNAs targeting NBS-LRR class of R genes

Pattern recognition receptors (PPRs) sense microbial MAMPs on the cell surface and trigger PTI (Dodds and Rathjen, 2010). Other type of receptors, encoded by resistance (R) genes are inside the cell and sense pathogen effectors to trigger effector-triggered-immunity (ETI). These intracellular receptors contain nucleotide-binding (NB) and protein-binding leucine-rich repeat (LRR) domains. The N-terminal domain of these NB-LRR proteins are often armed with a TIR (Toll interleukin-1 receptor) or CC domain (coiled-coil). NB-LRR proteins recognize bacterial, fungal, oomycete, insect and viral effectors, thereby inducing plant defense (Dodds and Rathjen, 2010; Li et al., 2012).

miR482 is a 22 nt long miRNA (Li et al., 2010a) that contains asymmetric bulges in its miRNA/miRNA\* duplex, leading to the production of 21 nt secondary siRNAs by RNA-dependent RNA polymerase RDR6 and DCL4 (Zhu et al., 2013). Some of its predicted targets are R genes (Li et al., 2010a). Infection with *P. syringae* represses miR482 in tomato plants and the concomitant induction of R genes protects the plant from the pathogen attack (Shivaprasad et al., 2012). Likewise, repression of this miRNA was observed in soybean infected with *P. sojae* (Wong et al., 2014). Consistent with this tendency, miR482 was down-regulated in the interaction of cotton and *V. dahliae*, probably leading to de-repression of R genes rapidly after infection (Zhu et al., 2013).

Remarkably, other 22 nt miRNAs targeting the NBS-LRR class of R genes have been found to be abundant and diverse in legumes and Solanum species (Zhai et al., 2011; Shivaprasad et al., 2012). miR482, miR2109 and miR1507 trigger the production of 21 nt secondary siRNAs by recruiting RDR6 and DCL4, amplifying the silencing event (Chen et al., 2010; Cuperus et al., 2010). Diversifying this secondary siRNA pool to target continuously evolving R genes seems to be an effective strategy to regulate R gene expression (Li et al., 2012). Additional examples of these 22 nt miRNAs are: miR2118 (the passenger strand of soybean miR482), which targets the conserved P-loop motif of *TIR-NBS-LRR*, miR2109 targeting TIR-1 motif of *TIR-NBS-LRR*, and miR1507 which targets the kinase-2 motif of *CC-NBS-LRR* (Zhai et al., 2011). miR2109 and miR1507 were induced in soybean only upon *P. sojae* infection but not by heat-inactivated *P. sojae* cells, hinting to a role in ETI (Wong et al., 2014). Up-regulation of these miRNAs keeps NB-LRR genes at low levels, while quick reversion of this process results in rapid expression of R genes, especially in response to infection (Wong et al., 2014). Importantly, in case of pathogen effectors suppressing RNAi, up-regulation of the miRNA targets (R genes in this case) would take place, thus endowing the plant with a plethora of R proteins to combat the pathogen (Shivaprasad et al., 2012).

### 3.9. miRNAs involved in growth and development also change upon biotic interactions

In the vegetative phase of Arabidopsis growth, miR156 and miR172 regulate the juvenile-to-adult transition (Wu et al., 2009). miR156 is highly expressed in the juvenile phase while miRNA172 follows the

opposite expression pattern and promotes adult traits. miR156 targets 10 Squamosa promoter binding protein like (SPL) transcription factors (Wu et al., 2009), which have different roles in plant development. SPL9 promotes the transcription of *MIR172* and the corresponding miRNA targets the *Ap2*-like transcription factors, which repress flowering (Wu and Poethig, 2006; Wu et al., 2009). Several studies show miR156 down-regulation when the plant was challenged by fungal pathogens. Infection with *C. quercuum* and *B. graminis* down-regulates miR156 in *Pinus taeda* and wheat, respectively (Lu et al., 2007; Xin et al., 2010). Lu et al. (2007) analyzed the infection site and the region in the stem above the infection site. Interestingly, they found that the miRNA targets, SPLs, were up-regulated above the infection site, possibly to limit the fungal growth by activating development and growth genes.

Li et al. (2014) found up-regulation of miR172 in either resistant or susceptible rice varieties in response to *M. oryzae*. Similarly, several studies show that nitrogen fixing bacteria up-regulate this miRNA in legumes (Subramanian et al., 2008; Wang et al., 2014; Lelandais-Brière et al., 2009; Nova-Franco et al., 2015).

Among the hundreds of members of the MYB transcription factors in Arabidopsis, five of them have a complementary region to miR159 (*AtMYB101*, *AtMYB104*, *AtMYB33*, *AtMYB65* and *At3g60460*) (Rhoades et al., 2002). The MYB transcription factors are involved in several processes in plants, such as development, defense, metabolism and response to biotic and abiotic stress (Ambawat et al., 2013). Interestingly, miR159 is also up-regulated in *V. dahliae* infected cotton and Arabidopsis, like miR166, and silences the *VdHic-15* virulence gene in the fungus (Zhang et al., 2016). Apart from this study, other reports showed that miR159, similar to miR156, was down-regulated in wheat and pine infected with *B. graminis* and *C. quercuum*, respectively (Xin et al., 2010; Lu et al., 2007).

### 3.10. miRNAs in mutualistic interactions between plants and beneficial microbes

Recent advances in *in silico* analysis approaches have elucidated a crucial role for miRNA-based regulation in legumes, which can form mutualistic symbiosis relationships with two major mutualist groups of organisms: nodule-forming nitrogen fixing bacteria (NFB) and arbuscular mycorrhizal fungi (AMF) (Bazin et al., 2013). Symbiotic inoculation and nodule development during colonization by NFB is one example of a plant-mutualist interaction process that has been shown to depend on miRNA regulation (de Luis et al., 2012). For example, miR172, targeting the *Ap2* (AP2) transcription factor was increased during infection of *Phaseolus vulgaris* with *Rhizobium etli* (Nova-Franco et al., 2015). Equally, miR172 was highly up-regulated during nodule development in soybean colonized by *Bradyrhizobium japonicum*, where it targets NNC1 (Nodule Number Control1) to regulate nodule formation (Wang et al., 2014). In contrast, a negative effect of miR396 over-expression in *Medicago truncatula* on *R. irregularis* mycorrhizal colonization has also been reported (Bazin et al., 2013).

Following the trend of miRNA-based regulation of auxin signalling in response to interaction with pathogenic microbes, several miRNAs modulating the auxin response also show differential regulation in interaction with mutualists. *B. japonicum* induces miR393 in soybean roots, facilitating an interplay of auxin signalling and miR393 expression during nodulation (Subramanian et al., 2008). In contrast, the role of miRNA-based auxin regulation in symbiosis was further cemented by showing the down-regulation of miR393 during arbuscular mycorrhizal (*Rhizophagus irregularis*) root colonization in tomato, *Medicago* (*M. truncatula*) and rice (Etemadi et al., 2014). Moreover, differential regulation of miR160 was found in soybean and *Medicago* in symbiosis with *B. japonicum* and *Sinorhizobium meliloti*, respectively (Subramanian et al., 2008; Lelandais-Brière et al., 2009), further substantiating the role of auxin signalling in nodulation. miR160 was up-regulated in *Medicago* but, on the contrary, down-regulated in soybean. Lastly, increased levels

of miR167 were also found in nodules of *M. truncatula* inoculated with *S. meliloti* (Lelandais-Brière et al., 2009). miR164 was down-regulated in soybean inoculated with *B. japonicum*, expanding the regulation to auxin homeostasis during nodulation (Subramanian et al., 2008). Supporting this hypothesis, D'haeseleer et al. (2011) observed differential regulation of miR164-NAC1 in *M. truncatula* inoculated with *S. meliloti*.

Up-regulation of miR169 has been found to be crucial for nodulation in *M. truncatula*-*S. meliloti* symbiosis (Combiér et al., 2006), with its expression increased in mature nodules, restricting the expression of its target *HAP2* to the meristematic zone. In contrast, down-regulation took place in soybean a few hours post inoculation with *B. japonicum* (Subramanian et al., 2008). Further miRNAs proposed to be involved in nodulation regulation are miR166, shown to be down-regulated in soybean-*B. japonicum* interaction (Subramanian et al., 2008), miR398, which accumulated in the colonization zone in *M. truncatula*-*S. meliloti* interactions (Lelandais-Brière et al., 2009) and miR482, whose expression increased over time in soybean inoculated with *B. japonicum* (Li et al., 2010a).

A set of known and novel miRNAs, including those from the miR156 family, was detected in *Oncidium* orchid roots when colonized with the mutualistic endophyte *Serendipita indica*, including miRNAs with targets involved in root growth and development, auxin signalling, hormone signal transduction and defence (Ye et al., 2014). Several miRNAs, including miR156, miR167 and miR168, were also found up-regulated in tomato roots in response to colonization by the endophyte *Pochonia chlamydosporia*, with predicted targets in pathways related to plant defence and apoptosis regulation (Pentimone et al., 2018). Further research is needed to elucidate the role of miRNAs in mutualistic plant-fungus interactions before we can answer the question of whether miRNAs are essential for this type of symbiosis.

### 4. miRNAs and agronomic application – potential for environmentally friendly plant protection

dsRNA-generating corn (commercial name SmartStax PRO), produced to target western corn rootworm (*Diabrotica virgifera virgifera*, DV) was approved by the Canadian Food Inspection Agency (CFIA) in 2016 and by the US Environmental Protection Agency (EPA) in 2017, making it the first RNAi-based crop protection strategy successfully introduced into commercial use. The dsRNA is designed to target the *Sucrose non-fermenting 7* (*DvSnf7*) gene (Bolognesi et al., 2012), and the resistance is further mediated by two insecticidal *Bacillus thuringiensis* (Bt)-derived proteins (Head et al., 2017). While SmartStax PRO is a good example of an HIGS-based protection strategy, integrated with chemical-based protection, such applications are limited in many other crop plants, including many fruit trees, vegetables and flowers (Capriotti et al., 2020; Imani and Kogel, 2020), due to a lack of efficient transformation technologies. Furthermore, consumer resistance to genetically modified (GMO) products is still present in many societies, resulting in GMOs being currently banned in European agriculture (Kleter et al., 2018). Under these circumstances, it is interesting to note the previous observation that fungal pathogens *Botrytis cinerea* and *Fusarium graminearum* can efficiently take up environmental dsRNAs and sRNAs duplexes, which induce the silencing of pathogen genes with complementary sequences (Koch et al., 2016; Wang et al., 2016). Thus, Spray-Induced Gene Silencing (SIGS), is a non-GMO alternative to HIGS (Cai et al., 2018; Šečić and Kogel, 2021).

Since many miRNAs have highly relevant roles in promoting tolerance to abiotic and resistance to biotic stress, and also contain the inherent potential to improve agronomically relevant developmental processes such as flowering, plant height and seed production (Zheng and Qu, 2015; Tang and Chu, 2017), utilization of plant miRNAs in crop protection seems like an obvious addition to the already existing RNAi-based strategies. A strategy using miRNAs could target different molecular mechanisms: i. the constitutive or induced expression of *MIR* genes, ii. the use of miRNA-resistant target genes, and iii. artificial

miRNAs or target mimics (Zhou and Luo, 2013). For example, introduction of mutations in the *SPL14* target site for miR156 in rice resulted in changes in plant architecture and enhanced grain yield (Jiao et al., 2010; Miura et al., 2010). Another example of an effect that absence of a proper miRNA target site can have on the phenotype is the overexpression of soybean (*Glycine max*) *NF-YA* (*HAP2*) without a 3' UTR, where miR169 would usually bind, which conferred increased drought tolerance in *Arabidopsis* (Ni et al., 2013). On the other hand, overexpression of a miRNA itself can improve plant traits, as shown in rice, where overexpression of miR319, which targets two members of a transcription factor family PCF/TCP (Teosinte branched/Cycloidea/PCF; PCF5 and PCF8), resulted in enhanced cold tolerance (Yang et al., 2013a). As mentioned above, overexpression of miR393 in *Arabidopsis* enhanced resistance against biotrophic pathogens and in turn increased susceptibility to necrotrophs (Navarro et al., 2006; Fahlgren et al., 2007; Robert-Seilanian et al., 2011; Hou et al., 2019), reinforcing the necessary elucidation of the miRNA role and effect before application considerations. Artificial miRNAs (amiRNAs) produced from native miRNA precursor backbone conferred resistance to Cucumber mosaic virus (CMV) in tobacco (Qu et al., 2007). Lastly, target mimicry has been shown as an effective mechanism for sequestration of native miRNAs, in the case of non-coding gene *IPS1*, which sequesters miR399 from its target mRNA *PHO2* (Phosphate 2; Franco-Zorrilla et al., 2007). This mechanism has been highlighted for its potential in introducing artificial target mimics that would sequester miRNAs that are negative regulators of desired enhancements (Gupta, 2015). A collection of target mimics in *Arabidopsis* was created (Todesco et al., 2010), along with several other options for inhibition of miRNA silencing activity, including molecular miRNA sponges and short tandem target MIMICS (STTMs) (Reichel et al., 2015). Excitingly, a CRISPR/Cas9-mediated genome editing technology has also been applied to targeted miRNA knock-downs (Chang et al., 2016). Taking all the available methods for miRNA/target recognition and expression manipulation, together with the abundance of information about stress response and development modulation that miRNA studies can provide, it is evident they are a crucial and useful tool in current and future agronomic applications.

## 5. miRNA discovery and analysis through bioinformatics approaches

Novel miRNA discovery and identification of conserved miRNA family members and their targets in non-model plant species and staple crops is of high importance for elucidation of the complex roles miRNAs can play in plants. Considering that their discovery, as well as target prediction is based on computational and prediction approaches, there is a multitude of available bioinformatics tools for miRNA analysis (reviewed in Chen et al., 2019). For example, tools like ShortStack (Axtell, 2013), miRA (Evers et al., 2015) and miRkwood (Guigon et al., 2019) are used for plant miRNA identification and *MIR* gene annotation. Because of a possible differential expression patterns of miRNAs and their targets in temporal and tissue-specific manner, the small RNA datasets used for these analyses should be as encompassing as possible.

Besides miRNA identification, target prediction is the second bottleneck of bioinformatics approaches, for which there are several tools available, the most wide-spread being TAPIR (Bonnet et al., 2010) and psRNATarget (Dai et al., 2018). An ongoing discussion about miRNA targets is based on opposing views of targets being a few major, highly relevant transcripts, validated by binding site modifications and, in contrast, a large network of targets that is modulated by miRNA silencing, hypothetically validated by simultaneous mutation of a large set of targets (Lai, 2015).

Lastly, the predicted miRNAs and their effect on the mRNAs have to be validated by experimental approaches, including stem-loop PCR, Northern blotting, degradome analysis and quantitative RT-PCR (Chen et al., 2005; German et al., 2009; Riolo et al., 2021). Importantly, integrated sequencing approaches that consider transcriptome, sRNA and

degradome data have been proven crucial for discovery of miRNA roles (Jin et al., 2020). Evidently, miRNA research supported by improved and optimized predictions and sequencing analysis pipelines hugely benefit the validation strategies, aiming towards a routine detection of (all) the needle(s) in the transcriptomic haystack.

## 6. Conclusion

As diverse as miRNAs can be in response to developmental and abiotic triggers, so too are their responses to different microbes. A range of conserved and microbe-specific interactions from which useful conclusions can be drawn about function and target conservation are yet to be investigated. While we are still some steps away from widespread use of miRNA-based regulatory modifications to improve plant protection strategies, the full picture of involved networks, hormonal regulation and the interplay between immunity and developmental processes is gradually becoming clearer.

## Author contributions

EŠ, KHK and MJLC wrote the text, conceptualized the figures and the table. EŠ and MJLC produced the figures. All authors edited and revised the manuscript, the figures and the table.

## Declaration of Competing Interest

The authors report no declarations of interest.

## Acknowledgements

The research was funded by the German Research Council (DFG) in the program RU5116 (exRNA).

## References

- Ambawat, S., Sharma, P., Yadav, N.R., Yadav, R.C., 2013. MYB transcription factor genes as regulators for plant responses: an overview. *Physiol. Mol. Biol. Plants* 19 (3), 307–321. <https://doi.org/10.1007/s12298-013-0179-1>.
- Axtell, M.J., 2013. ShortStack: comprehensive annotation and quantification of small RNA genes. *RNA* 19, 740–751. <https://doi.org/10.1261/rna.035279.112>.
- Axtell, M.J., Westholm, J.O., Lai, E.C., 2011. Vive la différence: biogenesis and evolution of microRNAs in plants and animals. *Genome Biol.* 12 (4), 1–13. <https://doi.org/10.1186/gb-2011-12-4-221>.
- Baker, C.C., Sieber, P., Wellmer, F., Meyerowitz, E.M., 2005. The early extra petals1 mutant uncovers a role for microRNA miR164c in regulating petal number in *Arabidopsis*. *Curr. Biol.* 15, 303–315. <https://doi.org/10.1016/j.cub.2005.02.017>.
- Balmer, A., De Paoli, E., Si-Ammour, A., Mauch-Mani, B., Balmer, D., 2017. Signs of silence: small RNAs and antifungal responses in *Arabidopsis thaliana* and *Zea mays*. *Plant Engineering. InTech*. <https://doi.org/10.5772/intechopen.69795>.
- Bartel, D.P., 2004. MicroRNAs: genomics, biogenesis, mechanism, and function. *Cell* 116 (2), 281–297. [https://doi.org/10.1016/S0092-8674\(04\)00045-5](https://doi.org/10.1016/S0092-8674(04)00045-5).
- Bazin, J., Khan, G.A., Combier, J.P., Bustos-Sanmamed, P., Debernardi, J.M., Rodriguez, R., Sorin, C., Palatnik, J., Hartmann, C., Crespi, M., Lelandais-Brière, C., 2013. MiR396 affects mycorrhization and root meristem activity in the legume *Medicago truncatula*. *Plant J.* 74, 920–934. <https://doi.org/10.1111/tpj.12178>.
- Bolognesi, R., Ramaseshadri, P., Anderson, J., Bachman, P., Clinton, W., Flannagan, R., Ilagan, O., Lawrence, C., Levine, S., Moar, W., Mueller, G., Tan, J., Uffman, J., Wiggins, E., Heck, G., Segers, G., 2012. Characterizing the mechanism of action of double-stranded RNA activity against western corn rootworm (*Diabrotica virgifera virgifera* LeConte). *PLoS One* 7, e47534. <https://doi.org/10.1371/journal.pone.0047534>.
- Bonnet, E., He, Y., Billiau, K., van de Peer, Y., 2010. TAPIR, a web server for the prediction of plant microRNA targets, including target mimics. *Bioinformatics* 26, 1566–1568. <https://doi.org/10.1093/bioinformatics/btq233>.
- Bouchie, A., 2013. First microRNA mimic enters clinic. *Nat. Biotechnol.* 31 (7), 577. <https://doi.org/10.1038/nbt0713-577>.
- Budak, H., Akpinar, B.A., 2015. Plant miRNAs: biogenesis, organization and origins. *Funct. Integr. Genomics* 15 (5), 523–531. <https://doi.org/10.1007/s10142-015-0451-2>.
- Cagliari, D., Dias, N.P., Galdeano, D.M., dos Santos, E.A., Smaghe, G., Zotti, M.J., 2019. Management of pest insects and plant diseases by non-transformative RNAi. *Front. Plant Sci.* 10, 1319. <https://doi.org/10.3389/fpls.2019.01319>.
- Cai, Q., He, B., Kogel, K.H., Jin, H., 2018. Cross-kingdom RNA trafficking and environmental RNAi — nature's blueprint for modern crop protection strategies. *Curr. Opin. Microbiol.* 46, 58–64. <https://doi.org/10.1016/j.mib.2018.02.003>.

- Calin, G.A., Dumitru, C.D., Shimizu, M., Bichi, R., Zupo, S., Noch, E., Alder, H., Rattan, S., Keating, M., Rai, K., Rassenti, L., Kipps, T., Negrini, M., Bullrich, F., Croce, C.M., 2002. Frequent deletions and down-regulation of micro-RNA genes miR15 and miR16 at 13q14 in chronic lymphocytic leukemia. *Proc. Natl. Acad. Sci. U. S. A.* 99, 15524–15529. <https://doi.org/10.1073/pnas.242606799>.
- Capriotti, L., Baraldi, E., Mezzetti, B., Limerica, C., Sabbadini, S., 2020. Biotechnological approaches: gene overexpression, gene silencing, and genome editing to control fungal and oomycete diseases in grapevine. *Int. J. Mol. Sci.* 21 (16), 1–29. <https://doi.org/10.3390/ijms21165701>.
- Chang, H., Yi, B., Ma, R., Zhang, X., Zhao, H., Xi, Y., 2016. CRISPR/cas9, a novel genomic tool to knock down microRNA in vitro and in vivo. *Sci. Rep.* 6, 1–12. <https://doi.org/10.1038/srep22312>.
- Chauhan, S., Yogindran, S., Rajam, M.V., 2017. Role of miRNAs in biotic stress reactions in plants. *Indian J. Plant Physiol.* 22 (4), 514–529. <https://doi.org/10.1007/s40502-017-0347-3>.
- Chen, C., Ridzon, D.A., Broomer, A.J., Zhou, Z., Lee, D.H., Nguyen, J.T., Barbisin, M., Xu, N.L., Mahuvakar, V.R., Andersen, M.R., Lao, K.Q., Livak, K.J., Guegler, K.J., 2005. Real-time quantification of microRNAs by stem-loop RT-PCR. *Nucleic Acids Res.* 33 <https://doi.org/10.1093/nar/gni178>.
- Chen, H.M., Chen, L.T., Patel, K., Li, Y.H., Baulcombe, D.C., Wu, S.H., 2010. 22-Nucleotide RNAs trigger secondary siRNA biogenesis in plants. *Proc. Natl. Acad. Sci. U. S. A.* 107, 15269–15274. <https://doi.org/10.1073/pnas.1001738107>.
- Chen, L., Heikkinen, L., Wang, C., Yang, Y., Sun, H., Wong, G., 2019. Trends in the development of miRNA bioinformatics tools. *Brief. Bioinform.* 20 (5), 1836–1852. <https://doi.org/10.1093/bib/bby054>.
- Combiere, J.P., Frugier, F., De Billy, F., Boualem, A., El-Yahyaoui, F., Moreau, S., Vernié, T., Ott, T., Gamas, P., Crespi, M., Niebel, A., 2006. MTHAP2-1 is a key transcriptional regulator of symbiotic nodule development regulated by microRNA169 in *Medicago truncatula*. *Genes Dev.* 20, 3084–3088. <https://doi.org/10.1101/gad.402806>.
- Cuperus, J.T., Carbonell, A., Fahlgren, N., Garcia-Ruiz, H., Burke, R.T., Takeda, A., Sullivan, C.M., Gilbert, S.D., Montgomery, T.A., Carrington, J.C., 2010. Unique functionality of 22-nt miRNAs in triggering RDR6-dependent siRNA biogenesis from target transcripts in Arabidopsis. *Nat. Struct. Mol. Biol.* 17, 997–1003. <https://doi.org/10.1038/nsmb.1866>.
- D'haeseleer, K., Den Herder, G., Laffont, C., Plet, J., Mortier, V., Lelandais-Brière, C., de Bodt, S., de Keyser, A., Crespi, M., Holsters, M., Frugier, F., Goormachtig, S., 2011. Transcriptional and post-transcriptional regulation of a NAC1 transcription factor in *Medicago truncatula* roots. *New Phytol.* 191, 647–661. <https://doi.org/10.1111/j.1469-8137.2011.03719.x>.
- Dai, X., Zhuang, Z., Zhao, P.X., 2018. PsRNATarget: a plant small RNA target analysis server (2017 release). *Nucleic Acids Res.* 46, W49–W54. <https://doi.org/10.1093/nar/gky316>.
- De Luis, A., Markmann, K., Cognat, V., Holt, D.B., Charpentier, M., Parniske, M., Stougaard, J., Voinnet, O., 2012. Two MicroRNAs linked to nodule infection and nitrogen-fixing ability in the legume *Lotus japonicus*. *Plant Physiol.* 160, 2137–2154. <https://doi.org/10.1104/pp.112.204883>.
- Dezulan, T., Palatnik, J., Huson, D., Weigel, D., 2005. Conservation and divergence of microRNA families in plants. *Genome Biol.* 6, 1–25. <https://doi.org/10.1186/gb-2005-6-11-p13>.
- Dharmasiri, N., Dharmasiri, S., Estelle, M., 2005a. The F-box protein TIR1 is an auxin receptor. *Nature* 435, 441–445. <https://doi.org/10.1038/nature03543>.
- Dharmasiri, N., Dharmasiri, S., Weijers, D., Lechner, E., Yamada, M., Hobbie, L., Ehrismann, J.S., Jürgens, G., Estelle, M., 2005b. Plant development is regulated by a family of auxin receptor F-box proteins. *Dev. Cell* 9, 109–119. <https://doi.org/10.1016/j.devcel.2005.05.014>.
- Dodds, P.N., Rathjen, J.P., 2010. Plant immunity: towards an integrated view of plant-pathogen interactions. *Nat. Rev. Genet.* 11 (8), 539–548. <https://doi.org/10.1038/nrg2812>.
- Du, J., Li, M., Huang, Q., Liu, W., Li, Wqun, Li, Yjian, Gong, Zcheng, 2019. The critical role of microRNAs in stress response: therapeutic prospect and limitation. *Pharmacol. Res.* 142, 294–302. <https://doi.org/10.1016/j.phrs.2018.12.007>.
- Etemadi, M., Gutjahr, C., Couzigou, J.M., Zouine, M., Laressergues, D., Timmers, A., Audran, C., Bouzayen, M., Bécard, G., Combiere, J.P., 2014. Auxin perception is required for arbuscule development in arbuscular mycorrhizal symbiosis. *Plant Physiol.* 166, 281–292. <https://doi.org/10.1104/pp.114.246595>.
- Evers, M., Huttner, M., Dueck, A., Meister, G., Engelmann, J.C., 2015. miRA: adaptable novel miRNA identification in plants using small RNA sequencing data. *BMC Bioinformatics* 16, 370. <https://doi.org/10.1186/s12859-015-0798-3>.
- Fahlgren, N., Howell, M.D., Kasschau, K.D., Chapman, E.J., Sullivan, C.M., Cumbie, J.S., Givan, S.A., Law, T.F., Grant, S.R., Dangl, J.L., Carrington, J.C., 2007. High-throughput sequencing of Arabidopsis microRNAs: evidence for frequent birth and death of MIRNA genes. *PLoS One* 2, e219. <https://doi.org/10.1371/journal.pone.0000219>.
- Fahlgren, N., Jogdeo, S., Kasschau, K.D., Sullivan, C.M., Chapman, E.J., Laubinger, S., Smith, L.M., Dasenko, M., Givan, S.A., Weigel, D., Carrington, J.C., 2010. MicroRNA gene evolution in *Arabidopsis lyrata* and *Arabidopsis thaliana*. *Plant Cell* 22, 1074–1089. <https://doi.org/10.1105/tpc.110.073999>.
- Fang, X., Qi, Y., 2015. RNAi in plants: an Argonaute-centered view. *Plant Cell* 28 (2), 272–285. <https://doi.org/10.1105/tpc.15.00920>.
- Feng, H., Duan, X., Zhang, Q., Li, X., Wang, B., Huang, L., Wang, X., Kang, Z., 2014. The target gene of tae-miR164, a novel NAC transcription factor from the NAM subfamily, negatively regulates resistance of wheat to stripe rust. *Mol. Plant Pathol.* 15, 284–296. <https://doi.org/10.1111/mpp.12089>.
- Fire, A., Xu, S., Montgomery, M.K., Kostas, S.A., Driver, S.E., Mello, C.C., 1998. Potent and specific genetic interference by double-stranded RNA in *Caenorhabditis elegans*. *Nature* 391, 806–811. <https://doi.org/10.1038/35888>.
- Franco-Zorrilla, J.M., Valli, A., Todesco, M., Mateos, I., Puga, M.I., Rubio-Somoza, I., Leyva, A., Weigel, D., García, J.A., Paz-Ares, J., 2007. Target mimicry provides a new mechanism for regulation of microRNA activity. *Nat. Genet.* 39, 1033–1037. <https://doi.org/10.1038/ng2079>.
- Gaiti, F., Calcino, A.D., Tanurdžić, M., Degnan, B.M., 2017. Origin and evolution of the metazoan non-coding regulatory genome. *Dev. Biol.* 427 (2), 193–202. <https://doi.org/10.1016/j.ydbio.2016.11.013>.
- German, M.A., Luo, S., Schroth, G., Meyers, B.C., Green, P.J., 2009. Construction of parallel analysis of RNA ends (PARE) libraries for the study of cleaved miRNA targets and the RNA degradome. *Nat. Protoc.* 4, 356–362. <https://doi.org/10.1038/nprot.2009.8>.
- González-Lamothe, R., El Oirdi, M., Brissin, N., Bouarab, K., 2012. The conjugated auxin indole-3-acetic acid-aspartic acid promotes plant disease development. *Plant Cell* 24, 672–777. <https://doi.org/10.1105/tpc.111.095190>.
- Griffiths-Jones, S., 2004. The microRNA registry. *Nucleic Acids Res.* 32, D109. <https://doi.org/10.1093/nar/gkh023>.
- Griffiths-Jones, S., Grocock, R.J., van Dongen, S., Bateman, A., Enright, A.J., 2006. miRBase: microRNA sequences, targets and gene nomenclature. *Nucleic Acids Res.* 34, D140–D144. <https://doi.org/10.1093/nar/gkj112>.
- Guigon, I., Legrand, S., Berthelot, J.F., Bini, S., Lanselle, D., Benmounah, M., Touzet, H., 2019. MiRkwood: a tool for the reliable identification of microRNAs in plant genomes. *BMC Genomics* 20, 532. <https://doi.org/10.1186/s12864-019-5913-9>.
- Guo, H.S., Xie, Q., Fei, J.F., Chua, N.H., 2005. MicroRNA directs mRNA cleavage of the transcription factor NAC1 to downregulate auxin signals for Arabidopsis lateral root development. *Plant Cell* 17, 1376–1386. <https://doi.org/10.1105/tpc.105.030841>.
- Gupta, P.K., 2015. MicroRNAs and target mimics for crop improvement. *Curr. Sci.* 108 (9), 1624–1633. <https://doi.org/10.18520/cs/v108/i9/1624-1633>.
- Hashemi, A., Gorji-bahri, G., 2020. MicroRNA: promising roles in cancer therapy. *Curr. Pharm. Biotechnol.* 21, 1186–1203. <https://doi.org/10.2174/1389201021666200420101613>.
- Head, G.P., Carroll, M.W., Evans, S.P., Rule, D.M., Willse, A.R., Clark, T.L., Storer, N.P., Flannagan, R.D., Samuel, L.W., Meinke, L.J., 2017. Evaluation of SmartStax and SmartStax PRO maize against western corn rootworm and northern corn rootworm: efficacy and resistance management. *Pest Manag. Sci.* 73, 1883–1899. <https://doi.org/10.1002/ps.4554>.
- Hou, Y., Zhai, Y., Feng, L., Karimi, H.Z., Rutter, B.D., Zeng, L., Choi, D.S., Zhang, B., Gu, W., Chen, X., Ye, W., Innes, R.W., Zhai, J., Ma, W., 2019. A Phytophthora effector suppresses trans-kingdom RNAi to promote disease susceptibility. *Cell Host Microbe* 25, 153–165. <https://doi.org/10.1016/j.chom.2018.11.007> e5.
- Hu, G., Lei, Y., Liu, J., Hao, M., Zhang, Z., Tang, Y., Chen, A., Wu, J., 2020. The ghr-miR164 and GhNAC100 modulate cotton plant resistance against *Verticillium dahlia*. *Plant Sci.* 293, 110438. <https://doi.org/10.1016/j.plantsci.2020.110438>.
- Hückelhoven, R., Kogel, K.H., 2003. Reactive oxygen intermediates in plant-microbe interactions: who is who in powdery mildew resistance? *Planta* 216 (6), 891–902. <https://doi.org/10.1007/s00425-003-0973-z>.
- Imani, J., Kogel, K.H., 2020. Plant transformation techniques: agrobacterium- and microparticle-mediated gene transfer in cereal plants. *Methods in Molecular Biology*. Humana Press Inc., pp. 281–294. [https://doi.org/10.1007/978-1-0716-0356-7\\_15](https://doi.org/10.1007/978-1-0716-0356-7_15).
- Jagadeeswaran, G., Saini, A., Sunkar, R., 2009. Biotic and abiotic stress down-regulate miR398 expression in Arabidopsis. *Planta* 229, 1009–1014. <https://doi.org/10.1007/s00425-009-0889-3>.
- Jiao, Y., Wang, Y., Xue, D., Wang, J., Yan, M., Liu, G., Dong, G., Zeng, D., Lu, Z., Zhu, X., Qian, Q., Li, J., 2010. Regulation of OsSPL14 by OsmiR156 defines ideal plant architecture in rice. *Nat. Genet.* 42, 541–544. <https://doi.org/10.1038/ng.591>.
- Jin, J., Xu, Y., Lu, P., Chen, Q., Liu, P., Wang, J., Zhang, J., Li, Z., Yang, A., Li, F., Cao, P., 2020. Degradome, small RNAs and transcriptome sequencing of a high-nicotine cultivated tobacco uncovers miRNA's function in nicotine biosynthesis. *Sci. Rep.* 10, 11751. <https://doi.org/10.1038/s41598-020-68691-y>.
- Jones-Rhoades, M.W., Bartel, D.P., 2004. Computational identification of plant microRNAs and their targets, including a stress-induced miRNA. *Mol. Cell* 14, 787–799. <https://doi.org/10.1016/j.molcel.2004.05.027>.
- Jones-Rhoades, M.W., Bartel, D.P., Bartel, B., 2006. MicroRNAs and their regulatory roles in plants. *Annu. Rev. Plant Biol.* 57, 19–53. <https://doi.org/10.1146/annurev.arplant.57.032905.105218>.
- Kleter, G., McFarland, S., Bach, A., Bernabucci, U., Bikker, P., Busani, L., Kok, E., Kostov, K., Nadal, A., Pla, M., Ronchi, B., Terre, M., Einspanier, R., 2018. Surveying selected European feed and livestock production chains for features enabling the case-specific post-market monitoring of livestock for intake and potential health impacts of animal feeds derived from genetically modified crops. *Food Chem. Toxicol.* 117, 66–78. <https://doi.org/10.1016/j.fct.2017.10.004>.
- Koch, A., Biedenkopf, D., Furch, A., Weber, L., Rossbach, O., Abdellatef, E., Linicua, L., Johannsmeier, J., Jelonek, L., Goemann, A., Cardoza, V., McMillan, J., Mentzel, T., Kogel, K.H., 2016. An RNAi-based control of *Fusarium graminearum* infections through spraying of long dsRNAs involves a plant passage and is controlled by the fungal silencing machinery. *PLoS Pathog.* 12, e1005901. <https://doi.org/10.1371/journal.ppat.1005901>.
- Kozomara, A., Birgaoanu, M., Griffiths-Jones, S., 2019. MiRBase: from microRNA sequences to function. *Nucleic Acids Res.* 47, D155–D162. <https://doi.org/10.1093/nar/gky1141>.
- Lagos-Quintana, M., Rauhut, R., Lendeckel, W., Tuschl, T., 2001. Identification of novel genes coding for small expressed RNAs. *Science* (80-) 294, 853–858. <https://doi.org/10.1126/science.1064921>.

- Lagos-Quintana, M., Rauhut, R., Yalcin, A., Meyer, J., Lendeckel, W., Tuschl, T., 2002. Identification of tissue-specific microRNAs from mouse. *Curr. Biol.* 12, 735–739. [https://doi.org/10.1016/S0960-9822\(02\)00809-6](https://doi.org/10.1016/S0960-9822(02)00809-6).
- Lai, E.C., 2015. Two decades of miRNA biology: lessons and challenges. *RNA* 21 (4), 675–677. <https://doi.org/10.1261/rna.051193.115>.
- Lamb, C., Dixon, R.A., 1997. The oxidative burst in plant disease resistance. *Annu. Rev. Plant Biol.* 48, 251–275. <https://doi.org/10.1146/annurev.arplant.48.1.251>.
- Lau, N.C., Lim, L.P., Weinstein, E.G., Bartel, D.P., 2001. An abundant class of tiny RNAs with probable regulatory roles in *Caenorhabditis elegans*. *Science* (80-) 294, 858–862. <https://doi.org/10.1126/science.1065062>.
- Lee, R.C., Ambros, V., 2001. An extensive class of small RNAs in *Caenorhabditis elegans*. *Science* (80-) 294, 862–864. <https://doi.org/10.1126/science.1065329>.
- Lee, R.C., Feinbaum, R.L., Ambros, V., 1993. The *C. elegans* heterochronic gene lin-4 encodes small RNAs with antisense complementarity to lin-14. *Cell* 75, 843–854. [https://doi.org/10.1016/0092-8674\(93\)90529-Y](https://doi.org/10.1016/0092-8674(93)90529-Y).
- Lee, M.-H., Jeon, H.S., Kim, H.G., Park, O.K., 2017. An Arabidopsis NAC transcription factor NAC4 promotes pathogen-induced cell death under negative regulation by microRNA164. *New Phytol.* 214, 343–360. <https://doi.org/10.1111/nph.14371>.
- Lelandais-Brière, C., Naya, L., Sallet, E., Calenge, F., Frugier, F., Hartmann, C., Gouzy, J., Crespi, M., 2009. Genome-wide medicago truncatula small RNA analysis revealed novel microRNAs and isoforms differentially regulated in roots and nodules. *Plant Cell* 21, 2780–2796. <https://doi.org/10.1105/tpc.109.068130>.
- Li, H., Deng, Y., Wu, T., Subramanian, S., Yu, O., 2010a. Misexpression of miR482, miR1512, and miR1515 increases soybean nodulation. *Plant Physiol.* 153, 1759–1770. <https://doi.org/10.1104/pp.110.156950>.
- Li, Y., Zhang, Q.Q., Zhang, J., Wu, L., Qi, Y., Zhou, J.M., 2010b. Identification of microRNAs involved in pathogen-associated molecular pattern-triggered plant innate immunity. *Plant Physiol.* 152, 2222–2231. <https://doi.org/10.1104/pp.109.151803>.
- Li, F., Pignatta, D., Bendix, C., Brunkard, J.O., Cohn, M.M., Tung, J., Sun, H., Kumar, P., Baker, B., 2012. MicroRNA regulation of plant innate immune receptors. *Proc. Natl. Acad. Sci. U. S. A.* 109, 1790–1795. <https://doi.org/10.1073/pnas.1118282109>.
- Li, Y., Lu, Y.G., Shi, Y., Wu, L., Xu, Y.J., Huang, F., Guo, X.Y., Zhang, Y., Fan, J., Zhao, J., Q., Zhang, H.Y., Xu, P.Z., Zhou, J.M., Wu, X.J., Wang, P.R., Wang, W.M., 2014. Multiple rice microRNAs are involved in immunity against the blast fungus *Magnaporthe oryzae*. *Plant Physiol.* 164, 1077–1092. <https://doi.org/10.1104/pp.113.230052>.
- Li, S., Castillo-González, C., Yu, B., Zhang, X., 2017. The functions of plant small RNAs in development and in stress responses. *Plant J.* 90, 654–670. <https://doi.org/10.1111/tpl.13444>.
- Li, M., Chen, W.D., Wang, Y.D., 2020. The roles of the gut microbiota-miRNA interaction in the host pathophysiology. *Mol. Med.* 26 (1), 101. <https://doi.org/10.1186/s10020-020-00234-7>.
- Liu, H., Yu, H., Tang, G., Huang, T., 2018. Small but powerful: function of microRNAs in plant development. *Plant Cell Rep.* 37 (3), 515–528. <https://doi.org/10.1007/s00299-017-2246-5>.
- Liu, S., Jaouannet, M., Dempsey, D.A., Imani, J., Coustau, C., Kogel, K.H., 2020. RNA-based technologies for insect control in plant production. *Biotechnol. Adv.* 39, 107463. <https://doi.org/10.1016/j.biotechadv.2019.107463>.
- Loreti, E., Betti, F., Ladera-Carmona, M.J., Fontana, F., Novi, G., Valeri, M.C., Perata, P., 2020. ARGONAUTE1 and ARGONAUTE4 regulate gene expression and auxin tolerance. *Plant Physiol.* 182, 287–300. <https://doi.org/10.1104/pp.19.00741>.
- Lu, S., Sun, Y.H., Amerson, H., Chiang, V.L., 2007. MicroRNAs in loblolly pine (*Pinus taeda* L.) and their association with fusiform rust gall development. *Plant J.* 51, 1077–1098. <https://doi.org/10.1111/j.1365-3113X.2007.03208.x>.
- Maity, S.N., De Crombrughe, B., 1998. Role of the CCAAT-binding protein CBF/NF-Y in transcription. *Trends Biochem. Sci.* 23 (5), 174–178. [https://doi.org/10.1016/S0968-0004\(98\)01201-8](https://doi.org/10.1016/S0968-0004(98)01201-8).
- Miura, K., Ikeda, M., Matsubara, A., Song, X.J., Ito, M., Asano, K., Matsuo, M., Kitano, H., Ashikari, M., 2010. OsSPL14 promotes panicle branching and higher grain productivity in rice. *Nat. Genet.* 42, 545–549. <https://doi.org/10.1038/ng.592>.
- Miyashima, S., Koi, S., Hashimoto, T., Nakajima, K., 2011. Non-cell-autonomous microRNA 165 acts in a dose-dependent manner to regulate multiple differentiation status in the Arabidopsis root. *Development* 138, 2303–2313. <https://doi.org/10.1242/dev.060491>.
- Moran, Y., Agron, M., Praher, D., Technau, U., 2017. The evolutionary origin of plant and animal microRNAs. *Nat. Ecol. Evol.* 1 (3) <https://doi.org/10.1038/s41559-016-0027>.
- Napoli, C., Lemieux, C., Jorgensen, R., 1990. Introduction of a chimeric chalcone synthase gene into *Petunia* results in reversible Co-suppression of homologous genes in trans. *Plant Cell* 2, 279–289. <https://doi.org/10.1105/tpc.2.4.279>.
- Naseem, M., Srivastava, M., Tehseen, M., Ahmed, N., 2015. Auxin crosstalk to plant immune networks: a plant-pathogen interaction perspective. *Curr. Protein Pept. Sci.* 16, 389–394. <https://doi.org/10.2174/1389203716666150330124911>.
- Navarro, L., Dunoyer, P., Jay, F., Arnold, B., Dharmasiri, N., Estelle, M., Voinnet, O., Jones, J.D.G., 2006. A plant miRNA contributes to antibacterial resistance by repressing auxin signaling. *Science* (80-) 312, 436–439. <https://doi.org/10.1126/science.1126088>.
- Ni, Z., Hu, Z., Jiang, Q., Zhang, H., 2013. GmNRYFA3, a target gene of miR169, is a positive regulator of plant tolerance to drought stress. *Plant Mol. Biol.* 82, 113–129. <https://doi.org/10.1007/s11103-013-0040-5>.
- Nova-Franco, B., Íñiguez, L.P., Valdés-López, O., Alvarado-Affantranger, X., Leija, A., Fuentes, S.I., Ramírez, M., Paul, S., Reyes, J.L., Girard, L., Hernández, G., 2015. The micro-RNA72c-APETALA2-1 node as a key regulator of the common bean *Rhizobium etli* nitrogen fixation symbiosis. *Plant Physiol.* 168, 273–291. <https://doi.org/10.1104/pp.114.255547>.
- Nowara, D., Schweizer, P., Gay, A., Lacomme, C., Shaw, J., Ridout, C., Douchkov, D., Hensel, G., Kümlehn, J., 2010. HIGS: host-induced gene silencing in the obligate biotrophic fungal pathogen *Blumeria graminis*. *Plant Cell* 22, 3130–3141. <https://doi.org/10.1105/tpc.110.077040>.
- O'Brien, J., Hayder, H., Zayed, Y., Peng, C., 2018. Overview of microRNA biogenesis, mechanisms of actions, and circulation. *Front. Endocrinol. (Lausanne)* 9 (Aug), 402. <https://doi.org/10.3389/fendo.2018.00402>.
- Orellana, E.A., Kasinski, A.L., 2015. MicroRNAs in cancer: a historical perspective on the path from discovery to therapy. *Cancers (Basel)* 7 (3), 1388–1405. <https://doi.org/10.3390/cancers7030842>.
- Pasquinelli, A.E., Reinhart, B.J., Slack, F., Martindale, M.Q., Kuroda, M.I., Maller, B., Hayward, D.C., Ball, E.E., Degnan, B., Müller, P., Spring, J., Srinivasan, A., Fishman, M., Finnerty, J., Corbo, J., Levine, M., Leahy, P., Davidson, E., Ruvkun, G., 2000. Conservation of the sequence and temporal expression of let-7 heterochronic regulatory RNA. *Nature* 408, 86–89. <https://doi.org/10.1038/35040556>.
- Pentimone, I., Lebrón, R., Hackenberg, M., Rosso, L.C., Colagiero, M., Nigro, F., Ciancio, A., 2018. Identification of tomato miRNAs responsive to root colonization by endophytic *Pochonia chlamydosporia*. *Appl. Microbiol. Biotechnol.* 102, 907–919. <https://doi.org/10.1007/s00253-017-8608-7>.
- Prigge, M.J., Otsuga, D., Alonso, J.M., Ecker, J.R., Drews, G.N., Clark, S.E., 2005. Class III homeodomain-leucine zipper gene family members have overlapping, antagonistic, and distinct roles in Arabidopsis development. *Plant Cell* 17, 61–76. <https://doi.org/10.1105/tpc.104.026161>.
- Pruss, G.J., Nester, E.W., Vance, V., 2008. Infiltration with *Agrobacterium tumefaciens* induces host defense and development-dependent responses in the infiltrated zone. *Mol. Plant Microbe Interact.* 21, 1528–1538. <https://doi.org/10.1094/MPMI-21-12-1528>.
- Qu, J., Ye, J., Fang, R., 2007. Artificial MicroRNA-mediated virus resistance in plants. *J. Virol.* 81, 6690–6699. <https://doi.org/10.1128/jvi.02457-06>.
- Reichel, M., Li, Y., Li, J., Millar, A.A., 2015. Inhibiting plant microRNA activity: molecular SPONGES, target MIMICs and STIMs all display variable efficacies against target microRNAs. *Plant Biotechnol. J.* 13, 915–926. <https://doi.org/10.1111/pbi.12327>.
- Reinhart, B.J., Slack, F.J., Basson, M., Pasquinelli, A.E., Bettinger, J.C., Rougvie, A.E., Horvitz, H.R., Ruvkun, G., 2000. The 21-nucleotide let-7 RNA regulates developmental timing in *Caenorhabditis elegans*. *Nature* 403, 901–906. <https://doi.org/10.1038/35002607>.
- Reinhart, B.J., Weinstein, E.G., Rhoades, M.W., Bartel, B., Bartel, D.P., 2002. MicroRNAs in plants. *Genes Dev.* 16, 1616–1626. <https://doi.org/10.1101/gad.1004402>.
- Rhoades, M.W., Reinhart, B.J., Lim, L.P., Burge, C.B., Bartel, B., Bartel, D.P., 2002. Prediction of plant microRNA targets. *Cell* 110, 513–520. [https://doi.org/10.1016/S0092-8674\(02\)00863-2](https://doi.org/10.1016/S0092-8674(02)00863-2).
- Riolo, G., Cantara, S., Marzocchi, C., Ricci, C., 2021. miRNA targets: from prediction tools to experimental validation. *Methods Protoc.* 4 (1), 1–20. <https://doi.org/10.3390/mps4010001>.
- Robert-Seilaniantz, A., MacLean, D., Jikumaru, Y., Hill, L., Yamaguchi, S., Kamiya, Y., Jones, J.D.G., 2011. The microRNA miR393 re-directs secondary metabolite biosynthesis away from camalexin and towards glucosinolates. *Plant J.* 67, 218–231. <https://doi.org/10.1111/j.1365-3113X.2011.04591.x>.
- Rogers, K., Chen, X., 2013. Biogenesis, turnover, and mode of action of plant microRNAs. *Plant Cell* 25 (7), 2383–2399. <https://doi.org/10.1105/tpc.113.113159>.
- Romano, N., Macino, G., 1992. Quelling: transient inactivation of gene expression in *Neurospora crassa* by transformation with homologous sequences. *Mol. Microbiol.* 6, 3343–3353. <https://doi.org/10.1111/j.1365-2958.1992.tb02202.x>.
- Sallie-Wondim, D., Gebremedhn, S., Hoelker, M., Tholen, E., Hailay, T., Tesfaye, D., 2020. The role of microRNAs in mammalian fertility: from gametogenesis to embryo implantation. *Int. J. Mol. Sci.* 21 (2) <https://doi.org/10.3390/ijms21020585>.
- Šečić, E., Kogel, K.H., 2021. Requirements for fungal uptake of dsRNA and gene silencing in RNAi-based crop protection strategies. *Curr. Opin. Biotechnol.* 70, 136–142. <https://doi.org/10.1016/j.copbio.2021.04.001>.
- Šečić, E., Zanini, S., Kogel, K.H., 2019. Further elucidation of the argonaute and dicer protein families in the model grass species *Brachypodium distachyon*. *Front. Plant Sci.* 10 <https://doi.org/10.3389/fpls.2019.01332>.
- Shivaprasad, P.V., Chen, H.M., Patel, K., Bond, D.M., Santos, B.A.C.M., Baulcombe, D.C., 2012. A microRNA superfamily regulates nucleotide binding site-leucine-rich repeats and other mRNAs. *Plant Cell* 24, 859–874. <https://doi.org/10.1105/tpc.111.095380>.
- Shriram, V., Kumar, V., Devarumath, R.M., Khare, T.S., Wani, S.H., 2016. MicroRNAs as potential targets for abiotic stress tolerance in plants. *Front. Plant Sci.* 7 (Jun), 817. <https://doi.org/10.3389/fpls.2016.00817>.
- Sieber, P., Wellmer, F., Gheyselinck, J., Riechmann, J.L., Meyerowitz, E.M., 2007. Redundancy and specialization among plant microRNAs: role of the MIR164 family in developmental robustness. *Development* 134, 1051–1060. <https://doi.org/10.1242/dev.02817>.
- Srivastava, P.K., Moturu, T.R., Pandey, P., Baldwin, I.T., Pandey, S.P., 2014. A comparison of performance of plant miRNA target prediction tools and the characterization of features for genome-wide target prediction. *BMC Genomics* 15, 348. <https://doi.org/10.1186/1471-2164-15-348>.
- Subramanian, S., Fu, Y., Sunkar, R., Barbazuk, W.B., Zhu, J.K., Yu, O., 2008. Novel and nodulation-regulated microRNAs in soybean roots. *BMC Genomics* 9, 160. <https://doi.org/10.1186/1471-2164-9-160>.
- Sugawara, S., Hishiyama, S., Jikumaru, Y., Hanada, A., Nishimura, T., Koshiba, T., Zhao, Y., Kamiya, Y., Kasahara, H., 2009. Biochemical analyses of indole-3-


- acetaldoximedependent auxin biosynthesis in Arabidopsis. *Proc. Natl. Acad. Sci. U. S. A.* 106, 5430–5435. <https://doi.org/10.1073/pnas.0811226106>.
- Sunkar, R., Zhu, J.K., 2004. Novel and stress regulated microRNAs and other small RNAs from Arabidopsis. *Plant Cell* 16, 2001–2019. <https://doi.org/10.1105/tpc.104.022830>.
- Tang, J., Chu, C., 2017. MicroRNAs in crop improvement: fine-tuners for complex traits. *Nat. Plants* 3. <https://doi.org/10.1038/nplants.2017.77>.
- Todesco, M., Rubio-Somoza, I., Paz-Ares, J., Weigel, D., 2010. A collection of target mimics for comprehensive analysis of microRNA function in *Arabidopsis thaliana*. *PLoS Genet.* 6, 1–10. <https://doi.org/10.1371/journal.pgen.1001031>.
- Ulmasov, T., Hagen, G., Guilfoyle, T.J., 1999. Dimerization and DNA binding of auxin response factors. *Plant J.* 19, 309–319. <https://doi.org/10.1046/j.1365-3113X.1999.00538.x>.
- Van Der Krol, A.R., Mur, L.A., Beld, M., Mol, J.N.M., Stuitje, A.R., 1990. Flavonoid genes in petunia: addition of a limited number of gene copies may lead to a suppression of gene expression. *Plant Cell* 2, 291–299. <https://doi.org/10.1105/tpc.2.4.291>.
- Vaucheret, H., Mallory, A.C., Bartel, D.P., 2006. AGO1 homeostasis entails coexpression of MIR168 and AGO1 and preferential stabilization of miR168 by AGO1. *Mol. Cell* 22, 129–136. <https://doi.org/10.1016/j.molcel.2006.03.011>.
- Wang, Y., Wang, L., Zou, Y., Cai, Z., Zhang, S., Zhang, S., Zhao, F., Tian, Y., Jiang, Q., Ferguson, B.J., Gresshoff, P.M., Li, X., 2014. Soybean miR172c targets the repressive AP2 transcription factor NNC1 to activate ENOD40 expression and regulate nodule initiation. *Plant Cell* 26, 4782–4801. <https://doi.org/10.1105/tpc.114.131607>.
- Wang, M., Weiberg, A., Lin, F.M., Thomma, B.P.H.J., Da Huang, H., Jin, H., 2016. Bidirectional cross-kingdom RNAi and fungal uptake of external RNAs confer plant protection. *Nat. Plants* 2. <https://doi.org/10.1038/nplants.2016.151>.
- Wang, J., Mei, J., Ren, G., 2019. Plant microRNAs: biogenesis, homeostasis, and degradation. *Front. Plant Sci.* 10, 360. <https://doi.org/10.3389/fpls.2019.00360>.
- Weiberg, A., Wang, M., Lin, F.M., Zhao, H., Zhang, Z., Kaloshian, I., Da Huang, H., Jin, H., 2013. Fungal small RNAs suppress plant immunity by hijacking host RNA interference pathways. *Science* (80-) 342, 118–123. <https://doi.org/10.1126/science.1239705>.
- Wienholds, E., Kloosterman, W.P., Miska, E., Alvarez-Saavedra, E., Berezikov, E., De Bruijn, E., Horvitz, H.R., Kauppinen, S., Plasterk, R.H.A., 2005. Cell biology: MicroRNA expression in zebrafish embryonic development. *Science* (80-) 309, 310–311. <https://doi.org/10.1126/science.1114519>.
- Wightman, B., Ha, I., Ruvkun, G., 1993. Posttranscriptional regulation of the heterochronic gene *lin-14* by *lin-4* mediates temporal pattern formation in *C. elegans*. *Cell* 75, 855–862. [https://doi.org/10.1016/0092-8674\(93\)90530-4](https://doi.org/10.1016/0092-8674(93)90530-4).
- Windels, D., Vazquez, F., 2011. Mir393: integrator of environmental cues in auxin signaling? *Plant Signal. Behav.* 6, 1672–1675. <https://doi.org/10.4161/psb.6.11.17900>.
- Wong, J., Gao, L., Yang, Y., Zhai, J., Arikiti, S., Yu, Y., Duan, S., Chan, V., Xiong, Q., Yan, J., Li, S., Liu, R., Wang, Y., Tang, G., Meyers, B.C., Chen, X., Ma, W., 2014. Roles of small RNAs in soybean defense against *Phytophthora sojae* infection. *Plant J.* 79, 928–940. <https://doi.org/10.1111/tpj.12590>.
- Wu, G., Poethig, R.S., 2006. Temporal regulation of shoot development in *Arabidopsis thaliana* by miR156 and its target SPL3. *Development* 133, 3539–3547. <https://doi.org/10.1242/dev.02521>.
- Wu, G., Park, M.Y., Conway, S.R., Wang, J.W., Weigel, D., Poethig, R.S., 2009. The sequential action of miR156 and miR172 regulates developmental timing in Arabidopsis. *Cell* 138, 750–759. <https://doi.org/10.1016/j.cell.2009.06.031>.
- Xin, M., Wang, Y., Yao, Y., Xie, C., Peng, H., Ni, Z., Sun, Q., 2010. Diverse set of microRNAs are responsive to powdery mildew infection and heat stress in wheat (*Triticum aestivum* L.). *BMC Plant Biol.* 10, 123. <https://doi.org/10.1186/1471-2229-10-123>.
- Yang, C., Li, D., Mao, D., Liu, X., Ji, C., Li, X., Zhao, X., Cheng, Z., Chen, C., Zhu, L., 2013a. Overexpression of microRNA319 impacts leaf morphogenesis and leads to enhanced cold tolerance in rice (*Oryza sativa* L.). *Plant Cell Environ.* 36, 2207–2218. <https://doi.org/10.1111/pce.12130>.
- Yang, L., Jue, D., Li, W., Zhang, R., Chen, M., Yang, Q., 2013b. Identification of miRNA from eggplant (*Solanum melongena* L.) by small RNA deep sequencing and their response to *Verticillium dahliae* infection. *PLoS One* 8. <https://doi.org/10.1371/journal.pone.0072840>.
- Ye, W., Shen, C.H., Lin, Y., Chen, P.J., Xu, X., Oelmüller, R., Yeh, K.W., Lai, Z., 2014. Growth promotion-related miRNAs in oncidium orchid roots colonized by the endophytic fungus *Piriformospora indica*. *PLoS One* 9, e84920. <https://doi.org/10.1371/journal.pone.0084920>.
- Yu, B., Yang, Z., Li, J., Minakhina, S., Yang, M., Padgett, R.W., Steward, R., Chen, X., 2005. Methylation as a crucial step in plant microRNA biogenesis. *Science* (80-) 307, 932–935. <https://doi.org/10.1126/science.1107130>.
- Zanini, S., Šečić, E., Busche, T., Galli, M., Zheng, Y., Kalinowski, J., Kogel, K.H., 2021. Comparative analysis of transcriptome and sRNAs expression patterns in the *Brachypodium distachyon* - *Magnaporthe oryzae* pathosystems. *Int. J. Mol. Sci.* 22, 1–33. <https://doi.org/10.3390/ijms22020650>.
- Zhai, J., Jeong, D.H., de Paoli, E., Park, S., Rosen, B.D., Li, Y., González, A.J., Yan, Z., Kitto, S.L., Grusak, M.A., Jackson, S.A., Stacey, G., Cook, D.R., Green, P.J., Sherrier, D.J., Meyers, B.C., 2011. MicroRNAs as master regulators of the plant NB-LRR defense gene family via the production of phased, trans-acting siRNAs. *Genes Dev.* 25, 2540–2553. <https://doi.org/10.1101/gad.177527.111>.
- Zhang, X., Zhao, H., Gao, S., Wang, W.C., Katiyar-Agarwal, S., Da Huang, H., Raikhel, N., Jin, H., 2011. Arabidopsis argonaute 2 regulates innate immunity via miRNA393\*-Mediated silencing of a Golgi-localized SNARE gene, MEMB12. *Mol. Cell* 42, 356–366. <https://doi.org/10.1016/j.molcel.2011.04.010>.
- Zhang, S., Liu, Y., Yu, B., 2015. New insights into pri-miRNA processing and accumulation in plants. *Wiley Interdiscip. Rev. RNA* 6 (5), 533–545. <https://doi.org/10.1002/wrna.1292>.
- Zhang, T., Zhao, Y.L., Zhao, J.H., Wang, S., Jin, Y., Chen, Z.Q., Fang, Y.Y., Hua, C.L., Ding, S.W., Guo, H.S., 2016. Cotton plants export microRNAs to inhibit virulence gene expression in a fungal pathogen. *Nat. Plants* 2. <https://doi.org/10.1038/nplants.2016.153>.
- Zhang, M., Hu, X., Zhu, M., Xu, M., Wang, L., 2017. Transcription factors NF-YA2 and NF-YA10 regulate leaf growth via auxin signaling in Arabidopsis. *Sci. Rep.* 7, 1–9. <https://doi.org/10.1038/s41598-017-01475-z>.
- Zhao, Y., Hull, A.K., Gupta, N.R., Goss, K.A., Alonso, J., Ecker, J.R., Normanly, J., Chory, J., Celenza, J.L., 2002. Trp-dependent auxin biosynthesis in Arabidopsis: involvement of cytochrome P450s CYP79B2 and CYP79B3. *Genes Dev.* 16, 3100–3112. <https://doi.org/10.1101/gad.1035402>.
- Zheng, L.L., Qu, L.H., 2015. Application of microRNA gene resources in the improvement of agronomic traits in rice. *Plant Biotechnol. J.* 13, 329–336. <https://doi.org/10.1111/pbi.12321>.
- Zhou, Man, Luo, Hong, 2013. MicroRNA-mediated gene regulation: potential applications for plant genetic engineering. *Plant Molecular Biology* 83, 59–75. <https://doi.org/10.1007/s11103-013-0089-1>.
- Zhou, X., Wang, G., Sutoh, K., Zhu, J.K., Zhang, W., 2008. Identification of cold-inducible microRNAs in plants by transcriptome analysis. *Biochim. Biophys. Acta - Gene Regul. Mech.* 1779, 780–788. <https://doi.org/10.1016/j.bbagrm.2008.04.005>.
- Zhu, Q.H., Fan, L., Liu, Y., Xu, H., Llewellyn, D., Wilson, I., 2013. miR482 regulation of NBS-LRR defense genes during fungal pathogen infection in cotton. *PLoS One* 8, e84390. <https://doi.org/10.1371/journal.pone.0084390>.

RESEARCH ARTICLE

Open Access



# A novel plant-fungal association reveals fundamental sRNA and gene expression reprogramming at the onset of symbiosis

Ena Šečić<sup>1</sup>, Silvia Zanini<sup>1</sup>, Daniel Wibberg<sup>2</sup>, Lukas Jelonek<sup>3</sup>, Tobias Busche<sup>2</sup>, Jörn Kalinowski<sup>2</sup>, Sabrine Nasfi<sup>1</sup>, Jennifer Thielmann<sup>1</sup>, Jafargholi Imani<sup>1</sup>, Jens Steinbrenner<sup>1</sup> and Karl-Heinz Kogel<sup>1\*</sup> 

## Abstract

**Background:** Beneficial associations between plants and microbes are widespread in nature and have been studied extensively in the microbial-dominant environment of the rhizosphere. Such associations are highly advantageous for the organisms involved, benefiting soil microbes by providing them access to plant metabolites, while plant growth and development are enhanced through the promotion of nutrient uptake and/or protection against (a)biotic stresses. While the establishment and maintenance of mutualistic associations have been shown to require genetic and epigenetic reprogramming, as well as an exchange of effector molecules between microbes and plants, whether short RNAs are able to effect such changes is currently unknown. Here, we established an interaction between the model grass species *Brachypodium distachyon* (*Bd*, Pooideae) and the beneficial fungal root endophyte *Serendipita indica* (*Si*, syn. *Piriformospora indica*, Sebaciniales) to elucidate RNA interference-based regulatory changes in gene expression and small (s)RNA profiles that occurred during establishment of a Sebacinalean symbiosis.

**Results:** Colonization of *Bd* roots with *Si* resulted in higher grain yield, confirming the mutualistic character of this interaction. Resequencing of the *Si* genome using the Oxford Nanopore technique, followed by de novo assembly yielded in 57 contigs and 9441 predicted genes, including putative members of several families involved in sRNA production. Transcriptome analysis at an early stage of the mutualistic interaction identified 2963 differentially expressed genes (DEG) in *Si* and 317 in *Bd* line 21-3. The fungal DEGs were largely associated with carbohydrate metabolism, cell wall degradation, and nutrient uptake, while plant DEGs indicated modulation of (a)biotic stress responses and defense pathways. Additionally, 10% of the upregulated fungal DEGs encode candidate protein effectors, including six DELD proteins typical for Sebaciniales. Analysis of the global changes in the sRNA profiles of both associated organisms revealed several putative endogenous plant sRNAs expressed during colonization belonging to known micro (mi)RNA families involved in growth and developmental regulation. Among *Bd*- and *Si*-generated sRNAs with putative functions in the interacting organism, we identified transcripts for proteins involved in circadian clock and flowering regulation as well as immunity as potential targets of fungal sRNAs, reflecting the beneficial activity of *Si*.

\* Correspondence: [Karl-Heinz.Kogel@agrar.uni-giessen.de](mailto:Karl-Heinz.Kogel@agrar.uni-giessen.de)

<sup>1</sup>Institute of Phytopathology, Centre for BioSystems, Land Use and Nutrition, Justus Liebig University, 35392 Giessen, Germany

Full list of author information is available at the end of the article



© The Author(s). 2021 **Open Access** This article is licensed under a Creative Commons Attribution 4.0 International License, which permits use, sharing, adaptation, distribution and reproduction in any medium or format, as long as you give appropriate credit to the original author(s) and the source, provide a link to the Creative Commons licence, and indicate if changes were made. The images or other third party material in this article are included in the article's Creative Commons licence, unless indicated otherwise in a credit line to the material. If material is not included in the article's Creative Commons licence and your intended use is not permitted by statutory regulation or exceeds the permitted use, you will need to obtain permission directly from the copyright holder. To view a copy of this licence, visit <http://creativecommons.org/licenses/by/4.0/>. The Creative Commons Public Domain Dedication waiver (<http://creativecommons.org/publicdomain/zero/1.0/>) applies to the data made available in this article, unless otherwise stated in a credit line to the data.

**Conclusions:** We detected beneficial effects of *Si* colonization on *Bd* growth and development, and established a novel plant-mutualist interaction model between these organisms. Together, the changes in gene expression and identification of interaction-induced sRNAs in both organisms support sRNA-based regulation of defense responses and plant development in *Bd*, as well as nutrient acquisition and cell growth in *Si*. Our data suggests that a Sebacinalean symbiosis involves reciprocal sRNA targeting of genes during the interaction.

**Keywords:** *Brachypodium distachyon*, Genome sequencing, Sebacinalean symbiosis, *Serendipita indica*, Small RNAs

## Background

Mutualistic associations between beneficial microbes and plants are widespread and highly advantageous, especially in the microbial-dominant environment of the rhizosphere. This relationship benefits soil microbes by providing them access to plant metabolites; in return, they enhance plant growth and development by promoting nutrient uptake and/or protection against (a)biotic stresses [1, 2]. The beneficial or parasitic outcome of a plant-microbe interaction is governed by the genotype and physiological status of the host, identity of the microbe, and environmental factors such as soil type and nutrient availability [3, 4]. The establishment and maintenance of mutualistic associations (here called symbiosis) require genetic and epigenetic reprogramming and metabolome modulation by the exchange of effector molecules between the beneficial microbe and the plant [5, 6]. Beneficial microbes have a significant impact on crop production, due to their effects on plant health and yield. However, considerable gaps in knowledge prior to their establishment in agricultural practice remain, including systemic identification of microbial abundance and diversity in various ecosystems, understanding the influence of climate, soil conditions, management practices, and, lastly, elucidating the intricacies of molecular mechanisms governing establishment of colonization and nutrient acquisition [7].

Crucial for regulation of gene expression, RNA interference (RNAi) is a well-known eukaryotic gene silencing mechanism [8], mediated by small RNAs (sRNAs) of 20–24 nucleotides (nt) in size and RNAi-associated proteins, primarily from the Argonaute (AGO), Dicer-like (DCL) and RNA-dependent RNA polymerase (RdRP) families [9]. DCLs generate sRNAs from longer RNA molecules, whereas AGOs bind sRNAs within an RNA-induced silencing complex (RISC). In the context of plant-microbe interactions, microbial protein effectors are known to promote pathogen colonization by suppressing host immune responses [10] and have been described in mutualistic associations as well [5], including the Sebacinalean symbiosis [11]. Recent findings suggest that sRNAs, through RNAi-based regulatory mechanisms, also can serve as effectors of pathogenic microbes [12], whereby the sRNA is secreted to suppress translation of a host mRNA via RNAi. Conversely, plants can

secrete sRNAs that target virulence-associated mRNAs in the microbe [13]. This transfer of sRNAs and subsequent gene silencing in the target organism is called cross-kingdom RNAi [12].

We studied the association of the beneficial fungus *Serendipita indica* (*Si*) with the model grass *Brachypodium distachyon* (*Bd*, purple false brome, Pooideae [14]). *Si* is an endophytic fungus belonging to the order Sebaciniales that colonizes the rhizodermis and cortex of a large spectrum of plants [15]. *Si* serves as an excellent model for beneficial microbes as it (i) primes plants for disease resistance against biotrophic [16] and necrotrophic [17] fungi, oomycetes [18], and viruses [19]; (ii) enhances the tolerance of plants against abiotic stress [20]; (iii) promotes growth and yield [21]; (iv) has a sequenced 25 Mb genome [22]; and (v) is genetically transformable and culturable in axenic conditions [23]. *Si* initially undergoes a biotrophic growth phase during *Arabidopsis* (*Arabidopsis thaliana*) and barley (*Hordeum vulgare*) colonization, with suppression of innate immune responses [24, 25] and activation of induced systemic resistance [16]. Subsequently, *Si* colonization of barley enters a cell-death associated phase and switches to a saprophytic lifestyle [26, 27].

*Bd* is a temperate grass species belonging to the Pooideae subfamily and a model for genetic studies of stress resistance and yield parameters of cereals [28]. *Bd* is self-pollinating, genetically transformable, easy to cultivate, and has a sequenced genome of 272 Mb [29–31]. It shares evolutionary proximity and broad synteny with complex crop genomes, such as wheat and rice [14], and is a host for major cereal pathogens [32]. Additionally, RNAi is operational in *Bd*, with proven alteration of micro RNA (miRNA) expression patterns in response to abiotic stresses [33, 34]. In silico analyses revealed that the *Bd* genome, similar to other cereals, contains an expansion of DCL and AGO families [35].

Currently, the significance of cross-kingdom RNAi in mutualistic interactions is largely unknown. A recent in silico study predicted that the arbuscular mycorrhizal fungus *Rhizophagus irregularis* generates sRNAs, which have predicted targets in the host plant *Medicago truncatula* [36]. Moreover, tRNA-derived sRNA fragments from rhizobial bacteria were shown to regulate host nodulation-associated genes by utilizing the host's RNAi machinery [37]. To investigate the role of sRNAs in

another agronomically relevant mutualistic interaction, we established a protocol for *Si* colonization of the model Pooideae *Bd*. Additionally, integrative high-throughput sequencing and transcriptome analysis assessed symbiosis-associated changes in the mRNA and sRNA expression patterns of both organisms. We discuss here possible sRNA-based regulation that might be critical for the establishment of the Sebacinalean symbiosis.

## Results

### *Brachypodium distachyon* Bd21-3 forms a mutualistic interaction with *Serendipita indica*

To investigate whether *Bd* can develop a beneficial interaction with *Si*, we established an inoculation protocol using one-week-old seedlings of *Bd* line Bd21-3, with dip-inoculation in  $5 \times 10^5$  chlamydospores ml<sup>-1</sup> for 3 h. Comparison of grain production in fully mature, colonized vs. non-colonized plants grown in soil showed that *Si* increased the number of filled grains/plant by 49.9% (Fig. 1a, Additional file 1), and total grain weight/plant increased by 38.1% (Fig. 1b, Additional file 1). Consistent with the observation that *Si*-colonized Bd21-3 plants flower several days earlier than control plants, they exhibited a 32.2% increase in the number of spikelets at 2 months after inoculation (Fig. 1c, Additional file 1). Concordantly, growth and biomass analyses of Bd21-3 seedlings revealed a significant 8.6% increase in shoot length (Fig. 1d) upon *Si* colonization.

Further analysis of Bd21-3 seedlings indicated that *Si* colonization increased lateral root growth, as early as 4 days post inoculation (4 DPI, Additional file 2: Figure S1a). By 25 DPI, roots showed a more extensively branched structure (Additional file 2: Figure S1b). Microscopy of *Si*-inoculated Bd21-3 roots confirmed root surface colonization and proliferation of fungal spores after staining with chitin-specific WGA-AF 488 at 4 DPI (Fig. 2a–d) and further on at 7 DPI and 14 DPI (Additional file 2: Figure S2). Inter- and intracellular colonization of Bd21-3 cells in the root differentiation zone also was visible after WGA-AF 488 and propidium iodide staining (Fig. 2e–h). These results suggest that establishment of a mutualistic symbiosis correlates with observable phenotypic changes by 4 DPI; thus, this time point was used to further investigate the Bd21-3-*Si* system.

### Resequencing of the *Si* genome

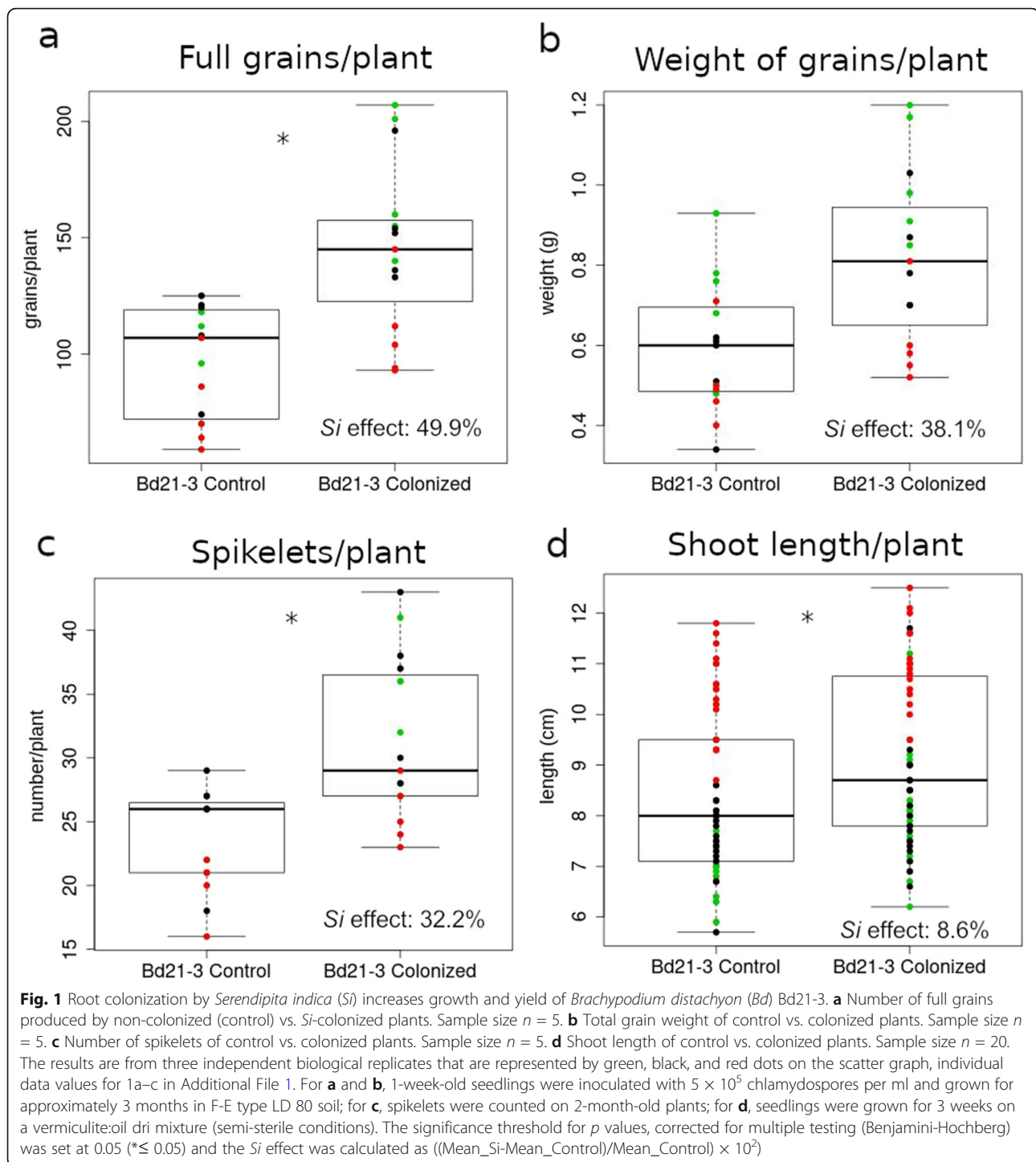
To improve *Si* assembly, the genome was resequenced using MinION (25,167 reads, 324 Mb) and MiSeq (18,225,814 reads, 5.46 Gb); together they yielded approx. 6.0 Gb of sequence information. *De novo* assembly of the Nanopore sequence reads generated 57 contigs, accounting for a total length of 24.7 Mb and a N50

of 1.3 Mb. The draft genome sequence features GC content of 50.8%, similar to the first genome version with 2,359 contigs and GC content of 50.7% [22]. Analyses using the eukaryotic gene prediction tool Genemark-ES 4.33 [38] revealed 9441 predicted genes (75% of the genome; 59,045 exons), 9498 intergenic regions (25% of the genome), and a gene density of 380.68 genes/Mbp (Additional file 2: Table S1). Annotation of the *Si* genes using a GenDB version designed to process eukaryotic genomes possessing multi-exon genes [39, 40] revealed that 4756 have a predicted function. Comparison of predicted genes from the resequenced *Si* genome (Si-2020) vs. the 2011 assembly [22] indicated that the vast majority are shared (90.3%), with 915 genes unique to the Si-2020 genome (Additional file 2: Figure S3). There is a reduction in gene model numbers relative to the 2011 assembly, which can be attributed to improved gene prediction tools for eukaryotic organisms and a considerably reduced number of contigs. Additionally, *Si* shares 2585 genes with another member of the Sebaciniales, *Serendipita vermifera*, while 156 genes are shared only with the ectomycorrhizal fungus *Laccaria bicolor* and 2729 genes are common in all three species (Additional file 2: Figure S4).

### Establishment of the *Si*-*Bd* symbiosis is associated with extensive transcriptional reprogramming

To assess how the symbiotic interaction affects gene expression in both organisms, mRNA was sequenced and analyzed (Additional file 2: Table S2) from the roots of *Si*-colonized Bd21-3 seedlings (sample Bd-Si) and mock-treated plants (Bd-C) at 4 DPI, and from 4-week-old axenic *Si* cultures (Si-ax). Comparison of reads between Bd-Si and Si-ax identified 2963 differentially expressed fungal genes (DEGs, DESeq2: Wald test, Benjamini-Hochberg (BH) adjustment, padj < 0.05), which accounts for 31.4% of the 9441 predicted *Si* genes. Comparison of reads from Bd-Si and Bd-C revealed 317 plant DEGs (0.66% out of approximately 47,917 protein-coding transcripts disclosed in the JGI v1.1 annotation, padj < 0.05). The interaction-responsive DEGs in *Si* and Bd21-3, split into up- and downregulated groups are shown in Fig. 3.

All significant DEGs were submitted to gene ontology term analysis against the reference background for *Bd* and a customized *Si*-specific background. The resulting enriched terms relate to metabolic, mainly redox processes and catalytic activity functions (Additional file 2: Table S3). Of the 25 highly downregulated *Si* DEGs, many encode proteins associated with metabolic reprogramming networks involved in nutrient exchange and adaptation to nutrient availability (Table 1). By contrast, highly upregulated *Si* DEGs encode for proteins involved in fungal catalytic and hydrolytic processes. This suggests that by 4 DPI, *Si* has entered a saprophytic-like



growth phase similar to that detected in barley roots [22]. To investigate whether any *Si* DEG encodes effector proteins, a computational pipeline [41] was used to mine 982 genes identified in the *Si*-2020 genome that encode signal peptide-containing proteins, resulting in 480 putative protein effector genes. In total, 174 (36%) of these were significantly upregulated during

colonization of Bd21-3 (Additional file 2: Table S4), including six DELD family proteins [22]. In Bd21-3, many of the highly downregulated interaction-responsive DEGs encode transcription factors or proteins associated with stress responses or circadian clock regulation. Those showing high levels of upregulation include genes linked to immune responses and hormone

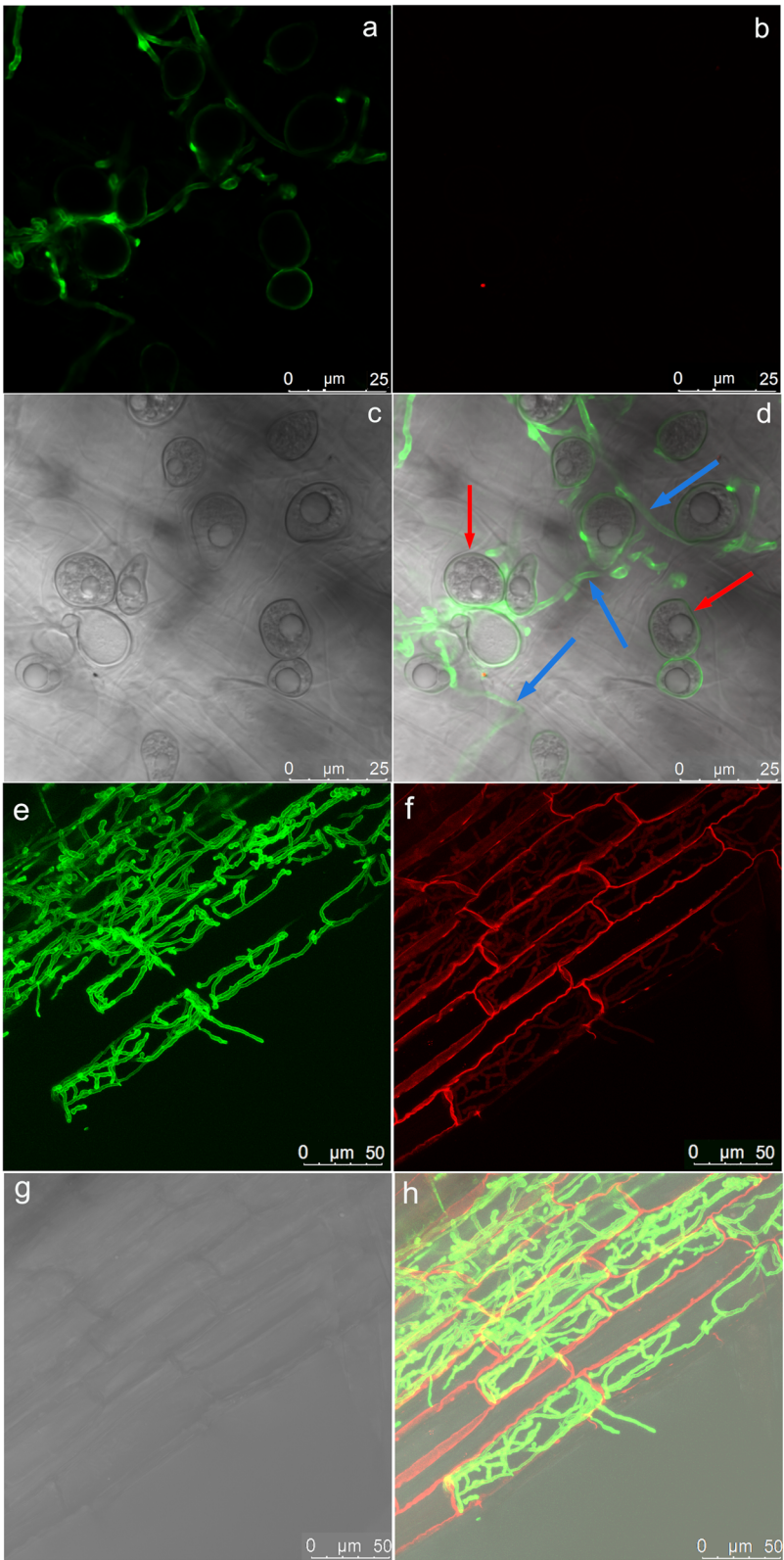


**Fig. 2** (See legend on next page.)

(See figure on previous page.)

**Fig. 2** Colonization pattern of *Serendipita indica* (Si) on *Brachypodium distachyon* Bd21-3 roots. **a–d** Colonization at 4 DPI. **a** Fluorescence microscopy showing WGA-AF488 staining of Si cell walls ( $\lambda_{exc}494$  nm,  $\lambda_{em}515$ ). **b** Fluorescence control ( $\lambda_{exc}631$  nm,  $\lambda_{em}642$ ). **c** Bright-field microscopy to visualize Si chlamydospores. **d** Overlay showing Si chlamydospores (red arrows), which have germinated and formed a hyphal network on the root surface (blue arrows). **e–h** Rhizodermal root colonization by Si at 4 DPI. **e** Fluorescence microscopy showing WGA-AF488 staining of Si cell walls ( $\lambda_{exc}494$  nm,  $\lambda_{em}515$ ). **f** Fluorescence microscopy to visualize propidium iodide staining of root cell walls ( $\lambda_{exc}535$  nm,  $\lambda_{em}617$ ). **g** Bright-field microscopy to visualize root cells. **h** Overlay showing extensive inter- and intracellular fungal growth on Bd21-3 roots. Imaging was done with a LEICA S8 confocal microscope (e–h: maximum projection; z-stack). For **a–d**, 1-week-old seedlings were inoculated with  $5 \times 10^5$  chlamydospores per ml and subsequently grown on a plastic mesh over 0.5X MS; for **e–h**, Si-inoculated seedlings were grown on vermiculite:oil dri mix before harvesting at 4 DPI

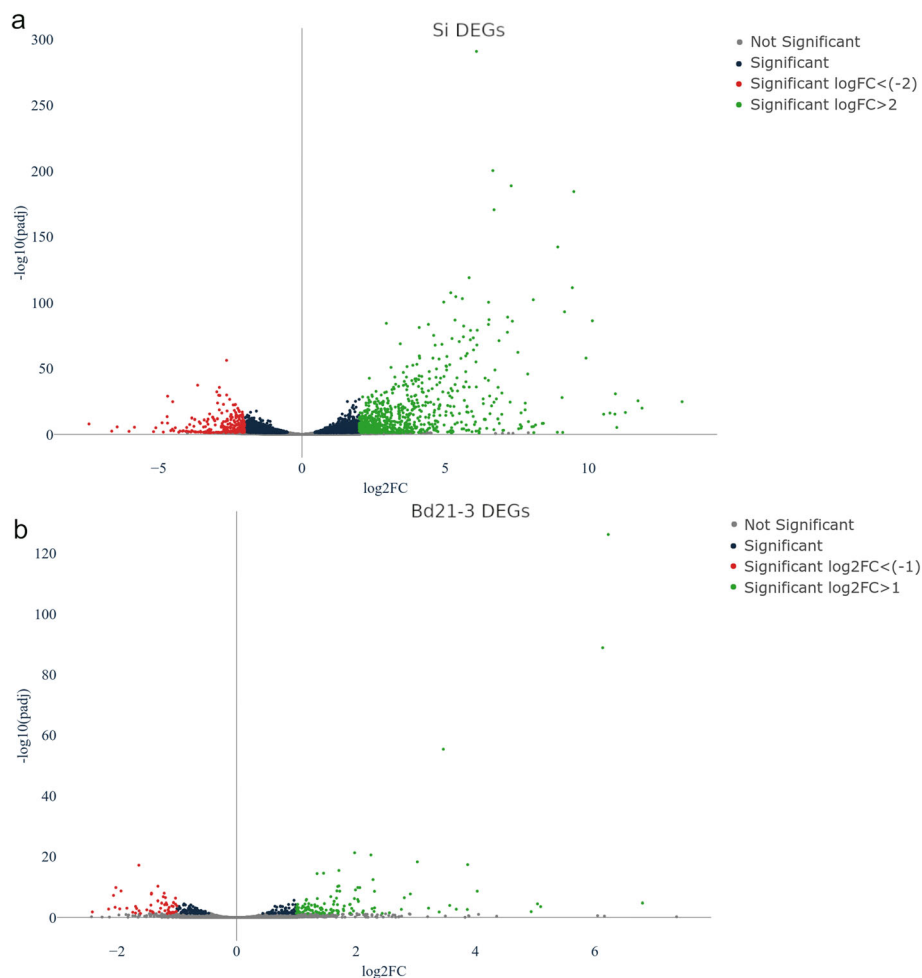


**Fig. 3** Volcano plots of colonization-associated, differentially expressed genes (DEGs). **a** *Serendipita indica* (Si) DEGs identified by comparing reads from colonized roots (Bd-Si) vs. axenic mycelium (Si-ax). **b** *Brachypodium distachyon* Bd21-3 DEGs identified by comparing colonized (Bd-Si) vs. mock-treated (Bd-C) roots. X-axis displays the  $\log_2$  FoldChange and Y-axis displays the negative  $\log_{10}$  of adjusted  $p$  values from DE analysis. The magnitude of up- or downregulation for the DEGs (represented by individual dots) is indicated by different colors, as designated in the legend for each plot

**Table 1** Top 25 *Serendipita indica* (Si) differentially expressed genes (DEGs) during colonization (4 DPI)

Gene	Description	log2FC
1937_g (PIIN_04746)	Related to mismatch base pair and cruciform DNA recognition protein HMP1	– 5.84
465_g (PIIN_02587)	Related to phenylalanine ammonia-lyase	– 5.1
281_g (PIIN_04449)	Probable succinate-fumarate transporter	– 4.7
1121_g (PIIN_02682)	Related to ADY2-protein essential for the acetate permease activity	– 4.68
7809_g (PIIN_07312)	Related to RTM1 protein	– 4.52
2544_g (PIIN_02778)	Probable ADH1-alcohol dehydrogenase I	– 4.42
4482_g (PIIN_08427)	Related to mixed-linked glucanase precursor MLG1	– 4.23
4969_g (PIIN_02119)	Related to meiotic nuclear division protein 1 homolog	– 3.54
1859_g (PIIN_00204)	Probable thioredoxin	– 3.45
5786_g (PIIN_00305)	Probable DHA14-like major facilitator; ABC transporter	– 3.41
4465_g (PIIN_06089)	Putative mitochondrial carnitine O-acetyltransferase	– 3.36
1392_g (PIIN_11719)	Putative alkaline ceramidase 3	– 3.22
8569_g (PIIN_01532)	Related to Ca <sup>2+</sup> -transport (H <sup>+</sup> /Ca <sup>2+</sup> exchange) protein	– 3.21
2933_g (PIIN_07440)	Related to monocarboxylate transporter 2	– 3.21
758_g (PIIN_02772)	Probable TOM40-mitochondrial import receptor MOM38	– 3.19
2855_g (PIIN_07067)	Related to L-asparaginase	– 3.18
5713_g (PIIN_07616)	Related to MFS transporter	– 3.17
3225_g (PIIN_08230)	Related to RSB1-integral membrane transporter	– 3.11
8602_g (PIIN_08742)	Putative maintenance of mitochondrial morphology protein 1	– 3.09
917_g (PIIN_03155)	Related to YTP1	– 3.05
6928_g (PIIN_00312)	Related to nitrogen metabolic regulation protein	– 2.96
6930_g (PIIN_00314)	Probable malate synthase	– 2.94
4348_g (PIIN_03103)	Putative ubiquitin-conjugating enzyme D4	– 2.9
6400_g (PIIN_07801)	Probable acyl-CoA dehydrogenase short-branched chain precursor	– 2.9
5097_g (PIIN_04235)	Related to acyl-CoA dehydrogenase	– 2.88
5186_g (PIIN_09750)	Probable pectate lyase	11.93
8239_g (PIIN_02110)	Related to family 61 glucanase	11.29
3289_g (PIIN_05863)	Endo-1,4-beta-xylanase	10.75
7464_g (PIIN_04708)	Alpha-L-arabinofuranosidase	10.14
5322_g (PIIN_05889)	Endo-1,4-beta-xylanase	10.14
1898_g (PIIN_08141)	Glutathione S-transferase	9.1
5131_g (PIIN_02752)	Cellulose 1,4-beta-cellobiosidase	8.93
3537_g (PIIN_10118)	Carboxylic ester hydrolase	8.83
6726_g (PIIN_08399)	Probable alpha-galactosidase B	8.29
4844_g (PIIN_06890)	Endo-1,4-beta-xylanase A	7.9
8585_g (PIIN_01553)	Probable beta-glucosidase	7.88
3597_g (PIIN_06117)	Related to endoglucanase B	7.78
5420_g (PIIN_07414)	Related to NACHT/WD40 domain-containing protein	7.64
1875_g (PIIN_06862)	Rhamnogalacturonan acetyltransferase	7.62
6520_g (PIIN_06360)	Endo-1,4-beta-xylanase C	7.53
3290_g (PIIN_05862)	Probable endo-1,4-beta-xylanase A	7.42
3615_g (PIIN_11270)	Probable feruloyl esterase C	7.37
5971_g (PIIN_04536)	Probable gEgh 16 protein	7.3
8031_g (PIIN_01484)	Related to CEL1 protein precursor	7.2

**Table 1** Top 25 *Serendipita indica* (Si) differentially expressed genes (DEGs) during colonization (4 DPI) (Continued)

Gene	Description	log2FC
6665_g (PIIN_03039)	Probable beta-glucoside glucohydrolase	7.15
720_g (PIIN_06594)	Cellulose 1,4-beta-cellobiosidase	7.08
3514_g (PIIN_09664)	Glucose oxidase	7.01
290_g (PIIN_04439)	Related to peroxisomal short-chain alcohol dehydrogenase	6.97
6967_g (PIIN_00353)	Exocellobiohydrolase 3	6.7
1893_g (PIIN_08147)	Probable glutathione S-transferase	6.57

DEGs are calculated as: colonized root vs. Si axenic culture exhibiting significant (padj. < 0.05) down- or up-regulation, log<sub>2</sub> FC (fold change) during colonization

signaling networks (Table 2 and Additional file 2: Table S3). In order to further validate our sequencing data, we confirmed the expression of five Si and five Bd21-3 DEGs from Tables 1 and 2 by RT-qPCR. Generally, the qPCR results show a similar fold change for the selected genes between the colonized root and the respective controls, compared to the mRNA-seq results (Additional file 2: Figure S5). Together, these results show that both organisms utilize a complex enzymatic arsenal to establish and control the symbiosis.

### Prediction of Si RNAi genes

Since RNAi-mediated gene silencing has been documented in most but not all fungi [42], we assessed whether the Si-2020 genome encodes RNAi-related proteins with conserved domain architecture and homology to RNAi components in the model filamentous fungus *Neurospora crassa* [43]. Genes encoding predicted DCLs (G4U2H0, G4TBW9) with typical domains (dsRNA-binding, RNase III and helicase, [44]), QDE2-like proteins with PIWI domains typical of AGOs (G4TEK0, G4TLO4, [45]), an AGO-like protein (G4T5G9), and RdRPs (G4TNU7, G4TQP0) were identified and were expressed in axenic culture and Bd21-3-associated Si samples (Additional file 2: Table S5). Thus, the Si genome is predicted to contain genes encoding critical components of the RNAi machinery. Based on these new data, and the earlier discovery that AGO and DCL families are expanded in the Bd genome [35], we decided to sequence the sRNAs of both organisms, in order to assess the role of RNAi-based regulation and communication in symbiosis.

### sRNA profiles undergo a substantial change at the onset of the Si-Bd symbiosis

To evaluate how the mutualistic interaction affects the sRNA profiles in the colonized root and respective Si and Bd controls, reads from Bd-C, Bd-Si, and Si-ax sRNA data sets were subjected to consecutive filtering steps (Additional file 2: Figure S6). This greatly reduced the number of raw reads to be analyzed and allowed us to distinguish between sRNAs

with potential targets in the interacting organism (putative ck-sRNAs) and sRNAs with potential functions in the same organism (putative endogenous sRNAs) (Additional file 2: Table S6).

Analysis of sRNAs from the Bd-Si dataset revealed that the total number of putative ck-sRNAs exceeds that of endogenous sRNAs in both Si (786,732 vs. 261,478) and Bd21-3 (17 million vs. 1.6 million), but the converse is true for unique sRNAs (36,163 endogenous vs. 35,895 putative ck-sRNAs in Si and 483,352 endogenous vs. 286,198 putative ck-sRNAs in Bd21-3).

### Size distribution profiles of Si and Bd21-3 sRNAs

Size distribution of sRNA reads from Bd21-3 and Si during colonization, and the respective controls was then assessed. For putative endogenous Bd21-3 sRNAs, peaks at 21 and 24 nt were identified, with the 24 nt sRNAs exhibiting greater diversity than those of 21 nt (Fig. 4a, b). These sizes are consistent with the expected peaks of RNAi-associated sRNAs in plants [46]. For putative endogenous Si sRNAs, a bimodal size distribution pattern was observed in the total fractions, with the first peak at 26 nt and second at 29–30 nt (Fig. 4c, d). A smaller peak of 21 nt long molecules was observed in the Bd-Si but not Si-ax samples, indicating that colonization affects the relative size distribution of Si sRNAs. Since previously identified ck-sRNAs range from 20 to 24 nt [12, 13], the size distribution of putative ck-sRNAs and corresponding reads in the control samples was assessed over a narrower window. Contrary to endogenous sRNAs, ck-sRNAs displayed no prominent peaks in the 20–24 nt window (Additional file 2: Figure S7).

Before sRNAs can guide RNAi-mediated gene silencing, they must be loaded onto AGO proteins and assembled into a RISC. Previously, Arabidopsis AGO proteins were shown to preferentially recruit sRNAs with specific 5' termini [47]. Hence, we analyzed the 5' terminal nt composition of Bd-C, Si-ax, and Bd-Si sRNAs. For unique putative endogenous and ck-sRNAs, the 5' nt composition was relatively consistent except for the 24 nt Bd21-3 sRNAs, which exhibited a strong bias towards 5' A (Additional file 2: Figure S8, Figure S9). The total sRNA

**Table 2** Top 25 *Brachypodium distachyon* (Bd) differentially expressed genes (DEGs) during root colonization (4 DPI)

Gene	Description	log2FC
BdiBd21-3.2G0197800	MYB-related transcription factor	– 2.41
BdiBd21-3.5G0123400	ABA/WDS induced protein	– 2.14
BdiBd21-3.3G0280400	Putative glycosyltransferase family 28	– 2.06
BdiBd21-3.3G0558500	Putative steroid 17-alpha-monooxygenase	– 2.03
BdiBd21-3.3G0660200	AP2 domain-containing protein	– 2.02
BdiBd21-3.1G0813200	GRAS transcription factor	– 1.96
BdiBd21-3.3G0264400	Homologous to barley constans-like protein CO8	– 1.94
BdiBd21-3.4G0000100	Fantastic four meristem regulator FAF	– 1.84
BdiBd21-3.1G0416000	Hydrophobic Protein RC12	– 1.69
BdiBd21-3.1G0002200	Ca <sup>2+</sup> -independent phospholipase A2	– 1.67
BdiBd21-3.1G0887100	Putative pseudo-response regulator 7	– 1.64
BdiBd21-3.4G0311800	Dirigent-like protein	– 1.6
BdiBd21-3.1G0815300	SPX domain-containing protein 3	– 1.43
BdiBd21-3.1G0972800	Cold regulated protein 27	– 1.42
BdiBd21-3.4G0303000	Putative protein kinase	– 1.32
BdiBd21-3.2G0034900	Putative sulfoquinovosyltransferase SQD2	– 1.21
BdiBd21-3.1G0281100	SPX – domain containing protein 3	– 1.23
BdiBd21-3.1G0554700	Anthranilate O-methyltransferase	– 1.18
BdiBd21-3.1G0584400	Peroxidase	– 1.17
BdiBd21-3.5G0205300	Putative calmodulin-dependent protein kinase	– 1.15
BdiBd21-3.2G0749200	Probable lipid transfer LTP2	– 1.13
BdiBd21-3.5G0303700	Wound-induced protein	– 1.1
BdiBd21-3.5G0024800	Heat shock protein 90-1	– 1.07
BdiBd21-3.1G0399200	bZIP transcription factor	– 1
BdiBd21-3.1G0557300	BURP domain protein	– 0.93
BdiBd21-3.3G0203000	Cupin-domain protein	6.13
BdiBd21-3.1G0469800	Glutathione S-Transferase	5.09
BdiBd21-3.4G0405200	Protein Hothead/ FAD binding	4.93
BdiBd21-3.3G0354800	Cytochrome P450 76C1	4.03
BdiBd21-3.3G0136300	Proprotein convertase subtilisin/kexin	3.87
BdiBd21-3.4G0068000	Pathogenesis-related protein Bet v I family	3.86
BdiBd21-3.1G0662500	LRR receptor-like serine/threonine protein kinase	3.57
BdiBd21-3.4G0556000	Alcohol dehydrogenase	3.39
BdiBd21-3.1G0772700	Pathogenesis-related protein 1 (PR1)	3.21
BdiBd21-3.4G0393500	Putative chalcone synthase	2.44
BdiBd21-3.3G0195800	Tryptophan decarboxylase	2.3
BdiBd21-3.4G0171000	Multicopper oxidase	2.28
BdiBd21-3.3G0639500	Glycosyl hydrolase protein/Chitinase-related	2.12
BdiBd21-3.1G0129100	Potato inhibitor I family	2.06
BdiBd21-3.2G0160100	Pipecolate/sarcosine oxidase	2.04
BdiBd21-3.4G0189100	Putative LRR protein kinase	1.99
BdiBd21-3.2G0418600	WRKY transcription factor	1.9
BdiBd21-3.4G0073800	Thaumatococcus family protein	1.8
BdiBd21-3.2G0545400	LRR protein	1.79

**Table 2** Top 25 *Brachypodium distachyon* (Bd) differentially expressed genes (DEGs) during root colonization (4 DPI) (Continued)

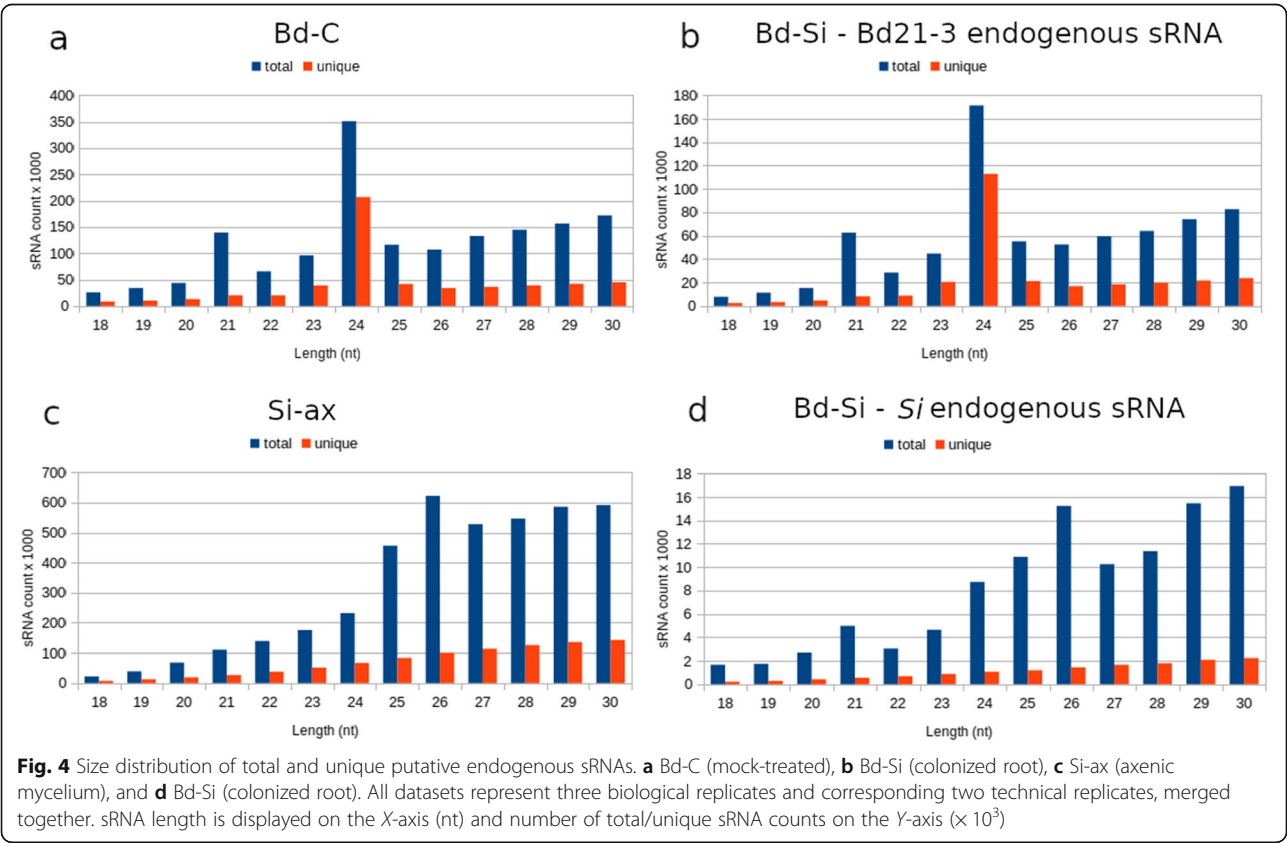
Gene	Description	log2FC
BdIBd21-3.4G0121800	Tryptophan biosynthesis protein	1.71
BdIBd21-3.4G0397700	Serine/threonine protein kinase	1.7
BdIBd21-3.4G0026800	Putative protein kinase	1.69
BdIBd21-3.2G0468100	Peroxidase	1.68
BdIBd21-3.2G0600500	Wall-associated receptor kinase	1.6
BdIBd21-3.2G0233800	PGP-like phosphoglycoprotein auxin transporter	1.58

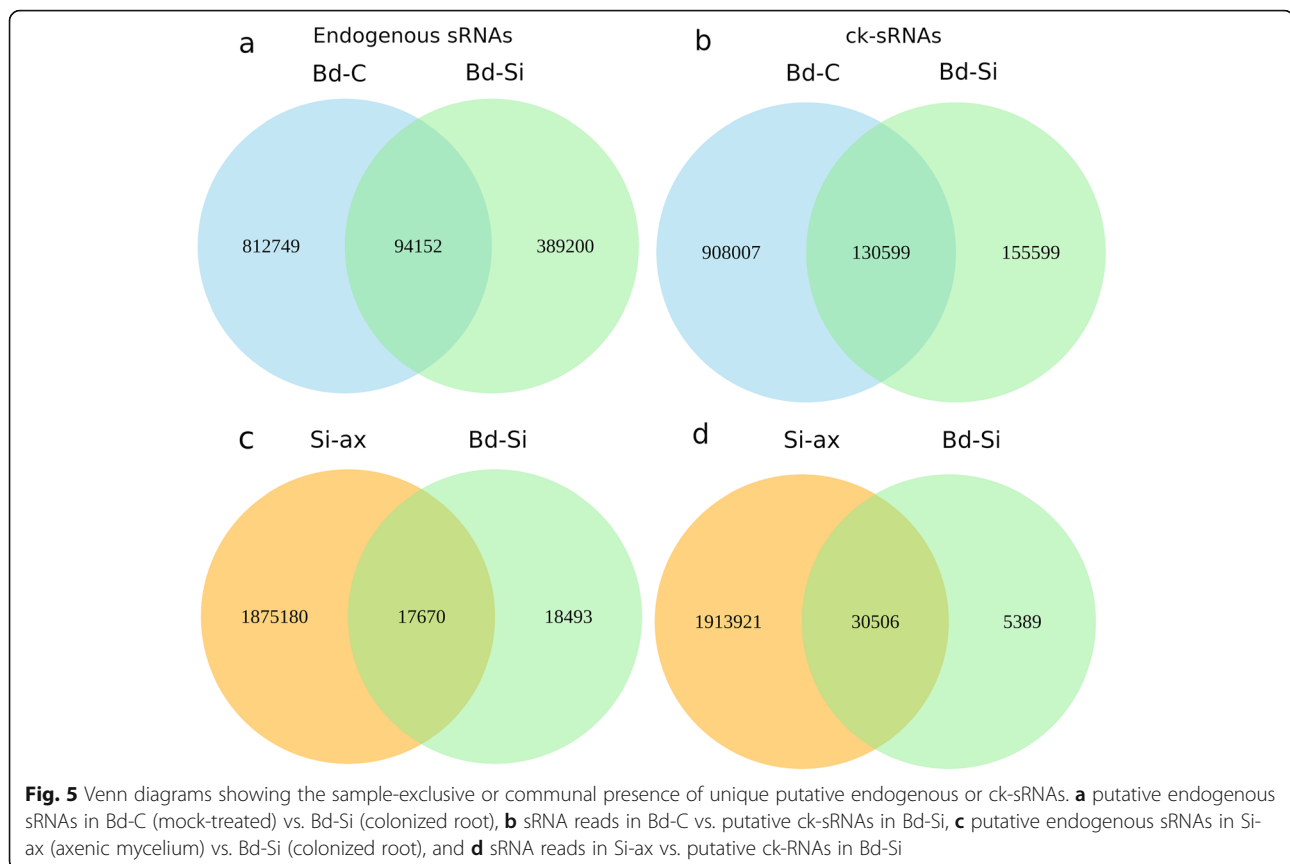
DEGs are calculated as: colonized root vs. mock-inoculated root exhibiting significant (padj. < 0.05) down- or upregulation, log<sub>2</sub> FC (fold change) during colonization

fractions exhibited somewhat greater variability in 5' nt composition. Of the total Bd21-3 endogenous sRNAs, 24 nt molecules from colonized and non-colonized tissue showed a strong bias towards 5' A, while 21 nt molecules were biased towards a terminal U (Additional file 2: Figure S10), and 20 nt ck-sRNAs had a higher percentage of 5' Cs (Additional file 2: Figure S11). Of the total endogenous *Si* sRNAs, those from colonized samples generally had a stronger bias towards 5' A than sRNA reads from *Si*-ax, especially at 26 nt and 21 nt (Additional file 2: Figure S10). A slightly higher percentage of 5' As also was detected in total putative ck-sRNAs of 21 nt (Additional file 2: Figure S11).

**Differentially expressed *Si* and Bd21-3 sRNAs**

Analysis of unique plant sRNAs in Bd-C vs. Bd-Si revealed that 63% of the putative endogenous sRNAs were exclusively present in Bd-C, 30% were exclusively in Bd-Si and 7% were present in both (Fig. 5). For the reads from the putative ck-sRNA pipeline, 76% of the reads were exclusively present in Bd-C, 13% were exclusive to Bd-Si, and 11% were found in both. Comparison between the unique fungal sRNAs in *Si*-ax and Bd-Si indicated that 98.1% of the putative endogenous sRNAs were exclusively present in axenic culture, 0.98% were exclusively found in Bd-Si, and 0.92% were in both. Similarly, from the putative ck-sRNA pipeline, 98.2% of





the sRNA reads were exclusive to the Si-ax sample, 0.3 % were exclusive to Bd-Si, and 1.5% were present in both. Considering only the *Si* sRNAs in the Bd-Si sample, 51.1% of the putative endogenous ones and 15% of the putative ck-sRNAs are exclusively present in the colonized sample. Among Bd21-3 sRNAs in the Bd-Si sample, there are 80.5% putative endogenous sRNAs and 54.3% ck-sRNAs exclusive for the colonized root. These data show that colonization induces many novel putative endogenous and ck-sRNAs in Bd21-3, and a smaller amount in *Si*, due to fungal quantity in the colonized roots.

#### Identification of Bd21-3 miRNAs during the *Bd-Si* interaction

Using the ShortStack analysis tool, we identified Bd21-3 loci that correspond to putative endogenous sRNAs expressed during *Si* colonization. The DicerCall function indicated loci whose predominant sRNAs are 20–24 nt. Comparison of these sRNAs with miRBase identified 16 sRNA-generating loci that correlate to known miRNAs (Table 3). These miRNAs belong to highly conserved plant miRNA families that regulate growth and development [33, 34]. We conducted the same analysis with *Si* sRNAs, but no predicted miRNA-like RNAs were

identified in the colonized sample, possibly due to a lack of data about the fungal sRNA-generating loci.

#### In silico target prediction of putative *Si* and Bd21-3 ck-sRNAs

Since most examples of sRNA-based communication in plant-microbe interactions have the commonality of 21 nt long sRNAs that silence transcripts in the target organism [12, 13, 48], we predicted the targets of 21 nt colonization-induced *Si* and *Bd* putative ck-sRNAs and assessed their expression after colonization. Of 16,003 unique Bd21-3 targets predicted for 412 induced 21 nt *Si* sRNAs, 49 were confirmed as downregulated at 4DPI. This represents 15.4% of all significantly changed genes in Bd21-3 during *Si* colonization. Some 89% of these transcripts are predicted as targets of *Si* sRNAs that are expressed exclusively in colonized tissue or with  $\log_2FC > 1$ . A representative set of sRNA-mRNA duplexes, chosen based on target identity and expression of target and sRNA, indicates that putative ck-sRNA targets in Bd21-3 are associated with transcription factor families, signaling pathways, and basal plant defense (Table 4, Additional file 2: Table S7).

To assess whether Bd21-3 generates ck-sRNAs that potentially target *Si* genes, we searched for predicted targets of 329 Bd21-3 sRNAs (21 nt long) induced in *Si*-

**Table 3** Predicted miRNA-generating loci identified in Bd21-3 roots colonized by *Serendipita indica*

Locus	Predominant sRNA	Known miRNA
Bd1:31073434-31073613	UCGGACCAGGCUUCAUCCCC	bdi-MIR166b
Bd2:10327043-10327213	CUGCACUGCCUCUCCCCUGGC	bdi-MIR408
Bd2:3991996-3992115	UGACAGAAGAGAGUGAGCAC	bdi-MIR156e
Bd2:3992232-3992320	UGACAGAAGAGAGUGAGCAC	bdi-MIR156f
Bd2:3992444-3992557	UUGACAGAAGAGAGUGAGCAC	bdi-MIR156g
Bd2:5570263-5570488	CUUGGAUUGAAGGGAGCUCU	bdi-MIR159a
Bd3:1968409-1968509	UCGCUUGGUGCAGAUCCGGAC	bdi-MIR168
Bd3:33173606-33173746	UCGGACCAGGCUUCAUCCCC	bdi-MIR166c
Bd3:39150748-39150893	GCUCACUUCUCUCUCUGUACC	bdi-MIR156b
Bd3:4482899-4483000	UUGACAGAAGAGAGUGAGCAC	bdi-MIR156c
Bd3:44836298-44836372	AGAAGAGAGAGAGUACAGCCU	bdi-MIR529
Bd3:7316295-7316393	GGGCAACUCCUCCGUUGGCAGA	bdi-MIR399d
Bd4:1654850-1654943	UGAAGCUGCCAGCAUGAUCUGA	bdi-MIR167e
Bd4:4893304-4893422	CGGAGGUCAGGAAUUCUACUGAUU	bdi-MIR9481b
Bd4:6029321-6029440	UCUCGGACCAGGCUUCAUCC	bdi-MIR166f
Bd5:18466111-18466202	UGACAGAAGAGAGUGAGCAC	bdi-MIR156d

**Table 4** Examples of deduced duplexes of *Serendipita indica* sRNAs and their downregulated targets in *Brachypodium distachyon*

sRNA name	sRNA Expression	Target transcript	Description	Transcript expression
SisRNA 1	NA	BdiBd21-3.1G0887100.1	Homologous to Arabidopsis pseudo-response regulator 3 and 7	– 1.63
		BdiBd21-3.2G0440200.1	Serine-carboxypeptidase-like 26-related	– 0.81
SisRNA 2	NA	BdiBd21-3.1G0399200.1	bZIP transcription factor	– 1.00
SisRNA 3	NA	BdiBd21-3.2G0288400.1	LURP1-related	– 1.20
SisRNA 4	NA	BdiBd21-3.1G0475100.1	Zinc-finger of the FCS-type	– 1.00
SisRNA 5	0.13	BdiBd21-3.1G0047100.1	Nitrogen metabolic regulation protein NMR-related	– 0.78
SisRNA 6	1.35	BdiBd21-3.3G0750900.1	Peroxygenase	– 0.77
SisRNA 7	NA	BdiBd21-3.1G0917100.1	Enolase	– 0.52
SisRNA 8	NA	BdiBd21-3.4G0303000.1	Protein kinase domain protein	– 1.31
SisRNA 9	NA	BdiBd21-3.1G0759800.1	Carboxyl-esterase 15 related	– 0.86
SisRNA 10	NA	BdiBd21-3.1G0813200.1	GRAS transcription factor	– 1.95
SisRNA 11	NA	BdiBd21-3.1G1017200.1	Expansin-like related	– 0.84
SisRNA 12	NA	BdiBd21-3.3G0134800.1	Copper transport protein ATOX1-related	– 1.11
SisRNA 13	1.95	BdiBd21-3.2G0288400.1	LURP1-related	– 1.20
SisRNA 14	NA	BdiBd21-3.1G0917100.1	Enolase	– 0.52
SisRNA 15	NA	BdiBd21-3.4G0303000.1	Protein kinase domain protein	– 1.31
	NA	BdiBd21-3.1G0411900.1	Serine-type carboxypeptidase activity (Blast2GO)	– 0.82
SisRNA 16	NA	BdiBd21-3.4G0507800.1	MYB transcription factor	– 0.70
SisRNA 17	NA	BdiBd21-3.1G0411900.1	Serine-type carboxypeptidase activity (Blast2GO)	– 0.82
SisRNA 18	NA	BdiBd21-3.2G0269000.1	Mannose-binding lectin family	– 0.85
SisRNA 19	NA	BdiBd21-3.3G0264400.1	Homologous to barley CONSTANS-like protein CO8	– 1.93
SisRNA 20	NA	BdiBd21-3.5G0237900.1	Aquaporin transporter	– 1.02

sRNA expression was calculated as  $\log_2(\text{colonized/control})$  from normalized reads, NA (not available) stands for sRNAs expressed exclusively in the colonized sample; transcript expression is indicated as the  $\log_2(\text{colonized/control})$  FC

colonized roots. Of 3,019 predicted unique *Si* targets, 358 were confirmed as downregulated after colonization. This represents 12% of all significantly changed *Si* genes. 35% of the 358 *Si* transcripts are predicted to be targeted by Bd21-3 sRNAs exclusive to colonized tissue and an additional 27.6 % are targeted by sRNAs that are highly upregulated in colonized tissue ( $\log_2FC > 1$ ). A set of sRNA-mRNA duplexes, selected with the same criteria as for the *Si* sRNA – Bd21-3 targets (Table 4), shows that predicted Bd21-3 ck-sRNAs have putative targets in *Si* which include proteins associated with nutrient acquisition, development of cell walls, hyphal networks, pathogenic fungal activities, fungal starvation, and signaling (Table 5, Additional file 2: Table S7). In order to confirm the expression of some of these sRNAs, we conducted stem-loop PCR and sRNA-specific sequencing on 10 *Si* and 10 Bd21-3-originating sRNAs from our Bd-*Si* sample and Table S7. All *Si* and all Bd21-3 sRNAs were amplified in the stem-loop PCR. To verify the nature of the amplification products, a subset of four *Sis*RNAs and three *Bds*RNAs were cloned and sent for Sanger

sequencing, confirming the expected sRNA sequences (Additional file 2: Figure S12, original gel pictures in Additional file 3 and Additional File 4, sequencing results in Additional file 2: Table S8). Thus, predicted targets of putative ck-sRNAs within this system imply another layer of expression control within the mutualistic interaction.

## Discussion

We established and studied the interaction between *Brachypodium distachyon*—a model Pooideae plant with shared synteny to major cereal crops—and *Serendipita indica*—a beneficial endophyte with an exceptionally large host range. This particular combination of traits adorning the *Bd-Si* interaction has great translational value towards filling in the gaps in knowledge about plant symbioses, especially their transcriptomic and sRNA expression profiles and the significance of RNAi. We show that *Si* colonizes *Bd*, resulting in shoot growth promotion, earlier flowering, and improved grain development. In comparison, earlier studies characterizing

**Table 5** Examples of deduced duplexes of *Brachypodium distachyon* sRNAs and their downregulated targets in *Serendipita indica*

sRNA	sRNA expression	Transcript	Description of target transcript	Transcript expression
<i>Bds</i> RNA 1	NA	CCA68723	Related to phenylalanine ammonia-lyase	– 5.1
<i>Bds</i> RNA 2	1.43	CCA69635	Probable acetyl-CoA synthetase	– 2.19
<i>Bds</i> RNA 3	0.04	CCA72153	Putative mitochondrial carnitine O-acetyltransferase	– 2.94
<i>Bds</i> RNA 4	0.58	CCA68099	Probable protein required for hyphal anastomosis HAM2	– 1.38
<i>Bds</i> RNA 5	0.59	CCA69082	Related to serine/threonine-protein kinase	– 1.65
<i>Bds</i> RNA 6	0.039	CCA67801	Probable isocitrate lyase	– 2.34
<i>Bds</i> RNA 7	4.37	CCA68918	Probable ADH1-alcohol dehydrogenase I	– 4.42
<i>Bds</i> RNA 8	NA	CCA77975	Related to peroxisomal membrane protein 4	– 2.39
		CCA68099	Probable protein required for hyphal anastomosis HAM2	– 1.38
<i>Bds</i> RNA 9	0.029	CCA73455	Related to phosphoprotein phosphatase 2C	– 0.89
<i>Bds</i> RNA 10	1.39	CCA72944	Protein TOXD	– 2.73
		CCA72668	Hypothetical protein	– 1.68
		CCA74115	Probable nucleolar rRNA processing protein GAR1	– 0.93
<i>Bds</i> RNA 11	0.19	CCA77931	Related to iron transport protein	– 2.4
<i>Bds</i> RNA 12	0.48	CCA68412	Related to ECM32-DNA dependent ATPase/DNA helicase B	– 1.96
<i>Bds</i> RNA 13	1.06	CCA75416	Related to estradiol 17 beta-dehydrogenase 4	– 2.12
<i>Bds</i> RNA 14	NA	CCA73650	Related to chitinase	– 1.37
<i>Bds</i> RNA 15	0.49	CCA77900	Related to LSB5-possible role in the regulation of actin cytoskeletal organization	– 1.27
<i>Bds</i> RNA 16	0.62	CCA69912	Related to acyl-CoA dehydrogenase	– 2.28
<i>Bds</i> RNA 17	0.88	CCA70015	Related to CAT1	– 1.84
<i>Bds</i> RNA 18	NA	CCA68373	Probable subtilisin-like serine protease	– 0.91
<i>Bds</i> RNA 19	1.38	CCA72980	Hypothetical protein	– 2.59
		CCA67021	Probable VID27-involved in vacuole import and degradation	– 0.93
<i>Bds</i> RNA 20	0.1	CCA73174	Related to ECM4-involved in cell wall biogenesis and architecture	– 2.48

sRNA expression was calculated as  $\log_2(\text{colonized/control})$  from normalized reads, NA stands for sRNAs expressed exclusively in the colonized sample; transcript expression is indicated as the  $\log_2(\text{colonized/control})$  FC

the interaction between *Si* and barley have demonstrated that fungal hyphae establish an interface with the root cell plasma membrane at an early colonization stage, followed by expansion of an extracellular hyphal network, intercellular growth, and intracellular penetration of cortical and rhizodermal cells [26]. Around 3 to 5 DPI, *Si* starts the switch from a biotrophic to a saprophytic lifestyle [26, 27]. Although this change involves intracellular hyphae extensively colonizing dead host cells and gradual digestion of cortical cell walls, the plant still benefits from the fungal presence. Consistent with these findings, our microscopic analyses confirmed proliferation of *Si* chlamydospores and both inter- and intracellular colonization of Bd21-3 cells in the root differentiation zone from 4 to 14 DPI. Detection of proliferating hyphae that were not wrapped in plasma membrane further suggests that *Si* is colonizing dead surface plant root cells at 4 DPI [25, 26].

#### Transcriptional changes detected during the *Bd-Si* interaction

To investigate colonization of Bd21-3 by *Si*, we analyzed *Si* DEGs in colonized vs. axenic mycelium samples. Gene ontology analysis indicated enrichment in genes involved in various metabolic and catalytic processes. DEGs with the greatest changes in expression play roles in plant cell wall degradation, carbohydrate metabolism and nutrient acquisition. These changes in nutritional reprogramming are to be expected, considering the different nutritional content that *Si* has accessible in planta vs. axenic CM plates and a more detailed look into the roles of the changed genes unveils a typical switch of fungal lifestyle. Examples of upregulated *Si* genes involved in cell wall degradation include a probable *Pectate lyase*, *Endo-1,4-beta-xylanases*, *Cellulose 1,4-beta-cellobiosidase*, and *Rhamnogalacturonan acetyltransferase*. The genes encoding these hydrolytic enzymes, which have undergone expansion in the *Si* genome [49], are similar to those upregulated in *Si* during saprophytic growth on autoclaved barley roots at 3 DPI and 5 DPI [22]. *PiAMT1*, encoding a high affinity ammonium transporter also was upregulated (logFC = 3.35; padj < 0.0001). Other upregulated genes encode enzymes involved in carbohydrate metabolism, including probable glucosidases, glucanase, and galactosidase. These proteins may modulate glucose concentration, which then regulates expression of some cell-wall degrading enzymes [22, 50]. Some of the 174 putative effector protein-encoding genes also are differentially expressed during *Si* colonization of barley and Arabidopsis [22, 27]. Six of these proteins (Additional file 2: Table S4) contain the *Si*-specific DELD domain, which suggests that *Si* utilizes a common protein effector arsenal to colonize various hosts. Considering highly downregulated *Si* DEGs, several encoded proteins

are associated with adaption to nutrient availability (*Accumulation of dyads protein 2*, *ADY2*; *Succinate-fumarate transporter*) and nutrient acquisition (*Acyl-CoA dehydrogenase*; *Carnitine acetyltransferase*, *CRAT*; *Phenylalanine ammonia-lyase*, *PAL* [51, 52]). Their reduced expression suggests ample nutrient availability at 4 DPI. Given the similarities in the *Si* transcriptome during colonization of *Bd* and barley, we propose that these fungal-plant interactions follow a pattern, and that by 4 DPI, a network of plant-endophyte communication cues has initiated a tightly controlled transcriptional program, leading to a shift from biotrophic to saprophytic growth.

Roots of Bd21-3 plants also displayed substantial transcriptional reprogramming following *Si* colonization. Gene ontology term analysis indicated enrichment in genes involved in catalytic and oxidoreduction-associated processes. Bd21-3 DEGs exhibiting the greatest changes in expression between colonized and non-colonized plants are related to stress-response, defense, and plant development. Of the downregulated Bd21-3 genes, several encode proteins commonly associated with stress responses, including a peroxidase, a wound-induced protein, and a putative protein kinase. Additionally, members of the *Heat-shock protein* gene family [53] are commonly induced in *Bd* during abiotic stress and members of the *Abscisic acid/water deficit stress (ABA/WDS)-induced protein* and the *Rare cold inducible (RCI2)* gene families enhance abiotic stress tolerance in various plant species [54, 55]. Circadian clock and flowering regulation genes such as *Pseudo-response regulator 7 (PRR7)*, *Cold regulated protein 27* and *Constans-like protein (CO8)*, also are downregulated during *Si* colonization. While members of the PRR and CO protein families work together to control flowering time [56, 57], any influence on early flowering in *Si*-colonized Bd21-3 is unclear. Circadian clock-associated genes also regulate lateral root development in Arabidopsis [58]; whether *Si*-induced changes in their expression influence root growth is unknown. Other downregulated development-associated DEGs include *Fantastic four meristem regulator (FAF)*, which regulates shoot and root development [59], and putative *Sulfoquinovosyltransferase (SQD2)*, which modulates seed setting and tiller development in rice [60]. Finally, several downregulated DEGs encode transcription factors, including MYB-related, GRAS, and bZIP.

In comparison, many of the upregulated Bd21-3 DEGs are associated with immune responses. Examples include genes encoding leucine-rich repeat (LRR) protein, a WRKY transcription factor, and thaumatin family protein. Increased expression of the defense gene *Pathogenesis-related protein 1 (PR1)* was similarly and transiently reported in *Si*-colonized Arabidopsis roots [61]. Upregulation of *Glutathione S-transferase (GST)* is consistent

with the increased antioxidant capacity of *Si*-colonized plants, which provides protection against attack by necrotrophic pathogens [21, 62]. The upregulation of genes in other hormonal networks (*PGP-like Phosphoglycoprotein auxin transporter*) and redox processes (*Multi-copper oxidase*) further suggests that *Si* colonization affects a range of signaling pathways.

### Bd miRNAs detected in the Bd-Si sample

The role of miRNAs as regulators of gene expression in the Sebacinalean symbiosis is largely unexplored. One report showed that *Si* induces growth promotion-associated miRNAs in *Oncidium* orchid roots [63]. Analysis of putative endogenous Bd21-3 sRNAs expressed during *Si* colonization identified 16 miRNAs. Some of them have known targets in transcription factors associated with plant growth and development. For example, the bdi-MIR166 family targets mRNAs encoding *Homeobox domain-leucine zipper* transcription factors [64]. In Arabidopsis, repression of these transcription factors by the miR165/166 family modulates root growth, maintenance of the shoot apical meristem, and development of leaf polarity [65]. Plant-specific transcription factors encoded by *Squamosa promoter-binding protein-like* (*SPL*) genes are the presumed targets of bdi-MIR156 and bdi-MIR529 [66]. In Arabidopsis, miR156-mediated downregulation of SPLs modulates developmental timing, lateral root development, branching, and leaf morphology [65]. Members of the *MYB* superfamily of transcription factors, which regulate many aspects of development, are the predicted targets of bdi-MIR159 [34]. Interestingly, miRNAs belonging to the miR159 and miR166 families in cotton are known ck-sRNAs that target virulence genes in *Verticillium dahliae* [13].

Other miRNAs identified in Bd21-3 include bdi-MIR168, predicted to target *AGO1* [64], and two miRNAs that regulate nutrition: bdi-MIR399, which is upregulated in *Bd* by phosphate starvation [64, 67], whereas bdi-MIR408 influences copper levels [34, 68]. Additionally, bdi-MIR408 (*BdsRNA* 10) has predicted ck targets in three *Si* transcripts: *CCA72944*, *CCA72668*, and *CCA74115*. Since various targets were predicted for bdi-MIR167 [34, 68] and no target was predicted for bdi-MIR9481, their endogenous functions in *Bd* are unclear. Interestingly, the miRNA families identified in our analysis, except bdi-MIR9481, also were detected in *Si*-colonized *Oncidium* [63]. Thus, this group of miRNAs may play an important role in reprogramming plant cells during Sebacinalean symbiosis establishment.

### Putative Si and Bd21-3 ck-sRNAs and their predicted targets

To date, cross-kingdom RNAi has been demonstrated in pathogenic plant-fungal interactions [12, 13, 69], and

while there are promising indications for its presence during plant-mycorrhiza interactions [36], whether it occurs in *Si*-plant associations is unknown. To investigate this possibility, we predicted targets for 21 nt putative ck-sRNAs from *Si* and Bd21-3 and confirmed their downregulation during colonization. This analysis uncovered 358 downregulated *Si* transcripts that are the predicted targets of 228 unique Bd21-3 sRNAs. Cross-kingdom RNAi-mediated downregulation of these targets might allow Bd21-3 to modulate *Si* growth during colonization. For example, *PAL*, *Acetyl-CoA synthetase*, *Carnitine acetyl transferase*, *Isocitrate lyase*, and *Acyl-CoA dehydrogenase*, which are targeted by *BdsRNA* 1, *BdsRNA* 2, *BdsRNA* 3, *BdsRNA* 6, and *BdsRNA* 16 (Table 5), are involved in fungal nutrient acquisition [22, 55, 70, 71]. Genes with important homologs in pathogenic fungi also are predicted targets, including *Subtilisin-like serine protease* (*BdsRNA* 18) [72], *Alcohol dehydrogenase 1* (*BdsRNA* 7) [73], and *Phosphoprotein phosphatase 2C* (*BdsRNA* 9) [74]. Targeting of *Hyphal anastomosis-2* (*HAM-2*) by *BdsRNA* 8 and *BdsRNA* 4 may provide another mechanism for controlling fungal growth, as *HAM-2* is required for hyphal fusion in *N. crassa* [75]. Similarly, targeting of *Chitinase* (*BdsRNA* 14) may help control *Si* growth.

Concurrently, we identified 49 downregulated Bd21-3 mRNAs that are the predicted targets of 63 unique *Si*-generated ck-sRNAs. Downregulation of these target genes via cross-kingdom RNAi might facilitate *Si* growth during colonization. For example, *Mannose-binding lectin* (targeted by *SisRNA* 18) belongs to a family of defense-related genes whose products trigger immune responses following pathogen recognition [76]. *SisRNA* 8 and *SisRNA* 15 target a protein kinase domain/LRR gene (*BdiBd21-3.4G0303000.1*) that may belong to the LRR receptor kinase family, which regulates defense and developmental-related processes [77]. Transcripts encoding serine-carboxypeptidase-like (SCPL) proteins *BdiBd21-3.2G0440200.1* and *BdiBd21-3.1G0411900.1* (targeted by *SisRNA* 1 and *SisRNA* 15) are associated with defense against (a)biotic stresses in monocots [78]. Members of various transcription factors families also were identified as predicted targets (*MYB* by *SisRNA* 16, *bZIP* by *SisRNA* 2, and *GRAS* by *SisRNA* 10). These families are associated with (a)biotic stress responses, as well as plant growth and development [79–81]. Lastly, transcripts for proteins involved in circadian clock and flowering regulation (*BdiBd21-3.1G0887100.1* and *BdiBd21-3.3G0264400.1* [56]) are the presumed targets of *SisRNA* 1 and *SisRNA* 19. Together, these findings suggest that *Si*-derived ck-sRNAs may promote fungal colonization by targeting signaling processes associated with plant development and responses to (a)biotic stresses.

In combination with earlier studies on *Bd* RNAi proteins [35] and *Bd* interaction with the pathogen *Magnaporthe oryzae* [82], the in silico analyses presented here suggest that *Si* and *Bd* contain functional RNAi components and that both organisms generate ck-sRNAs, which potentially modulate this mutualistic interaction. However, further studies are necessary to validate cross-kingdom RNAi in a Sebacinales symbiosis. Namely, degradome analysis is needed to confirm target degradation and evidence that Bd21-3 and *Si* AGOs associate with sRNAs expressed by the interacting organism is necessary for confirmation of cross-kingdom RNAi.

## Conclusions

We report that Bd21-3 and *Si* form a mutualistic symbiosis with a promoting effect on plant yield and development, accompanied by changes in gene expression in both organisms, including putative protein *Si* effectors and RNAi-related genes. sRNA profiles of both organisms also changed, indicating that this model system will provide important insights into the multiple layers of regulation and interaction between beneficial fungi and cereal hosts. Within the broader scope of plant-mutualist interactions, we show that detection of putative RNAi-involved sRNAs in an interaction highly benefits from simultaneous transcriptome analysis and indicate an involvement of sRNA-based regulation in defense responses, nutritional reprogramming, and colonization maintenance. Alongside other experimental approaches in plant-microbe interactions (eg. sRNA uptake studies [83]), developing a deeper understanding of the communication mechanisms that modulate mutualistic interactions is highly relevant for establishing robust growth promotion and protection strategies in crops.

## Methods

### *Bd* and *Si* cultivation and inoculation

The seeds of *Brachypodium distachyon* (*Bd*) line Bd21-3 (gift from R. Sibout, INRA Versailles, France) were surface sterilized (3% active chlorine, sodium hypochlorite solution) for 15 min, washed three times, and placed on half-strength MS [84] medium in dark at 4 °C for 2 days and then 7 days at 24 °C and 16 h light/8 h dark cycle ( $47 \mu\text{mol m}^{-2} \text{s}^{-1}$  photon flux density). *Serendipita indica* (*Si*) (IPAZ-11827, Institute of Phytopathology, Giessen, Germany) was grown on complete media plates (CM [85]) at 23 °C in dark for 4–5 weeks.

For inoculation, *Si* mycelium was collected in 0.002% aqueous Tween 20 solution, filtered (Miracloth, Calbiochem), and pelleted by centrifugation (10 min/4000 rpm/20 °C) twice. Chlamydospore

concentration of  $5 \times 10^5$  conidia  $\text{ml}^{-1}$  in 0.002% Tween 20 solution was used to inoculate 7-day-old plant seedlings for 2–3 h. Control plants were mock treated with the 0.002% Tween 20 solution for the same time. Grain yield analyses were done on mature plants grown on soil (F-E type LD 80, Fruhstorfer Erde, Germany) under 16 h light ( $160 \mu\text{mol m}^{-2} \text{s}^{-1}$ , 22 °C) and 8 h dark (18 °C) conditions at 60% relative humidity for 1 month, and then greenhouse conditions until seed maturity. Number of spikelets was assessed after 2 months. Shoot biomass was assessed 3 weeks after inoculation of seedlings grown on a mixture (2:1, v/v) of vermiculite (Deutsche Vermiculite GmbH) and oil dri (oil binder Typ III R Coarse grain, Damolin, Mettmann, Germany) under comparable conditions as for grain yield, and fertilized every 3 days with an aqueous solution of Wuxal Super NPK-8/8/6 ( $1:10^3$  v/v; Haug, Düsseldorf, Germany). Samples for RNA-seq, RT-qPCR, stem-loop PCR, and microscopy were also grown under these conditions. To assess growth promotion in *Si* inoculated *Bd* relative to the control, we used the pairwise *t* test or the Mann-Whitney-Wilcoxon test on each of the three repetitions of experiments, after checking for normality and homogenous variances. Benjamini-Hochberg correction for multiple testing was used to correct the *p* values and the significance asterisks were assigned to the average *p*-value as follows: \* for  $p \leq 0.05$ , \*\* for  $p \leq 0.001$ , and \*\*\* for  $p \leq 0.0001$ .

### Microscopy

Following *Si* inoculation, one-week-old seedlings were grown on plastic mesh ( $\sim 90 \mu\text{m}$ ) placed over half-strength MS medium or on vermiculite/oil dri prior to assessing root colonization. *Si* was visualized with the chitin-specific dye WGA-AF 488 (wheat germ agglutinin; Molecular Probes, Karlsruhe, Germany), as described in Deshmukh et al. (2006) [26], with boiling in KOH (10%) for 30 s, prior to incubation in phosphate-buffered saline (PBS, pH 7.4). Root cells were visualized by incubating with propidium iodide ( $10 \mu\text{g ml}^{-1}$ ) for 10 min and washing with sterile water. Confocal laser scanning microscopy was done (TCS SP8 microscope, Leica, Bensheim, Germany) and the Leica LAS X software was utilized for visualization and maximum (z-stack) projections.

### Resequencing, assembly, and annotation of the *Si* genome

The MasterPure Yeast DNA Purification Kit (Epicentre, Illumina) was used to extract genomic DNA from 4-week-old axenic *Si* cultures. The *Si* genome was resequenced, assembled [86], and annotated as described [87], whereby a MinION sequencing library

was prepared using the Nanopore Rapid DNA Sequencing kit. Sequencing was performed on an Oxford Nanopore MinION Mk1b sequencer using a R9.5 flow cell. Additionally, sequencing of an Illumina Nexera XT library was performed on the MiSeq platform (Illumina; 2 × 300 bp paired-end sequencing, v3 chemistry). Adapters and low-quality reads were removed by an in-house software pipeline prior to polishing [88]. MinKNOW (v1.13.1, Oxford Nanopore Technologies) was used to control the run with the 48 h sequencing run protocol, and base calling was performed offline using albacore (v2.3.1, Oxford Nanopore Technologies). The assembly was performed using Canu v1.6 ([89], default settings). The resulting contigs were polished with Illumina short read data using Pilon [90] for eight iterative cycles. BWA-MEM [91] was used for read mapping in the first four iterations and Bowtie2 v2.3.2 [92] in the second set. Gene prediction was performed with GeneMark-ES 4.3.3. ([38], default settings). Predicted genes were functionally annotated using a modified version of the genome annotation platform GenDB 2.0 [39] for eukaryotic genomes [40]. RNAi-associated proteins were predicted by searching the proteome [22] for typical domain structure and highest homology to *Neurospora crassa* RNAi proteins (NC12 genome assembly [93]). A modified version of the pipeline from Rafiqi et al. (2013) [41] was used to predict protein effectors. After identifying proteins with signal peptides (signalp-4.1 [94]), those predicted as transmembrane helix proteins (tmhmm [95]), mitochondrial proteins (target-1.1 [96]), and cell wall hydrolysis-associated proteins were removed. For comparative analysis of the *Si* (Si-2020 and DSM11827 ASM31354 v.1 [22]), *Serendipita vermifera* [97] and *Laccaria bicolor* [98] genomes, software platform EDGAR 2.3 [99] was used.

#### RNA extraction, library preparation, and mRNA/sRNA sequencing

Roots inoculated with *Si* (Bd-Si) or mock-inoculated (Bd-C), as described above, were grown for 4 days and pooled (three roots per sample). *Si* mycelium and spores were collected from 4-week-old axenic cultures grown on CM medium. All samples in triplicates were shock frozen, stored at − 80 °C, and ground in liquid N<sub>2</sub>. Total RNA was isolated using the ZymoBIOMICS RNA Mini Kit (Zymo Research, USA), quantified with DropSense16/Xpose (BIOKÉ, Netherlands), and analyzed with an Agilent 2100 Bioanalyzer Nano Chip (Agilent, Germany). RNA Clean and Concentrator 25 and 5 kits (Zymo Research) were utilized to separate total RNA into fractions: 17–200 nt and > 200 nt. 1.5 µg of the larger fractions were processed for mRNA library

preparation (TruSeq Stranded mRNA protocol, Illumina, USA). Fragment Analyzer Automated CE System (Advanced Analytical Technologies, Austria) determined the quality of the generated polyA mRNA libraries. Quantity and quality of the smaller RNA fractions were assessed with the Qubit fluorometer (Invitrogen, Germany) and Agilent 2100 Bioanalyzer Pico Chip. sRNA library preparation was done with 50 ng of RNA (TruSeq Small RNA Library Prep, Illumina) and size selection with the BluePippin (Sage Science, USA) for fragments between 140 and 160 nt (15–35 nt without adapters) applied. Sequencing was accomplished on the Illumina HiSeq 1500.

#### Transcriptome analysis

Raw reads from mRNA sequencing [100] were submitted to quality check using FastQC [101] and aligned to the Bd21-3 v1.1 (DOE-JGI, <http://phytozome.jgi.doe.gov/> [102]) or resequenced *Si* (Si-2020) genomes with HISAT2 [103]. An intron length of 20–2000 nt was allowed for *Si* [104] and 20–10,000 nt for Bd21-3 [105]. The reads were counted using HTSeq-count [106], differential gene expression was performed with DESeq2 [107], and gene enrichment analysis with AgriGO v.2 [108], with reference Bd21 setting for Bd21-3 (Bd 21 synonyms) and a customized background for *Si*. Volcano plots were generated using plotly [109] and ggplot2 [110] R [111] libraries. Gene descriptions were obtained from the organism annotations or Blast2GO [112].

#### sRNA analysis and prediction of putative endogenous and ck-sRNAs

Raw reads from sRNA sequencing [113] were submitted to FastQC [101] and adapter trimming [114]. Bowtie [115] was used for alignment as detailed in Additional file 2: Fig. S6. The resequenced *Si* genome was used for alignments of fungal origin. tRNA/rRNA sequences were downloaded from RNACentral ([116], EMBL-EBI). Putative endogenous sRNA reads were submitted to ShortStack [117]. For filtering putative ck-sRNAs, a previously established pipeline [118] was utilized. Reads were normalized to the total number of mapped reads for a single genome and reads per million (RPM) and log<sub>2</sub> (colonized/mock-treated) values calculated. Thus, a sRNA read was selected as a putative ck-sRNA if it was present exclusively or at a higher quantity (i.e., induced) in the colonized vs. control sample. Putative ck-sRNAs were submitted to psRNAtarget [119]. Since the separation of sRNA and mRNA fractions from each biological sample was facilitated, we checked for downregulation of mRNAs corresponding to predicted sRNA target genes within the DEGs. Transcriptomes used for these predictions were Bd 21-3 v1.1 (DOE-JGI, <http://phytozome.jgi.doe.gov/> [102]) and *Si* DSM11827 ASM31354 v.1 [22].

Venn diagrams were generated using the VennDiagram R package [120].

### Quantitative real-time PCR and stem-loop PCR for validation of sequencing results

To validate gene expression detected in the sequencing, we used quantitative real-time PCR (qRT-PCR). RNA extraction from mock treated and *Si* inoculated Bd21-3 roots, as well as *Si* axenic cultures, under the same conditions as explained above for the sequencing, was done with TRIzol (Thermo Fisher Scientific, Waltham, MA, USA), cDNA synthesized using qScript™ cDNA kit (Quantabio, Beverly, MA, USA) and 10 ng of cDNA used as template in the QuantStudio 5 Real-Time PCR system (Applied Biosystems), with SYBR® green JumpStart Taq ReadyMix (Sigma-Aldrich, St. Louis, MO, USA). Each sample had three technical replicates. Primers used for these amplifications are listed in Table S9 (Additional file 2: Table S9). Transcript levels were calculated using the  $2^{-\Delta\Delta C_t}$  method [121], relatively to *BdUbi4-3* for Bd21-3 and *Si ITS* sequence for *Si*.

For the identification of sRNAs in the interaction of *Si* with Bd21-3 stem-loop RT-PCR was employed [122]. cDNA was synthesized from DNase I-treated total RNA extracted from *Si* axenic culture or inoculated Bd21-3 roots. The folding of the hairpin primer was performed according to Kramer (2011) [123]. For each stem-loop reaction, six hairpin primers were multiplexed in a 20-μL reaction using the Revertaid RT enzyme according to the manufacturer's instructions (Thermo Scientific). For primer annealing, the reaction was incubated for 30 min at 16 °C followed by an extension step at 42 °C for 30 min. The reaction was stopped at 85 °C for 5 min. cDNA was stored at -80 °C until further use. Endpoint PCR was performed using an universal stem-loop primer and specific sRNA primer (Additional file 2: Table S10) under the following conditions: initial denaturation at 95 °C for 5 min followed by 35 cycles: 95 °C for 30 s, primer annealing at 60 °C for 30 s, and extension at 72 °C for 30 s. PCR products were separated by gel electrophoresis on a 2% (w/v) agarose gel. To obtain sequence information of the amplified sRNAs of the stem-loop reaction, PCR products were purified and cloned into the pGEM®-T Easy Vector Systems (Promega, Madison, WI, USA) following the manufacturer's instructions. From each cloned sRNA, six colonies were further analyzed by Sanger sequencing using a M13 reverse primer.

### Abbreviations

AGO: Argonaute; Bd: *Brachypodium distachyon*; Bd-C: Mock-inoculated Bd root sample; Bd-Si: *Si*-inoculated Bd root sample; BdsRNA: *Brachypodium distachyon*-derived sRNA; ck-sRNA: Cross-kingdom sRNA; DCL: Dicer-like; DEG: Differentially expressed gene; DPI: Day(s) post inoculation; FC: Fold change; miRNA: MicroRNA; nt: Nucleotide; RdRP: RNA-dependent RNA polymerase; RNAi: RNA interference; *Si*: *Serendipita indica*; Si-ax: *Si* axenic culture sample; *Si*sRNA: *Serendipita indica*-derived sRNA; sRNA: Small RNA

### Supplementary Information

The online version contains supplementary material available at <https://doi.org/10.1186/s12915-021-01104-2>.

**Additional file 1.** Supporting individual data values displayed in Figure 1a-c and Additional File 2: Figure S5.

**Additional file 2: Fig. S1.** *Serendipita indica* (*Si*) colonization has an effect on *Brachypodium distachyon* (*Bd*) root structure. **Fig. S2.** Progress of *Serendipita indica* (*Si*) spore proliferation during colonization of *Brachypodium distachyon* Bd21-3. **Fig. S3.** Comparison of the resequenced *Serendipita indica* (*Si*) genome to the 2011 assembly. **Fig. S4.** Comparison of the resequenced *Serendipita indica* (*Si*) genome to *Serendipita vermifera* and *Laccaria bicolor*. **Fig. S5.** qRT-PCR confirmation of DEGs identified during mRNA sequencing. **Fig. S6.** Filtering pipelines applied in the analysis. **Fig. S7.** Size distribution of total and unique putative ck (cross-kingdom) -sRNAs. **Fig. S8.** Percentage distribution of the 5' terminal nucleotide in unique putative endogenous sRNAs. **Fig. S9.** Percentage distribution of the 5' terminal nucleotide in unique putative ck-sRNAs. **Fig. S10.** Percentage distribution of the 5' terminal nucleotide in total putative endogenous sRNAs. **Fig. S11.** Percentage distribution of the 5' terminal nucleotide in total putative ck-sRNAs. **Fig. S12.** Stem-loop PCR (gel electrophoresis) of some *Si* and Bd21-3 sRNAs expressed in the Bd-Si sample. **Table S1.** Quantification of identified features in the resequenced genome of *Serendipita indica* (*Si*). **Table S2.** Total reads from the Bd-C (mock-treated), Bd-Si (colonized root) and Si-ax (axenic culture) samples and their alignment rate (HISAT2) to the corresponding genomes. **Table S3.** Significant gene ontology terms of molecular function in the differentially expressed genes (DEGs) datasets. **Table S4.** Predicted protein effectors identified in the resequenced *Serendipita indica* (*Si*) genome. **Table S5.** Candidate RNAi machinery proteins predicted from the resequenced *Serendipita indica* (*Si*) genome. **Table S6.** Total and unique reads for filtered sRNAs from Bd-C (mock-treated), Bd-Si (colonized root) and Si-ax (axenic culture). **Table S7.** Sequences of putative sRNAs in Tables 4 and 5. **Table S8.** sRNA sequences after stem-loop PCR amplification. **Table S9.** Primers used for qRT-PCR (Figure S5). **Table S10.** Primers used for stem-loop PCR and sequencing (Figure S12, Table S8).

**Additional file 3.** Uncropped gel picture annotated in Additional file 2: Figure S12a.

**Additional file 4.** Uncropped gel picture annotated in Additional file 2: Figure S12b.

### Acknowledgements

We thank Elke Stein, Dagmar Biedenkopf, Ute Micknass and Christina Birkenstock for technical assistance. We thank Dr. John Vogel and the DOE-JGI for permission to use the Bd21-3 genome under early access conditions. *Brachypodium distachyon* Bd21-3 is a gift of R. Sibout, INRA Versailles. We are very thankful to D'Maris Dempsey for her assistance in preparation of the manuscript.

### Authors' contributions

EŠ, SZ, DW, and KHK wrote the text and drafted the figures. EŠ and SZ designed and conducted the establishment experiments. EŠ, SZ, TB, DW, LJ, and JK conducted the RNAseq and genome resequencing experiments and analyzed the data. SN and JS conducted the stem-loop PCR experiments and sequencing analysis. JI and JT performed microscopy in sterile conditions. All authors read and approved the final manuscript.

### Funding

This work was supported by the Deutsche Forschungsgemeinschaft (DFG), Research Training Group (RTG) 2355, and Research Unit FOR5116 to KHK. We gratefully acknowledge the bioinformatics support of the BMBF-funded project Bielefeld-Gießen Center for Microbial Bioinformatics-BiGi (grant number 031A533) within the German Network for Bioinformatics Infrastructure (de.NBI). Open Access funding enabled and organized by Projekt DEAL.

### Availability of data and materials

All data generated or analyzed during this study are included in this published article, its supplementary information files (Additional files 1, 2, 3 and 4) and publicly available repositories. mRNA and sRNA-seq of

*Brachypodium distachyon* roots inoculated with *Serendipita indica* datasets are available in the ArrayExpress database at EMBL-EBI ([www.ebi.ac.uk/arrayexpress](http://www.ebi.ac.uk/arrayexpress)) under accession numbers E-MTAB-10649 and E-MTAB-10650, respectively. The genome assembly data for *Serendipita indica* resequencing study is available in the European Nucleotide Archive (ENA) at EMBL-EBI under accession numbers: assembly GCA\_910890315 and study PRJEB45884 (<https://www.ebi.ac.uk/ena/browser/view/PRJEB45884>). Additional publicly available datasets have been accessed from the corresponding European Nucleotide Archive accessions and EnsemblFungi: *Serendipita indica* 2011 genome (GCA\_000313545.1) [22], NC12 of *Neurospora crassa* (GCA\_000182925.2) [93], *Serendipita vermifera* subsp. *besicii* [97] has been accessed from JGI MycoCosm (<https://mycocosm.jgi.doe.gov/Sebbe1/Sebbe1.home.html>), as was the *Laccaria bicolor* genome ([98], <https://mycocosm.jgi.doe.gov/Lacbi2/Lacbi2.home.html>). The Bd21-3 v1.1 genome [102] was accessed under early access conditions and these sequence data were produced by the US Department of Energy Joint Genome Institute - DOE-JGI, <http://phytozome.jgi.doe.gov/>.

## Declarations

### Ethics approval and consent to participate

Not applicable.

### Consent for publication

Not applicable.

### Competing interests

The authors declare that they have no competing interests.

### Author details

<sup>1</sup>Institute of Phytopathology, Centre for BioSystems, Land Use and Nutrition, Justus Liebig University, 35392 Giessen, Germany. <sup>2</sup>Center for Biotechnology - CeBITec, Bielefeld University, 33615 Bielefeld, Germany. <sup>3</sup>Institute of Bioinformatics and Systems Biology, Justus Liebig University, 35392 Giessen, Germany.

Received: 17 December 2020 Accepted: 16 July 2021

Published online: 24 August 2021

## References

- Marschner P, Yang C-H, Lieberei R, Crowley DE. Soil and plant specific effects on bacterial community composition in the rhizosphere. *Soil Biol Biochem*. 2001;33(11):1437–45. [https://doi.org/10.1016/S0038-0717\(01\)00052-9](https://doi.org/10.1016/S0038-0717(01)00052-9).
- Lagunas B, Schäfer P, Gifford ML. Housing helpful invaders: the evolutionary and molecular architecture underlying plant root-mutualist microbe interactions. *J Exp Bot*. 2015;66(8):2177–86. <https://doi.org/10.1093/jxb/erv038>.
- Kogel KH, Franken P, Hückelhoven R. Endophyte or parasite – what decides? *Curr Opin Plant Biol*. 2006;9(4):358–63. <https://doi.org/10.1016/j.pbi.2006.05.001>.
- Fesel PH, Zuccaro A. Dissecting endophytic lifestyle along the parasitism/mutualism continuum in Arabidopsis. *Curr Opin Microbiol*. 2016;32:103–12. <https://doi.org/10.1016/j.mib.2016.05.008>.
- Kloppholz S, Kuhn H, Requena N. A secreted fungal effector of *Glomus intraradices* promotes symbiotic biotrophy. *Curr Biol*. 2011;21(14):1204–9. <https://doi.org/10.1016/j.cub.2011.06.044>.
- Doehlemann G, Requena N, Schaefer P, Brunner F, O'Connell R, Parker JE. Reprogramming of plant cells by filamentous plant-colonizing microbes. *New Phytol*. 2014;204(4):803–14. <https://doi.org/10.1111/nph.12938>.
- Vishwakarma K, Kumar N, Shandilya C, Mohapatra S, Bhayana S, Varma A. Revisiting plant-microbe interactions and microbial consortia application for enhancing sustainable agriculture: a review. *Front Microbiol*. 2020;11:3195. <https://doi.org/10.1038/nature02874>.
- Baulcombe D. RNA silencing in plants. *Nature*. 2004;431(7006):356–63. <https://doi.org/10.1038/nature02874>.
- Fang X, Qi Y. RNAi in plants: an Argonaute-centered view. *Plant Cell*. 2016;28(2):272–85. <https://doi.org/10.1105/tpc.15.00920>.
- Uhse S, Djamei A. Effectors of plant-colonizing fungi and beyond. *PLOS Pathog*. 2018;14(6):e1006992. <https://doi.org/10.1371/journal.ppat.1006992>.
- Akum FN, Steinbrenner J, Biedenkopf D, Imani J, Kogel KH. The *Piriformospora indica* effector PIIN\_08944 promotes the mutualistic Sebacinalean symbiosis. *Front Plant Sci*. 2015;6:1–12.
- Weiberg A, Wang M, Lin F-M, Zhao H, Zhang Z, Kaloshian I, et al. Fungal small RNAs suppress plant immunity by hijacking host RNA interference pathways. *Science* (80-). 2013;342(6154):118–23.
- Zhang T, Zhao YL, Zhao JH, Wang S, Jin Y, Chen ZQ, et al. Cotton plants export microRNAs to inhibit virulence gene expression in a fungal pathogen. *Nat Plants*. 2016;2(10):1–6.
- Kellogg EA. *Brachypodium distachyon* as a genetic model system. *Annu Rev Genet*. 2015;49(1):1–20. <https://doi.org/10.1146/annurev-genet-112414-055135>.
- Qiang X, Weiss M, Kogel KH, Schäfer P. *Piriformospora indica*-a mutualistic basidiomycete with an exceptionally large plant host range. *Mol Plant Pathol*. 2012;13(5):508–18. <https://doi.org/10.1111/j.1364-3703.2011.00764.x>.
- Stein E, Molitor A, Kogel KH, Waller F. Systemic resistance in Arabidopsis conferred by the mycorrhizal fungus *Piriformospora indica* requires jasmonic acid signaling and the cytoplasmic function of NPR1. *Plant Cell Physiol*. 2008;49(11):1747–51. <https://doi.org/10.1093/pcp/pcn147>.
- Deshmukh SD, Kogel KH. *Piriformospora indica* protects barley from root rot caused by *Fusarium graminearum*. *J Plant Dis Prot*. 2007;114(6):263–8. <https://doi.org/10.1007/BF03356227>.
- Trzewik A, Maciorowski R, Klocke E, Orlikowska T. The influence of *Piriformospora indica* on the resistance of two rhododendron cultivars to *Phytophthora cinnamomi* and *P. plurivora*. *Biol Control*. 2020;140:104121.
- Fakhro A, Andrade-Linares DR, von Barga S, Bandte M, Büttner C, Grosch R, et al. Impact of *Piriformospora indica* on tomato growth and on interaction with fungal and viral pathogens. *Mycorrhiza*. 2010;20(3):191–200. <https://doi.org/10.1007/s00572-009-0279-5>.
- Baltruschat H, Fodor J, Harrach BD, Niemczyk E, Barna B, Gullner G, et al. Salt tolerance of barley induced by the root endophyte *Piriformospora indica* is associated with a strong increase in antioxidants. *New Phytol*. 2008;180(2):501–10. <https://doi.org/10.1111/j.1469-8137.2008.02583.x>.
- Waller F, Achatz B, Baltruschat H, Fodor J, Becker K, Fischer M, et al. The endophytic fungus *Piriformospora indica* reprograms barley to salt-stress tolerance, disease resistance, and higher yield. *Proc Natl Acad Sci U S A*. 2005;102(38):13386–91. <https://doi.org/10.1073/pnas.0504423102>.
- Zuccaro A, Lahrmann U, Güldener U, Langen G, Pfiffi S, Biedenkopf D, et al. Endophytic life strategies decoded by genome and transcriptome analyses of the mutualistic root symbiont *Piriformospora indica*. *PLoS Pathog*. 2011;7(10):Serendipita indica genome assembly. 2011. GCA accession number: GCA\_000313545.1 ([https://www.ebi.ac.uk/ena/browser/view/GCA\\_000313545.1](https://www.ebi.ac.uk/ena/browser/view/GCA_000313545.1)).
- Zuccaro A, Basiewicz M, Zurawska M, Biedenkopf D, Kogel KH. Karyotype analysis, genome organization, and stable genetic transformation of the root colonizing fungus *Piriformospora indica*. *Fungal Genet Biol*. 2009;46(8):543–50. <https://doi.org/10.1016/j.fgb.2009.03.009>.
- Schäfer P, Pfiffi S, Voll LM, Zajic D, Chandler PM, Waller F, et al. Manipulation of plant innate immunity and gibberellin as factor of compatibility in the mutualistic association of barley roots with *Piriformospora indica*. *Plant J*. 2009;59(3):461–74. <https://doi.org/10.1111/j.1365-3113X.2009.03887.x>.
- Jacobs S, Zechmann B, Molitor A, Trujillo M, Petutschnig E, Lipka V, et al. Broad-spectrum suppression of innate immunity is required for colonization of Arabidopsis roots by the fungus *Piriformospora indica*. *Plant Physiol*. 2011;156(2):726–40. <https://doi.org/10.1104/pp.111.176446>.
- Deshmukh S, Hückelhoven R, Schäfer P, Imani J, Sharma M, Weiss M, et al. The root endophytic fungus *Piriformospora indica* requires host cell death for proliferation during mutualistic symbiosis with barley. *Proc Natl Acad Sci U S A*. 2006;103(49):18450–7. <https://doi.org/10.1073/pnas.0605697103>.
- Lahrmann U, Ding Y, Banhara A, Rath M, Hajirezaei MR, Döhlemann S, et al. Host-related metabolic cues affect colonization strategies of a root endophyte. *Proc Natl Acad Sci U S A*. 2013;110(34):13965–70. <https://doi.org/10.1073/pnas.1301653110>.
- Scholtz K-BG, Irigoyen S, Catalan P, Mandadi KK. *Brachypodium*: a monocot grass model genus for plant biology. *Plant Cell*. 2018;30(8):1673–94. <https://doi.org/10.1105/tpc.18.00083>.
- Vogel J, Hill T. High-efficiency Agrobacterium-mediated transformation of *Brachypodium distachyon* inbred line Bd21-3. *Plant Cell Rep*. 2008;27(3):471–8. <https://doi.org/10.1007/s00299-007-0472-y>.
- Vogel JP, Garvin DF, Mockler TC, Schmutz J, Rokhsar D, Bevan MW, et al. Genome sequencing and analysis of the model grass *Brachypodium distachyon*. *Nature*. 2010;463(7282):763–8.
- Hsia MM, O'Malley R, Cartwright A, Nieu R, Gordon SP, Kelly S, et al. Sequencing and functional validation of the JGI *Brachypodium distachyon* T-DNA collection. *Plant J*. 2017;91(3):361–70. <https://doi.org/10.1111/tpj.13582>.

32. Fitzgerald TL, Powell JJ, Schneebeil K, Hsia MM, Gardiner DM, Bragg JN, et al. Brachypodium as an emerging model for cereal-pathogen interactions. *Ann Bot*. 2015;115(5):717–31. <https://doi.org/10.1093/aob/mcv010>.
33. Zhang J, Xu Y, Huan Q, Chong K. Deep sequencing of Brachypodium small RNAs at the global genome level identifies microRNAs involved in cold stress response. *BMC Genomics*. 2009;10(1):449. <https://doi.org/10.1186/1471-2164-10-449>.
34. Bertolini E, Verelst W, Horner DS, Gianfranceschi L, Piccolo V, Inzé D, et al. Addressing the role of microRNAs in reprogramming leaf growth during drought stress in *Brachypodium distachyon*. *Mol Plant*. 2013;6(2):423–43. <https://doi.org/10.1093/mp/sss160>.
35. Šečić E, Zanini S, Kogel KH. Further elucidation of the Argonaute and Dicer protein families in the model grass species *Brachypodium distachyon*. *Front Plant Sci*. 2019;10:1332. <https://doi.org/10.3389/fpls.2019.01332>.
36. Silvestri A, Fiorilli V, Miozzi L, Accotto GP, Turina M, Lanfranco L. In silico analysis of fungal small RNA accumulation reveals putative plant mRNA targets in the symbiosis between an arbuscular mycorrhizal fungus and its host plant. *BMC Genomics*. 2019;20(1):1–18.
37. Ren B, Wang X, Duan J, Ma J. Rhizobial tRNA-derived small RNAs are signal molecules regulating plant nodulation. *Science* (80- ). 2019;365:919–22.
38. Ter-Hovhannisyán V, Lomsadze A, Chernoff YO, Borodovsky M. Gene prediction in novel fungal genomes using an *ab initio* algorithm with unsupervised training. *Genome Res*. 2008;18(12):1979–90. <https://doi.org/10.1101/gr.081612.108>.
39. Meyer F, Goesmann A, McHardy AC, Bartels D, Bekel T, Clausen J, et al. GenDB—an open source genome annotation system for prokaryote genomes. *Nucleic Acids Res*. 2003;31(8):2187–95. <https://doi.org/10.1093/nar/gkg312>.
40. Rupp O, Becker J, Brinkrolf K, Timmermann C, Borth N, Pühler A, et al. Construction of a public CHO cell line transcript database using versatile bioinformatics analysis pipelines. *PLoS One*. 2014;9(1):e85568. <https://doi.org/10.1371/journal.pone.0085568>.
41. Rafiqi M, Jelonek L, Akum NF, Zhang F, Kogel KH. Effector candidates in the secretome of *Piriformospora indica*, a ubiquitous plant-associated fungus. *Front Plant Sci*. 2013;4:228.
42. Billmyre RB, Calo S, Feretaki M, Wang X, Heitman J. RNAi function, diversity, and loss in the fungal kingdom. *Chromosome Res*. 2013;21(6–7):561–72. <https://doi.org/10.1007/s10577-013-9388-2>.
43. Dang Y, Yang Q, Xue Z, Liu Y. RNA interference in fungi: pathways, functions, and applications. *Eukaryot Cell*. 2011;10(9):1148 LP–1155.
44. Lau P-W, Guiley KZ, De N, Potter CS, Carragher B, MacRae IJ. The molecular architecture of human Dicer. *Nat Struct Mol Biol*. 2012;19(4):436–40. <https://doi.org/10.1038/nsmb.2268>.
45. Cenik ES, Zamore PD. Argonaute proteins. *Curr Biol*. 2011;21(12):R446–9. <https://doi.org/10.1016/j.cub.2011.05.020>.
46. Meyers BC, Axtell MJ. MicroRNAs in plants: key findings from the early years. *Plant Cell*. 2019;31(6):1206–7. <https://doi.org/10.1105/tpc.19.00310>.
47. Mi S, Cai T, Hu Y, Chen Y, Hodges E, Ni F, et al. Sorting of small RNAs into Arabidopsis Argonaute complexes is directed by the 5' terminal nucleotide. *Cell*. 2008;133(1):116–27. <https://doi.org/10.1016/j.cell.2008.02.034>.
48. Cai Q, Qiao L, Wang M, He B, Lin F-M, Palmquist J, et al. Plants send small RNAs in extracellular vesicles to fungal pathogen to silence virulence genes. *Science* (80- ). 2018;360:eaar4142.
49. Lahmann U, Strehmel N, Langen G, Frerigmann H, Leson L, Ding Y, et al. Mutualistic root endophytism is not associated with the reduction of saprotrophic traits and requires a noncompromised plant innate immunity. *New Phytol*. 2015;207(3):841–57. <https://doi.org/10.1111/nph.13411>.
50. Tonukari NJ, Scott-Craig JS, Walton JD. The *Cochliobolus carbonum* SNF1 gene is required for cell wall-degrading enzyme expression and virulence on maize. *Plant Cell*. 2000;12(2):237–47.
51. Zhou H, Lorenz MC. Carnitine acetyltransferases are required for growth on non-fermentable carbon sources but not for pathogenesis in *Candida albicans*. *Microbiology*. 2008;154(2):500–9. <https://doi.org/10.1099/mic.0.2007/014555-0>.
52. Hyun MW, Yun YH, Kim JY, Kim SH. Fungal and plant phenylalanine ammonia-lyase. *Mycobiology*. 2011;39(4):257–65. <https://doi.org/10.5941/MYCO.2011.39.4.257>.
53. Zhang M, Shen Z, Meng G, Lu Y, Wang Y. Genome-wide analysis of the *Brachypodium distachyon* (L.) P. Beauv. Hsp90 gene family reveals molecular evolution and expression profiling under drought and salt stresses. *PLoS One*. 2017;12(12):e0189187. <https://doi.org/10.1371/journal.pone.0189187>.
54. Brunetti SC, Arseneault MKM, Gulick PJ. Characterization of the Esi3/RCI2/PMP3 gene family in the Triticeae. *BMC Genomics*. 2018;19(1):898. <https://doi.org/10.1186/s12864-018-5311-8>.
55. Liang Y, Jiang Y, Du M, Li B, Chen L, Chen M, et al. ZmASR3 from the maize ASR gene family positively regulates drought tolerance in transgenic Arabidopsis. *Int J Mol Sci*. 2019;20(9):2278. <https://doi.org/10.3390/ijms20092278>.
56. Hayama R, Sarid-Krebs L, Richter R, Fernández V, Jang S, Coupland G. PSEUDO RESPONSE REGULATORS stabilize CONSTANS protein to promote flowering in response to day length. *EMBO J*. 2017;36(7):904–18. <https://doi.org/10.15252/embj.201693907>.
57. Li Y, Xu M. CCT family genes in cereal crops: A current overview. *Crop J*. 2017;5(6):449–58. <https://doi.org/10.1016/j.cj.2017.07.001>.
58. Voß U, Wilson MH, Kenobi K, Gould PD, Robertson FC, Peer WA, et al. The circadian clock rephases during lateral root organ initiation in *Arabidopsis thaliana*. *Nat Commun*. 2015;6(1):7641. <https://doi.org/10.1038/ncomms8641>.
59. Wahl V, Brand LH, Guo Y-L, Schmid M. The FANTASTIC FOUR proteins influence shoot meristem size in *Arabidopsis thaliana*. *BMC Plant Biol*. 2010;10(1):285. <https://doi.org/10.1186/1471-2229-10-285>.
60. Zhan X, Shen Q, Wang X, Hong Y. The Sulfoquinovosyltransferase-like enzyme SQD2.2 is involved in flavonoid glycosylation, regulating sugar metabolism and seed setting in rice. *Sci Rep*. 2017;7(1):4685.
61. Pedrotti L, Mueller MJ, Waller F. *Piriformospora indica* root colonization triggers local and systemic root responses and inhibits secondary colonization of distal roots. *PLoS One*. 2013;8(7):e69352. <https://doi.org/10.1371/journal.pone.0069352>.
62. Harrach B, Baltruschat H, Barna B, Fodor J, Kogel KH. The mutualistic fungus *Piriformospora indica* protects barley roots from a loss of antioxidant capacity caused by the necrotrophic pathogen *Fusarium culmorum*. *Mol Plant Microbe Interact*. 2013;26(5):599–605. <https://doi.org/10.1094/MPMI-09-12-0216-R>.
63. Ye W, Shen C-H, Lin Y, Chen P-J, Xu X, Oelmüller R, et al. Growth promotion-related miRNAs in *Oncidium* orchid roots colonized by the endophytic fungus *Piriformospora indica*. *PLoS One*. 2014;9(1):e84920. <https://doi.org/10.1371/journal.pone.0084920>.
64. Jeong D-H, Schmidt SA, Rymarquis LA, Park S, Ganssmann M, German MA, et al. Parallel analysis of RNA ends enhances global investigation of microRNAs and target RNAs of *Brachypodium distachyon*. *Genome Biol*. 2013;14(12):R145. <https://doi.org/10.1186/gb-2013-14-12-r145>.
65. Šečić E, Kogel KH, Ladera-Carmona MJ. Biotic stress-associated microRNA families in plants. *J Plant Physiol*. 2021;263:153451. <https://doi.org/10.1016/j.jplph.2021.153451>.
66. Morea E, Silva E, Silva G, Valente G, Barrera C, Vincenz M, et al. Functional and evolutionary analyses of the miR156 and miR529 families in land plants. *BMC Plant Biol*. 2016;16:40.
67. Hackenberg M, Shi B-J, Gustafson P, Langridge P. Characterization of phosphorus-regulated miR399 and miR827 and their isomirs in barley under phosphorus-sufficient and phosphorus-deficient conditions. *BMC Plant Biol*. 2013;13(1):214. <https://doi.org/10.1186/1471-2229-13-214>.
68. Baev V, Milev I, Naydenov M, Apostolova E, Minkov G, Minkov I, et al. Implementation of a de novo genome-wide computational approach for updating *Brachypodium* miRNAs. *Genomics*. 2011;97(5):282–93. <https://doi.org/10.1016/j.ygeno.2011.02.008>.
69. Wang B, Sun Y, Song N, Zhao M, Liu R, Feng H, et al. *Puccinia striiformis* f. sp. tritici microRNA-like RNA 1 (Pst-miR1), an important pathogenicity factor of Pst, impairs wheat resistance to Pst by suppressing the wheat pathogenesis-related 2 gene. *New Phytol*. 2017;215(1):338–50. <https://doi.org/10.1111/nph.14577>.
70. Lammers PJ, Jun J, Abubaker J, Arreola R, Gopalan A, Bago B, et al. The glyoxylate cycle in an arbuscular mycorrhizal fungus. Carbon flux and gene expression. *Plant Physiol*. 2001;127(3):1287–98. <https://doi.org/10.1104/pp.010375>.
71. Hynes MJ, Murray SL, Andrianopoulos A, Davis MA. Role of carnitine acetyltransferases in acetyl coenzyme A metabolism in *Aspergillus nidulans*. *Eukaryot Cell*. 2011;10(4):547–55. <https://doi.org/10.1128/EC.00295-10>.
72. Li J, Yu L, Yang J, Dong L, Tian B, Yu Z, et al. New insights into the evolution of subtilisin-like serine protease genes in Pezizomycotina. *BMC Evol Biol*. 2010;10(1):68. <https://doi.org/10.1186/1471-2148-10-68>.
73. Corrales Escobosa AR, Rangel Porras RA, Meza Carmen V, Gonzalez Hernandez GA, Torres Guzman JC, Wrobel K, et al. *Fusarium oxysporum* Adh1 has dual fermentative and oxidative functions and is involved in

- fungus virulence in tomato plants. Fungal Genet Biol. 2011;48(9):886–95. <https://doi.org/10.1016/j.fgb.2011.06.004>.
74. Jiang J, Yun Y, Yang Q, Shim W-B, Wang Z, Ma Z. A type 2C protein phosphatase FgPtc3 is involved in cell wall integrity, lipid metabolism, and virulence in *Fusarium graminearum*. PLoS One. 2011;6(9):e25311. <https://doi.org/10.1371/journal.pone.0025311>.
75. Xiang Q, Rasmussen C, Glass NL. The ham-2 locus, encoding a putative transmembrane protein, is required for hyphal fusion in *Neurospora crassa*. Genetics. 2002;160(1):169–80. <https://doi.org/10.1093/genetics/160.1.169>.
76. Lannoo N, Van Damme EJM. Lectin domains at the frontiers of plant defense. Front Plant Sci. 2014;5:397.
77. Torii KU. Leucine-rich repeat receptor kinases in plants: structure, function, and signal transduction pathways. Int Rev Cytol. 2004;234:1–46. [https://doi.org/10.1016/S0074-7696\(04\)34001-5](https://doi.org/10.1016/S0074-7696(04)34001-5).
78. Mugford ST, Osbourn A. Evolution of serine carboxypeptidase-like acyltransferases in the monocots. Plant Signal Behav. 2010;5(2):193–5. <https://doi.org/10.4161/psb.5.2.11093>.
79. Corréa LGG, Riaño-Pachón DM, Schrago CG, dos Santos RV, Mueller-Roeber B, Vincentz M. The role of bZIP transcription factors in green plant evolution: adaptive features emerging from four founder genes. PLoS One. 2008;3(8):e2944. <https://doi.org/10.1371/journal.pone.0002944>.
80. Hirsch S, Oldroyd GED. GRAS-domain transcription factors that regulate plant development. Plant Signal Behav. 2009;4(8):698–700. <https://doi.org/10.4161/psb.4.8.9176>.
81. Ambawat S, Sharma P, Yadav NR, Yadav RC. MYB transcription factor genes as regulators for plant responses: an overview. Physiol Mol Biol Plants. 2013;19(3):307–21. <https://doi.org/10.1007/s12298-013-0179-1>.
82. Zanini S, Šečić E, Busche T, Galli M, Zheng Y, Kalinowski J, et al. Comparative analysis of transcriptome and sRNAs expression patterns in the *Brachypodium distachyon*-*Magnaporthe oryzae* pathosystems. Int J Mol Sci. 2021;22(2). <https://doi.org/10.3390/ijms22020650>.
83. Šečić E, Kogel KH. Requirements for fungal uptake of dsRNA and gene silencing in RNAi-based crop protection strategies. Curr Opin Biotech. 2021;70:136–42. <https://doi.org/10.1016/j.copbio.2021.04.001>.
84. Murashige T, Skoog F. A revised medium for rapid growth and bio assays with tobacco tissue cultures. Physiol Plant. 1962;15(3):473–97. <https://doi.org/10.1111/j.1399-3054.1962.tb08052.x>.
85. Pontecorvo G, Roper JA, Hemmons LM, Macdonald KD, Bufton AW. The genetics of *Aspergillus nidulans*. Ad Genet. 1953;5:141–238. [https://doi.org/10.1016/S0065-2660\(08\)60408-3](https://doi.org/10.1016/S0065-2660(08)60408-3).
86. Resequencing and genome assembly of *Serendipita indica* (syn. *Piriformospora indica*). European Nucleotide Archive. 2021. <https://www.ebi.ac.uk/ena/browser/view/PRJEB45884>.
87. Wibberg D, Stadler M, Lambert C, Bunk B, Spröer C, Rückert C, et al. High quality genome sequences of thirteen Hypoxylaceae (Ascomycota) strengthen the phylogenetic family backbone and enable the discovery of new taxa. Fungal Divers. 2021;106:7–28.
88. Wibberg D, Andersson L, Tzelepis G, Rupp O, Blom J, Jelonek L, et al. Genome analysis of the sugar beet pathogen *Rhizoctonia solani* AG2-2/IIIB revealed high numbers in secreted proteins and cell wall degrading enzymes. BMC Genomics. 2016;17(1):245. <https://doi.org/10.1186/s12864-016-2561-1>.
89. Koren S, Walenz BP, Berlin K, Miller JR, Bergman NH, Phillippy AM. Canu: scalable and accurate long-read assembly via adaptive k-mer weighting and repeat separation. Genome Res. 2017;27(5):722–36. <https://doi.org/10.1101/gr.215087.116>.
90. Walker BJ, Abeel T, Shea T, Priest M, Abouelliel A, Sakthikumar S, et al. Pilon: an integrated tool for comprehensive microbial variant detection and genome assembly improvement. PLoS One. 2014;9(11):e112963. <https://doi.org/10.1371/journal.pone.0112963>.
91. Li H. Aligning sequence reads, clone sequences and assembly contigs with BWA-MEM. ArXiv. 2013;1303.3997:1–3.
92. Langmead B, Salzberg SL. Fast gapped-read alignment with Bowtie 2. Nat Methods. 2012;9(4):357–9. <https://doi.org/10.1038/nmeth.1923>.
93. Galagan JE, Calvo SE, Borkovich KA, Selker EU, Read ND, Jaffe D, et al. The genome sequence of the filamentous fungus *Neurospora crassa*. Nature. 2003;422(6934):859–68 NC12 genome assembly. 2014. GCA accession number: GCA\_000182925.2 ([https://www.ebi.ac.uk/ena/browser/view/GCA\\_000182925.2](https://www.ebi.ac.uk/ena/browser/view/GCA_000182925.2)).
94. Petersen TN, Brunak S, von Heijne G, Nielsen H. SignalP 4.0: discriminating signal peptides from transmembrane regions. Nat Methods. 2011;8(10):785–6. <https://doi.org/10.1038/nmeth.1701>.
95. Krogh A, Larsson B, von Heijne G, Sonnhammer ELL. Predicting transmembrane protein topology with a hidden markov model: application to complete genomes. J Mol Biol. 2001;305(3):567–80. <https://doi.org/10.1006/jmbi.2000.4315>.
96. Emanuelsson O, Nielsen H, Brunak S, von Heijne G. Predicting subcellular localization of proteins based on their N-terminal amino acid sequence. J Mol Biol. 2000;300(4):1005–16. <https://doi.org/10.1006/jmbi.2000.3903>.
97. Ray P, Chi M-H, Guo Y, Chen C, Adam C, Kuo A, et al. Genome sequence of the plant growth promoting fungus *Serendipita vermifera* subsp. bescii: The First Native Strain from North America. Phytobiomes J. 2018;2(2):62–3 *Serendipita vermifera* ssp. bescii NFPB0129 v1.0. (<https://mycocosm.jgi.doe.gov/Sebbeve1/Sebbeve1.home.html>).
98. Martin F, Aerts A, Ahrén D, Brun A, Danchin EGJ, Duchaussoy F, et al. The genome of *Laccaria bicolor* provides insights into mycorrhizal symbiosis. Nature. 2008;452(7183):88–92 *Laccaria bicolor* v2.0. (<https://mycocosm.jgi.doe.gov/Lacbi2/Lacbi2.home.html>).
99. Blom J, Kreis J, Spänig S, Juhre T, Bertelli C, Ernst C, et al. EDGAR 2.0: an enhanced software platform for comparative gene content analyses. Nucleic Acids Res. 2016;44(W1):W22–8. <https://doi.org/10.1093/nar/gkw255>.
100. mRNA-seq of *Brachypodium distachyon* roots inoculated with *Serendipita indica* (syn. *Piriformospora indica*). ArrayExpress database at EMBL-EBI. 2021. <https://www.ebi.ac.uk/arrayexpress/experiments/E-MTAB-10649>.
101. Andrews S, Krueger F, Segonds-Pichon A, Biggins L, Krueger C, Wingett S. FastQC: a quality control tool for high throughput sequence data. Babraham; 2016. <http://www.bioinformatics.babraham.ac.uk/projects/fastqc> [Accessed 1 Feb 2019].
102. *Brachypodium distachyon* Bd21-3 v1.1 DOE-JGI, <http://phytozome.jgi.doe.gov/>.
103. Kim D, Paggi JM, Park C, Bennett C, Salzberg SL. Graph-based genome alignment and genotyping with HISAT2 and HISAT-genotype. Nat Biotechnol. 2019;37(8):907–15. <https://doi.org/10.1038/s41587-019-0201-4>.
104. Kupfer DM, Drabenstot SD, Buchanan KL, Lai H, Zhu H, Dyer DW, et al. Introns and splicing elements of five diverse fungi. Eukaryot Cell. 2004;3(5):1088–100. <https://doi.org/10.1128/EC.3.5.1088-1100.2004>.
105. Walters B, Lum G, Sablok G, Min XJ. Genome-wide landscape of alternative splicing events in *Brachypodium distachyon*. DNA Res. 2013;20(2):163–71. <https://doi.org/10.1093/dnares/dss041>.
106. Anders S, Pyl PT, Huber W. HTSeq—a Python framework to work with high-throughput sequencing data. Bioinformatics. 2015;31(2):166–9. <https://doi.org/10.1093/bioinformatics/btu638>.
107. Love MI, Huber W, Anders S. Moderated estimation of fold change and dispersion for RNA-seq data with DESeq2. Genome Biol. 2014;15(12):550. <https://doi.org/10.1186/s13059-014-0550-8>.
108. Du Z, Zhou X, Ling Y, Zhang Z, Su Z. agriGO: a GO analysis toolkit for the agricultural community. Nucleic Acids Res. 2010 Jul;38(suppl\_2):W64–70. <https://doi.org/10.1093/nar/gkq310>.
109. Sievert C. Interactive web-based data visualization with R, plotly, and shiny: Chapman and Hall/CRC; 2020. Available from: <https://plotly-r.com>. <https://doi.org/10.1201/9780429447273>.
110. Wickham H. ggplot2: Elegant graphics for data analysis. New York: Springer-Verlag; 2016. Available from: <http://ggplot2.org>.
111. R Core Team. R: A language and environment for statistical computing. Vienna; 2017. Available from: <https://www.r-project.org/>.
112. Götz S, García-Gómez JM, Terol J, Williams TD, Nagaraj SH, Nueda MJ, et al. High-throughput functional annotation and data mining with the Blast2GO suite. Nucleic Acids Res. 2008;36(10):3420–35. <https://doi.org/10.1093/nar/gkn176>.
113. sRNA-seq of *Brachypodium distachyon* roots inoculated with *Serendipita indica* (syn. *Piriformospora indica*). ArrayExpress database at EMBL-EBI. 2021. <https://www.ebi.ac.uk/arrayexpress/experiments/E-MTAB-10650>.
114. Martin M. Cutadapt removes adapter sequences from high-throughput sequencing reads. EMBnetjournal. 2011;17(1):10–12. Next Gener Seq Data Anal - 1014806/ej171200.
115. Langmead B, Trapnell C, Pop M, Salzberg SL. Ultrafast and memory-efficient alignment of short DNA sequences to the human genome. Genome Biol. 2009;10(3):R25. <https://doi.org/10.1186/gb-2009-10-3-r25>.
116. The RNAcentral Consortium, Petrov AI, Kay SJE, Kalvari I, Howe KL, Gray KA, et al. RNAcentral: a comprehensive database of non-coding RNA sequences. Nucleic Acids Res. 2017;45(D1):D128–34. <https://doi.org/10.1093/nar/gkw1008>.
117. Johnson NR, Yeoh JM, Coruh C, Axtell MJ. Improved placement of multi-mapping small RNAs. G3 (Bethesda). 2016;6(7):2103–11.

118. Zanini S, Šečić E, Jelonek L, Kogel KH. A bioinformatics pipeline for the analysis and target prediction of RNA effectors in bidirectional communication during plant–microbe interactions. *Front Plant Sci.* 2018;9. <https://doi.org/10.3389/fpls.2018.01212>.
119. Dai X, Zhao PX. psRNATarget: a plant small RNA target analysis server. *Nucleic Acids Res.* 2011;39(suppl\_2):W155–9. <https://doi.org/10.1093/nar/gkr319>.
120. Chen H, Boutros PC. VennDiagram: a package for the generation of highly-customizable Venn and Euler diagrams in R. *BMC Bioinformatics.* 2011;12(1):35. <https://doi.org/10.1186/1471-2105-12-35>.
121. Livak KJ, Schmittgen TD. Analysis of relative gene expression data using real-time quantitative PCR and the 2<sup>−</sup> $\Delta\Delta$ CT Method. *Methods.* 2001;25(4):402–8. <https://doi.org/10.1006/meth.2001.1262>.
122. Chen C, Ridzon DA, Broomer AJ, Zhou Z, Lee DH, Nguyen JT, et al. Real-time quantification of microRNAs by stem–loop RT–PCR. *Nucleic Acids Res.* 2005;33(20):e179. <https://doi.org/10.1093/nar/gni178>.
123. Kramer MF. Stem-Loop RT-qPCR for miRNAs. *Curr Protoc Mol Biol.* 2011;95:15.10.1.

# Publisher's Note

Springer Nature remains neutral with regard to jurisdictional claims in published maps and institutional affiliations.

**Ready to submit your research? Choose BMC and benefit from:**

- fast, convenient online submission
- thorough peer review by experienced researchers in your field
- rapid publication on acceptance
- support for research data, including large and complex data types
- gold Open Access which fosters wider collaboration and increased citations
- maximum visibility for your research: over 100M website views per year

**At BMC, research is always in progress.**

Learn more [biomedcentral.com/submissions](https://biomedcentral.com/submissions)



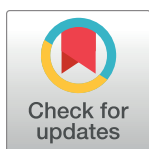
RESEARCH ARTICLE

# *Fusarium graminearum* DICER-like-dependent sRNAs are required for the suppression of host immune genes and full virulence

Bernhard Timo Werner<sup>1</sup>, Aline Koch<sup>2</sup>, Ena Šečić<sup>1</sup>, Jonas Engelhardt<sup>1</sup>, Lukas Jelonek<sup>3</sup>, Jens Steinbrenner<sup>1</sup>, Karl-Heinz Kogel<sup>1\*</sup>

**1** Institute of Phytopathology, Centre for BioSystems, Land Use and Nutrition, Justus Liebig University, Giessen, Germany, **2** Institute for Phytomedicine, University of Hohenheim, Stuttgart, Germany, **3** Institute of Bioinformatics and Systems Biology, Justus Liebig University, Giessen, Germany

\* [Karl-Heinz.Kogel@agr.uni-giessen.de](mailto:Karl-Heinz.Kogel@agr.uni-giessen.de)



## OPEN ACCESS

**Citation:** Werner BT, Koch A, Šečić E, Engelhardt J, Jelonek L, Steinbrenner J, et al. (2021) *Fusarium graminearum* DICER-like-dependent sRNAs are required for the suppression of host immune genes and full virulence. PLoS ONE 16(8): e0252365. <https://doi.org/10.1371/journal.pone.0252365>

**Editor:** Richard A Wilson, University of Nebraska-Lincoln, UNITED STATES

**Received:** May 11, 2021

**Accepted:** July 19, 2021

**Published:** August 5, 2021

**Copyright:** © 2021 Werner et al. This is an open access article distributed under the terms of the [Creative Commons Attribution License](https://creativecommons.org/licenses/by/4.0/), which permits unrestricted use, distribution, and reproduction in any medium, provided the original author and source are credited.

**Data Availability Statement:** Data used in this study are available from the NCBI (Bioproject) repository at accession number: PRJNA749737 (<https://www.ncbi.nlm.nih.gov/bioproject/PRJNA749737>).

**Funding:** This work was supported by the Deutsche Forschungsgemeinschaft ([www.dfg.de](https://www.dfg.de/); Research Unit FOR5116) to KHK. BTW, AK, ES, JE, LJ and JS received no specific funding for this work. The funders had no role in study design, data

## Abstract

In filamentous fungi, gene silencing by RNA interference (RNAi) shapes many biological processes, including pathogenicity. Recently, fungal small RNAs (sRNAs) have been shown to act as effectors that disrupt gene activity in interacting plant hosts, thereby undermining their defence responses. We show here that the devastating mycotoxin-producing ascomycete *Fusarium graminearum* (*Fg*) utilizes DICER-like (DCL)-dependent sRNAs to target defence genes in two Poaceae hosts, barley (*Hordeum vulgare*, *Hv*) and *Brachypodium distachyon* (*Bd*). We identified 104 *Fg*-sRNAs with sequence homology to host genes that were repressed during interactions of *Fg* and *Hv*, while they accumulated in plants infected by the DCL double knock-out (dKO) mutant PH1-*dcl1/2*. The strength of target gene expression correlated with the abundance of the corresponding *Fg*-sRNA. Specifically, the abundance of three tRNA-derived fragments (tRFs) targeting immunity-related *Ethylene overproducer 1-like 1* (*HvEOL1*) and three Poaceae orthologues of *Arabidopsis thaliana* *BRI1-associated receptor kinase 1* (*HvBAK1*, *HvSERK2* and *BdSERK2*) was dependent on fungal DCL. Additionally, RNA-ligase-mediated Rapid Amplification of cDNA Ends (RLM-RACE) identified infection-specific degradation products for the three barley gene transcripts, consistent with the possibility that tRFs contribute to fungal virulence via targeted gene silencing.

## Introduction

RNA interference (RNAi) is a biological process in which small RNA (sRNA) molecules mediate gene silencing at the transcriptional or post-transcriptional level. In agriculture, RNAi-mediated silencing strategies have the potential to protect crops from pests and microbial pathogens [1–5]. Expression of non-coding double-stranded (ds) RNA targeting essential genes in a pest, a pathogen or a virus can render host plants more resistant by a process known as host-induced gene silencing (HIGS) [6–9]. Alternatively, plants can be protected by foliar application of dsRNA to plants [10–16]. While these RNAi-based crop protection strategies are

collection and analysis, decision to publish, or preparation of the manuscript.

**Competing interests:** The authors have declared that no competing interests exist.

proving to be efficient and agronomically practical in the control of insects [17] and viruses [18], many questions remain unanswered with regard to the control of fungi.

The blueprint for using RNA to fight disease comes from nature [7]. During infection of *Arabidopsis thaliana* (*At*), the necrotrophic ascomycete *Botrytis cinerea* (*Bc*) secretes DICER-like (DCL)-dependent sRNAs that are taken up into plant cells to interact with the Arabidopsis ARGONAUTE protein *AtAGO1* and initiate silencing of plant immune genes [19, 20]. For instance, sRNA *Bc-siR3.2* targets mitogen-activated protein kinases, including *MPK2* and *MPK1* in *At*, and *MAPKKK4* in tomato (*Solanum lycopersicum*), while *Bc-siR37* targets several immune-related transcription factors including *WRKY7*, *PMR6* and *FEI2* [21]. Likewise, the oomycete *Hyaloperonospora arabidopsidis* produces 133 AGO1-bound sRNAs, which are crucial for virulence [22], and microRNA-like RNA1 (*Pst-milR1*) from the yellow rust causing biotrophic basidiomycete *Puccinia striiformis* f.sp. *tritici* (*Pst*) reduced expression of the defence gene *Pathogenesis-related 2* (*PR2*) in wheat (*Triticum aestivum*) [23]. Notably, when comparing sRNA in the leaf rust fungus *Puccinia triticina* (*Pt*), 38 *Pt*-sRNAs were homologous to sRNAs previously identified in *Pst* [24, 25], hinting to the possibility that sRNA effectors are conserved among related fungal species as it is known for plant miRNAs [26, 27]. One group of conserved sRNAs with putative effector function are transfer RNA (tRNA)-derived fragments (tRFs). Bacterial tRFs play a role in the symbiotic interaction between soybean (*Glycine max*) and its nitrogen fixing symbiont *Bradyrhizobium japonicum* during root nodulation [28]. Similarly, the protozoan pathogen *Trypanosoma cruzi* secretes tRF-containing microvesicles resulting in gene expression changes in mammalian host cells [29].

Fungal species of the genus *Fusarium* belong to the most devastating pathogens of cereals causing Fusarium head blight and crown rot [30], and contaminate the grain with mycotoxins such as the B group trichothecenes deoxynivalenol (DON), nivalenol (NIV), and their acetylated derivatives (3A-DON, 15A-DON, and 4A-NIV) [31–33]. Viability, aggressiveness, and virulence of Fusaria are under control of the RNAi machinery [8, 34, 35]. In tomato, a *Fol-milR1* produced by *F. oxysporum* f.sp. *lycopersici* (*Fol*) was shown to target the protein kinase *SlyFRG4* via AGO4a [36]. Moreover, in wheat, *Fg-sRNA1* produced by *Fg* targets and silences the pattern recognition receptor gene *TaCEBiP* (*Chitin Elicitor Binding Protein*) [37].

To further test the possibility of *Fg* producing sRNAs that exert effector function and promote pathogenesis, we predicted *Fg*-sRNA targets in two Poaceae hosts, *Hordeum vulgare* (*Hv*) and *Brachypodium distachyon* (*Bd*). Among the many predicted plant targets of fungal sRNA, three fungal tRFs had sequence similarity to *BRI1-associated receptor kinase 1* (*BAK1*) homologs and *EOL1* (*Ethylene overproducer 1-like 1*) in *Hv* and *Bd*. Upon infection with the wild type *Fg* strain, transcripts of genes were strongly reduced, while in contrast they were increased upon infection with *Fg* strains compromised for DCL activity. Degradation products of target mRNAs were detected by RNA-ligase-mediated Rapid Amplification of cDNA Ends (RLM-RACE), supporting the possibility that DCL-dependent sRNAs play a critical role in the interaction of *Fg* with cereal hosts.

## Results

### *Fusarium graminearum* DCL mutants are less virulent on barley and *Brachypodium* leaves

The *Fusarium* mutant IFA65-*dcl1* is partially impaired in infecting wheat ears and causing Fusarium Head Blight [8]. We extended this earlier study to examine the effects of impaired DCL activity on the plant defence response. To this end, two to three-week-old detached second leaves of barley cv. Golden Promise (GP) were drop-inoculated with 3 µl of a solution containing 150,000 conidia per ml of *Fg* isolate PH1 or the double knock-out (dKO) mutant

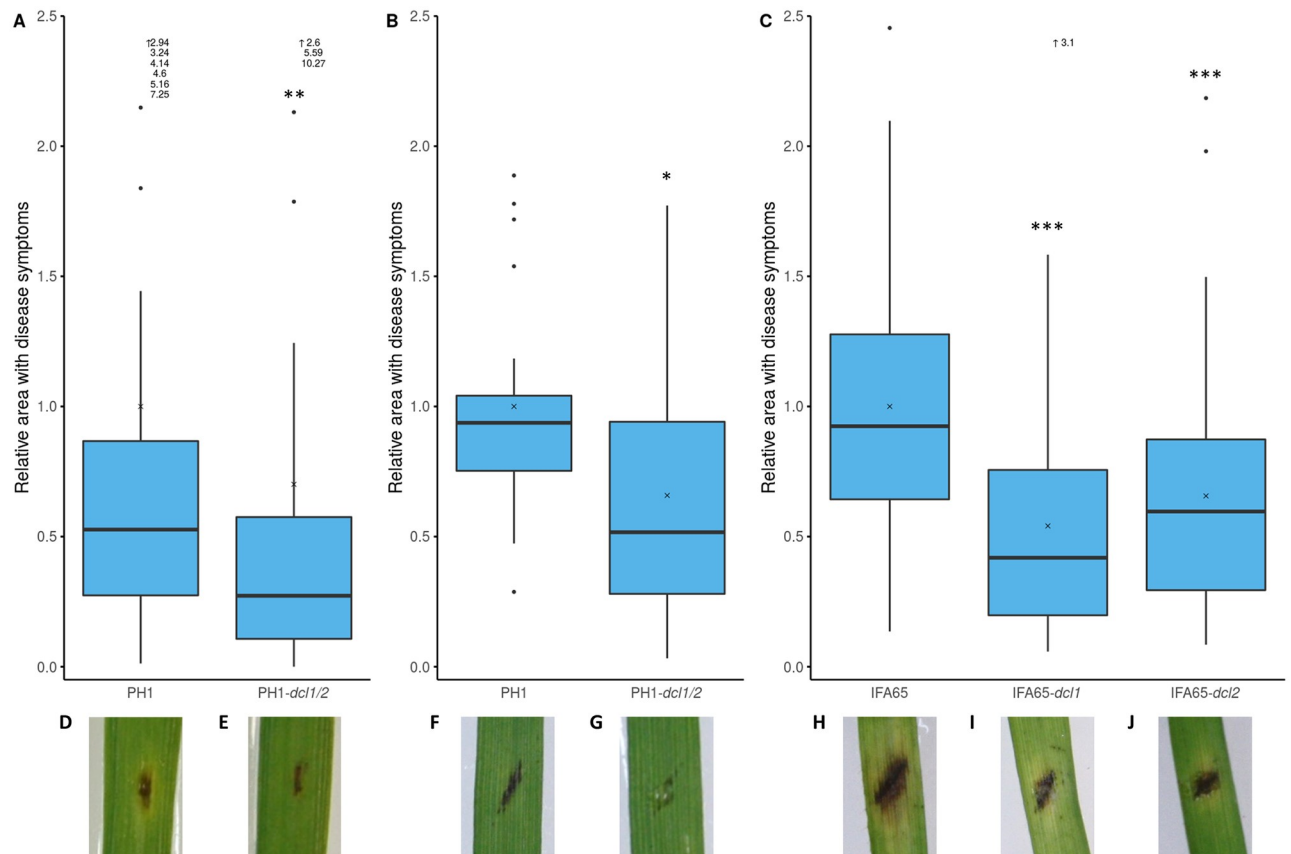


**Fig 1. Virulence of *Fusarium graminearum* DCL single and dKO mutants on barley and *Brachypodium*.** A: Relative infected area on leaves of barley cv. Golden Promise (GP) at 5 dpi. Detached leaves were inoculated with 3  $\mu$ l of a solution containing 150,000 conidia per mL. The area with leaf necrosis was measured with the free image analysis software package PlantCV. Boxplots represent the median and quartiles of three independent biological experiments ( $n = 56$ ). (Wilcoxon Rank Sum Test,  $P = 7.1 \times 10^{-3}$ ,  $x = \text{mean}$ ). B and C: Relative infected leaf area on leaves of *Brachypodium distachyon* Bd21-3 at 4 dpi (B) or 5 dpi (C). Detached leaves were inoculated with 10  $\mu$ l of a solution containing 10,000 conidia per mL. The area with leaf necrosis was measured with ImageJ. Boxplots represent the median and quartiles of three (B) or nine (C) independent biological experiments ( $n = 21$  (B),  $n = 63$  (C)). (B: Wilcoxon Rank Sum Test,  $P = 0.013$ ; C: Pairwise Wilcoxon Rank Sum Test, Bonferroni corrected,  $P_{dcl1} = 4.9 \times 10^{-8}$ ,  $P_{dcl2} = 2.6 \times 10^{-4}$ ;  $x = \text{mean}$ ). Outliers ( $>2.5$ ) are not shown but indicated as written values next to the upward arrow (!). D-J: Representative pictures of disease symptoms of PH1 (D and F), PH1-dcl1/2 (E and G), IFA65 (H), IFA65-dcl1 (I) and IFA65-dcl2 (J) on barley (D and E) and Bd (F-J).

<https://doi.org/10.1371/journal.pone.0252365.g001>

PH1-dcl1/2. At five days post inoculation (dpi), the dKO mutant produced significantly smaller necrotic lesions (30%; median (MED) (27%); interquartile range (IQR) (47%) Wilcoxon rank sum test,  $p = 0.007$ ) than the wild type (wt) strain, confirming that DCL activity is required for full *Fg* virulence (Fig 1A).

Next, we determined the virulence of DCL mutants on *Brachypodium distachyon* Bd21-3. Flag leaves of three-week-old plants were inoculated with 10  $\mu$ l (10,000 conidia  $\text{ml}^{-1}$ ) of fungal inoculum. Single mutants IFA65-dcl1 and IFA65-dcl2 and dKO mutant PH1-dcl1/2 produced significantly smaller lesions than the wt (PH1-dcl1/2, 66%; MED (52%); IQR (66%); Wilcoxon rank sum test;  $p = 0.013$ , IFA65-dcl1, 54%; MED (42%); IQR (56%) and IFA65-dcl2, 66%; MED (60%); IQR (58%); pairwise Wilcoxon rank sum test; Bonferroni corrected;  $p < 0.005$ ) (Fig 1B and 1C). These results substantiate the earlier findings [8] that fungal DCL activity is required for *Fusarium* virulence on graminaceous plants.

## Selection of sRNAs with sequence homology to plant genes

We looked for interaction-related fungal sRNAs that potentially could interfere with plant gene expression by sequence-specific silencing. To this end, a previously published sRNA sequencing data set of *Fg* sRNAs from an axenic IFA65 culture [10] was analysed for sRNAs with sequence complementarity to barley genes. In order to identify a wide range of potential targets, we applied only two selection criteria, namely *i.* size (21–24 nt) and *ii.* a minimal number of reads (at least 400 reads in the dataset). From a total of 35,997,924 raw reads, 5,462,596 (comprising 589,943 unique sequences) had a length of 21–24 nt. From the unique sequences, 1,987 had at least 400 reads. Since the IFA65 genome has not been sequenced, we used the published genome information of *Fg* strain PH1 (genome assembly ASM24013v3 from International Gibberella zeae Genomics Consortium: GCA\_000240135.3) for further analysis. The majority of the 1,987 unique sRNAs mapped to rRNA (64.4%) and intergenic regions (21.6%), while 3.7% and 2.4% mapped to protein coding genes and tRNAs, respectively, and 7.8% did not perfectly match the reference genome (S1 Fig). According to the TAPIR algorithm, the 1,987 sequences overall matched mRNAs of 2,492 genes (*Hordeum vulgare* IBSC PGSB v2 reference genome; [38]) sufficiently close according to the refined target prediction criteria suggested by Srivastava et al. [39]. GO-enrichment analysis revealed an enrichment in functions of nucleotide binding, motor activity and kinase activity and processes such as transport and localization (S2 Fig). Most of the 14,156 transcripts of the 2,492 target genes, which we nominated as potential sRNA targets, showed partially homologous sequences to more than one sRNA accounting for a total of 17,275 unique pairs of potential target gene—sRNA combinations. Target prediction results are presented with only one transcript (splice variant) for every combination (S1 Table). Of note, merely 101 out of the 1,987 sRNAs had no predicted target among the total number of 248,391 plant mRNAs in the IBSC\_PGSB\_v2 annotation.

## Barley immune genes accumulate to higher levels in PH1-dcl1/2-infected leaves

From the set of 2,492 barley genes with partial sequence homology to *Fg* sRNAs, we selected 16 genes for further analysis, based on an educated guess that they are potentially involved in biotic stress reactions during plant-fungal interaction (Table 1). When tested with RT-qPCR, we found eight genes, being targeted by a total of 104 unique *Fg* sRNAs, significantly higher expressed (Student's *t*-test, paired, \**p*<0.1, \*\**p*<0.05, \*\*\**p*<0.01) in leaves infected with PH1-*dcl1/2* vs. PH1 (Fig 2). Among these genes are three that encode proteins involved in the regulation of either ethylene (ET) (Ethylene overproducer 1-like 1, *HvEOL1*) or auxin responses (Auxin response transcription factors *HvARF10* and *HvARF19*) and three kinases, of which Somatic embryogenesis receptor-like kinase 2 (*HvSERK2*) and BRI1-associated receptor kinase 1 (*HvBAK1*) are likely involved in recognition of microbe-associated molecular patterns (MAMPs). Moreover, genes encoding the plastid kinase 2-Phosphoglycolate phosphatase 2 (*HvPGLP2*), Resurrection 1 (*HvRST1*, with a rather elusive function in cuticle formation and embryo development), and the histone-lysine N-methyltransferase Su(var)3-9-related protein 5 (*HvSUVR5*, involved in transcriptional gene silencing) were also strongly expressed.

The first column gives the name of the respective gene abbreviated as in Fig 1 and in full. The second column shows the respective accession. In the third column selected GO terms are shown. The fourth and fifth columns give the accession and abbreviated name of the closest homologue in *At*.

Table 1. Selected GO-terms of tested genes and closest homologs in *A. thaliana*.

Name	ensembl_gene_id	GO_term	<i>A.thaliana</i> Homolog	Abbr.
<i>HvARF3</i>	HORVU1Hr1G076690	auxin-activated signaling pathway	AT2G33860	<i>ARF3</i>
Auxin response transcription factor 3		regulation of transcription, DNA-templated		
		nucleus		
<i>HvSUB1</i>	HORVU2Hr1G028070	Golgi apparatus	AT4G08810	<i>SUB1</i>
Short under blue light 1		transferase activity, transferring glycosyl groups		
		fucose metabolic process		
<i>HvPPR</i>	HORVU2Hr1G078260	protein binding	AT2G06000	
Pentatricopeptide repeat superfamily protein				
<i>HvSERK2</i>	HORVU2Hr1G080020	integral component of membrane	AT1G34210	<i>SERK2</i>
Somatic embryogenesis receptor-like kinase 2_1		positive regulation of innate immune response		
		regulation of defense response to fungus		
<i>HvARF10</i>	HORVU2Hr1G089670	auxin-activated signaling pathway	AT2G28350	<i>ARF10</i>
Auxin response transcription factor 10		regulation of transcription, DNA-templated		
		nucleus		
<i>HvEOL1</i>	HORVU2Hr1G119180	regulation of ethylene biosynthetic process	AT4G02680	<i>EOL1</i>
ETO1-like 1		protein binding		
<i>HvRST1</i>	HORVU3Hr1G016630	integral component of membrane	AT3G27670	<i>RST1</i>
Resurrection 1		membrane		
<i>HvPIX7</i>	HORVU3Hr1G051080	protein serine/threonine kinase activity	AT5G15080	<i>PIX7</i>
Putative interactor of XopAC 7		ATP binding		
		protein kinase activity		
<i>Hvemb2726</i>	HORVU5Hr1G024470	translation elongation factor activity	AT4G29060	<i>emb2726</i>
Embryo defective 2726		mitochondrion		
		intracellular		
<i>HvPGLP2</i>	HORVU5Hr1G052320	chloroplast	AT5G47760	<i>PGLP2</i>
2-Phosphoglycolate phosphatase 2		phosphoglycolate phosphatase activity		
		hydrolase activity		
<i>HvATG2</i>	HORVU6Hr1G034660	autophagy of peroxisome	AT3G19190	<i>ATG2</i>
Autophagy-related 2		autophagy		
<i>HvSUVR5</i>	HORVU6Hr1G069350	histone-lysine N-methyltransferase activity	AT2G23740	<i>SUVR5</i>
Su(var)3-9-related protein 5		chromosome		
		methyltransferase activity		
<i>HvRDR1</i>	HORVU6Hr1G074180	RNA-directed 5'-3' RNA polymerase activity	AT1G14790	<i>RDR1</i>
RNA-dependent RNA polymerase 1		RNA binding		
		gene silencing by RNA		
<i>HvGDH</i>	HORVU6Hr1G076880	glycine decarboxylation via glycine cleavage system	AT2G35370	<i>GDH1</i>
Glycine decarboxylase complex H		glycine cleavage complex		
		mitochondrion		
<i>HvBAK1</i>	HORVU7Hr1G068990	integral component of membrane	AT1G34210	<i>SERK2</i>
Somatic embryogenesis receptor-like kinase 2_2		transmembrane receptor protein serine/threonine kinase signaling pathway		
<i>HvARF19</i>	HORVU7Hr1G096460	auxin-activated signaling pathway		
Auxin response transcription factor 19		regulation of transcription, DNA-templated		
		nucleus		
<i>BdSERK2</i>	BRADI_5g12227v3	integral component of membrane	AT1G34210	<i>SERK2</i>
Somatic embryogenesis receptor-like kinase 2		positive regulation of innate immune response		
		regulation of defense response to fungus		

<https://doi.org/10.1371/journal.pone.0252365.t001>

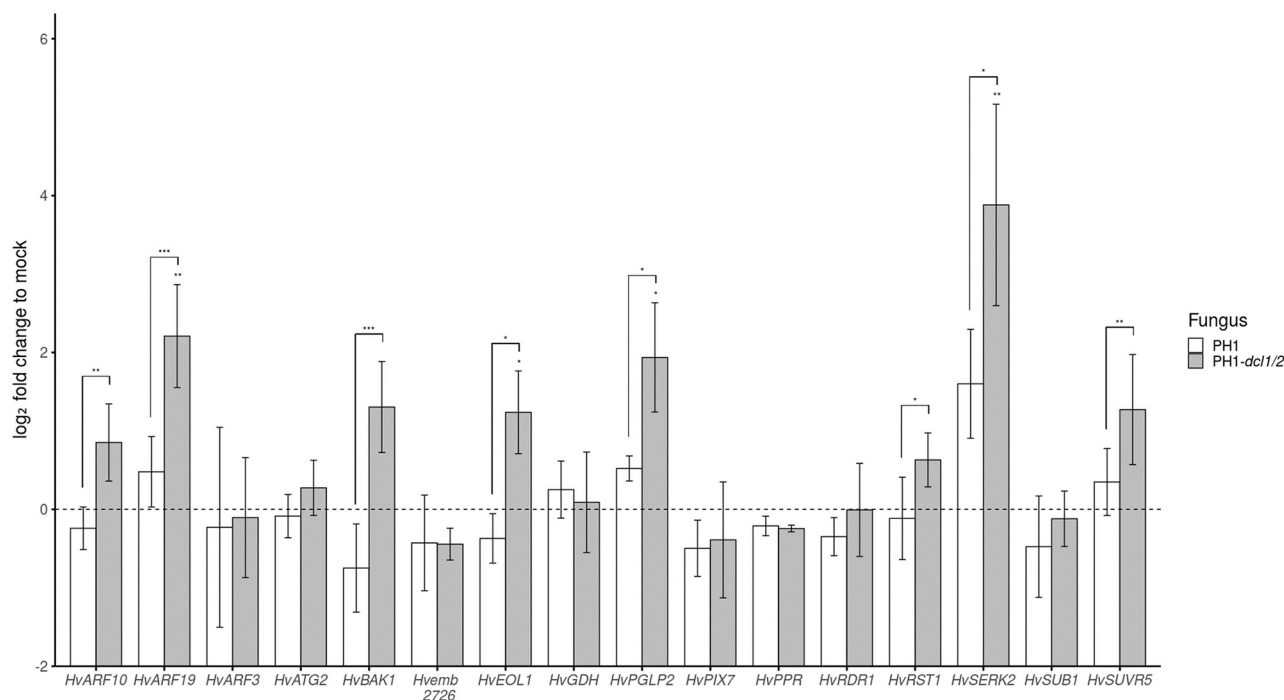


**Fig 2. Relative expression (log2 fold) of potential barley target genes for fungal sRNAs in leaves infected with *Fusarium graminearum* wt strain PH1 vs. PH1-dcl1/2.** Expression was normalized against barley *Ubiquitin* (*HvUBQ*) and subsequently against the  $\Delta$ ct of the uninfected control (mock treatment). Bars represent the mean  $\pm$  SE of three independent biological replicates. Significant differences were calculated for the expression of a respective gene in PH1 vs. PH1-dcl1/2-infected samples and PH1 vs. controls. The dotted line shows the expression level of mock treatment. (Student's *t*-test, (paired) one sided, \**P*<0.1, \*\**P*<0.05, \*\*\**P*<0.01).

<https://doi.org/10.1371/journal.pone.0252365.g002>

### HvEOL1 transcripts also accumulate to higher levels upon DCL knock-down via spray induced gene silencing (SIGS)

We selected *HvEOL1* (*HORVU2Hr1G119180*), which is a homologue of *At Ethylene overproducer1* (*AtETO1*; *AT4GO2680.1*), for further analysis. The alignment of the respective protein sequences of *HvEOL1* and *AtETO1* is shown in [S3 Fig](#). *AtETO1* negatively regulates ethylene synthesis in *At* by ubiquitination of type-2 1-Aminocyclopropane-1-carboxylate synthases (ACSs), which produce the direct precursor of ET [40] ([S4 Fig](#)). Upon inoculation with PH1, *HvEOL1* expression was reduced by 23% as compared to non-inoculated barley leaves. In contrast, *HvEOL1* was strongly expressed in PH1-dcl1/2-infected leaves well above the levels measured either in PH1- or mock-inoculated leaves. To further substantiate that *HvEOL1* expression is under the control of fungal DCL activity, we used a SIGS strategy [10] to partially inactivate DCL function in *Fg*. Two-week-old detached leaves were sprayed with 20 ng  $\mu$ l<sup>-1</sup> of dsRNA-*dcl1/2*, a 1,782 nt long dsRNA derived from the sequences of IFA65-DCL1 and IFA65-DCL2 ([S5A and S5B Fig](#)). 48 h later, leaves were drop inoculated with conidia and harvested at 5 dpi. Consistent with the expectation that exogenous dsRNA-*dcl1/2* mediates silencing of their DCL gene targets, RT-qPCR analysis confirmed that the transcript levels of IFA65-DCL1 and IFA65-DCL2 were reduced to 22% and 42%, respectively, as compared with the Tris-EDTA (TE) buffer control ([Fig 3A](#)). In accordance with the results obtained with strain PH1, *HvEOL1* was also significantly (*p* = 0.029, Student's *t*-test ( $\Delta$ ct), one sided, paired) downregulated in response to IFA65 infection compared to mock controls treated with 0.02% Tween20 ([Fig 3B](#)). In contrast, however, when leaves were sprayed with dsRNA-*dcl1/2* prior to

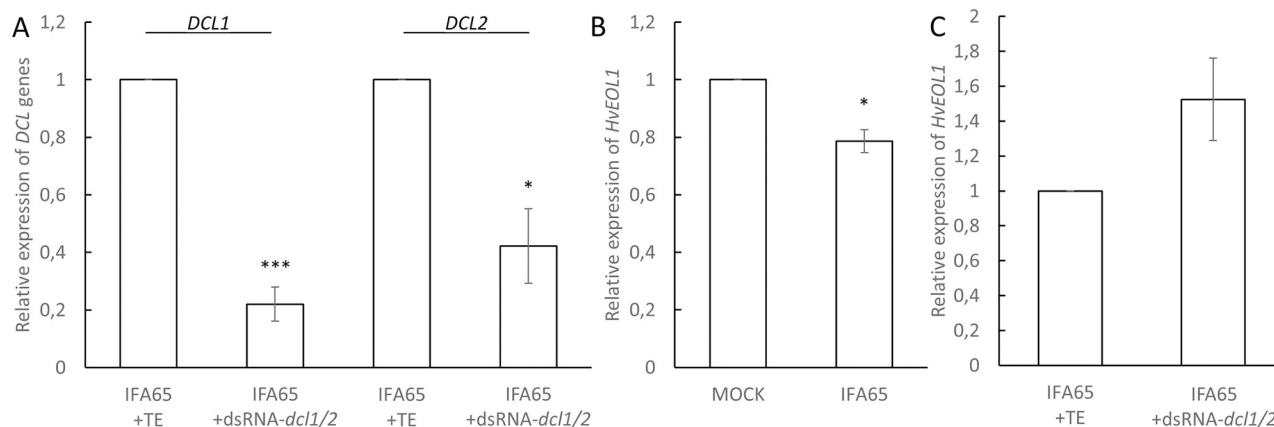


**Fig 3. Relative expression of HvEOL1 in response to inoculation of barley leaves with *Fusarium graminearum*.** A, Relative expression of *FgDCL1* and *FgDCL2* on detached barley cv. Golden Promise leaves at 5 dpi in wt strain IFA65 and 7 days post spray application of the 1,782 nt long dsRNA construct *dsRNA-dcl1/2* vs. TE buffer. B, Relative expression of *HvEOL1* at 5 dpi with IFA65 vs. mock control. C, Relative expression of *HvEOL1* 5 dpi with wt strain IFA65 and 7 days post spray application of *dsRNA-dcl1/2* vs. TE buffer. Gene expression was first normalized against the reference gene *HvUBQ* (*HORVU1Hr1G023660*) and subsequently against the  $\Delta$ ct of the respective control for B (mock = 0.002% Tween20) and for A,C (IFA65 / TE). Bars represent the mean  $\pm$  SE of three (B) and four (A, C) independent biological replicates. (Student's *t*-test, \**P*<0.05, \*\*\**P*<0.005).

<https://doi.org/10.1371/journal.pone.0252365.g003>

inoculation with IFA65, *HvEOL1* transcripts accumulated ( $p = 0.055$ , Student's *t*-test ( $\Delta$ ct), one sided, paired) in comparison with the inoculated leaves sprayed with TE buffer (Fig 3C).

### Fungal sRNAs targeting HvBAK1, HvEOL1, and HvSERK2 mRNAs are less abundant in PH1-dcl1/2 vs. PH1

To detect the abundance of specific *Fg*-sRNAs, originally identified by sequencing of axenic IFA65 mycelium, in PH1-infected plant tissue, we performed reverse transcription stem-loop qPCR [41]. From the above defined pool of 1,987 *Fg*-sRNAs (axenic, 21–24 nt length,  $> 400$  reads) 22 unique sRNAs matched partial sequences of *HvEOL1*, 10 matched *HvBAK1* and five matched *HvSERK2*. *Fg*-sRNA-1921 matched all three genes and *Fg*-sRNA-321 matched both *HvEOL1* and *HvBAK1* (Table 2 and S2 Table). These two sRNAs show high sequence similarities among each other. To identify their origin, they were aligned to the genomic sequence of strain PH1 (GCA\_900044135.1). We found that they match the gene *Fg\_CS3005\_tRNA-Gly-GCC-1-9* encoding tRNA-Gly for the anticodon GCC. Of note, a larger cluster of 27 overlapping tRNA-derived fragments (tRFs) with more than 50 reads matching the tRNA-Gly gene sequence were detected (S6 Fig). To assess differential accumulation of tRFs from the *Fg\_CS3005\_tRNA-Gly-GCC-1-9* cluster in leaves infected with PH1 vs. PH1-*dcl1/2*, sRNAs were reverse transcribed using hairpin-priming followed by qPCR amplification [41]. For this analysis, we chose *Fg*-sRNA-321, the most abundant tRF from this cluster, along with *Fg*-sRNA-1921, which targets all three GOIs and an additional tRF (*Fg*-sRNA-6717), which targets *HvEOL1* and *HvBAK1* (see Table 2) to assess the sensitivity of the assay. In the initial IFA65 dataset the *Fg*-sRNA-321 had a read count of 2,106, *Fg*-sRNA-1921 had 416 and *Fg*-sRNA-6717 had 86 from a total of more than 5 million reads (S7 Fig). This equals 386 reads per million (rpm) for *Fg*-sRNA-321, while in average unique reads had only 1.7 rpm. Using TAPIR [42], we also calculated the target score values for all three tRFs, which is a measure for the similarity between sRNA and target. A high value refers to more dissimilarities. Mismatches (MMs) increase the score by one point and G-U pairs by 0.5 points. These values are doubled if the respective MMs and G-U pairs are located between the second and 12<sup>th</sup> nt of the sRNA

Table 2. Target prediction results of Fg-sRNAs with more than 400 reads in IFA65 axenic culture.

sRNA-Name	Reads	Score	Alignment			Length
Fg-sRNA-321	2106	4.5	3'	GCUUGGGUCCCGAGGGGCUACC	5'	22
				.. .o       o		
HvEOL1			5'	GAAUUCAGGGCUCGGUGG	3'	
Fg-sRNA-1921	416	3.5	3'	CUUGGGUCCCGAGGGGCUACC	5'	21
				.. .o       o		
HvEOL1			5'	AAUUCAGGGCUCGGUGG	3'	
Fg-sRNA-6717	86	4.5	3'	UAGCUUGGGUCCCGAGGGGCUAC	5'	23
				.. .o       o		
HvEOL1			5'	AUGAAUUCAGGGCUCGGUG	3'	
Fg-sRNA-1921	416	6	3'	CUUGGGUCCCGAGGGGCUACC	5'	21
				.. .o       o		
HvSERK2			5'	GCACGAGGGGUCACGAUGG	3'	
Fg-sRNA-321	2106	4.5	3'	GCUUGGGUCCCGAGGGGCUACC	5'	22
				o .  .. .o       o		
HvBAK1			5'	UGCACACAGGGCUCGGUGG	3'	
Fg-sRNA-1921	416	4	3'	CUUGGGUCCCGAGGGGCUACC	5'	21
				.. .o       o		
HvBAK1			5'	GCACACAGGGCUCGGUGG	3'	
Fg-sRNA-6717	86	5.5	3'	UAGCUUGGGUCCCGAGGGGCUAC	5'	23
				.. .o .  .. .o       o		
HvBAK1			5'	UUUGCACACAGGGCUCGGUG	3'	
Fg-sRNA-321	2106	5.5	3'	GCUUGGGUCCCGAGGGGCUACC	5'	22
				.. .o       o   o		
BdEOL1			5'	GAAUUCAGGGCUCGGUGG	3'	
Fg-sRNA-1921	416	4.5	3'	CUUGGGUCCCGAGGGGCUACC	5'	21
				.. .o       o   o		
BdEOL1			5'	AAUUCAGGGCUCGGUGG	3'	
Fg-sRNA-6717	86	5.5	3'	UAGCUUGGGUCCCGAGGGGCUAC	5'	23
				.. .o       o   o		
BEOL1			5'	AUGAAUUCAGGGCUCGGUG	3'	
Fg-sRNA-321	2106	3.5	3'	GCUUGGGUCCCGAGGGGCUACC	5'	22
				o .  .. .o       o		
BdSERK2			5'	UGCACGAAGGCUCGGUGG	3'	
Fg-sRNA-1921	416	3	3'	CUUGGGUCCCGAGGGGCUACC	5'	21
				.. .o       o		
BdSERK2			5'	GCACGAAGGCUCGGUGG	3'	
Fg-sRNA-6717	86	5.5	3'	UAGCUUGGGUCCCGAGGGGCUAC	5'	23
				..o .  .. .o       o		
BdSERK2			5'	UCUGCACGAAGGCUCGGUG	3'	

Mismatches (MMs) between mRNA and sRNA are marked as “.”, while G-U pairs are marked as “o”.

<https://doi.org/10.1371/journal.pone.0252365.t002>

(5'-3') because a high similarity in the seed region of the sRNA is especially important for RNAi [43]. Fg-sRNA-321 has a score of 4.5 for *HvBAK1* and *HvEOL1*, Fg-sRNA-1921 has a score of 4, 3.5 and 6 for *HvBAK1*, *HvEOL1* and *HvSERK2*, respectively and Fg-sRNA-6717 has a score of 5.5 and 4.5 with *HvBAK1* and *HvEOL1*. In plants other than Arabidopsis, such as

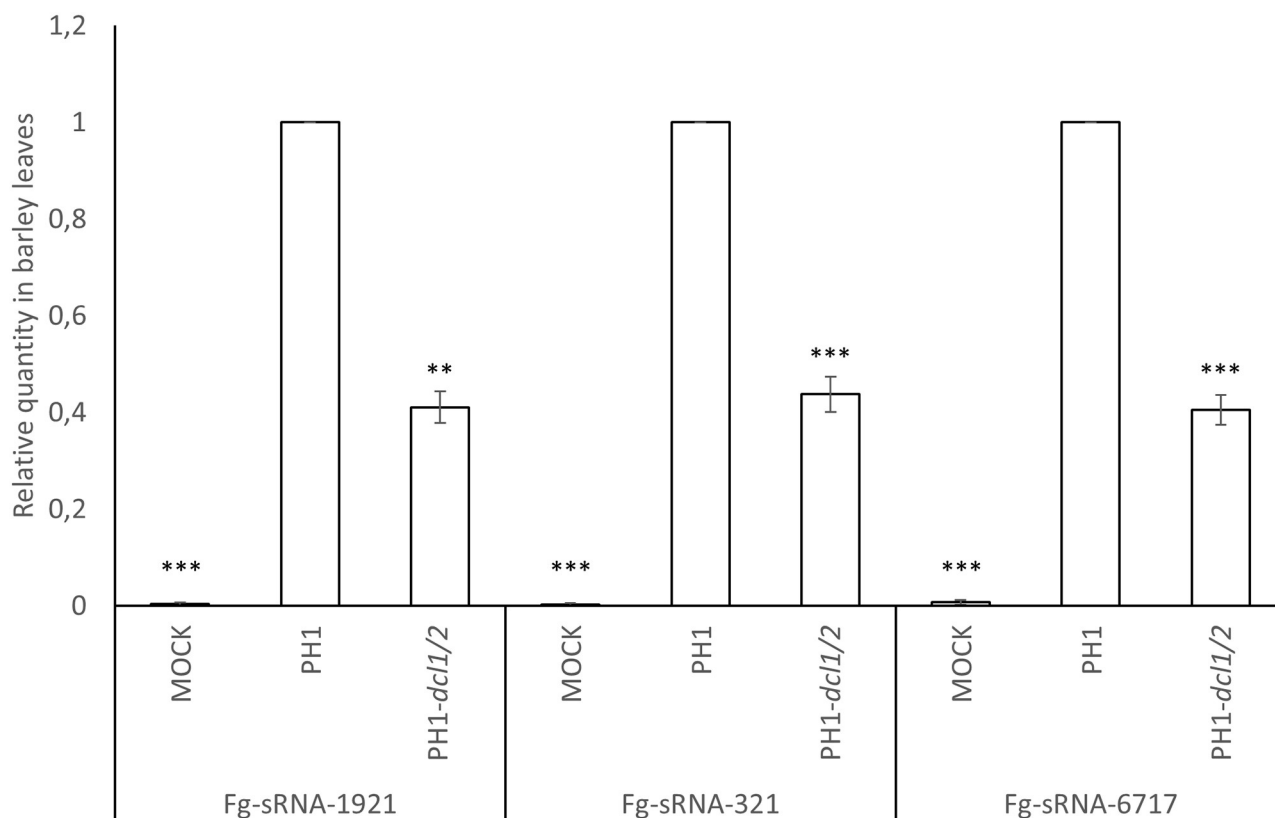


**Fig 4. Relative amount of different fungal tRFs with homology to *HvEOL1* mRNA.** Relative amount of different fungal tRFs with homology to *HvEOL1* mRNA during infection of barley leaves with PH1 and PH1-*dcl1/2* normalized to fungal biomass and relative quantity of sRNAs normalized to wt PH1 measured by qPCR. Fg-sRNA-1921, Fg-sRNA-321 and Fg-sRNA-6717 quantity was normalized to *Hvu-miR159* and *Hvu-miR168* and fungal biomass as determined by *FgEF1a* expression was normalized to *HvUBQ*. Subsequently the amount of sRNAs was normalized with fungal biomass. The amount of sRNA in PH1-infected leaves was set to 1. Values and error bars represent the mean  $\pm$  SE of three independent biological replicates. Significance was calculated via a one-sample *t*-test. (\*\* $P < 0.01$ , \*\*\* $P < 0.005$ ).

<https://doi.org/10.1371/journal.pone.0252365.g004>

wheat and rice, a score cut off at 4 or 6 points lead to a precision of 82% or 62% and a recall of known interactions of 39% or 58% respectively according to Srivastava et al. [39].

All three fungal tRFs were detected in infected leaves, while they could not be found in uninfected leaves (Fig 4). Significantly lower amounts of Fg-sRNA-1921 (59%), Fg-sRNA-321 (56%), and Fg-sRNA-6717 (60%) were detected in PH1-*dcl1/2* vs. PH1-infected leaves (Fig 4), showing that their biogenesis is DCL-dependent.

### **Fg-sRNA-321 and Fg-sRNA-1921 also match *SERK2* in *Brachypodium distachyon* Bd21-3**

Next, we assessed the possibility that Fg-sRNA-321, Fg-sRNA-1921 and Fg-sRNA-6717 also have sequence homologies in *At* and the model grass *Bd*. Target prediction with the TAPIR algorithm using the optimised parameters for *At* (score = 4; mfe = 0.7), could not detect potential targets in *At* ecotype Col-0. In contrast, these three tRFs matched the sequence of *Brachypodium somatic embryogenesis receptor-like kinase 2* (*BdSERK2*) in Bd21-3 with a score of 3.5, 3 and 5.5, respectively (Table 2). We examined the expression pattern of *BdSERK2* in response to leaf infection: *BdSERK2* is relatively weakly expressed in uninfected plants and is not further suppressed after inoculation with PH1, whereas it strongly accumulated in PH1-*dcl1/2* vs.

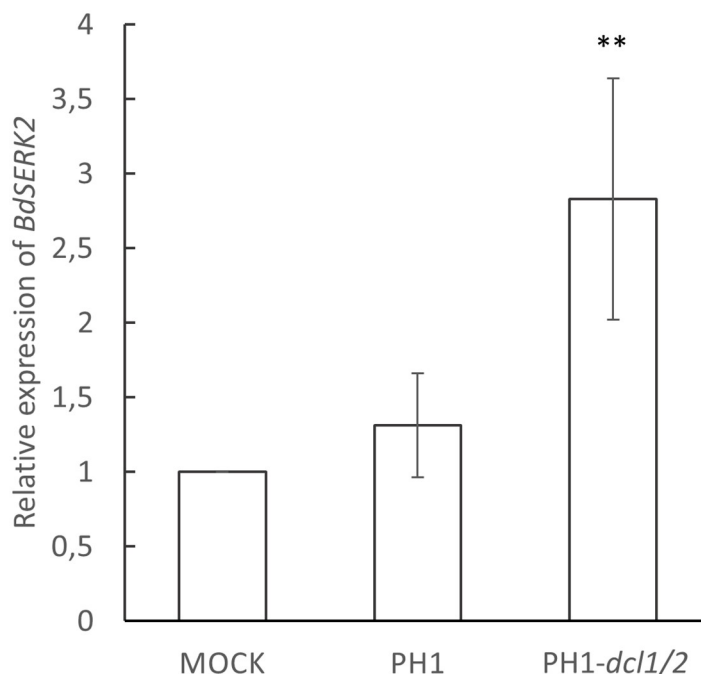


**Fig 5. Relative expression of *BdSERK2* in response to inoculation of *Brachypodium distachyon* leaves with *Fusarium graminearum*.** Relative expression of *BdSERK2* in detached Bd21-3 leaves at 4 dpi with PH1 vs. PH1-*dcl1/2*. The gene expression was first normalized against the reference gene *BdUBI4* and subsequently against the  $\Delta$ ct of the mock treated control. Values and error bars represent the mean  $\pm$  SE of three independent biological replicates. (Student's t-test, paired, one sided, \*\* $P < 0.01$ ).

<https://doi.org/10.1371/journal.pone.0252365.g005>

PH1-infected Bd21-3 (Fig 5). This finding further supports the possibility that the control of *SERK2* expression via RNAi pathways by *Fg* is evolutionary conserved in cereals.

### RLM-RACE shows infection specific degradation products of *HvBAK1*, *HvEOL1* and *HvSERK2*

We assessed the sRNA-mediated cleavage of *HvBAK1*, *HvEOL1*, and *HvSERK2* mRNAs, using a modified RNA-ligase-mediated Rapid Amplification of cDNA Ends (RLM-RACE) assay. Control samples were prepared both from uninfected tissue and from infected tissue without the reverse transcription step (no-RT control) and PCR products were visualized on an EtBr-Agarose gel. In these no-RT controls no amplification was visible.

For each gene more than one infection-specific product was amplified (blue and red arrows), which could not be amplified from the uninfected sample (Fig 6D–6F). We excised three bands (red arrows) of the expected size for a *Fg*-sRNA-1921 guided cleavage of *HvBAK1* (Fig 6D) and one band for *HvEOL1* (Fig 6E) and *HvSERK2* (Fig 6F) and cloned them into the pGEM-T easy vector system. According to the IBSC\_PGSEB\_v2 assembly, *HvBAK1* has splice variants, which could produce cleavage products of different lengths while for *HvSERK2* and *HvEOL1* there are no introns between sRNA target site and primer. From each band, five colonies were picked and for 23 of these extracted plasmids sequences were obtained. 16 sequences perfectly matched the reference genome, four with one MM and one with four MMs. Two sequences did not match the reference sufficiently enough to be aligned over the full length. The observed cleavage products are close to but do not match the canonical slice site between the 10<sup>th</sup> and 11<sup>th</sup> nt of *Fg*-sRNA-1921 and *Fg*-sRNA-321 (Fig 6A–6C).

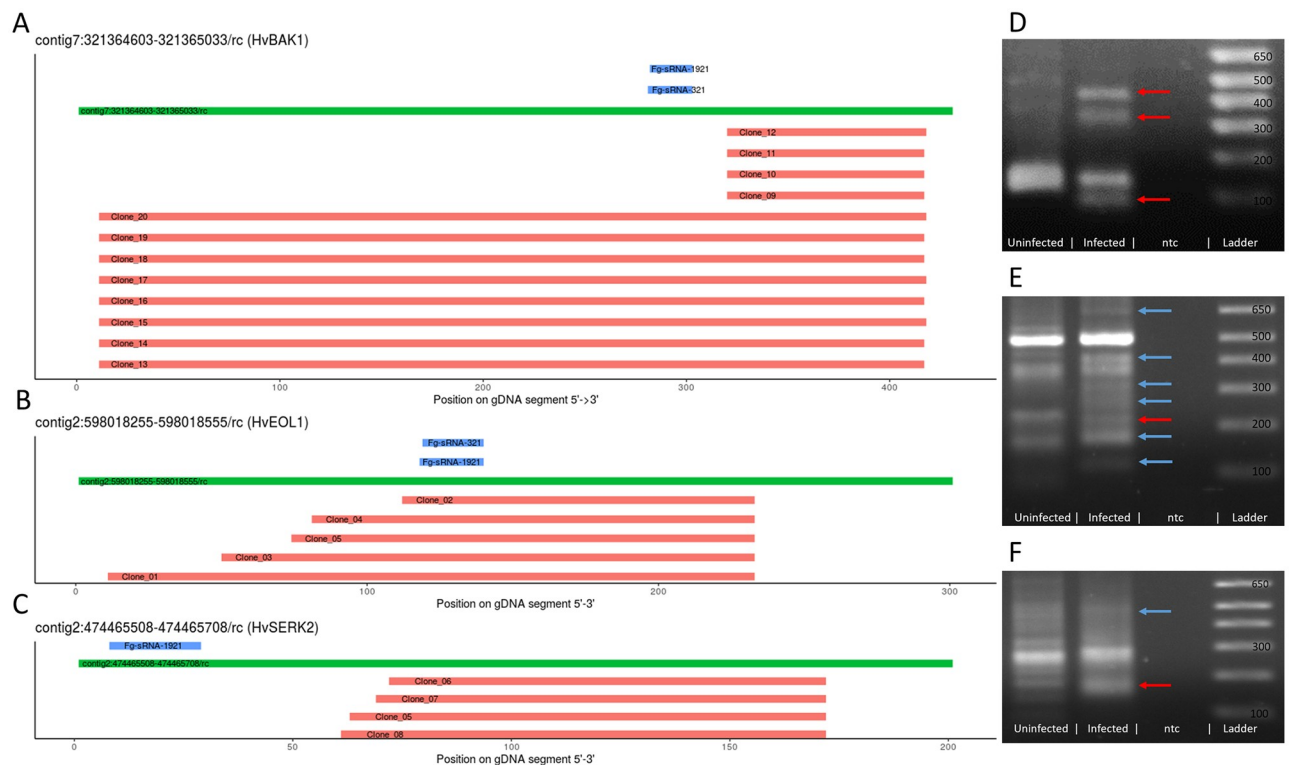


**Fig 6. Analysis of potential target sites of *Fg*-sRNAs as determined by RLM-RACE products.** A,B,C Potential target sites of *Fg*-sRNA-321 and *Fg*-sRNA-1921 predicted by TAPIR (blue), genomic DNA (GPv1, GCA\_902500625.1, A: contig7:321364603–321365033, B: contig2:598018255–598018555, C: contig2:474465508–474465708) of barley cv. Golden Promise (green), and the alignment of sequences derived from the RLM-RACE PCR (red) relative to the *Hv*-gDNA and *Fg*-sRNAs. D,E,F PCR-products of the second nested RLM-RACE-PCR visualized in an EtBr-Agarose gel. Red arrows indicate excised bands and blue arrows indicate infection specific products.

<https://doi.org/10.1371/journal.pone.0252365.g006>

## Total sRNAs predicted to target a gene in barley are correlated with the de-repression strength

Not all potential targets of *Fg*-sRNAs are downregulated nor do all potential targets show a re-accumulation upon infection with PH1-*dcl1/2* (see Fig 3). To address this bias we conducted a more focused target prediction exclusively for the 16 genes already tested by RT-qPCR. This allowed a much more thorough search, where targets for all sRNAs with at least two reads were predicted. From these 136,825 unique sRNAs (axenic, 21–24 nt length,  $\geq 2$  reads) representing 4,997,312 reads of the total of 5,439,472 reads 21–24 nt in length, 5,052 have potential target sequences in the 16 mRNA sequences selected for further investigation in the *Hordeum vulgare* cv. GP assembly GCA\_902500625. An additional filter step was employed to select for sRNAs with a maximum of one MM to the PH1 assemblies GCA\_000240135.3 and GCA\_900044135.1. Subsequently, sRNAs with up to one MM to *Fg*-rRNAs were removed leaving a total of 1,212 sRNAs with 1,311 potential sRNA-mRNA interactions representing 85,531 reads in the analysis.

To establish a correlation of the observed resurgence of potential target genes and targeting sRNAs, we analysed the DCL-dependent expression change using  $\Delta\Delta\text{Act}$  values. To compare the expression of a GOI in two samples, the difference between the ct-values for a reference gene and the GOI can be determined ( $\Delta\text{ct}$ ) and to calculate the expression difference between the control and treated sample the difference between the  $\Delta\text{ct}$  values ( $\Delta\Delta\text{ct}$ ) is calculated. We

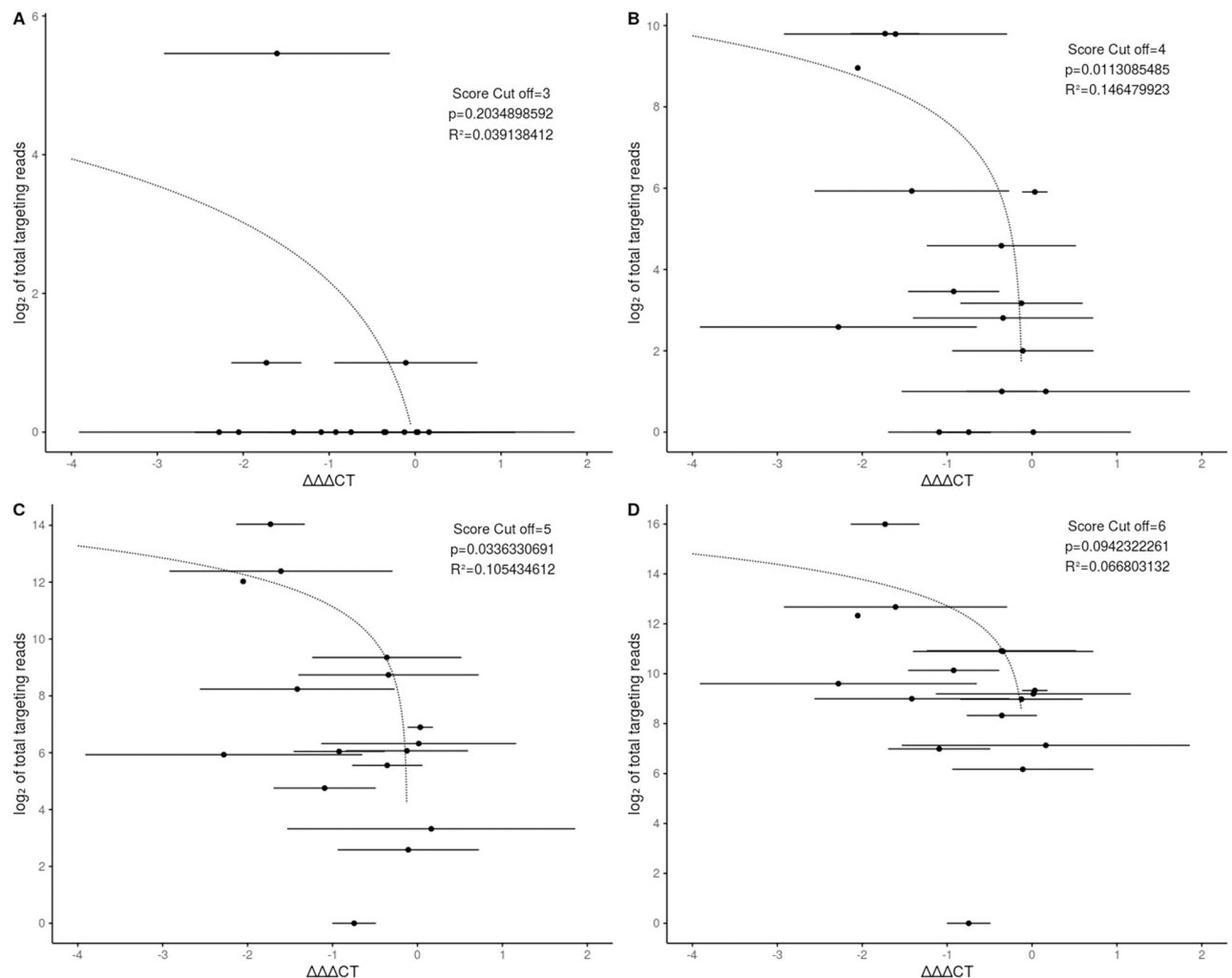


**Fig 7. The degree of DCL-dependent gene silencing is correlated with the number of homologous fungal sRNAs.** Each dot represents a predicted target gene of *Fg*-sRNAs. On the x-axis the  $\Delta\Delta\Delta\text{CT}$ -value is shown with bars representing SD. On the y-axis the  $\log_2$  of the number of total sRNAs potentially targeting each gene are shown. The dotted line represents a linear regression model. P indicates the significance (t-test) of the model and the score cut-off indicates the score limit used during the target prediction. Plot A, B, C and D are the calculations for a score cut off of 3, 4, 5 and 6 respectively.

<https://doi.org/10.1371/journal.pone.0252365.g007>

further defined the  $\Delta\Delta\Delta\text{CT}$  value as the difference between the  $\Delta\Delta\text{CT}$  values for a GOI in PH1 and PH1-*dcl1/2*-infected samples. From this follows a gene with a negative  $\Delta\Delta\Delta\text{CT}$  value shows a higher transcript accumulation during the infection with a fungal strain with compromised DCL function and the stronger the accumulation the lower this  $\Delta\Delta\Delta\text{CT}$  value is. We found a negative correlation between the  $\Delta\Delta\Delta\text{CT}$  value and the number of total sRNAs targeting a GOI (Fig 7). This correlation becomes more significant if a lower score cut-off for the target prediction is chosen until the cut-off of four. The most significant correlation is for all predicted interactions with a score equal or below four with a p-value of 0.011 (t-test) (Fig 7B). The p-value for a correlation with a cut-off of five (Fig 7C) is 0.033 (t-test) and six (Fig 7D) is 0.094 (t-test), while a score cut-off of 3 leads to a situation, where there are no predicted sRNA interactions for all genes except for three (Fig 7A).

## Discussion

We show here that full virulence of the ascomycete fungus *Fusarium graminearum* on graminaceous leaves depends on the activity of fungal DCLs. The dKO mutant PH1-*dcl1/2* is less virulent on barley and the two single KO mutants IFA65-*dcl1* and IFA65-*dcl2* also are less virulent on *Brachypodium*. These results are consistent with our previous studies showing that knock-down or SIGS-mediated silencing of *Fusarium* DCLs and other components of the RNAi machinery reduced the virulence of the fungus on barley [8, 44]. DCL enzymes are key components of the fungal RNAi machinery required for the biogenesis of sRNAs directing silencing of sequence-complementary endogenous and foreign genes [45]. The latter case involves DCL-dependent pathogen-derived sRNAs that target plant defense genes to increase virulence as shown for *Botrytis cinerea* [19, 21], *Puccinia striiformis* [23] and *Magnaporthe oryzae* [46].

In the present work we found potential host target genes for fungal small RNAs (Fg-sRNAs) that were differentially regulated in response to plant infection with Fg wt vs. Fg DCL KO mutants, and the same effect was confirmed when DCLs were silenced by SIGS. This suggests a scenario in which impaired DCL function resulting in reduced fungal RNAi activity ultimately leads to de-repression of host target genes. Of note, target gene de-repression was also observed when the transcript was not significantly downregulated by the wt fungus during infection. This could be explained by a mutually neutralizing effect in which Fg-sRNAs continuously target genes for silencing, while concurrent plant immune responses are a trigger for up-regulation. Thus, one can speculate that these described effects reflect an abrogation of host-favouring upregulation by host immunity vs. pathogen-favouring downregulation by sRNA effectors.

We identified three tRFs predicted to target *BdSERK2*, *HvBAK1*, *HvEOL1* and *HvSERK2*. Unexpectedly, these tRFs are partially DCL-dependent, with a reduced abundance by more than 50% during infections with the dKO mutant PH1-*dcl1/2* vs. wt PH1 based on fungal biomass. Current knowledge of tRFs in fungi and oomycetes suggests that their silencing activity is independent of DCL, as shown for *Sclerotinia sclerotiorum* [47] and *Phytophthora infestans*, where the production is partially dependent on AGO [48]. Furthermore, analysis of tRFs in *Cryptococcus* spp. revealed a RNAi-independent generation of tRFs and possible compensatory effects in an RNAi-deficient genotype [49]. Interestingly however, the tRFs Fg-sRNA-321, Fg-sRNA-1921 and Fg-sRNA-6717 are neither 5'- or 3' tRNA halves nor do they belong to any of the described tRF-1, tRF-2, tRF-4 or tRF-5 classes [50] applied by the tRFtarget database for animals, yeast (*Schizosaccharomyces pombe*) and the bacterium *Rhodobacter sphaeroides* [51]. When following the classification of the tsRBase used for all eukaryotic kingdoms and bacteria [52], the three tRFs are classified as internal tRFs based on the origin within the mature tRNA. Interestingly, there are tRFs found in *Phytophthora sojae* starting in the anticodon loop and ending in the T loop of mature tRNAs [53], which resembles the Fg-sRNA tRFs (S8 Fig).

We observed several infection-specific degradation products of the predicted host target genes *HvBAK1*, *HvEOL1* and *HvSERK2* for tRFs Fg-sRNA-321, Fg-sRNA-1921 and Fg-sRNA-6717. However, cleavage occurred outside the canonical miRNA cleavage site as defined by Mallory et al. [43], though these genes are partially silenced during infection and silencing is apparently abolished upon infection with the DCL dKO mutant. While the canonical cleavage site for miRNA-directed cleavage in *At* is well defined, the tRF-directed cleavage observed by 5' RACE of transposable elements in *At* [54] and of defence-related genes during the infection of black pepper (*Piper nigrum*) with *Phytophthora capsici* [55] was found outside of the canonical cleavage site. Additionally, the identification of sRNA-directed cleavage sites in barley often leads to divergent findings. Ferdous et al. [56] predicted ~400 target genes for 11

presumably drought responsive miRNAs and found cleavage products for 15 targets overlapping the respective miRNAs alignment through degradome sequencing in the two barley cultivars Golden Promise (GP) and Pallas. From these confirmed targets, 13 were cleaved at the canonical 10<sup>th</sup>-11<sup>th</sup> nt site, one was cleaved at 19<sup>th</sup>-20<sup>th</sup> nt, and one at the 5<sup>th</sup>-6<sup>th</sup> nt. Hackenberg et al. [57] predicted 97 target genes of drought responsive miRNAs in GP and identified eight targets through degradome sequencing, which were all cleaved outside of the 10<sup>th</sup>-11<sup>th</sup> nt site. Thus, both studies suggest the presence of non-canonical miRNA directed cleavage. Of note, both studies relied on the same degradome sequencing dataset from GP, while Ferdous et al. also observed non-canonical cleavage in an independent Pallas dataset. Moreover, in a study performed by Curaba et al. [58] 96 target genes of GP for miRNAs involved in seed development and germination were identified by degradome sequencing and only 16 targets were cleaved exclusively at the 10<sup>th</sup>-11<sup>th</sup> nt site, while the other targets were sporadically cleaved with an offset (24) and 56 were cleaved in majority in a non-canonical site. Finally, Deng et al. [59] identify in the barley cultivar Morex 65 target genes of 39 miRNAs, and for only 32% of the identified targets the canonical 10<sup>th</sup>-11<sup>th</sup> nt cleavage product was the major degradome product. Together these studies highlight the challenges in the identification of cleavage sites of sRNAs in barley and cleavage sites of tRFs in plants. The absence of canonical cleavage products for tRFs does therefore not exclude the tRF-directed cleavage of *HvBAK1*, *HvEOL1* and *HvSERK2*.

We found that 22 *Fg*-sRNAs target *HvEOL1*, a putative negative regulator of ET biosynthesis in barley. In *Arabidopsis thaliana* the EOL1 homolog *AtETO1* acts together with *AtEOL1* and *AtETO1-like 2* (EOL2) in directing the ubiquitination and subsequent degradation of type-2 1-aminocyclopropane-1-carboxylate synthase (ACS) proteins (e.g. ET overproducer 2 (ETO2)) [40, 60]. ET is a gaseous plant hormone that plays an important role in regulating plant growth and development, and is critical for pathogen interaction and abiotic stresses [61]. Generally, ET acts synergistically with jasmonate (JA) in the defence response against necrotrophic pathogens and this ET/JA response has antagonistic effects on salicylic acid (SA) signalling against biotrophic pathogens. Yet in low amounts JA and SA act synergistically [62, 63]. Therefore, controlling both ET biosynthesis and ET signalling is crucial for plants. Towards this, plants have evolved complex mechanisms that allow tight regulation of ET pathways e.g. at the level of (i) ET production mainly by regulating ACS gene family members, (ii) ET perception through constitutive triple response 1 (CTR1)-mediated inhibition of positive regulator ET insensitive 2 (EIN2) [64, 65], and (iii) expression of ET-responsive TFs (e.g. ET response factor 1 (ERF1)) via EBF-mediated degradation of ET insensitive 3 (EIN3) [66] (S4 Fig). According to the anticipated role of ET in the plant response to necrotrophic pathogens, such as *Fg*, targeting negative regulators of ET synthesis such as *HvEOL1* would be detrimental to *Fg* colonization. Of note, our findings are consistent with previous results demonstrating that *Fg* exploits ET signalling to enhance colonization of *Arabidopsis*, wheat and barley [67], supposedly through an increase in DON-induced cell death through ET. These findings further challenge the role of ET in defence against necrotrophic pathogens. Strikingly, the authors showed that in *Arabidopsis* ET overproducing mutants (ETO1 and ETO2) and a negative regulator of ET signalling (CTR1) are more susceptible to *Fg*, while *At* mutants in ET perception (ETR1) and signalling (EIN2 and EIN3) are resistant. These findings were confirmed by the direct application of ET during the infection of wheat and barley, which lead to increased susceptibility to *Fg*. Based on these findings, we suggest that negative regulators of ET are efficient targets for sRNA-directed manipulation of host immunity by *Fg*.

The bacterial pathogen *Pseudomonas syringae* secretes two effector molecules, AvrPto and AvrPtoB, into host plants. These effectors interact with the receptor-like kinase BRI1-associated receptor kinase 1 (BAK1), also known as SERK3, thereby preventing the recognition of

various MAMPs through the association of BAK1 with pattern recognition receptors (PRRs) such as flagellin-sensitive 2 (FLS2) and Ef-Tu receptor (EFR) [68]. We observed *FgDCL*-dependent silencing of the cereal BAK1 homologs *HvBAK1*, *HvSERK2* and *BdSERK2*. While these genes have a higher similarity to *AtSERK2* than to *AtSERK3* (*AtBAK1*), they still are among the closest homologs to *AtBAK1* found in cereals (S9 Fig). It is tempting to speculate that further experiments will uncover additional hubs that are targeted both by protein and sRNA effectors.

## Conclusion

Our data show that in the necrotrophic ascomycete *Fusarium graminearum* gene silencing by RNAi shapes its ability to cause disease, which is consistent with earlier results on the significance of the RNAi machinery in *Fg* [8, 35]. Pathogenicity relies on DICER-like (DCL)-dependent sRNAs that were identified as potential candidates for fungal effectors targeting defence genes in two Poaceae hosts, barley and *Brachypodium*. We identified *Fg*-sRNAs with sequence homology to host genes that were down-regulated by *Fg* during plant colonisation, while they were expressed above their level in healthy plants after infection with a DCL dKO mutant. In PH1-*dcl1/2* vs. PH1 the strength of target gene accumulation correlated with the abundance of the corresponding *Fg*-sRNA. Our data hint to the possibility that three DCL-dependent tRFs with sequence homology to immunity-related *Ethylene overproducer 1-like 1* (*HvEOL1*) and three Poaceae orthologues of *Arabidopsis thaliana* *BRI1-associated receptor kinase 1* (*HvBAK1*, *HvSERK2* and *BdSERK2*) contribute to fungal virulence via targeted gene silencing.

## Experimental procedures

### Plants, fungi and plant infection

*Fusarium graminearum* (*Fg*) strain PH1, the double knock-out (dKO) PH1-*dcl1/2* (Dr. Martin Urban, Rothamsted Research, England), strain IFA65 (IFA, Department for Agrobiotechnology, Tulln, Austria) and single mutants IFA65-*dcl1* and IFA65-*dcl2* [8] were cultured on synthetic nutrient poor agar (SNA). Preparation of fungal inoculum was performed as described [69]. *Arabidopsis thaliana* ecotype Col-0 and *Atago1-27* ([70]; Polymorphism:3510706481) were grown in 8 h photoperiod at 22°C with 60% relative humidity in a soil—sand mixture (4:1) (Fruhstorfer Type T, Hawita, Germany). For infection, 15 rosette leaves were detached and transferred in square Petri plates containing 1% water-agar. Drop-inoculation of *At* leaves was done with 5 µl of a suspension of  $5 \times 10^4$  *Fg* conidia ml<sup>-1</sup> at two spots per leaf. Infection strength was recorded as infection area (size of chlorotic lesions relative to total leaf area) using the ImageJ software (<https://imagej.nih.gov/ij/>).

For infection of barley (*Hordeum vulgare* cv. Golden Promise, GP) and *Brachypodium distachyon* (Bd21-3), plants were grown in a 16 h photoperiod at 20°C/18°C day/night and 60% relative humidity in soil (Fruhstorfer Type LD80, Hawita). Ten detached second leaves were transferred into square Petri plates containing 1% water-agar. GP leaves were drop-inoculated with 3 µl of  $1.5 \times 10^5$  conidia ml<sup>-1</sup> conidia suspension. Bd21-3 leaves were drop-inoculated on two spots with 10 µl of  $1 \times 10^4$  conidia ml<sup>-1</sup> conidia suspension. Infection strength was measured with the PlantCV v2 software package (<https://plantcv.danforthcenter.org/>) (*Hv*) by training a machine learning algorithm to recognize necrotic lesions or by ImageJ (*Bd*). For gene expression analysis, a suspension of  $5 \times 10^4$  *Fg* conidia ml<sup>-1</sup> was used and leaves were either inoculated on 3 spots with 20 µl (*Hv*) or on 2 spots with 10 µl (*Bd*), respectively and experiments were evaluated 5 dpi or 4 dpi for strain PH1 on *Bd*.

## Fungal transcript analysis

Gene expression analysis was performed using reverse transcription quantitative PCR (RT-qPCR). RNA extraction was performed with GENEzol reagent (Geneaid) following the manufacturer's instructions. DNA was digested with DNase I (Thermo Scientific) according to manufacturer protocol and remaining RNA was used for cDNA synthesis using qScript™ cDNA kit (Quantabio). For RT-qPCR, 10 ng of cDNA was used as template in the QuantStudio 5 Real-Time PCR system (Applied Biosystems). Amplifications were performed with 5 µl of SYBR® green JumpStart Taq ReadyMix (Sigma-Aldrich) with 5 pmol oligonucleotides. Each sample had three technical repetitions. After an initial activation step at 95°C for 5 min, 40 cycles (95°C for 30 sec, 60°C for 30 sec, 72°C for 30 sec) were performed followed by a melt curve analysis (60°C–95°C, 0.075°C/s). Ct values were determined with the QuantStudio design and analysis software supplied with the instrument. Transcript levels were determined via the  $2^{-\Delta\Delta C_t}$  method [71] by normalizing the amount of target transcript to the amount of the reference transcript *Elongation factor 1-alpha* (*EF1-a*, FGSG\_08811) gene (S2 Table).

## Plant transcript analysis

Leaves were shock frozen at 5 dpi and RT-qPCR was performed as for fungal transcript analysis. Reference genes were *Ubiquitin-40S ribosomal protein S27a-3* (HORVU1Hr1G023660) for GP and *Ubi4* (Bradi3g04730) for Bd21-3 according to Chambers et al. [72] (S1 Table). Primers were designed using Primer3 v2.4.0 [73].

## Spray application of dsRNA

Second leaves of 2 to 3-week-old GP were detached and transferred to square Petri plates containing 1% water agar. dsRNA was diluted in 500 µl water to a final concentration of 20 ng µl<sup>-1</sup>. As control, Tris-EDTA (TE) buffer was diluted in 500 µl water corresponding to the amount used for dilution of the dsRNA. Typical RNA concentration after elution was 500 ng µl<sup>-1</sup>, with 400 µM Tris-HCL and 40 µM EDTA in the final dilution. Each plate containing 10 detached leaves was evenly sprayed with either dsRNAs or TE buffer with 500 µl, and subsequently kept at room temperature [10]. Two days after spraying, leaves were drop-inoculated with three 20 µl drops of *Fg* suspension containing  $5 \times 10^4$  conidia ml<sup>-1</sup>. After inoculation, plates were closed and incubated for five days at room temperature.

## Target prediction for sRNAs

RNA was purified and enriched for sRNAs from fungal axenic culture (PRJNA749737) using the mirVana miRNA Isolation Kit (Life Technologies). Indexed sRNA libraries were constructed from these sRNA fractions with the NEBNext Multiplex Small RNA Library Prep Set for Illumina (New England Biolabs) according to the manufacturer's instructions. Reads were trimmed with the cutadapt tool v2.1 [74] by removing adapters and retaining reads with a length of 21–24 nt and quality checked with the fastQC tool v0.11.9 (<http://www.bioinformatics.babraham.ac.uk/projects/fastqc/>). For S1 Fig reads were aligned to the *Fg* reference genome (GCF\_000240135.3\_ASM24013v3) with bowtie2 [75] following a sensitive alignment policy (-D 100, -R 10, -L 19). The aligned reads were assigned to the additional attribute "gene\_biotype" with htseq-count [76] according to the latest assembly ([ftp://ftp.ensemblgenomes.org/pub/release-44/fungi/gff3/fungi\\_ascomycota3\\_collection/fusarium\\_graminearum\\_gca\\_000240135](ftp://ftp.ensemblgenomes.org/pub/release-44/fungi/gff3/fungi_ascomycota3_collection/fusarium_graminearum_gca_000240135)). Remaining reads were collapsed with the fastx toolkit v0.0.14 [77] and reads with at least 400 reads were targeted against the IBSC\_PGSG\_v2 cDNA annotation with the plant miRNA target prediction algorithm TAPIR [42], following the optimized

parameters according to Srivastava et al. [39]. The results of the target prediction were further analysed with RStudio [78] and the package biomaRt [79] to find targets associated with stress and immunity associated Gene ontology (GO) terms in the database “plants\_mart” from plants.ensembl.org hosted by the EBI (European Bioinformatics Institute) and the Wellcome Trust Sanger Institute. The same method was used for the identification of target genes in *B. distachyon* (GCA\_000005505.4) and *A. thaliana* (Araport11).

### Stemloop-RT-qPCR of sRNAs

RNA was extracted and genomic DNA was digested as described for the transcript analyses. The sequences of sRNAs found in axenic fungal culture were used to design specific stem loop (SL) primers matching the sRNA over 6 nt at the 3' end. For the primer design, the tool of Adhikari et al. [80] was used. SL-primers were diluted to 10 pM and folded in a cyclor (95°C for 15 min, 90°C 5 min, 85°C 5 min, 80°C 5 min, 75°C 1 h, 68°C 1 h, 65°C 1 h, 62°C 1 h, 60°C 3 h). These primers were used for cDNA synthesis (Thermo Scientific RevertAid RT Reverse Transcription Kit) according to manufacturer's instruction with an annealing step at 16°C instead of 25°C and were used in multiplex to target respective fungal sRNAs and barley miRNAs *Hvu-mir159* and *Hvu-mir168* as references. To obtain amplification efficiencies, a mix from all RNAs was diluted in a four step dilution series with a factor of ten and reverse transcribed. Reactions were set up with the highest concentration of 15 ng  $\mu\text{l}^{-1}$  and the lowest of 15 pg  $\mu\text{l}^{-1}$  cDNA. All sRNA amplifications showed an efficiency of 80–82% and an  $R^2$  between 1 and 0.997 except for Fg-sRNA-6717 with an efficiency of 66.4%. For RT-qPCR, 1.5  $\mu\text{l}$  of 3 ng  $\mu\text{l}^{-1}$  cDNA was used as template in the QuantStudio 5 Real-Time PCR system (Applied Biosystems). Amplifications were performed with 5  $\mu\text{l}$  of SYBR<sup>®</sup> green JumpStart Taq ReadyMix (Sigma-Aldrich) with 1.5 pmol or 3 pmol oligonucleotides. Each sample had three technical repetitions. As forward primer the unused nucleotides of the remaining sequence of the sRNA were used, which were extended to achieve optimal melting temperature, and as reverse primer the universal stem loop primer developed by Chen et al. [41] was used. Relative abundance of the sRNAs was calculated with the  $\Delta\Delta\text{Ct}$ -method with incorporation of amplification efficiencies. sRNAs were normalized against the reference miRNAs *Hvu-mir-159a* and 168-5p and after this against the fungal biomass measured as *EF1- $\alpha$*  against *HvUBQ* (*HORVUIHr1G023660*).

### Statistics

To assess the differential expression of genes via RT-qPCRs the  $\Delta\text{Ct}$  values were compared via a one or two sided paired Students *t*-test. Disease symptoms were either compared via Students *t*-test if the data showed a normal distribution in Shapiro-Wilk test or via a Wilcoxon rank sum test.

### RLM-RACE

RNA from GP barley infected with Fg-IFA65 at 5 dpi and an uninfected control was extracted with the Isolate II plant miRNA kit (Bioline). 1  $\mu\text{g}$  of RNA (>200 nt) of infected, uninfected and a mix of both samples for a-RT-control were assembled. 1  $\mu\text{l}$  of the 5'RACE Adapter [0.3  $\mu\text{g}/\mu\text{l}$ ], 1  $\mu\text{l}$  of the 10x Reaction Buffer, 1  $\mu\text{l}$  of 1mg/ $\mu\text{l}$  BSA, 0.5  $\mu\text{l}$  of T4 RNA Ligase [10U/ $\mu\text{l}$ ] (Thermo Scientific) and DEPC-treated water up to 10  $\mu\text{l}$  were prepared and incubated at 37°C for 60 min. Subsequently, the whole reaction was used for reverse transcription (RevertAid Reverse Transcriptase, Thermo Scientific). 10  $\mu\text{l}$  ligation reaction, 1  $\mu\text{l}$  Random Hexamer [100pmol/ $\mu\text{l}$ ], 4  $\mu\text{l}$  5x Reaction Buffer, 0.5  $\mu\text{l}$  RiboLock RNase Inhibitor (Thermo Scientific), 2  $\mu\text{l}$  dNTP Mix [10 mM] and 1  $\mu\text{l}$  RevertAid Reverse Transcriptase (or water (–RT control))

and 1.5 µl water were mixed and run for 10 min at 25°C, 60 min at 42°C and 10 min at 70°C. Then, a nested hot-start touch-down PCR for each target gene was performed. The primer sequences for the outer (first) and inner (second) PCR are shown in S1 Table. 5 µl of 10x Buffer B, 1 µl of a dNTP Mix [10 mM], 2 µl MgCl<sub>2</sub> [25 mM], 1 µl Adapter specific Primer [10 pmol µl<sup>-1</sup>] and 1 µl gene specific primer (GSP) [10 pmol µl<sup>-1</sup>], 0.6 µl DCS DNA Polymerase (DNA Cloning Service) [5 U/µl] and 2 µl cDNA or outer PCR reaction and 37.4 µl water were mixed and run at 95°C for 5 min, (95°C for 30 s, 68°C-0.5°C/cycle for 30 s, 72°C for 30 s)\*15, (95°C for 30 s, 60°C for 30 s, 72°C for 30 s)\*18 and 72°C for 5 min. PCR products were evaluated in a 1.5% agarose gel and bands of the expected size, which were present in the infected but not uninfected samples, were excised. Products were cleaned with the Wizard SV Gel and PCR Clean-Up System (Promega) and cloned with the pGEM-T easy Vector Systems (Promega). For each band, five clones were picked for sequencing. Plasmids from O/N cultures were extracted with the Monarch Plasmid Miniprep Kit (New England Biolabs) and sent for sequencing to LGC genomics.

### Analysis of target genes and targeting sRNAs

After the initial target prediction an additional target prediction for the newly released cultivar specific genome (GCA\_902500625) of barley cv. Golden Promise (GP) was conducted. Adapters were removed and reads were collapsed as described before for the target prediction. All sRNA sequences were read with SeqinR v3.6-1 [81] and stored in a list of SeqFastadna objects. To identify the homologous genes to the already identified targets in GP, the cDNA library was blasted with the command-line blast application (Nucleotide-Nucleotide BLAST 2.6.0+) [82] against the identified target sequences from the IBSC\_PGSEB\_v2 cDNA library with percent identity of 90 and a query coverage of 55% as cut-off values. All sRNAs with at least two reads were written to a file in chunks of 2000 each and ran against each individual target gene with TAPIR via the system2 function in R [83] in the RStudio software. Results were collected, stored in a data.frame, and further analysed with R. sRNAs identified to target a gene of interest (GOI) were written to a fasta file with SeqinR and blasted against the rRNAs from the assemblies GCA\_900044135.1 (*Fg*-PH1), GCA\_000240135.3 (*Fg*-PH1) and the *Fusarium* rRNAs from the RNACentral fungal ncRNA dataset ([ftp://ftp.ebi.ac.uk/pub/databases/RNACentral/current\\_release/sequences/by-database/ensembl\\_fungi.fasta](ftp://ftp.ebi.ac.uk/pub/databases/RNACentral/current_release/sequences/by-database/ensembl_fungi.fasta) (12/Sep/2020)) with the options wordsize = 4, perc\_identity = 95, qcov\_hsp\_perc = 95. All sRNAs matching rRNAs were removed. Thereafter, sRNAs were compared to the *Fg* assemblies GCA\_900044135.1 (*Fg*-PH1) and GCA\_000240135.3 (*Fg*-PH1) with the same blast strategy and only perfectly matching sRNAs were retained.

To derive the relative expression of a GOI between two samples the following formula is used.

$$Relativeexpression_{GOI} = 2^{-\Delta\Delta ct_{GOI}}$$

We further defined the  $\Delta\Delta ct$  value as the difference between the  $\Delta\Delta ct$  values for a GOI in PH1 and PH1-*dcl1/2*-infected samples.

$$\Delta\Delta ct = \Delta\Delta ct_{PH1-dcl1/2} - \Delta\Delta ct_{PH1}$$

This enables the calculation of the re-accumulation between the two samples as follows.

$$DCL - dependent \ resurgence \ factor = \frac{Relativeexpression_{PH1-dcl1/2}}{Relativeexpression_{PH1}} = 2^{-\Delta\Delta ct_{GOI}}$$

The sum of all reads and the corresponding  $\Delta\Delta ct$ -value were plotted with ggplot2 [84] and

a linear regression was added to the plot. To allow a log2-transformation of the plots genes with zero targeting reads were set to one targeting read. The plots were arranged using ggpubr v.0.4.0 [85].

### GO enrichment analysis

Gene ontology (GO) enrichment analysis was performed via the AgriGO v.2.0 analysis toolkit [86] with the standard parameters singular enrichment analysis (SEA).

### Phylogenetic analysis of SERK homologs

Homologs of *HvBAK1* and *HvSERK2* were searched in *At*, *Hv* and *Bd* with biomaRt v.2.40.5 [79] and downloaded from the EMBL's European Bioinformatics Institute plants genome page (plants.ensembl.org) in the plants\_mart dataset hvulgare\_eg\_gene (Ensembl Plants Genes v. 50). For these homologs the CDS of all homologs within the respective datasets athaliana\_eg\_gene, hvulgare\_eg\_gene and bdistachyon\_eg\_gene were downloaded. The CDS were subsequently aligned with the muscle algorithm in MEGA7 [87] and a phylogenetic tree was constructed via a bootstrap method with 200 iterations.

### Supporting information

**S1 Fig. Feature mapping of *Fg*-sRNAs with a read length of 21–24 nt.** Reads were trimmed as described earlier and aligned to the PH1 reference genome (GCF\_000240135.3\_ASM24013v3) with bowtie2 [75].  
(TIF)

**S2 Fig. GO-enrichment analysis of all potential targets of *Fg*-sRNAs with more than 400 reads.** The plot shows all significantly enriched GO-terms in the target gene set for (A) molecular function and (B) biological process. The analysis was done using agriGo v2.0. Each box contains information regarding one term. GO: indicates the GO accession, in brackets the p-value is stated (Fisher; Yekutieli (FDR)). After the bracket the GO-term description is written followed by the number of genes associated with said term 1. in the gene set and 2. In the background.  
(TIF)

**S3 Fig. Alignment of *At*ETO1 and *Hv*EOL1.** Identical amino acids are marked blue and similar amino acids are marked red. The alignment and visualization was done with the msa package for R [88].  
(TIF)

**S4 Fig. Regulation of ET synthesis in *At*.** *At*ETO1 negatively regulates ethylene (ET) synthesis in *At*. *At*ETO1 acts together with *At*EOL1 and *At*ETO1-like 2 (EOL2) in directing the ubiquitination and subsequent degradation of type-2 1-aminocyclopropane-1-carboxylate synthase (ACS) proteins (e.g. ET overproducer 2 (ETO2)), which produce the direct precursor of ET.  
(TIF)

**S5 Fig. Sequences of dsRNA-dcl1/2.** Coding Sequences (CDS) of the respective *FgDCL* genes with the sequences comprising the dsRNAs marked in red. A. *FgDCL1*-FGSG\_09025 (912 nt long dsRNA-*FgDCL1*). B. *FgDCL2*-FGSG\_04408 (870 nt long dsRNA-*FgDCL2*).  
(TIF)

**S6 Fig. Position and read count of all tRFs from *Fg*-tRNA-Gly(GCC).** Alignment position of all *Fg*-sRNAs from axenic culture with more than 50 reads perfectly matching the *Fg*-tRNA-Gly(GCC)-9 gene (*Fusarium\_graminearum\_CS3005*-tRNA-Gly-GCC-1-9) colored by read count.

(TIF)

**S7 Fig. Abundance of unique *Fg*-sRNAs in axenic culture of IFA65.** A: Histogram of the read count of every unique sRNA. The plot is truncated to make abundances recognizable. Most sRNAs have very low read counts and very few sRNAs have more reads than 3,000. Maximum read count per sRNA is 42,866. B: Violin plot of log<sub>2</sub>-transformed reads counts untruncated.

(TIF)

**S8 Fig. Origin of tRFs in *Fg*-tRNA-Gly(GCC).** The centroid secondary structure of the *Fg*-tRNA-Gly(GCC) generated on the RNAfold web server (<http://rna.tbi.univie.ac.at/cgi-bin/RNAWebSuite/RNAfold.cgi>) with the origin and alignment of *Fg*-sRNA-321, *Fg*-sRNA-1921 and *Fg*-sRNA-6717. The colors of bases indicate the base pair probabilities.

(TIF)

**S9 Fig. Molecular Phylogenetic analysis by maximum likelihood method.** The evolutionary history was inferred by using the Maximum Likelihood method based on the General Time Reversible model [89]. The tree with the highest log likelihood (-25430.37) is shown. Initial tree(s) for the heuristic search were obtained automatically by applying Neighbor-Join and BioNJ algorithms to a matrix of pairwise distances estimated using the Maximum Composite Likelihood (MCL) approach, and then selecting the topology with superior log likelihood value. The tree is drawn to scale, with branch lengths measured in the number of substitutions per site. The analysis involved 77 nucleotide sequences. Codon positions included were 1st +2nd+3rd. There were a total of 2427 positions in the final dataset. Evolutionary analyses were conducted in MEGA7 [87].

(TIF)

**S10 Fig. Unedited gel images from Fig 6.**

(PDF)

**S1 Table. Primer sequences.**

(DOCX)

**S2 Table. Target prediction results.** Results of the target prediction with the TAPIR algorithm for all *Fg*-sRNAs with more than 400 reads.

(XLSX)

## Acknowledgments

We thank the Salk Institute Genomic Analysis Laboratory for providing the sequence-indexed *Arabidopsis* TDNA insertion mutants.

## Author Contributions

**Conceptualization:** Bernhard Timo Werner, Aline Koch, Karl-Heinz Kogel.

**Data curation:** Bernhard Timo Werner, Aline Koch, Lukas Jelonek.

**Formal analysis:** Bernhard Timo Werner, Ena Šečić, Jonas Engelhardt, Lukas Jelonek.

**Funding acquisition:** Aline Koch, Jens Steinbrenner, Karl-Heinz Kogel.

**Investigation:** Aline Koch, Ena Šečić, Karl-Heinz Kogel.

**Methodology:** Bernhard Timo Werner, Aline Koch, Ena Šečić, Jonas Engelhardt, Jens Steinbrenner.

**Project administration:** Aline Koch, Jens Steinbrenner, Karl-Heinz Kogel.

**Resources:** Bernhard Timo Werner.

**Software:** Bernhard Timo Werner, Ena Šečić, Jonas Engelhardt, Lukas Jelonek.

**Supervision:** Aline Koch, Jens Steinbrenner, Karl-Heinz Kogel.

**Validation:** Bernhard Timo Werner.

**Visualization:** Bernhard Timo Werner.

**Writing – original draft:** Bernhard Timo Werner, Aline Koch, Karl-Heinz Kogel.

**Writing – review & editing:** Bernhard Timo Werner, Aline Koch, Ena Šečić, Lukas Jelonek, Jens Steinbrenner, Karl-Heinz Kogel.

## References

1. Koch A., & Kogel K. H. (2014). New wind in the sails: improving the agronomic value of crop plants through RNA i-mediated gene silencing. *Plant biotechnology journal*, 12(7), 821–831. <https://doi.org/10.1111/pbi.12226> PMID: 25040343
2. Guo Q., Liu Q., Smith N.A., Liang G., & Wang M.B. (2016). RNA Silencing in plants: mechanisms, technologies and applications in horticultural crops. *Current Genomics*, 17, 476–489. <https://doi.org/10.2174/1389202917666160520103117> PMID: 28217004
3. Liu S., Jaouannet M., Dempsey D. M. A., Imani J., Coustau C., & Kogel K. H. (2020). RNA-based technologies for insect control in plant production. *Biotechnology advances*, 39, 107463. <https://doi.org/10.1016/j.biotechadv.2019.107463> PMID: 31678220
4. Šečić E and Kogel KH (2021). Requirements for fungal uptake of dsRNA and gene silencing in RNAi-based crop protection strategies. *Current Opinion in Biotechnology*, COBIOT-D-21-00048. <https://doi.org/10.1016/j.copbio.2021.04.001> PMID: 34000482
5. Koch A., & Wassenegger M. (2021). Host-induced gene silencing—mechanisms and applications. *New Phytologist*, 231(1), 54–59. <https://doi.org/10.1111/nph.17364> PMID: 33774815
6. Rosa C., Kuo Y. W., Wuriyanghan H., & Falk B. W. (2018). RNA interference mechanisms and applications in plant pathology. *Annual review of phytopathology*, 56, 581–610. <https://doi.org/10.1146/annurev-phyto-080417-050044> PMID: 29979927
7. Cai Q., He B., Kogel K. H., & Jin H. (2018). Cross-kingdom RNA trafficking and environmental RNAi—nature's blueprint for modern crop protection strategies. *Current opinion in microbiology*, 46, 58–64. <https://doi.org/10.1016/j.mib.2018.02.003> PMID: 29549797
8. Gaffar F. Y., Imani J., Karlovsky P., Koch A., & Kogel K.-H. (2019). Different components of the RNA interference machinery are required for conidiation, ascosporeogenesis, virulence, deoxynivalenol production, and fungal inhibition by exogenous double-stranded RNA in the Head Blight pathogen *Fusarium graminearum*. *Frontiers in Microbiology*, 10, 1662. <https://doi.org/10.3389/fmicb.2019.01662> PMID: 31616385
9. Niehl A., & Heinlein M. (2019). Perception of double-stranded RNA in plant antiviral immunity. *Molecular plant pathology*, 20(9), 1203–1210. <https://doi.org/10.1111/mpp.12798> PMID: 30942534
10. Koch A., Biedenkopf D., Furch A., Weber L., Rossbach O., Abdellatif E., et al. (2016). An RNAi-based control of *Fusarium graminearum* infections through spraying of long dsRNAs involves a plant passage and is controlled by the fungal silencing machinery. *PLoS pathogens*, 12(10), e1005901. <https://doi.org/10.1371/journal.ppat.1005901> PMID: 27737019
11. Wang M., Weiberg A., Lin F.-M., Thomma B. P. H. J., Huang H.D., & Jin H. (2016). Bidirectional cross-kingdom RNAi and fungal uptake of external RNAs confer plant protection. *Nature Plants*, 2, 16151. <https://doi.org/10.1038/nplants.2016.151> PMID: 27643635
12. Konakalla N. C., Kaldis A., Berbati M., Masarapu H., & Voloudakis A. E. (2016). Exogenous application of double-stranded RNA molecules from TMV p126 and CP genes confers resistance against

- TMV in tobacco. *Planta*, 244(4), 961–969. <https://doi.org/10.1007/s00425-016-2567-6> PMID: 27456838
13. Mitter N., Worrall E. A., Robinson K. E., Li P., Jain R. G., Taochy C., et al. (2017). Clay nanosheets for topical delivery of RNAi for sustained protection against plant viruses. *Nature plants*, 3(2), 1–10. <https://doi.org/10.1038/nplants.2016.207> PMID: 28067898
  14. Kaldis A., Berbaty M., Melita O., Reppa C., Holeva M., Otten P., et al. (2018). Exogenously applied dsRNA molecules deriving from the Zucchini yellow mosaic virus (ZYMV) genome move systemically and protect cucurbits against ZYMV. *Molecular plant pathology*, 19(4), 883–895. <https://doi.org/10.1111/mpp.12572> PMID: 28621835
  15. McLoughlin A. G., Wytinck N., Walker P. L., Girard I. J., Rashid K. Y., de Kievit T., et al. (2018). Identification and application of exogenous dsRNA confers plant protection against *Sclerotinia sclerotiorum* and *Botrytis cinerea*. *Scientific Reports*, 8(1), 1–14. <https://doi.org/10.1038/s41598-017-17765-5> PMID: 29311619
  16. Sang H., & Kim J. I. (2020). Advanced strategies to control plant pathogenic fungi by host-induced gene silencing (HIGS) and spray-induced gene silencing (SIGS). *Plant Biotechnology Reports*, 14(1), 1–8.
  17. Head G. P., Carroll M. W., Evans S. P., Rule D. M., Willse A. R., Clark T. L., et al. (2017). Evaluation of SmartStax and SmartStax PRO maize against western corn rootworm and northern corn rootworm: efficacy and resistance management. *Pest management science*, 73(9), 1883–1899. <https://doi.org/10.1002/ps.4554> PMID: 28195683
  18. Niehl A., Soininen M., Poranen M. M., & Heinlein M. (2018). Synthetic biology approach for plant protection using ds RNA. *Plant biotechnology journal*, 16(9), 1679–1687.
  19. Weiberg A., Wang M., Lin F. M., Zhao H., Zhang Z., Kaloshian I., et al. (2013). Fungal small RNAs suppress plant immunity by hijacking host RNA interference pathways. *Science*, 342(6154), 118–123. <https://doi.org/10.1126/science.1239705> PMID: 24092744
  20. Cai Q., Qiao L., Wang M., He B., Lin F. M., Palmquist J., et al. (2018). Plants send small RNAs in extracellular vesicles to fungal pathogen to silence virulence genes. *Science*, 360(6393), 1126–1129. <https://doi.org/10.1126/science.aar4142> PMID: 29773668
  21. Wang M., Weiberg A., Dellota E. Jr, Yamane D., & Jin H. (2017). Botrytis small RNA Bc-siR37 suppresses plant defense genes by cross-kingdom RNAi. *RNA Biology*, 14, 421–428. <https://doi.org/10.1080/15476286.2017.1291112> PMID: 28267415
  22. Dunker F., Trutzenberg A., Rothenpieler J. S., Kuhn S., Pröls R., Schreiber T., et al. (2020). Oomycete small RNAs bind to the plant RNA-induced silencing complex for virulence. *Elife*, 9, e56096. <https://doi.org/10.7554/eLife.56096> PMID: 32441255
  23. Wang B., Sun Y.F., Song N., Zhao M.X., Liu R., Feng H., et al. (2017). *Puccinia striiformis* f. sp. *tritici* microRNA-like RNA 1 (Pst-milR1), an important pathogenicity factor of Pst, impairs wheat resistance to Pst by suppressing the wheat pathogenesis-related 2 gene. *New Phytologist*, 215, 338–350.
  24. Dubey H., Kiran K., Jaswal R., Jain P., Kayastha A. M., Bhardwaj S. C., et al. (2019). Discovery and profiling of small RNAs from *Puccinia triticina* by deep sequencing and identification of their potential targets in wheat. *Functional & integrative genomics*, 19(3), 391–407. <https://doi.org/10.1007/s10142-018-00652-1> PMID: 30618015
  25. Mueth N. A., Ramachandran S. R., & Hulbert S. H. (2015). Small RNAs from the wheat stripe rust fungus (*Puccinia striiformis* f. sp. *tritici*). *Bmc Genomics*, 16(1), 1–16.
  26. Reinhart B. J., Weinstein E. G., Rhoades M. W., Bartel B., & Bartel D. P. (2002). MicroRNAs in plants. *Genes & development*, 16(13), 1616–1626. <https://doi.org/10.1101/gad.1004402> PMID: 12101121
  27. Ren B., Wang X., Duan J., & Ma J. (2019). Rhizobial tRNA-derived small RNAs are signal molecules regulating plant nodulation. *Science*, 365(6456), 919–922. <https://doi.org/10.1126/science.aav8907> PMID: 31346137
  28. Jones-Rhoades M. W. (2012). Conservation and divergence in plant microRNAs. *Plant molecular biology*, 80(1), 3–16. <https://doi.org/10.1007/s11103-011-9829-2> PMID: 21996939
  29. Garcia-Silva M. R., Cabrera-Cabrera F., Cura das Neves R. F., Souto-Pradón T., de Souza W., & Cayota A. (2014). Gene expression changes induced by *Trypanosoma cruzi* shed microvesicles in mammalian host cells: relevance of tRNA-derived halves. *BioMed Research International*, 2014, 1–11. <https://doi.org/10.1155/2014/305239> PMID: 24812611
  30. Dean R., Van Kan J. A., Pretorius Z. A., Hammond-Kosack K. E., Di Pietro A., Spanu P. D., et al. (2012). The Top 10 fungal pathogens in molecular plant pathology. *Molecular plant pathology*, 13(4), 414–430. <https://doi.org/10.1111/j.1364-3703.2011.00783.x> PMID: 22471698
  31. Desjardins A. E., Hohn T. M., & McCORMICK S. P. (1993). Trichothecene biosynthesis in *Fusarium* species: chemistry, genetics, and significance. *Microbiology and Molecular Biology Reviews*, 57(3), 595–604.

32. Jansen C., Von Wettstein D., Schäfer W., Kogel K. H., Felk A., & Maier F. J. (2005). Infection patterns in barley and wheat spikes inoculated with wild-type and trichodiene synthase gene disrupted *Fusarium graminearum*. *Proceedings of the National Academy of Sciences*, 102(46), 16892–16897. <https://doi.org/10.1073/pnas.0508467102> PMID: 16263921
33. Ilgen P., Hadeler B., Maier F. J., & Schäfer W. (2009). Developing kernel and rachis node induce the trichothecene pathway of *Fusarium graminearum* during wheat head infection. *Molecular plant-microbe interactions*, 22(8), 899–908. <https://doi.org/10.1094/MPMI-22-8-0899> PMID: 19589066
34. Kim H. K., Jo S. M., Kim G. Y., Kim D. W., Kim Y. K., & Yun S. H. (2015). A large-scale functional analysis of putative target genes of mating-type loci provides insight into the regulation of sexual development of the cereal pathogen *Fusarium graminearum*. *PLoS Genet*, 11(9), e1005486. <https://doi.org/10.1371/journal.pgen.1005486> PMID: 26334536
35. Son H., Park AR, Lim JY, Shin C, Lee Y-W (2017) Genome-wide exonic small interference RNA-mediated gene silencing regulates sexual reproduction in the homothallic fungus *Fusarium graminearum*. *PLoS Genet* 13(2): e1006595. <https://doi.org/10.1371/journal.pgen.1006595> PMID: 28146558
36. Ji H., Mao H., Li S., Feng T., Zhang Z., Cheng L., et al. (2021). *Fol-milR1*, a pathogenicity factor of *Fusarium oxysporum*, confers tomato wilt disease resistance by impairing host immune responses. *New Phytologist*, nph.17436. <https://doi.org/10.1111/nph.17436> PMID: 33960431
37. Jian J., & Liang X. (2019). One small RNA of *Fusarium graminearum* targets and silences CEBiP gene in common wheat. *Microorganisms*, 7(10), 425. <https://doi.org/10.3390/microorganisms7100425> PMID: 31600909
38. Mascher M., Gundlach H., Himmelbach A., Beier S., Twardziok S. O., Wicker T., et al. (2017). A chromosome conformation capture ordered sequence of the barley genome. *Nature*, 544(7651), 427–433. <https://doi.org/10.1038/nature22043> PMID: 28447635
39. Srivastava P. K., Moturu T. R., Pandey P., Baldwin I. T., & Pandey S. P. (2014). A comparison of performance of plant miRNA target prediction tools and the characterization of features for genome-wide target prediction. *BMC genomics*, 15(1), 1–15. <https://doi.org/10.1186/1471-2164-15-348> PMID: 24885295
40. Christians M. J., Gingerich D. J., Hansen M., Binder B. M., Kieber J. J., & Vierstra R. D. (2009). The BTB ubiquitin ligases ETO1, EOL1 and EOL2 act collectively to regulate ethylene biosynthesis in Arabidopsis by controlling type-2 ACC synthase levels. *The Plant Journal*, 57(2), 332–345. <https://doi.org/10.1111/j.1365-3113X.2008.03693.x> PMID: 18808454
41. Chen C., Ridzon D. A., Broomer A. J., Zhou Z., Lee D. H., Nguyen J. T., et al. (2005). Real-time quantification of microRNAs by stem-loop RT-PCR. *Nucleic acids research*, 33(20), e179–e179. <https://doi.org/10.1093/nar/gni178> PMID: 16314309
42. Bonnet E., He Y., Billiau K., & Van de Peer Y. (2010). TAPIR, a web server for the prediction of plant microRNA targets, including target mimics. *Bioinformatics*, 26(12), 1566–1568. <https://doi.org/10.1093/bioinformatics/btq233> PMID: 20430753
43. Mallory A. C., Reinhart B. J., Jones-Rhoades M. W., Tang G., Zamore P. D., Barton M. K., et al. (2004). MicroRNA control of PHABULOSA in leaf development: importance of pairing to the microRNA 5' region. *The EMBO journal*, 23(16), 3356–3364. <https://doi.org/10.1038/sj.emboj.7600340> PMID: 15282547
44. Werner B. T., Gaffar F. Y., Schuermann J., Biedenkopf D., & Koch A. M. (2020). RNA-spray-mediated silencing of *Fusarium graminearum* AGO and DCL genes improve barley disease resistance. *Frontiers in Plant Science*, 11, 476. <https://doi.org/10.3389/fpls.2020.00476> PMID: 32411160
45. Lax C., Tahiri G., Patiño-Medina J. A., Cánovas-Márquez J. T., Pérez-Ruiz J. A., Osorio-Concepción M., et al. (2020). The Evolutionary Significance of RNAi in the Fungal Kingdom. *International Journal of Molecular Sciences*, 21(24), 9348. <https://doi.org/10.3390/ijms21249348> PMID: 33302447
46. Zanini S., Šečić E., Busche T., Galli M., Zheng Y., Kalinowski J., et al. (2021). Comparative Analysis of Transcriptome and sRNAs Expression Patterns in the *Brachypodium distachyon*—*Magnaporthe oryzae* Pathosystems. *International Journal of Molecular Sciences*, 22(2), 650. <https://doi.org/10.3390/ijms22020650> PMID: 33440747
47. Lee Marzano S. Y., Neupane A., Mochama P., Feng C., & Saleem H. (2019). Roles of argonautes and dicers on *Sclerotinia sclerotiorum* antiviral RNA silencing. *Frontiers in Plant Science*, 10, 976. <https://doi.org/10.3389/fpls.2019.00976> PMID: 31440265
48. Åsman A. K., Vetukuri R. R., Jahan S. N., Fogelqvist J., Corcoran P., Avrova A. O., et al. (2014). Fragmentation of tRNA in *Phytophthora infestans* asexual life cycle stages and during host plant infection. *BMC microbiology*, 14(1), 308. <https://doi.org/10.1186/s12866-014-0308-1> PMID: 25492044
49. Streit R. S. A., Ferrareze P. A. G., Vainstein M. H., & Staats C. C. (2021). Analysis of tRNA-derived RNA fragments (tRFs) in *Cryptococcus* spp.: RNAi-independent generation and possible compensatory

- effects in a RNAi-deficient genotype. *Fungal Biology*, 125(5), 389–399. <https://doi.org/10.1016/j.funbio.2020.12.003> PMID: 33910680
50. Kumar P., Kuscu C., & Dutta A. (2016). Biogenesis and function of transfer RNA-related fragments (tRFs). *Trends in biochemical sciences*, 41(8), 679–689. <https://doi.org/10.1016/j.tibs.2016.05.004> PMID: 27263052
  51. Li N., Shan N., Lu L., & Wang Z. (2021). tRFtarget: a database for transfer RNA-derived fragment targets. *Nucleic Acids Research*, 49(D1), D254–D260. <https://doi.org/10.1093/nar/gkaa831> PMID: 33035346
  52. Zuo Y., Zhu L., Guo Z., Liu W., Zhang J., Zeng Z., et al. (2021). tsRBase: a comprehensive database for expression and function of tsRNAs in multiple species. *Nucleic Acids Research*, 49(D1), D1038–D1045. <https://doi.org/10.1093/nar/gkaa888> PMID: 33068436
  53. Wang Q., Li T., Xu K., Zhang W., Wang X., Quan J., et al. (2016b). The tRNA-derived small RNAs regulate gene expression through triggering sequence-specific degradation of target transcripts in the oomycete pathogen *Phytophthora sojae*. *Frontiers in plant science*, 7, 1938.
  54. Martinez G., Choudury S. G., & Slotkin R. K. (2017). tRNA-derived small RNAs target transposable element transcripts. *Nucleic acids research*, 45(9), 5142–5152. <https://doi.org/10.1093/nar/gkx103> PMID: 28335016
  55. Asha S., & Soniya E. V. (2016). Transfer RNA derived small RNAs targeting defense responsive genes are induced during *Phytophthora capsici* infection in black pepper (*Piper nigrum* L.). *Frontiers in plant science*, 7, 767. <https://doi.org/10.3389/fpls.2016.00767> PMID: 27313593
  56. Ferdous J., Sanchez-Ferrero J. C., Langridge P., Milne L., Chowdhury J., Brien C., et al. (2017). Differential expression of microRNAs and potential targets under drought stress in barley. *Plant, cell & environment*, 40(1), 11–24. <https://doi.org/10.1111/pce.12764> PMID: 27155357
  57. Hackenberg M., Gustafson P., Langridge P., & Shi B. J. (2015). Differential expression of micro RNA s and other small RNA s in barley between water and drought conditions. *Plant biotechnology journal*, 13(1), 2–13. <https://doi.org/10.1111/pbi.12220> PMID: 24975557
  58. Curaba J., Spriggs A., Taylor J., Li Z., & Helliwell C. (2012). miRNA regulation in the early development of barley seed. *BMC plant biology*, 12(1), 1–16. <https://doi.org/10.1186/1471-2229-12-120> PMID: 22838835
  59. Deng P., Wang L., Cui L., Feng K., Liu F., Du X., et al. (2015). Global identification of microRNAs and their targets in barley under salinity stress. *PLoS One*, 10(9), e0137990. <https://doi.org/10.1371/journal.pone.0137990> PMID: 26372557
  60. Yoshida H., Wang K.L., Chang C.M., Mori K., Uchida E., Ecker J.R. (2006). The ACC synthase TOE sequence is required for interaction with ETO1 family proteins and destabilization of target proteins. *Plant Mol Biol*. 62(3):427–37. <https://doi.org/10.1007/s11103-006-9029-7> PMID: 16897471
  61. Abeles F. B., Morgan P. W., & Saltveit M. E. (1992). CHAPTER 5—Roles and Physiological Effects of Ethylene in Plant Physiology: Dormancy, Growth, and Development. In *Ethylene in Plant Biology* (2nd ed., pp. 120–181). Academic Press.
  62. Glazebrook J. (2005). Contrasting mechanisms of defense against biotrophic and necrotrophic pathogens. *Annu. Rev. Phytopathol.*, 43, 205–227. <https://doi.org/10.1146/annurev.phyto.43.040204.135923> PMID: 16078883
  63. Li N., Han X., Feng D., Yuan D., & Huang L. J. (2019). Signaling crosstalk between salicylic acid and ethylene/jasmonate in plant defense: do we understand what they are whispering?. *International Journal of Molecular Sciences*, 20(3), 671. <https://doi.org/10.3390/ijms20030671> PMID: 30720746
  64. Kieber J. J., Rothenberg M., Roman G., Feldmann K. A., & Ecker J. R. (1993). CTR1, a negative regulator of the ethylene response pathway in Arabidopsis, encodes a member of the raf family of protein kinases. *Cell*, 72(3), 427–441. [https://doi.org/10.1016/0092-8674\(93\)90119-b](https://doi.org/10.1016/0092-8674(93)90119-b) PMID: 8431946
  65. Alonso J. M., Hirayama T., Roman G., Nourizadeh S., & Ecker J. R. (1999). EIN2, a bifunctional transducer of ethylene and stress responses in Arabidopsis. *Science*, 284(5423), 2148–2152. <https://doi.org/10.1126/science.284.5423.2148> PMID: 10381874
  66. Potuschak T., Lechner E., Parmentier Y., Yanagisawa S., Grava S., Koncz C., et al. (2003). EIN3-dependent regulation of plant ethylene hormone signaling by two Arabidopsis F box proteins: EBF1 and EBF2. *Cell*, 115(6), 679–689. [https://doi.org/10.1016/s0092-8674\(03\)00968-1](https://doi.org/10.1016/s0092-8674(03)00968-1) PMID: 14675533
  67. Chen X., Steed A., Travella S., Keller B., & Nicholson P. (2009). *Fusarium graminearum* exploits ethylene signalling to colonize dicotyledonous and monocotyledonous plants. *New Phytologist*, 182(4), 975–983. <https://doi.org/10.1111/j.1469-8137.2009.02821.x> PMID: 19383094
  68. Shan L., He P., Li J., Heese A., Peck S. C., Nürnberger T., et al. (2008). Bacterial effectors target the common signaling partner BAK1 to disrupt multiple MAMP receptor-signaling complexes and impede

- plant immunity. *Cell host & microbe*, 4(1), 17–27. <https://doi.org/10.1016/j.chom.2008.05.017> PMID: 18621007
69. Koch A., Kumar N., Weber L., Keller H., Imani J., & Kogel K. H. (2013). Host-induced gene silencing of cytochrome P450 lanosterol C14 $\alpha$ -demethylase-encoding genes confers strong resistance to *Fusarium* species. *Proceedings of the National Academy of Sciences*, 110(48), 19324–19329. <https://doi.org/10.1073/pnas.1306373110> PMID: 24218613
  70. Morel J. B., Godon C., Mourrain P., Béclin C., Boutet S., Feuerbach F., et al. (2002). Fertile hypomorphic ARGONAUTE (ago1) mutants impaired in post-transcriptional gene silencing and virus resistance. *The Plant Cell*, 14(3), 629–639. <https://doi.org/10.1105/tpc.010358> PMID: 11910010
  71. Livak K. J., & Schmittgen T. D. (2001). Analysis of relative gene expression data using real-time quantitative PCR and the 2 $^{-\Delta\Delta CT}$  method. *methods*, 25(4), 402–408. <https://doi.org/10.1006/meth.2001.1262> PMID: 11846609
  72. Chambers J. P., Behpouri A., Bird A., & Ng C. K. (2012). Evaluation of the use of the Polyubiquitin Genes, Ubi4 and Ubi10 as reference genes for expression studies in *Brachypodium distachyon*. *PLoS One*, 7(11), e49372. <https://doi.org/10.1371/journal.pone.0049372> PMID: 23166649
  73. Untergasser A., Cutcutache I., Koressaar T., Ye J., Faircloth B. C., Remm M., et al. (2012). Primer3—new capabilities and interfaces. *Nucleic acids research*, 40(15), e115–e115. <https://doi.org/10.1093/nar/gks596> PMID: 22730293
  74. Martin M. (2011). Cutadapt removes adapter sequences from high-throughput sequencing reads. *EMB-net. journal*, 17(1), 10–12.
  75. Langmead B., & Salzberg S. L. (2012). Fast gapped-read alignment with Bowtie 2. *Nature methods*, 9(4), 357. <https://doi.org/10.1038/nmeth.1923> PMID: 22388286
  76. Anders S., Pyl P. T., & Huber W. (2015). HTSeq—a Python framework to work with high-throughput sequencing data. *Bioinformatics*, 31(2), 166–169. <https://doi.org/10.1093/bioinformatics/btu638> PMID: 25260700
  77. Hannon, G. "Fastx-toolkit." FASTQ/A Short-reads Preprocessing Tools (2010)
  78. RStudio Team (2016). RStudio: Integrated Development for R. RStudioInc., Boston, MA URL <http://www.rstudio.com/>.
  79. Durinck S., Moreau Y., Kasprzyk A., Davis S., De Moor B., Brazma A., et al. (2005). BioMart and Bioconductor: a powerful link between biological databases and microarray data analysis. *Bioinformatics*, 21(16), 3439–3440. <https://doi.org/10.1093/bioinformatics/bti525> PMID: 16082012
  80. Adhikari S., Turner M., & Subramanian S. (2013). Hairpin priming is better suited than in vitro polyadenylation to generate cDNA for plant miRNA qPCR. *Molecular plant*, 6(1), 229–231. <https://doi.org/10.1093/mp/sss106> PMID: 23024207
  81. Charif D., & Lobry J. R. (2007). SeqinR 1.0–2: a contributed package to the R project for statistical computing devoted to biological sequences retrieval and analysis. In *Structural approaches to sequence evolution* (pp. 207–232). Springer, Berlin, Heidelberg.
  82. Camacho C., Coulouris G., Avagyan V., Ma N., Papadopoulos J., Bealer K., et al. (2009). BLAST+: architecture and applications. *BMC bioinformatics*, 10(1), 1–9. <https://doi.org/10.1186/1471-2105-10-421> PMID: 20003500
  83. R Core Team, R. (2019). R: A language and environment for statistical computing.
  84. Wickham, H. (2016). ggplot2: elegant graphics for data analysis. springer.
  85. Kassambara, A. (2017). ggpubr: "ggplot2" based publication ready plots. R package version 0.1. 6.
  86. Tian T., Liu Y., Yan H., You Q., Yi X., Du Z., et al. (2017). agriGO v2. 0: a GO analysis toolkit for the agricultural community, 2017 update. *Nucleic acids research*, 45(W1), W122–W129. <https://doi.org/10.1093/nar/gkx382> PMID: 28472432
  87. Kumar S., Stecher G., & Tamura K. (2016). MEGA7: molecular evolutionary genetics analysis version 7.0 for bigger datasets. *Molecular biology and evolution*, 33(7), 1870–1874. <https://doi.org/10.1093/molbev/msw054> PMID: 27004904
  88. Bodenhofer U., Bonatesta E., Horejš-Kainrath C., & Hochreiter S. (2015). msa: an R package for multiple sequence alignment. *Bioinformatics*, 31(24), 3997–3999. <https://doi.org/10.1093/bioinformatics/btv494> PMID: 26315911
  89. Nei M., & Kumar S. (2000). Molecular evolution and phylogenetics. Oxford university press.

## Selbstständigkeitserklärung

Hiermit versichere ich, die vorgelegte Arbeit selbstständig und ohne unerlaubte fremde Hilfe und nur mit den Hilfen angefertigt zu haben, die ich in der Thesis angegeben habe. Alle Textstellen, die wörtlich oder sinngemäß aus veröffentlichten Schriften entnommen sind, und alle Angaben die auf mündlichen Auskünften beruhen, sind als solche kenntlich gemacht. Bei den von mir durchgeführten und in der Thesis erwähnten Untersuchungen habe ich die Grundsätze guter wissenschaftlicher Praxis, wie sie in der ‚Satzung der Justus-Liebig-Universität zur Sicherung guter wissenschaftlicher Praxis‘ niedergelegt sind, eingehalten. Gemäß § 25 Abs. 6 der Allgemeinen Bestimmungen für modularisierte Studiengänge dulde ich eine Überprüfung der Thesis mittels Anti-Plagiatssoftware.

Datum

08.10.2021

Ena Šečić



## Acknowledgments

During the course of my work at the Institute of Phytopathology, there are numerous people I have to express gratitude towards, for both professional and personal support.

Firstly, to Prof. Dr. Karl-Heinz Kogel, for the opportunity to work on these exciting projects and for all the support and expertise provided and shared with me during my studies and scientific career so far.

Secondly, to my Master thesis supervisor, for her support, dedication and patience, I thank Dr. Aline Koch.

During my PhD project, many coworkers and collaboration partners without which this work would be impossible to accomplish, and my own expertise would not have been built at all – I thank Dr. Jens Steinbrenner, Dr. Jafargholi Imani, Dr. Maria José Ladera Carmona, Dr. Lukas Jelonek, Dr. Tobias Busche, Dr. Daniel Wibberg and Prof. Dr. Jörn Kalinowski.

I thank all the technical and administration assistants of the Institute, for all of their help, shared knowledge and insight, as well as patience and wisdom in guiding me through experimental work. Especially, I have to thank Dagmar Biedenkopf, whose lab assistance and efforts dedicated to all the work she does make all the challenges we meet in scientific work so much easier.

Of course, great gratitude goes to all the PhD students who worked in the Institute during my years here. Regardless of collaborative or individual projects, you all have been a great source of inspiration and knowledge. Especially, I have to thank Dr. Silvia Zanini, who worked on related projects with me, and provided excellent research and publication cooperation.

Special thanks goes to all the Bachelor and Master students who I had the privilege to co-supervise . Last but not least, I thank my parents for their unconditional love and support throughout my life and academic career.

## Supplementary material

Supplements to:

Šečić E, Zanini S, Kogel K-H: Further elucidation of the Argonaute and Dicer protein families in the model grass species *Brachypodium distachyon*. *Front Plant Sci* 2019, 10:1332.  
<https://doi.org/10.3389/fpls.2019.01332>

and

Šečić E, Zanini S, Wibberg D, Jelonek L, Busche T, Kalinowski J, Nasfi S, Thielmann J, Imani J, Steinbrenner J, Kogel K-H: A novel plant-fungal association reveals fundamental sRNA and gene expression reprogramming at the onset of symbiosis. *BMC Biol* 2021, 19:171.  
<https://doi.org/10.1186/s12915-021-01104-2>

(Additional File 2)

## *Supplementary Material*

### 1 Supplementary Tables

**Table S1: Accession numbers of *AtAGO* and *AtDCL* gene IDs, as acquired from TAIR.**

<b>Assigned name of protein</b>	<b>Gene ID (TAIR)</b>
AtAGO1	AT1G48410.2
AtAGO2	AT1G31280.1
AtAGO3	AT1G31290.1
AtAGO4	AT2G27040.1
AtAGO5	AT2G27880.1
AtAGO6	AT2G32940.1
AtAGO7	AT1G69440.1
AtAGO8	AT5G21030.1
AtAGO9	AT5G21150.1
AtAGO10	AT5G43810.1
AtDCL1	AT1G01040.1
AtDCL2	AT3G03300.1
AtDCL3	AT3G43920.2
AtDCL4	AT5G20320.1

Supplementary Material

**Table S2: Domain structure of Bd AGO-like proteins, as identified by domain search by SMART, with PFAM overlaps of higher confidence shown in some cases. Domains are indicated with a start-end residue interval, followed by E-values. Domains shown: N domain, Linker 1 (DUF1785), PAZ, Linker 2 (L2), MID and PIWI.**

Protein	N domain	DUF1785	PAZ	L2	MID	PIWI
BdAGO1		46-97 (1.34e-17)	101-225 (1.1e-23)	234-281 (4.4e-13)		325-623 (2.02e-56)
BdAGO2	56-218 (3.3e-34)	228-280 (2.37e-18)	284-412 (3e-26)	421-467 (4.8e-14)		565-874 (8.55e-110)
BdAGO3	68-228 (8.8e-34)	238-290 (7.82e-19)	294-424 (1.3e-27)	433-479 (6e-16)		576-883 (5.43e-112)
BdAGO4	38-196 (2.3e-31)	206-258 (2.27e-15)	262-389 (2.4e-25)	398-444 (2.1e-16)		541-850 (1.21e-109)
BdAGO5	42-170 (8.4e-35)	179-230 (8.4e-35)	237-368 (0.000638)	369-415 (1.6e-17)	425-496 (3.9e-11)	507-827 (5.21e-123)
BdAGO6	1-132 (5.9e-32)	141-193 (1.6e-24)	198-330 (0.00339)	334-380 (1e-13)	390-469 (1.1e-11)	481-803 (5.01e-125)
BdAGO7	169-304 (7.1e-31)	318-370 (9.7e-24)	375-504 (0.00000249)	508-554 (1.2e-14)	564-621 (6.6e-9)	658-964 (5.77e-116)
BdAGO8	191-335 (3.5e-24)	344-396 (4.07e-17)	404-544 (0.000953)	539-586 (1.1e-7)	601-673 (0.0077)	692-1000 (5.03e-107)
BdAGO9	110-245 (2.1e-34)	254-306 (1.1e-22)	311-443 (0.00232)	447-493 (9e-18)	503-583 (6e-15)	595-916 (7.09e-125)
BdAGO10	195-323 (2.6e-33)	332-383 (3.38e-23)	394-522 (0.00188)	523-569 (3.4e-17)	579-658 (4.1e-12)	664-983 (2.75e-122)
BdAGO11	186-321 (9.7e-35)	330-382 (1.18e-22)	387-522 (0.0000324)	523-569 (3.2e-15)	579-656 (5.4e-9)	673-986 (1.48e-113)
BdAGO12	233-372 (5.4e-37)	381-433 (2.11e-24)	438-570 (0.00184)	574-620 (1.1e-18)	630-710 (2e-11)	724-1045 (1.22e-128)
BdAGO13		218-278 (0.000311)	286-423 (2.7e-18)	434-481 (2.8e-13)		599-899 (3.56e-98)
BdAGO14	251-373 (7.5e-14)	374-419 (0.000167)	423-550 (3.8e-23)	560-607 (1.6e-10)		699-996 (1.6e-10)
BdAGO15	213-352 (2.7e-36)	361-413 (1.28e-23)	418-550 (0.00155)	554-600 (1.1e-17)	610-689 (1.3e-10)	704-1026 (1.36e-126)
BdAGO16	183-317 (3.7e-37)	326-378 (9.7e-24)	383-518 (0.000464)	519-565 (8.5e-18)	575-652 (4.5e-10)	669-990 (7.9e-123)

**Table S3: Domain structure of BdDCLs, as identified by domain search by SMART, with PFAM overlaps of higher confidence shown in some cases. Domains are indicated with a start-end residue interval, followed by E-values. Domains shown: DEXDc, HELICc, Dicer\_dimer, PAZ, RIBOc, DSRM.**

Protein	DEXDc	HELICc	Dicer_dimer	PAZ	RIBOc	RIBOc	DSRM	DSRM
BdDCL1	266-469 (9.68e-20)	703-789 (5.28e-12)	862-952 (6.6e-24)	1203-1366 (1.43e-29)	1381-1564 (6.27e-34)	1600-1756 (5.62e-45)	1760-1821 (1.53e-6)	1845-1918 (2.15e-10)
BdDCL2a	23-223 (3.78e-22)	406-493 (1.35e-18)	561-642 (1.6e-18)	810-952 (2.08e-8)	972-1127 (1.12e-21)	1159-1314 (5.06e-29)	1318-1382 (0.0221)	
BdDCL2b	1-201 (3.93e-20)	379-466 (1.54e-13)		766-908 (0.0000604)	928-1086 (2.76e-21)	1116-1271 (9.08e-31)	1275-1339 (0.000000573)	
BdDCL3a	22-219 (4.62e-17)	410-500 (3.76e-17)	567-653 (1.3e-26)	849-1014 (0.000611)	1031-1204 (2.65e-23)	1240-1396 (2.51e-33)	1400-1463 (0.0000011)	1530-1612 (0.423)
BdDCL3b				434-577 (6.8e-15)	596-772 (6.73e-25)	805-961 (2.22e-34)	965-1028 (0.201)	1090-1172 (0.806)
BdDCL4	17-211 (2e-21)	404-486 (2.64e-12)	550-636 (8.5e-24)	813-967 (5.81e-7)	988-1156 (9.04e-17)	1192-1344 (2.63e-27)	1348-1413 (0.912)	1539-1613 (9.59e-8)

**Table S4: Validation of predicted 3D structures of BdAGO-like proteins. Prediction with CPH and Swiss Model, validation by QMEAN, PROCHECK, WHATCHECK and dFIRE. Last column indicates the template used for the model and coverage.**

Protein	3D Modelling software	QMEAN (Z-score)	Residues in favored region (PROCHECK)	Ramachandran z-score (WHATCHECK)	dDFIRE total energy	Model used (coverage)
BdAGO1	CPH	-6.14	79.3%	-5.375	-1173.77	
	Swiss Model	-3.14	86.70%	-1.536	-1294.89	Protein argonaute-1 – 4kxt.1.A (0.94)
BdAGO2	CPH	-5.48	81.1%	-4.973	-1678.64	
	Swiss Model	-3.28	87.00%	-1.786	-1869.75	Protein argonaute-2 – 4f3t.1.A (0.87)
BdAGO3	CPH	-5.67	79.5%	-5.237	-1679.2	
	Swiss Model	-3.32	86.50%	-2.586	-1706.52	Protein argonaute-2 – 4w5n.1.A (0.82)
BdAGO4	CPH	-7.65	79.4%	-5.321	-1552.69	
	Swiss Model	-3.64	85.30%	-2.321	-1847.83	Protein argonaute-2 – 4w5n.1.A (0.91)
BdAGO5	CPH	-4.74	81.6%	-4.936	-1783.77	
	Swiss Model	-2.85	88.40%	-1.206	-1920.25	Protein argonaute-2 – 4z4f.1.A (0.94)
BdAGO6	CPH	-4.33	82.30%	-4.94	-1769.1	
	Swiss Model	-2.67	87.50%	-2.23	-1889.91	Protein argonaute-2 – 4w5n.1.A (0.96)
BdAGO7	CPH	-4.99	80.8%	-4.814	-1753.88	
	Swiss Model	-3.35	86.20%	-2.068	-1867.99	Protein argonaute-2 – 4w5n.1.A (0.82)
BdAGO8	CPH	-4.94	82.7%	-5.319	-1777.54	
	Swiss Model	-3.38	86.10%	-2.074	-1930.16	Protein argonaute-2 – 4w5n.1.A (0.79)
BdAGO9	CPH	-3.61	84.6%	-4.933	-1803.08	
	Swiss Model	-2.77	87.00%	-1.643	-1928.83	Protein argonaute-2 – 4w5n.1.A (0.87)
BdAGO10	CPH	-3.98	83.7%	-4.673	-1766.73	
	Swiss Model	-2.68	88.20%	-1.34	-1903.52	Protein argonaute-2 - 4z4f.1.A (0.80)
BdAGO11	CPH	-3.77	84.1%	-4.942	-1778.22	
	Swiss Model	-2.46	88.20%	-1.749	-1796.97	Protein argonaute-2 – 4w5n.1.A (0.80)
BdAGO12	CPH	-4.16	83.6%	-5.042	-1806.27	
	Swiss Model	-2.98	86.20%	-1.992	-1944.46	Protein argonaute-1 – 4kxt.1.A (0.76)
BdAGO13	CPH	-8.48	76.2%	-5.955	-1502.92	
	Swiss Model	-3.26	86.60%	-2.38	-1726.87	Protein argonaute-2 – 4w5n.1.A (0.83)
BdAGO14	CPH	-5.36	79.8%	-5.108	-1567.95	
	Swiss Model	-2.63	89.30%	-1.744	-1758.43	Protein argonaute-2- 5f7b.1.B (0.75)
BdAGO15	CPH	-4.42	83.4%	-5.035	-1777.14	
	Swiss Model	-3.2	87.40%	-1.706	-1946.8	Protein argonaute-2 – 4w5n.1.A (0.78)
BdAGO16	CPH	-3.58	83.4%	-5.044	-1806.1	
	Swiss Model	-2.2	89.00%	-1.575	-1940.92	Protein argonaute-2- 4z4f.1.A (0.80)

**Table S5: Validation of predicted 3D structures of AtAGO proteins. Prediction with CPH and Swiss Model. validation by QMEAN, PROCHECK, WHATCHECK and dFIRE. Last column indicates the template used for the model and coverage.**

Protein	3D Modelling software	QMEAN (Z-score)	Residues in favored region (PROCHECK)	Ramachandran z-score (WHATCHECK)	dFIRE total energy	Template used (coverage)
AtAGO1	CPH	-4.21	83.6%	-4.76	-1789.47	
	Swiss Model	-2.15	89.2%	-1.28	-1987.42	Protein argonaute-1-4kre.1.A (0.79)
AtAGO2	CPH	-5.47	80.80%	-5.282	-1698.99	
	Swiss Model	-3.76	86.3%	-1.825	-1851.7	Protein argonaute-2-4w5n.1.A (0.81)
AtAGO3	CPH	-4.96	82.0%	-5.318	-1714.79	
	Swiss Model	-3.23	87.8%	-1.902	-1901.54	Protein argonaute-2 -4f3t.1.A (0.70)
AtAGO4	CPH	-4.76	80.7%	-4.976	-1695.86	
	Swiss Model	-3.08	86.3%	-1.997	-1896.01	Protein argonaute-2-4w5n.1.A (0.87)
AtAGO5	CPH	-3.78	83.8%	-4.96	-1767.24	
	Swiss Model	-2.75	88.5%	-1.457	-1903.68	Protein argonaute-2-4w5n.1.A (0.83)
AtAGO6	CPH	-4.72	82.4%	-4.847	-1782.18	
	Swiss Model	-2.81	87.8%	-1.613	-1878.9	Protein argonaute-2-5js2.1.A (0.91)
AtAGO7	CPH	-5.23	78.9%	-5.275	-1690.98	
	Swiss Model	-2.81	88.2%	-1.472	-1923.34	Protein argonaute-2-4z4h.1.A (0.82)
AtAGO8	CPH	-6.4	77.4%	-5.105	-1569.03	
	Swiss Model	-3.26	90.0%	-1.922	-1646.43	Protein argonaute-1-4kre.1.A (0.86)
AtAGO9	CPH	-4.28	80.5%	-5.024	-1685.77	
	Swiss Model	-3.26	84.6%	-2.29	-1875.11	Protein argonaute-2-4w5n.1.A (0.90)
AtAGO10	CPH	-5.59	84.0%	-5.135	-1726.53	
	Swiss Model	-2.56	91.2%	-1.397	-1954.61	Protein argonaute-2-5t7b.1.B (0.84)

**Table S6: Interacting proteins of BdAGOs predicted with STRING (coexpression and experimental validation only connections shown)**

BdAGO Protein	Interacts with:	Interacting protein description	Coexpression Score	Experimental Validation Score	Combined Score	Reference
BdAGO9	BRADI1G07247.1	Hypothetical protein	0	0.486	0.485	Ding et al., 2015
BdAGO9	BRADI1G10047.1	Hypothetical protein	0	0.486	0.485	Ding et al., 2015
BdAGO9	BRADI1G12677.1	homeobox protein knotted-1-like 4	0	0.486	0.485	Ding et al., 2015
BdAGO9	BRADI1G12690.1	homeobox protein knotted-1-like 4 isoform X1	0	0.486	0.485	Ding et al., 2015
BdAGO1; BdAGO2; BdAGO3	BRADI1G36340.1	110 kDa U5 small nuclear ribonucleoprotein component CLO	0.043	0.453	0.454	Kallgren et al., 2014
BdAGO4; BdAGO5; BdAGO6; BdAGO7; BdAGO8; BdAGO9; BdAGO10; BdAGO11; BdAGO12; BdAGO13; BdAGO14; BdAGO15; BdAGO16			0		0.453	
BdAGO9	BRADI1G57607.1	homeobox protein knotted-1-like 12	0	0.486	0.485	Ding et al., 2015
BdAGO9	BRADI2G14890.1	GATA transcription factor 15	0.047	0.481	0.484	Ding et al., 2015
BdAGO1; BdAGO2; BdAGO3	BRADI2G30160.1	GTP binding/ Transcription factor	0.043	0.453	0.454	Kallgren et al., 2014
BdAGO4; BdAGO5; BdAGO6; BdAGO7; BdAGO8; BdAGO9; BdAGO10; BdAGO11; BdAGO12; BdAGO13; BdAGO14; BdAGO15; BdAGO16			0		0.453	
BdAGO9	BRADI2G45750.1	GATA transcription factor 19	0.047	0.481	0.484	Ding et al., 2015
BdAGO1; BdAGO2; BdAGO3; BdAGO4; BdAGO5; BdAGO6; BdAGO7; BdAGO8; BdAGO9; BdAGO10; BdAGO11; BdAGO12; BdAGO13; BdAGO14; BdAGO15; BdAGO16	BRADI4G45065.1	DNA-directed RNA polymerase V subunit 1	0.045	0.626	0.627	Zhong et al., 2015

**Table S7: Prediction of location of BdAGO-like proteins. as done by PSI (Plant Subcellular-localization Integrative predictor). Displayed are the scores (0-1) representing the confidence the protein is present in a cellular part. All scores have p-values < 0.01.**

<b>Protein name</b>	<b>Predicted location</b>	<b>Score</b>
BdAGO1	cytosol	0.59008
BdAGO2	cytosol	0.58123
BdAGO3	nucleus	0.56674
BdAGO4	cytosol	0.53687
BdAGO5	cytosol	0.56023
BdAGO6	cytosol	0.56837
BdAGO7	plastid	0.47348
BdAGO8	cytosol	0.65765
BdAGO9	cytosol	0.647
BdAGO10	cytosol	0.48456
BdAGO11	cytosol	0.60782
BdAGO12	cytosol	0.56826
BdAGO13	cytosol	0.6786
BdAGO14	nucleus	0.51582
BdAGO15	cytosol	0.6013
BdAGO16	cytosol	0.36562

**Figure S1: 3D structure prediction of BdAGO8, as modeled by SWISS-MODEL. AtAGO7 3D structure prediction is displayed as the closest homolog in Arabidopsis. PAZ (yellow), Mid (red) and PIWI (blue) domains as predicted by SMART and PFAM displayed. The catalytic tetrad within the PIWI domain (DEDH) marked by magenta spheres. Visualization by PyMOL.**

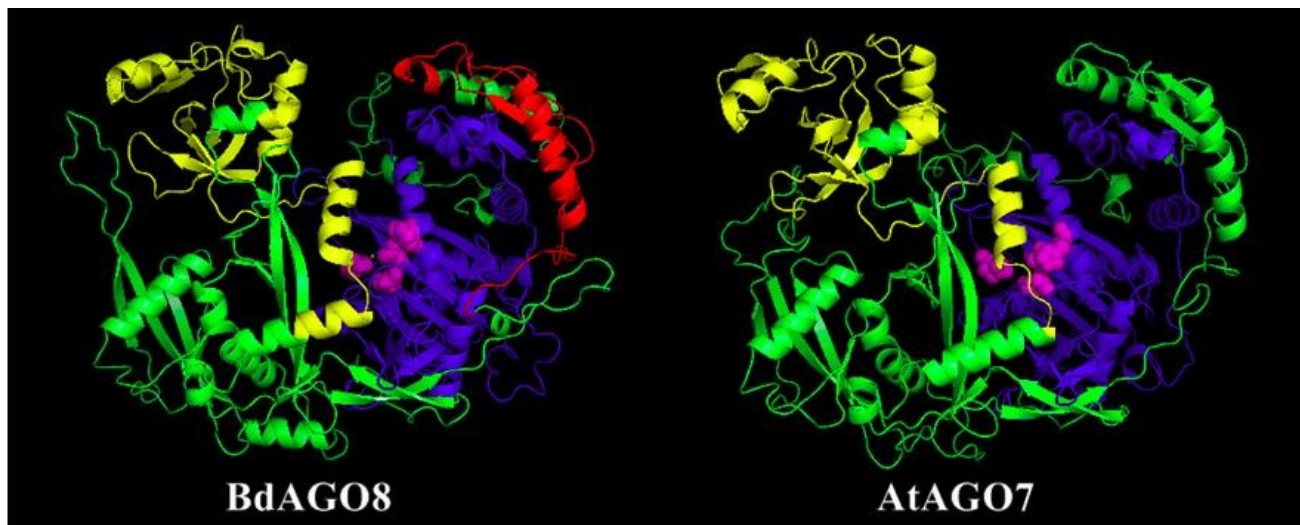
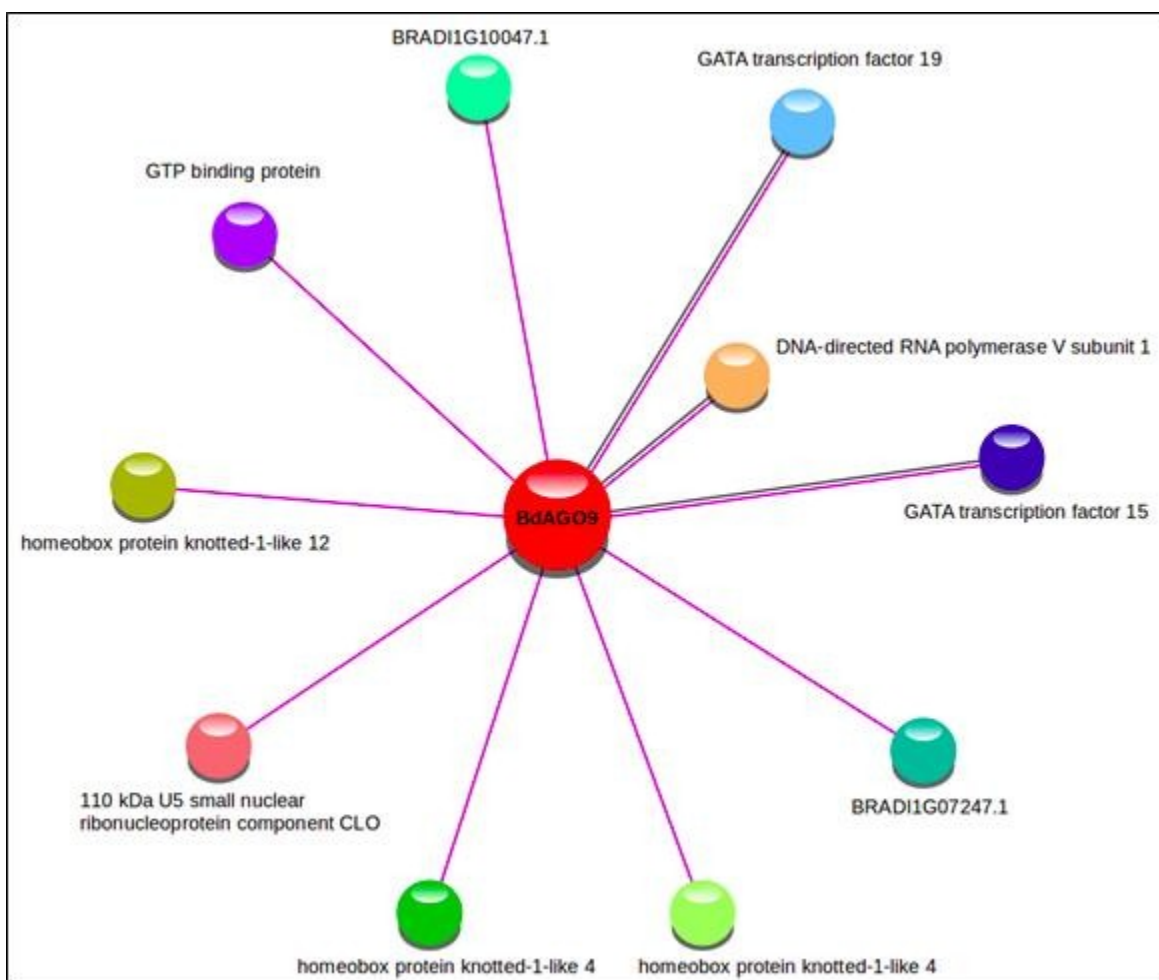


**Figure S2: Interacting proteins of BdAGO9 predicted with STRING (coexpression and experimental validation only connections valid). Pink connection: based on experimental data. Black connection: based on coexpression.**



## Additional File 2: Supporting Information

### Title: A novel plant-fungal association reveals fundamental sRNA and gene expression reprogramming at the onset of symbiosis

**Authors:** Ena Šečić, Silvia Zanini, Daniel Wibberg, Lukas Jelonek, Tobias Busche, Jörn Kalinowski, Sabine Nasfi, Jennifer Thielmann, Jafargholi Imani, Jens Steinbrenner and Karl-Heinz Kogel

**Figure S1: *Serendipita indica* (Si) colonization alters *Brachypodium distachyon* Bd21-3 root structure.** One-week-old Bd21-3 seedlings were mock treated (Bd-C) or dip-inoculated with  $5 \times 10^5$  chlamydospores per ml (Bd-Si) and subsequently grown for four days (a) or 25 days (b) on a vermiculite:oil dri mix.

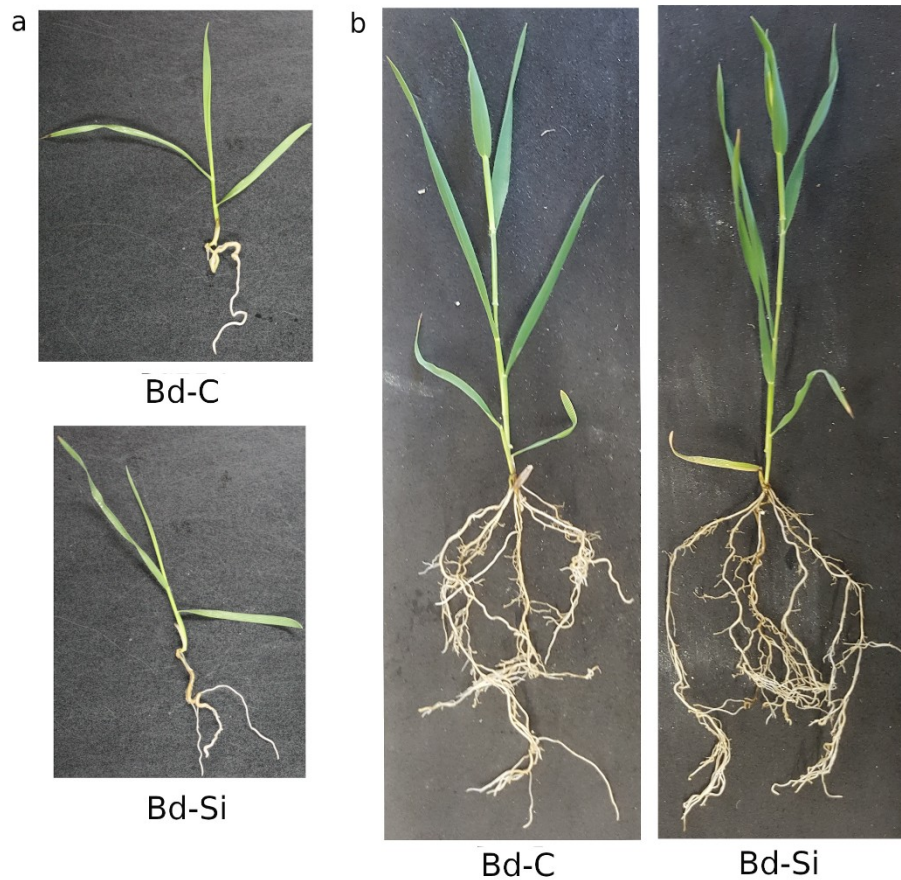


**Figure S2: Progress of *Serendipita indica* (Si) spore proliferation during colonization of *Brachypodium distachyon* Bd21-3.** Displayed at 4DPI (days post inoculation), when new spores were first observed, and at 7DPI and 14 DPI, with an increasing number of chlamydospores. Fluorescence microscopy showing WGA-AF488 staining of Si cell walls ( $\lambda_{exc}494$  nm,  $\lambda_{em}515$ ). Imaging was done with a LEICA S8 confocal microscope.

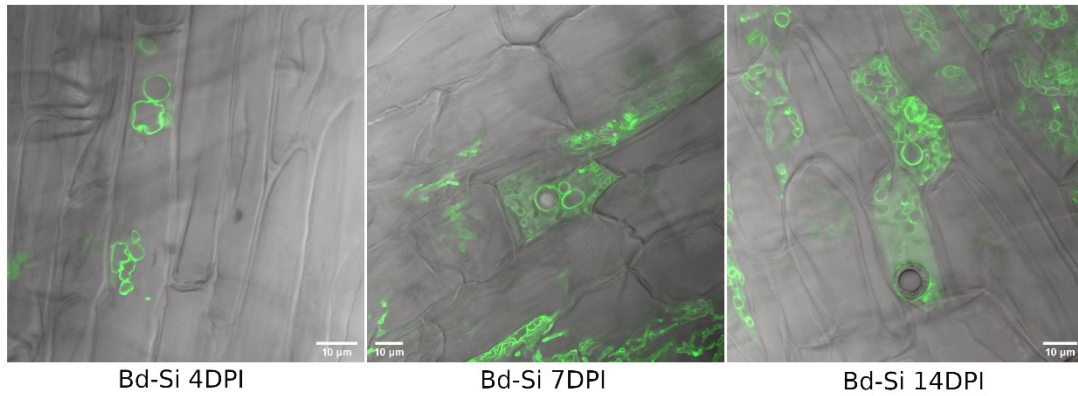


**Figure S3: Shared and unique genes of *Serendipita indica* between the originally sequenced and resequenced genome.** Venn diagram (as displayed by EDGAR 2.3) showing the number of genes that are shared between (core) or are unique to (single color) the resequenced *Serendipita indica* (Si) genome and the Zuccaro *et al.*, 2011 (22) assembly.

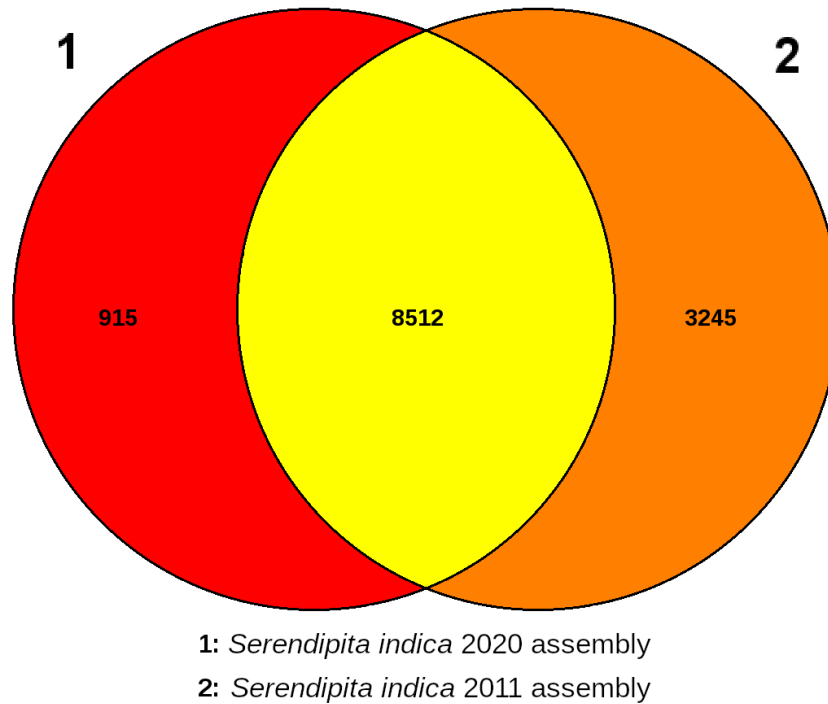


**Figure S4: Shared and unique genes of the *Serendipita indica* with *Serendipita vermifera* and *Laccaria bicolor*.** Venn diagram (as displayed by EDGAR 2.3) showing the number of genes that are shared between (core) or are unique to (single color) the resequenced *Serendipita indica* (Si) genome and those of *Serendipita vermifera* and *Laccaria bicolor*.

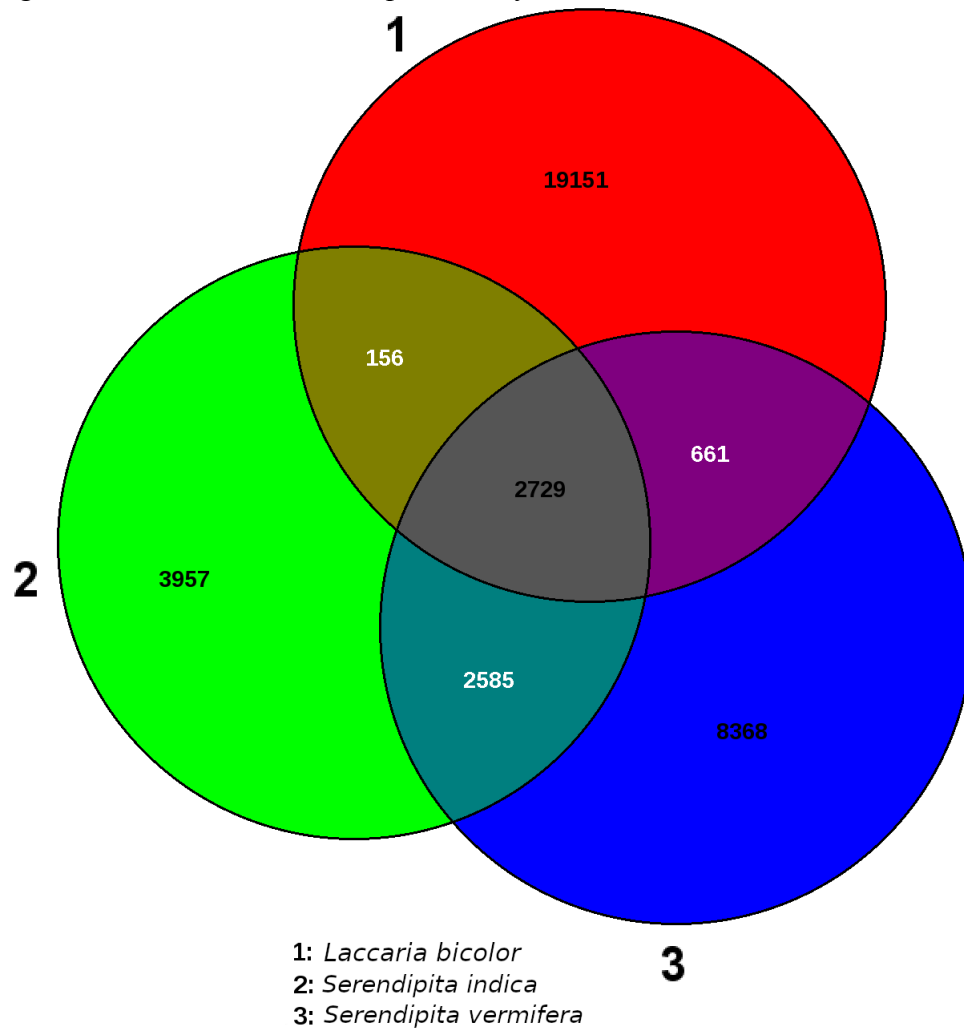


**Figure S5: Quantitative real-time PCR (qRT-PCR) of selected DEG transcripts during *Si* colonization of Bd21-3.** Expression was measured in mock-treated and *Si*-inoculated *Bd* roots (a) and axenic *Si* control and *Si*-inoculated *Bd* roots (b). One-week-old seedlings were inoculated with  $5 \times 10^5$  chlamydospores per ml and subsequently grown for four days on a vermiculite:oil dri mixture (semi-sterile conditions). Sample size (n) = 3 biological samples, each containing 3-4 pooled roots. Two independent biological replicates (inoculations) were performed for each gene, standard error (SE) bars indicated. Individual data values of fold change are available in Additional File 1. The significance threshold after t-test or Mann-Whitney-Wilcoxon test was set at .05 (\*= $<.05$ ; \*\*= $<.001$ ). *Bd* transcripts tested (in Table 2): glycosyl-hydrolase (BdiBd21-3.3G0639500.1), HSP 90-1 (BdiBd21-3.5G0024800.1), PRR7 (BdiBd21-3.1G0887100.1), RCI2 (BdiBd21-3.1G0416000.1), WAK (BdiBd21-3.2G0600500.1). Primers used in Table S9.

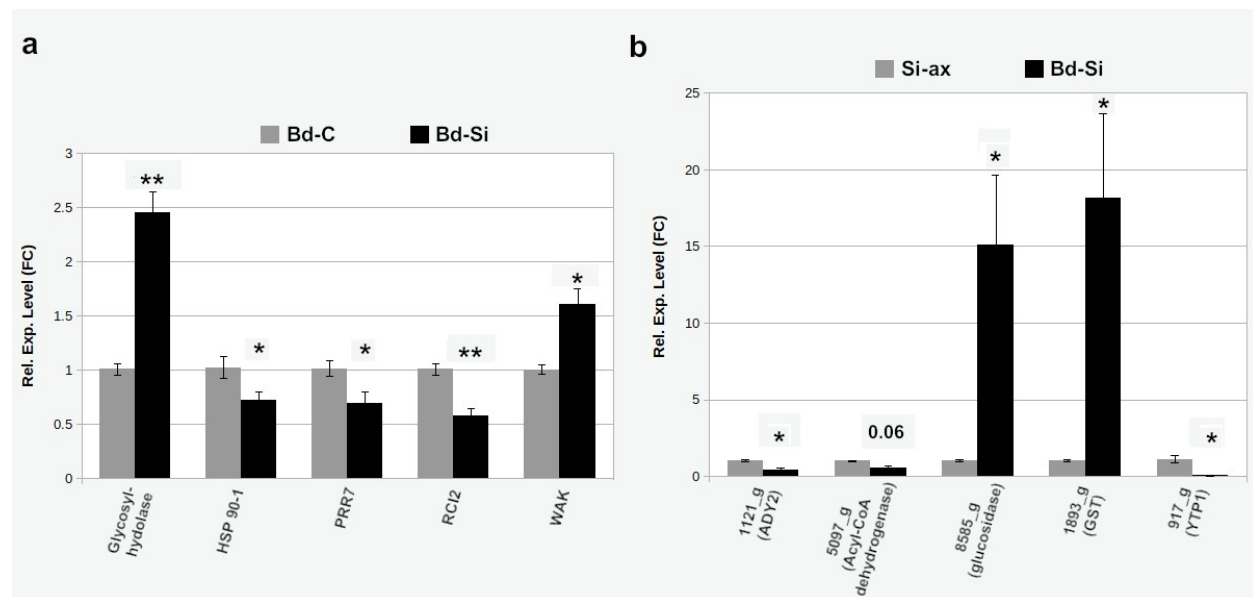


**Figure S6: Filtering pipelines utilized in sRNA analysis.** These pipelines were used to identify putative cross-kingdom (ck-sRNAs) and putative endogenous sRNAs in *Serendipita indica* (Si) and *Brachypodium distachyon* Bd21-3.

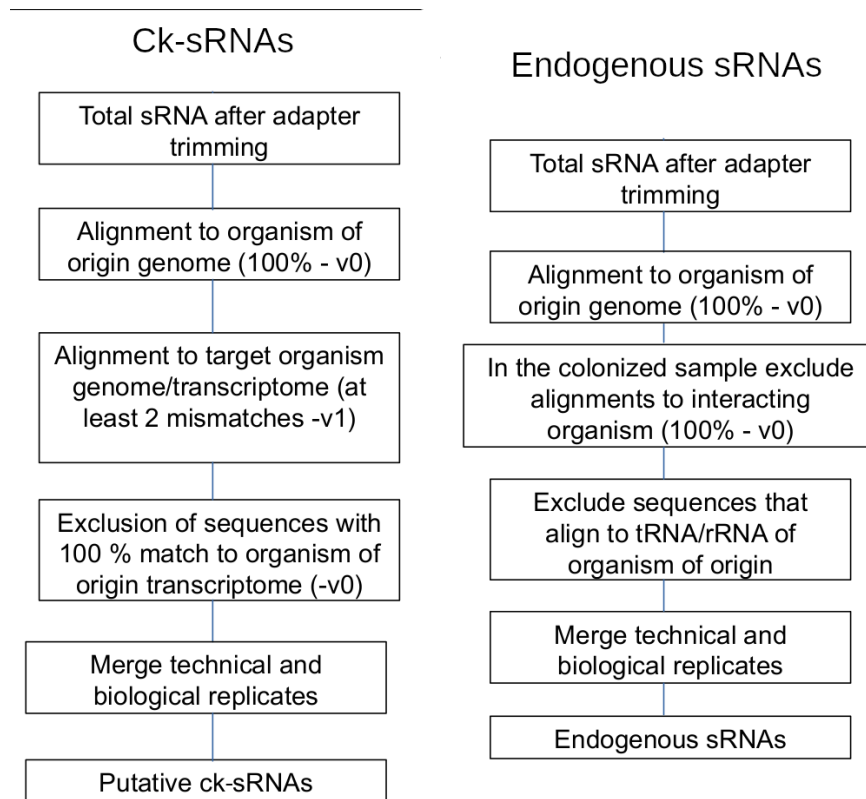


**Figure S7: Size distribution of total and unique putative ck-sRNAs in the interaction and reads from controls.** a) Bd-C (mock-treated), b) Bd-Si (colonized root), c) Si-ax (axenic *Si* culture), and d) Bd-Si. All datasets represent three biological replicates and corresponding two technical replicates, merged together. sRNA length is displayed on the X-axis (nt) and number of total/unique sRNA counts on the Y-axis ( $\times 10^3$ ).

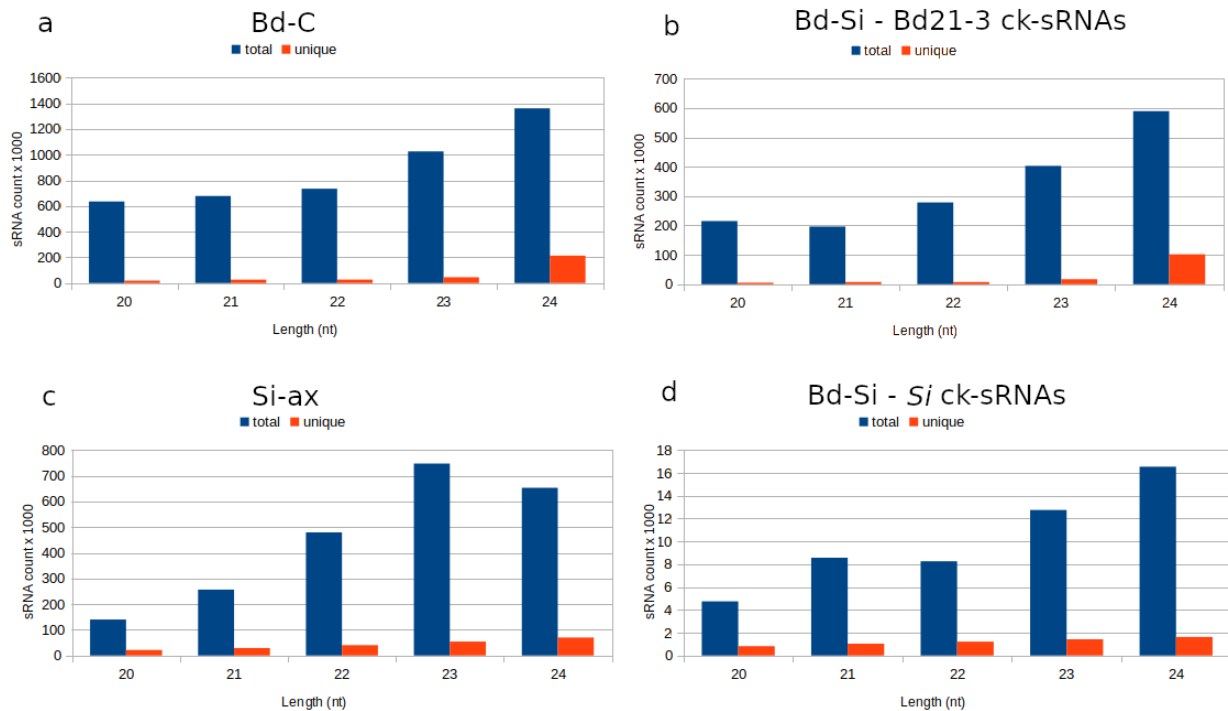


**Figure S8: 5' terminal nucleotide distribution of unique putative endogenous sRNAs.**

Percentage distribution of the 5' terminal nucleotide in unique putative endogenous sRNAs (18 – 30 nt) from Bd-C (mock-treated), Bd-Si (colonized root) and Si-ax (axenic culture).

*Brachypodium distachyon* Bd21-3- and *Serendipita indica*-associated endogenous sRNAs were identified from the colonized root sample by aligning filtered sRNAs with the plant or fungal genome; they are presented as Bd-Si Bd endg or Bd-Si Si endg, respectively.

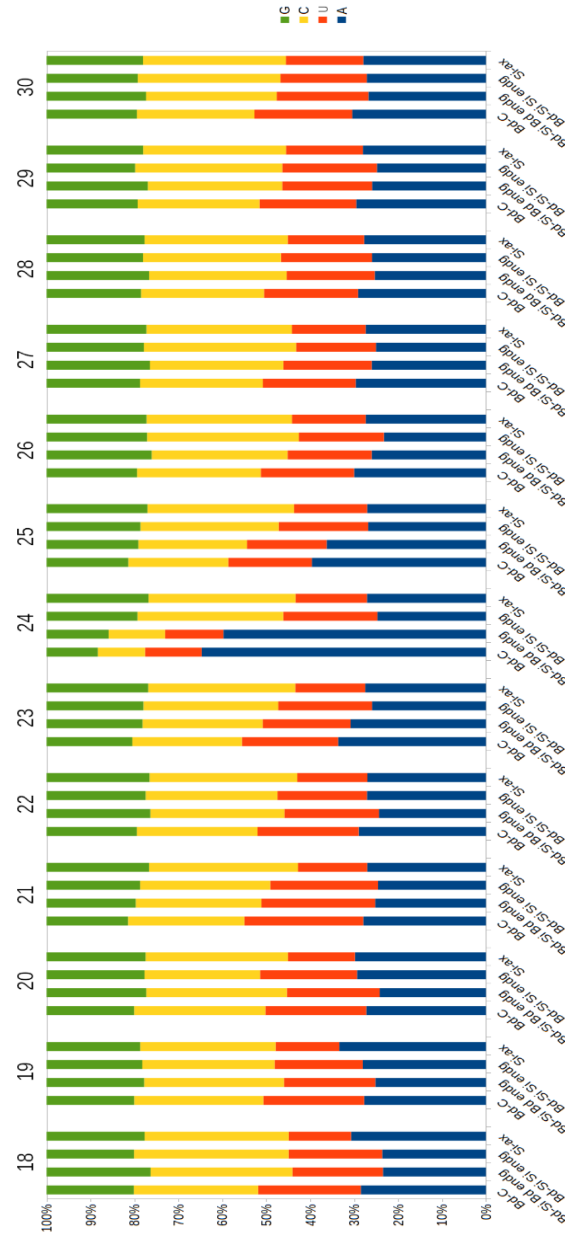


**Figure S9: 5' terminal nucleotide distribution of unique putative ck-sRNAs.** Percentage distribution of the 5' terminal nucleotide in unique reads (20-24 nt long) from Bd-C (mock-treated) and Si-ax (axenic culture) samples, putative ck-sRNAs from Bd-Si (colonized root) sample. *Brachypodium distachyon* Bd21-3- and *Serendipita indica*-associated ck-sRNAs were identified from the colonized root sample by aligning filtered sRNAs with the plant or fungal genome; they are presented as Bd-Si Bd ck or Bd-Si Si ck, respectively.

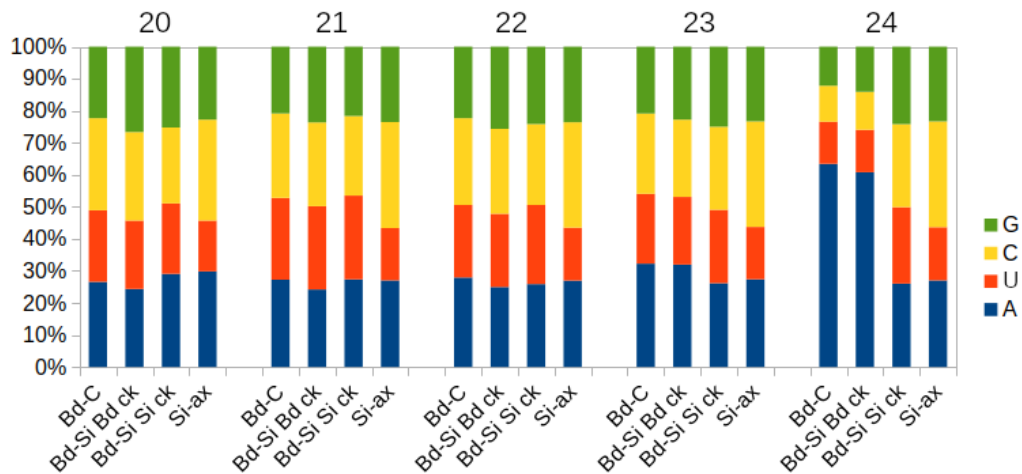


**Figure S10: 5' terminal nucleotide distribution of total putative endogenous sRNAs.**  
 Percentage distribution of the 5' terminal nucleotide in total putative endogenous sRNAs (18 – 30 nt long) from Bd-C (mock-treated), Bd-Si (colonized root) and Si-ax (axenic culture). *Brachypodium distachyon* Bd21-3- and *Serendipita indica*-associated endogenous sRNAs were identified from the colonized root sample by aligning filtered sRNAs with the plant or fungal genome; they are presented as Bd-Si Bd endg or Bd-Si Si endg, respectively.

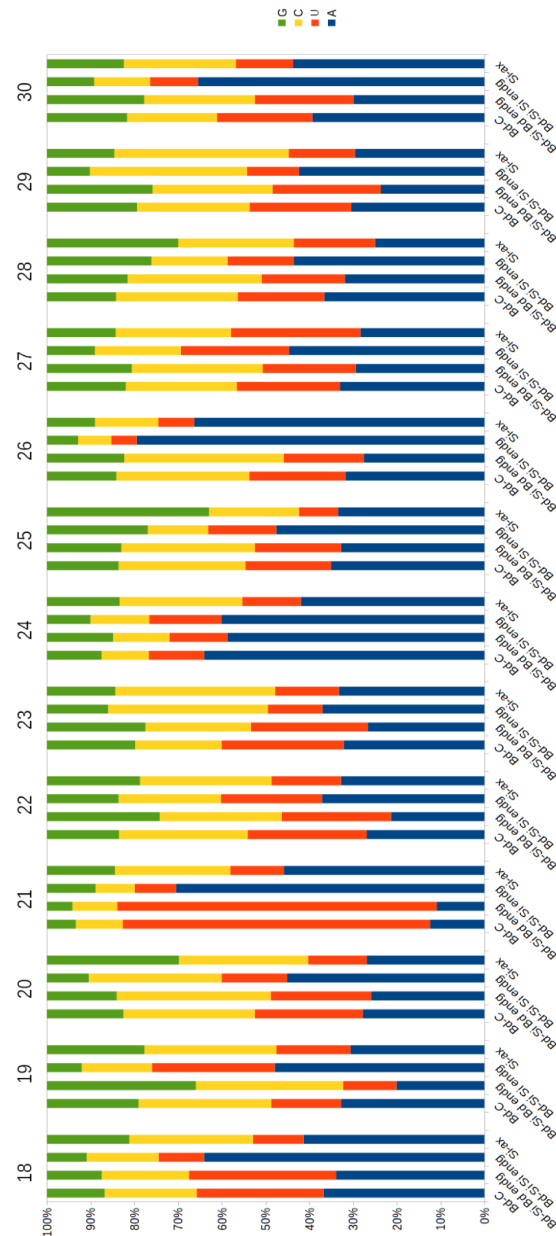


**Figure S11: 5' terminal nucleotide distribution of total putative ck-sRNAs.** Percentage distribution of the 5' terminal nucleotide in total reads (20-24 nt long) from Bd-C (mock-treated) and Si-ax (axenic culture) samples, putative ck-sRNAs from Bd-Si (colonized root) sample. *Brachypodium distachyon* Bd21-3- and *Serendipita indica*-associated ck-sRNAs were identified from the colonized root sample by aligning filtered sRNAs with the plant or fungal genome; they are presented as Bd-Si Bd ck or Bd-Si Si ck, respectively.

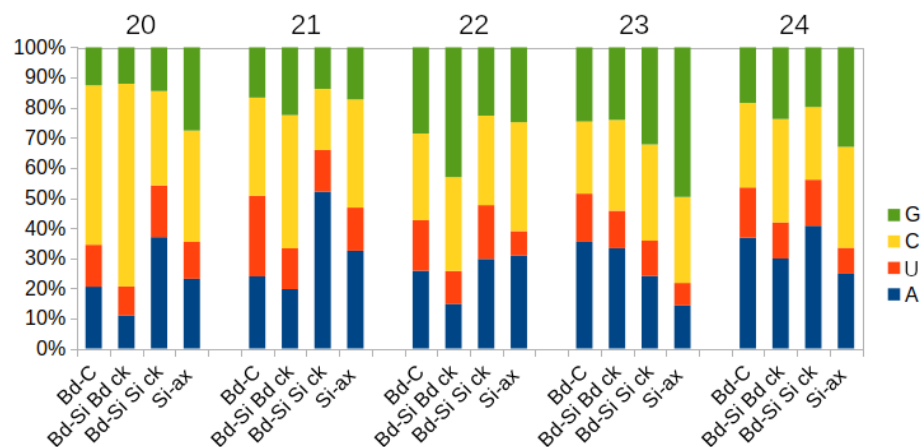


**Figure S12: Stem-loop PCR to show expression of selected sRNAs during the interaction.** Gel electrophoresis after stem-loop PCR of *Si* (a) and *Bd21-3* (b) sRNAs identified in the Bd-Si sample during sequencing. Length of amplicon (sRNA+hairpin) is 65bp. Small RNAs marked with (\*) were further confirmed by sequencing (Table S8), and the primers used are displayed in Table S10. Original gel pictures are available as Additional File 3 and Additional File 4.

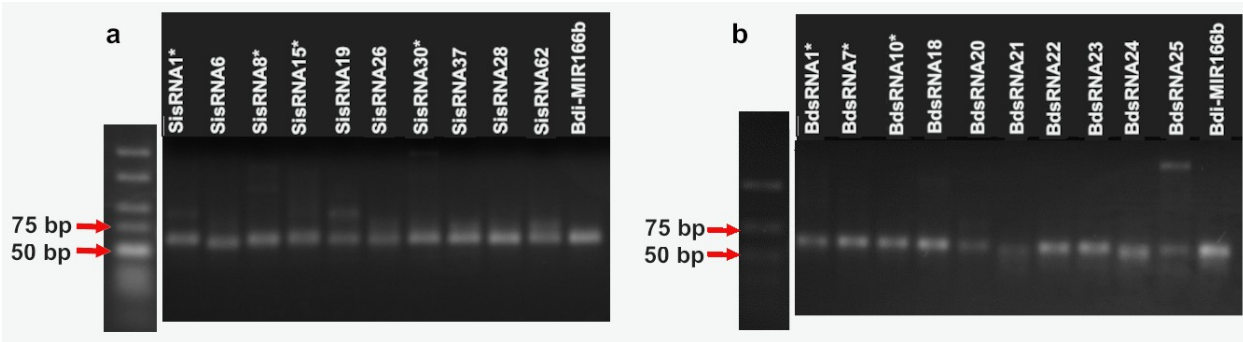


**Table S1:** Quantification of identified features in the resequenced genome of *Serendipita indica* (Si).

Genome feature	Value
Gene density	380.68 genes/Mbp
Contigs	57
Total Genome Size	24.8Mbp (24724951 bp)
Gene/mRNA number	9441
Exon number	59045
Intron number	49604
Intergenic region	9498
Mean (median) gene length	1955.36bp (1554.00bp)
Mean (median) exon length	259.97bp (149.00bp)
Mean (median) intron length	62.71bp (48.00bp)
Mean (median) intergenic region	659.54bp (363.00bp)
Exons/Gene	6.25
Cumulative length of genes (% of genome)	18.5M bp (18460589 bp) (0.75)
Cumulative length of exons (% of genome)	15.4M bp (15350115 bp) (0.62)
Cumulative length of introns (% of genome)	3.2M bp (3110474 bp) (0.13)
Cumulative length of intergenic regions (% of genome)	6.3M bp (6264362 bp) (0.25)

**Table S2:** Total reads from the Bd-C (mock-treated), Bd-Si (colonized root) and Si-ax (axenic culture) samples.

<b>Sample description</b>	<b>Total reads (PE)</b>	<b>Overall alignment rate to genome</b>
<i>Si</i> axenic culture (Si-ax)	53 million	96.54 % reads align to <i>Si</i> genome
Bd21-3 mock treated control (Bd-C)	53.2 million	98 % reads align to Bd21-3 genome
Bd21-3 + <i>Si</i> 4 DPI (Bd-Si)	55 million	96.55 % reads align to Bd21-3 genome
		2.13 % reads align to <i>Si</i> genome

**Table S3:** Significant GO terms of molecular function in the differentially expressed gene (DEG) datasets.\*

Term ID	P-value (FDR)	Term
<b>Si DEGs</b>		
GO:0016491	0.00007	oxidoreductase activity
GO:0004553	0.00007	hydrolase activity hydrolyzing O-glycosyl compounds
GO:0016798	0.00007	hydrolase activity acting on glycosyl bonds
GO:0030246	0.00007	carbohydrate binding
GO:0030247	0.00007	polysaccharide binding
GO:0001871	0.00007	pattern binding
GO:0030248	0.00007	cellulose binding
GO:0016876	0.00007	ligase activity forming aminoacyl-tRNA and related compounds
GO:0004812	0.00007	aminoacyl-tRNA ligase activity
GO:0016875	0.00007	ligase activity forming carbon-oxygen bonds
GO:0003824	0.00017	catalytic activity
GO:0016874	0.00028	ligase activity
GO:0003995	0.0055	acyl-CoA dehydrogenase activity
GO:0048037	0.01	cofactor binding
GO:0016627	0.01	oxidoreductase activity acting on the CH-CH group of donors
GO:0016684	0.012	oxidoreductase activity acting on peroxide as acceptor
GO:0004601	0.012	peroxidase activity
GO:0016829	0.019	lyase activity
GO:0016620	0.028	oxidoreductase activity acting on the aldehyde or oxo group of donors NAD or NADP as acceptor
GO:0070003	0.028	threonine-type peptidase activity
GO:0004298	0.028	threonine-type endopeptidase activity
GO:0002161	0.033	aminoacyl-tRNA editing activity
GO:0016903	0.04	oxidoreductase activity acting on the aldehyde or oxo group of donors NAD or NADP as acceptor
GO:0000287	0.044	magnesium ion binding
GO:0050662	0.045	coenzyme binding
GO:0016840	0.045	carbon-nitrogen lyase activity
GO:0004725	0.047	protein tyrosine phosphatase activity
<b>Bd21-3 DEGs</b>		
GO:0046906	0.00000039	tetrapyrrole binding
GO:0020037	0.00000039	heme binding
GO:0003824	0.00000072	catalytic activity
GO:0016829	0.000016	lyase activity
GO:0005506	0.000018	iron ion binding
GO:0016491	0.000018	oxidoreductase activity
GO:0016705	0.000035	oxidoreductase activity acting on paired donors with incorporation or reduction of molecular oxygen
GO:0048037	0.0036	cofactor binding
GO:0016830	0.0039	carbon-carbon lyase activity
GO:0016831	0.0066	carboxy-lyase activity
GO:0043168	0.014	anion binding
GO:0016684	0.014	oxidoreductase activity acting on peroxide as acceptor
GO:0004601	0.014	peroxidase activity
GO:0030170	0.016	pyridoxal phosphate binding
GO:0016209	0.017	antioxidant activity
GO:0016887	0.017	ATPase activity
GO:0016758	0.027	transferase activity transferring hexosyl groups
GO:0043167	0.031	ion binding
GO:0016757	0.034	transferase activity transferring glycosyl groups

\* Analysis was done on *Serendipita indica* and *Brachypodium distachyon* Bd21-3 with AgriGO v2.0. Hochberg (FDR) adjustment for multiple testing was used and is reported in the table.

**Table S4:** A representative set of potential protein effectors identified in the resequenced *Serendipita indica* (*Si*) genome.\*

Putative effector gene	log2FC	Description	DE putative effector
5323_g(PIIN_05891)	13.26	Hypothetical protein	
2999_g(PIIN_05674)	10.99	Hypothetical protein	
7143_g(PIIN_07595)	10.53	Hypothetical protein, DELD	<i>Hv</i> colonization
4184_g(PIIN_06901)	9.16	Hypothetical protein	
3615_g(PIIN_11270)	7.36	Related to esterase D	
5279_g(PIIN_10706)	7.36	Hypothetical protein, DELD	<i>Hv</i> and <i>At</i> colonization
3514_g(PIIN_09664)	7.01	Related to glucose oxidase	
2829_g(PIIN_07952)	6.66	Hypothetical protein	
2677_g(PIIN_08766)	6.5	Related to hydrophobin	
6427_g(PIIN_07750)	6.42	Related to triacylglycerol lipase precursor	
7044_g(PIIN_07884)	6.38	Hypothetical protein	
4610_g(PIIN_01386)	6.36	Hypothetical protein	
4303_g(PIIN_03861)	6.21	Hypothetical protein	
7637_g(PIIN_08723)	6.2	Hypothetical protein, lectin-like LysM	<i>Hv</i> colonization
3661_g(PIIN_09859)	6.18	Hypothetical protein, DELD	<i>Hv</i> and <i>At</i> colonization
6698_g(PIIN_06410)	6.18	Hypothetical protein	
6458_g(PIIN_05098)	5.71	Hypothetical protein, DELD	<i>Hv</i> and <i>At</i> colonization
7883_g(PIIN_05242)	5.6	Related to peptidyl-Lys metalloendopeptidase	
9216_g(PIIN_03736)	5.5	Probable acetylxylan esterase	
6575_g(PIIN_01273)	4.9	Hypothetical protein	
7037_g(PIIN_08942)	4.78	Related to metalloprotease	
4183_g(PIIN_06900)	4.75	Hypothetical protein	
6634_g(PIIN_03075)	4.58	Hypothetical protein	
767_g(PIIN_08824)	4.23	Related to WD40-repeat protein (notchless protein)	
7142_g(N/A)	3.91	Hypothetical protein, DELD	
5200_g(PIIN_07639)	3.9	Hypothetical protein	
5275_t(PIIN_06837)	4.02	Hypothetical protein, DELD	<i>Hv</i> and <i>At</i> colonization
3238_g(PIIN_09643)	1.9	PiDld2	<i>Hv</i> and <i>At</i> colonization
6196_g(PIIN_04163)	1.44	Related to HSP82-Heat shock protein	
8967_g(PIIN_03461)	6.09	Hypothetical protein	
2675_g(PIIN_08764)	2.66	Probable ADE12-adenylosuccinate synthetase	
8386_g(PIIN_00425)	0.91	Probable extracellular elastolytic metalloproteinase precursor	

\*Those with the highest level of upregulation during Bd21-3 colonization are displayed. Prior detection of differentially expressed (DE) putative effector proteins in *Si*-colonized barley (*Hordeum vulgare* - *Hv*) or Arabidopsis (*At*) is indicated (22, 27).

**Table S5:** Candidate RNAi machinery proteins predicted from the resequenced *Serendipita indica* (Si) genome.\*

Gene	Protein	Description / Domains	<i>N. crassa</i> homolog	Score (E-value) / Identity (BlastP)	baseMean Deseq2
1587_g (PIIN_03414)	G4U2H0	Dicer-like protein, Helicase, dicer ds-RNA binding, RNase III	NCU08270	330 (3E-52) / 30.71 %	54.36
7403_g (PIIN_02669)	G4TBW9			273 (9E-75) / 24.15 %	51.81
5425_g (PIIN_06945)	G4TNU7	Related to qde-1 RNA-dependent RNA polymerase (RdRP)	NCU07534	111(9E-25)/25.97 %	102.65
2067_g (PIIN_07582)	G4TQP0			92.4 (5E-19) / 30.32 %	49.21
3379_g (PIIN_03690)	G4TEK0	QDE2 – like protein, PIWI domain	NCU04730	354 (2E-106) / 36.26 %	16.05
3261_g (PIIN_05928)	G4TL04			224 (1E-61) / 31.05 %	2.11
5826_g (PIIN_00261)	G4T5G9	Related to argonaute-like protein- <i>Laccaria bicolor</i>		233 (5E-64) / 28.59 %	124.7
1551_g (PIIN_06323)	G4TM47	Related to QDE3 protein, helicase domains	NCU08598	339 (3E-101) / 44.5 %	47.47
5685_g (PIIN_06751)	G4TND7	Probable DNA-directed RNA polymerase I	NCU01638	1208 (0.0) / 41.22 %	60.38

\* Homology with quelling-typical *Neurospora crassa* proteins is indicated. The baseMean (Deseq2; 107) is presented as an average of normalized count values across all samples.

**Table S6:** Total and unique reads for filtered sRNAs from Bd-C, Bd-Si and Si-ax.\*

sRNA dataset	Description	Number of sRNA
Si-ax	Total reads after adapter trimming	48 mil
	Total sRNAs, 100 % alignment to Si genome	33.9 mil
	Unique sRNAs, 100 % alignment to Si genome	1.9 mil
	Total endogenous sRNAs	11 mil
	Unique endogenous sRNAs	1.8 mil
Bd-Si	Total reads after adapter trimming	32.7 mil
<i>Si</i> → Bd21-3	Total putative ck sRNAs	786732
	Unique putative ck sRNAs	35895
Bd21-3 → <i>Si</i>	Total putative ck sRNAs	17 mil
	Unique putative ck sRNAs	286198
<i>Si</i> aligned sRNAs	Total endogenous sRNAs	261478
	Unique endogenous sRNAs	36163
Bd21-3 aligned sRNAs	Total endogenous sRNAs	1.6 mil
	Unique endogenous sRNAs	483352
Bd-C	Total reads after adapter trimming	55 mil
	Total sRNAs, 100 % alignment to Bd21-3 genome	34.6 mil
	Unique sRNAs, 100 % alignment to Bd21-3 genome	1 mil
	Total endogenous sRNAs	3 mil
	Unique endogenous sRNAs	906901

**Table S7:** Sequences of putative *Serendipita indica* and *Brachypodium distachyon* Bd21-3 ck-sRNA displayed in Table 4 and Table 5.

sRNA name	sRNA sequence
<i>Sis</i> RNA 1	AACUUCUCGAAUCGCAUGGCC
<i>Sis</i> RNA 2	AAUGCUGGGUGGAACGGCCCC
<i>Sis</i> RNA 3	AGCACCGCAUCCCGUCCGAUC
<i>Sis</i> RNA 4	AUGAAAGUGAAAGGUCGGGAA
<i>Sis</i> RNA 5	AUGGUUAGGAUUUGUCGCUCU
<i>Sis</i> RNA 6	CAAACCCGGACGCGUAAUGAA
<i>Sis</i> RNA 7	CCAUAGGACUCUGAAAGCACC
<i>Sis</i> RNA 8	CGAGUAGGCAGGCGUGGGGGU
<i>Sis</i> RNA 9	CUCGAAUCGCAUGGCCUUGUG
<i>Sis</i> RNA 10	CUUAAUUUUUGACGCCGUCGCC
<i>Sis</i> RNA 11	GACGCAUCCGCGGUAGAGCGU
<i>Sis</i> RNA 12	GAGGGAAAAAGGCUUGGGGAA
<i>Sis</i> RNA 13	GCACCGCAUCCCGUCCGAUCU
<i>Sis</i> RNA 14	GCCAUAGGACUCUGAAAGCAC
<i>Sis</i> RNA 15	GGGUCCGGUGCGUCCUCGACA
<i>Sis</i> RNA 16	GGUUCGAUUCCCCGAUUCGGA
<i>Sis</i> RNA 17	GUAAGCGUUGGAUUGUUCACC
<i>Sis</i> RNA 18	UCCGGCAACGGAACCCCGUUG
<i>Sis</i> RNA 19	UUGGGGAUCCGGCAACGGAAC
<i>Sis</i> RNA 20	UUGUCGUGCUGGGGAUAGAGC
<i>Bds</i> RNA 1	ACGGUGGUCAUGGAAGUCGAA
<i>Bds</i> RNA 2	ACUGUUGUCGGCCGUGCUGGC
<i>Bds</i> RNA 3	AGCCCCGUCCGGCCCGACCC
<i>Bds</i> RNA 4	AGUUAAGCGUGCUUGGGCGAG
<i>Bds</i> RNA 5	CCGGGCGGAGCGGCCGUCGGU
<i>Bds</i> RNA 6	CCUGGACGGGGUCUAUGGCCG
<i>Bds</i> RNA 7	CGGGGGACGGACCGGGAGUCG
<i>Bds</i> RNA_8	CGUGCUUGGGCGAGAGUAGUA
<i>Bds</i> RNA 9	CUGACAUGCGUGCGAGUCGAC
<i>Bds</i> RNA_10	CUGCACUGCCUCUUCCUGGC
<i>Bds</i> RNA 11	CUUAAUCCGUGGGUCGGAAGC
<i>Bds</i> RNA 12	CUUUGAACGCAAGUUGCGCCC
<i>Bds</i> RNA 13	GAGUCGACGGGUUCUGAAACC
<i>Bds</i> RNA 14	GCCACCCGGUCGAGGGCACGC
<i>Bds</i> RNA 15	GCGAGUCGACGGGUUCUGAAA
<i>Bds</i> RNA 16	GCUCGUAGUUGGACUUUGGGC
<i>Bds</i> RNA 17	GGCCGUGCCGUCCGAAUUGUA
<i>Bds</i> RNA 18	GGCGAGCGAACCGGGAGCAGC
<i>Bds</i> RNA_19	GGCUUUUGCUGGUCCGCCGCU
<i>Bds</i> RNA 20	UCGAGUCUUUGAACGCAAGUU

\* Putative endogenous and ck-sRNAs were identified via the filtering pipelines shown in Figure S6.

**Table S8:** Sequencing results from stem-loop PCR amplification of the selected *Si* and *Bd* sRNAs.\*

sRNA name	sRNA sequence	Stem_Loop Hairpin	Sequencing results
<i>SisRNA1</i>	AACUUCUCGAAUCGCAUGGCC	GTCGTATCCAGTGCAGG GTCCGAGGTATTCGCAC TGGATACGACggccat	5'- TCGCTAACTTCTCGAATCGCATG <u>GCCGTCGTATCCAGTGCGAAT</u> <b>ACCTCGGACCCTGCACTGGAT</b> <b>ACAATCACTAGTGAAT-3'</b>
<i>SisRNA30</i>	UACCCAUACCUCGCCGUCGGC	GTCGTATCCAGTGCAGG GTCCGAGGTATTCGCAC TGGATACGACgccgac	5'- TCGCTTACCCATACCTCGCCGTC <u>GGCGTCGTATCCAGTGCGAAT</u> <b>ACCTCGGACCCTGCACTGGAT</b> <b>ACAATCACTAGTGA-3'</b>
<i>SisRNA8</i>	CGAGUAGGCAGGCGUGGGGGU	GTCGTATCCAGTGCAGG GTCCGAGGTATTCGCAC TGGATACGACaccccc	5'- TCGCTCGAGTAGGCAGGCGTGG <u>GGGTGTCGTATCCAGTGCGAA</u> <b>TACCTCGGACCCTGCACTGGA</b> <b>TACAATCACTAGTGA-3'</b>
<i>SisRNA15</i>	GGGUCCGGUGCGUCCUCGACA	GTCGTATCCAGTGCAGG GTCCGAGGTATTCGCAC TGGATACGACtgtga	5'- TCGCTGGGTCCGGTGCGTCCTCG <u>ACAGTCGTATCCAGTGCGAAT</u> <b>ACCTCGGACCCTGCACTGGAT</b> <b>ACAATCACTAGTGAAT-3'</b>
<i>BdsRNA1</i>	ACGGUGGUCAUGGAAGUCGAA	GTCGTATCCAGTGCAGG GTCCGAGGTATTCGCAC TGGATACGACttegac	5'- TCGCTACGGTGGTCATGGAAGTC <u>GAAAGTCGTATCCAGTGCGAAT</u> <b>ACCTCGGACCCTGCACTGGAT</b> <b>ACAATCGAATTCCCGC-3'</b>
<i>BdsRNA7</i>	CGGGGGACGGACCGGGAGUCG	GTCGTATCCAGTGCAGG GTCCGAGGTATTCGCAC TGGATACGACcgactc	5'- TCGCTCGGGGGACGGACCGGGA <u>GTCCGTGTCGTATCCAGTGCGAA</u> <b>TACCTCGGACCCTGCACTGGA</b> <b>TACAATCACTAGTGAAT-3'</b>
<i>BdsRNA10</i>	CUGCACUGCCUCUCCCCUGGC	GTCGTATCCAGTGCAGG GTCCGAGGTATTCGCAC TGGATACGACgccagg	5'- TCGCTCTGCACTGCCTCTTCCCT <u>GGCGTCGTATCCAGTGCGAAT</u> <b>ACCTCGGACCCTGCACTGGGT</b> <b>ACAATCGAATTCCCGCATCACTA</b> <b>GTGAAT-3'</b>

\* Performed after cloning into pGEMT-Easy vector (Figure S12). Small RNA sequence in the sequencing results is underlined and the stem-loop hairpin is in bold.

**Table S9:** List of primers used for qPCR validation of DEGs from mRNA sequencing.

Primer name	Sequence
Ubi4-3Fw	GCTGTTGGAAGTCTGCTATACCT
Ubi4-3Rv	TTGCACCAAACCAACACACACCAG
Bd213_PRR7_F	CAGTTGATGGTGGGTGCCT
Bd213_PRR7_R	TCGTCATTACCGCTCCTCCA
Bd213_PR5_F	CTACGTGTGCGAGCAGTCTT
Bd213_PR5_R	CTTTGAGTGTGCCCTTGATGC
Bd213_HSP90_F	TGAGGTTTCAGAGTTGGTCGC
Bd213_HSP90_R	CCCGAGCCTTTGGATCACTT
Bd213_Chit_rel_F	CGTCGCCTATTACGAGCAGT
Bd213_Chit_rel_R	ATGCCACAAATCAAACGCCC
Bd213_RCI2_F	CCTGTGGTCGCCAATGACAC
Bd213_RCI2_R	CGCAGGAGAGCCTATTCGTT
Piri_ITS_F	CAACACATGTGCACGTCGAT
Piri_ITS_R	CCAATGTGCATTCAGAACGA
1121_t_ADY2_F	CCACCACGACTACCCAACAA
1121_t_ADY2_R	AGGACCAGGATTGCCAAGTG
5097_t_acCOdh_F	CGGTGTCTTTGCCGACTACT
5097_t_acCOdh_R	ACTGGGACCTTGACGTTGTC
917_t_YTP1_F	GCAAACATCCAGGAGACCCA
917_t_YTP1_R	CCAGCCCCAAAACATGACAGC
8585_t_glucosidase_F	CTCACCGTCCTCGACAACAA
8585_t_glucosidase_R	CCCCGCTTCAATCTTCCACT
1893_t_GST_F	ATGAGCTGACCTATGCCGAC
1893_t_GST_R	TTCCTCCCTTGGCTTTCTGC

**Table S10:** Hairpin primers and specific primers used in stem-loop PCR confirmation of sequencing-detected sRNAs.

hairpin Primer name	hairpin Primer sequence
qPSisRNA1_cDNAhp	GTCGTATCCAGTGCAGGGTCCGAGGTATTCGCACTGGATACGACggccat
qPSisRNA6_cDNAhp	GTCGTATCCAGTGCAGGGTCCGAGGTATTCGCACTGGATACGACttcatt
qPSisRNA8_cDNAhp	GTCGTATCCAGTGCAGGGTCCGAGGTATTCGCACTGGATACGACaccccc
qPSisRNA15_cDNAhp	GTCGTATCCAGTGCAGGGTCCGAGGTATTCGCACTGGATACGACtgtcga
qPSisRNA19_cDNAhp	GTCGTATCCAGTGCAGGGTCCGAGGTATTCGCACTGGATACGACgttcgg
qPSisRNA26_cDNAhp	GTCGTATCCAGTGCAGGGTCCGAGGTATTCGCACTGGATACGACgatccg
qPSisRNA30_cDNAhp	GTCGTATCCAGTGCAGGGTCCGAGGTATTCGCACTGGATACGACgccgac
qPSisRNA37_cDNAhp	GTCGTATCCAGTGCAGGGTCCGAGGTATTCGCACTGGATACGACacaaat
qPSisRNA28_cDNAhp	GTCGTATCCAGTGCAGGGTCCGAGGTATTCGCACTGGATACGACagatcc
qPSisRNA62_cDNAhp	GTCGTATCCAGTGCAGGGTCCGAGGTATTCGCACTGGATACGACcagagt
qPBdsRNA1_cDNAhp	GTCGTATCCAGTGCAGGGTCCGAGGTATTCGCACTGGATACGACttcgac
qPBdsRNA7_cDNAhp	GTCGTATCCAGTGCAGGGTCCGAGGTATTCGCACTGGATACGACcgactc
qPBdsRNA10_cDNAhp	GTCGTATCCAGTGCAGGGTCCGAGGTATTCGCACTGGATACGACgccagg
qPBdsRNA18_cDNAhp	GTCGTATCCAGTGCAGGGTCCGAGGTATTCGCACTGGATACGACgctgct
qPBdsRNA_20_cDNAhp	GTCGTATCCAGTGCAGGGTCCGAGGTATTCGCACTGGATACGACaacttg
qPBdsRNA_21_cDNAhp	GTCGTATCCAGTGCAGGGTCCGAGGTATTCGCACTGGATACGACgccggc
qPBdsRNA_22_cDNAhp	GTCGTATCCAGTGCAGGGTCCGAGGTATTCGCACTGGATACGACaggaat
qPBdsRNA_23_cDNAhp	GTCGTATCCAGTGCAGGGTCCGAGGTATTCGCACTGGATACGACgccggc
qPBdsRNA_24_cDNAhp	GTCGTATCCAGTGCAGGGTCCGAGGTATTCGCACTGGATACGACgccagc
qPBdsRNA_25_cDNAhp	GTCGTATCCAGTGCAGGGTCCGAGGTATTCGCACTGGATACGACgaggcc
qPBdi-MIR166b_cDNAhp	GTCGTATCCAGTGCAGGGTCCGAGGTATTCGCACTGGATACGACggggaa
Specific forward primer name	specific forward primer sequence
qPSisRNA1_F	TCGCTaacttctcgaatcgc
qPSisRNA6_F	TCGCTcaaaccggacgcgt
qPSisRNA8_F	TCGCTcgagtaggcaggcgt
qPSisRNA15_F	TCGCTgggtccggtgcgtcc
qPSisRNA19_F	TCGCTttgggatccggcaa
qPSisRNA26_F	TCGCTtacaactttcaaaa
qPSisRNA30_F	TCGCTtaccataacctgcc
qPSisRNA37_F	TCGCTgctcacgttctatag
qPSisRNA28_F	TCGCTacaactttcaacaac
qPSisRNA62_F	TCGCTatccacggccatagg

qPBdsRNA1_F	TCGCTacggtggatcatggaa
qPBdsRNA7_F	TCGCTcgggggacggaccgg
qPBdsRNA10_F	TCGCTctgcactgcctcttc
qPBdsRNA18_F	TCGCTggcgagcgaaccggg
qPBdsRNA20_F	TCGCTtcgagtctttgaacg
qPBdsRNA_21_F	TCGCTagcgggtcgccgcgt
qPBdsRNA_22_F	TCGCTaagtcctcgtgttc
qPBdsRNA_23_F	TCGCTtgettataaggactcc
qPBdsRNA_24_F	TCGCTactgttgctggccgt
qPBdsRNA_25_F	TCGCTggagacgccggcggg
qPBdi-MIR166b_F	TCGCTtcggaccaggctca
primer name	primer sequence
M13_F	GTTTTCCCAGTCACGAC
M13_R	AACAGCTATGACCATG
univ_stemloop_PCR_rev	GTATCCAGTGCAGGGTCCGAGGT